

Synthesis and Biomedical Applications of Fluorescent Organophosphorus Compounds



Charlotte Hepples

Submitted in fulfilment of the requirements for the degree of
Doctor of Philosophy

December 2020

Supervisor of Research: Dr Lee J. Higham

School of Natural and Environmental Sciences
Newcastle University
Newcastle upon Tyne, NE1 7RU

Abstract

An important and ongoing area of research is the treatment and imaging of diseases such as cancer and heart disease, as these are two of the leading causes of death worldwide. Prior research in this area has led to the development of effective agents such as the chemotherapeutic agent, cisplatin, and Myoview, a cardiac perfusion imaging agent. However, with the number of cases of cancer and heart disease continuing to rise, there is still an urgent requirement for further development of these agents. Thus, the synthesis of effective imaging agents and, in particular, probes with multiple modalities which can harness the benefits of multiple imaging techniques are of interest. Organophosphorus compounds provide a versatile platform to build such probes that could be applied in fluorescence imaging, SPECT, PET and MRS. Therefore, this thesis explores the functionalisation of organophosphorus compounds to afford a range of novel, fluorescent, phosphine probes with potential medicinal applications.

Auranofin is a triethylphosphine containing, FDA approved therapeutic agent that has recently shown potential for its repurposing in new areas including neurodegenerative disorders, parasitic infections, HIV and cancers. Thus, Chapter 2 explores the synthesis of a series of analogues of auranofin by altering the triethylphosphine ligand. A series of fluorescent analogues of auranofin are also introduced which may hold potential as theranostic agents and perhaps aid in the derivation or elucidation of the mechanism of action of the pharmaceutical.

Azacycles are nitrogen containing cyclic compounds which are commonly found in natural products and bioactive compounds. Chapter 3 introduces three novel fluorescent phosphacycles which are far less studied than their nitrogen derivatives. We investigate a highly strained three-membered cycle, a phosphirane, where we explore its air- and thermal-stability and its coordination to group 6 metal carbonyl complexes. The methylation of the phosphirane to afford a phosphiranium salt is detailed for which the product has potential application as a dual optical and magnetic resonance imaging agent.

We also look briefly at two six-membered 1,3,5-diazaphosphanes, which were synthesised in collaboration with Dr Randolph Köhn, at the University of Bath are detailed. Coordination of one of the diazaphosphanes to chromium(III) centres and the subsequent preliminary experiments to test for its application in catalytic 1-hexene trimerization will then be

described. A short collaborative project with Professor Bill Henderson at the University of Waikato is introduced to detail how one of the fluorescent phosphines can be applied in the fluorescent labelling of amine modified surfaces.

The final phosphacycles introduced are the seven-membered phosphacycles, the phosphepines. The synthesis of two group 6 phosphepine complexes will be described followed by a study of their electronic properties. Preliminary experiments were then carried out in an effort to afford the free ligand which would allow for its further functionalisation.

Chapter 4 describes the synthesis of BodP₃, a fluorescent tridentate phosphine, via a platinum-catalysed hydrophosphination of the fluorescent primary phosphine. Exploration into its coordination to group 10 metals will be detailed, with particular attention focused on the square planar platinum complexes as potential theranostic agents.

Combined imaging agents are becoming increasingly popular in order to harness the benefits of multiple imaging techniques, such as optical imaging and radioimaging, to overcome the limitations of the individual techniques. Thus, Chapter 5 introduces a series of phosphonium salts which have potential as trifunctional imaging agents. These novel phosphonium salts contain i) a fluorescent Bodipy backbone suitable for *in vitro* fluorescence imaging, ii) a positively charged phosphonium centre to enable specific localisation within the mitochondria, and iii) an alkyne functional group to enable radiolabelling by click chemistry to facilitate *in vivo* PET imaging. Finally, preliminary click chemistry reactions will be described to demonstrate the synthesis of a cold standard of this trifunctional imaging agent.

Acknowledgements

First of all, I would like to thank my supervisor, Dr Lee J. Higham, for giving me the chance to carry out this PhD – it has led to a great deal of opportunities for which I'm very grateful for. Particular thanks for letting me escape Newcastle for a year for San Diego! Finally, thank you for the sheer amount of time and red pen you spent to help me get this thesis to where it is today, I really do appreciate it (no sarcasm intended, I promise)!

I am also very thankful to Newcastle University for funding my PhD, and to the Capstaff Fellowship for giving me the incredible opportunity to join the lab of Dr Peter Wang and Dr Kathy Lu at the University of California, San Diego. A special thank you to Peter and Kathy for welcoming me into your lab, and to all my co-workers, specifically Rinoka, Shannon, Chi-Wei and Yijia; I miss you all a lot! Also, the 'behind-the-scenes' work of Francesca in Newcastle – I never got to meet you, but your hard work didn't go unnoticed – thank you!

I could not have completed this work without the help of the exceptional: Dr Paul Waddell (X-ray), Professor William McFarlane, Dr Corinne Wills, Dr Casey Dixon (NMR), Alex Charlton (MS) and Dr Magda Borrás Pascual (DFT). I must also give appreciation to the School's glassblowing, technical, workshop and administrative staff for their approachability and services provided.

To our fantastic academic collaborators: Dr Randolph Köhn, Prof. Bill Henderson, Prof. Sofia I. Pascu, Dr Kogularamanan (Rama) Suntharalingam and Prof. Steve Archibald – this thesis wouldn't be same without you all – thank you.

I feel very privileged to have joined an exceptional research group for my PhD. I'm grateful to Antonio, Graeme and Muhammad for your helpful discussions and advice. To Roger and Manraj, sadly, lockdown cut our time in the lab together short, but it has been great working with you! Finally, to the LJH alumni, Arne, Manuel, Connor, James and Jenny, thanks for taking me under your wing and keeping the LJH team alive! A special thanks to Manuel, Jenny and Laura; Manuel for being my running partner throughout my write up months (and lockdown) which undoubtedly helped to keep me sane. And to Jenny and Laura, for doing an incredible job of setting the foundations of this Bodipy phosphine research project and for teaching me everything I needed to know. I hope you will be pleased to see how it has progressed!

I was fortunate enough to meet some fantastic people throughout my PhD and so I would like to extend my thanks to all my colleagues in the School, particularly those in the Johnston Lab and to the Erasmus and MChem students that I have had the pleasure of working with over the years; Rosie, Rosie, Linh and Charlotte, thanks for contributing to the Bodipy research!

An immense thank you to my friends Lok and Dom, who always went out of their way to help me wherever they could; thanks for keeping my caffeine levels high and proof-reading my terrible first drafts (and my *slightly less terrible* second and third drafts) – you guys are the best, I owe you!

Finally, I absolutely would not be the person I am today without the support and friendship from all of my wonderful friends: Sam, Abbie, Chloe, Tiph, AJ, Matt, Jack, Tom, Vicky and Violeta, and my family, especially Mum, Dad and Laura. Thanks for keeping my spirits high and being my ultimate cheer team! Maybe one day you'll read this book and finally understand what I do...!

I finally did it!! – I hope I made you all proud! xx

List of Abbreviations

General:

β	Beta particle
B3LYP	Becke Parameter Lee-Yang-Parr
C–C	Carbon–Carbon
C–P	Carbon–Phosphorus
CT	Computed Tomography
CuAAC	Copper-catalysed Azide-Alkyne Cycloaddition
Cy	Cyclohexyl
DFT	Density Functional Theory
Et	Ethyl
γ	Gamma ray
HOMO	Highest Occupied Molecular Orbital
HPLC	High-Performance Liquid Chromatography
LUMO	Lowest Unoccupied Molecular Orbital
99m	Metastable isotope
M	Metal
Me	Methyl
MRI	Magnetic Resonance Imaging
MRS	Magnetic Resonance Spectroscopy
PET	Positron Emission Tomography
PeT	Photoinduced Electron Transfer
Ph	Phenyl
RT	Room Temperature
SOMO	Singly Occupied Molecular Orbital
SPECT	Single Photon Emission Computed Tomography
TLC	Thin Layer Chromatography
$t_{1/2}$	Half-life

UV	Ultraviolet
Chemicals:	
Bodipy	4,4-difluoro-4-borata-3a-azonia-4a-aza-s-indacene
CBr_4	Tetrabromomethane
CDCl_3	Deuterated chloroform
cod	1,5-Cyclooctadiene
CDCl_3	Deuterated Chloroform
DCM	Dichloromethane
DDQ	2,3-Dicyano-5,6-dichloro-1,4-benzoquinone
DMSO	Dimethylsulfoxide
DPPB	1,4-Bis-(diphenylphosphino)-butane
Et_2O	Diethyl ether
EtOH	Ethanol
HBr	Hydrogen Bromide
HP(O)(OEt)_2	Diethyl phosphite
LiAlH_4	Lithium aluminium hydride
MeLi	Methyl lithium
MeOH	Methanol
MgSO_4	Magnesium sulfate
(<i>S</i>)-H-MOPH ₂	(<i>S</i>)-2-Phosphino-1',1'-binaphthyl
(<i>R</i>)-MeO-MOPH ₂	(<i>R</i>)-2-Phosphino-2'-methoxy-1',1'-binaphthyl
NEt_3	Triethylamine
Pd(OAc)_2	Palladium(II) acetate
PPh_3	Triphenylphosphine
PTA	1,3,5-Triaza-7-phosphaadamantane
R	Arbitrary Organic Substituent
TFA	Trifluoroacetic acid
THF	Tetrahydrofuran
TMSCl	Trimethylsilyl chloride

NMR Spectroscopy:

δ	Chemical shift
br	Broad
d	Doublet
dd	Doublet of Doublets
I	Nuclear Spin
J	Coupling Constant
m	Multiplet
NMR	Nuclear Magnetic Resonance
<i>NOE</i>	Nuclear Overhauser Effect
q	Quartet
s	Singlet
t	Triplet

UV-Visible and Fluorescence Spectroscopy:

ϵ	Molar Absorption Coefficient
Φ_F	Fluorescence Quantum Yield

IR Spectroscopy:

br	Broad
FT-IR	Fourier Transform Infrared Spectroscopy
IR	Infrared
ν	Frequency
m	Medium/Moderate
s	Strong
w	Weak

Mass Spectrometry:

ESI	Electrospray Ionisation
HRMS	High Resolution Mass Spectrometry
TOF	Time-of-Flight

Fluorescence Imaging:

ECFP	Cyan Fluorescent Protein
FRET	Förster Resonance Energy Transfer
H3K9me3	Histone-3 Lysine-9 trimethylation
YPet	Yellow Fluorescent Protein

List of Units

Å	Angstroms
cm	Centimetres
°	Degrees
°C	Degrees Celsius
eq	Equivalents
eV	Electron Volts
Hz	Hertz
h	Hours
L	Litres
mg	Milligrams
MHz	MegaHertz
mmol	Millimolar
mins	Minutes
M	Molar
nm	Nanometres
ppm	Parts per million

s	Seconds
Å	Angstroms
cm	Centimetres
°	Degrees
°C	Degrees Celsius
eq	Equivalents
eV	Electron Volts
Hz	Hertz
h	Hours
L	Litres
mg	Milligrams
MHz	MegaHertz
mmol	Millimolar
mins	Minutes
M	Molar
nm	Nanometres
ppm	Parts per million
s	Seconds

Table of Contents

1	Background and Introduction	2
1.1	Cancer and Disease.....	2
1.2	Current Approaches to Treatment	3
1.2.1	Cisplatin and Platinum-Based Therapeutic Agents	3
1.2.2	Auranofin and Drug Repurposing.....	4
1.2.3	Ruthenium-Based Therapeutic Agents.....	5
1.3	Fluorescence Labelling.....	6
1.3.1	Fluorescence	7
1.4	Mitochondrial Dysfunction	8
1.4.1	Incorporation of an Imaging Modality	9
1.4.2	Click Chemistry	10
1.4.3	Positron Emission Tomography.....	12
1.5	Heart Disease	14
1.5.1	Single Photon Emission Computed Tomography (SPECT)	15
1.6	Magnetic Resonance Spectroscopy.....	17
1.6.1	Magnetic Resonance Imaging (MRI) and Magnetic Resonance Spectroscopy (MRS)	19
1.7	Organophosphorus Compounds	20
1.7.1	Phosphines	20
1.1.1	Steric and Electronic Parameters of Phosphine Ligands	21
1.8	Primary Phosphines.....	22
1.8.1	Steric Effects on Stability.....	23
1.1.2	Electronic Stability.....	25
1.9	Bodipy.....	27
1.1.3	Photoinduced electron Transfer (PeT)	28
1.10	Thesis Outline.....	30
1.11	References	33
2	Auranofin and its Analogues	41
2.1	Auranofin	41
2.1.1	Auranofin Analogues in the Literature.....	42
2.2	Analogues of Auranofin	43
2.2.1	Gold(I) Phosphine Complexes	44
2.2.2	Synthesis of Chlorogold(I) Phosphine Complexes [Au(16a-g)Cl] 17a-g	45

2.2.3	Synthesis of Gold(I) Phosphine Thioglucose Tetraacetate Complexes [Au(16a-g)SR]	46
2.3	Fluorescent Analogues of Auranofin	48
2.3.1	Towards the Synthesis of Fluorescent Auranofin Analogues.....	48
2.3.2	Synthesis of Fluorescent Tertiary Phosphines 24a-b	50
2.3.3	An Alternative Synthetic Approach via Primary Phosphine 14	51
2.3.4	Synthesis of Fluorescent Chlorogold(I) Phosphine Complexes [Au(24a-d)Cl] 25a-d	54
2.3.5	X-ray Crystal Structures.....	55
2.3.6	Synthesis of Fluorescent Gold(I) Phosphine Thioglucose Tetraacetate Complexes 26a-d	56
2.4	Photophysical Data	57
2.5	Summary and Future Work	62
2.6	Experimental Procedures and Analytical Data.....	65
2.6.1	General Procedure	65
2.7	General Procedure for the Synthesis of Chlorogold(I) Complexes (17a-g)	66
2.7.1	[Au(16a)Cl] (17a).....	66
2.7.2	[Au(16b)Cl] (17b)	66
2.7.3	[Au(16c)Cl] (17c)	67
2.7.4	[Au(16d)Cl] (17d)	67
2.7.5	[Au(16e)Cl] (17e).....	68
2.7.6	[Au(16f)Cl] (17f)	68
2.7.7	[Au(16g)Cl] (17g).....	69
2.8	General Procedure for the Synthesis of Gold(I)Thiosugar Phosphine Complexes (18a-g) 70	
2.8.1	[Au(16a)SR] (18a).....	70
2.8.2	[Au(16b)SR] (18b)	71
2.8.3	[Au(16c)SR] (18c)	71
2.8.4	[Au(16d)SR] (18d)	72
2.8.5	[Au(16e)SR] (18e).....	72
2.8.6	[Au(16f)SR] (18f)	73
2.9	Synthesis of Fluorescent Analogues of Auranofin.....	74
2.9.1	8-(4-Bromophenyl)-4,4-difluoro-1,3,5,7-tetramethyl-2,6-diethyl-4-bora-3a,4a-diaza-s-indacene (19)	74
2.9.2	8-(4-Bromophenyl)-4,4-dimethyl-1,3,5,7-tetramethyl-2,6-diethyl-4-bora-3a,4a-diaza-s-indacene (20)	75
2.9.3	8-((4-Diethylphosphonato)phenyl)-4,4-difluoro-1,3,5,7-tetramethyl-2,6-diethyl-4-bora-3a,4a-diaza-s-indacene (21)	75
2.9.4	8-((4-Diethylphosphonato)phenyl)-4,4-dimethyl-1,3,5,7-tetramethyl-2,6-diethyl-4-bora-3a,4a-diaza-s-indacene (22)	76

2.9.5	8-((4-Phosphino)phenyl)-4,4-dimethyl-1,3,5,7-tetramethyl-2,6-diethyl-4-bora-3a,4a-diaza-s-indacene (14)	77
2.10	General Procedure for the Synthesis of Fluorescent Tertiary Phosphines (24a-d)	78
2.10.1	Route 1	78
2.10.2	Route 2	78
2.10.3	8-((4-Diphenylphosphino)phenyl)-4,4-dimethyl-1,3,5,7-tetramethyl-2,6-diethyl-4-bora-3a,4a-diaza-s-indacene (24a)	78
2.10.4	8-((4-Dicyclohexylphosphino)phenyl)-4,4-dimethyl-1,3,5,7-tetramethyl-2,6-diethyl-4-bora-3a,4a-diaza-s-indacene (24b)	79
2.10.5	8-((4-Diethylphosphino)phenyl)-4,4-dimethyl-1,3,5,7-tetramethyl-2,6-diethyl-4-bora-3a,4a-diaza-s-indacene (24c)	80
2.10.6	8-(4-(Bis(hydroxymethyl)phosphino)phenyl)-4,4-dimethyl-1,3,5,7-tetramethyl-2,6-diethyl-4-bora-3a,4a-diaza-s-indacene (24d)	81
2.11	General Procedure for the Synthesis of Fluorescent Gold(I) Complexes (25a-d)	82
2.11.1	[Au(24a)Cl] (25a)	82
2.11.2	[Au(24b)Cl] (25b)	83
2.11.3	[Au(24c)Cl] (25c)	83
2.11.4	[Au(24d)Cl] (25d)	84
2.12	General Procedure for the Synthesis of Fluorescent Gold(I)Thiosugar Complexes (26a-d)	85
2.12.1	[Au(24a)SR] (26a)	85
2.12.2	[Au(24b)SR] (26b)	86
2.12.3	[Au(24c)SR] (26c)	86
2.12.4	[Au(24d)SR] (26d)	87
2.13	References	88
3	Phosphacycles from a Fluorescent Air Stable Primary Phosphine	93
3.1	Phosphacycles	94
3.1.1	Three-Membered Heterocycles	94
3.1.2	Three-Membered Phosphacycles	95
3.1.3	Four-Membered Heterocycles	97
3.1.4	Five-Membered Heterocycles	99
3.1.5	Six-Membered Heterocycles	101
3.1.6	Seven-Membered Heterocycles	103
3.2	Results and Discussion	105
3.2.1	Highly Stable Phosphirane	105
3.3	Multimodal Imaging	106

3.4	Synthesis of a Novel Fluorescent Phosphirane 47	107
3.5	Phosphirane Air- and Thermal-Stability Studies	110
3.5.1	Air-Stability Studies of Phosphirane 47	110
3.5.2	Thermal-Stability Studies of Phosphirane 47	111
3.6	Coordination Studies	111
3.6.1	Synthesis of a <i>cis</i> -Platinum(II) Complex	111
3.6.2	Synthesis of Metal Carbonyl Complexes	112
3.6.3	Photophysical Properties	116
3.7	Towards the Synthesis of a Fluorescent Phosphiranium Salt 48	118
3.7.1	Synthesis of Phosphiranium Salt 48	118
3.7.2	Density Functional Theory Calculations	120
3.8	Phosphirane Summary	122
3.9	1,3,5-Diazaphosphinanes	123
3.9.1	Six-Membered Heterocycles	123
3.9.2	Synthesis of a Novel Fluorescent 1,3,5-Diazaphosphinane	125
3.10	Photophysical Data	127
3.11	Complexation reactions with Chromium(III) Complexes	129
3.11.1	Testing in Catalytic Reactions	131
3.12	1,3,5-Diazaphosphinane Summary	131
3.13	Surface Modification with a Fluorescent Label	131
3.13.1	Surface Modification	133
3.14	Seven-Membered Phosphacycle	134
3.14.1	Synthesis of Primary Phosphine Group 6 Carbonyl Complexes [M(CO) ₅ (14)]	134
3.14.2	Synthesis of Metal Carbonyl Complexes	134
3.14.3	Synthesis of 1,2-Diethynylbenzene	135
3.14.4	Synthesis of Fluorescent Group 6 3-Benzophosphepine Complexes	136
3.14.5	IR and NMR Spectroscopic Characterisation	139
3.14.6	Photophysical Properties of [M(CO) ₅ (PR ₃)] Complexes 68a, 68b, 69a and 69b	140
3.15	Free Phosphepine	142
3.15.1	Attempted Synthesis of a Metal-Free Phosphepine	142
3.16	DFT Calculations	145
3.17	Phosphepine Summary	146
3.18	Chapter Summary	147

3.19	Experimental Procedures and Analytical Data	149
3.19.1	General Procedure	149
3.20	Phosphirane and Phosphiranium Experimental	150
3.20.1	8-((4-Phosphirane)phenyl)-4,4-dimethyl-1,3,5,7-tetramethyl-2,6-diethyl-4-bora-3a,4a-diaza-s-indacene (47).....	150
3.20.2	(<i>R</i>)-1-(2'-Methoxy-1,1'-binaphthyl-2-yl)phosphirane (32a).....	151
3.20.3	Solid-State Oxidation Experiments	152
3.20.4	Solution-State Oxidation Experiments.....	152
3.20.5	Thermal Stability Experiments	152
3.20.6	<i>cis</i> -[Pt(47) ₂ Cl ₂] (50)	152
3.20.7	<i>cis</i> -[Pt(32a) ₂ Cl ₂] (49a)	152
3.20.8	General Procedure for the Preparation of [M(CO) ₅ (32a/47)]	153
3.20.9	[Mo(CO) ₅ (47)] (52a).....	153
3.20.10	[W(CO) ₅ (47)] (52b)	153
3.20.11	[Mo(CO) ₅ (32a)] (51a).....	154
3.20.12	[W(CO) ₅ (32a)] (51b)	154
3.20.13	(<i>R</i>)-1-(2'-Methoxy-[1,1'-binaphthalen]-2-yl)-1-methylphosphiranium triflate (44a)	155
3.20.14	4,4-Dimethyl-1,3,5,7-tetramethyl-2,6-diethyl-4-bora-3a,4a-diaza-s-indacene-8-methylphosphiranium triflate (48).....	155
3.21	1,3,5-Diazaphosphinane Experimental.....	156
3.21.1	General Procedure	156
3.21.2	Calculation Details.....	156
3.21.3	8-(4-(1,3-Dimethyl-1,3,5-diazaphosphinan-5-yl)phenyl)-4,4-dimethyl-1,3,5,7-tetramethyl-2,6-diethyl-4-bora-3a,4a-diaza-s-indacene (62a)	157
3.21.4	8-(4-(1,3-Diethyl-1,3,5-diazaphosphinan-5-yl)phenyl)-4,4-dimethyl-1,3,5,7-tetramethyl-2,6-diethyl-4-bora-3a,4a-diaza-s-indacene (62b)	158
3.21.5	8-(4-(1,3-Dimethyl-1,3,5-diazaphosphinane-5-oxide)phenyl)-4,4-dimethyl-1,3,5,7-tetramethyl-2,6-diethyl-4-bora-3a,4a-diaza-s-indacene (63a).....	159
3.21.6	8-(4-(1,3-Diethyl-1,3,5-diazaphosphinane-5-oxide)phenyl)-4,4-dimethyl-1,3,5,7-tetramethyl-2,6-diethyl-4-bora-3a,4a-diaza-s-indacene (63b)	159
3.21.7	8-(4-(1,3-Dimethyl-1,3,5-diazaphosphinane-5-sulfide)phenyl)-4,4-dimethyl-1,3,5,7-tetramethyl-2,6-diethyl-4-bora-3a,4a-diaza-s-indacene (64a).....	160
3.21.8	8-(4-(1,3-Diethyl-1,3,5-diazaphosphinane-5-sulfide)phenyl)-4,4-dimethyl-1,3,5,7-tetramethyl-2,6-diethyl-4-bora-3a,4a-diaza-s-indacene (64b)	160
3.22	Surface Modification General Procedure	161
3.22.1	Synthesis of 3-Aminopropyl SBA-15	161
3.22.2	Reaction of Aminopropyl SBA-15 with 24d	161
3.22.3	Control Experiment	161

3.23	Phosphepine Experimental	162
3.23.1	General Procedure	162
3.23.2	1,2-Bis(2,2-dibromovinyl)benzene (71).....	163
3.23.3	1,2-Diethynylbenzene (66) ⁸⁹	163
3.23.4	General Procedure for the Synthesis of Metal Carbonyl Complexes	164
3.23.5	[Mo(CO) ₅ (14)] (68a)	164
3.23.6	[W(CO) ₅ (14)] (68b)	164
3.23.7	[Mo(CO) ₅ (72)] (69a)	165
3.23.8	[W(CO) ₅ (72)] (69b)	166
3.23.9	1,2-Bis((Z)-2-bromovinyl)benzene (73)	167
3.23.10	Attempted Synthesis of a Metal-Free Phosphepine (72)	167
3.24	References.....	169
4	A Fluorescent Tridentate Phosphine and its Coordination to Group 10 Metals	179
4.1	Polydentate Ligands.....	180
4.1.1	Polydentate Ligands in Catalysis	180
4.1.2	Polydentate Ligands in Medicine	181
4.1.3	Dual-Modality Tridentate Phosphine.....	182
4.1.4	Synthesis of Fluorescent Tridentate Phosphine (75)	184
4.2	Group 10 Metal Coordination Studies	185
4.2.1	Synthesis of Nickel(II) Complex from Fluorescent Tridentate BodP ₃	185
4.2.2	Palladium	187
4.2.3	Synthesis of Palladium(II) Complex 83 from Fluorescent Tridentate BodP ₃	188
4.2.4	Synthesis of Platinum(II) Complex 84a from Fluorescent Tridentate BodP ₃	189
4.2.5	Cell Imaging Studies	191
4.2.6	Effect of the Halide Ligand on Platinum(II) Complexes.....	192
4.2.7	Synthesis of Novel Platinum(II) Complexes from Fluorescent Tridentate BodP ₃	194
4.3	Photophysical Data	196
4.4	DFT Calculations	198
4.5	Summary and Future Work	201
4.6	Experimental Procedures and Analytical Data	202
4.6.1	General Procedure	202
4.6.2	8-(4-(Bis-2-ethyldiphenylphosphino)-phenylphosphino)-4,4-dimethyl-1,3,5,7-tetramethyl-2,6-diethyl-4-bora-3a,4a-diaza-s-indacene (75)	203
4.6.3	[Ni(75)Cl]Cl (81).....	204
4.6.4	[Pd(75)Cl]Cl (83)	204
4.6.5	[PtCl ₂ (η ² :η ² -cod)]	205

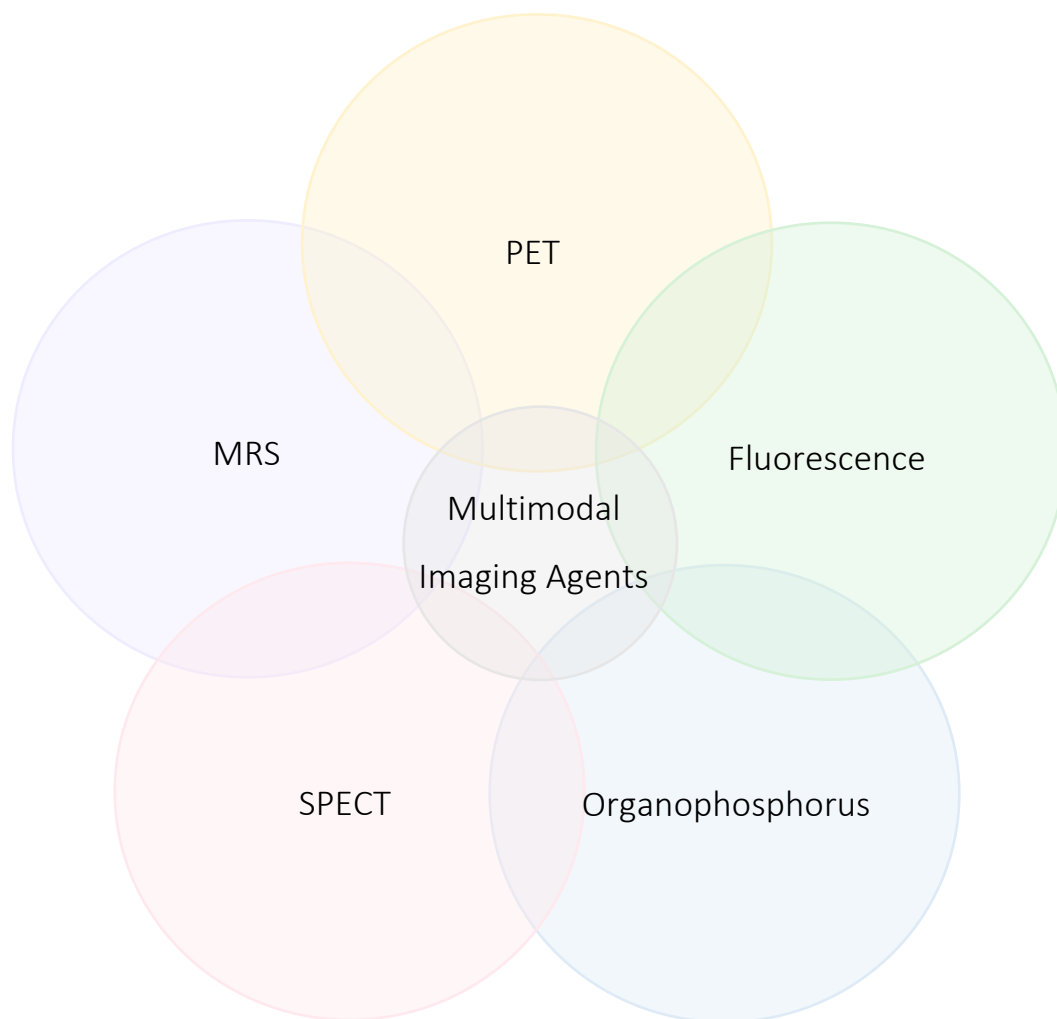
4.6.6	[PtBr ₂ (η ² :η ² -cod)]	205
4.6.7	[PtI ₂ (η ² :η ² -cod)]	205
4.6.8	General Procedure for the Synthesis of Platinum Complexes (84a-c)	205
4.6.9	[Pt(75)Cl]Cl (84a)	206
4.6.10	[Pt(75)Br]Br (84b)	206
4.6.11	[Pt(75)I]I (84c)	206
4.7	References	208
5	Towards a Trifunctional Mitochondrial Imaging Agent	213
5.1	Mitochondria	213
5.1.1	Phosphonium Cations	214
5.2	Towards a Multimodal Imaging Agent	215
5.3	Synthesis of Fluorescent Phosphonium Salt 85a	217
5.4	Cell Imaging Studies of 85a in Pancreatic Ductal Adenocarcinoma Cells	217
5.4.1	Pancreatic Cancer	217
5.4.2	Mitochondrial Uptake Tests	218
5.5	Radiolabelling of the Fluorescent Phosphonium Salt to Convert 85a into a PET Probe	220
5.6	Development of Probes for Radiolabelling by the Direct Exchange Method	221
5.6.1	Synthesis of Triphenylphosphonium Salts	222
5.6.2	Synthesis of the Third-Generation Fluorescent Triphenylphosphonium Salts 85b-c	224
5.7	Attempted ¹⁸F Radiolabelling Reactions	224
5.8	Radiolabelling by Click Chemistry	226
5.9	Development of Probes for Radiolabelling by Click Chemistry	227
5.9.1	Synthesis of Alkynyl Triphenylphosphonium Salts	227
5.9.2	Synthesis of Fluorescent Alkynyl Phosphonium Salts	230
5.9.3	Synthesis of Fluorescent Alkynyl Phosphonium Salts (97a and 97b)	236
5.10	Photophysical Data	237
5.11	Preliminary Copper-Catalysed Azide-Alkyne Cycloaddition Experiments	239
5.12	Summary and Future Work	242
5.13	Experimental Procedures and Analytical Data	244
5.13.1	General Procedure	244
5.14	Cell Imaging Studies of 85a in Pancreatic Ductal Adenocarcinoma Cells	244
5.14.1	Cell Culture	244
5.14.2	Cell Plating for Microscopy	245

5.14.3	Image Acquisition and Analysis	245
5.15	General Procedure for the Synthesis of the Triphenylphosphonium Salts 88a-c	246
5.15.1	(4-Fluorobutyl)triphenylphosphonium bromide (88a).....	246
5.15.2	(4-Bromobutyl)triphenylphosphonium bromide (88b)	246
5.15.3	(4-Iodobutyl)triphenylphosphonium iodide (88c).....	247
5.16	General Procedure for the Synthesis of the Halobutane Phosphonium Salts 85a-c	248
5.16.1	8-((4-Dicyclohexylphosphino)(fluorobutyl)phenyl)-4,4-dimethyl-1,3,5,7-tetramethyl-2,6-diethyl-4-bora-3a,4a-diaza-s-indacene (85a) ¹⁵	248
5.16.2	8-((4-Dicyclohexylphosphino)(bromobutyl)phenyl)-4,4-dimethyl-1,3,5,7-tetramethyl-2,6-diethyl-4-bora-3a,4a-diaza-s-indacene (85b)	249
5.16.3	8-((4-Dicyclohexylphosphino)(iodobutyl)phenyl)-4,4-dimethyl-1,3,5,7-tetramethyl-2,6-diethyl-4-bora-3a,4a-diaza-s-indacene (85c)	249
5.17	Attempted ¹⁸F-Radiolabelling Experiments by Direct Exchange	250
5.17.1	¹⁸ F Generation	250
5.17.2	Direct Exchange Experiments.....	250
5.17.3	Attempted Two-step Radiolabelling with a ¹⁸ F-Bu-Br Prosthetic Group	250
5.18	Synthesis of the Propyne Phosphonium Bromide Salts.....	251
5.18.1	Prop-2-yn-1-yltriphenylphosphonium bromide (89a).....	251
5.18.2	Prop-2-yn-1-yl-dicyclohexylphenylphosphonium bromide (89c)	251
5.18.3	Cyclohexyldiphenylphosphonium bromide (92)	252
5.19	General Procedure for the Synthesis of the Butyne Phosphonium Bromide Salts	253
5.19.1	But-3-yn-1-yltriphenylphosphonium bromide (95a).....	253
5.19.2	But-3-yn-1-ylcyclohexyldiphenylphosphonium bromide (95b).....	253
5.19.3	But-3-yn-1-yl-dicyclohexylphenylphosphonium bromide (95c)	254
5.19.4	But-3-yn-1-yl-tricyclohexylphosphonium bromide (95d)	255
5.20	General Procedure for the Synthesis of the Hexyne Phosphonium Iodide Salts	255
5.20.1	Hex-5-yn-1-yltriphenylphosphonium iodide (96a).....	255
5.20.2	Hex-5-yn-1-ylcyclohexyldiphenylphosphonium iodide (96b).....	256
5.20.3	Hex-5-yn-1-yl-dicyclohexylphenylphosphonium iodide (96c)	256
5.20.4	Hex-5-yn-1-yl-tricyclohexylphosphonium iodide (96d)	257
5.20.5	8-((4-Diphenylphosphino)(hex-5-yn-1-yl)phenyl)-4,4-dimethyl-1,3,5,7-tetramethyl-2,6-diethyl-4-bora-3a,4a-diaza-s-indacene iodide (97a)	258
5.20.6	8-((4-Dicyclohexylphosphino)(hex-5-yn-1-yl)phenyl)-4,4-dimethyl-1,3,5,7-tetramethyl-2,6-diethyl-4-bora-3a,4a-diaza-s-indacene iodide (97b)	259
5.21	General Procedure for the Copper-Catalysed Azide-Alkyne Cycloaddition³¹	260
5.21.1	1-Azido-4-fluorobutane ⁴⁸	260
5.21.2	(4-(1-(4-Fluorobutyl)-1H-1,2,3-triazol-4-yl)butyl)triphenylphosphonium iodide (98a)	260

5.21.3	8-((4-Dicyclohexylphosphino)phenyl)-4,4-dimethyl-1,3,5,7-tetramethyl-2,6-diethyl-4-bora-3a,4a-diaza-s-indacene(4-(1-(4-fluorobutyl)-1H-1,2,3-triazol-4-yl)butyl) phosphonium iodide (99b)	261
5.22	References	262
6	Appendices.....	265
6.1	Chapter 2 X-ray Crystallographic Data	267
6.1.1	[Au(16g)Cl] (17g)	267
6.1.2	[Au(16f)SR] (18f)	268
6.1.3	[Au(24a)Cl] (25a)	269
6.1.4	[Au(24d)Cl] (25d).....	270
6.2	Chapter 3 X-ray Crystallographic Data	271
6.2.1	8-((4-Phosphirane)phenyl)-4,4-dimethyl-1,3,5,7-tetramethyl-2,6-diethyl-4-bora-3a,4a-diaza-s-indacene (47)	271
6.2.2	(R)-1-(2'-Methoxy-1,1'-binaphthyl-2-yl)phosphirane (32a)	272
6.2.3	[Mo(CO) ₅ (47)] (52a)	273
6.2.4	[W(CO) ₄ (32a) ₂] (51b)	274
6.2.5	8-(4-(1,3-Dimethyl-1,3,5-diazaphosphinan-5-yl)phenyl)-4,4-dimethyl-1,3,5,7-tetramethyl-2,6-diethyl-4-bora-3a,4a-diaza-s-indacene (62a)	275
6.2.6	8-(4-(1,3-Diethyl-1,3,5-diazaphosphinan-5-yl)phenyl)-4,4-dimethyl-1,3,5,7-tetramethyl-2,6-diethyl-4-bora-3a,4a-diaza-s-indacene (62b)	276
6.2.7	8-(4-(1,3-Dimethyl-1,3,5-diazaphosphinane-5-sulfide)phenyl)-4,4-dimethyl-1,3,5,7-tetramethyl-2,6-diethyl-4-bora-3a,4a-diaza-s-indacene (64a)	277
6.2.8	8-(4-(1,3-Diethyl-1,3,5-diazaphosphinane-5-sulfide)phenyl)-4,4-dimethyl-1,3,5,7-tetramethyl-2,6-diethyl-4-bora-3a,4a-diaza-s-indacene (64b)	278
6.2.9	[Mo(CO) ₅ (72)] (69a)	279
6.2.10	[W(CO) ₅ (72)] (69b)	280
6.3	Chapter 4 X-ray Crystallographic Data	281
6.3.1	[Ni(75)Cl]Cl (81).....	281
6.3.2	[Pd(75)Cl]Cl (83)	282
6.3.3	[Pt(75)Cl]Cl (84a)	283
6.4	Chapter 5 X-ray Crystallographic Data	284
6.4.1	(4-Bromobutyl)triphenylphosphonium fluoride (88a)	284
6.4.2	(4-Bromobutyl)triphenylphosphonium bromide (88b)	285
6.4.3	(4-Iodobutyl)triphenylphosphonium iodide (88c).....	286
6.4.4	Prop-2-yn-1-yl-dicyclohexylphenylphosphonium bromide (89c)	287
6.4.5	Cyclohexyldiphenylphosphonium bromide (92)	288
6.4.6	1-Bromo-2-((4-(diphenylphosphaneyl)phenyl)(4-ethyl-3,5-dimethyl-3H-pyrrol-2-yl)methyl)-4-ethyl-3,5-dimethyl-1H-pyrrole (94)	289

6.4.7	But-3-yn-1-ylcyclohexyldiphenylphosphonium bromide (95b)	290
6.4.8	But-3-yn-1-ylcyclohexylphenylphosphonium bromide (95c)	291
6.4.9	But-3-yn-1-yltricyclohexylphosphonium bromide (95d)	292
6.4.10	Hex-5-yn-1-ylcyclohexyldiphenylphosphonium iodide (96b)	293
6.4.11	Hex-5-yn-1-ylcyclohexylphenylphosphonium iodide (96c)	294
6.4.12	Hex-5-yn-1-yltricyclohexylphosphonium iodide (96d)	295
6.4.13	8-((4-Diphenylphosphino)(hex-5-yn-1-yl)phenyl)-4,4-dimethyl-1,3,5,7-tetramethyl-2,6-diethyl-4-bora-3a,4a-diaza-s-indacene iodide (97a)	296
6.5	Calculated Molecular Orbital Surfaces for 4-(2-Diphenylphosphinoethylamino)-7-nitro-2,1,3-benzoxadiazole	298
6.6	Calculated Molecular Orbital Surfaces for BodP₃ Complexes	299
6.7	Epigenetic Mechanisms of Cancer Drug Resistance	302
6.7.1	Pancreatic Cancer	302
6.7.2	Treatments for Pancreatic Cancer	302
6.7.3	Epigenetics	303
6.7.4	Förster Resonance Energy Transfer (FRET)	303
6.7.5	Histone H3K9me3 FRET Biosensor	304
6.7.6	Live Cell Fluorescence Imaging	305
6.8	Results and Discussion	306
6.8.1	Initial Comparative Studies	306
6.8.2	Effect of Gemcitabine Treatment	307
6.8.3	Time Series Experiments	307
6.8.4	RNA Sequencing	309
6.8.5	Summary	310
6.9	Experimental Procedures and Analytical Data	310
6.9.1	Cell lines	310
6.10	Cell Culture	310
6.10.1	Cell Plating for Microscopy	310
6.10.2	Image Acquisition and Analysis	311
6.10.3	RNA Extraction and Isolation	311
6.11	References	312

Chapter 1



Background and Introduction

The treatment and imaging of diseases such as cancer and heart disease is a highly important and active area of research. This has led to the development of effective reagents such as cisplatin as a chemotherapeutic agent, and Myoview as a cardiac perfusion imaging agent.

We are interested in the development of effective imaging agents, and in particular, probes with multiple modalities which can harness the benefits of two imaging techniques. With this in mind, organophosphorus compounds provide a versatile platform to build such probes that could be applied in fluorescence imaging, SPECT, PET and MRS. Developing probes of this kind requires a detailed understanding of phosphorus chemistry which will be introduced in the second half of the chapter.

1 Background and Introduction

1.1 Cancer and Disease

As highlighted by the World Health Organisation¹ and Our World in Data,² cancer and heart disease are two of the leading causes of death worldwide. In the UK alone, there are over 367,000 new cases of cancer every year and 164,901 fatalities, with the number of cases continuing to rise.³ An estimated four million people will be living with cancer by 2030, up from 2.5 million people in 2015.⁴ The two most common types of cancer in the UK are breast and prostate cancer which make up over 100,000 cases each year, with over 55,000 people diagnosed with breast cancer and over 47,500 cases of prostate cancer.³

Though it is not the most common cancer, pancreatic cancer is one of the most lethal malignancies; it is the 10th most common but the 5th most fatal cancer within the UK.³ Its abysmal five-year survival rate of only 7.3% can be attributed to the lack of early symptoms which make late stage diagnosis common; at the time of diagnosis, the cancer has often reached an advanced or metastatic stage (shown in Figure 1.1) where surgery is no longer an option. Thus, there is an urgent requirement for earlier diagnosis and screening to allow treatment of pancreatic cancer at an earlier stage and therefore improve the survival rate.^{5,6}

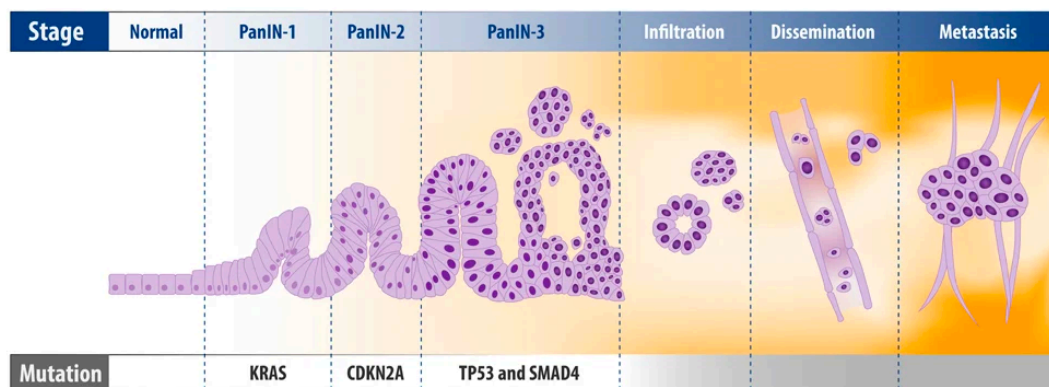


Figure 1.1 Development and stages of pancreatic cancer and the corresponding gene mutations. Pancreatic cancer is often not diagnosed until it has reached metastasis.⁷

A further reason for the poor survival statistics of pancreatic cancer patients is the weak response of pancreatic cancer cells to chemotherapy. Its notable cellular resistance to chemotherapeutics is thought to be caused, not only by genotype factors, but can mostly be attributed to non-genetic, phenotype mechanisms. Therefore, understanding the phenotype changes that occur in pancreatic cancer cells is fundamental to the development of efficient treatments, and in the development of earlier diagnosis.⁸

As mentioned, the two major problems associated with cancer are its late diagnosis and the resistance of the cancers to treatment. To help counter these issues, there is an urgent requirement to develop new methods for early diagnosis; the 10-year survival of cancer is three times higher when diagnosed in the first two stages, with 81% survival which drops to 26% survival when diagnosed in stage three and four (Figure 1.2).⁹

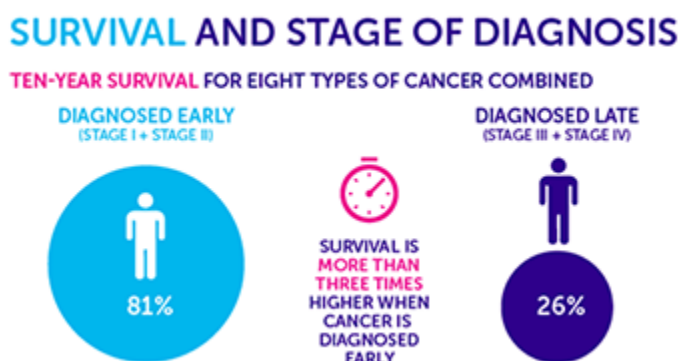


Figure 1.2 Percentage of ten-year survival of cancer patients with respect to the stage of diagnosis.⁹

1.2 Current Approaches to Treatment

1.2.1 Cisplatin and Platinum-Based Therapeutic Agents

A helpful introduction to the subject of drug resistance is the widely used inorganic platinum drug, cisplatin. Cisplatin, shown in Figure 1.3 is one of the most potent chemotherapy agents that is used in the treatment of cancers including: testicular, ovarian, bladder, head and neck, lung and cervical cancer. The mode of action of cisplatin is linked to the intracellular hydrolysis of the two labile chloride groups which enables the drug to crosslink with the purine bases of DNA resulting in DNA damage and cell apoptosis.¹⁰ This has been illustrated in Figure 1.3.

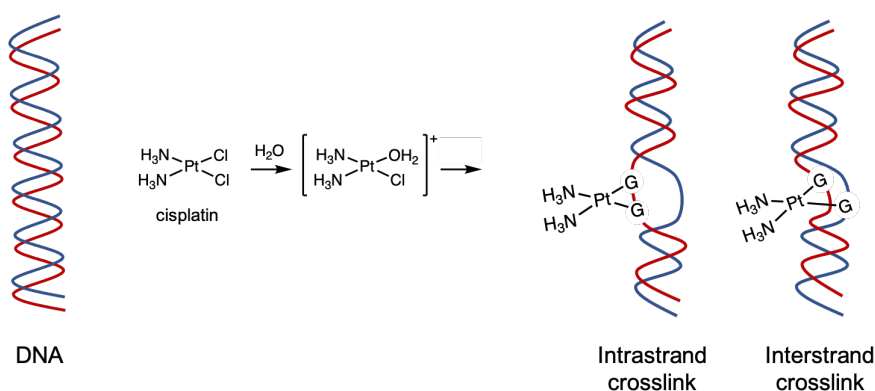


Figure 1.3 The sequential hydrolysis of cisplatin within the body and figure to depict the mode of action of cisplatin which results in the crosslinking of the therapeutic to DNA via both intrastrand and interstrand crosslinks.

Despite the overall success of cisplatin, many cancers have displayed an acquired or intrinsic resistance to the chemotherapy agent.¹¹ Due to this resistance and the numerous toxic side effects associated with cisplatin, including: allergic reactions, increased risk of infection,

severe kidney problems, anaemia and hearing loss, additional platinum containing anticancer drugs have been developed. Carboplatin and oxaliplatin shown in Figure 1.4 are two additional platinum-containing FDA approved anticancer agents; oxaliplatin was developed to help overcome cisplatin resistance and carboplatin treatment has less severe side effects.¹⁰ Both of these second-generation platinum-containing anticancer agents feature a bidentate ligand which makes them much less chemically reactive than the first-generation agent cisplatin.¹²

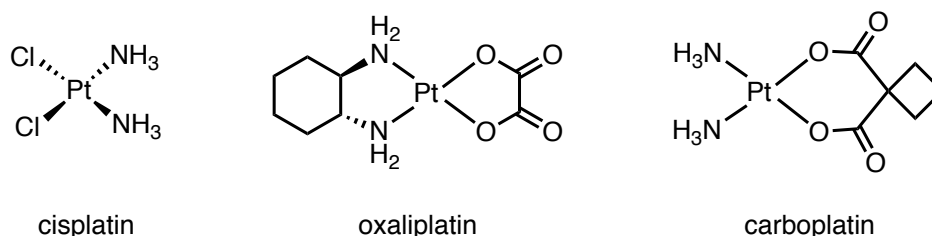


Figure 1.4 FDA approved, platinum(II)-containing anticancer agents.

1.2.2 Auranofin and Drug Repurposing

An alternative approach to the development of novel therapeutics for the treatment of diseases is drug repurposing. Drug repurposing identifies novel therapeutic areas and uses for already clinically established drugs. This strategy holds promise due to the reduced costs and time associated in comparison to drug development, owing to the already derived safety profile of the drug.¹³

A therapeutic agent that has attracted attention for its activity in the treatment of a number of different areas and thus, holds potential to be repurposed,¹⁴ is the gold(I) complex, auranofin, shown in Figure 1.5. Auranofin was originally approved by the FDA in 1985 for the treatment of rheumatoid arthritis, although, it is now seldom used for this purpose due to the rise of more effective therapeutics with less adverse effects.¹⁵ More recently, studies have shown its potential in neurodegenerative disorders (Parkinson's and Alzheimer's disease),^{16,17} parasitic¹⁸ and bacterial infections,^{19–23} cancers^{24–26} and HIV.^{27,28}

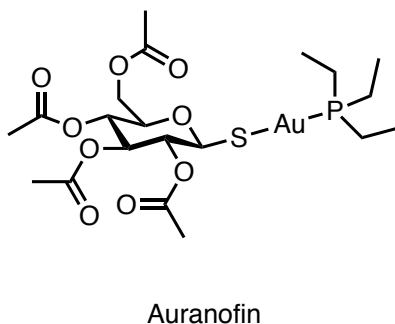


Figure 1.5 The structure of auranofin, a linear gold(I) therapeutic, stabilised by an acetate protected thiosugar (1-thio-β-D-glucose tetraacetate) and a triethylphosphine ligand to aid in lipophilicity.

Auranofin is composed of an acetate protected thiosugar (1-thio- β -D-glucose tetraacetate) which is coordinated to a gold(I) metal centre and stabilised by a triethylphosphine ligand. Both ligands are reported to enhance the stability of the +1 oxidation state of the gold metal centre and provide lipophilicity for ease of transfer of auranofin across the cell membrane.²⁹ Auranofin is taken orally and gets metabolised in the body; the deacetylation of the thiosugar moiety occurs in the intestine.³⁰ The gold(I) complex is found to be highly reactive towards thiols and thus, ligand exchange is likely and has been supported by *in vitro* and *in vivo* animal and human studies. It has also been proposed that ligand exchange with membrane associated thiols could aid with transfer into the cell. Once inside the cell membrane, the triethylphosphine ligand is lost, metabolised to triethylphosphine oxide and subsequent ligand exchange is thought to occur.²⁹

At the time of FDA approval, the mechanism of action of auranofin was controversial, whereas, it is now thought that the main mechanism of action, for anticancer activity, is through the inhibition of thioredoxin reductase (TrxR).¹³ TrxR is an enzyme that is particularly important in maintaining the redox state within cells; the inhibition of TrxR results in an increase in intracellular oxidative stress and thus, induces apoptosis. The overexpression of this enzyme is linked to aggressive tumour progression and low survival of patients with breast, ovarian and lung cancers, and therefore auranofin may be a suitable candidate as an anticancer agent.^{31,32}

Auranofin will be discussed in greater detail in Chapter 2 where the synthesis of a small library of analogues, prepared by varying the tertiary phosphine ligand, are reported.

1.2.3 Ruthenium-Based Therapeutic Agents

Ruthenium complexes are gaining popularity for their bioactivity as alternatives to platinum-based drugs due to their desirable properties.^{33,34} Some of the favourable properties of ruthenium-based therapeutics include, i) an alternative mode of action, ii) activity against some cisplatin resistant cell lines, iii) low side effects which are likely to be attributed to the higher selective uptake of these compounds in cancer cells and iv) ruthenium can bind to some biological molecules, mimicking iron.³⁴

Shown in Figure 1.6 are four ruthenium complexes that have been studied for their potential anticancer activity; NAMI-A, KP1019 and (N)KP1339 have all been assessed in clinical investigations. NAMI-A showed low therapeutic efficiency which resulted in its failure in

clinical trials. In addition, the low solubility of KP1019 prevented its further development, but its more soluble sodium salt derivative, (N)KP1339, is currently undergoing clinical trials.³⁴

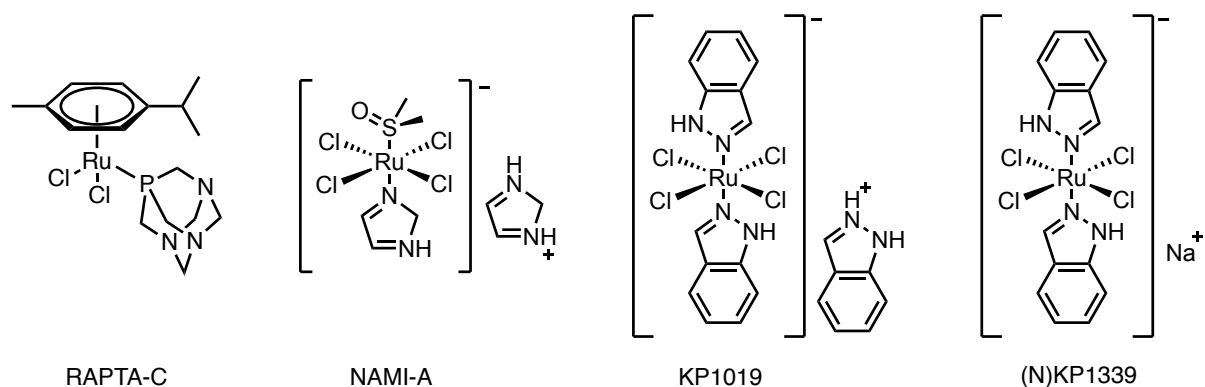


Figure 1.6 Ruthenium containing anticancer agents. NAMI-A, KP1019 and (N)KP1339 have been tested in clinical studies, with (N)KP1339 clinical trials currently underway. RAPTA-C is a promising candidate for clinical trials.

In the case of RAPTA-C, this complex is in pre-clinical trials and shows promising anticancer activity.³⁵ The ruthenium(II) metal centre is coordinated to two chloride ligands, a *para*-cymene ligand and 1,3,5-triaza-7-phosphaadamantane (PTA) ligand. Similar to cisplatin, the two chloride groups readily hydrolyse, yet, unlike cisplatin, RAPTA-C preferentially binds to histones resulting in the altered secondary and tertiary structure of the DNA helix.³⁵ Complexes bearing PTA ligands typically have high aqueous solubility, a factor that is of great importance in pharmaceutical chemistry, and therefore they have been intensively studied by Dyson *et al.*^{36,37} RAPTA-C is a part of a larger class of ruthenium-based complexes coined RAPTA (ruthenium arene PTA) which differ by the coordinated arene group. Small changes such as altering the arene group, or through the introduction of a chelating ligand allow for the fine tuning of the kinetics of aquation and cellular uptake.³⁶ This phosphine-containing complex has shown efficacy both *in vitro* and *in vivo* and, in addition, it has a desirable safety profile. These properties warrant its further research and trials as an anticancer agent.³⁵

1.3 Fluorescence Labelling

It was highlighted earlier that a key challenge of medicinal chemists today is understanding the mechanism of action of drugs. Fluorescence labelling has been applied to aid in the visualisation of therapeutic agents at a subcellular level to provide information on the localisation and interactions of the compounds within the cell.

Fluorescence microscopy is a powerful tool that enables the visualisation of physiological processes at subcellular levels of resolution via the detection of light emitted by fluorophores present in an imaging agent. It can provide higher spatial resolution (μm resolution) than that

available to radioimaging techniques (mm resolution).³⁸ For a more detailed insight into the technique, see Box 1.1 below.

Bodio *et al.* synthesised a boron-dipyrromethene (Bodipy) phosphine compound which they coordinated to ruthenium, gold and osmium to afford complexes **1a-c**, shown in Figure 1.7. In contrast to the previously discussed compounds, due to the Bodipy fluorophore, these agents are highly fluorescent as illustrated in Figure 1.7 by the green colour-coding. In the case of the ruthenium complex **1a**, this is a fluorescent analogue of RAPTA-C. They described their complexes as theranostic agents due to their potential in both imaging and therapeutic applications.³⁹

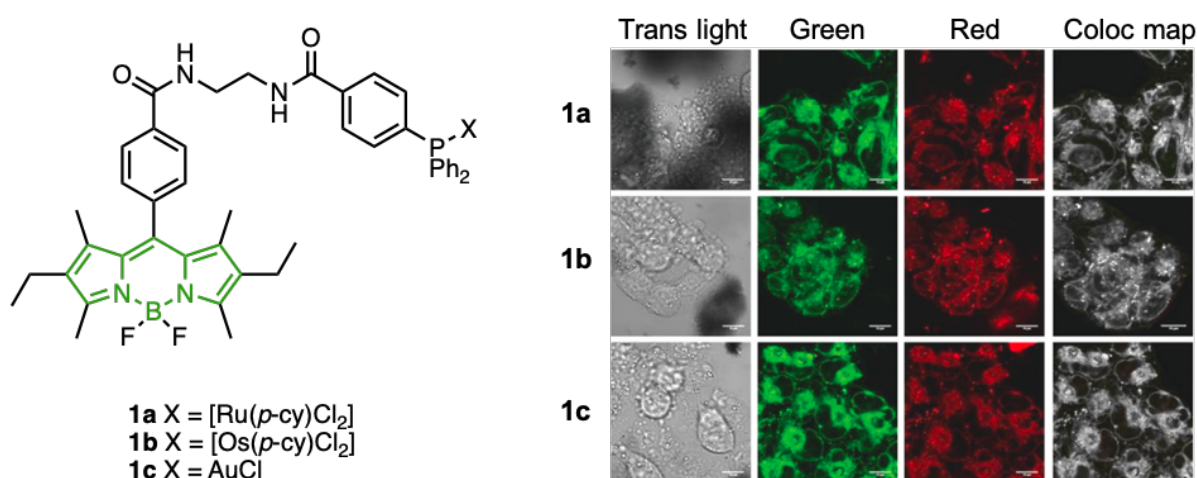


Figure 1.7 Bodio *et al.* synthesised Bodipy-phosphine metal complexes **1a**, **1b** and **1c** as organometallic imaging complexes. Confocal microscopy images show A2780S cells which were incubated for 2 hours at 37 °C with **1a-1c**. Pictures display cells in transmitted light (trans light), green channel (exc 488 nm, em 520 nm), red channel (exc 515 nm, em 550 nm) and a co-localised pixel map (Coloc map), where grey pixels show complete co-localisation.³⁹

Complexes **1a-c** were tested for their bioactivity against human ovarian cancer cell lines, sensitive (A2780S) and resistant (A2780cisR) to cisplatin; they were found to have moderate cytotoxic properties with respect to cisplatin with the most active compound being the gold derivative **1c**. They noted that **1a** had an improved cytotoxic profile in comparison to the non-fluorescent derivative, RAPTA-C. The fluorescent Bodipy moiety allowed for *in vitro* imaging of the cancer cells and showed the localisation of the agent; all the complexes demonstrated accumulation within the cell membrane, without specificity.³⁹

Box 1.1 Information on fluorescence and fluorescence imaging.

1.3.1 Fluorescence

Fluorescence is a type of photoluminescence that results in the emission of light following the absorption of a photon. Photoluminescence can be split into fluorescence and phosphorescence which differ by the nature of the excited state; these two phenomena

have been illustrated in the Jablonski diagram in Figure 1.8. Fluorescence occurs when the relaxation from the singlet excited state to the singlet ground state (usually from S_1-S_0) results in the emission of a photon. In the case of phosphorescence, the emission of a photon occurs as the excited electron first relaxes via intersystem crossing to the excited triplet state and relaxes to the singlet ground state (T_1-S_0) in a spin forbidden transition.^{40,41}

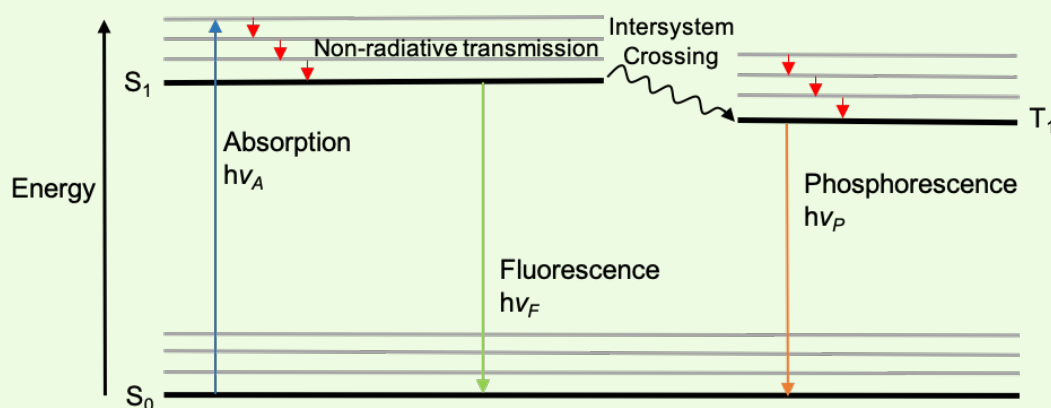


Figure 1.8 Jablonski diagram illustrating photoluminescence phenomena, fluorescence ($h\nu_F$ the energy of the emitted photon) and phosphorescence ($h\nu_P$ the energy of the emitted photon) which occurs following the absorption of a photon ($h\nu_A$ is the energy of an absorbed photon).⁴²

Currently, fluorescence imaging is mainly used as an *in vitro* technique, fundamental to biomedical scientific research. Fluorescence plays a key role in many biological applications due to its remarkable sensitivity with capability of ‘single molecule detection’.⁴¹ Fluorophores are used in a range of applications including i) visualising cells *in vitro*, with probes available to image each individual organelle separately,⁴³ ii) monitoring of subcellular processes,⁴⁴ iii) labelling of biologically active compounds to aid in the determination of the mechanism of action⁴⁵ and iv) fluorescent sensors.⁴⁶

As was demonstrated by Bodio *et al.* in the fluorescence labelling of RAPTA-C, Chapter 2 will see the introduction of a fluorescent label to auranofin through the coordination of a fluorescent phosphine to a gold(I) metal centre.

1.4 Mitochondrial Dysfunction

Mitochondria are a common target for therapeutic and diagnostic agents due to their dysfunction in a range of diseases⁴⁷ including cancers,^{48,49} Alzheimer’s disease,⁵⁰ and Parkinson’s disease.⁵¹ Positively charged species are known to accumulate in the mitochondria due to its negatively charged membrane (*ca.* -150 mV to -170 mV in healthy cells)^{52,53} and thus, this has seen cationic compounds developed for this purpose, as a way of introducing site specificity.⁵² Many solid tumours and ischaemic heart cells have a more negative

mitochondrial membrane potential (MMP) compared to their healthy counterparts⁵⁴ and thus, the reported accumulation of mitochondrial specific compounds is tenfold higher in these cells. This has been exploited to allow for selective localisation of compounds in tumour cells for both treatment⁵⁴ and diagnostic purposes.⁵⁵

Three lipophilic phosphonium salts that have demonstrated specific mitochondrial localisation are the triphenyl phosphonium cations developed by Neamati *et al.*,^{54,56} shown in Figure 1.9.

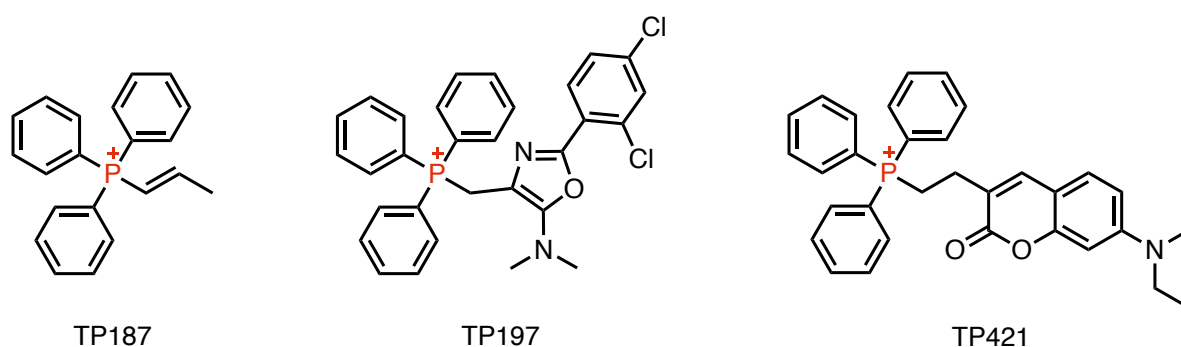


Figure 1.9 Three phosphonium salts developed by Neamati *et al.* which have shown to specifically localise within the mitochondria.

The researchers tested the phosphonium salts containing a triphenyl moiety against a panel of cancer cell lines and a mouse model of human breast cancer. The compounds displayed remarkable anticancer activity which the authors attributed to their mitochondrial localisation which caused decreased oxygen consumption and increased superoxide production.⁵⁴

1.4.1 Incorporation of an Imaging Modality

The incorporation of an ¹⁸F radiolabel to triphenylphosphonium salts has been carried out as a way of introducing an imaging modality to these mitochondrial-specific compounds.⁵⁷ An ¹⁸F radiolabel enables imaging via positron emission tomography (PET), a technique used to visualise metabolic processes and tumours within the body.⁵⁸ A more detailed discussion of the technique and applicable radionuclides can be found in Box 1.2.

Three examples of ¹⁸F radiolabelled triphenylphosphonium salts are shown in Figure 1.10; to highlight their dual-modality, the compounds have been colour-coded: i) red to illustrate site specificity to the mitochondria, and ii) blue to display application in *in vivo* imaging by PET imaging. All three phosphonium salts have shown application in myocardial imaging with [¹⁸F]-FBnTP showing additional potential as a myocardial perfusion agent.⁵⁷ Myocardial perfusion is a non-invasive, radioactive scan which provides information on the blood flow (perfusion) through the heart muscle.

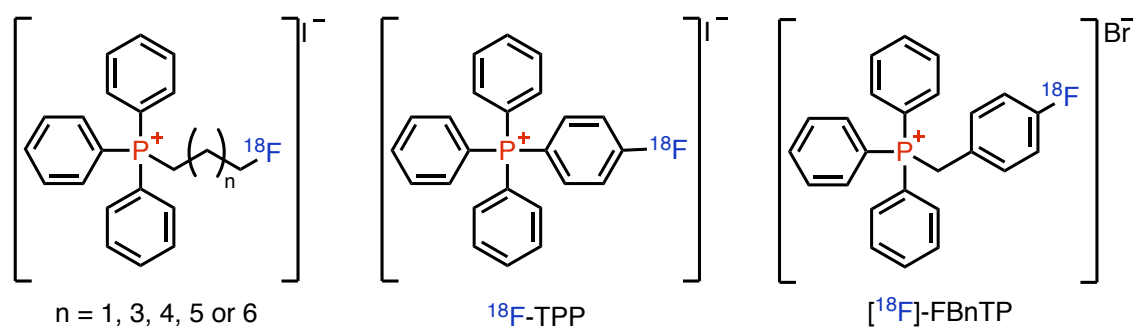
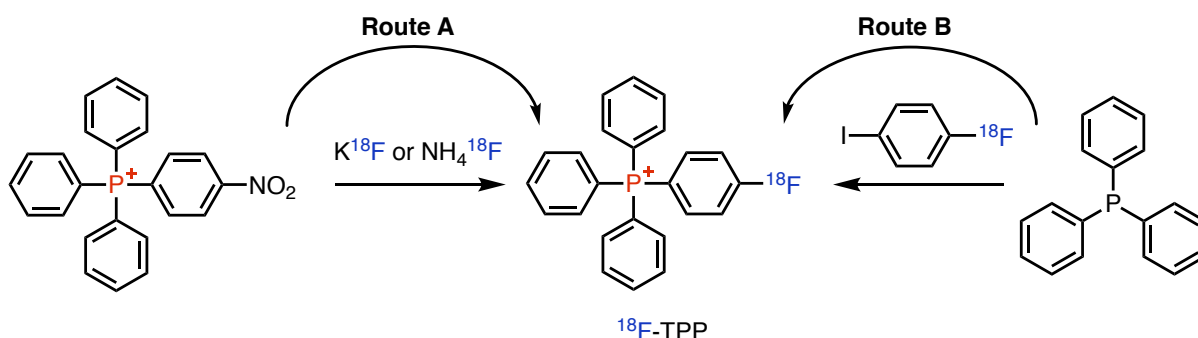


Figure 1.10 Examples of ^{18}F radiolabelled triphenylphosphonium salts with application in myocardial imaging.

Radiolabels such as ^{18}F can be integrated into a compound by nucleophilic substitution, the only requirement being the presence of a good leaving group such as triflate, tosylate, mesylate, iodide or bromide.^{59,60} Two examples of the radiolabelling of ^{18}F -TPP are shown in Scheme 1.1. Route A shows a direct exchange reaction of the nitro-group for ^{18}F via a nucleophilic source of ^{18}F , whereas Route B requires a two-step labelling method which first requires the labelling of the iodobenzene (not shown) followed by a substitution reaction with triphenylphosphine.⁵⁷



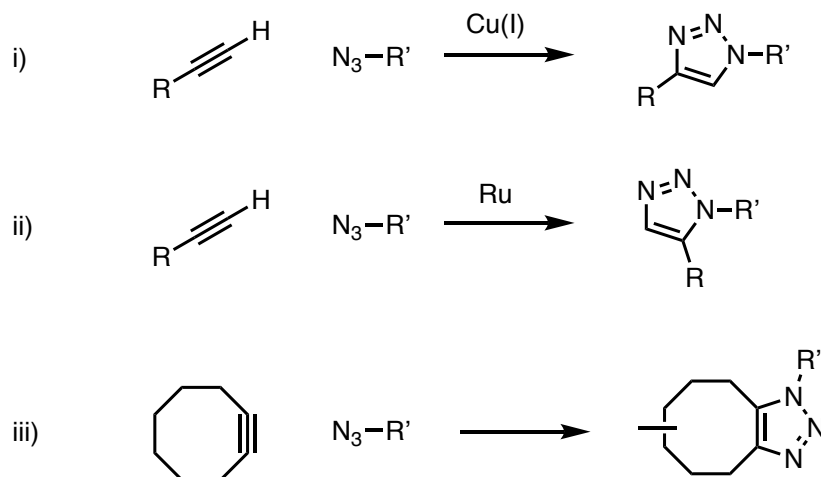
Scheme 1.1 Two routes to afford the ^{18}F radiolabelled phosphonium salt ^{18}F -TPP.⁵⁷

There are limitations to using direct exchange to radiolabel compounds. For instance, any additional potential sites for reactivity must first be protected and subsequently deprotected following radiolabelling. These additional steps usually equate to a lengthier synthetic procedure which can be detrimental when using radionuclides with short half-lives.⁶¹ The reactions have to be held to a very high standard in terms of safety, requiring clean reactions with effective purification before administering to a patient. An additional challenge is the poor nucleophilicity of the ^{18}F anion which has limited reactivity in protic environments.⁶²

1.4.2 Click Chemistry

Some of the limitations and challenges associated with the nucleophilic aromatic substitution by ^{18}F , as discussed in the previous section, can be circumvented through the use of click chemistry.

Click chemistry is a term first coined by Professor K. B. Sharpless in 1998 for a group of reactions that must meet a stringent criteria which he later described; the reactions must be high yielding, work in ambient conditions, have a short reaction time and the products must be easily isolable (non-chromatographic methods) and regiospecific.⁶³ A common example of click chemistry is the cycloaddition between an azide and alkyne. Three variations of this reaction are known which are shown in Scheme 1.2.

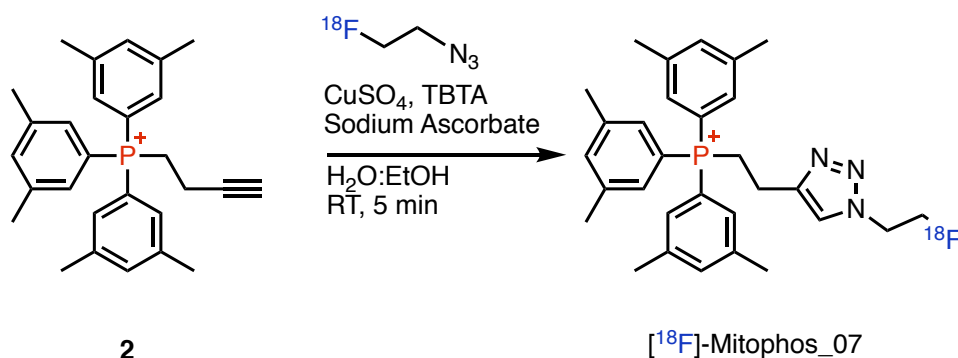


Scheme 1.2 Three variations of the azide-alkyne click reaction. i) copper catalysed (CuAAC), ii) ruthenium catalysed (RuAAC) and iii) strain-promoted (SPAAC).

The first and most well-known variation is the copper azide-alkyne cycloaddition (CuAAC) which specifically gives the 1,4-disubstituted triazole isomer; in the case of the ruthenium catalysed variation (RuAAC), this affords the 1,5-isomer and the strain promoted cycloaddition (SPAAC) removes the need for catalysts altogether. Click reactions are often exploited in biochemistry in the investigation of biological systems, or in drug development. The addition of a radiolabel, a targeting agent or a fluorophore are some of the ways that people have exploited this type of reaction to result in the addition of functionality to a compound. Click chemistry enables the use of mild reaction conditions and short reaction times to allow for the labelling of more delicate biomolecules in a time considerate manner.

In 2013, Haslop *et al.* employed CuAAC click chemistry in the rapid radiolabelling of an alkyne substituted phosphonium salt **2**. Haslop's synthesis of an ¹⁸F labelled phosphonium salt, [¹⁸F]-Mitophos_07, starts with the preparation of [¹⁸F]fluoroethyl azide from 2-azidoethyl-4-tosylate which was subsequently reacted with **2** to afford [¹⁸F]-Mitophos_07 (step two is illustrated in Scheme 1.3). The total synthesis time, from aqueous [¹⁸F]fluoride, was just over one hour and resulted in an average radiochemical yield, defined as "the amount of activity in

the product expressed as the percentage of starting activity used in the considered process”,⁶⁴ of 9% following purification by HPLC, with a radiochemical purity of >99%.⁶⁵



Scheme 1.3 The ^{18}F radiolabelling of phosphonium salt **2** with ^{18}F fluoroethyl azide via CuAAC to afford ^{18}F -Mitophos_07.

The resulting radiolabelled compound, ^{18}F -Mitophos_07, has since been reported for its potential as a PET tracer for the imaging of evolving mitochondrial cardiotoxicity.⁶⁶ This radiolabelled compound, ^{18}F -Mitophos_07, displayed improved pharmacokinetic properties over clinically used compounds with respect to cardiac imaging. The lipophilic salt showed fast washout from the heart and liver and stable retention in the myocardium. In addition, it was shown to be responsive to doxorubicin (DOX) induced cardiotoxicity, suggesting its promise as an early diagnostic agent. ^{18}F -Mitophos_07 displayed specific localisation within the mitochondria, key to its success in the imaging of mitochondrial cardiotoxicity.⁶⁶

The Higham group sought to synthesise a fluorescent phosphonium salt with the aim of developing an agent with an additional imaging modality. The probe would have: i) a fluorescent backbone to enable *in vitro* imaging through fluorescence microscopy, ii) an ^{18}F radiolabel to enable *in vivo* imaging via PET and iii) a phosphonium salt to provide specificity to the mitochondria. This work will be introduced in further detail in Chapter 5 and will show the development of this project to date.

Box 1.2 Information on the radioimaging technique, Positron Emission Tomography (PET).

1.4.3 Positron Emission Tomography

PET is a radioimaging technique which measures physiological functions and metabolic activity of cells and tissues and is commonly used in patients with cancer, brain⁶⁷ or heart⁶⁸ conditions.⁶⁹ It enables the visualisation of biochemical changes in the body (i.e. metabolism) and allows for the monitoring of disease progression or response to a stimulus.⁶⁰ Example images from a PET scan on the brain are shown in Figure 1.11.

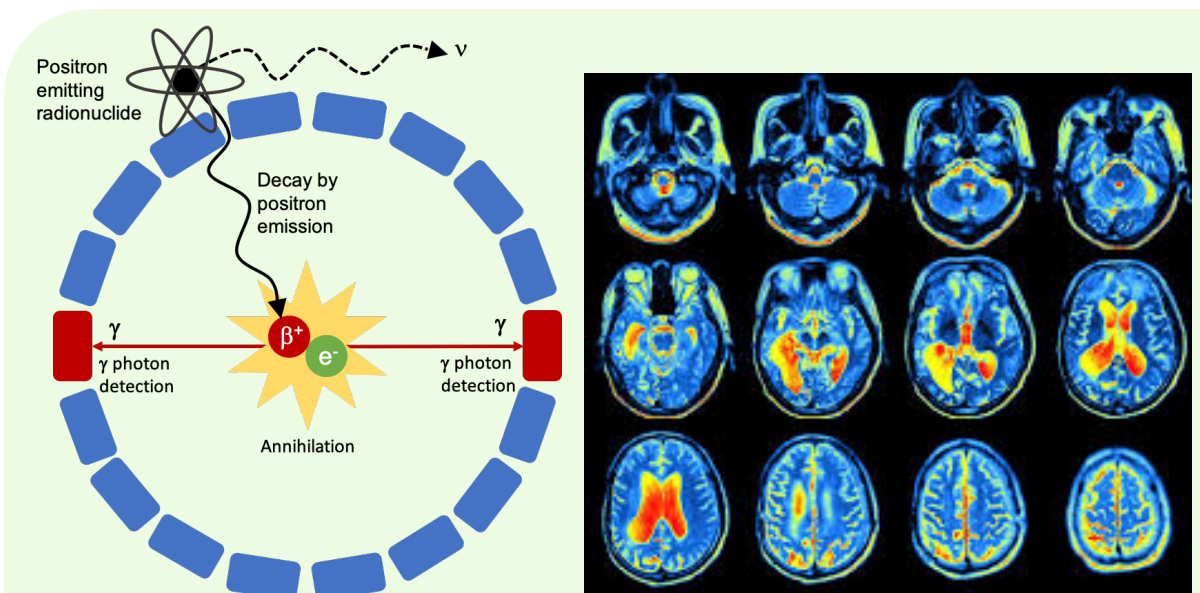


Figure 1.11 Diagram illustrating the principles behind PET imaging (left) and an example of the images obtained following a PET scan on the brain (right).

PET requires radionuclides that decay by emission of a positron. The positron travels a short distance into the tissue and gets annihilated on combining with an electron; this annihilation converts to energy and two γ -rays are emitted simultaneously at 180° from each other. The γ -rays are detected by scintillators and information on the positron annihilation is recorded. This has been illustrated in Figure 1.11. Once a sufficient number of γ -rays have been recorded, image reconstruction can occur, which provides spatial distribution of radioactivity as a function of time.⁶⁰

Many nuclides that decay by emission of a positron are available and are shown in Table 1.1.

Table 1.1 Nuclides commonly used for PET imaging⁶⁰

Nuclide	Half-life/min	Type of emission	Max. energy/MeV
^{11}C	20.3	β^+	0.97
^{13}N	10	β^+	1.20
^{15}O	2	β^+	1.74
^{18}F	110	β^+	0.64
^{64}Cu	762	β^+ /electron capture	0.66
^{68}Ga	68.1	β^+ /electron capture	1.90
^{76}Br	972	β^+ /electron capture	4.00
^{124}I	60192	β^+ /electron capture	2.14

For optimal selection of an isotope, the time taken to image the biochemical process must be considered and be comparable to that of the nuclide. Too short and one cannot image the process (most of the nuclei have decayed before the image is obtained), too long and one exposes the patient to unnecessary amounts of radiation. The half-life of the nuclei is a factor as soon as the nuclei are generated. This means synthesis, purification, administration, and imaging all need to be done in an appropriate time-efficient process. Two of the most common nuclides⁷⁰ used are ^{11}C and ^{18}F due to the ability for radiolabelled imaging agents to be almost indistinguishable from their cold counterparts. It should be noted that ^{18}F is an excellent steric mimic for hydrogen, but this is notwithstanding the considerably higher electronegativity of fluorine over hydrogen. This electronic difference can be advantageous however, when it results in compounds with increased potency; the risk of metabolism of the probe, which would lead to the loss of the isotope, can be reduced due to the strong C-F bond ($105.4 \text{ kcal mol}^{-1}$).⁷¹

^{18}F has a half-life of 109.7 minutes which is favourable for longer, more complex *in vivo* studies. An additional benefit is the low positron energy of ^{18}F which results in the generation of high-resolution images.⁶⁰

1.5 Heart Disease

Heart and circulatory diseases make up 27% of all deaths in the UK each year with 167,116 deaths in 2018. More specifically, coronary heart disease (ischaemic heart disease) which occurs when coronary arteries narrow due to a build-up of fatty material (Figure 1.12), is responsible for 64,000 deaths in the UK each year.⁷²

Myoview, shown in Figure 1.12 is an example of a radioactive probe which has been developed for clinical use as a SPECT imaging agent in myocardial perfusion imaging.⁷³ To diagnose coronary heart disease, Myoview is administered and imaging of the heart is carried out at both resting state and whilst exercising. Further information on SPECT is reported in Box 1.3. The probe consists of two bidentate phosphine ligands which provide kinetic stability and prevent leaching of the radioactive $^{99\text{m}}\text{Tc}$ metal centre.⁷³ It can be prepared in high radiochemical purity via commercially available kits; $^{99\text{m}}\text{Tc}$ is produced from a $^{99\text{m}}\text{Tc}$ generator in the form of $[\text{}^{99\text{m}}\text{Tc}]\text{-pertechnetate}$ in oxidation state +7, which can then be reduced by stannous ions to favour the coordination of ligands to the reduced metal centre. In the case of Myoview, two chelating 1,2-bis[di(2-ethoxyethyl)phosphino]ethane ligands and two oxo ligands afford a *trans* octahedral complex in the +5 oxidation state.⁷⁴ The resulting radioactive

complex has an overall charge of +1 which promotes myocardial uptake due to its negative membrane potential.⁷⁵ The specific and substantial myocardial uptake of Myoview provides rapid diagnostic information on the heart; this, combined with the fast non-target clearance has resulted in its routine clinical use. The rapid non-target clearance has been attributed to the ethoxyethyl groups on the phosphine ligands and is not observed with alkyl phosphine derivatives.^{73,75}

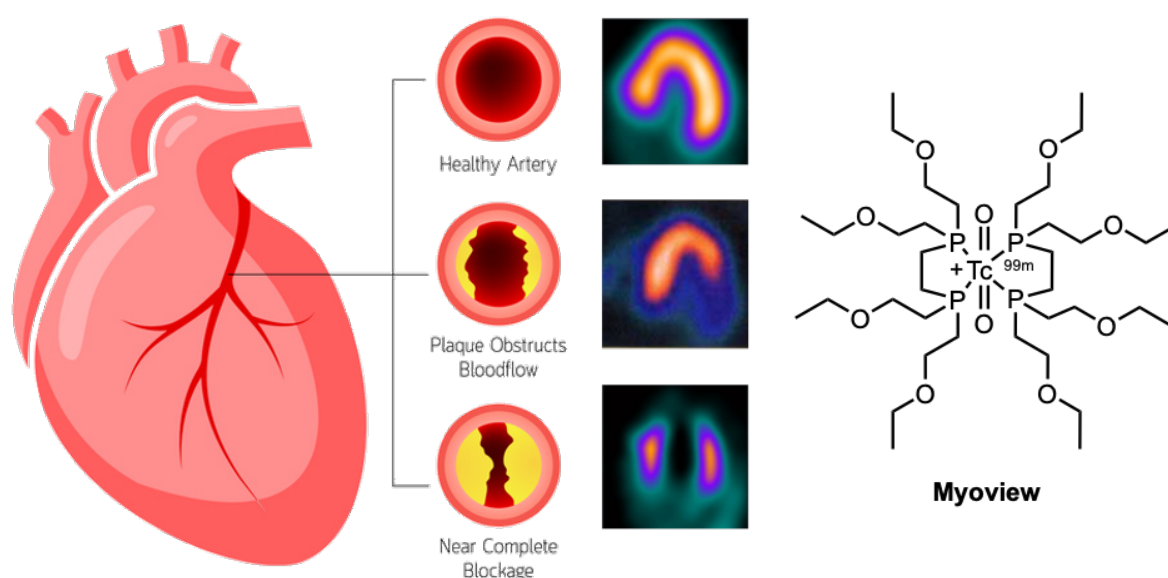


Figure 1.12 ^{99m}Tc -Tetrafosmin, commercially known as Myoview, a clinically used SPECT imaging agent with two bidentate phosphine ligands to provide kinetic stability to prevent the leaching of the radioactive ^{99m}Tc .⁷⁴

Box 1.3 Information on the radioimaging technique, Single Photon Emission Computed Tomography (SPECT).

1.5.1 Single Photon Emission Computed Tomography (SPECT)

SPECT is a radioimaging technique used for the imaging of metabolic processes. The imaging process requires radionuclides that emit γ -rays; in the case of Myoview a technetium-99m nuclide is present. Some additional γ -ray emitters are displayed in Table 1.2. In SPECT imaging, a collimator is placed in front of a gamma camera which is used to define the angle of incidence of the emitted γ -rays, obtaining directional information and resulting in multiple 2D images which are subsequently converted to 3D images following tomographic reconstruction. Relative to PET, SPECT has a lower cost and thus is a more widely available technique. However, it has lower detection efficiency and therefore, lower resolution. Nevertheless, the nuclides used for SPECT generally have a longer half-life than those used for PET, which allows for longer imaging procedures.⁶⁰

Table 1.2 Nuclides commonly used for SPECT imaging⁶⁰

Nuclide	Half-life/h	Type of emission	Principal photon emission energies/MeV
¹²³ I	13.2	Electron capture	0.16
^{99m} Tc	6	Isomeric transition	0.14
¹¹¹ In	67.9	Electron capture	0.17/0.25
⁶⁷ Ga	78.3	Electron capture	0.09
²⁰¹ Tl	73.1	Electron capture	0.17

One drawback of radioimaging probes is their low (mm) resolution which prevents the imaging of their fate at a cellular or subcellular level. In an attempt to alleviate this limitation, Valliant *et al.* developed a multimodal imaging agent capable of both *in vitro* fluorescence imaging and *in vivo* SPECT imaging.⁷⁶ The probe, shown in Figure 1.13, has four modalities which have been colour coded for the reader: i) a quinoline fluorophore to enable *in vitro* fluorescence imaging (green), ii) a ^{99m}Tc radionuclide to enable *in vivo* imaging by SPECT (blue), iii) a targeting sequence (fMLF) to provide localisation to a specific formyl peptide receptor (red) and iv) a tridentate nitrogen ligand to provide kinetic inertness and thermodynamic stability (pink).

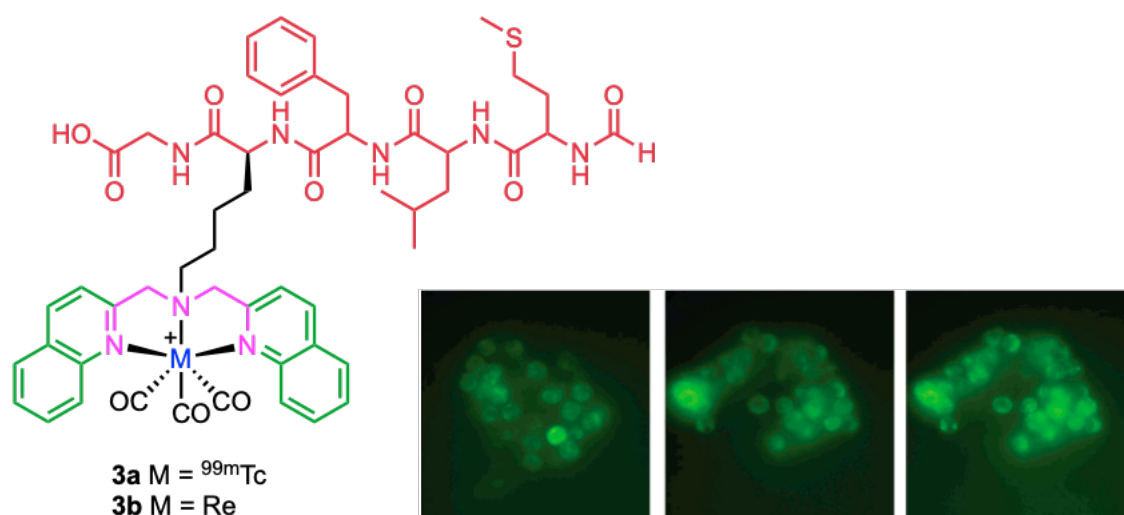


Figure 1.13 Multifunctional imaging agent developed by Valliant *et al.* suitable for *in vitro* fluorescent imaging and *in vivo* SPECT imaging.⁷⁶ The fluorescent microscopy images show human leukocytes incubated with **3b** (1 nM) (left), fluorescein labelled fNLFNTK (a reference ligand) (middle) and **3b** (50 nM) (right).

On heating of **3b** to 37 °C, no metal dissociation was observed over 24 hours and thus, it was deemed to be suitably robust for *in vivo* imaging, aided by the tridentate ligand enabling kinetic stability.⁷⁶ Polydentate or chelating ligands have been utilised in the design of

radioactive complexes for SPECT imaging, due to their ability to enhance the kinetic stability of the metal complexes to ensure the complex remains intact for long enough to reach its target or be cleared from the body.⁷⁷

Following this work, the Higham group developed a multimodal imaging agent suitable for both fluorescence and SPECT imaging based on a fluorescent tridentate phosphine ligand.⁷⁸ This research will be introduced in Chapter 4 where the reader will see the application of the same fluorescent tridentate phosphine in its coordination to group 10 metal complexes in the development of diagnostic or theranostic imaging agents.

1.6 Magnetic Resonance Spectroscopy

An additional medical imaging technique is magnetic resonance imaging which is used to produce images of the body and physiological processes. A companion technique to this, that is much less exploited, is *in vivo* magnetic resonance spectroscopy (MRS).⁷⁹ Whilst MRI ascertains the spatial distribution of water and fat protons in a region of interest, MRS can determine the chemical composition of the scanned tissue and map metabolic and physiological processes through the resonances of species containing heteronucleides such as ³¹P, ¹⁹F, ¹³C, ¹⁵N and ²³Na.⁸⁰ Further information on these techniques can be found in Box 1.4.

³¹P MRS is a non-invasive, *in vivo* technique which can be used to measure the levels of endogenous phosphorus compounds such as adenosine triphosphate (ATP), phosphocreatine (PCr) and inorganic phosphate (Pi), which are critically important in normal cellular functions e.g. metabolism.⁷⁹ The absence of ionising radiation allows for repeated measurements which enables the monitoring of disease progression and treatment response without ionising radiation. ³¹P MRS has been applied to study diabetes mellitus (DM), a disease which can lead to muscle atrophy and impaired metabolic activity. A study by Greenman *et al.* found that differences in regional muscle can be identified by ³¹P MRS by providing data on the metabolic activity of muscle, to assess the biochemical pathways for the use and supply of energy in muscle through a non-invasive method. It has been validated that the ratio of the concentrations of inorganic phosphate (Pi) to phosphocreatine (PCr) is a marker of metabolic oxidative capacity in skeletal muscle; an increased resting Pi/PCr ratio has been observed with DM.⁸¹

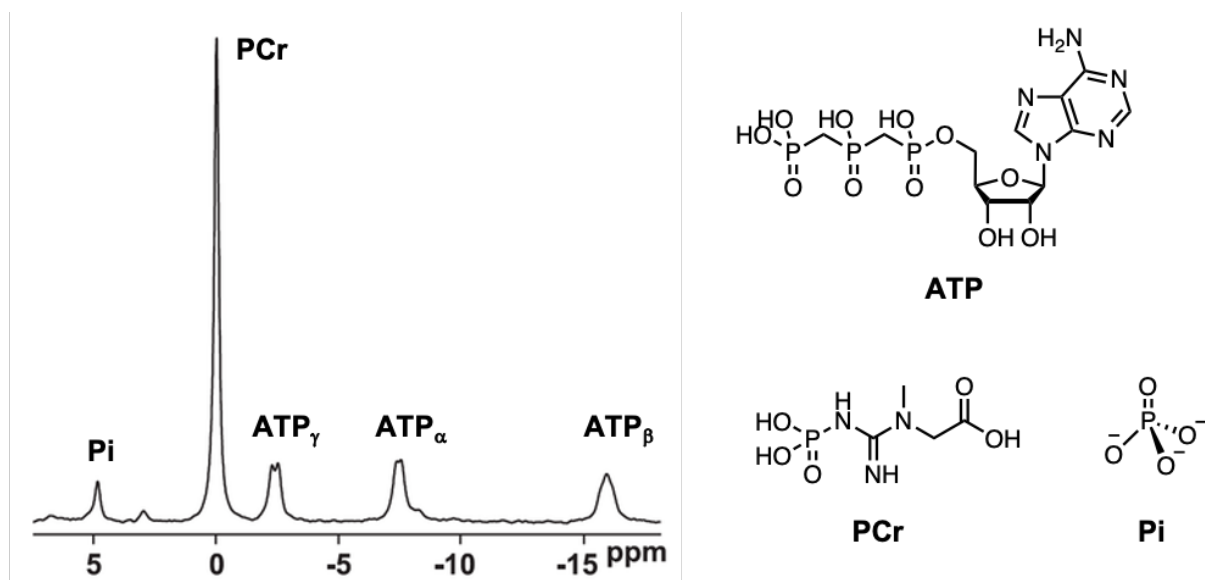


Figure 1.14 ^{31}P MRS spectrum displaying signals for endogenous phosphorus species adenosine triphosphate (ATP) phosphocreatine (PCr) and inorganic phosphate (Pi).⁷⁹

^{31}P MRS has also been applied in metabolic characterisation investigations in a range of areas including: skeletal muscle,^{82–84} heart,⁸⁵ brain,⁸⁶ liver,⁸³ cancer,⁸⁷ myocardial disease⁸⁸ and obesity,⁸⁹ thus displaying its versatility and potential for diagnostic applications.

Two important factors for successful MRS are i) the enhancement of the endogenous or probe signal against the background and ii) the crucial need for the signal to be observed well away from the endogenous resonances.⁹⁰

The Parker group at Durham University have shown that paramagnetic metal ions can be used to shift the proton NMR signals of chelating ligands away from the diamagnetic range of endogenous proton resonances. This allows paramagnetic complexes to be exploited as imaging probes for MRI which can be detected directly against zero background (Figure 1.15).⁸⁰

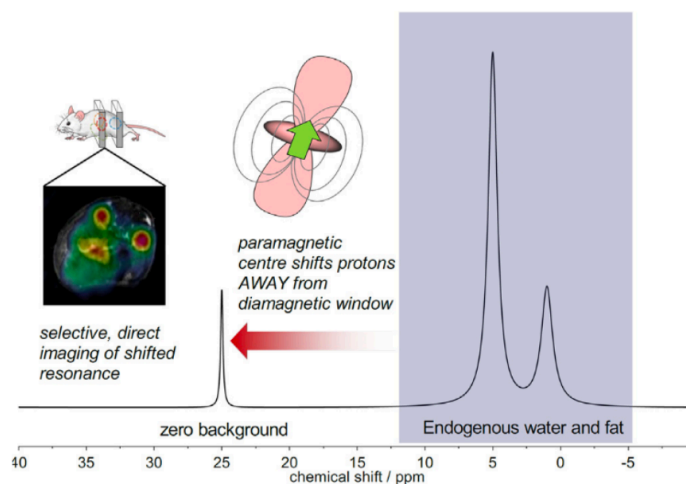


Figure 1.15 Imaging of paramagnetically-shifted proton resonances away from endogenous signals⁸⁰

An alternative method to the addition of paramagnetic metal ions to shift the signal away from endogenous resonances could perhaps involve the addition of a probe with a chemical shift outside the region of endogenous signals. Chapter 3 will explore the synthesis of a cyclic phosphine with an unusual ^{31}P NMR chemical shift that could potentially act as a probe for ^{31}P MRS.

Box 1.4 Information on the non-invasive imaging techniques, Magnetic Resonance Imaging (MRI) and Magnetic Resonance Spectroscopy (MRS).

1.6.1 Magnetic Resonance Imaging (MRI) and Magnetic Resonance Spectroscopy (MRS)

A non-invasive imaging technique used routinely for treatment monitoring, disease detection and diagnosis is magnetic resonance imaging (MRI). MRI works by aligning the protons in the body, which are usually spinning with their axes randomly aligned, using a strong magnetic field. This creates a magnetic vector oriented along the axis of the MRI scanner. Radio waves are applied, resulting in the deflection of the magnetic vector, causing the nuclei to resonate. When the radiofrequency is switched off, the magnetic vector returns to its resting state, emitting a radio wave in the process. This resulting radio wave signal is used to create the MR image (receiver coils are used to improve detection). The intensity of the signal is plotted, enabling the build-up of cross-sectional images. Several transmitted radiofrequencies can be used to emphasise abnormalities, made possible by the different relaxation times of different tissues. The relaxation time of the protons is measured in two ways, i) T1 is the time for the magnetic vector to return to the resting state and ii) T2 is the time for the axial spin to return to the resting state. Fat and water have different relaxation times and thus can be differentiated from each other. Most diseases manifest as an increase in water content, but, it can be difficult to ascertain the exact nature of the pathology.⁹¹

Currently, MRS is used as a research tool to obtain biochemical information about the body; it provides a non-invasive method to characterise the tissue. Where MRI can be used to form anatomical images, MRS uses this information to determine the concentration of metabolites present. For example, this information can be used to differentiate a high-grade from a low-grade tumour. MRS can be performed using a number of different nuclei such as ^{13}C , ^{15}N , ^{19}F , ^{23}Na , ^{31}P and ^1H , although only ^{31}P and ^1H exist in high enough concentration *in vivo* for clinical studies.⁹²

A key focus of this thesis is the synthesis of probes with the potential to act as imaging agents. A particular emphasis is placed on probes with multiple functionalities which can harness the

benefits of multiple imaging techniques. The advantage of designing such probes, is the potential to gain greater insight into the particular subject being imaged by overcoming the limitations of using just a single technique.⁶⁰

Displayed in Table 1.3 are the corresponding spatial resolution and sensitivities of PET, SPECT and MRI imaging to highlight the strengths and limitations of each technique.

Table 1.3 The respective spatial resolution, sensitivities and amount of molecular probe required for PET, SPECT and MRI agents.⁶⁰

Imaging technique	Spatial resolution	Sensitivity	Amount of molecular probe used
PET	1–2 mm	10^{-11} to 10^{-12} mole L ⁻¹	Nanograms
SPECT	1–2 mm	10^{-10} to 10^{-11} mole L ⁻¹	Nanograms
MRI	25–100 μ m	10^{-3} to 10^{-5} mole L ⁻¹	Micrograms to milligrams

1.7 Organophosphorus Compounds

From the first half of this introduction, the versatile nature of phosphine ligands in medicine is apparent. Examples of phosphines used to enhance lipophilicity, kinetic stability, aqueous solubility and site specificity have been described, demonstrating their application in both therapeutic and diagnostic areas. To understand why phosphines have found applications in these areas, a discussion of their fundamental properties and synthesis will be given.

1.7.1 Phosphines

Phosphines are neutral ligands that can behave as both σ -donors and π -acceptors, illustrated in Figure 1.16. They can act as Lewis bases through the donation of their lone pair of electrons to the empty d orbitals of a transition metal centre. In addition, they can accept electron density from d-orbitals on the metal centre into their empty P–R antibonding σ^* -orbitals.^{93,94}

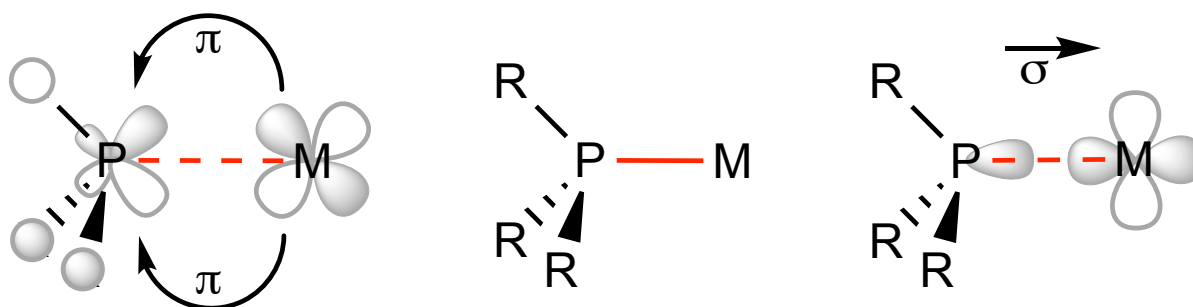


Figure 1.16 The binding of organophosphorus ligands to metal complexes. Phosphines act as both π -acceptor ligands (left) and σ -donor ligands (right).

Phosphines are generally regarded as strong σ -donors and weak π -acceptors, although it is well established that the nature of the ligand can be tuned by modifying the substituents.⁹⁵ This enables the development of versatile ligands that can be tailored to a specific role, for example, in the case of auranofin, the ethyl substituents on the phosphine enhance the lipophilicity of the complex.²⁹

1.1.1 Steric and Electronic Parameters of Phosphine Ligands

Tolman's cone angle (θ_T) is a measure of the steric bulk of a phosphine ligand on a transition metal complex.⁹⁶ When all three substituents are the same, θ_T is defined as the apex angle of a cylindrical cone that touches the Van der Waals radii of the outermost atoms when centred 2.28 Å away from the phosphorus atom, this has been illustrated in Figure 1.17. As the size of the ligand varies, so does Tolman's cone angle. As expected, larger substituents, such as *t*-butyl groups, produce large angles ($182 \pm 2^\circ$), while the opposite is true for smaller functionalities, for instance, the methyl group ($118 \pm 4^\circ$).⁹⁷

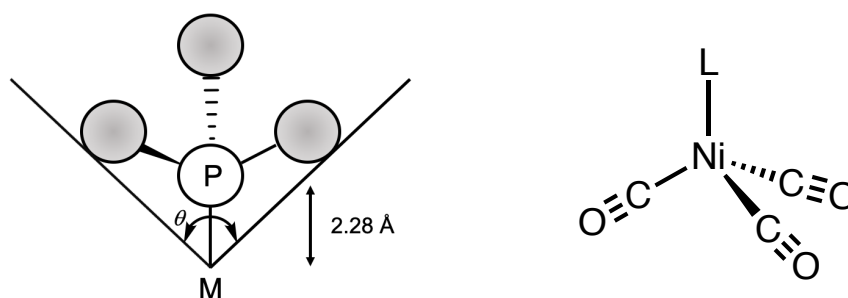


Figure 1.17 Figure to illustrate Tolman's cone angle (left) and an example complex, $[\text{Ni}(\text{CO})_3\text{L}]$, which can be used to determine the electron donating or withdrawing ability of L through the A_1 -symmetrical carbonyl stretching mode (ν_{CO}).

Tolman also established that IR carbonyl stretches could be used to infer the electronic parameter, ν , of phosphine ligands, to determine their electron-donating or electron-withdrawing ability. By analysing the IR spectra of $[\text{Ni}(\text{CO})_3\text{L}]$ complexes, Tolman found the frequency of the A_1 -symmetrical carbonyl stretching mode (ν_{CO}) to be dependent on the other ligands in the complex. Phosphine ligands act as σ -donors, increasing the electron density of the metal centre which in turn is transferred to the π^* antibonding orbitals of the carbonyl group (Figure 1.18). As a result, this reduces the carbonyl $\text{C}\equiv\text{O}$ bond order which is reflected in a lower vibrational frequency. Thus, a shift of the $\text{C}\equiv\text{O}$ stretching frequency to a lower wavenumber signifies good σ -donor ligands. Tuning the groups on the phosphorus to be good π -acceptors, for example in the case of phosphites, results in a reduction in electron density on the metal and therefore, less donation into the π^* antibonding orbital of the CO. This

results in a stronger C≡O bond, which is shown by a higher stretching frequency in the IR spectra.^{97,98}

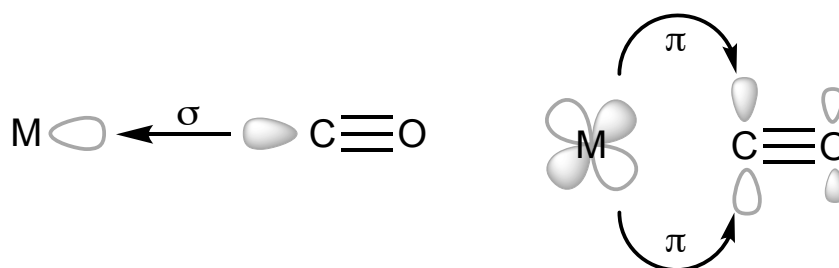


Figure 1.18 The molecular orbitals involved in metal carbonyl bonding: σ -donation from the carbonyl group (left) and π -back-donation from the metal centre.

In addition to Tolman's cone angle and electronic parameters, alternative approaches have since been explored. The Quantitative Analysis of Ligand Effects (QALE) approach takes additional experimental values into account including pKa, enthalpy of formation, reduction potentials and IR data to form parameters to describe trends in reactivity and classification of ligands.^{99–102} The Ligand Knowledge Base (LKB) approach, developed by Fey and co-workers, utilises principle component analysis to model organophosphorus ligands. For a representative overview, they are modelled not only as the free ligand but in a range of coordination environments including the protonated form ([HL]⁺), the borane adduct (BH₃•L), three metal complexes, ([ClAuL], [Cl₃PdL][−] and [(H₃P)₃PtL]) and a ring of eight helium atoms (He₈.L) to simulate the steric hinderance encountered in an octahedral coordination environment. From the DFT calculations, parameters can be extracted and applied to map chemical space and to visualise ligands in chemically meaningful groups. Calculation of LKB parameters and comparison with known compounds before ligand synthesis can potentially allow for the prediction of a range of properties and reactivity.^{103,104} This could be beneficial in the development of phosphorus-containing compounds for therapeutic applications to predict their reactivity.

1.8 Primary Phosphines

The synthesis of tertiary phosphines from primary phosphines is a key feature in this thesis. A primary phosphine consists of two highly reactive phosphorus-hydrogen bonds on an alkyl or aryl substituent. The P–H bonds enable their facile functionalisation and thus makes them extremely valuable starting materials in synthetic procedures.^{105,106} Shown in Figure 1.19 are the functionalisation reactions that will be discussed throughout this thesis.

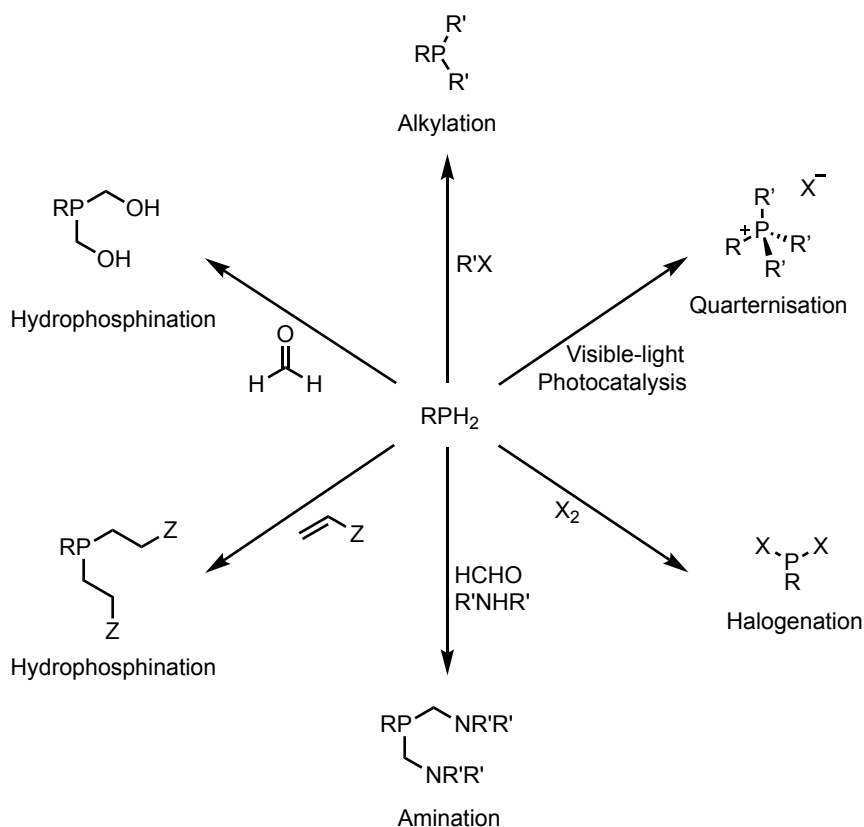
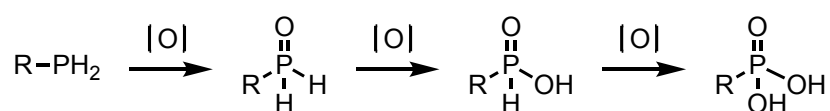


Figure 1.19 A range of primary phosphine functionalisation reactions that will be discussed in this thesis.

Although primary phosphines are valuable starting materials, their highly reactive and pyrophoric nature previously limited the fulfilment of their potential. Their decomposition via oxidation occurs first to the phosphine oxide which is driven by the formation of the strong P=O bond (544 kJ/mol).¹⁰⁷ This phosphine oxide can further oxidise to the analogous phosphinic then phosphonic acid, as has been depicted in Scheme 1.4.⁹⁵



Scheme 1.4 Oxidation of a primary phosphine to phosphine oxide, phosphinic and phosphonic acid.

The tuning of stereoelectronic properties has proven to be a viable method for producing more ‘user friendly’ air-stable primary phosphines which will be discussed in the following sections. It should be noted that in this thesis, the term ‘air-stability’ is defined as, the degree of resistance of a primary phosphine to degradation via oxidation in air, with primary phosphines being considered “stable” if they are inert to oxidation over a period of several weeks.

1.8.1 Steric Effects on Stability

There are a small number of examples in the literature where steric protection of the phosphino group has been employed which successfully resulted in the formation of air-stable

primary phosphines. Two examples, **4** and **5**, are shown in Figure 1.20. Brynda *et al.* used a bicyclic barrelene backbone to afford triptycylphosphine **4**; the bulky backbone around the phosphino group afforded a crystalline air-stable product.^{108,109} For **5**, the addition of steric bulk around the phosphino group in the form of the supermesityl group, resulted in the air-stable, odourless product.^{110,111} This can be contrasted with phenylphosphine **6** which undergoes rapid reaction with dioxygen in a pyrophoric reaction.¹¹²

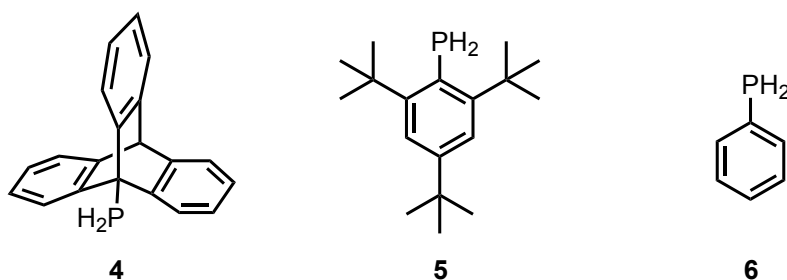


Figure 1.20 Examples of air-stable primary phosphines **4** and **5** with their air-stability attributed to steric protection in contrast to highly reactive phenylphosphine **6** which has no steric protection.

Thus, steric protection is known, but by definition, this limits further functionalisation. Remarkably, Figure 1.21 shows three examples of primary phosphines whose air-stability cannot be attributed to steric effects.

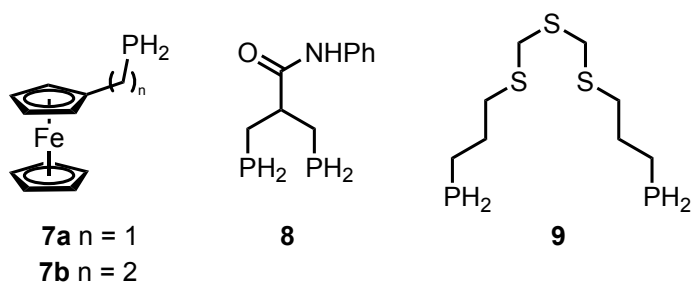


Figure 1.21 Examples of primary phosphines where steric effects cannot account for their stability.

Interestingly, both (ferrocenylmethyl)phosphine **7a** and (ferrocenylethyl)phosphine **7b** show complete air-stability over two years in the solid state.^{113,114} The presence of the alkyl spacer appears to be key for the stability, as the corresponding derivative without a spacer is sensitive to air oxidation. It was noted that the phosphine group points away from the ferrocenyl group in the crystal structure and thus any stabilising interactions with the iron could be ruled out in the solid state. However, it is perhaps possible that the iron affects the primary phosphine through bonds electronically. Bisphosphine **8** was also deemed inert to oxidation in air and demonstrated air-stability over 12 months in a glass vial. The authors deduced from the crystal structure of **8** that there were no direct hydrogen bonding interactions from the phosphorus and thus discounted that the oxidative inertness could be attributable to

this.¹¹⁵ Thioether-functionalised phosphine **9** is a further example of a surprisingly air-stable primary phosphine. This phosphine can be isolated as a crystalline solid and resisted oxidation over a two year period after storage in an unsealed glass vial. It was postulated that the stability could be due to negative hyperconjugation of the heteroatoms, but this explanation was not fully articulated.^{116,117}

It is apparent that the air-stability of the aforementioned examples in Figure 1.21 cannot be attributed to steric effects and thus, in these cases, there must be an alternative explanation. The Higham group also synthesised two air-stable primary phosphines **10a** and **10b** with a chiral binaphthyl backbone shown in Figure 1.22, which also contain no steric encumbrance and therefore, electronic effects were considered.

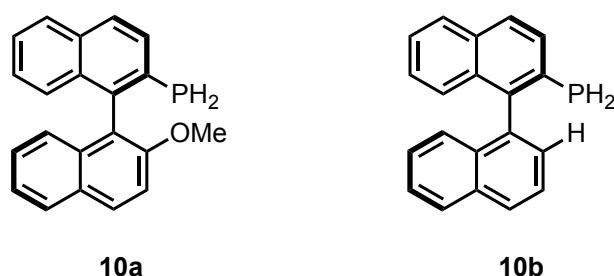
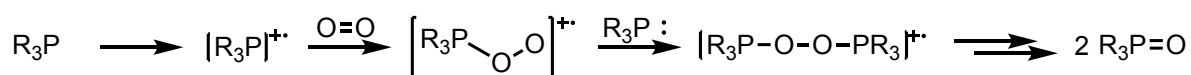


Figure 1.22 Air-stable atropisomeric primary phosphines (*R*)-MeO-MOPH₂ **10a** and (*S*)-H-MOPH₂ **10b**.

1.1.2 Electronic Stability

A family of structurally diverse, air-stable primary phosphines had now been reported, some with unexplained stability. Therefore, the Higham group attempted to find a common cause of this phenomenon using DFT calculations.

The Higham group developed a model to predict the air-stability of primary phosphines which was based on the proposed mechanism for phosphine oxidation by Yasui *et al.* which is shown in Scheme 1.5.¹¹⁸ The mechanism, supported by photolysis and radiolysis experiments, relies on the formation of a phosphine radical cation which reacts with dioxygen in the air. This step is proposed to proceed via an interaction between the radical cation and dioxygen, which indicates the importance of the SOMO energy.



Scheme 1.5 Proposed mechanism of phosphine oxidation via the reaction of a phosphine radical with dioxygen.

The model is based on density functional theory (DFT) calculations using a B3LYP function with a 6-31G* basis set which was applied to calculate the optimised geometries, the HOMO/LUMO

for the neutral phosphines and the SOMO energy for the phosphine radical cations which, as described, is expected to play a role in the oxidation of the phosphine.

Initially, these calculations were performed on a series of phosphines containing increasing amounts of π -conjugation; experimentally, phenyl phosphine **6** is much more sensitive to oxidation than **10a** and **10b** and therefore, this was a rational starting point. The calculations revealed some important qualitative trends. Firstly, it was apparent that the relative amount of phosphorus character present in the HOMO (i.e. the degree to which the HOMO is localised on phosphorus) varied with the extent of π -conjugation, with phosphines with more conjugation displaying lower phosphorus character in the HOMO. Phosphines with lower phosphorus character in the HOMO were also found to be those which are more stable with respect to oxidation in air.

Furthermore, a trend between the HOMO and SOMO energies with the extent of π -conjugation was observed. It was found that as the extent of π -conjugation increased, so too did the HOMO (as expected) and SOMO energy. This can be correlated with an increase in the experimentally determined resistance to air oxidation; phosphines with a higher energy HOMO have a higher energy SOMO, and this leads to decreased reactivity with dioxygen. This revealed an apparent threshold value for air-stability of approximately -10 eV for the SOMO energy. If the SOMO is below this value, the phosphine displayed sensitivity to air, if above, the compound is found to be air stable. This appears to tie-in with the proposed mechanism based on photolysis and radiolysis as discussed earlier.

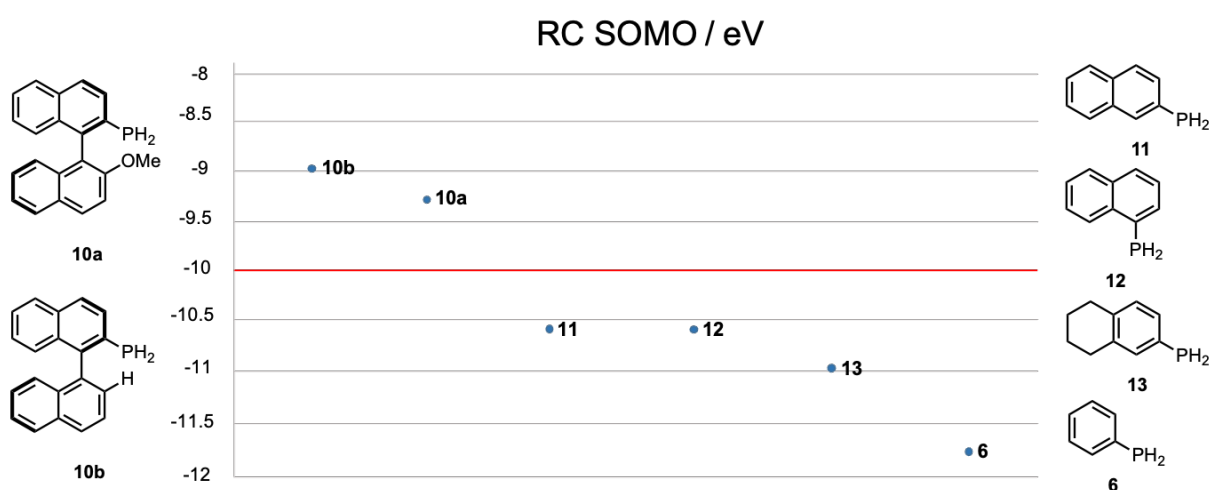


Figure 1.23 A plot showing the SOMO energies for a range of air-stable and air-sensitive primary phosphine radical cations, separated by an evident threshold value of -10 eV (red line).

The model was applied to additional phosphines and was able to rationalise the stability of those with previously unexplained stability, including those in Figures 1.20 and 1.21. The

group concluded that air-stability of phosphines can be achieved both by steric hinderance around the phosphino group and through the incorporation of sufficient π -conjugation or heteroatom presence in the backbone. Two effects are observed when the extent of the π -conjugation is increased: i) the shift of the localisation of the neutral HOMO away from the phosphorus and ii) the increase of the SOMO of the corresponding radical cation.¹¹⁹ The group postulated that the radical cation SOMO energy can be used as a predictor for primary phosphine air stability. This enables the use of a safe and convenient starting material for further functionalisation, without the concern of the dangers normally associated with this class of compound. Note, novel primary phosphines should always be treated with caution in the first instance.

Bodipy primary phosphine **14** shown in Figure 1.24 is a member of the second class of air-stable primary phosphines developed by the Higham group to be stabilised through extended π -conjugation. The DFT model gave a SOMO value of -8.82 eV which is in line with the apparent threshold for air-stability; the compound was subsequently found to be air-stable, experimentally.¹²⁰ It was the first example of an air-stable, fluorescent primary phosphine, and is the primary phosphine of choice for this project; the added chromophore enables its application in fluorescence imaging, a key concept in this thesis.

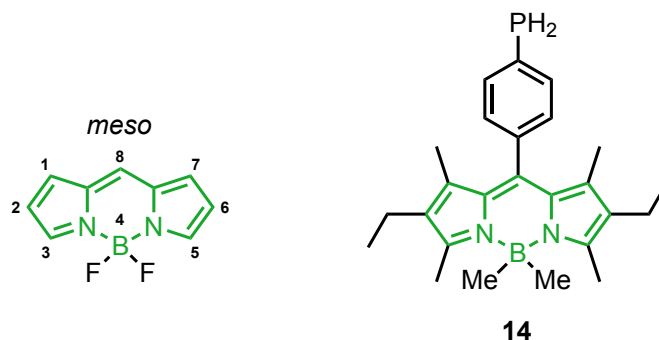
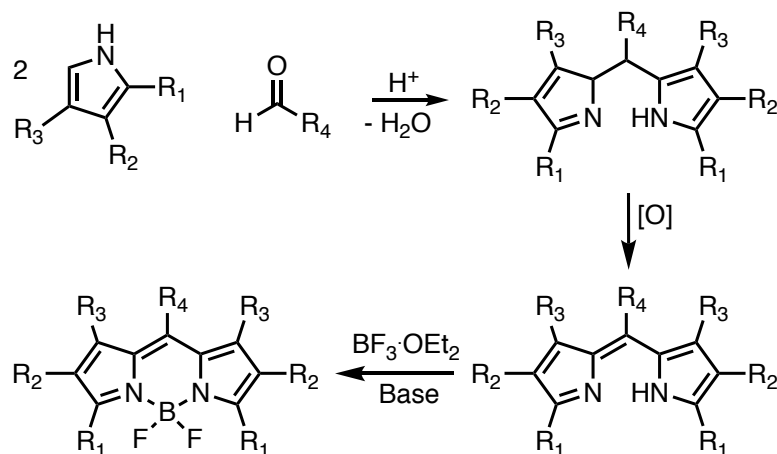


Figure 1.24 The chemical structure of the Bodipy (4,4-difluoro-4-borata-3a-azonia-4a-aza-s-indacene) fluorophore (left): position 8 is also known as the *meso* position. The first example of an air-stable, fluorescent primary phosphine stabilised through extended π -conjugation is also illustrated (right).

1.9 Bodipy

Bodipy compounds are an exceedingly popular class of fluorescent dyes due to their wealth of desirable properties including i) high quantum yields, ii) thermal and photochemical stability, iii) an intense absorption profile and sharp fluorescence emission peaks, iv) good solubility, and v) chemical robustness. The ability to functionalise the Bodipy core at all positions (1–8) makes for a highly versatile fluorophore which can be modified to tune the fluorescent characteristics.^{121,122}

The synthesis of a symmetrical Bodipy core can be achieved with a pyrrole condensation reaction which has been illustrated in Scheme 1.6. Two pyrrole units first undergo a condensation reaction with an aldehyde and the resulting dipyrromethane structure can then be oxidised to dipyrromethene. The complexation with boron trifluoride diethyl etherate in the presence of a base such as a tertiary amine afforded the conjugated structure.¹²¹



Scheme 1.6 Synthesis of a symmetrical Bodipy core from a pyrrole condensation reaction with an aldehyde, the subsequent oxidation of the resulting dipyrromethane structure followed by complexation with boron trifluoride diethyl etherate in the presence of a base.

1.1.3 Photoinduced electron Transfer (PeT)

Photoinduced electron transfer (PeT) is a process that can occur intramolecularly in fluorescent molecules which can result in fluorescence quenching. Nagano *et al.* compared calculated orbital energy levels with experimental photophysical and electrochemical properties to aid in rationalising this behaviour. They first used fluorescein derivatives^{123,124} as an example, and later expanded their research to include Bodipy systems.^{125,126} Both reductive- and oxidative-PeT processes can occur and are illustrated in Figure 1.25, demonstrating how *meso*-substituted Bodipy compounds can act as a donor or acceptor group. Oxidative-PeT or d-PeT (d = donor) occurs when the excited-state of the fluorophore donates electrons to the substituent's LUMO. This process becomes apparent when strongly electron withdrawing acceptors such as aryl nitro, ketone, ester or nitrile groups are present.

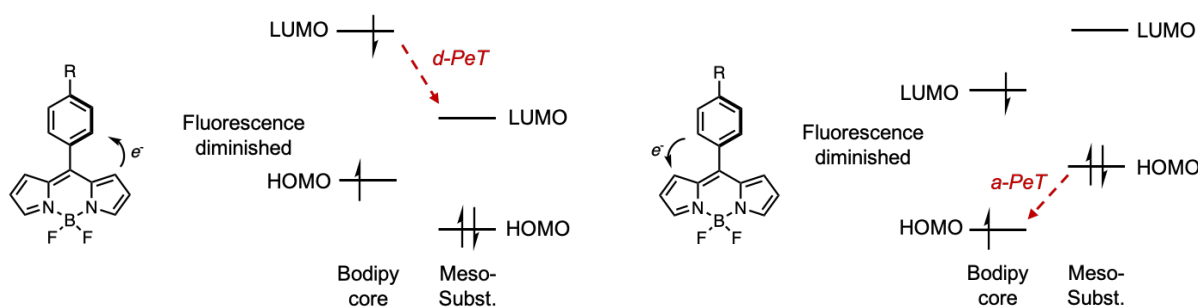


Figure 1.25 Schematic of oxidative PeT (d-PeT) (left) and of reductive-PeT (a-PeT) (right).

The opposite process, known as reductive-PeT or a-PeT (a = acceptor), can occur when donor molecules such as aryl amines, thiols and alcohols are present on the substituent of the molecule. The donation of an electron from the HOMO of the substituent on the fluorophore to the fluorophore, reduces the excited state of the fluorophore, resulting in the quenching of the fluorescence. Inoue *et al.* have reported Bodipy-based phosphine examples where a phosphino group acts as a donor in reductive-PeT. They exploited this to develop a sensing system for the detection of hydroperoxides.⁴⁶ When neither a suitable donor or acceptor is present on the fluorophore then PeT is disfavoured and fluorescence dominates (Figure 1.26).

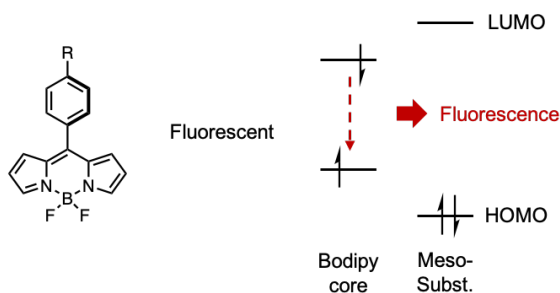


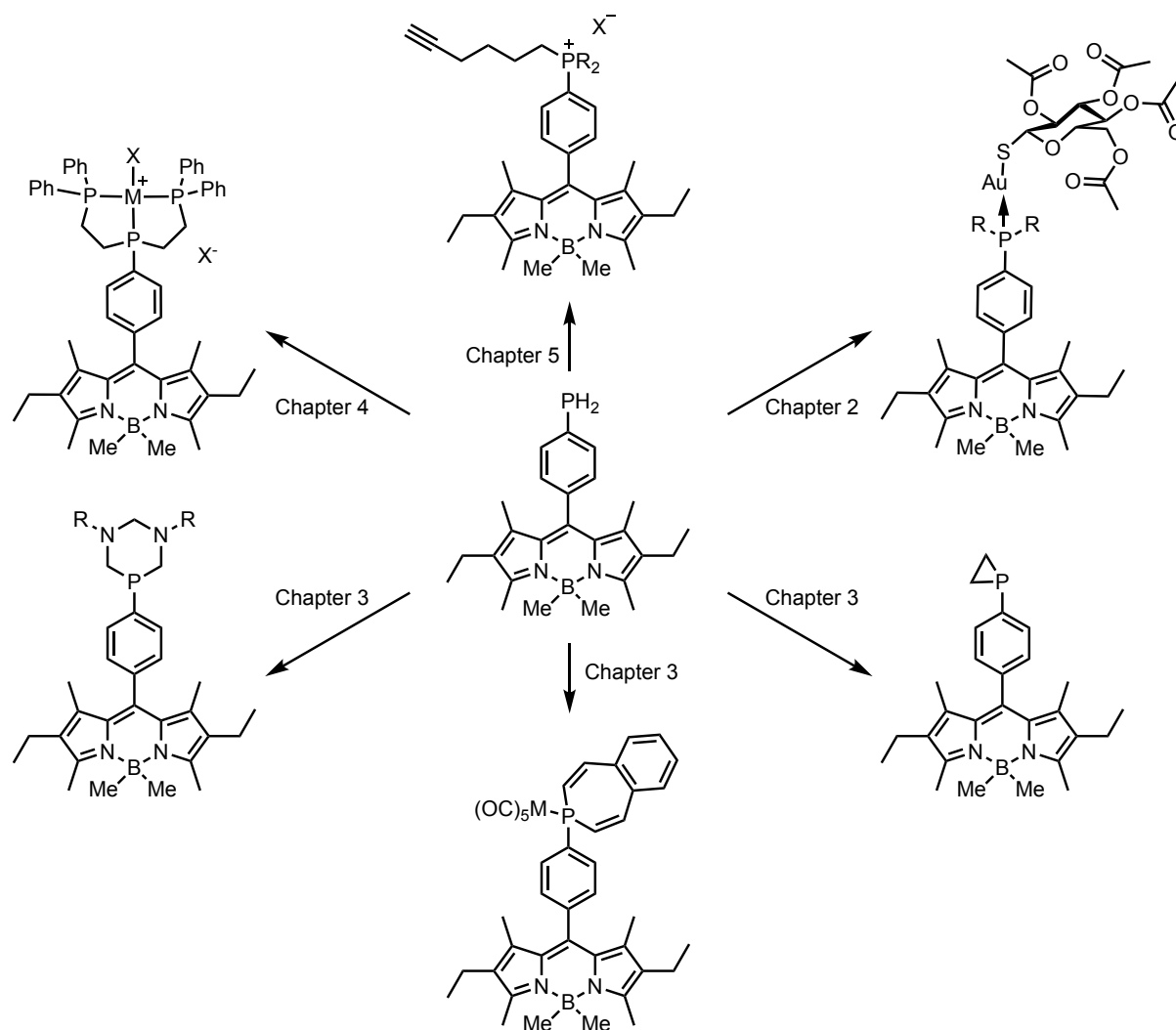
Figure 1.26 Schematic of when there is no electronic significant perturbation, which results in fluorescence.

The Higham group established that in the case of the Bodipy-based primary phosphine **14**, adding a potential 'reductive-PeT donor' phosphorus atom to the Bodipy core did not result in the quenching of fluorescence by reductive-PeT, as might have been expected. This was reflected by the high quantum yields displayed by primary phosphine, **14** of $\Phi = 0.33$.

The fluorescence quantum yield (QY) is a method of quantifying fluorescence that can be defined as the ratio of photons emitted to the number of photons absorbed. It is given as a percentage or a value between zero and one where zero represents no radiative emission from the singlet state, and values close to one are typical for the fluorophores present in highly fluorescent compounds. The fact that the fluorescence persisted upon the addition of a versatile PH₂ moiety opened up the possibility of synthesising and investigating the properties of a range of diverse fluorescent phosphines which are explored in detail in this thesis.

1.10 Thesis Outline

This thesis will describe the synthesis of a fluorescent, Bodipy-based, primary phosphine – this being the first example of a fluorescent, air-stable, primary phosphine with the air-stability attributed to increased π -conjugation, as reported by our group. The functionalisation of this primary phosphine to generate a range of tertiary phosphine ligands and phosphonium salts is reported, with the intention of synthesising probes with biomedical applications.



Chapter two details the synthesis of fluorescent analogues of the therapeutic agent, auranofin. Four fluorescent tertiary phosphines have been synthesised, complexed to Au(I) and coordinated to a thiosugar to afford auranofin derivatives with a fluorescent Bodipy motif. These compounds have been characterised by NMR spectroscopy and their photophysical properties determined. They hold potential as theranostic agents, or as a way to aid in the elucidation or derivation of mechanisms of action.

Chapter three introduces the synthesis of three novel phosphacycles of different sizes. Firstly, a fluorescent phosphirane, a highly strained three-membered organophosphorus ring with

remarkably high thermal-stability and resistance to air oxidation was characterised by NMR spectroscopy and X-ray crystallography, and the photophysical properties were determined. The stereoelectronic properties of the phosphirane were explored through its coordination to group 6 carbonyl complexes. In addition, preliminary investigations into the phosphirane's reactivity with methyl trifluoromethanesulfonate to produce a phosphiranium salt were carried out; a fluorescent phosphiranium salt may hold potential as a mitochondrial specific ^{31}P MRS agent. The results are compared to the previously reported (*R*)-1-(2'-methoxy-1,1'-binaphthyl-2-yl)phosphirane. Secondly, two six-membered phosphacycles, 1,3,5-diazaphosphanes, have been synthesised in collaboration with Dr Randolph Köhn at the University of Bath and will be introduced. These fluorescent phosphacycles were also characterised by NMR spectroscopy, X-ray crystallography and photophysics. Their coordination to chromium(III) and preliminary catalytic studies in hexene trimerization will also be detailed. A short collaborative project with Dr Bill Henderson at the University of Waikato explores the application of a potential precursor to the fluorescent 1,3,5-diazaphosphanes in the fluorescent labelling of amine-modified surfaces. Finally, the synthesis, characterisation and photophysical properties of a seven-membered, unsaturated phosphorus ring, a phosphepine, will be discussed. Initially, the ligand was synthesised by functionalisation of primary phosphine-bound group 6 metal complexes, which were characterised by NMR spectroscopy and X-ray crystallography. Preliminary studies were then carried out to investigate the generation of the free ligand.

Chapter four presents the synthesis of a fluorescent tridentate phosphine, BodP₃, and explores its coordination with the group 10 metal complexes. The resultant fluorescent metal complexes were characterised by NMR spectroscopy, photophysical properties and in addition, the nickel(II), palladium(II) and platinum(II) chloride complexes were characterised by X-ray crystallography. Particular focus is on the synthesis of a novel series of fluorescent platinum complexes due to the prominence of platinum in chemotherapeutic agents. Preliminary studies of one of these fluorescent platinum complexes in prostate cancer (PC-3) cells and their analysis via fluorescence microscopy is described.

Chapter five describes the synthesis of fluorescent phosphonium salts for mitochondrial imaging. The initial work focused on the synthesis of phosphonium salts containing a haloalkyl chain, to allow for the substitution of the halogen atom by ^{18}F , to give applications in both PET and fluorescence imaging. A short ongoing collaborative project with Dr Peter (Yingxiao) Wang and Dr Kathy (Shaoying) Lu at the University of California, San Diego resulted in one

phosphonium salt being tested as an imaging agent in pancreatic cancer cells. Finally, the synthesis of fluorescent phosphonium salts with an alkynyl moiety is explored, which would provide both an alternative route to radiolabelling and enables additional bioconjugation reactions for further probe development.

1.11 References

- 1 World Health Organisation - The top 10 causes of death, <https://www.who.int/news-room/fact-sheets/detail/the-top-10-causes-of-death>, (accessed 15 September 2020).
- 2 Our World in Data - Causes of Death, <https://ourworldindata.org/causes-of-death>, (accessed 15 September 2020).
- 3 Cancer Research UK, <https://www.cancerresearchuk.org/health-professional/cancer-statistics/statistics-by-cancer-type/pancreatic-cancer/>, (accessed 19 May 2020).
- 4 J. Maddams, M. Utley and H. Møller, *Br. J. Cancer*, 2012, **107**, 1195–1202.
- 5 P. E. Oberstein and K. P. Olive, *Therap. Adv. Gastroenterol.*, 2013, **6**, 321–337.
- 6 S. P. Pereira, L. Oldfield, A. Ney, P. A. Hart, M. G. Keane, S. J. Pandol, D. Li, W. Greenhalf, C. Y. Jeon, E. J. Koay, C. V. Almario, C. Halloran, A. M. Lennon and E. Costello, *Lancet Gastroenterol. Hepatol.*, 2020, **5**, 698–710.
- 7 Challenges and Opportunities in Pancreatic Cancer Research, <https://blog.crownbio.com/pancreatic-cancer-research>, (accessed 15 September 2020).
- 8 M. Swayden, J. Iovanna and P. Soubeyran, *Heliyon*, 2018, **4**, e01055.
- 9 Early Detection Cambridge, <https://www.earlydetectioncambridge.org.uk/about/why-early-detection>, (accessed 15 September 2020).
- 10 S. A. Aldossary, *Biomed. Pharmacol. J.*, 2019, **12**, 7–15.
- 11 C. J. Jones and J. R. Thornback, in *Medicinal Applications of Coordination Chemistry*, 2007, pp. 324–339.
- 12 A. J. Di Pasqua, J. Goodisman and J. C. Dabrowiak, *Inorg. Chim. Acta*, 2012, **389**, 29–35.
- 13 C. Roder and M. J. Thomson, *Drugs R. D.*, 2015, **15**, 13–20.
- 14 J. M. Madeira, D. L. Gibson, W. F. Kean and A. Klegeris, *Inflammopharmacology*, 2012, **20**, 297–306.
- 15 W. F. Kean, L. Hart and W. W. Buchanan, *Rheumatology*, 1997, **36**, 560–572.
- 16 J. M. Madeira, C. J. Renschler, B. Mueller, S. Hashioka, D. L. Gibson and A. Klegeris, *Life Sci.*, 2013, **92**, 1072–1080.
- 17 J. M. Madeira, E. Bajwa, M. J. Stuart, S. Hashioka and A. Klegeris, *J. Neuroimmunol.*, 2014, **276**, 71–79.
- 18 E. V Capparelli, R. Bricker-Ford, M. J. Rogers, J. H. McKerrow and S. L. Reed, *Antimicrob.*

Agents Chemother., 2017, **61**, e01947-16.

- 19 S. Jackson-Rosario, D. Cowart, A. Myers, R. Tarrien, R. L. Levine, R. A. Scott and W. T. Self, *J. Biol. Inorg. Chem.*, 2009, **14**, 507–519.
- 20 S. Jackson-Rosario and W. T. Self, *J. Bacteriol.*, 2009, **191**, 4035–4040.
- 21 Y. Hokai, B. Jurkowicz, J. Fernández-Gallargo, N. Zakirkhodjaev, M. Sanaú, T. R. Muth and M. Contel, *J. Inorg. Biochem.*, 2014, **138**, 81–88.
- 22 C. Roder and E. Athan, *Drugs R. D.*, 2020, **20**, 209–216.
- 23 B. Wu, X. Yang and M. Yan, *J. Med. Chem.*, 2019, **62**, 7751–7768.
- 24 C. Fan, W. Zheng, X. Fu, X. Li, Y.-S. Wong and T. Chen, *Cell Death Dis.*, 2014, **5**, e1191–e1191.
- 25 W. Fiskus, N. Saba, M. Shen, M. Ghias, J. Liu, S. Das Gupta, L. Chauhan, R. Rao, S. Gunewardena, K. Schorno, C. P. Austin, K. Maddocks, J. Byrd, A. Melnick, P. Huang, A. Wiestner and K. N. Bhalla, *Cancer Res.*, 2014, **74**, 2520–2532.
- 26 C. Marzano, V. Gandin, A. Folda, G. Scutari, A. Bindoli and M. P. Rigobello, *Free Radic. Biol. Med.*, 2007, **42**, 872–881.
- 27 I. L. Shytaj, B. Chirullo, W. Wagner, M. G. Ferrari, R. Sgarbanti, A. Della Corte, C. LaBranche, L. Lopalco, A. T. Palamara, D. Montefiori, M. G. Lewis, E. Garaci and A. Savarino, *Retrovirology*, 2013, **10**, 71.
- 28 B. Chirullo, R. Sgarbanti, D. Limongi, I. L. Shytaj, D. Alvarez, B. Das, A. Boe, S. DaFonseca, N. Chomont, L. Liotta, E. III Petricoin, S. Norelli, E. Pelosi, E. Garaci, A. Savarino and A. T. Palamara, *Cell Death Dis.*, 2013, **4**, e944–e944.
- 29 R. M. Snyder, C. K. Mirabelli and S. T. Crooke, *Semin. Arthritis Rheum.*, 1987, **17**, 71–80.
- 30 K. Tepperman, R. Finer, S. Donovan, R. Elder, J. Doi, D. Ratliff and K. Ng, *Science*, 1984, **225**, 430–432.
- 31 T. C. Karlenius and K. F. Tonissen, *Cancers (Basel)*, 2010, **2**, 209–232.
- 32 T. Onodera, I. Momose and M. Kawada, *Chem. Pharm. Bull.*, 2019, **67**, 186–191.
- 33 K. Lin, Z.-Z. Zhao, H.-B. Bo, X.-J. Hao and J.-Q. Wang, *Front. Pharmacol.*, 2018, **9**, 1323.
- 34 S. Thota, D. A. Rodrigues, D. C. Crans and E. J. Barreiro, *J. Med. Chem.*, 2018, **61**, 5805–5821.
- 35 M. Rausch, P. J. Dyson and P. Nowak-Sliwinska, *Adv. Ther.*, 2019, **2**, 1900042.
- 36 W. H. Ang, A. Casini, G. Sava and P. J. Dyson, *J. Organomet. Chem.*, 2011, 696, 989–998.

- 37 C. S. Allardyce, P. J. Dyson, D. J. Ellis and S. L. Heath, *Chem. Commun.*, 2001, **2**, 1396–1397.
- 38 C. A. Combs, *Curr. Protoc. Neurosci.*, 2010, **50**, 2.1.1-2.1.14.
- 39 S. Tasan, O. Zava, B. Bertrand, C. Bernhard, C. Goze, M. Picquet, P. Le Gendre, P. Harvey, F. Denat, A. Casini and E. Bodio, *Dalton Trans.*, 2013, **42**, 6102–6109.
- 40 J. R. Lakowicz, *Principles of Fluorescence Spectroscopy*, Springer, 3rd edn., 2006.
- 41 B. Valeur and M. N. Berberan-Santos, *Molecular Fluorescence*, Wiley-VCH Verlag GmbH & Co. KGaA, Weinheim, Germany, 2012.
- 42 B. Valeur and I. Leray, *Coord. Chem. Rev.*, 2000, **205**, 3–40.
- 43 P. Gao, W. Pan, N. Li and B. Tang, *Chem. Sci.*, 2019, **10**, 6035–6071.
- 44 K. A. Myers and C. Janetopoulos, *F1000Research*, 2016, **5**, 1–14.
- 45 M. Piccolo, G. Misso, M. G. Ferraro, C. Riccardi, A. Capuozzo, M. R. Zarone, F. Maione, M. Trifuoggi, P. Stiuso, G. D’Errico, M. Caraglia, L. Paduano, D. Montesarchio, C. Irace and R. Santamaria, *Sci. Rep.*, 2019, **9**, 7006.
- 46 N. Inoue, Y. Suzuki, K. Yokoyama and I. Karube, *Biosci. Biotechnol. Biochem.*, 2009, **73**, 1215–1217.
- 47 D. C. Wallace, *Science*, 1999, **283**, 1482–1488.
- 48 N. Hail, *Apoptosis*, 2005, **10**, 687–705.
- 49 G. Kroemer, *Oncogene*, 2006, **25**, 4630–4632.
- 50 X. Chen, D. Stern and S. Du Yan, *Curr. Alzheimer Res.*, 2006, **3**, 515–520.
- 51 H. E. Moon and S. H. Paek, *Exp. Neurobiol.*, 2015, **24**, 103–116.
- 52 M. P. Murphy, *Biochim. Biophys. Acta, Bioenerg.*, 2008, **1777**, 1028–1031.
- 53 J. S. Modica-Napolitano and J. R. Aprille, *Adv. Drug Deliv. Rev.*, 2001, **49**, 63–70.
- 54 M. Millard, D. Pathania, Y. Shabaik, L. Taheri, J. Deng and N. Neamati, *PLoS One*, 2010, **5**, e13131.
- 55 D.-Y. Kim, H.-S. Kim, U. N. Le, S. N. Jiang, H.-J. Kim, K.-C. Lee, S.-K. Woo, J. Chung, H.-S. Kim, H.-S. Bom, K.-H. Yu and J.-J. Min, *J. Nucl. Med.*, 2012, **53**, 1779–1785.
- 56 Y. H. Shabaik, M. Millard and N. Neamati, *PLoS One*, 2013, **8**, e54346.
- 57 D.-Y. Kim and J.-J. Min, *Nucl. Med. Mol. Imaging*, 2016, **50**, 185–195.
- 58 J. J. Vaquero and P. Kinahan, *Annu. Rev. Biomed. Eng.*, 2015, **17**, 385–414.

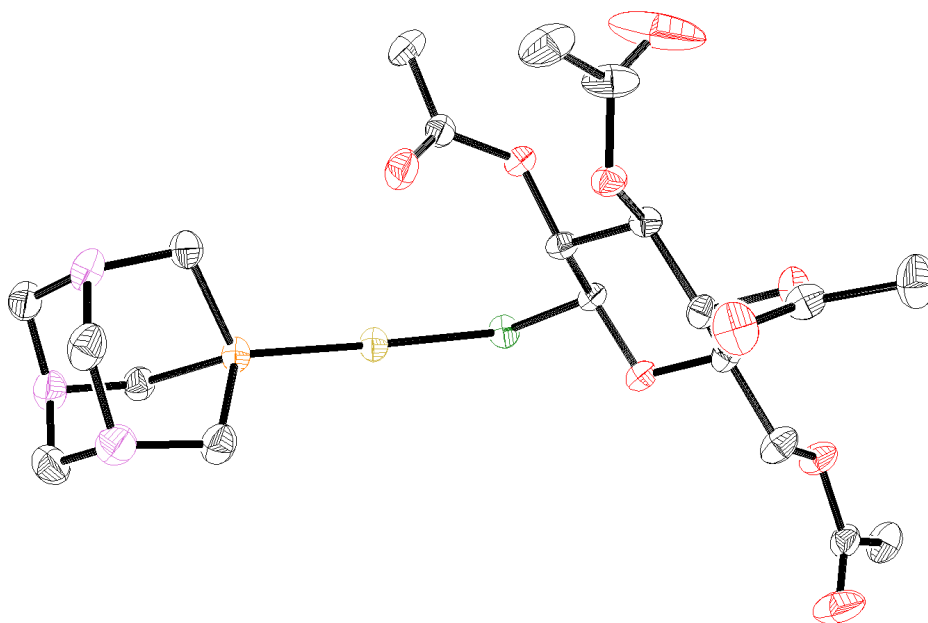
- 59 P. W. Miller, N. J. Long, R. Vilar and A. D. Gee, *Angew. Chemie Int. Ed.*, 2008, **47**, 8998–9033.
- 60 S. L. Pimlott and A. Sutherland, *Chem. Soc. Rev.*, 2011, **40**, 149–162.
- 61 F. Buckingham and V. Gouverneur, *Chem. Sci.*, 2016, **7**, 1645–1652.
- 62 J. C. Knight and B. Cornelissen, in *Radiopharmaceutical Chemistry*, eds. J. S. Lewis, A. D. Windhorst and B. M. Zeglis, Springer International Publishing, 2019, pp. 467–479.
- 63 H. C. Kolb, M. G. Finn and K. B. Sharpless, *Angew. Chemie Int. Ed.*, 2001, **40**, 2004–2021.
- 64 H. H. Coenen, A. D. Gee, M. Adam, G. Antoni, C. S. Cutler, Y. Fujibayashi, J. M. Jeong, R. H. Mach, T. L. Mindt, V. W. Pike and A. D. Windhorst, *Nucl. Med. Biol.*, 2017, **55**, v–xi.
- 65 A. Haslop, A. Gee, C. Plisson and N. Long, *J. Label. Compd. Radiopharm.*, 2013, **56**, 313–316.
- 66 S. P. McCluskey, A. Haslop, C. Coello, R. N. Gunn, E. W. Tate, R. Southworth, C. Plisson, N. J. Long and L. A. Wells, *J. Nucl. Med.*, 2019, **60**, 1750–1756.
- 67 J.-M. Werner, P. Lohmann, G. R. Fink, K.-J. Langen and N. Galldiks, *Molecules*, 2020, **25**, 1471.
- 68 A. Zhu, A. Daniel Lee and H. Shim, *Semin Oncol*, 2011, **38**, 55–69.
- 69 Z. Li, A. A. Gupte, A. Zhang and D. J. Hamilton, *Methodist Debakey Cardiovasc. J.*, 2017, **13**, 29–33.
- 70 M. Silindir and A. Y. Özer, *Fabad J. Pharm. Sci.*, 2008, **33**, 153–162.
- 71 D. O’Hagan, *Chem. Soc. Rev.*, 2008, **37**, 308–319.
- 72 British Heart Foundation, <https://www.bhf.org.uk/what-we-do/news-from-the-bhf/contact-the-press-office/facts-and-figures>, (accessed 16 September 2020).
- 73 J. D. Kelly, A. M. Forster, B. Higley, C. M. Archer, F. S. Booker, L. R. Canning, K. Wai Chiu, B. Edwards, H. K. Gill, M. McPartlin, K. R. Nagle, I. A. Latham, R. D. Pickett, A. E. Storey and P. M. Webbon, *J. Nucl. Med.*, 1993, **34**, 222–227.
- 74 G. T. Woolley, S. L. Kitson and R. Gordon Reid, *J. Label. Compd. Radiopharm.*, 2007, **50**, 468–470.
- 75 H. Spies and H.-J. Pietzsch, in *Technetium-99m Pharmaceuticals*, ed. I. Zolle, Springer Berlin Heidelberg, Berlin, Heidelberg, 2007, pp. 59–66.
- 76 K. A. Stephenson, S. R. Banerjee, T. Besanger, O. O. Sogbein, M. K. Levadala, N. McFarlane, J. A. Lemon, D. R. Boreham, K. P. Maresca, J. D. Brennan, J. W. Babich, J.

- Zubieta and J. F. Valliant, *J. Am. Chem. Soc.*, 2004, **126**, 8598–8599.
- 77 W. A. Volkert and S. Jurisson, in *Technetium and Rhenium Their Chemistry and Its Applications*, eds. K. Yoshihara and T. Omori, Springer Berlin Heidelberg, Berlin, Heidelberg, 1996, pp. 123–148.
- 78 L. H. Davies, B. B. Kasten, P. D. Benny, R. L. Arrowsmith, H. Ge, S. I. Pascu, S. W. Botchway, W. Clegg, R. W. Harrington and L. J. Higham, *Chem. Commun.*, 2014, **50**, 15503–15505.
- 79 D. E. Befroy and G. I. Shulman, *Diabetes*, 2011, **60**, 1361–1369.
- 80 A. C. Harnden, D. Parker and N. J. Rogers, *Coord. Chem. Rev.*, 2019, 383, 30–42.
- 81 Y.-C. Lin, J. Wu, D. Baltzis, A. Veves and R. Greenman, *J. Magn. Reson. Imaging*, 2016, **44**, 1132–1142.
- 82 M. D. Campbell and D. J. Marcinek, *Biochim. Biophys. Acta - Mol. Basis Dis.*, 2016, **1862**, 716–724.
- 83 L. Valkovič, M. Chmelík and M. Krššák, *Anal. Biochem.*, 2017, 529, 193–215.
- 84 G. J. Kemp and K. M. Brindle, *Diabetes*, 2012, **61**, 1927–1934.
- 85 R. G. Weiss, G. A. Hirsch and P. A. Bottomley, ed. R. Y. Kwong, Humana Press, Totowa, NJ, 2008, pp. 673–694.
- 86 A. Bainbridge, I. Tachtsidis, S. D. Faulkner, D. Price, T. Zhu, E. Baer, K. D. Broad, D. L. Thomas, E. B. Cady, N. J. Robertson and X. Golay, *Neuroimage*, 2014, 102, 173–183.
- 87 A. A. K. Abdel Razek and H. Poptani, *Eur. J. Radiol.*, 2013, **82**, 982–989.
- 88 R. Beadle and M. Frenneaux, *Expert Rev. Cardiovasc. Ther.*, 2010, 8, 269–277.
- 89 J. H. Hwang and C. S. Choi, *Exp. Mol. Med.*, 2015, **47**, 1–8.
- 90 K. L. N. A. Finney, A. C. Harnden, N. J. Rogers, P. K. Senanayake, A. M. Blamire, D. O’Hogain and D. Parker, *Chem. Eur. J.*, 2017, **23**, 7976–7989.
- 91 A. Berger, *BMJ*, 2002, **324**, 35.
- 92 J. Neil and J. J. H. Ackerman, *Encycl. Neurol. Sci.*, 2014, **25**, 973–976.
- 93 A. G. Orpen and N. G. Connelly, *J. Chem. Soc. Chem. Commun.*, 1985, 1310–1311.
- 94 A. G. Orpen and N. G. Connelly, *Organometallics*, 1990, **9**, 1206–1210.
- 95 L. D. Quin, *A Guide to Organophosphorus Chemistry*, John Wiley & Sons, Inc., New York, 2000.

- 96 C. A. Tolman, *Chem. Rev.*, 1977, **77**, 313–348.
- 97 C. A. Tolman, *J. Am. Chem. Soc.*, 1970, **92**, 2956–2965.
- 98 C. A. Tolman, *J. Am. Chem. Soc.*, 1970, **92**, 2953–2956.
- 99 M. Rahman, H. Y. Liu, K. Eriks, A. Prock and W. P. Giering, *Organometallics*, 1989, **8**, 1–7.
- 100 M. N. Golovin, M. M. Rahman, J. E. Belmonte and W. P. Giering, *Organometallics*, 1985, **4**, 1981–1991.
- 101 M. M. Rahman, H. Y. Liu, A. Prock and W. P. Giering, *Organometallics*, 1987, **6**, 650–658.
- 102 M. R. Wilson, D. C. Woska, A. Prock and W. P. Giering, *Organometallics*, 1993, **12**, 1742–1752.
- 103 N. Fey, A. C. Tsipis, S. E. Harris, J. N. Harvey, A. G. Orpen and R. A. Mansson, *Chem. Eur. J.*, 2005, **12**, 291–302.
- 104 N. Fey, S. Papadouli, P. G. Pringle, A. Ficks, J. T. Fleming, L. J. Higham, J. F. Wallis, D. Carmichael, N. Mézailles and C. Müller, *Phosphorus Sulfur Silicon Relat Elem*, 2015, **190**, 706–714.
- 105 K. V. Katti, N. Pillarsetty and K. Raghuraman, 2003, 121–141.
- 106 J. T. Fleming and L. J. Higham, *Coord. Chem. Rev.*, 2015, **297–298**, 127–145.
- 107 E. Lippert, *Angew. Chemie*, 1960, **72**, 602.
- 108 M. Brynda, M. Geoffroy and G. Bernardinelli, *Chem. Commun.*, 1999, 961–962.
- 109 G. Ramakrishnan, A. Jouaiti, M. Geoffroy and G. Bernardinelli, *J. Phys. Chem.*, 1996, **100**, 10861–10868.
- 110 M. Yoshifuji, K. Shibayama, N. Inamoto, T. Matsushita and K. Nishimoto, *J. Am. Chem. Soc.*, 1983, **105**, 2495–2497.
- 111 M. Yoshifuji, K. Shibayama, K. Toyota and N. Inamoto, *Tetrahedron Lett.*, 1983, **24**, 4227–4228.
- 112 J. T. Fleming and L. J. Higham, *Coord. Chem. Rev.*, 2015, **297–298**, 127–145.
- 113 N. J. Goodwin, W. Henderson, B. K. Nicholson, J. Fawcett and D. R. Russell, *J. Chem. Soc. Dalt. Trans.*, 1999, 1785–1793.
- 114 W. Henderson and S. R. Alley, *J. Organomet. Chem.*, 2002, **656**, 120–128.

- 115 N. Pillarsetty, K. Raghuraman, C. L. Barnes and K. V. Katti, *J. Am. Chem. Soc.*, 2005, **127**, 331–336.
- 116 K. V. Katti, H. Gali, C. J. Smith and D. E. Berning, *Acc. Chem. Res.*, 1999, **32**, 9–17.
- 117 H. Gali, S. R. Karra, V. S. Reddy and K. V Katti, *Angew. Chemie Int. Ed.*, 1999, **38**, 2020–2023.
- 118 Z. B. Alfassi, P. Neta and B. Beaver, *J. Phys. Chem. A*, 1997, **101**, 2153–2158.
- 119 B. Stewart, A. Harriman and L. J. Higham, *Organometallics*, 2011, **30**, 5338–5343.
- 120 L. H. Davies, B. Stewart, R. W. Harrington, W. Clegg and L. J. Higham, *Angew. Chemie Int. Ed.*, 2012, **51**, 4921–4924.
- 121 A. Loudet and K. Burgess, *Chem. Rev.*, 2007, **107**, 4891–4932.
- 122 G. Ulrich, R. Ziessel and A. Harriman, *Angew. Chemie Int. Ed.*, 2008, **47**, 1184–1201.
- 123 T. Ueno, Y. Urano, K. Setsukinai, H. Takakusa, H. Kojima, K. Kikuchi, K. Ohkubo, S. Fukuzumi and T. Nagano, *J. Am. Chem. Soc.*, 2004, **126**, 14079–14085.
- 124 K. Tanaka, T. Miura, N. Umezawa, Y. Urano, K. Kikuchi, T. Higuchi and T. Nagano, *J. Am. Chem. Soc.*, 2001, **123**, 2530–2536.
- 125 Y. Gabe, Y. Urano, K. Kikuchi, H. Kojima and T. Nagano, *J. Am. Chem. Soc.*, 2004, **126**, 3357–3367.
- 126 H. Sunahara, Y. Urano, H. Kojima and T. Nagano, *J. Am. Chem. Soc.*, 2007, **129**, 5597–5604.

Chapter 2



Auranofin and its Analogues

This chapter introduces the gold(I) phosphine complex, auranofin, and outlines its pharmaceutical importance, not only as an FDA approved arthritis drug, but in a range of applications that have more recently been discovered.

A series of analogues of auranofin have been prepared by varying the phosphine donor to incorporate different R groups. A further series of fluorescent derivatives are prepared to enable their application in fluorescence imaging.

The gold(I) containing complexes have been characterised by NMR and IR spectroscopy, mass spectrometry and some by X-ray crystallography. In addition, the photophysical properties of the fluorescent analogues are studied.

2 Auranofin and its Analogues

2.1 Auranofin

The use of gold for therapeutic benefits can be dated back to 2500 BC in ancient China with the belief that consuming it would bring longevity.¹ In recent years, a number of gold complexes have been demonstrated to be effective as therapeutic agents for rheumatoid arthritis.² Some examples, shown in Figure 2.1, include aurothioglucose (Solganal), sodium aurothiomalate (Myocrisin) and auranofin (Ridaura), where the main focus of this chapter lies.

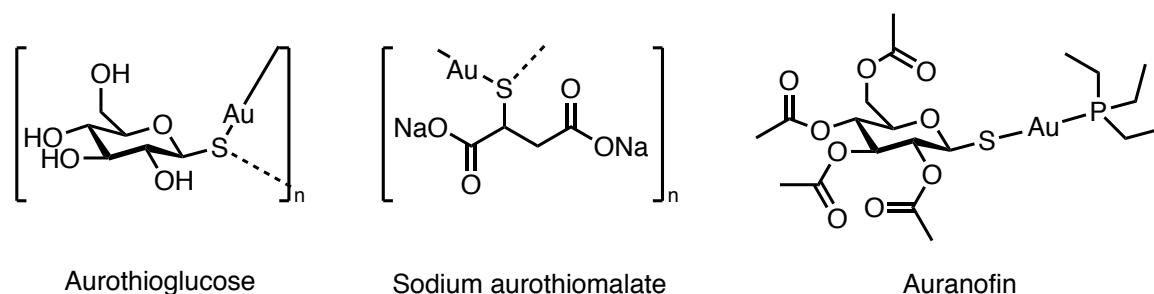


Figure 2.1 Gold(I)thiolate therapeutic agents, aurothioglucose (Solganal), sodium aurothiomalate (Myocrisin) and auranofin (Ridaura).

Auranofin is a two coordinate, linear gold(I) complex with triethylphosphine and thioglucose tetraacetate ligands. It was developed by Smith Kline and French Laboratories in 1976, and later received clinical approval from the FDA in 1985 as an oral treatment for rheumatoid arthritis.³⁻⁵ Auranofin was initially deemed beneficial over aurothioglucose and sodium aurothiomalate due to its improved method of administration (oral as opposed to intramuscular injection) and increased potency in its anti-inflammatory abilities. However, auranofin is no longer the drug of choice in treating rheumatoid arthritis, as sodium aurothiomalate proved to be more effective and novel medications have since been developed.⁶ Since the decline of the clinical use of auranofin in rheumatoid arthritis, it has been given orphan drug status by the FDA for the treatment of the rare disease amebiasis.⁷ Orphan drug status allows for the repurposing of drugs with an already established safety profile, to be used in the treatment of rare diseases^{8,9} and therefore highlights the continued importance of auranofin.

Although auranofin was approved by the FDA over 30 years ago, its precise mechanism of action against rheumatoid arthritis still remains unclear.^{5,10,11} Nevertheless, auranofin has demonstrated activity as an antiparasitic agent where the major mode of action is the inhibition of redox enzymes such as thioredoxin reductase.⁴ The thiol ligand of auranofin forms stable, irreversible adducts with thiol and selenol groups and consequently, has a strong

affinity towards thioredoxin reductase. These redox enzymes are essential for maintaining the levels of reactive oxygen species (ROS) within the cell but thioredoxin reductase is overexpressed in cells in a number of diseases including cancer,¹² and parasitic infections.¹³ This overexpression results in an increased affinity of auranofin towards the diseased cells which results in the increased formation of ROS which subsequently leads to oxidative stress and apoptosis.¹⁴ Studies have shown promising results of auranofin in areas including neurodegenerative disorders (Parkinson's and Alzheimer's disease),^{15,16} parasitic⁴ and bacterial infections,^{3,17–20} cancers^{12,21–23} and HIV.^{24,25} Consequently, there are high hopes for the repurposing of auranofin. These areas have been covered in detail in the thorough review by Roder and Thomson.¹⁴

2.1.1 Auranofin Analogues in the Literature

The bioactivity of auranofin has led to the development of analogues by the modification of the phosphine and/or thiolate ligands to tune the properties to fit the application.

Epstein *et al.* developed a small library of sugar modified analogues of auranofin in an attempt to yield superior antibiotics for the treatment of *Helicobacter pylori* to help mitigate mammalian cell toxicity. Their results suggested that by modifying the sugar, the target enzyme inhibition was maintained and in addition, caused reduced mammalian cytotoxicity.²⁶

Wu *et al.* tested 40 different auranofin analogues against ESKAPE (*Enterococcus faecium*, *Staphylococcus aureus*, *Klebsiella pneumoniae*, *Acinetobacter baumannii*, *Pseudomonas aeruginosa* and *Enterobacters*) pathogens with the intention of finding therapies for pathogenic diseases, in particular, those caused by Gram-negative bacteria which auranofin is inactive towards. Their library of analogues consisted of gold(I) complexes with modification at both the thiol and phosphine ligands. The authors showed that both thiol and the phosphine moieties influence the activities of the analogues. The alkyl phosphines, trimethyl- and triethylphosphine gave the highest activity against both Gram-negative and positive bacteria and all of the complexes gave similar or lower mammalian cell toxicities in comparison to auranofin.³ Gunatilleke *et al.* demonstrated that by tuning the ligands on the gold(I) metal centre, that their potency against cathepsin B could be altered. They studied both the thiolate thiosugar derived gold phosphine complexes, $[\text{Au}(\text{PR}_3)\text{SR}]$, and their metabolite complexes, $[\text{Au}(\text{PR}_3)\text{Cl}]$, with varying phosphine ligands. They reported that larger and more lipophilic phosphines showed an increased cellular uptake and biodistribution. In particular, $[\text{Au}(\text{PPh}_3)\text{Cl}]$ was over 700 times more potent than $[\text{Au}(\text{PEt}_3)\text{Cl}]$. Furthermore, they found that changing the thiolate ligand had little effect on the inhibition of cathepsin B.^{27,28} In

addition to these studies, a 2012 review by Lima *et al.* has been published on *Phosphine-Gold(I) Complexes as Anticancer Agents*.²⁹

Many of these analogues have comparable or improved bioactivity in comparison to auranofin, and have novel applications. This has provided the motivation for the development of a library of triaryl, diarylalkyl, arylalkyl and trialkyl phosphine complexes of auranofin, in order to produce a systematic series of complexes with the intent of altering the bioactivity. In addition, the synthesis of a series of fluorescent derivatives could provide insight into the mechanisms of action through fluorescence microscopy.

2.2 Analogues of Auranofin

The first aim of this project is to synthesise analogues of auranofin by varying the tertiary phosphine ligand. Changing the substituents on the tertiary phosphine allows for the tuning of the steric and electronic properties of the ligand.³⁰ As we have seen with the analogues reported in the literature, this will likely have an effect on the bioactivity of the complexes. Knowing how these different analogues perform in comparison to auranofin could aid in building a clearer picture of how the phosphine ligand affects the bioactivity of the metal complexes.

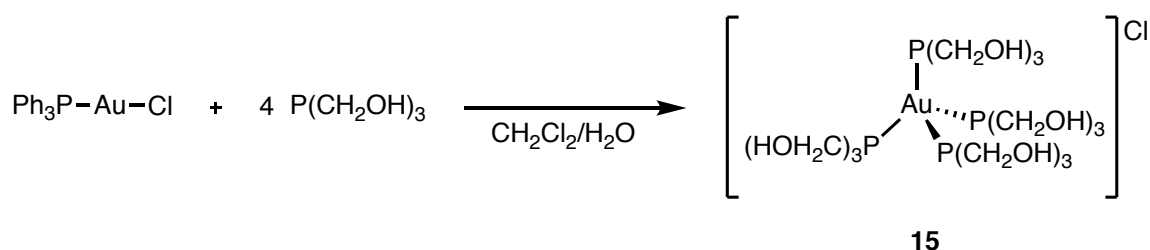
Seven tertiary phosphines were selected for this study; the first four were triphenylphosphine **16a**, cyclohexyldiphenylphosphine **16b**, dicyclohexylphenylphosphine **16c** and tricyclohexylphosphine **16d**. This would enable the comparison of the bioactivity of these complexes within a series. Next, diethylphenylphosphine **16e**, was chosen due to its close similarity to the triethylphosphine ligand of auranofin. Finally, two phosphines of biological interest due to their water solubility, 1,3,5-triaza-7-phosphaadamantane (PTA) **16f** and tris(hydroxymethyl)phosphine (THP) **16g** were also selected.

The phosphine gold(I)chloride complexes **17a-f** are known in the literature,³¹⁻³⁴ whereas [Au(**16g**)Cl] **17g** is unreported. Although these complexes typically act as precursors to those of biological interest, some studies have been carried out to test the biological activity of these [Au(PR₃)Cl] complexes themselves. **17a**, **17b**, **17d** and **17e** were studied as part of a larger library reported by Karver *et al.* and were screened for their selective protein tyrosine phosphatase inhibitor properties, with some derivatives demonstrating significant selectivity and potency.³³

17a has recently been studied by Chrysouli *et al.* for its antiproliferation activity against human breast adenocarcinoma cells (MCF-7) and normal human fetal lung fibroblast cells (MRC-5). It

displayed higher activity than cisplatin against MCF-7 cells, resulting in the induction of cell death via apoptosis, in a similar manner to cisplatin. These encouraging results highlight the potential of **17a** as a candidate as a breast cancer therapeutic agent.³²

Although **17g** has not previously been reported, the closely related four-coordinate complex, tetrakis((trihydroxymethyl)phosphine)gold(I) chloride, [Au(THP)₄]Cl **15** is known in the literature and can be synthesised from the reaction of trishydroxymethylphosphine with triphenylphosphine gold(I)chloride (Scheme 2.1). **15** has been tested for its antitumor properties both *in vitro* and *in vivo*; it demonstrated activity against HCT-15, AGS, PC-3 and LNCaP tumour cells, leading to their growth inhibition.³⁵ The testing of **15** against murine malaria parasite *Plasmodium berghei* has also been reported where it demonstrated potential for the development of this water-soluble gold(I) complex to act as an antimalarial agent.³⁶

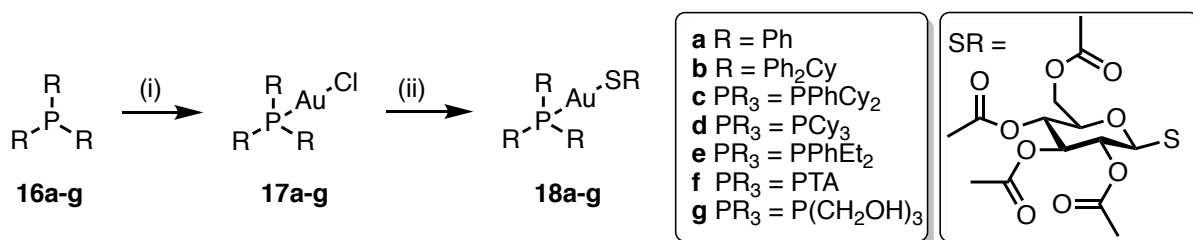


Scheme 2.1 The synthesis of tetrakis((trihydroxymethyl)phosphine)gold(I) chloride, [Au(THP)₄]Cl **15**.

The success of these studies provides motivation, not only to synthesise the thioglucose tetraacetate auranofin analogues, but to synthesise and assess the bioactivity of these precursors.

2.2.1 Gold(I) Phosphine Complexes

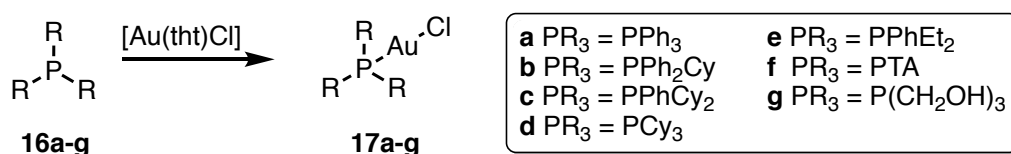
A proposed route to the synthesis of the auranofin analogues is shown in Scheme 2.2. This two-step procedure first requires the coordination of the tertiary phosphines to a gold(I) metal centre through reaction with [chloro(tetrahydrothiophene)gold(I)]. The resulting gold(I) complexes **17a-g** could be prepared from the treatment of **16a-g** with 1-thio-β-D-glucose tetraacetate under basic conditions.³⁷



Scheme 2.2 Proposed route to the synthesis of the analogues of auranofin **18a-g**. (i) [Au(tht)Cl], dichloromethane or ethanol, (ii) 1-thio-β-D-glucose tetraacetate, potassium carbonate, dichloromethane, H₂O.

2.2.2 Synthesis of Chlorogold(I) Phosphine Complexes [Au(**16a-g**)Cl] **17a-g**

To synthesise the corresponding [Au(PR₃)Cl] complexes, tertiary phosphines **16a-g** were treated with [chloro(tetrahydrothiophene)gold(I)] ([Au(tht)Cl]). Tertiary phosphines **16d**, **16e** and **16f** were dissolved in anhydrous dichloromethane and added dropwise to an anhydrous dichloromethane solution of [Au(tht)Cl]. In the case of the phosphines **16a**, **16b**, **16c** and **16g**, these were dissolved in anhydrous ethanol and added dropwise to a suspension of [Au(tht)Cl] in anhydrous ethanol. The respective reaction mixtures were stirred for 1-2 hours; in this time, a white precipitate formed. The precipitates were isolated by filtration, washed with ethanol and dried *in vacuo* to yield pure products in moderate to good yields (49-79%).



Scheme 2.3 The synthesis of [Au(**16a-g**)Cl] **17a-g** complexes by reaction of tertiary phosphines **16a-g** with [Au(tht)Cl].

The desired products were initially characterised by ¹H, ³¹P{¹H} and ¹³C{¹H} NMR spectroscopy which gave resonances consistent with those found in the literature^{28,31,38-45} with the exception of **17g**, which is novel. In all cases, the ³¹P{¹H} NMR spectra displayed downfield resonances from the free phosphines **16a-g** (δ –104.3 to 11.2 ppm) to the Au(I) complexes **17a-g** (δ –52.3 to 54.0 ppm). This data has been tabulated and is shown in Table 2.1.

The novel chlorogold(I) complex **17g** was further characterised by X-ray crystallography. Crystals suitable for analysis by X-ray diffraction were grown from the slow evaporation of a water solution of **17g**. The solid-state structure showed a dimeric structure with aurophilic interactions, and is shown in Figure 2.2.

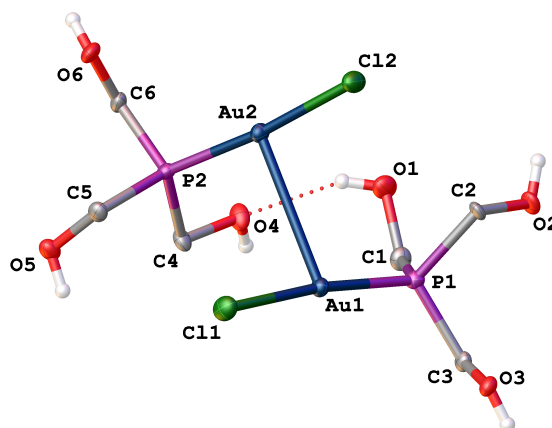


Figure 2.2 View of the molecular structure of **17g**. Hydrogen atoms bound to carbon have been omitted for clarity. Selected bond distances [Å] and angles [°]: Au1-Au2 3.1935(10), Au1-Cl1 2.293(5), Au1-P1 2.229(5), Au2-Cl2 2.300(5), Au2-P2 2.221(5), O4-H 2.110, P1-Au1-Cl1 173.41(18), P2-Au2-Cl2 174.25(17).

The two Au1-P1 and Au2-P2 bond lengths of 2.229(5) and 2.221(5) Å respectively, are in agreement with similar complexes within the literature. The P1-Au1-Cl1 bond angle of 173.41(18)° is slightly lower than the well documented near linear angles seen for gold(I) complexes,⁴⁶ presumably due to the interaction to a second Au atom (Au1-Au2 3.1935(10) Å). The complex also displayed a hydrogen bond (O-H) with a distance of 2.110 Å.

Although their chloro-substituted gold(I) precursors **17a-f** are known, to the best of our knowledge, only the triphenyl- **18a**, tricyclohexylphosphine **18d** and PTA **18f** gold(I) 1-thiolate-β-D-glucose tetraacetate (SR) analogues of auranofin have been reported.

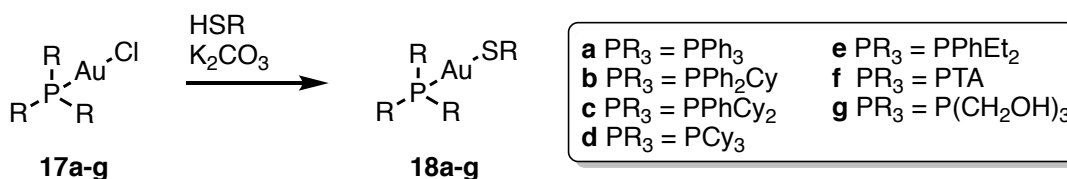
Both [Au(**16a**)SR] **18a** and [Au(**16f**)SR] **18f** have been tested for their bioactivity, **18a** for its antimicrobial activity²⁷ and **18f** in anticancer studies.⁴⁷ [Au(**16d**)SR] **18d** has been reported, however only ¹H NMR studies have been carried out.⁴⁸ **18a** was reported and tested for its activity in the inhibition of lysosomal cysteine proteases. It was found to be the best inhibitor with an IC₅₀ of 339 nM and over 700 times more potent than auranofin.^{27,48,49} **18f** was previously synthesised by Vergara *et al.* as part of a larger study of cytotoxic water-soluble gold(I) complexes with anticancer properties. These complexes were screened against the human ovarian carcinoma cell lines (A2780/S) and its cisplatin-resistant variant (A2780/R). The PTA complex **18f** showed a lower resistance factor than cisplatin, but, an inferior IC₅₀ to both cisplatin and auranofin.^{47,50}

These studies, along with those discussed in Section 2.1.1 show promise for the development of further, more effective bioactive gold(I)phosphine complexes. Therefore, chlorogold(I) complexes **17a-g** were reacted with 1-thio-β-D-glucose tetraacetate (HSR) to afford a small library of auranofin analogues.

2.2.3 Synthesis of Gold(I) Phosphine Thioglucose Tetraacetate Complexes [Au(**16a-g**)SR]

The reaction of 1-thio-β-D-glucose tetraacetate (HSR) with **17a-g** was accomplished using a biphasic reaction. The gold(I)phosphine complexes were dissolved in dichloromethane in the case of **17a-e** and **17g**, or ethanol in the case of **17f**, and stirred with 1-thio-β-D-glucose tetraacetate (HSR) at 0 °C. A cooled aqueous solution of K₂CO₃ was then added dropwise to this stirred solution. The reaction mixtures were warmed to room temperature and stirred rapidly for 1-2 hours. The completion of the reactions was confirmed, in all cases, by a slight downfield shift from their respective precursors in the ³¹P{¹H} NMR spectra which have been tabulated (Table 2.1). The separation and isolation of the organic layer or extraction from the aqueous layer afforded [Au(**16a-f**)SR] **18a-f** in near quantitative yields (97-98%) and no further

purification was required. Unfortunately, **18g** could not be extracted from the reaction mixture and thus, the synthesis of **18g** was not confirmed.



Scheme 2.4 Synthesis of [Au(**16a-g**)SR] complexes, **18a-g**.

The complexes **18a-f** were fully characterised by ¹H, ¹³C{¹H} and ³¹P{¹H} NMR and IR spectroscopy and mass spectrometry. In all cases, the ¹H NMR spectra showed additional peaks (when compared to their respective precursors) corresponding to those of the protected glucose. Four characteristic methyl peaks with shifts consistent with those of the acetate protons from the protected glucose were observed for all of the analogues of auranofin. In addition, the signals relating to the protons on the ring of the glucose were observed as four multiplets. The carbonyl carbons are visible in the ¹³C{¹H} NMR spectra as four downfield singlets for all of the derivatives.

Table 2.1 The ³¹P{¹H} NMR signals from tertiary phosphines **16a-g**, their Au(I)chloride complexes **17a-g** and the corresponding auranofin analogues **18a-f**. (i) [Au(tht)Cl], EtOH (**16a-c**, **16g**) or DCM (**16d-f**) (ii) 1-Thio-β-D-glucose tetraacetate, K₂CO₃, H₂O and DCM (**17a-e**) or EtOH (**17f**). Data obtained in *d*-chloroform unless otherwise stated.

$$\begin{array}{c} \text{R} \\ | \\ \text{R}-\text{P}-\text{R} \end{array} \xrightarrow{\text{(i)}} \begin{array}{c} \text{R} \\ | \\ \text{R}-\text{P}-\text{Au}-\text{Cl} \\ | \\ \text{R} \end{array} \xrightarrow{\text{(ii)}} \begin{array}{c} \text{R} \\ | \\ \text{R}-\text{P}-\text{Au}-\text{SR} \\ | \\ \text{R} \end{array}$$

Compound	PR ₃ (16)	R ₃ P-Au-Cl (17)	R ₃ P-Au-SR (18)
PPh ₃ (a)	−5.3 ppm	33.2 ppm	38.8 ppm
PPh ₂ Cy (b)	−3.6 ppm	43.4 ppm	46.7 ppm
PCy ₂ Ph (c)	3.2 ppm	51.4 ppm	54.4 ppm
PCy ₃ (d)	11.2 ppm	54.0 ppm	56.7 ppm
PEt ₂ Ph (e)	−15.6 ppm	35.7 ppm	40.4 ppm
PTA (f)	−104.3 ppm ^a	−52.3 ppm ^a	−50.7 ppm ^a
P(CH ₂ OH) ₃ (g)	−27.3 ppm ^{51 a}	25.8 ppm ^a	–

^a NMR taken in *d*₆-DMSO

Further confirmation of the synthesis of **18f** was obtained by X-ray diffraction. **18f** has been synthesised previously by Laguna *et al.*^{47,50} however, the X-ray crystal structure had not been reported. Crystals were obtained from a *d*₆-DMSO solution of **18f** and were analysed by X-ray crystallographic diffraction. **18f** crystallised as an orthorhombic structure. Selected bond lengths and angles are given in Figure 2.3.

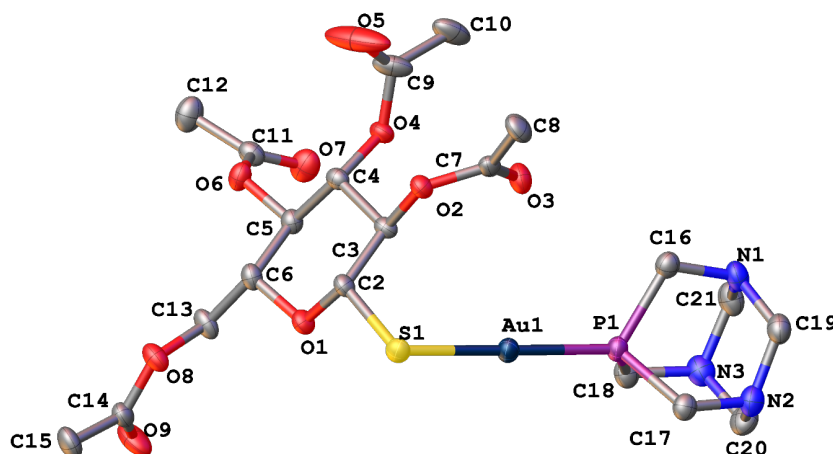


Figure 2.3 View of the molecular structure of **18f**. Hydrogen atoms bound to carbon have been omitted for clarity. Selected bond distances [Å] and angles [°]: Au1-S1 2.3093(14), Au1-P1 2.2591(14), S1-C2 1.813(6), P1-C16 1.849(7), P1-C17 1.837(6), P1-C18 1.846(7), P1-Au1-S1 178.20(7), C2-S1-Au1 107.36(19), C16-P1-Au1 119.2(2), C17-P1-Au1 117.88(19), C18-P1-Au1 118.2(2).

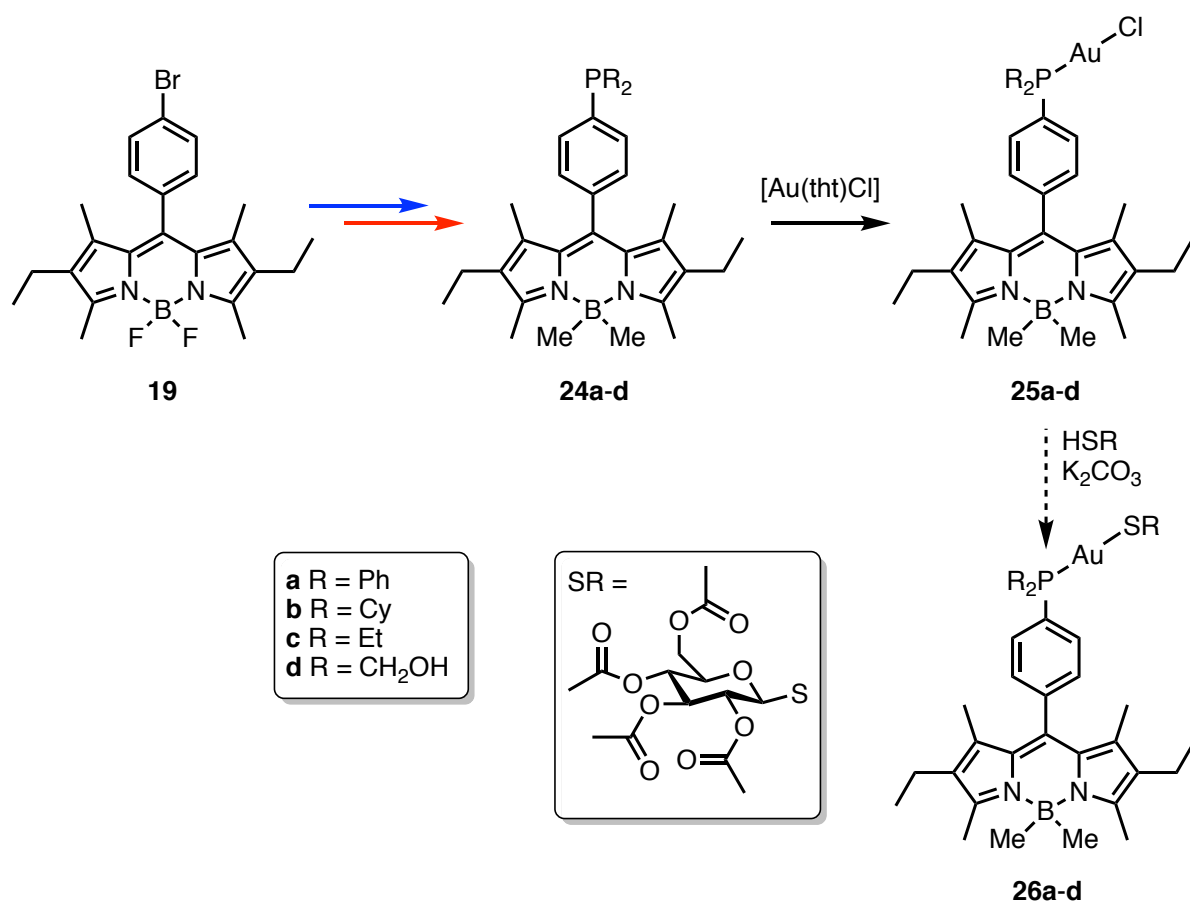
The Au1-P1 bond length of 2.2591(14) Å corresponds to similar compounds in the literature,⁴⁶ including auranofin which has a Au-P bond length of 2.26 Å.⁵² The complex has a slightly distorted linear geometry at the gold centre, which is typical for gold(I) complexes, shown by the P1-Au1-S1 bond angle of 178.20(7)°. The angle is slightly larger than the one observed for auranofin (173.6°).^{46,53}

2.3 Fluorescent Analogues of Auranofin

The focus in this section is now directed towards a second aim, the synthesis of fluorescent auranofin analogues. The addition of a fluorescent label to auranofin could allow for the observation of how these complexes act at a subcellular level, notwithstanding the fact that the addition of a fluorophore could alter the biological properties of the complex. It has previously been reported that fluorescent labels have aided in the elucidation of mechanisms of action of compounds,^{54–57} something which remains unclear for auranofin in rheumatoid arthritis, and thus, providing the motivation for this work. Therefore, the synthesis of the fluorescently tagged derivatives of auranofin with a Bodipy backbone will be discussed in the following sections.

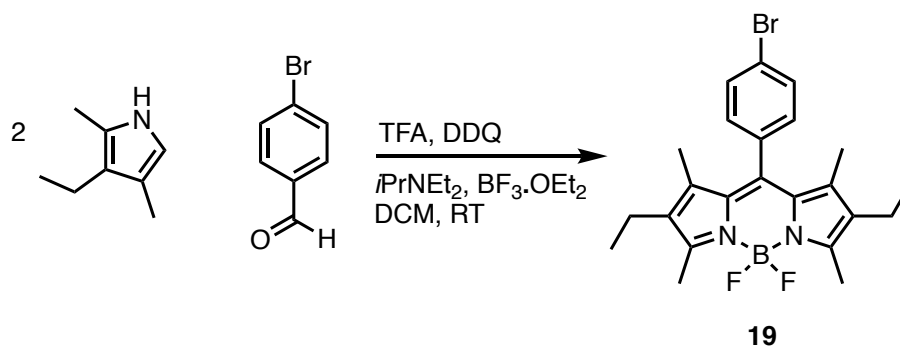
2.3.1 Towards the Synthesis of Fluorescent Auranofin Analogues

The proposed synthetic route has been illustrated in Scheme 2.5. The first step towards the synthesis of a fluorescently labelled auranofin derivative, was to synthesise the Bodipy backbone. From here, different synthetic routes to the fluorescent tertiary phosphines were taken which will be described in detail.



Scheme 2.5 Proposed synthetic route for the synthesis of fluorescently labelled analogues of auranofin **26a-d**.

The synthesis of the Bodipy backbone was achieved by a one-pot pyrrole condensation reaction between 3-ethyl-2,4-dimethyl-1-pyrrole and 4-bromobenzaldehyde which has previously been reported and subsequently used by the Higham group (Scheme 2.6).⁵⁸

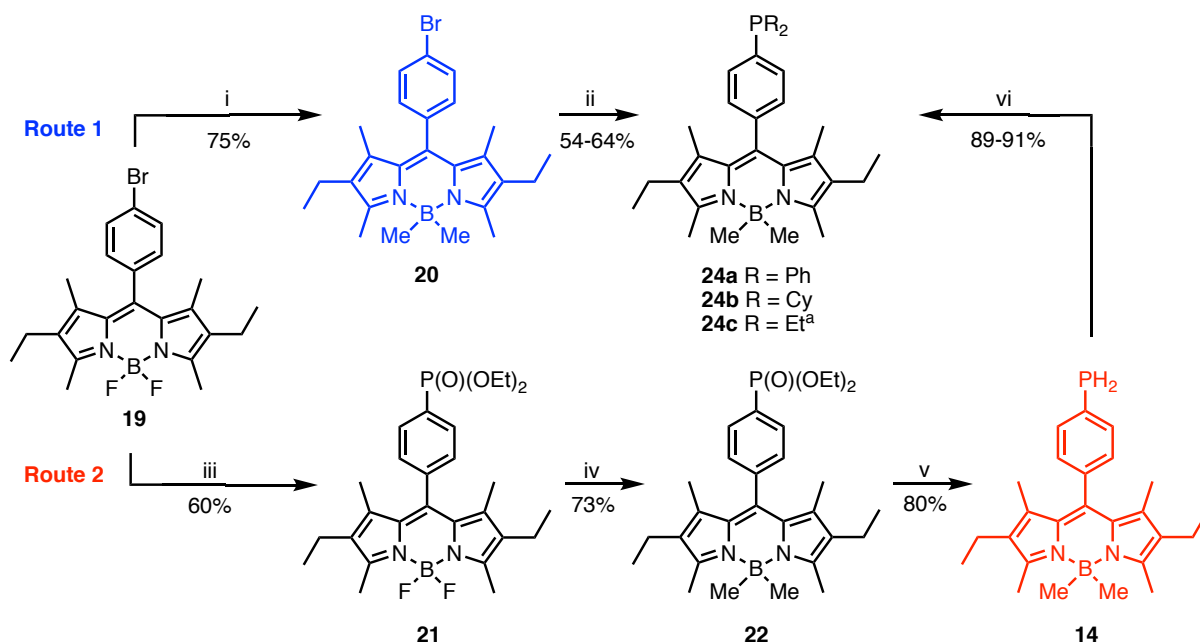


Scheme 2.6 Synthesis of *F*-Bodipy aryl bromide **19** following a one-pot pyrrole condensation reaction.

The reaction was analysed by NMR spectroscopy, which confirmed the synthesis of the desired product. The ¹⁹F{¹H} NMR spectrum showed a quartet with peaks of equal intensity at δ −145.4 ppm (¹J_{FB} = 31.8 Hz) and the ¹¹B{¹H} NMR spectrum showed a triplet at δ −0.2 ppm with a coupling constant of 31.8 Hz for ¹J_{BF}. The compound was purified by column chromatography to give **19** in a moderate yield of 59%. From here, we looked to synthesise the fluorescent tertiary phosphine ligands **24a-d** through the functionalisation of **19**.

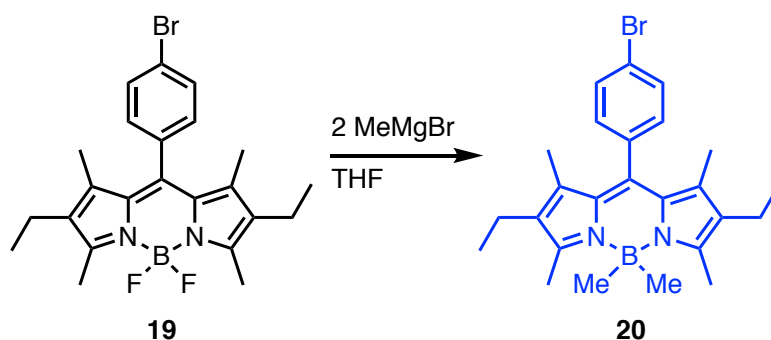
2.3.2 Synthesis of Fluorescent Tertiary Phosphines **24a-b**

Two routes were utilised in the synthesis of the fluorescent tertiary phosphines, which have been illustrated in Scheme 2.7. The synthetic procedures are described in turn below.



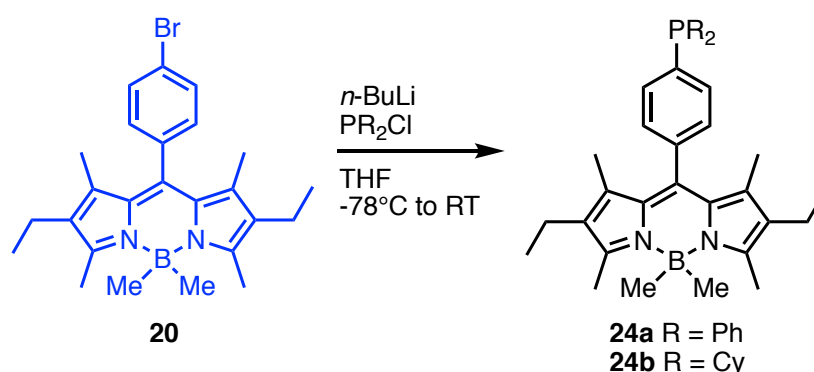
Scheme 2.7 Original synthesis via the blue route and the alternative synthesis shown in red. i) 2 MeMgBr, THF, RT, ii) *n*-BuLi, PR₂Cl (R = Ph or Cy), Et₂O -78 °C to RT iii) Pd(OAc)₂, DPPB, *i*Pr₂NEt, HP(O)(OEt)₂, DMSO, 90 °C iv) 2 MeMgBr, THF, RT v) LiAlH₄/TMSCl, THF, -78 °C to RT, vi) PCl₅, Tol, RMgX (R = Ph, Cy or Et, X = Cl or Br), THF; ^a only synthesised via route 2.

The first route for the synthesis of the tertiary phosphines **24a** and **24b** was from the fluorescent arylbromide **19** and has previously been reported by the Higham group.⁵⁹ Before the introduction of the phosphine group, the BF₂ moiety was first protected to prevent its attack by *n*-butyllithium, which has previously shown to result in dechelation. A carbon-boron bond is less likely to be attacked than a boron-fluoride bond and thus, methylmagnesium bromide was used in the methylation of **19** to afford **20** with a BMe₂ moiety, as illustrated in Scheme 2.8.



Scheme 2.8 Synthesis of the dimethyl derivative **20** from **19** with two equivalents of methylmagnesium bromide in tetrahydrofuran.

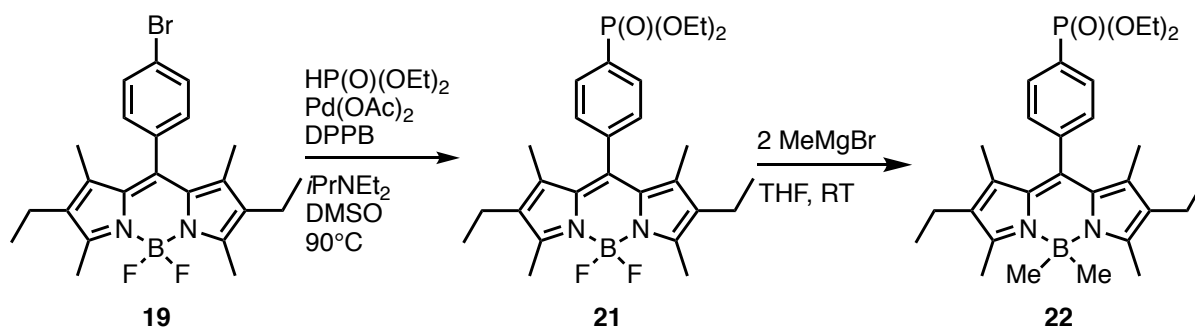
Following the protection of the boron moiety, **20** was subjected to a lithium-halogen exchange reaction to afford tertiary phosphines **24a** and **24b**. As illustrated in Scheme 2.9, **20** was reacted with *n*-butyllithium at $-78\text{ }^{\circ}\text{C}$, in diethyl ether, followed by the addition of the corresponding chlorodiphenyl- or chlorodicyclohexylphosphine and brought to room temperature. The reactions were monitored by TLC and $^{31}\text{P}\{^1\text{H}\}$ NMR spectroscopy where the appearance of peaks at $\delta -6.1\text{ ppm}$ for **24a** and $\delta 2.2\text{ ppm}$ for **24b**, consistent with the published values, were observed.⁵⁹ Following purification by an aqueous work up and column chromatography, the compounds **24a** and **24b** were isolated in adequate yields 54-64%.



Scheme 2.9 Lithium-halogen exchange of **20** with *n*-butyllithium followed by reaction of chlorodiphenyl- or chlorodicyclohexylphosphine to yield **24a** and **24b** respectively.

2.3.3 An Alternative Synthetic Approach via Primary Phosphine **14**

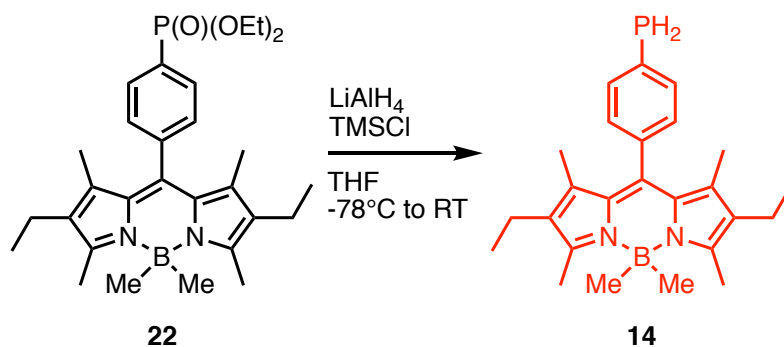
The second route for the synthesis of **24a**, **24b** and **24c** required the preparation of the primary phosphine **14**, by the multigram synthetic procedure reported by the Higham group and shown in Schemes 2.10 and 2.11. Bodipy **19** was converted into Bodipy phosphonate **21** by a palladium-catalysed cross-coupling reaction with diethylphosphite in dimethyl sulfoxide at $90\text{ }^{\circ}\text{C}$. The resulting product was isolated following an aqueous work-up and purification by column chromatography in 60% yield. It displayed a characteristic singlet at $\delta 18.3\text{ ppm}$ in the $^{31}\text{P}\{^1\text{H}\}$ NMR spectrum.



Scheme 2.10 Synthesis of phosphonate **22** by a palladium-catalysed cross-coupling reaction from **19** and subsequent dimethylation of **21**.

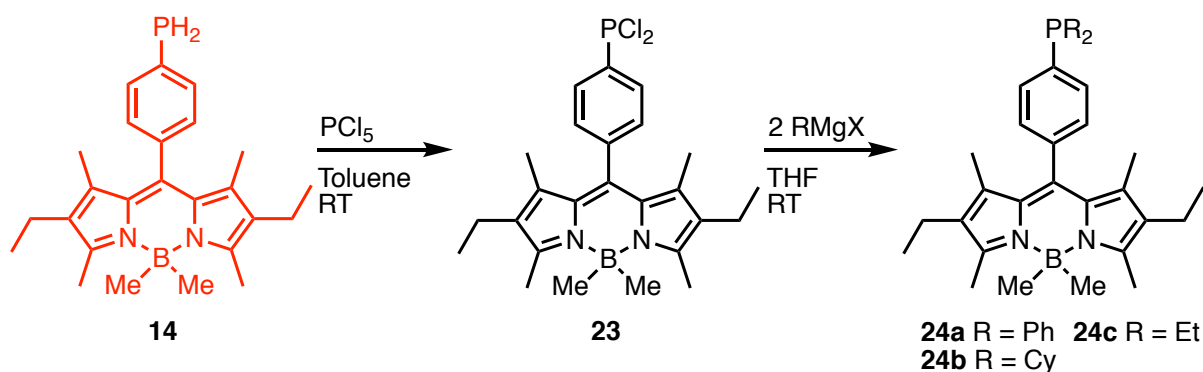
Before the reduction of the phosphonate group to a phosphino group, the boron moiety first had to be protected. Thus, **21** was reacted with two equivalents of methylmagnesium bromide to afford **22**. The reaction could be monitored by following either the $^{19}\text{F}\{^1\text{H}\}$ or the $^{11}\text{B}\{^1\text{H}\}$ NMR spectra. The absence of a resonance in the $^{19}\text{F}\{^1\text{H}\}$ NMR spectrum, and the transformation from triplet to a singlet in the $^{11}\text{B}\{^1\text{H}\}$ NMR spectrum signalled the completion of the reaction. Following an aqueous work up, **22** was isolated by column chromatography in 73% yield.

The phosphonate group was then reduced using lithium aluminium hydride and trimethylsilyl chloride to afford the fluorescent primary phosphine **14**, as illustrated in Scheme 2.11. Following an aqueous work-up with diethyl ether, purification was achieved by column chromatography or by recrystallisation from ethyl acetate to afford **14** in excellent yields of over 80%.



Scheme 2.11 Synthesis of primary phosphine **14** by reduction of the phosphonate **22**.

The conversion of the air-stable primary phosphine **14** to tertiary phosphines **24a-c**, could be achieved via the dichlorophosphine intermediate **23** and its subsequent reaction with a Grignard reagent (Scheme 2.12). Phosphorus pentachloride and primary phosphine **14** were dissolved in anhydrous toluene at room temperature. After one hour, the reaction was monitored by $^{31}\text{P}\{^1\text{H}\}$ NMR spectroscopy and displayed no starting material and only a single peak at $\delta -159.7$ ppm corresponding to dichlorophosphine **23**. The volatiles were removed *in vacuo*, and **23** was re-dissolved in anhydrous tetrahydrofuran followed by the addition of two equivalents of phenylmagnesium bromide for **24a**, cyclohexylmagnesium chloride for **24b** or ethylmagnesium bromide for **24c**. In all cases, an immediate colour change from red to orange was observed. The reaction mixtures were stirred for 30 minutes to ensure the completion of the reaction, which was confirmed by the absence of the dichlorophosphine intermediate **23** at $\delta -159.7$ ppm in the $^{31}\text{P}\{^1\text{H}\}$ NMR spectra and new resonances at δ 5.9 ppm for **24a**, δ 2.2 ppm for **24b** and $\delta -16.1$ ppm for **24c**.



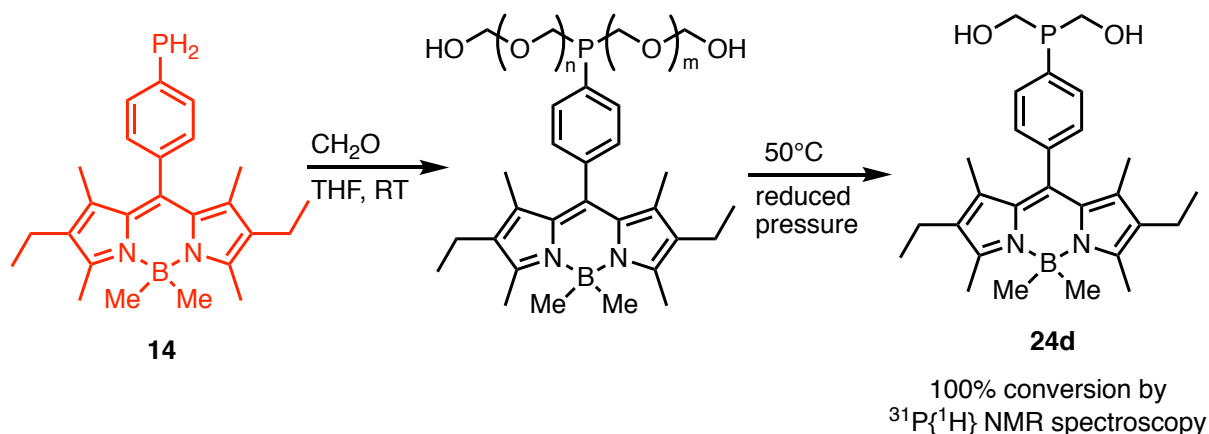
Scheme 2.12 Synthesis of the tertiary phosphines **24a-c** from primary phosphine **14** via the dichlorophosphine intermediate **23** and its subsequent reactions with a suitable Grignard reagent.

The compounds **24a-c** were purified by an aqueous work-up and trituration with acetonitrile, which afforded compounds **24a-c** in high yields (89-92%). The NMR spectroscopic data for the fluorescent tertiary phosphines **24a** and **24b** was consistent with those previously reported by the Higham group. The novel Bodipy diethylphosphine derivative **24c** was fully characterised by NMR and IR spectroscopy and mass spectrometry. The ^1H NMR spectrum revealed two new resonances corresponding to the ethyl groups; as expected, a doublet of triplets ($^3J_{\text{HP}} = 15.0$ Hz and $^3J_{\text{HH}} = 7.6$ Hz) corresponding to the two methyl groups was present; this was further confirmed by the $^1\text{H}\{^{31}\text{P}\}$ NMR spectrum where this signal collapsed to a single triplet ($^3J_{\text{HH}} = 7.6$ Hz). However, the expected doublet of quartets corresponding to the methylene protons was not observed. Instead, a quartet ($^3J_{\text{HH}} = 7.6$ Hz) was present suggesting that the $^2J_{\text{HP}}$ coupling is too small to be observed. This occurrence is also seen for the non-fluorescent analogue, diethylphenylphosphine, which has previously been discussed by Randall and Shaw.⁶⁰ Two additional doublets were observed in the ^{13}C NMR spectrum corresponding to the ethyl groups of the phosphine. The methylene carbon was observed at 20.0 ppm, with a one-bond carbon-phosphorus coupling constant of 10.8 Hz, and the methyl carbon at 9.7 ppm, with a two-bond carbon-phosphorus coupling constant of 12.6 Hz. The larger two bond coupling is also observed in for diethylphenylphosphine.⁶¹

Although this synthetic route is longer, its advantage lies in the number of potential phosphines available due to the significant number of Grignard reagents readily accessible. In comparison, the number of chlorophosphines available is low, and additionally, these are often expensive.

In order to synthesise a more hydrophilic phosphine, **14** was subjected to a hydrophosphination reaction with an excess of formaldehyde, which is shown in Scheme 2.13. The reaction was monitored by $^{31}\text{P}\{^1\text{H}\}$ NMR spectroscopy, which showed the complete

consumption of the starting material after two days. The reaction formed an equilibrium of hemiacetals with formaldehyde, indicated by a series of resonances in the $^{31}\text{P}\{^1\text{H}\}$ NMR spectrum. The hemiacetals were converted exclusively to **24d** under reduced pressure whilst heating at 50 °C for two weeks. The removal of the hemiacetals was confirmed by the observation of a single resonance in the $^{31}\text{P}\{^1\text{H}\}$ NMR spectrum at $\delta -14.1$ ppm.

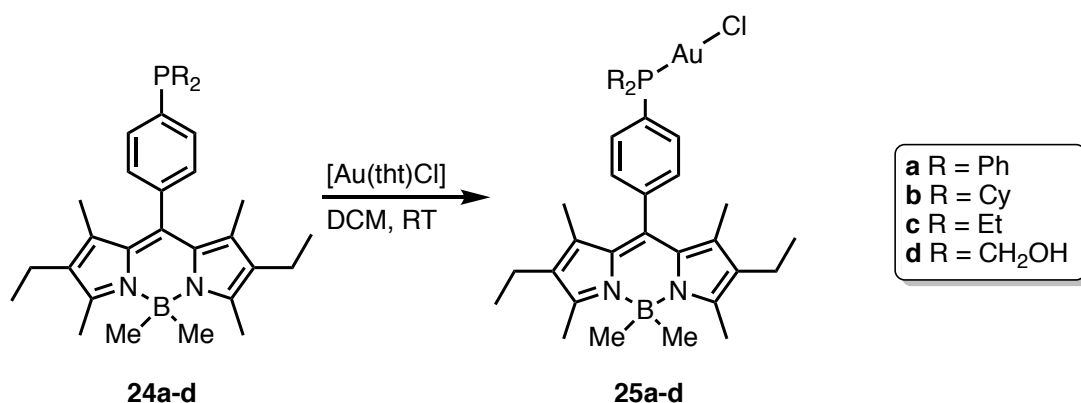


Scheme 2.13 Hydrophosphination of primary phosphine **14** to yield Bodipy bis(hydroxymethyl)phosphine **24d**.

Following the successful synthesis of the tertiary phosphines **24a-d**, efforts towards the synthesis of the fluorescent auranofin analogues were then made.

2.3.4 Synthesis of Fluorescent Chlorogold(I) Phosphine Complexes $[\text{Au}(\mathbf{24a-d})\text{Cl}]$ **25a-d**

The fluorescent tertiary phosphines **24a-d** were reacted with $[\text{Au}(\text{tht})\text{Cl}]$ in anhydrous dichloromethane at room temperature. Following the consumption of the starting materials by $^{31}\text{P}\{^1\text{H}\}$ NMR spectroscopy, the volatiles were removed *in vacuo* and the resulting solids were triturated with petroleum ether to remove the excess thiophene ligand, and further purified by column chromatography. In each case, this led to the formation of the gold(I) complexes $[\text{Au}(\mathbf{24a-d})\text{Cl}]$ **25a-d** in moderate to good yields (29-67%). This has been illustrated in Scheme 2.14.



Scheme 2.14 Synthesis of $[\text{Au}(\mathbf{24a-d})\text{Cl}]$ complexes, **25a-d**.

In all cases, the coordination of the phosphines to [Au(tht)Cl] led to a single downfield shift of their $^{31}\text{P}\{^1\text{H}\}$ NMR resonances from δ -6.1, 2.2, -16.1 and -14.1 ppm for **24a-24d** to δ 32.7, 50.9, 35.7 and 25.4 ppm for their gold(I) complexes **25a**, **25b**, **25c** and **25d** respectively.

The NMR spectroscopic data of complexes **25a** and **25b** was found to be consistent with the data reported by the Higham group.⁵⁹ The novel diethylphosphine complex **25c** was fully characterised by NMR and IR spectroscopy and mass spectrometry. The hydroxymethyl complex **25d** was sparingly soluble in chloroform and so, full NMR spectroscopic data was obtained using d_6 -acetone – **25d** was also found to be soluble in more polar solvents such as methanol.

2.3.5 X-ray Crystal Structures

Crystals of **25a** suitable for X-ray diffraction were grown by the slow diffusion of petroleum ether into a dichloromethane solution. The molecular structure is shown in Figure 2.4.

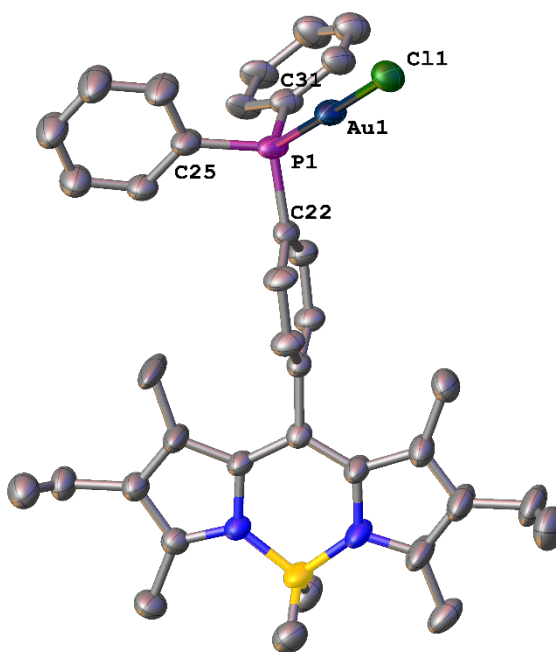


Figure 2.4 View of the molecular structure of **25a** Hydrogen atoms bound to carbon have been omitted for clarity. Selected bond distances [Å] and angles [°]: Au1-Cl1 2.274(4), Au1-P1 2.248(4), P1-C22 1.821(11), P1-C25 1.807(13), P1-C31 1.811(19), P1-Au1-Cl1 179.21(12), C22-P1-Au1 111.6(4), C25-P1-Au1 112.5(5), C31-P1-Au1 114.3(5).

25a exhibited a near linear geometry around the gold(I) centre, shown by the P1-Au1-Cl1 bond angle of 179.12(12)° typical for gold(I) complexes.⁵³ The structure is fully disordered across a mirror plane.

Crystals of **25d** suitable for X-ray diffraction were grown by the slow evaporation of a toluene solution of **25d**. The molecular structure is shown in Figure 2.5. **25d** crystallised as a 1D coordination polymer,⁶² which was formed by aurophilic interactions, in a similar way to the

closely related THP-Au(I) complex, **25g**. The loosely bound gold atoms, indicated by the Au1-Au2 bond length of 3.1525(4) Å, form distorted square planar geometry with each other and the P1-Au-Cl bond.

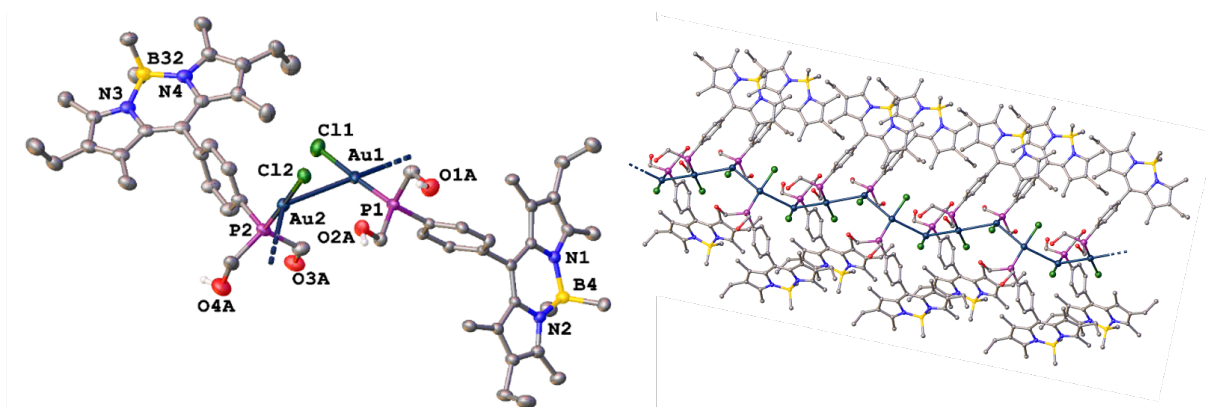


Figure 2.5 View of the molecular structure of **25d**. Hydrogen atoms bound to carbon and oxygen have been omitted for clarity. Selected bond distances [Å] and angles [°]: Au1-Au2 3.1525(4), Au1-Cl1 2.303(2), Au1-P1 2.2399(19), Au2-Cl2 2.3316(17), Au2-P2 2.2408(18), P1-Au1-Cl1 177.19(7), P2-Au2-Cl2 176.60(7).

Au1-P1 and Au1-Cl1 bond lengths of 2.2399(19) and 2.303(2) respectively, and P1-Au1-Cl1 and P2-Au2-Cl2 bond angles of 177.19(7) and 176.60(7) respectively, are consistent with those reported in the literature.⁵³ Auophilic interactions, displayed by the Au1-Au2 bond length of 3.1525(4) is similar to the value for the non-fluorescent analogue, **17g**, of 3.1935(10), reported earlier in the chapter. Similar auophilic interactions have also been reported.⁶²

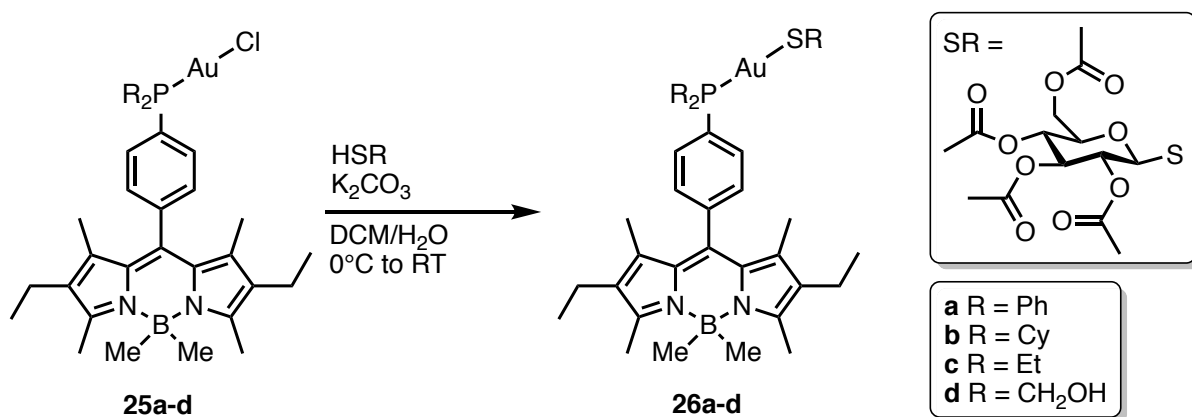
Following the successful synthesis of the [Au(**24a-d**)Cl] complexes **25a-d**, efforts towards the synthesis of their thioglucose tetraacetate gold(I) complexes, to afford fluorescent analogues of auranofin, were made.

2.3.6 Synthesis of Fluorescent Gold(I) Phosphine Thioglucose Tetraacetate Complexes **26a-d**

In an analogous method to the preparation of [Au(PR₃)SR] complexes reported earlier in the chapter, fluorescent auranofin analogues were synthesised from a biphasic substitution reaction of the gold(I) complexes **25a**, **25b**, **25c** and **25d** respectively with 1-thio-β-D-glucose tetraacetate in basic conditions.

A dichloromethane solution of the corresponding phosphine complex **25a**, **25b**, **25c** or **25d** and one equivalent of 1-thio-β-D-glucose tetraacetate was cooled to 0 °C. A cooled aqueous solution of excess potassium carbonate was then added. The biphasic reaction mixture was stirred rapidly for one hour which led to the formation of the thiolate gold(I) complexes **26a**, **26b**, **26c** and **26d** in the organic layer, as depicted in Scheme 2.15. Purification of the complexes was achieved by the separation of the layers and further extraction from the

aqueous layer. The organics were filtered through Celite and the solvent was removed *in vacuo* to afford **26a**, **26b**, **26c** and **26d** in near quantitative yields (88-97%).



Scheme 2.15 Synthesis of [Au(**24a-d**)SR] complexes, **26a-d**.

Full characterisation of the complexes **26a**, **26b**, **26c** and **26d** was obtained by ¹H, ³¹P{¹H}, ¹³C{¹H} NMR and IR spectroscopy and mass spectrometry. In all cases, new resonances were observed in ¹H NMR spectra; the methyl peaks of the acetate groups were observed as four characteristic singlets, and the protons on the ring of the protected glucose were observed as four multiplets. These observations were consistent to those displayed by the non-fluorescent analogues earlier described. The ³¹P{¹H} NMR spectra displayed minor downfield shifts from **26a**, **26b**, **26c** and **26d** which have been tabulated against the free phosphines **24a**, **24b**, **24c** and **24d** and chlorogold(I) complexes **25a**, **25b**, **25c** and **25d** for comparison in Table 2.2.

Table 2.2 ³¹P{¹H} NMR signals from tertiary phosphines **24a-d**, their Au(I)Cl complexes **25a-d** and the corresponding auranofin analogues **26a-d**. NMR data was obtained in *d*-chloroform unless otherwise stated.

Compound	24	[Au(24)Cl] (25)	[Au(24)SR] (26)
BodPPh ₂ (a)	−6.1 ppm	32.4 ppm	38.3 ppm
BodPCy ₂ (b)	2.2 ppm	50.9 ppm	54.1 ppm
BodPEt ₂ (c)	−16.1 ppm	35.7 ppm	40.7 ppm
BodP(CH ₂ OH) ₂ (d)	−14.1 ppm	25.4 ppm ^a	28.4 ppm

^a NMR taken in Acetone-*d*₆

2.4 Photophysical Data

After the successful synthesis of the fluorescent tertiary phosphines **24a**, **24b**, **24c** and **24d**, their chlorogold(I) complexes **25a**, **25b**, **25c** and **25d** and the gold(I)thiosugar auranofin analogues **26a**, **26b**, **26c** and **26d**, it was essential to determine their photophysical properties to determine whether the complexes would be appropriate for cell testing studies. Thus, photophysical data was collected in dry degassed tetrahydrofuran in all cases to minimise photobleaching and phosphine oxidation in solution. The data is shown in Table 2.3.

Table 2.3 Photophysical data for tertiary phosphines **24a**, **24b**, **24c** and **24d**, their Au(I)Cl complexes **25a**, **25b**, **25c** and **25d** and the corresponding auranofin analogues **26a**, **26b**, **26c** and **26d**. Measured in dry, degassed tetrahydrofuran at room temperature.

	λ_{abs} (nm)	λ_{em} (nm) ^a	$\Phi_{\text{F}}^{\text{a,b}}$	ϵ (M ⁻¹ cm ⁻¹)
BodPPh ₂ 24a ⁵⁹	513	527	0.29	92,000
[Au(24a)Cl] 25a ⁵⁹	514	529	0.20	74,000
[Au(24a)SR] 26a	514	532	0.24	66,000
BodPCy ₂ 24b ⁵⁹	512	526	0.44	82,000
[Au(24b)Cl] 25b ⁵⁹	514	529	0.39	85,000
[Au(24b)SR] 26b	514	531	0.31	62,000
BodPET ₂ 24c	514	529	0.33	39,000
[Au(24c)Cl] 25c	514	531	0.29	21,000
[Au(24c)SR] 26c	514	531	0.19	44,000
BodP(CH ₂ OH) ₂ 24d	513	529	0.32	89,000
[Au(24d)Cl] 25d	514	531	0.24	100,000
[Au(24d)SR] 26d	514	531	0.21	47,000

^a Dyes were excited at 485 nm; ^b Fluorescence quantum yields were measured with respect to 4,4-difluoro-8-phenyl-1,3,5,7-tetramethyl-2,6-diethyl-4-bora-3a,4a-diaza-s-indacene.

The four phosphine ligands **24a**, **24b**, **24c** and **24d** all show a characteristic Bodipy absorption profile with a maximum between 512 and 514 relating to the S₀-S₁ (π - π^*) transition, which is assigned to the Bodipy core. The ligands have typically high molar absorption coefficients ranging between 82,000-92,000 M⁻¹ cm⁻¹ with the exception of **24c** which had a value of 39,000 M⁻¹ cm⁻¹. The absorption spectra for the tertiary phosphines **24a**, **24b**, **24c** and **24d** and their gold(I) complexes **25a**, **25b**, **25c** and **25d** and **26a**, **26b**, **26c** and **26d** are shown in Figures 2.6-2.9.

The absorption spectra of the gold(I) complexes are mostly comparable to those of their free ligands; the molar absorption coefficients of the chlorogold(I) complexes **25a**, **25b**, and **25d** retained similar values to those of the uncoordinated ligands **24a**, **24b** and **24d** (ϵ = 74,000-100,000 M⁻¹ cm⁻¹); although, the molar absorption coefficient of **25c** lowered to 21,000 M⁻¹ cm⁻¹. Finally, the absorption spectra of the gold(I) thiosugar complexes **26a**, **26b** and **26d** show identical maxima to their chloride precursors, yet their molar absorption coefficients lowered in all cases (ϵ = 47,000-66,000 M⁻¹ cm⁻¹), except that of **26c** which increased to 44,000 M⁻¹

cm^{-1} . The molar absorption coefficients displayed by the Bodipy diethylphosphine compounds, particularly **24c** and **25c**, are uncharacteristically low in comparison to the diphenyl-, dicyclohexyl- and dihydroxymethylphosphine derivatives. This could be due to an impurity within the sample and thus, additional purification methods should be considered.

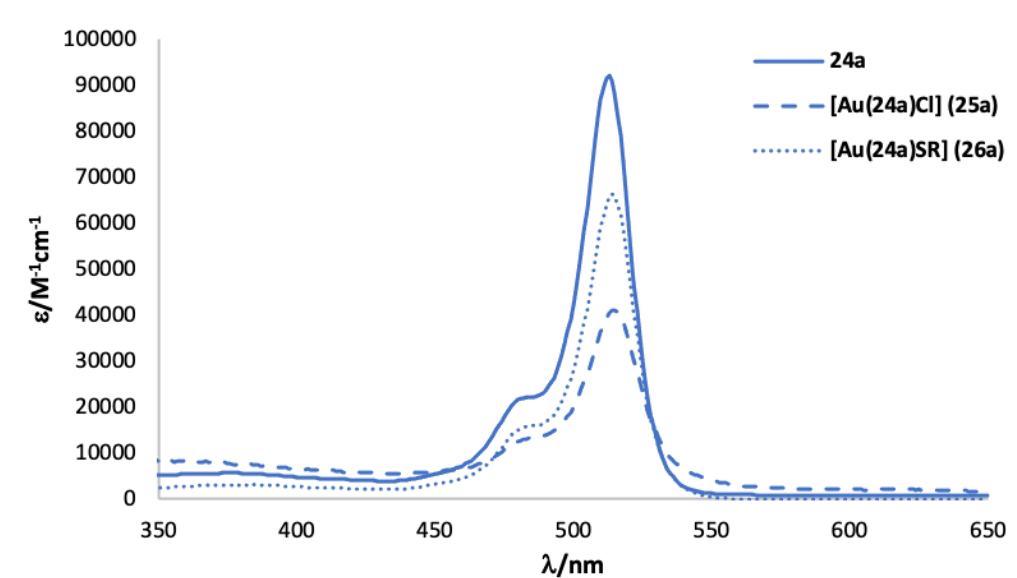


Figure 2.6 Absorption spectra of **24a**, and its complexes **[Au(24a)Cl] 25a** and **[Au(24a)SR] 26a**, in tetrahydrofuran at room temperature.

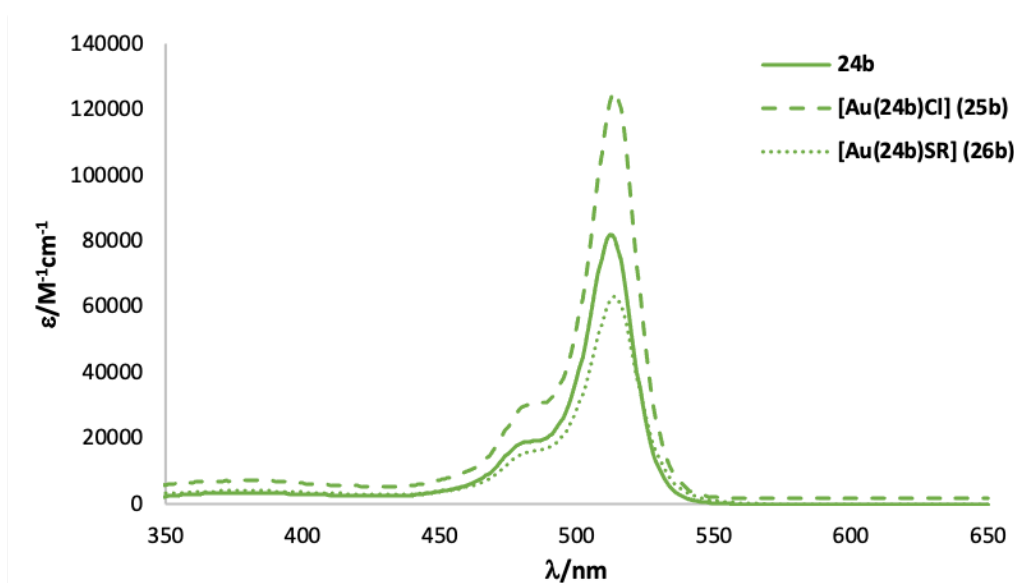


Figure 2.7 Absorption spectra of **24b**, and its complexes **[Au(24b)Cl] 25b** and **[Au(24b)SR] 26b**, in tetrahydrofuran at room temperature.

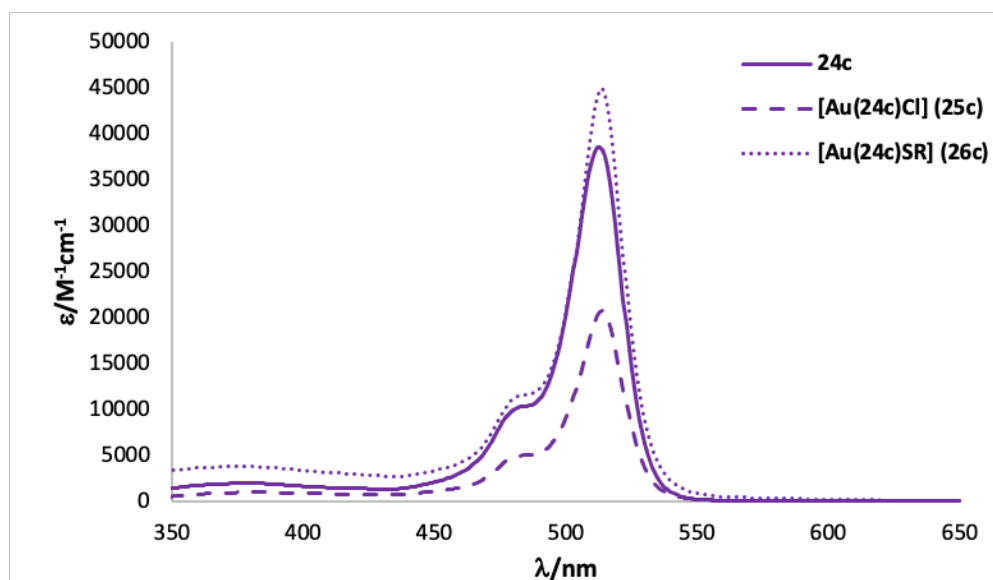


Figure 2.8 Absorption spectra of **24c**, and its complexes [Au(**24c**)Cl] **25c** and [Au(**24c**)SR] **26c**, in tetrahydrofuran at room temperature.

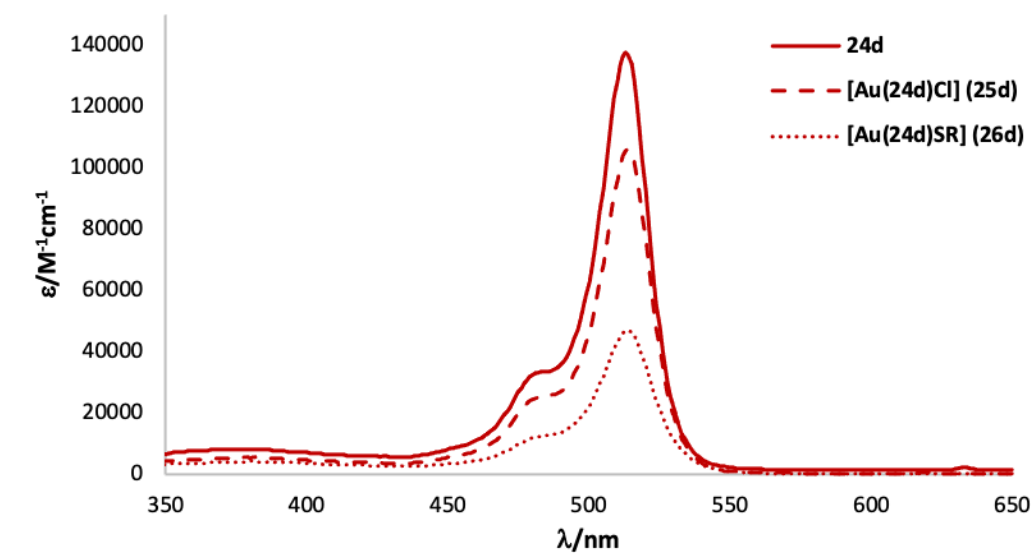


Figure 2.9 Absorption spectra of **24d**, and its complexes [Au(**24d**)Cl] **25d** and [Au(**24d**)SR] **26d**, in tetrahydrofuran at room temperature.

Room temperature fluorescence of the tertiary phosphines was detected, with emission maxima at 526–529 nm. The Stokes shifts of 14–16 nm are small and suggests that there are only minor structural changes on excitation, which is common for the Bodipy fluorophore.

The fluorescence quantum yields of the tertiary phosphines **24a** ($\Phi_F = 0.29$), **24b** ($\Phi_F = 44$), **24c** ($\Phi_F = 0.33$) and **24d** ($\Phi_F = 0.26$). **24a** and **24b** have previously been reported by our group,⁵⁹ it was noted that the phosphorus donor did not quench the fluorescence which was contradictory to several examples of phosphines in the literature.^{63–70} They rationalised this observation using DFT calculations which showed that the orbitals in the compounds

displayed no phosphorus character until the HOMO-2 and that the difference in energy between the HOMO and the HOMO-2 (the first phosphorus containing orbital) was 0.9 eV.

The fluorescence spectra of the gold(I) complexes show a slight red-shift of 2–5 nm from the free ligands and are shown in Figures 2.10-2.13. On coordination, a slight decrease in the fluorescence quantum yields was observed (**25a**: $\Phi_F = 0.20$, **25b**: $\Phi_F = 0.39$, **25c**: $\Phi_F = 0.29$, **25d**: $\Phi_F = 0.24$) and on reaction with the thiosugar, the quantum yields decreased slightly in the cases of **26b** to **26d** ($\Phi_F = 0.31$ for **26b**, $\Phi_F = 0.19$ for **26c** and $\Phi_F = 0.21$ **26d**) however, in the case of **26a**, increased to $\Phi_F = 0.24$.

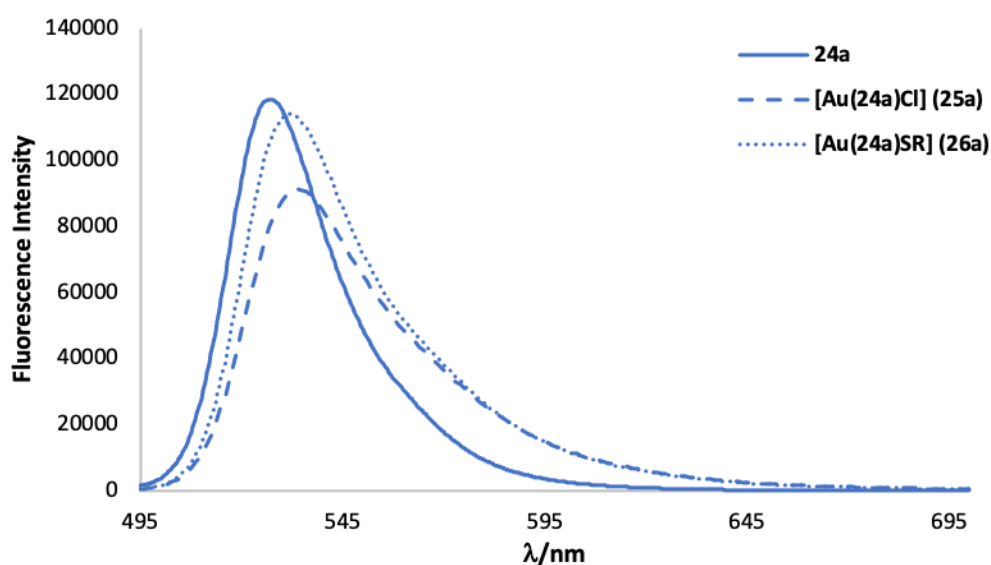


Figure 2.10 Emission spectra of **24a** and complexes [Au(**24a**)Cl] **25a** and [Au(**24a**)SR] **26a**, in tetrahydrofuran at room temperature (excitation at 485 nm).

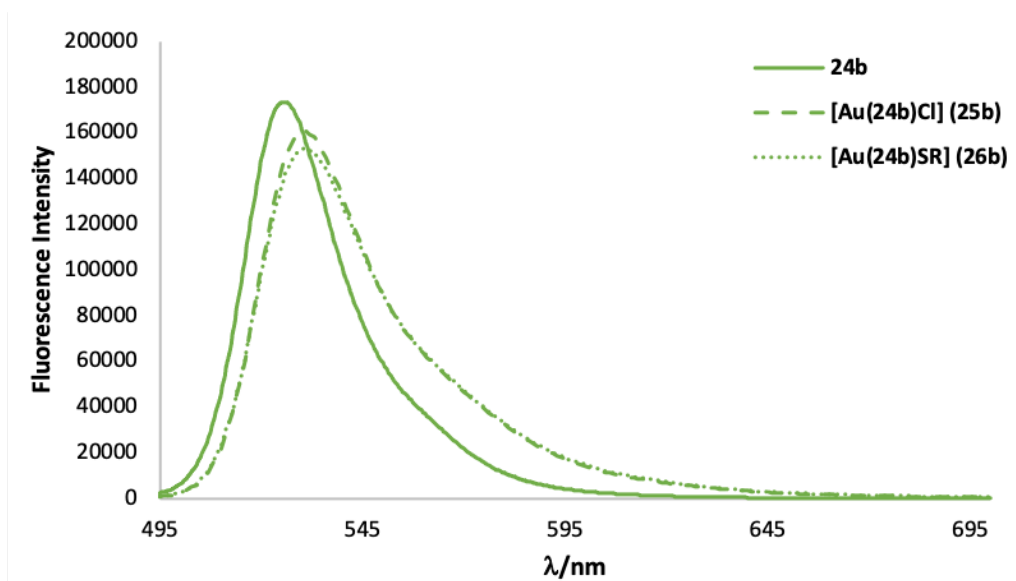


Figure 2.11 Emission spectra of **24b** and complexes [Au(**24b**)Cl] **25b** and [Au(**24b**)SR] **26b**, in tetrahydrofuran at room temperature (excitation at 485 nm).

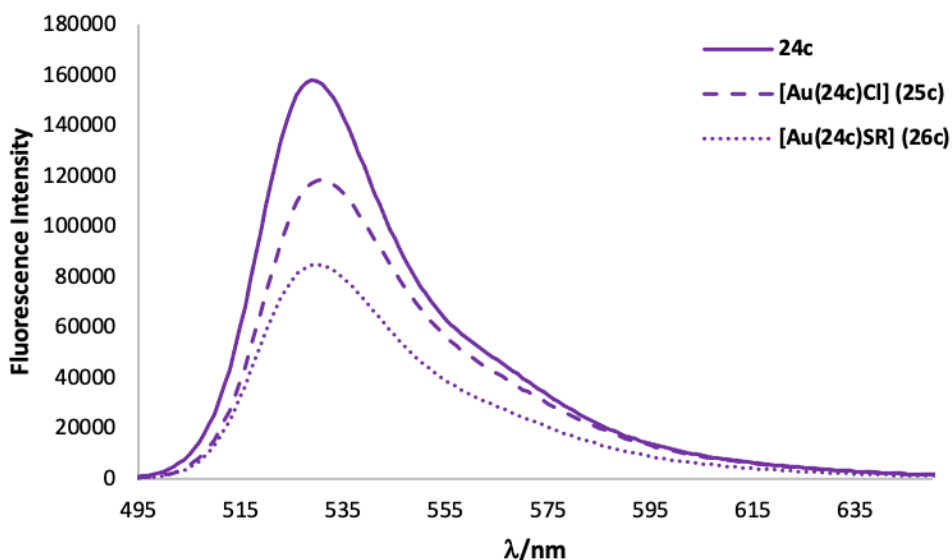


Figure 2.12 Emission spectra of **24c** and complexes [Au(**24c**)Cl] **25c** and [Au(**24c**)SR] **26c**, in tetrahydrofuran at room temperature (excitation at 485 nm).

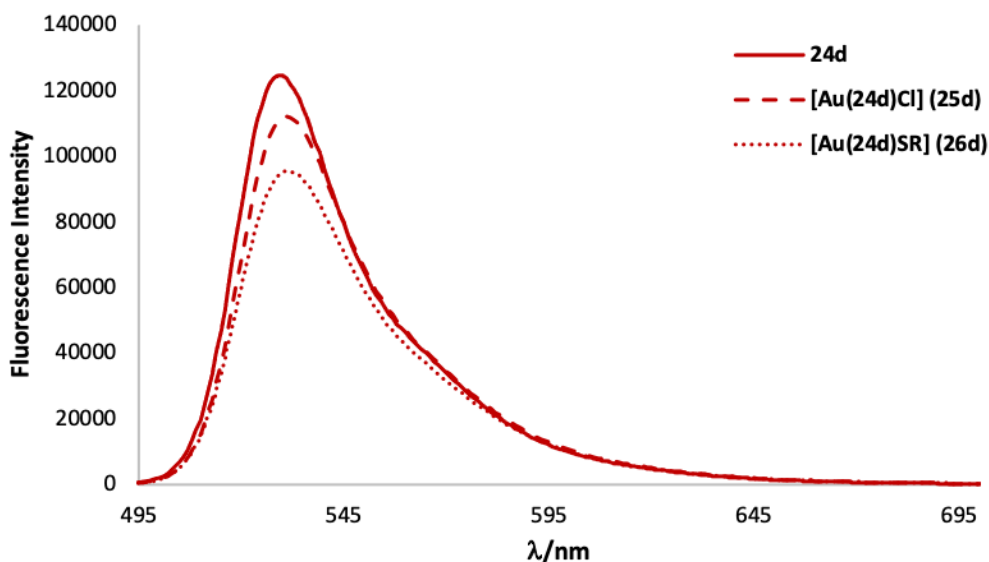


Figure 2.13 Emission spectra of **24d** and complexes [Au(**24d**)Cl] **25d** and [Au(**24d**)SR] **26d**, in tetrahydrofuran at room temperature (excitation at 485 nm).

All the auranofin analogues **26a**, **26b**, **26c** and **26d** retained their fluorescent properties and therefore have potential applications as cell imaging agents or perhaps as theranostic agents with a dual diagnostic and therapeutic element.

2.5 Summary and Future Work

To summarise, seven chlorogold(I) phosphine complexes **17a-g** were prepared from [Au(tht)Cl] and the corresponding tertiary phosphines **16a-g**, to afford [Au(**16a-g**)Cl] from the exchange of the labile tetrahydrothiophene (tht) ligand by the respective phosphine ligands. Crystals of the novel gold(I) complex, **17g** suitable for analysis by X-ray diffraction, were grown by slow evaporation of water. This analysis identified aurophilic interactions in the compound

as shown by the Au1-Au2 distance of Au1-Au2 3.1935(10) Å. To convert these complexes to analogues of auranofin, a reaction with 1-thio-β-D-glucose tetraacetate in the presence of potassium carbonate was carried out to afford six auranofin analogues [Au(**16a-f**)SR], **18a-f**, in near quantitative conversion (97-98%).

It is likely that these analogues will exhibit different biological properties from auranofin due to their differing phosphine ligands. Therefore, it would be of interest to test them *in vitro*, to compare their bioactivity to auranofin. It would be appropriate to test these complexes in cells which overexpress thioredoxin reductase, such as gastrointestinal stromal tumor cells,¹² and parasitic *giardia lamblia* cells,¹³ to see whether they are effective in its inhibition, as auranofin is. Thus, this work provides an opportunity to develop a collaboration to see how altering the steric and electronic properties of the phosphine affects the bioactivity of the drug.

The second aim of this chapter was to synthesise fluorescent analogues of auranofin. Therefore, four fluorescent tertiary phosphines were synthesised. The synthesis of the fluorescent tertiary phosphines **24a** and **24b** has been achieved via two routes. The first route followed the lithium-halogen exchange reaction which was reported by our group in 2014.⁵⁹ The lithiation of **20** with *n*-butyllithium, followed by the addition of the corresponding chlorophosphine afforded **24a** and **24b** in moderate yields (54% and 64% respectively). This route is limited by the number of chlorophosphines available and so an alternative route was considered.

The second route to the fluorescent tertiary phosphines was carried out from the primary phosphine **14**. A double chlorination of **14** with phosphorus pentachloride, led to the reactive dichlorophosphine intermediate **23**, which was subsequently converted to triaryl **24a** and arylalkyl **24b** and **24c** tertiary phosphines via reaction with the corresponding Grignard reagent in quantitative yields (by ³¹P{¹H} NMR spectroscopy). This route could provide an excellent alternative for the synthesis of a library of fluorescent tertiary phosphines due to the large availability of Grignard reagents.

In addition, a more hydrophilic tertiary phosphine **24d** was synthesised from a hydrophosphination reaction of primary phosphine **14** with formaldehyde. The reaction initially formed hemiacetals, which could be transformed purely into **24d** by subsequent heating at 50 °C whilst under vacuum for two weeks.

In an effort to synthesise fluorescent analogues of the FDA approved drug, auranofin, the fluorescent tertiary phosphines **24a-d** were reacted with the gold(I) complex, [Au(tht)Cl]. The

coordination was readily achieved by the exchange of the labile tetrahydrothiophene (tht) group with the fluorescent phosphines **24a-d**, which afforded [Au(**24a-d**)Cl] **25a-d** in moderate yields (29-67%). Crystals of **25a** and **25d** were grown and subsequently analysed by X-ray diffraction. The analysis of **25d** revealed its solid-state structure as a 1D coordination polymer formed by aurophilic interactions. The gold(I) phosphine complexes **25a**, **25b**, **25c** and **25d** were subsequently reacted with 1-thio- β -D-glucose tetraacetate (HSR) and potassium carbonate to yield [Au(**24a**)SR] **26a**, [Au(**24b**)SR] **26b**, [Au(**24c**)SR] **26c** and [Au(**24d**)SR] **26d** in good to near quantitative yields, 78-97%.

The photophysical properties of the Bodipy tertiary phosphines **24a**, **24b**, **24c** and **24d**, their chlorogold(I) complexes **25a**, **25b**, **25c** and **25d**, and their gold(I)thiosugar complexes **26a**, **26b**, **26c** and **26d**, were obtained and confirmed the retention of the fluorescent properties in all cases. Thus, these fluorescent analogues of auranofin have the potential to help with the elucidation of the mechanism of action, which has repeatedly been reported as unclear (in rheumatoid arthritis). Therefore, this work presents an opportunity for a collaboration to test these complexes within cells and establish their subcellular behaviour.

2.6 Experimental Procedures and Analytical Data

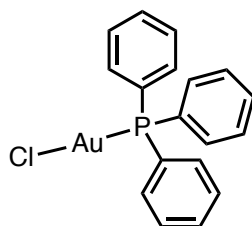
2.6.1 General Procedure

All air- and/or water-sensitive reactions were performed under a nitrogen atmosphere using standard Schlenk line techniques. Tetrahydrofuran was dried over sodium/benzophenone, toluene over sodium, dichloromethane over calcium hydride, ethanol over magnesium ethoxide and *d*-chloroform over phosphorus pentoxide; all solvents were distilled prior to use. Chloro(tetrahydrothiophene)gold(I) was prepared according to literature procedures.⁷¹ All other chemicals were purchased from Sigma Aldrich, Fisher Scientific, Alfa Aesar or Fluorochem and used as received. Flash chromatography was performed on silica gel from Fluorochem (silica gel, 40-63 μ , 60 Å). Thin-layer chromatography was performed on Fisher aluminium-based plates with silica gel and fluorescent indicator (254 nm). ^1H , $^{13}\text{C}\{^1\text{H}\}$, $^{31}\text{P}\{^1\text{H}\}$, and $^{11}\text{B}\{^1\text{H}\}$ NMR spectra were recorded on a Bruker Avance III 300 MHz (^1H 300.13 Hz), Bruker Avance II 400 MHz (^1H 399.78 MHz) or Bruker Avance III HD 500 MHz (^1H 500.16 MHz) spectrometer at room temperature (21 °C) using the indicated solvent as internal reference; ^1H and ^{13}C shifts were relative to tetramethylsilane, ^{31}P relative to 80% H_3PO_4 , and ^{11}B relative to $\text{BF}_3\cdot\text{Et}_2\text{O}$. IR spectra were recorded on a Varian 800 FT-IR spectrometer and mass spectrometry was carried out by the EPSRC National Mass Spectrometry Service Centre, Swansea or the SAgE Mass Spectrometry Facility (Newcastle University) performed by Dr Rachael Dack and Dr Alex Charlton. The X-ray crystallographic data were collected on an Xcalibur, Atlas, Gemini ultra diffractometer equipped with a fine-focus sealed X-ray tube ($\lambda_{\text{CuK}\alpha} = 1.54184 \text{ \AA}$) and an Oxford Cryosystems CryostreamPlus open-flow N_2 cooling device. The analysis of the X-ray diffraction data of the compounds was performed by Dr Paul Waddell (Newcastle University).

2.7 General Procedure for the Synthesis of Chlorogold(I) Complexes (**17a-g**)

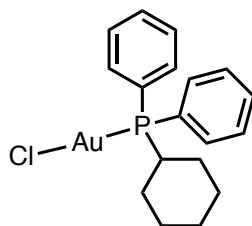
Tertiary phosphine (**16a-g**) (1 eq) and [chloro(tetrahydrothiophene)gold(I)] (1 eq) were added to a Schlenk flask, dissolved in anhydrous solvent and stirred under nitrogen for one hour, by when, the consumption of the starting material was confirmed by $^{31}\text{P}\{^1\text{H}\}$ NMR. The solvent was removed *in vacuo* and the solid was washed with hexane to remove tetrahydrothiophene.

2.7.1 [Au(**16a**)Cl] (**17a**)



Reacting 0.116 g (0.36 mmol) of chloro(tetrahydrothiophene)gold(I) with 0.10 g (0.38 mmol) of triphenylphosphine in 1.5 mL ethanol afforded **17a** as a white solid (0.14 g, 79%). ^1H NMR (300 MHz, CDCl_3) δ 7.58–7.43 (m, 15H) ppm; $^{13}\text{C}\{^1\text{H}\}$ NMR (75 MHz, CDCl_3) δ 134.3 (d, J_{CP} = 13.8 Hz), 132.1 (d, J_{CP} = 2.6 Hz), 129.4 (d, J_{CP} = 11.7 Hz), 128.9 (d, J_{CP} = 62.5 Hz) ppm; $^{31}\text{P}\{^1\text{H}\}$ NMR (121 MHz, CDCl_3) δ 31.2 (s, 1P) ppm; IR (neat): $\tilde{\nu}$ = 1479 (w), 1433 (m), 1313 (w), 1179 (w), 1102 (m), 1026 (w), 999 (w), 748 (s), 713 (m), 691 (s), 545 (s), 500 (s), 449 (m) cm^{-1} ; TOF MS (ES^+) calcd for $\text{C}_{18}\text{H}_{15}\text{NaPClAu}$ [$\text{M}+\text{Na}$] $^+$ requires m/z 517.0193, found m/z 517.0163 (5.8 ppm). These spectroscopic data are in agreement with literature values.²⁷

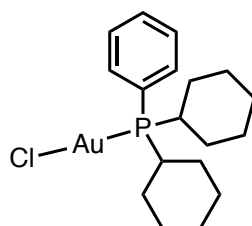
2.7.2 [Au(**16b**)Cl] (**17b**)



Reacting 0.119 g (0.37 mmol) of [chloro(tetrahydrothiophene)gold(I)] with 0.10 g (0.37 mmol) of diphenylcyclohexylphosphine in 3 mL ethanol afforded **17b** as a white solid (0.116 g, 63%). ^1H NMR (300 MHz, CDCl_3) δ 7.79–7.68 (m, 4H), 7.54–7.40 (m, 6H), 1.90–1.66 (m, 5H), 1.63–1.42 (m, 2H), 1.42–1.20 (m, 4H) ppm; $^{13}\text{C}\{^1\text{H}\}$ NMR (75 MHz, CDCl_3) δ 134.1 (d, J_{CP} = 12.8 Hz), 132.0 (d, J_{CP} = 2.7 Hz), 129.3 (d, J_{CP} = 11.4 Hz), 128.4 (d, J_{CP} = 57.5 Hz), 36.3 (d, J_{CP} = 38.0 Hz), 29.2 (d, J_{CP} = 3.7 Hz), 26.3 (d, J_{CP} = 14.9 Hz), 25.7 ppm; $^{31}\text{P}\{^1\text{H}\}$ NMR (121 MHz, CDCl_3) δ 43.4 (s, 1P) ppm; IR (neat): $\tilde{\nu}$ = 2929 (m), 2842 (w), 1573 (w), 1434 (m), 1309 (w), 1100 (m), 998 (m),

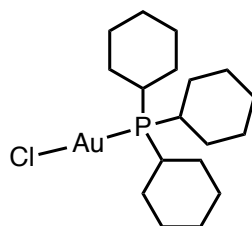
886 (w), 744 (m), 709 (m), 693 (s), 525 (s), 497 (s), 486 (m), 411 (m) cm^{-1} . These spectroscopic data are in agreement with literature values.⁷²

2.7.3 [Au(**16c**)Cl] (**17c**)



Reacting 0.116 g (0.36 mmol) of [chloro(tetrahydrothiophene)gold(I)] with 0.10 g (0.36 mmol) of phenyldicyclohexylphosphine in 3 mL ethanol afforded **17c** as a white solid (0.090 g, 49%). **¹H NMR** (300 MHz, CDCl_3) δ 7.76–7.62 (m, 2H), 7.59–7.43 (m, 3H), 2.32–2.16 (m, 2H), 2.13–2.00 (m, 2H), 1.93–1.80 (m, 2H), 1.80–1.72 (m, 2H), 1.74–1.59 (m, 4H), 1.46–1.04 (m, 10H); **¹³C{¹H} NMR** (75 MHz, CDCl_3) δ 135.2 (d, J_{CP} = 11.7 Hz), 132.1, 129.0 (d, J_{CP} = 10.7 Hz), 125.4 (d, J_{CP} = 53.0 Hz), 33.9 (d, J_{CP} = 34.7 Hz), 29.7 (d, J_{CP} = 3.2 Hz), 26.6 (d, J_{CP} = 4.5 Hz), 25.8 ppm; **³¹P{¹H} NMR** (121 MHz, CDCl_3) δ 51.4 (s, 1P) ppm. **IR** (neat): $\tilde{\nu}$ = 2924 (s), 2854 (m), 1478 (w), 1447 (m), 1433 (m), 1314 (w), 1298 (w), 1268 (w), 1172 (w), 1113 (m), 1037 (w), 999 (m), 918 (w), 885 (w), 852 (m), 819 (w), 758 (m), 752 (s), 702 (m), 693 (m), 539 (s), 524 (s), 504 (s), 486 (m), 447 (m), 427 (w), 411 (w) cm^{-1} . **TOF MS (ES⁺)** calcd for $\text{C}_{18}\text{H}_{27}\text{NaPClAu}$ [$\text{M}+\text{Na}$]⁺ requires m/z 529.1130, found m/z 529.1102 (5.3 ppm).

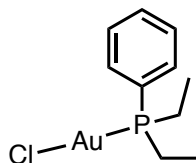
2.7.4 [Au(**16d**)Cl] (**17d**)



Reacting 0.114 g (0.36 mmol) of [chloro(tetrahydrothiophene)gold(I)] with 0.10 g (0.36 mmol) of tricyclohexylphosphine in 3 mL dichloromethane afforded **17d** as a white solid (0.118 g, 63%). **¹H NMR** (300 MHz, CDCl_3) δ 2.04–1.91 (m, 9H), 1.91–1.81 (m, 6H), 1.77–1.68 (m, 3H), 1.54–1.38 (m, 7H), 1.38–1.30 (m, 2H), 1.30–1.15 (m, 6H). ppm; **¹³C{¹H} NMR** (75 MHz, CDCl_3) δ 33.4 (d, J_{CP} = 31.0 Hz), 30.8, 27.0 (d, J_{CP} = 12.1 Hz), 25.8 ppm; **³¹P{¹H} NMR** (121 MHz, CDCl_3) δ 53.9 (s, 1P) ppm; **IR** (neat): $\tilde{\nu}$ = 2920 (s), 2851 (m), 1446 (m), 1293 (w), 1265 (w), 1209 (w), 1174 (m), 1112 (w), 1039 (w), 1004 (m), 914 (w), 888 (m), 849 (m), 820 (w), 756 (m), 739 (m), 708 (w), 530 (s), 523 (s), 481 (m), 465 (m), 437 (w), 424 (w) cm^{-1} ; **TOF MS (ES⁺)** calcd for

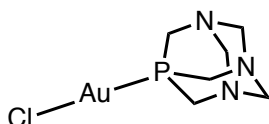
$\text{C}_{18}\text{H}_{33}\text{NaPClAu}$ $[\text{M}+\text{Na}]^+$ requires m/z 535.1596, found m/z 535.1572 (4.5 ppm). These spectroscopic data are in agreement with literature values.³³

2.7.5 $[\text{Au}(\mathbf{16e})\text{Cl}]$ (**17e**)



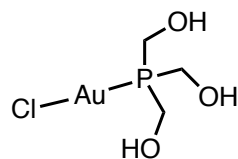
Reacting 0.10 g (0.31 mmol) of [chloro(tetrahydrothiophene)gold(I)] with 0.054 mL (0.31 mmol) of diethylphenylphosphine in 3 mL dichloromethane afforded **17e** as a colourless oil (0.084 g, 68%). ^1H NMR (300 MHz, CDCl_3) δ 7.77–7.67 (m, 2H), 7.58–7.44 (m, 3H), 2.11 (dq, $^2J_{\text{HP}} = 10.3$ Hz, $^3J_{\text{HH}} = 7.6$ Hz, 4H), 1.13 (dt, $^3J_{\text{HP}} = 20.2$ Hz, $^3J_{\text{HH}} = 7.6$ Hz, 6H) ppm; $^{13}\text{C}\{^1\text{H}\}$ NMR (75 MHz, CDCl_3) δ 133.4 (d, $J_{\text{CP}} = 12.5$ Hz), 132.4 (d, $J_{\text{CP}} = 2.6$ Hz), 129.4 (d, $J_{\text{CP}} = 11.3$ Hz), 127.9 (d, $J_{\text{CP}} = 57.8$ Hz), 21.4 (d, $J_{\text{CP}} = 37.9$ Hz), 9.5 ppm; $^{31}\text{P}\{^1\text{H}\}$ NMR (121 MHz, CDCl_3) δ 35.7 (s, 1P) ppm; IR (neat): $\tilde{\nu} = 2965$ (w), 2929 (w), 2872 (w), 1572 (w), 1452 (m), 1435 (s), 1412 (m), 1378 (m), 1311 (w), 1259 (w), 1159 (w), 1108 (s), 1016 (m), 999 (m), 768 (s), 753 (s), 693 (s), 663 (m) cm^{-1} ; TOF MS (ES^+) calcd for $\text{C}_{10}\text{H}_{15}\text{NaPClAu}$ $[\text{M}+\text{Na}]^+$ requires m/z 421.0163, found m/z 421.0103 (–14.3 ppm). These spectroscopic data are in agreement with literature values.²⁸

2.7.6 $[\text{Au}(\mathbf{16f})\text{Cl}]$ (**17f**)



Reacting 0.204 g (0.64 mmol) of [chloro(tetrahydrothiophene)gold(I)] with 0.10 g (0.64 mmol) of 1,3,5-triaza-7-phosphaadamantane in 6 mL dichloromethane afforded **17f** as a white solid (0.184 g, 74%). ^1H NMR (300 MHz, $\text{DMSO}-d_6$) δ 4.50 (d, $^2J_{\text{HP}} = 13.0$ Hz, 6H), 4.34 (d, $^4J_{\text{HP}} = 7.5$ Hz, 6H) ppm; $^{13}\text{C}\{^1\text{H}\}$ NMR (75 MHz, $\text{DMSO}-d_6$) δ 71.8 (d, $^3J_{\text{CP}} = 8.6$ Hz), 50.9 (d, $^1J_{\text{CP}} = 23.2$ Hz) ppm; $^{31}\text{P}\{^1\text{H}\}$ NMR (121 MHz, $\text{DMSO}-d_6$) δ 52.3 (s, 1P) ppm. IR (neat): $\tilde{\nu} = 2908$ (w), 1446 (w), 1407 (w), 1278 (m), 1242 (m), 1097 (m), 1040 (m), 1013 (m), 975 (s), 948 (m), 898 (m), 809 (m), 741 (s), 584 (s), 494 (m), 451 (m) cm^{-1} ; TOF MS (ES^+) calcd for $\text{C}_6\text{H}_{13}\text{N}_3\text{PClAu}$ $[\text{M}+\text{H}]^+$ requires m/z 390.0215, found m/z 390.0201 (3.6 ppm).

2.7.7 [Au(**16g**)Cl] (**17g**)

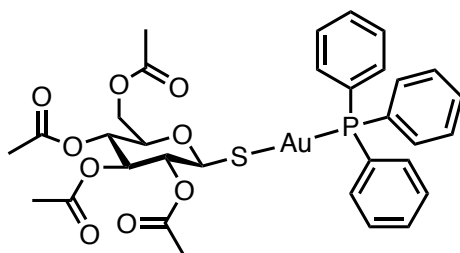


Reacting 0.395 g (1.23 mmol) of [chloro(tetrahydrothiophene)gold(I)] with 0.153 g (1.23 mmol) of *tris*(hydroxymethyl)phosphine in 5 mL ethanol afforded **17g** as a white solid (0.213 g, 49%) after separation from the blue/black precipitate that formed on the addition of chloro(tetrahydrothiophene)gold(I). Crystals suitable for X-ray diffraction were grown from slow evaporation of water. ^1H NMR (300 MHz, DMSO- d_6) δ 5.62 (s, 3H), 4.14 (s, 6H) ppm; $^{13}\text{C}\{^1\text{H}\}$ NMR (75 MHz, DMSO- d_6) δ 54.1 (d, $^1J_{\text{CP}} = 41.2$ Hz) ppm; $^{31}\text{P}\{^1\text{H}\}$ NMR (121 MHz, DMSO- d_6) δ 25.8 ppm; IR (neat): $\tilde{\nu} = 3430$ (w), 3203 (br), 2891 (w), 1423 (w), 1399 (w), 1291 (w), 1192 (w), 1043 (m), 1020 (s), 911 (m), 887 (m), 837 (m), 786 (w), 723 (m), 629 (m), 465 (s), 412 (m) cm^{-1} . HRMS (TOF MS ES+) calcd for $\text{C}_6\text{H}_{18}\text{Au}_2\text{ClO}_6\text{P}_2$ [2M-Cl] 676.9598, found m/z 676.8788.

2.8 General Procedure for the Synthesis of Gold(I)Thiosugar Phosphine Complexes (**18a-g**)

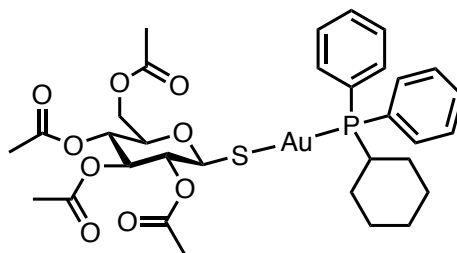
K₂CO₃ was dissolved in deionised water, cooled to 0 °C and added to a cooled (0 °C) solution of the corresponding gold(I) phosphine complex (1 eq) and 1-thio-β-D-glucose tetraacetate (1 eq) in dichloromethane (unless stated otherwise). The biphasic reaction mixture was warmed to RT and stirred rapidly. The completion of reaction was confirmed by ³¹P{¹H} NMR spectroscopy and the layers were separated and extracted with dichloromethane (3x). The solvent was removed *in vacuo* to yield the desired product in near quantitative yields.

2.8.1 [Au(**16a**)SR] (**18a**)



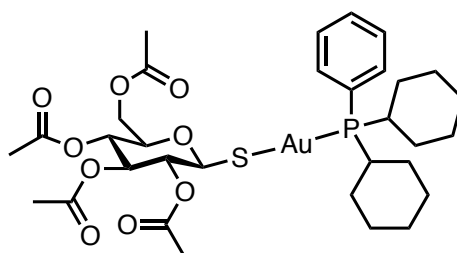
Using 0.037 g (0.10 mmol) of 1-thio-β-D-glucose tetraacetate and 0.050 g (0.10 mmol) of **17a** in 2 mL dichloromethane, 0.017 g (0.12 mmol) of potassium carbonate in 1 mL H₂O afforded **18a** as a white oily solid. (0.08 g, 98%). ¹H NMR (300 MHz, CDCl₃) δ 7.65–7.40 (m, 15H), 5.18–4.99 (m, 4H), 4.20 (dd, ²J_{HH} = 12.2 Hz, ³J_{HH} = 4.7 Hz, 1H), 4.09 (dd, ²J_{HH} = 12.2 Hz, ³J_{HH} = 2.4 Hz, 1H), 3.74 (m, 1H), 2.03 (s, 3H), 1.99 (s, 3H), 1.96 (s, 3H), 1.89 (s, 3H) ppm; ¹³C{¹H} NMR (75 MHz, CDCl₃) δ 170.9, 170.4, 169.7, 169.7, 134.4 (d, J_{CP} = 13.9 Hz), 131.8 (d, J_{CP} = 2.6 Hz), 129.9 (d, J_{CP} = 33.6 Hz), 129.3 (d, J_{CP} = 11.4 Hz), 83.2, 77.7, 75.8, 74.3, 69.1, 62.9, 53.6, 21.2, 20.8, 20.8 ppm; ³¹P{¹H} NMR (121 MHz, CDCl₃) δ 38.8 (s, 1P) ppm; IR (neat): $\tilde{\nu}$ = 2957 (w), 1744 (s), 1471 (w), 1436 (m), 1365 (m), 1218 (s), 1100 (m), 1033 (s), 998 (m), 912 (m), 815 (w), 730 (m), 711 (m), 693 (m), 646 (w), 599 (w), 538 (s), 509 (m), 433 (w) cm⁻¹; TOF MS (ES⁺) calcd for C₃₂H₃₅O₉PSAu [M+H]⁺ requires m/z 823.1405, found m/z 823.1405 (0.0 ppm). These spectroscopic data are in agreement with literature values.^{27,48}

2.8.2 [Au(**16b**)SR] (**18b**)



Using 0.037 g (0.10 mmol) of 1-thio-β-D-glucose tetraacetate and 0.050 g (0.10 mmol) of **17b** in 2 mL dichloromethane, 0.017 g (0.12 mmol) of potassium carbonate in 1 mL H₂O afforded **18b** as a white oily solid (0.08 g, 97%). ¹H NMR (300 MHz, CDCl₃) δ 7.85 – 7.69 (m, 4H), 7.51–7.41 (m, 6H), 5.24–5.00 (m, 4H), 4.22 (dd, ²J_{HH} = 12.2 Hz, ³J_{HH} = 4.7 Hz, 1H), 4.10 (dd, ²J_{HH} = 12.2 Hz, ³J_{HH} = 2.4 Hz, 1H), 3.76 (m, 1H), 2.61 (m, 1H), 2.07 (s, 3H), 1.99 (s, 3H), 1.96 (s, 3H), 1.86 (s, 3H), 1.84–1.21 (m, 10H) ppm; ¹³C{¹H} NMR (75 MHz, CDCl₃) δ 170.9, 170.4, 169.7 (overlapping peaks), 134.2 (d, J_{CP} = 13.0 Hz), 131.6 (d, J_{CP} = 2.5 Hz), 129.2 (d, J_{CP} = 10.9 Hz), 129.4 (d, J_{CP} = 51.5 Hz), 83.3, 77.9, 75.7, 74.3, 69.1, 62.9, 53.5, 36.4 (d, J_{CP} = 34.6 Hz), 29.1 (dd, J_{CP} = 16.3, 4.8 Hz), 26.4 (dd, J_{CP} = 14.1, 3.0 Hz), 25.7, 21.3, 20.8, 20.7 ppm; ³¹P{¹H} NMR (121 MHz, CDCl₃) δ 46.7 (s, 1P) ppm; IR (neat): $\tilde{\nu}$ = 2933 (w), 2853 (w), 1743 (s), 1482 (w), 1436 (w), 1366 (m), 1217 (s), 1099 (m), 1032 (s), 973 (m), 912 (m), 815 (w), 729 (s), 697 (m), 646 (w), 599 (w), 520 (m), 493 (m), 410 (w) cm⁻¹; TOF MS (ES⁺) calcd for C₃₂H₄₁O₉PSAu [M+H]⁺ requires m/z 829.1875, found m/z 829.1873 (–0.2 ppm).

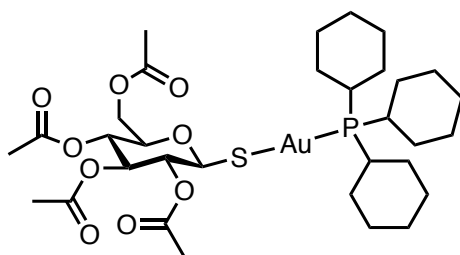
2.8.3 [Au(**16c**)SR] (**18c**)



Using 0.036 g (0.10 mmol) of 1-thio-β-D-glucose tetraacetate and 0.051 g (0.10 mmol) of **17c** in 2 mL dichloromethane, 0.017 g (0.12 mmol) of potassium carbonate in 1 mL H₂O afforded **18c** as a white oily solid (0.082 g, 98%). ¹H NMR (300 MHz, CDCl₃) δ 7.78–7.65 (m, 2H), 7.56–7.43 (m, 3H), 5.22–5.01 (m, 4H), 4.21 (dd, ²J_{HH} = 12.2 Hz, ³J_{HH} = 4.8 Hz, 1H), 4.08 (dd, ²J_{HH} = 12.2 Hz, ³J_{HH} = 2.5 Hz, 1H), 3.73 (m, 1H), 2.40–2.23 (m, 2H), 2.08 (s, 3H), 1.99 (s, 3H), 1.96 (s, 3H), 1.94 (s, 3H), 1.90–1.60 (m, 8H), 1.44–1.13 (m, 12H) ppm; ¹³C{¹H} NMR (75 MHz, CDCl₃) δ 170.9, 170.4, 169.7 (overlapping peaks), 135.2 (d, J_{CP} = 11.7 Hz), 131.7 (d, J_{CP} = 2.4 Hz), 128.8 (d, J_{CP} = 10.4 Hz), 126.6 (d, J_{CP} = 47.5 Hz), 83.4, 78.0, 75.7, 74.4, 69.1, 63.1, 53.6, 33.9 (dd, J_{CP} =

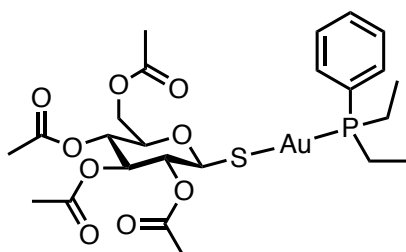
31.2, 3.5 Hz), 29.5 (dd, $J_{CP} = 9.0, 4.2$ Hz), 28.5 (d, $J_{CP} = 14.9$ Hz), 25.8 (d, $J_{CP} = 1.6$ Hz), 21.3, 20.8, 20.8 ppm; $^{31}\text{P}\{^1\text{H}\}$ NMR (121 MHz, CDCl_3) δ 54.4 (s, 1P) ppm; IR (neat): $\tilde{\nu} = 2928$ (m), 2852 (w), 1745 (s), 1448 (m), 1435 (m), 1365 (m), 1219 (s), 1089 (m), 1032 (s), 956 (w), 913 (m), 889 (w), 817 (w), 733 (s), 697 (m), 645 (w), 599 (w), 538 (m), 503 (w) cm^{-1} ; TOF MS (ES^+) calcd for $\text{C}_{32}\text{H}_{47}\text{O}_9\text{PSAu}$ $[\text{M}+\text{H}]^+$ requires m/z 835.2344, found m/z 835.2394 (6.0 ppm).

2.8.4 $[\text{Au}(\mathbf{16d})\text{SR}]$ (**18d**)



Using 0.036 g (0.10 mmol) of 1-thio- β -D-glucose tetraacetate and 0.051 g (0.10 mmol) of **17d** in 2 mL dichloromethane, 0.017 g (0.12 mmol) of potassium carbonate in 1 mL H_2O afforded **18d** as a white solid (0.079 g, 94%). ^1H NMR (300 MHz, CDCl_3) δ 5.18–4.94 (m, 4H), 4.22 (dd, $^2J_{\text{HH}} = 12.1$ Hz, $^3J_{\text{HH}} = 4.9$ Hz, 1H), 4.06 (dd, $^2J_{\text{HH}} = 12.3$ Hz, $^3J_{\text{HH}} = 2.5$ Hz, 1H), 3.72 (m, 1H), 2.11–2.01 (m, 12H), 2.03–1.92 (m, 3H), 1.99 (s, 3H), 1.96 (s, 3H), 1.92–1.65 (m, 8H), 1.71 (m, 6H), 1.57–1.17 (m, 10H) ppm; $^{13}\text{C}\{^1\text{H}\}$ NMR (75 MHz, CDCl_3) δ 170.9, 170.4, 169.7, 169.6, 83.3, 74.4, 69.1, 63.1, 53.6, 33.5 (d, $J_{CP} = 27.7$ Hz), 31.5 (d, $J_{CP} = 55.4$ Hz), 30.8 (d, $J_{CP} = 8.0$ Hz), 27.2 (d, $J_{CP} = 11.9$ Hz), 26.0, 21.3, 20.9, 20.8, 20.8 ppm; $^{31}\text{P}\{^1\text{H}\}$ NMR (121 MHz, CDCl_3) δ 56.7 (s, 1P) ppm; IR (neat): $\tilde{\nu} = 2928$ (m), 2852 (w), 1749 (s), 1447 (w), 1366 (m), 1224 (s), 1034 (s), 914 (w), 853 (w), 817 (w), 735 (w), 599 (w), 520 (w) cm^{-1} ; TOF MS (ES^+) calcd for $\text{C}_{32}\text{H}_{53}\text{O}_9\text{PSAu}$ $[\text{M}+\text{H}]^+$ requires m/z 841.2814, found m/z 841.2852 (4.5 ppm). These spectroscopic data are in agreement with literature values.⁴⁸

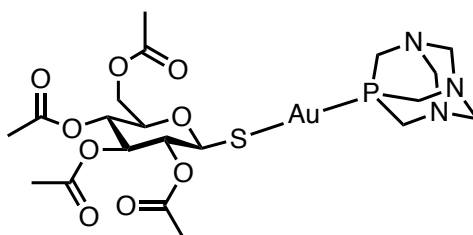
2.8.5 $[\text{Au}(\mathbf{16e})\text{SR}]$ (**18e**)



Using 0.031 g (0.08 mmol) of 1-thio- β -D-glucose tetraacetate and 0.034 mg (0.08 mmol) of **17e** in 2 mL dichloromethane, 0.013 g (0.09 mmol) of potassium carbonate in 1 mL H_2O afforded **18e** as a white oily solid (0.057 g, 98%). ^1H NMR (300 MHz, CDCl_3) δ 7.80–7.71 (m, 2H), 7.54–7.46 (m, 3H), 5.23–4.98 (m, 4H), 4.24 (dd, $^2J_{\text{HH}} = 12.3$ Hz, $^3J_{\text{HH}} = 4.8$ Hz, 1H), 4.10 (dd,

$^2J_{\text{HH}} = 12.3$ Hz, $^3J_{\text{HH}} = 2.4$ Hz, 1H), 3.74 (m, 1H), 2.20–2.05 (m, 4H), 2.08 (s, 3H), 2.00 (s, 3H), 1.98 (s, 3H), 1.97 (s, 3H), 1.16 (dtd, $^3J_{\text{HP}} = 19.8$, $^3J_{\text{HH}} = 7.6$, $^4J_{\text{HH}} = 4.0$ Hz, 6H) ppm; $^{13}\text{C}\{^1\text{H}\}$ NMR (75 MHz, CDCl_3) δ 170.9, 170.4, 169.8, 169.8, 133.5 (d, $J_{\text{CP}} = 12.6$ Hz), 131.9 (d, $J_{\text{CP}} = 2.5$ Hz), 129.3 (d, $J_{\text{CP}} = 51.6$ Hz), 129.3 (d, $J_{\text{CP}} = 10.9$ Hz), 83.3, 77.4, 75.9, 74.4, 69.0, 62.9, 21.4, 21.3, 21.3, 20.9, 20.8 (d, $^1J_{\text{CP}} = 3.6$ Hz), 9.4 ppm; $^{31}\text{P}\{^1\text{H}\}$ NMR (121 MHz, CDCl_3) δ 40.4 (s, 1P) ppm; IR (neat): $\tilde{\nu} = 2965$ (w), 1743 (s), 1436 (w), 1366 (m), 1219 (s), 1108 (w), 1090 (w), 1032 (s), 956 (w), 913 (m), 816 (w), 734 (m), 696 (w), 599 (w) cm^{-1} ; TOF MS (ES^+) calcd for $\text{C}_{27}\text{H}_{34}\text{AuO}_9\text{PSNa}$ $[\text{M}+\text{Na}]^+$ requires m/z 749.1224, found m/z 749.1249.

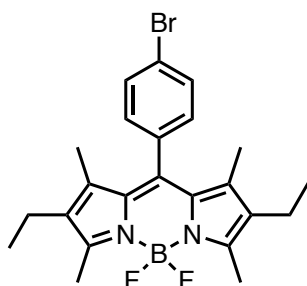
2.8.6 $[\text{Au}(\mathbf{16f})\text{SR}]$ (**18f**)



Using 0.047 g (0.13 mmol) of 1-thio- β -D-glucose tetraacetate, and 0.050 mg (0.13 mmol) of **17f** in 5 mL ethanol, 0.020 g (0.14 mmol) of potassium carbonate in 5 mL H_2O afforded **18f** as a white solid. (0.089 g, 95%). Crystals suitable for X-ray crystallography were formed from slow evaporation of dimethyl sulfoxide. ^1H NMR (300 MHz, $\text{DMSO}-d_6$) δ 5.09 (pseudo-t, $^3J_{\text{HH}} = 9.5$ Hz, 2H), 4.84 (pseudo-t, $^3J_{\text{HH}} = 9.8$ Hz, 1H), 4.61 (pseudo-t, $^3J_{\text{HH}} = 9.4$ Hz, 1H), 4.56–4.29 (m, 6H, NCH_2N), 4.23 (s, 6H, NCH_2P), 4.10 (dd, $^2J_{\text{HH}} = 12.3$ Hz, $^3J_{\text{HH}} = 4.9$ Hz, 1H), 3.95 (dd, $^2J_{\text{HH}} = 12.3$ Hz, $^3J_{\text{HH}} = 2.3$ Hz, 1H), 3.76 (ddd, $^2J_{\text{HH}} = 9.5$ Hz, $^2J_{\text{HH}} = 4.7$ Hz, $^3J_{\text{HH}} = 2.5$ Hz, 1H), 2.02 (s, 3H), 1.98 (s, 3H), 1.96 (s, 3H), 1.90 (s, 3H); $^{31}\text{P}\{^1\text{H}\}$ NMR (121 MHz, $\text{DMSO}-d_6$) δ -50.7 (br s, 1P) ppm; IR (neat): $\tilde{\nu} = 2942$ (w), 1742 (s), 1443 (w), 1368 (m), 1223 (s), 1098 (w), 1033 (s), 1014 (m), 973 (m), 947 (m), 914 (w), 813 (w), 740 (w), 582 (w) cm^{-1} . These spectroscopic data are in agreement with literature values.⁵⁰

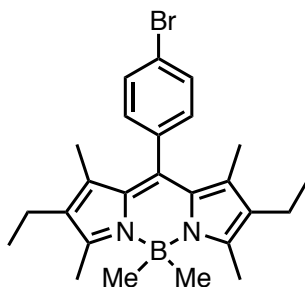
2.9 Synthesis of Fluorescent Analogues of Auranofin

2.9.1 8-(4-Bromophenyl)-4,4-difluoro-1,3,5,7-tetramethyl-2,6-diethyl-4-bora-3a,4a-diaza-s-indacene (**19**)



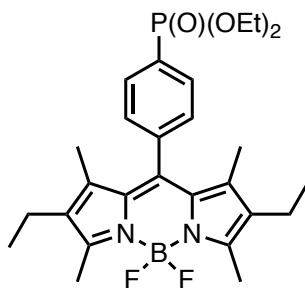
4-Bromobenzaldehyde (10.0 g, 54.0 mmol) was dissolved in anhydrous dichloromethane (800 mL), and to this stirred solution, 3-ethyl-2,4-dimethyl-1H-pyrrole (14.5 mL, 108.0 mmol) was added, followed by TFA (2 drops). The reaction was stirred in a darkened flask at room temperature, overnight, under a nitrogen atmosphere. DDQ (12.3 g, 54.0 mmol) was added in a single portion and the reaction was stirred for a further three hours. *N,N*-diisopropylethylamine (56.4 mL, 324.0 mmol) was added, followed by the dropwise addition of $\text{BF}_3 \cdot \text{OEt}_2$ (53.3 mL, 432.0 mmol) and was stirred overnight at room temperature. The reaction mixture was washed with water (3 x 100 mL) and extracted with DCM (3 x 50 mL). The organics were combined and dried over MgSO_4 , filtered and dried *in vacuo*. Purification by column chromatography on silica gel (toluene) yielded a purple solid with a green tint (14.6 g, 59%). **^1H NMR** (300 MHz, CDCl_3) δ 7.64 (d, $^3J_{\text{HH}} = 8.5$ Hz, 2H), 7.18 (d, $^3J_{\text{HH}} = 8.5$ Hz, 2H), 2.53 (s, 6H), 2.30 (q, $^3J_{\text{HH}} = 8.2$ Hz, 4H), 1.31 (s, 6H), 0.98 (t, $^3J_{\text{HH}} = 7.6$ Hz, 6H) ppm; **$^{11}\text{B}\{^1\text{H}\}$ NMR** (128 MHz, CDCl_3) δ -0.2 (t, $^1J_{\text{BF}} = 31.8$ Hz, 1B) ppm; **$^{19}\text{F}\{^1\text{H}\}$ NMR** (376 MHz, CDCl_3) δ -145.4 (q (equal intensity), $^1J_{\text{FB}} = 31.8$ Hz, 2F) ppm; **$^{13}\text{C}\{^1\text{H}\}$ NMR** (101 MHz, CDCl_3) δ 154.3, 138.6, 138.3, 138.2, 134.9, 133.2, 132.5, 130.3, 123.2, 17.2, 14.7, 12.7, 12.1 ppm. These spectroscopic data are in agreement with literature values.⁵⁸

2.9.2 8-(4-Bromophenyl)-4,4-dimethyl-1,3,5,7-tetramethyl-2,6-diethyl-4-bora-3a,4a-diaza-s-indacene (20)



Methylmagnesium bromide (5.7 mL, 3.0 M solution in diethyl ether, 16.9 mmol) was added dropwise to a stirred solution of **19** (3.91 g, 8.49 mmol) in anhydrous tetrahydrofuran (120 mL). The reaction was monitored by TLC. Purification by column chromatography on silica gel (toluene/petroleum ether, 1:9) afforded an orange solid (2.90 g, 75%). ^1H NMR (300 MHz, CDCl_3) δ 7.72 (m, 2H), 7.21 (m, 2H), 2.45 (s, 6H), 2.32 (q, $^3J_{\text{HH}} = 7.6$ Hz, 4H), 1.30 (s, 6H), 0.99 (t, $^3J_{\text{HH}} = 7.6$ Hz, 6H), 0.27 (s, 6H); $^{11}\text{B}\{^1\text{H}\}$ NMR (96 MHz, CDCl_3) δ -1.8 (s, 1B) ppm; $^{13}\text{C}\{^1\text{H}\}$ NMR (101 MHz, CDCl_3) δ 150.8, 138.5, 136.3, 133.6, 132.6, 132.1, 130.5, 128.6, 122.2, 17.5, 14.7, 14.3, 12.0, 10.4 (br) ppm. These spectroscopic data are in agreement with literature values.⁵⁹

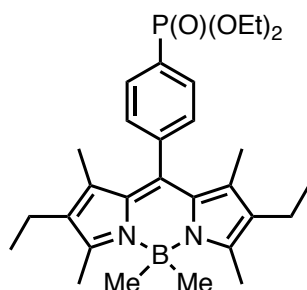
2.9.3 8-((4-Diethylphosphonato)phenyl)-4,4-difluoro-1,3,5,7-tetramethyl-2,6-diethyl-4-bora-3a,4a-diaza-s-indacene (21)



19 (6.0 g, 13.1 mmol), palladium acetate (0.293 g, 1.3 mmol) and 1,4-bis(diphenylphosphino)-butane (0.557 g, 1.3 mmol) were added to a Schlenk flask and dissolved in anhydrous dimethyl sulfoxide (300 mL) under nitrogen atmosphere. *N,N*-diisopropylethylamine (6.8 mL, 39.2 mmol) was added to the stirred solution followed by diethyl phosphite (2.0 mL, 15.7 mmol). The reaction mixture was heated to 90 °C and stirred for 72 hours. The reaction mixture was diluted with dichloromethane (200 mL) and washed with water (5 x 200 mL). The organic layers were combined and dried over MgSO_4 , filtered and the solvent removed *in vacuo* to yield a purple solid. Purification by column chromatography on silica gel (ethyl acetate/petroleum ether, 3:1) yielded a red solid (4.08 g, 60%). ^1H NMR (300 MHz, CDCl_3) δ

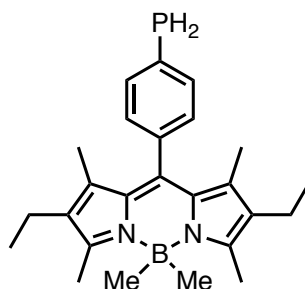
7.93 (dd, $^3J_{\text{HH}} = 8.3$ Hz, $^3J_{\text{HP}} = 13.1$ Hz, 2H), 7.41 (dd, $^3J_{\text{HH}} = 8.1$ Hz, $^4J_{\text{HP}} = 3.9$ Hz, 2H), 4.14 (m, 4H), 2.50 (s, 6H), 2.27 (q, $^3J_{\text{HH}} = 7.5$ Hz, 4H), 1.32 (t, $^3J_{\text{HH}} = 7.1$ Hz, 6H), 1.23 (s, 6H), 0.95 (t, $^3J_{\text{HH}} = 7.6$ Hz, 6H) ppm; $^{31}\text{P}\{^1\text{H}\}$ NMR (121 MHz, CDCl_3) δ 17.6 ppm; $^{11}\text{B}\{^1\text{H}\}$ NMR (96 MHz, CDCl_3) δ 0.8 (t, $^1J_{\text{BF}} = 32.8$ Hz, 1B) ppm; $^{19}\text{F}\{^1\text{H}\}$ NMR (282 MHz, CDCl_3) δ -145.8 (q (equal intensity), $^1J_{\text{FB}} = 32.8$ Hz, 2F ppm); $^{13}\text{C}\{^1\text{H}\}$ NMR (101 MHz, CDCl_3) δ 154.3, 140.2, 138.4, 138.0, 133.1, 132.4 (d, $J_{\text{CP}} = 10.1$ Hz), 130.3, 129.7 (d, $^1J_{\text{CP}} = 121.7$ Hz), 128.7 (d, $J_{\text{CP}} = 15.2$ Hz), 62.4 (d, $^2J_{\text{CP}} = 5.5$ Hz), 17.1, 16.3 (d, $^3J_{\text{CP}} = 6.1$ Hz), 14.6, 12.5, 11.8 ppm. These spectroscopic data are in agreement with literature values.⁵⁸

2.9.4 8-((4-Diethylphosphonato)phenyl)-4,4-dimethyl-1,3,5,7-tetramethyl-2,6-diethyl-4-bora-3a,4a-diaza-s-indacene (**22**)



Methylmagnesium bromide (6.6 mL, 3.0 M solution in diethyl ether, 19.8 mmol) was added dropwise to a stirred solution of **21** (4.08 g, 7.9 mmol) in anhydrous tetrahydrofuran (100 mL). The reaction was monitored by TLC. Purification by column chromatography on silica gel (ethyl acetate:petroleum ether, 3:1) afforded an orange solid (2.94 g, 73%). ^1H NMR (300 MHz, CDCl_3) δ 7.91 (dd, $^3J_{\text{HH}} = 8.2$ Hz, $^3J_{\text{HP}} = 13.1$ Hz, 2H), 7.44 (dd, $^3J_{\text{HH}} = 8.2$ Hz, $^4J_{\text{HP}} = 3.9$ Hz, 2H), 4.13 (m, 4H), 2.43 (s, 6H), 2.28 (q, $^3J_{\text{HH}} = 7.5$ Hz, 4H), 1.32 (t, $^3J_{\text{HH}} = 7.1$ Hz, 6H), 1.21 (s, 6H), 0.95 (t, $^3J_{\text{HH}} = 7.5$ Hz, 6H), 0.26 (s, 6H) ppm; $^{31}\text{P}\{^1\text{H}\}$ NMR (202 MHz, CDCl_3) δ 18.1 ppm; $^{11}\text{B}\{^1\text{H}\}$ NMR (128 MHz, CDCl_3) δ -0.9 ppm; $^{13}\text{C}\{^1\text{H}\}$ NMR (126 MHz, CDCl_3) δ 151.2, 141.8 (d, $J_{\text{CP}} = 3.4$ Hz), 138.9, 133.6, 132.9, 132.3 (d, $J_{\text{CP}} = 10.1$ Hz), 129.3 (d, $J_{\text{CP}} = 15.2$ Hz), 128.8 (d, $^1J_{\text{CP}} = 188.5$ Hz), 128.7, 62.4 (d, $^2J_{\text{CP}} = 5.6$ Hz), 17.6, 16.5 (d, $^3J_{\text{CP}} = 5.6$ Hz), 14.8, 14.5, 12.0, 10.2 (br) ppm. These spectroscopic data are in agreement with literature values.⁵⁸

2.9.5 8-((4-Phosphino)phenyl)-4,4-dimethyl-1,3,5,7-tetramethyl-2,6-diethyl-4-bora-3a,4a-diaza-s-indacene (**14**)



Trimethylsilyl chloride (0.95 mL, 7.5 mmol) was added to cooled ($-78\text{ }^{\circ}\text{C}$) lithium aluminium hydride (7.5 mL, 1 M solution in tetrahydrofuran, 7.5 mmol). This reducing mixture was warmed to room temperature over 45 minutes and then cooled again to $-78\text{ }^{\circ}\text{C}$. **14** (1.91 g, 3.76 mmol) was dissolved in anhydrous tetrahydrofuran (150 mL) and this was added slowly to the cooled mixture. The reaction mixture was warmed to room temperature and stirred overnight. The reaction mixture was concentrated *in vacuo* and cooled in an ice bath, before water was added dropwise to quench the reaction. The product was extracted with diethyl ether (3 x 100 mL), the organic layers were then combined and dried over MgSO_4 , filtered and dried *in vacuo*. Purification by column chromatography on silica gel (chloroform:petroleum ether, 1:3) yielded an orange solid (1.22 g, 80%). $^1\text{H NMR}$ (300 MHz, CDCl_3) δ 7.61 (m, 2H), 7.26 (m, 2H), 4.11 (d, $^1J_{\text{HP}} = 202.6\text{ Hz}$, 2H), 2.47 (s, 6H), 2.33 (q, $^3J_{\text{HH}} = 7.8\text{ Hz}$, 4H), 1.29 (t, 6H), 1.00 (t, $^3J_{\text{HH}} = 7.5\text{ Hz}$, 6H), 0.30 (s, 6H) ppm; $^{31}\text{P}\{^1\text{H}\}$ NMR (121 MHz, CDCl_3) δ -122.4 ppm; $^{11}\text{B}\{^1\text{H}\}$ NMR (96 MHz, CDCl_3) δ -0.96 ppm; $^{13}\text{C}\{^1\text{H}\}$ NMR (75 MHz, CDCl_3) δ 150.8, 139.9, 137.4, 135.1 (d, $J_{\text{CP}} = 15.2\text{ Hz}$), 133.9, 132.6, 129.1, 129.0, 128.9, 17.6, 14.8, 14.5, 12.1, 10.4 (br) ppm. IR (neat): $\tilde{\nu} = 2955$ (w), 2923 (w), 2867 (w), 2287 (w), 1545 (s), 1529 (s), 1467 (m), 1358 (m), 1313 (s), 1289 (m), 1167 (s), 1142 (s), 1109 (s), 1065 (m), 1023 (m), 977 (s), 942 (s), 906 (s), 785 (s), 669 (m), 608 (w), 558 (w), 518 (s), 505 (m) cm^{-1} . These spectroscopic data are in agreement with literature values.⁵⁸

2.10 General Procedure for the Synthesis of Fluorescent Tertiary Phosphines (**24a-d**)

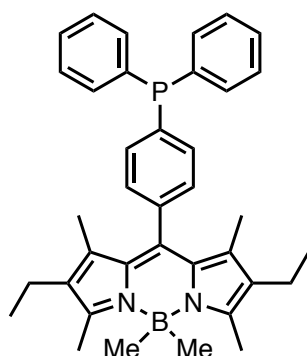
2.10.1 Route 1

n-Butyllithium (1.1 eq) was added dropwise to a cooled (−78 °C) solution of aryl bromide **20** (1.0 eq) in anhydrous diethyl ether and the reaction mixture was warmed to room temperature over 45 minutes. The reaction mixture was cooled to −78 °C and the corresponding chlorodiphenyl- or chlorodicyclohexylphosphine (1.1 eq) was added dropwise. The reaction mixture was warmed to room temperature and stirred overnight. The following day, the reaction mixture was washed with water (3x) and extracted with diethyl ether. The organic fractions were combined, dried over MgSO₄ and filtered. The solvent was removed *in vacuo* and the crude product was purified by column chromatography (chloroform/petroleum ether, 1:4).

2.10.2 Route 2

Primary phosphine **14** (1.0 eq) and phosphorus pentachloride (2.2 eq) were added to a Schlenk flask; the flask was then cycled three times between vacuum and nitrogen. Anhydrous toluene was added, and the reaction mixture was stirred vigorously for one hour. Completion of the reaction was confirmed by the absence of **14** in the ³¹P{¹H} NMR spectra and a new resonance at −159.7 ppm relating to the dichlorophosphine, **23**. The volatiles were removed *in vacuo* and **23** was dissolved in anhydrous tetrahydrofuran. The corresponding Grignard reagent (2.2 eq) was added drop-wise and the reaction was monitored by ³¹P{¹H} NMR spectroscopy. On completion of the reaction, the reaction mixture was washed with water (3x) and extracted with diethyl ether, the organic fractions were combined, dried over MgSO₄ and filtered. The crude product was then triturated with acetonitrile to remove any soluble impurities.

2.10.3 8-((4-Diphenylphosphino)phenyl)-4,4-dimethyl-1,3,5,7-tetramethyl-2,6-diethyl-4-bora-3a,4a-diaza-s-indacene (**24a**)



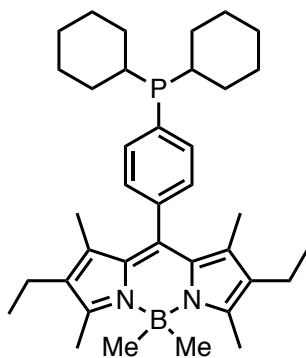
Route 1 used 0.8 mL (1.22 mmol) of *n*-butyllithium (1.6 M in hexane) and 0.50 g (1.11 mmol) of **20** and 0.22 mL (1.22 mmol) of chlorodiphenylphosphine in diethyl ether (40 mL). The

complex was purified by column chromatography on silica gel (chloroform:petroleum ether 1:4) and yielded **24a** as an orange solid. (0.298 g, 54%).

Route 2 used 0.200 mg (0.49 mmol) of primary phosphine **14**, 0.216 mg (1.04 mmol) of phosphorus pentachloride in 12 mL of anhydrous toluene and 1.04 mL of phenylmagnesium bromide (1 M in tetrahydrofuran, 1.04 mmol) in 12 mL tetrahydrofuran to yield **24a** as an orange solid (0.24 g, 89%).

¹H NMR (300 MHz, CDCl₃) δ 7.87–7.68 (m, 1H), 7.65–7.47 (m, 1H), 7.48–7.29 (m, 12H), 2.49 (s, 6H), 2.36 (q, ³J_{HH} = 7.5 Hz, 4H), 1.38 (s, 6H), 1.03 (t, ³J_{HH} = 7.5 Hz, 6H), 0.33 (s, 6H) ppm; **¹³C{¹H} NMR** (75 MHz, CDCl₃) δ 150.8, 139.9, 137.9, 137.8, 136.9 (d, J_{CP} = 11.0 Hz), 134.0, 133.8, 133.7, 132.6, 132.3, 132.1, 129.0, 128.7 (d, J_{CP} = 7.2 Hz), 17.6, 14.9, 14.4, 12.0, 10.6 (br) ppm; **³¹P{¹H} NMR** (121 MHz, CDCl₃) δ –6.1 (s, 1P) ppm; **¹¹B{¹H} NMR** (96 MHz, CDCl₃) δ –0.9 (s, 1B) ppm; **IR (neat)**: $\tilde{\nu}$ = 3054 (w), 2959 (w), 2928 (w), 2868 (w), 1547 (s), 1433 (m), 1359 (m), 1319 (s), 1262 (w), 1171 (s), 1145 (s), 1112 (m), 1063 (m), 1020 (m), 980 (s), 644 (s), 907 (s), 847 (w), 800 (s), 730 (s), 694 (s), 673 (m), 647 (w), 599 (w), 516 (m) cm^{–1}. These spectroscopic data are in agreement with literature values.⁵⁹

2.10.4 8-((4-Dicyclohexylphosphino)phenyl)-4,4-dimethyl-1,3,5,7-tetramethyl-2,6-diethyl-4-bora-3a,4a-diaza-s-indacene (**24b**)

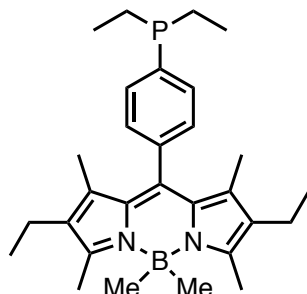


Route 1 used 0.4 mL (0.98 mmol) of *n*-butyllithium and 0.40 g (0.89 mmol) of **20** and 0.22 mL (0.98 mmol) of chlorodicyclohexylphosphine in diethyl ether (40 mL). Purification by column chromatography on silica gel (chloroform:petrol 1:4) to afford **24b** as an orange solid (0.32 g, 64%).

Route 2 used 0.10 g (0.25 mmol) of primary phosphine **14**, 0.112 g (0.54 mmol) of phosphorus pentachloride in 6 mL of anhydrous toluene and 0.1 mL of cyclohexylmagnesium chloride (2 M solution in diethyl ether, 0.5 mmol) in 6 mL tetrahydrofuran to yield **24b** as an orange solid. (0.13 mg, 91%). **¹H NMR** (300 MHz, CDCl₃) δ 7.55 (m, 2H), 7.31 (m, 2H), 2.47 (s, 6H), 2.32 (q, ³J_{HH} = 7.5 Hz, 4H), 2.02–1.62 (m, 12H), 1.28 (s, 6H), 1.21–0.78 (m, 10H), 1.00 (t, ³J_{HH} = 7.5 Hz,

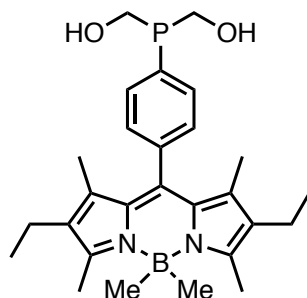
6H), 0.30 (s, 6H) ppm; $^{31}\text{P}\{^1\text{H}\}$ NMR (121 MHz, CDCl_3) δ 2.2 (s, 1P) ppm; $^{11}\text{B}\{^1\text{H}\}$ NMR (96 MHz, CDCl_3) δ -0.8 ppm. These spectroscopic data are in agreement with literature values.⁵⁹

2.10.5 8-((4-Diethylphosphino)phenyl)-4,4-dimethyl-1,3,5,7-tetramethyl-2,6-diethyl-4-bora-3a,4a-diaza-s-indacene (**24c**)



Route 2 used 0.100 g (0.25 mmol) of primary phosphine **14**, 0.108 g (0.49 mmol) of phosphorus pentachloride in 6 mL of anhydrous toluene and 0.17mL of ethylmagnesium bromide (3 M in diethyl ether, 0.49 mmol) in 6 mL tetrahydrofuran to yield **24c** as an orange solid. The crude compound was triturated with acetonitrile and the solid was filtered and dried *in vacuo* to afford an orange solid (0.105 g, 92% yield). ^1H NMR (300 MHz, CDCl_3) δ 7.63–7.55 (m, 2H), 7.35–7.30 (m, 2H), 2.47 (s, 6H), 2.33 (q, $^3J_{\text{HH}} = 7.6$ Hz, 4H), 1.76 (q, $^3J_{\text{HH}} = 7.6$ Hz, 4H), 1.28 (s, 6H), 1.10–0.96 (m, overlapping peaks, 12H), 0.30 (s, 6H) ppm; $^1\text{H}\{^{31}\text{P}\}$ NMR (300 MHz, CDCl_3) δ 7.63–7.55 (m, 2H), 7.35–7.30 (m, 2H), 2.47 (s, 6H), 2.33 (q, $^3J_{\text{HH}} = 7.6$ Hz, 4H), 1.76 (q, $^3J_{\text{HH}} = 7.6$ Hz, 4H), 1.28 (s, 6H), 1.04 (t, $^3J_{\text{HH}} = 7.6$ Hz, 6H), 1.00 (t, $^3J_{\text{HH}} = 7.5$ Hz, 6H), 0.30 (s, 6H) ppm; $^{31}\text{P}\{^1\text{H}\}$ NMR (121 MHz, CDCl_3) δ -16.1 (s, 1P) ppm; $^{13}\text{C}\{^1\text{H}\}$ NMR (75 MHz, CDCl_3) δ 150.7, 140.2, 138.9 (d, $J_{\text{CP}} = 16.3$ Hz), 137.7, 133.9, 132.8, 132.6, 129.1, 128.8 (d, $J_{\text{CP}} = 6.6$ Hz), 20.0 (d, $^1J_{\text{CP}} = 10.8$ Hz), 17.6, 14.9, 14.4, 11.9, 10.5 (br), 9.7 (d, $^2J_{\text{CP}} = 12.6$ Hz) ppm; $^{11}\text{B}\{^1\text{H}\}$ NMR (96 MHz, CDCl_3) δ -1.0 (s, 1B) ppm; IR (neat): $\tilde{\nu} = 2961$ (w), 2929 (w), 2870 (w), 1548 (s), 1470 (m), 1453 (m), 1404 (m), 1360 (w), 1319 (s), 1262 (w), 1171 (s), 1145 (s), 1112 (m), 981 (m), 944 (s), 904 (s), 800 (m), 728 (s), 704 (s), 647 (m), 557 (m), 516 (s) cm^{-1} ; TOF MS (ES^+) calcd for $\text{C}_{29}\text{H}_{42}\text{BN}_2\text{P}$ $[\text{M}+\text{H}]^+$ requires m/z 461.3257, found m/z 461.2892; TOF MS (ES^+) calcd for $\text{C}_{29}\text{H}_{42}\text{BN}_2\text{OP}$ $[\text{M}+\text{O}+\text{H}]^+$ requires m/z 477.3206, found m/z 477.3220.

2.10.6 8-(4-(Bis(hydroxymethyl)phosphino)phenyl)-4,4-dimethyl-1,3,5,7-tetramethyl-2,6-diethyl-4-bora-3a,4a-diaza-s-indacene (**24d**)

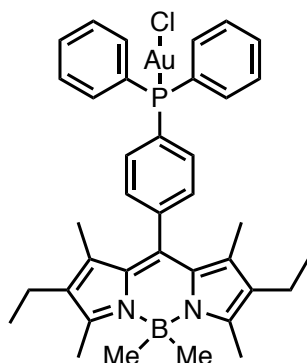


Aqueous formaldehyde (37 wt. % in H₂O) was purged with nitrogen gas for two hours. **14** (0.10 g, 0.25 mmol) was dissolved in anhydrous tetrahydrofuran (3 mL) and the purged aqueous formaldehyde (0.1 mL, 1.33 mmol) was added. The reaction was monitored by ³¹P{¹H} NMR spectroscopy where the gradual consumption of the primary phosphine **14** (peak at δ –122.4 ppm) was observed; the complete consumption of **14** was seen after three days. Removal of the solvent and excess formaldehyde *in vacuo* at 50 °C afforded **24d** as an orange solid in quantitative conversion by ³¹P{¹H} NMR spectroscopy. ¹H NMR (300 MHz, CDCl₃) δ 7.67 (m, 2H), 7.39 (m, 2H), 4.94 (m, 4H), 3.40 (s, 2H), 2.46 (s, 6H), 2.31 (q, ³J_{HH} = 7.5 Hz, 4H), 1.26 (s, 6H), 0.98 (t, ³J_{HH} = 7.5 Hz, 6H), 0.28 (s, 6H). ³¹P{¹H} NMR (121 MHz, CDCl₃) δ –14.1 (s, 1P) ppm; ¹¹B{¹H} NMR (96 MHz, CDCl₃) δ –2.0 (s, 1B) ppm; ¹³C{¹H} NMR (101 MHz, CDCl₃) δ 150.8, 139.5, 138.1, 133.6, 133.1 (d, ¹J_{CP} = 11.6 Hz), 132.7, 132.7, 129.3 (d, J_{CP} = 5.8 Hz), 129.2, 62.0 (d, ¹J_{CP} = 20.1 Hz), 17.5, 14.8, 14.4, 12.0, 10.5 (br) ppm; IR (neat): $\tilde{\nu}$ = 3255 (br), 2960 (w), 2868 (w), 1553 (s), 1532 (m), 1470 (m), 1451 (m), 1322 (s), 1294 (m), 1261 (m), 1172 (s), 1146 (s), 1112 (m), 1020 (s), 980 (s), 944 (s), 909 (m), 798 (s), 673 (m), 515 (m) cm^{–1}.

2.11 General Procedure for the Synthesis of Fluorescent Gold(I) Complexes (**25a-d**)

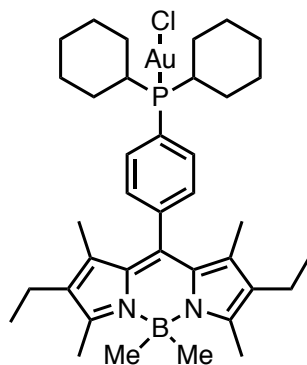
The tertiary phosphine (1 eq) and [chloro(tetrahydrothiophene)gold(I)] (1 eq) were added to a Schlenk flask, dissolved in anhydrous dichloromethane and stirred under nitrogen for one hour, by which time consumption of the starting material was confirmed by $^{31}\text{P}\{^1\text{H}\}$ NMR spectroscopy. The solvent was removed *in vacuo* and the solid was washed with hexane (3x) to remove tetrahydrothiophene.

2.11.1 [Au(**24a**)Cl] (**25a**)



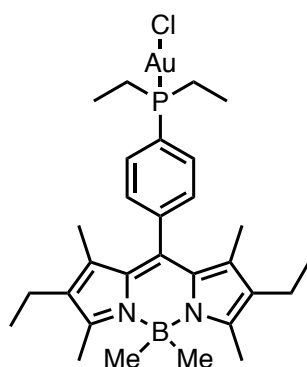
Reacting 0.115 g (0.36 mmol) of [chloro(tetrahydrothiophene)gold(I)] with 0.200 g (0.36 mmol) of **24a** in 3 mL dichloromethane. The complex was purified by column chromatography on silica gel (dichloromethane/petroleum ether 2:1) and yielded **25a** as an orange solid. (0.110 g, 40%). ^1H NMR (300 MHz, CDCl_3) δ 7.69–7.62 (m, 2H), 7.62–7.54 (m, 4H), 7.54–7.44 (m, 8H), 2.46 (s, 6H), 2.33 (q, $^3J_{\text{HH}} = 7.5$ Hz, 4H), 1.29 (s, 6H), 1.00 (t, $^3J_{\text{HH}} = 7.5$ Hz, 6H), 0.29 (s, 6H) ppm; $^{13}\text{C}\{^1\text{H}\}$ NMR (75 MHz, CDCl_3) δ 151.4, 141.7, 138.1, 134.4 (d, $J_{\text{CP}} = 14.1$ Hz), 134.2 (d, $J_{\text{CP}} = 13.8$ Hz), 133.2, 133.0, 132.3 (d, $J_{\text{CP}} = 2.8$ Hz), 130.1 (d, $J_{\text{CP}} = 11.9$ Hz), 129.5 (d, $J_{\text{CP}} = 12.0$ Hz), 128.9, 128.6, 128.0, 17.5, 14.8, 14.4, 12.2, 10.5 (br) ppm; $^{31}\text{P}\{^1\text{H}\}$ NMR (121 MHz, CDCl_3) δ 32.7 (s, 1P) ppm; $^{11}\text{B}\{^1\text{H}\}$ NMR (128 MHz, CDCl_3) δ –1.0 (s, 1B) ppm; IR (neat): $\tilde{\nu} = 2960$ (w), 2927 (w), 2868 (w), 1551 (s), 1471 (m), 1436 (m), 1360 (m), 1321 (s), 1263 (w), 1173 (s), 1146 (s), 1102 (m), 1021 (w), 945 (s), 910 (w), 801 (m), 734 (w), 693 (m), 673 (m) cm^{-1} . These spectroscopic data are in agreement with literature.⁵⁹

2.11.2 [Au(**24b**)Cl] (**25b**)



Reacting 0.032 g (0.1 mmol) of [chloro(tetrahydrothiophene)gold(I)] with 0.057 g (0.1 mmol) of **24b** in 1.5 mL dichloromethane. The complex was purified by column chromatography on silica gel (dichloromethane/petroleum ether 1:1) and yielded **25b** as an orange solid. (0.054 g, 67%). $^1\text{H NMR}$ (300 MHz, CDCl_3) δ 7.79 (m, 2H), 7.49 (m, 2H), 2.46 (s, 6H), 2.31 (q, $^3J_{\text{HH}} = 7.5$ Hz, 4H), 1.95–1.63 (m, 10H), 1.42–0.79 (m, 12H), 1.21 (s, 6H), 1.00 (t, $^3J_{\text{HH}} = 7.5$ Hz, 6H), 0.29 (s, 6H) ppm; $^{13}\text{C}\{^1\text{H}\}$ NMR (101 MHz, CDCl_3) δ 151.4, 141.7 (d, $J_{\text{CP}} = 2.4$ Hz), 138.3, 135.4 (d, $J_{\text{CP}} = 11.8$ Hz), 133.2 (d, $J_{\text{CP}} = 13.0$ Hz), 129.7 (d, $J_{\text{CP}} = 10.8$ Hz), 128.4, 125.5, 125.4, 33.5 (d, $^1J_{\text{CP}} = 34.2$ Hz), 29.7 (d, $^3J_{\text{CP}} = 3.2$ Hz), 26.6 (d, $^3J_{\text{CP}} = 5.3$ Hz), 26.5 (d, $^3J_{\text{CP}} = 2.7$ Hz), 17.6, 14.8, 14.5, 12.0, 10.6 (br) ppm; $^{31}\text{P}\{^1\text{H}\}$ NMR (121 MHz, CDCl_3) δ 50.9 ppm; $^{11}\text{B}\{^1\text{H}\}$ NMR (128 MHz, CDCl_3) δ -1.3 (s, 1B) ppm. These spectroscopic data are in agreement with literature values.⁵⁹

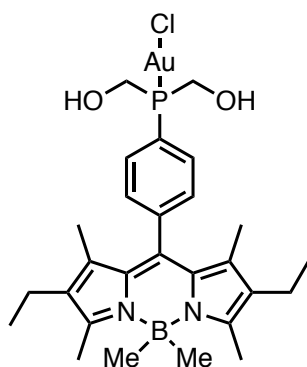
2.11.3 [Au(**24c**)Cl] (**25c**)



Reacting 0.056 g (0.17 mmol) of [chloro(tetrahydrothiophene)gold(I)] with 0.080 g (0.17 mmol) of **24c** in 3 mL dichloromethane. The complex was purified by column chromatography on silica gel (ethyl acetate/petroleum ether 1:1) and afforded **25c** as an orange solid. (0.035 g, 29%). $^1\text{H NMR}$ (300 MHz, CDCl_3) δ 7.89–7.81 (m, 2H), 7.53–7.48 (m, 2H), 2.45 (s, 6H), 2.30 (q, $^3J_{\text{HH}} = 7.6$ Hz, 4H), 2.20 (q, $^3J_{\text{HH}} = 7.6$ Hz, 4H), 1.20 (s, 6H), 1.16 (dt, $^3J_{\text{HP}} = 20.2$ Hz, $^3J_{\text{HH}} = 7.5$ Hz, 6H), 0.98 (t, $^3J_{\text{HH}} = 7.5$ Hz, 6H), 0.28 (s, 6H) ppm; $^{13}\text{C}\{^1\text{H}\}$ NMR (75 MHz, CDCl_3) δ 151.4, 142.0 (d, $J_{\text{CP}} = 2.8$ Hz), 138.2, 133.8 (d, $J_{\text{CP}} = 12.7$ Hz), 133.2 (d, $J_{\text{CP}} = 14.5$ Hz), 130.1 (d, $J_{\text{CP}} =$

11.4 Hz), 128.6, 128.6, 128.4, 21.5 (d, $J_{CP} = 37.7$ Hz), 17.6, 14.8, 14.5, 12.0, 10.5 (br), 9.3 ppm; $^{31}\text{P}\{^1\text{H}\}$ NMR (121 MHz, CDCl_3) δ 35.7 ppm $^{11}\text{B}\{^1\text{H}\}$ NMR (128 MHz, CDCl_3) δ -0.9 ppm; IR (neat): $\tilde{\nu} = 2964$ (w), 2929 (w), 2871 (w), 1548 (s), 1453 (m), 1387 (w), 1360 (m), 1319 (s), 1261 (m), 1172 (s), 1145 (s), 1111 (s), 1063 (m), 1015 (m), 981 (s), 945 (s), 799 (s), 734 (m), 714 (m), 672 (m), 516 (m) cm^{-1} .

2.11.4 $[\text{Au}(\mathbf{24d})\text{Cl}]$ (**25d**)

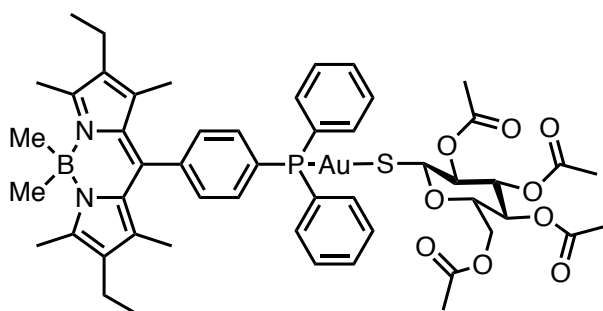


Reacting 0.08 g (0.25 mmol) of [chloro(tetrahydrothiophene)gold(I)] with 0.116 g (0.25 mmol) of **24d** in 4 mL anhydrous dichloromethane. The complex was purified by column chromatography on silica gel (dichloromethane/methanol 20:1) and yielded **25d** as an orange solid. (0.096 g, 55%). Crystals suitable for X-ray diffraction were formed from slow evaporation of toluene. ^1H NMR (300 MHz, Acetone- d_6) δ 8.18–8.09 (m, 2H), 7.57–7.51 (m, 2H), 4.75–4.60 (m, 4H), 2.88 (br s, 2H), 2.46 (s, 6H), 2.33 (q, $^3J_{\text{HH}} = 7.5$ Hz, 4H), 1.26 (s, 6H), 0.96 (t, $^3J_{\text{HH}} = 7.5$ Hz, 6H), 0.26 (s, 6H) ppm; $^{13}\text{C}\{^1\text{H}\}$ NMR (75 MHz, Acetone- d_6) δ 151.7, 141.8 (d, $J_{CP} = 2.7$ Hz), 139.9, 135.6 (d, $J_{CP} = 11.3$ Hz), 134.5, 133.5, 130.2 (d, $J_{CP} = 11.0$ Hz), 129.5, 128.3, 58.8 (d, $^1J_{CP} = 43.4$ Hz), 17.8, 15.0, 14.6, 12.3, 10.5 (br) ppm; $^{31}\text{P}\{^1\text{H}\}$ NMR (121 MHz, Acetone- d_6) δ 25.4 (s, 1P) ppm; $^{31}\text{P}-^1\text{H}$ NMR (121 MHz, Acetone- d_6) δ 25.4 (t, $J_{\text{PH}} = 11.6$ Hz) ppm; $^{11}\text{B}\{^1\text{H}\}$ NMR (96 MHz, Acetone- d_6) δ -1.2 (s, 1B) ppm; IR (neat): $\tilde{\nu} = 3399$ (br), 2960 (m), 2927 (w), 2868 (w), 1549 (s), 1452 (m), 1387 (m), 1359 (m), 1319 (s), 1262 (m), 1172 (s), 1145 (s), 1111 (m), 1034 (s), 981 (s), 944 (s), 909 (w), 799 (s), 735 (w), 703 (w), 672 (w) cm^{-1} ; TOF MS (ES^+) calcd for $\text{C}_{27}\text{H}_{39}\text{BN}_2\text{O}_2\text{PClAu}$ $[\text{M}+\text{H}]^+$ requires m/z 697.2196, found m/z 697.2341 (20.8 ppm).

2.12 General Procedure for the Synthesis of Fluorescent Gold(I)Thiosugar Complexes (**26a-d**)

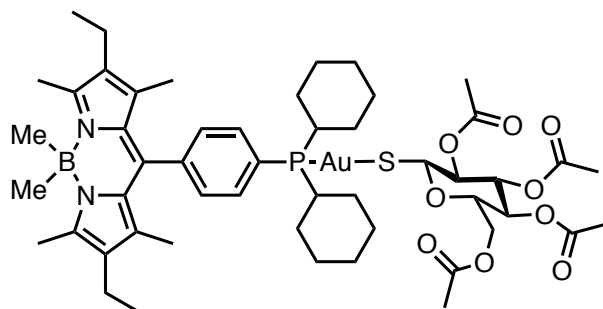
K₂CO₃ (1.2 eq) was dissolved in deionised water, cooled to 0 °C and added to a cooled (0 °C) solution of the corresponding gold(I) phosphine complex (1 eq) and 1-thio-β-D-glucose tetraacetate (1 eq) in dichloromethane. The biphasic reaction mixture was warmed to RT and stirred rapidly. Completion of reaction was confirmed by ³¹P{¹H} NMR and the layers were separated and extracted with dichloromethane (3 x 3 mL), then filtered through Celite. The solvent was removed *in vacuo* to yield the desired product.

2.12.1 [Au(**24a**)SR] (**26a**)



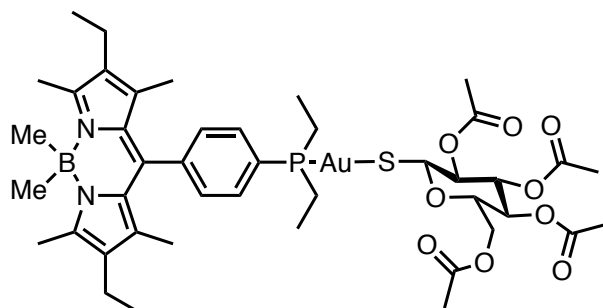
Reacting 0.05 g (0.14 mmol) of 1-thio-β-D-glucose tetraacetate, with 0.110 g (0.14 mmol) of **25a** in dichloromethane (4 mL), 0.021 g (0.15 mmol) of potassium carbonate in water (2 mL) to yield **26a** as an orange solid. (0.147 g, 97%). ¹H NMR (300 MHz, CDCl₃) δ 7.75–7.42 (m, 14H), 5.24–5.01 (m, 4H), 4.24 (dd, ²J_{HH} = 12.2 Hz, ³J_{HH} = 4.8 Hz, 1H), 4.12 (dd, ²J_{HH} = 12.2 Hz, ³J_{HH} = 2.5 Hz, 1H), 3.77 (m, 1H), 2.45 (s, 6H), 2.32 (q, ³J_{HH} = 7.5 Hz, 4H), 2.06 (s, 3H), 2.01 (s, 3H), 1.97 (s, 3H), 1.92 (s, 3H), 1.29 (s, 6H), 0.99 (t, ³J_{HH} = 7.5 Hz, 6H), 0.27 (s, 6H); ¹³C{¹H} NMR (75 MHz, CDCl₃) δ 170.8, 170.3, 169.6, 169.6, 151.2, 134.5 (d, J_{CP} = 14.1 Hz), 134.3 (dd, J_{CP} = 14.0, 2.9 Hz), 133.2, 132.9, 131.8 (d, J_{CP} = 2.5 Hz), 129.9, 129.8, 129.8, 129.3 (d, J_{CP} = 11.5 Hz), 129.2, 128.6, 83.1, 77.6, 77.2, 75.8, 74.2, 68.9, 62.9, 53.4, 21.2, 20.8, 20.7, 17.5, 14.7, 14.4, 12.1, 10.4 (br) ppm; ³¹P{¹H} NMR (121 MHz, CDCl₃) δ 38.3 (s, 1P) ppm; ¹¹B{¹H} NMR (96 MHz, CDCl₃) δ –1.5 (s, 1B) ppm; IR (neat): $\tilde{\nu}$ = 2962 (w), 2929 (w), 2255 (w), 1748 (s), 1549 (s), 1437 (m), 1361 (m), 1320 (m), 1221 (s), 1172 (s), 1145 (m), 1112 (m), 1033 (s), 981 (m), 945 (m), 907 cm^{–1}; TOF MS (ES⁺) calcd for C₅₁H₆₁AuBN₂O₉PSNa [M+Na]⁺ requires m/z 1139.3489, found m/z 1139.3508.

2.12.2 [Au(**24b**)SR] (**26b**)



Reacting 0.083 g (0.012 mmol) of 1-thio-β-D-glucose tetraacetate with 0.010 g (0.012 mmol) of **25b** in 1 mL dichloromethane and 0.002 g (0.014 mmol) of potassium carbonate in 1 mL water to yield **26b** as an orange solid. (0.013 g, 96%). ¹H NMR (300 MHz, CDCl₃) δ 7.82 (m, 2H), 7.48 (m, 2H), 5.31–5.00 (m, 4H), 4.25 (dd, ²J_{HH} = 12.1 Hz, ³J_{HH} = 5.0 Hz, 1H), 4.10 (dd, ²J_{HH} = 12.2 Hz, ³J_{HH} = 2.5 Hz, 1H), 3.80–3.71 (m, 1H), 2.46 (s, 6H), 2.31 (q, ³J_{HH} = 7.5 Hz, 4H), 2.09 (s, 3H), 2.02 (s, 3H), 2.01 (s, 3H), 1.97 (s, 3H), 1.94–1.56 (m, 10H), 1.47–1.03 (m, 12H), 1.23 (s, 6H), 0.98 (t, ³J_{HH} = 7.5 Hz, 6H), 0.28 (s, 6H) ppm; ³¹P{¹H} NMR (121 MHz, CDCl₃) δ 54.1 (s, 1P) ppm; ¹³C{¹H} NMR (75 MHz, CDCl₃) δ 170.9, 170.5, 169.7 (overlapping peaks), 151.3, 141.2, 138.6, 135.5 (d, J_{CP} = 11.9 Hz), 133.3, 133.0, 129.5 (d, J_{CP} = 10.3 Hz), 128.7, 126.7, 83.4, 75.8, 74.4, 69.2, 63.1, 53.6, 33.7, 33.4, 29.6, 28.5 (d, J_{CP} = 17.0 Hz), 26.5, 26.0, 21.3, 20.9, 20.8 (d, J_{CP} = 2.9 Hz), 17.6, 14.8, 14.5, 12.0, 10.5 (br) ppm; IR (neat): $\tilde{\nu}$ = 2961.7 (w), 2928.6 (w), 2853.4 (w), 1749.6 (s), 1551.6 (m), 1448.2 (w), 1361.6 (m), 1321.1 (w), 1258.3 (s), 1221.1 (s), 1172.9 (s), 1146.0 (m), 1090.2 (s), 1030.9 (s), 982.4 (m), 946.4 (m), 911.2 (w), 800.6 (s), 734.5 (w), 702.1 (w) cm⁻¹; TOF MS (ES⁺) calcd for C₅₁H₇₃AuBN₂O₉PSNa [M+Na]⁺ requires m/z 1151.4425, found m/z 1151.4446.

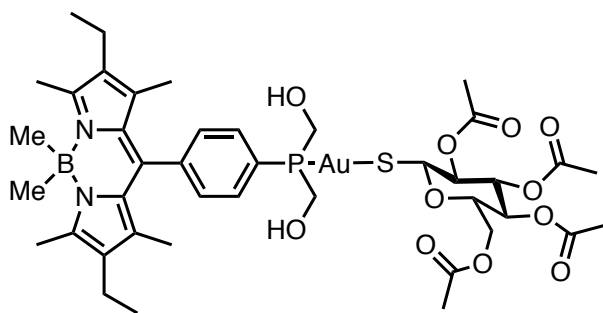
2.12.3 [Au(**24c**)SR] (**26c**)



Reacting 0.030 g (0.04 mmol) of 1-thio-β-D-glucose tetraacetate with 0.016 g (0.04 mmol) of **25c** in 1 mL dichloromethane, 0.007 g (0.05 mmol) of potassium carbonate in 0.5 mL water to yield **26c** as an orange solid. (0.034 g, 78%). ¹H NMR (300 MHz, CDCl₃) δ 7.97–7.71 (m, 2H), 7.54–7.41 (m, 2H), 5.27–4.93 (m, 4H), 4.25–4.16 (m, 1H), 4.11 (dd, ³J = 12.2 Hz, ⁴J_{HH} = 2.4 Hz,

1H), 3.84–3.69 (m, 1H), 2.44 (s, 6H), 2.30 (q, $^3J_{\text{HP}} = 7.6$ Hz, 4H), 2.18 (m, 4H), 2.12 (s, 3H), 2.09 (s, 3H), 2.08 (s, 3H), 2.02 (s, 3H), 1.21 (s, 6H), 0.97 (t, $^3J_{\text{HP}} = 7.5$ Hz, 6H), 0.97–0.77 (m, 6H), 0.27 (s, 6H) ppm; $^{13}\text{C}\{^1\text{H}\}$ NMR (75 MHz, CDCl_3) δ 170.8, 170.2, 169.4, 169.3, 151.3, 141.5, 138.5, 133.9 (d, $J_{\text{CP}} = 12.7$ Hz), 133.4, 132.9, 129.9 (d, $J_{\text{CP}} = 10.9$ Hz), 129.7, 128.9, 83.4, 74.4, 73.9, 69.8, 62.9, 61.7, 53.6, 21.3, 20.9, 20.8, 20.7 (d, $^1J_{\text{CP}} = 6.9$ Hz), 17.6, 14.8, 14.5, 11.9, 10.4 (br), 9.3 (d, $^2J_{\text{CP}} = 4.1$ Hz) ppm; $^{31}\text{P}\{^1\text{H}\}$ NMR (121 MHz, CDCl_3) δ 40.7 (s, 1P) ppm; $^{11}\text{B}\{^1\text{H}\}$ NMR (128 MHz, CDCl_3) δ –0.7 ppm; IR (neat): $\tilde{\nu} = 2963$ (w), 2931 (w), 1749 (s), 1551 (m), 1455 (m), 1407 (m), 1362 (m), 1291 (m), 1219 (s), 1173 (s), 1146 (m), 1090 (m), 1031 (s), 946 (m), 910 (m), 801 (s), 733 (m), 673 (w), 598 (w), 531 (w), 517 (w) cm^{-1} ; TOF MS (ES^+) calcd for $\text{C}_{43}\text{H}_{62}\text{AuBN}_2\text{O}_9\text{PS}$ $[\text{M}+\text{H}]^+$ requires m/z 1021.3672, found m/z 1021.3663.

2.12.4 [Au(24d)SR] (26d)



Reacting 0.021 g (0.06 mmol) of 1-thio- β -D-glucose tetraacetate with 0.040 g (0.06 mmol) of **25d** in 2 mL dichloromethane, 0.009 g (0.06 mmol) of potassium carbonate in 1 mL water to yield **26d** as an orange solid. (0.054 g, 88%). ^1H NMR (300 MHz, CDCl_3) δ 7.99 (m, 2H), 7.54–7.45 (m, 2H), 5.31–5.04 (m, 4H), 4.73–4.61 (m, 4H), 4.28 (dd, $^2J_{\text{HH}} = 12.4$ Hz, $^3J_{\text{HH}} = 4.8$ Hz, 1H), 4.16 (d, $^2J_{\text{HH}} = 12.1$ Hz, 1H), 3.93 (br s, 1H), 3.77 (br s, 2H), 2.45 (s, 6H), 2.30 (q, $^3J_{\text{HH}} = 7.4$ Hz, 4H), 2.12 (s, 3H), 2.05 (s, 3H), 2.02 (s, 3H), 1.98 (s, 3H), 1.22 (s, 6H), 0.97 (t, $^3J_{\text{HH}} = 7.4$ Hz, 6H), 0.27 (s, 6H) ppm; $^{13}\text{C}\{^1\text{H}\}$ NMR (75 MHz, CDCl_3) δ 171.0, 170.3, 169.8 (overlapping peaks), 151.4, 142.0, 138.4, 134.4 (d, $J_{\text{CP}} = 11.6$ Hz), 133.5, 133.0, 130.0 (d, $J_{\text{CP}} = 10.5$ Hz), 128.7, 126.8, 83.4, 77.9, 77.4, 76.1, 74.2, 68.8, 62.7, 59.9–59.1 (m), 21.5, 21.00, 20.8 (d, $^1J_{\text{CP}} = 3.9$ Hz), 17.6, 14.8, 14.5, 12.2, 10.5 ppm; $^{11}\text{B}\{^1\text{H}\}$ NMR (128 MHz, CDCl_3) δ –0.3 (s, 1B) ppm; IR (neat): $\tilde{\nu} = 3457$ (br), 2963 (w), 2931 (w), 2871 (w), 2255 (w), 1749 (s), 1549 (s), 1471 (m), 1433 (m), 1361 (m), 1321 (m), 1220 (s), 1172 (s), 1146 (m), 1112 (m), 1033 (s), 981 (m), 906 (s), 799 (m), 727 (s), 672 (m), 647 (m), 598 (m), 556 (w) cm^{-1} ; TOF MS (ES^+) calcd for $\text{C}_{41}\text{H}_{57}\text{BN}_2\text{O}_{11}\text{PSAuNa}$ $[\text{M}+\text{Na}]^+$ requires m/z 1047.3077, found m/z 1047.3591.

2.13 References

- 1 Z. Huaizhi and N. Yuantao, *Gold Bull.*, 2000, **33**, 103–105.
- 2 C. Frank Shaw III, *Chem. Rev.*, 1999, **99**, 2589–2600.
- 3 B. Wu, X. Yang and M. Yan, *J. Med. Chem.*, 2019, **62**, 7751–7768.
- 4 E. V Capparelli, R. Bricker-Ford, M. J. Rogers, J. H. McKerrow and S. L. Reed, *Antimicrob. Agents Chemother.*, 2017, **61**, e01947-16.
- 5 T. Onodera, I. Momose and M. Kawada, *Chem. Pharm. Bull.*, 2019, **67**, 186–191.
- 6 J. M. Madeira, D. L. Gibson, W. F. Kean and A. Klegeris, *Inflammopharmacology*, 2012, **20**, 297–306.
- 7 A. Debnath, M. Ndao and S. L. Reed, *Gut Microbes*, 2013, **4**, 66–71.
- 8 R. Y. Cheung, J. C. Cohen and P. Illingworth, *Health Law J.*, 2004, **12**, 183–200.
- 9 O. Wellman-Labadie and Y. Zhou, *Health Policy*, 2010, **95**, 216–228.
- 10 B. M. Sutton, *Gold Bull.*, 1986, **19**, 15–16.
- 11 S. T. Crooke and C. K. Mirabelli, *Am. J. Med.*, 1983, **75**, 109–113.
- 12 Z. Y. Pessetto, S. J. Weir, G. Sethi, M. A. Broward and A. K. Godwin, *Mol. Cancer Ther.*, 2013, **12**, 1299–1309.
- 13 N. Tejman-Yarden, Y. Miyamoto, D. Leitsch, J. Santini, A. Debnath, J. Gut, J. H. McKerrow, S. L. Reed and L. Eckmann, *Antimicrob. Agents Chemother.*, 2013, **57**, 2029–2035.
- 14 C. Roder and M. J. Thomson, *Drugs R. D.*, 2015, **15**, 13–20.
- 15 J. M. Madeira, C. J. Renschler, B. Mueller, S. Hashioka, D. L. Gibson and A. Klegeris, *Life Sci.*, 2013, **92**, 1072–1080.
- 16 J. M. Madeira, E. Bajwa, M. J. Stuart, S. Hashioka and A. Klegeris, *J. Neuroimmunol.*, 2014, **276**, 71–79.
- 17 S. Jackson-Rosario, D. Cowart, A. Myers, R. Tarrien, R. L. Levine, R. A. Scott and W. T. Self, *J. Biol. Inorg. Chem.*, 2009, **14**, 507–519.
- 18 S. Jackson-Rosario and W. T. Self, *J. Bacteriol.*, 2009, **191**, 4035–4040.
- 19 Y. Hokai, B. Jurkowicz, J. Fernández-Gallargo, N. Zakirkhodjaev, M. Sanaú, T. R. Muth and M. Contel, *J. Inorg. Biochem.*, 2014, **138**, 81–88.
- 20 C. Roder and E. Athan, *Drugs R. D.*, 2020, **20**, 209–216.

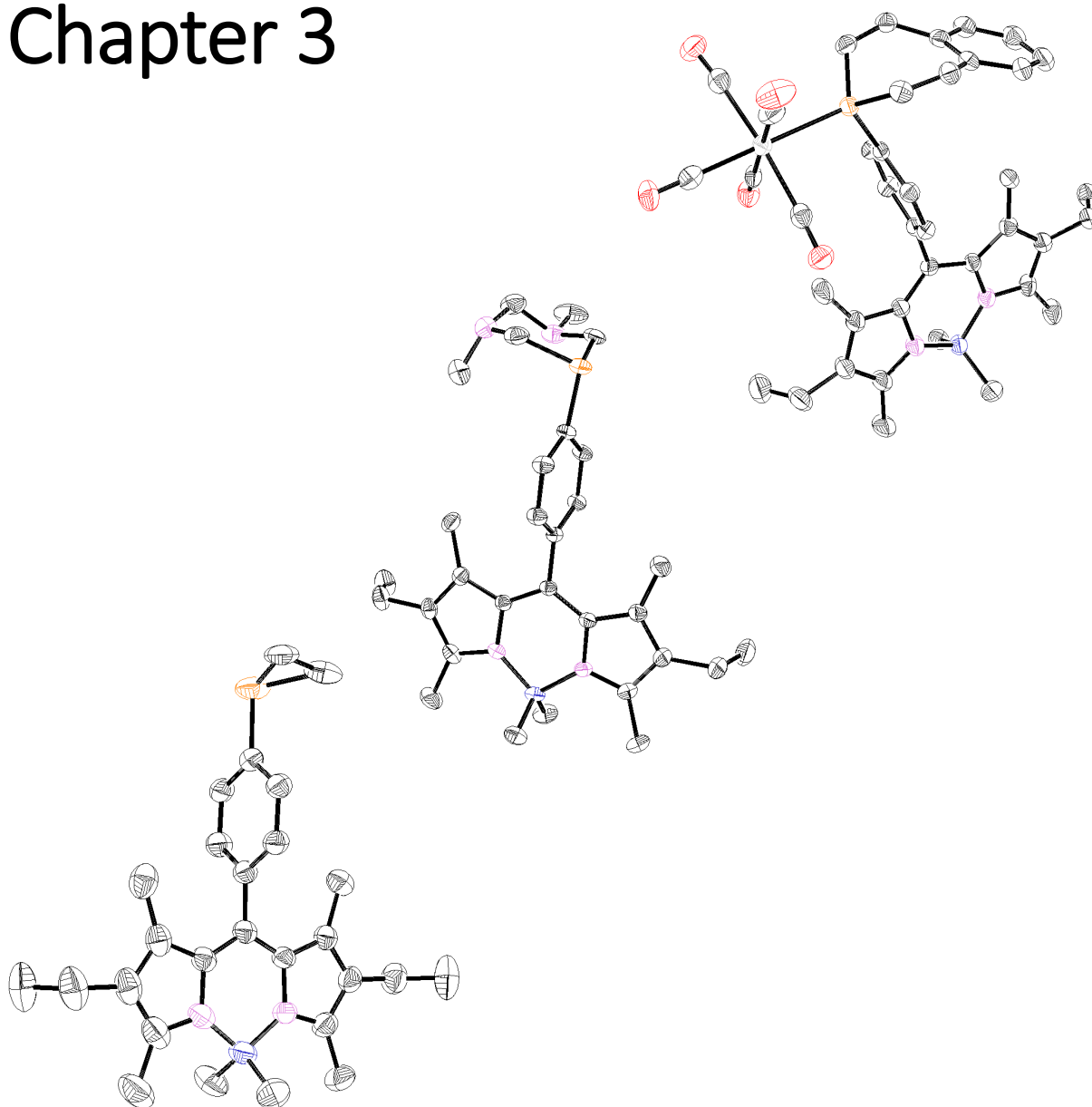
- 21 C. Fan, W. Zheng, X. Fu, X. Li, Y.-S. Wong and T. Chen, *Cell Death Dis.*, 2014, **5**, e1191–e1191.
- 22 W. Fiskus, N. Saba, M. Shen, M. Ghias, J. Liu, S. Das Gupta, L. Chauhan, R. Rao, S. Gunewardena, K. Schorno, C. P. Austin, K. Maddocks, J. Byrd, A. Melnick, P. Huang, A. Wiestner and K. N. Bhalla, *Cancer Res.*, 2014, **74**, 2520–2532.
- 23 C. Marzano, V. Gandin, A. Folda, G. Scutari, A. Bindoli and M. P. Rigobello, *Free Radic. Biol. Med.*, 2007, **42**, 872–881.
- 24 I. L. Shytaj, B. Chirullo, W. Wagner, M. G. Ferrari, R. Sgarbanti, A. Della Corte, C. LaBranche, L. Lopalco, A. T. Palamara, D. Montefiori, M. G. Lewis, E. Garaci and A. Savarino, *Retrovirology*, 2013, **10**, 71.
- 25 B. Chirullo, R. Sgarbanti, D. Limongi, I. L. Shytaj, D. Alvarez, B. Das, A. Boe, S. DaFonseca, N. Chomont, L. Liotta, E. III Petricoin, S. Norelli, E. Pelosi, E. Garaci, A. Savarino and A. T. Palamara, *Cell Death Dis.*, 2013, **4**, e944–e944.
- 26 T. D. Epstein, B. Wu, K. D. Moulton, M. Yan and D. H. Dube, *ACS Infect. Dis.*, 2019, **5**, 1682–1687.
- 27 S. S. Gunatilleke and A. M. Barrios, *J. Med. Chem.*, 2006, **49**, 3933–3937.
- 28 S. S. Gunatilleke, C. A. F. de Oliveira, J. A. McCammon and A. M. Barrios, *J. Biol. Inorg. Chem.*, 2008, **13**, 555–561.
- 29 J. Carlos Lima and L. Rodriguez, *Anticancer. Agents Med. Chem.*, 2012, **11**, 921–928.
- 30 C. A. Tolman, *Chem. Rev.*, 1977, **77**, 313–348.
- 31 N. C. Baenziger, W. E. Bennett and D. M. Soboroff, *Acta Crystallogr. Sect. B*, 1976, **32**, 962–963.
- 32 M. P. Chrysouli, C. N. Banti, N. Kourkouvelis, N. Panayiotou, G. S. Markopoulos, A. J. Tasiopoulos and S. K. Hadjikakou, *J. Inorg. Biochem.*, 2018, **179**, 107–120.
- 33 M. R. Karver, D. Krishnamurthy, R. A. Kulkarni, N. Bottini and A. M. Barrios, *J. Med. Chem.*, 2009, **52**, 6912–6918.
- 34 J. A. Muir, S. I. Cuadrado and M. M. Muir, *Acta Crystallogr. Sect. C*, 1991, **47**, 1072–1074.
- 35 N. Pillarsetty, K. K. Katti, T. J. Hoffman, W. A. Volkert, K. V Katti, H. Kamei and T. Koide, *J. Med. Chem.*, 2003, **46**, 1130–1132.
- 36 S. Tapanelli, A. Habluetzel, M. Pellei, L. Marchiò, A. Tombesi, A. Capparè and C. Santini,

J. Inorg. Biochem., 2017, **166**, 1–4.

- 37 J. Wang, X. Mi, J. Wang and Y. Yang, *Green Chem.*, 2017, **19**, 634–637.
- 38 V. A. Rassadin, V. P. Boyarskiy and V. Yu. Kukushkin, *Org. Lett.*, 2015, **17**, 3502–3505.
- 39 I. A. Guzei, I. Arachchige and S. A. Ivanov, *Acta Crystallogr. Sect. C*, 2010, **66**, m55–m57.
- 40 J. A. Muir, S. I. Cuadrado and M. M. Muir, *Acta Crystallogr. Sect. C*, 1991, **47**, 1072–1074.
- 41 K. Kang, S. Liu, T. Xu, D. Wang, X. Leng, R. Bai, Y. Lan and Q. Shen, *Organometallics*, 2017, **36**, 4727–4740.
- 42 J. A. Muir, M. M. Muir, L. B. Pulgar, P. G. Jones and G. M. Sheldrick, *Acta Crystallogr. Sect. C*, 1985, **41**, 1174–1176.
- 43 S. Linert, S. Wagner, P. Schmidt, L. Higham, C. Hepples, P. Waddell and K. Karaghiosoff, *Phosphorus Sulfur Silicon Relat Elem*, 2019, **194**, 565–568.
- 44 Z. Assefa, M. A. Omary, B. G. McBurnett, A. A. Mohamed, H. H. Patterson, R. J. Staples and J. P. Fackler, *Inorg. Chem.*, 2002, **41**, 6274–6280.
- 45 M. Weishäupl, C. Robl, W. Weigand, S. Kowalski and F. Mohr, *Inorg. Chim. Acta*, 2011, **374**, 171–174.
- 46 S. Kenzler, M. Kotsch and A. Schnepf, *Eur. J. Inorg. Chem.*, 2018, 3840–3848.
- 47 E. Vergara, E. Cerrada, C. Clavel, A. Casini and M. Laguna, *Dalton Trans.*, 2011, **40**, 10927–10935.
- 48 P. S. Pregosin and E. D. Becker, *Helv. Chim. Acta*, 1983, **66**, 1436–1440.
- 49 L. K. Batchelor, E. Păunescu, M. Soudani, R. Scopelliti and P. J. Dyson, *Inorg. Chem.*, 2017, **56**, 9617–9633.
- 50 E. Vergara, S. Miranda, F. Mohr, E. Cerrada, E. R. T. Tiekink, P. Romero, A. Mendía and M. Laguna, *Eur. J. Inorg. Chem.*, 2007, 2926–2933.
- 51 L. J. Higham, M. K. Whittlesey and P. T. Wood, *Dalton Trans.*, 2004, 4202–4208.
- 52 R. C. Elder and M. K. Eidsness, *Chem. Rev.*, 2002, **87**, 1027–1046.
- 53 J.-G. Kang, H.-K. Cho, C. Park, S.-S. Yun, J.-K. Kim, G. A. Broker, D. R. Smyth and E. R. T. Tiekink, *Inorg. Chem.*, 2007, **46**, 8228–8237.
- 54 S. Chen, G. Dong, S. Wu, N. Liu, W. Zhang and C. Sheng, *Acta Pharm. Sin. B*, 2019, **9**, 144–156.

- 55 B. Zhou, P. Jiang, J. Lu and C. Xing, *Arch. Pharm. (Weinheim)*., 2016, **349**, 1–14.
- 56 W. L. Yu, G. Guizzunti, T. L. Foley, M. D. Burkart and J. J. La Clair, *J. Nat. Prod.*, 2010, **73**, 1659–1666.
- 57 M. R. L. Stone, M. S. Butler, W. Phetsang, M. A. Cooper and M. A. T. Blaskovich, *Trends Biotechnol.*, 2018, **36**, 523–536.
- 58 L. H. Davies, J. F. Wallis, M. R. Probert and L. J. Higham, *Synthesis*, 2014, **46**, 2622–2628.
- 59 L. H. Davies, R. W. Harrington, W. Clegg and L. J. Higham, *Dalton Trans.*, 2014, **43**, 13485–13499.
- 60 E. W. Randall and D. Shaw, *Mol. Phys.*, 1965, **10**, 41–48.
- 61 B. E. Mann, *J. Chem. Soc. Perkin Trans. 2*, 1972, 30.
- 62 M. J. Irwin, J. J. Vittal, G. P. A. Yap and R. J. Puddephatt, *J. Am. Chem. Soc.*, 1996, **118**, 13101–13102.
- 63 N. Inoue, Y. Suzuki, K. Yokoyama and I. Karube, *Biosci. Biotechnol. Biochem.*, 2009, **73**, 1215–1217.
- 64 N. Soh, O. Sakawaki, K. Makihara, Y. Odo, T. Fukaminato, T. Kawai, M. Irie and T. Imato, *Bioorg. Med. Chem.*, 2005, **13**, 1131–1139.
- 65 M. Onoda, S. Uchiyama, A. Endo, H. Tokuyama, T. Santa and K. Imai, *Org. Lett.*, 2003, **5**, 1459–1461.
- 66 K. Akasaka, T. Suzuki, H. Ohruai and H. Meguro, *Anal. Lett.*, 1987, **20**, 731–745.
- 67 J. Pan, J. A. Downing, J. L. McHale and M. Xian, *Mol. Biosyst.*, 2009, **5**, 918–920.
- 68 T. Hatakeyama, S. Hashimoto and M. Nakamura, *Org. Lett.*, 2011, **13**, 2130–2133.
- 69 S. Cai, Y. Lu, S. He, F. Wei, L. Zhao and X. Zeng, *Chem. Commun.*, 2013, **49**, 822–824.
- 70 J. C. Vaughan, G. T. Dempsey, E. Sun and X. Zhuang, *J. Am. Chem. Soc.*, 2013, **135**, 1197–1200.
- 71 R. Uson, A. Laguna, M. Laguna, D. A. Briggs, H. H. Murray and J. P. Fackler Jr., *Inorg. Synth.*, 1989, 85–91.
- 72 S. S. Zalesskiy, A. E. Sedykh, A. S. Kashin and V. P. Ananikov, *J. Am. Chem. Soc.*, 2013, **135**, 3550–3559.

Chapter 3



Phosphacycles from a Fluorescent Air-Stable Primary Phosphine

A detailed discussion regarding azacycles of ring sizes three to seven which are prevalent in natural products, and their less known analogous phosphacycles is presented.

We then describe the synthesis of three fluorescent phosphacycles of varying ring sizes. Their structural characteristics and σ -donor/ π -acceptor properties have been evaluated by X-ray crystallographic studies and their coordination to group 6 metal complexes.

We will see that this opens up potential applications in areas as diverse as cell imaging and ethylene trimerization.

3 Phosphacycles from a Fluorescent Air Stable Primary Phosphine

This chapter will focus on the synthesis and characterisation of three fluorescent compounds containing a phosphorus atom within different sized ring systems – the general name for which are phosphacycles. The chapter will begin by reviewing phosphacycles of increasing ring size (three to seven) in the literature, with particular attention given to their geometries, syntheses and reactivities. A short discussion on the nitrogen-containing analogues will be detailed in order to set our work in context, with emphasis on their prevalence in nature and their biological applications. The synthesis of the three novel, fluorescent phosphacycles from an air stable primary phosphine will then be discussed.

Firstly, the synthesis of a three membered phosphacycle (a phosphirane) will be presented, and its air and thermal stability will be explored. Coordination studies with group-six molybdenum and tungsten metal carbonyl complexes were carried out to determine the stereoelectronic properties of the ligand. The attempted quarternisation of this phosphirane to afford a phosphiranium salt will be detailed, for which it was envisaged that the resultant product could have applications as a multimodal imaging agent.

Secondly, research into a fluorescent six-membered phosphacycle which has been carried out in a collaborative project with Dr Randolph Köhn at the University of Bath will be introduced. The synthesis of this 1,3,5-diazaphosphinane, from its 1,3,5-triaza precursor and a fluorescent primary phosphine will be detailed. Comparisons to its triaza-analogue will be highlighted and initial studies into its properties as a ligand in catalytic hexene trimerization will be reported. The initial findings of a collaborative project with Professor Bill Henderson at the University of Waikato, New Zealand will then be highlighted. We will introduce how our fluorescent hydroxymethylphosphine (potential precursor to the 1,3,5-diazaphosphinane) can be used in the fluorescent labelling of amine modified surfaces.


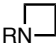
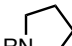
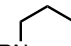
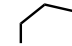

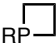
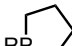
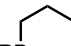
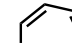
Finally, an unsaturated seven-membered phosphorus ring, a phosphepine, will be introduced. Initially, the synthesis of this ring structure from pre-bound primary phosphine group 6 pentacarbonyl complexes will be detailed and the electronic properties discussed. In addition, a short synthetic study was carried out to explore the possible synthesis of this phosphepine without the pre-bound metal.

3.1 Phosphacycles

Phosphacycles are few and far between in comparison to their nitrogen analogues, which are common in both natural products¹ and biologically active compounds.² Azetidines, for example, are commonly found in antibiotics including penicillin in the form of a β -lactam.³

Table 3.1 displays the structures and nomenclature of both aza- and phosphacycles from ring sizes three to seven. A discussion of each cycle will be carried out in turn, in order of their increasing ring sizes.

Table 3.1 Nomenclature and structures for aza and phosphacycles of $L(CH_2)_n$ where $n = 2-6$, $L = P$ or N .

$L(CH_2)_n$	$n = 2$	$n = 3$	$n = 4$	$n = 5$	$n = 6$
L = N	Aziridine	Azetidine	Pyrrolidine	Piperidine	Azepane
					
L = P	Phosphirane	Phosphetane	Phospholane	Phosphinane	Phosphepine ^a
					

^aThe saturated rings are termed phosphhepanes, however, the focus here is on the more commonly known, unsaturated phosphepines.

3.1.1 Three-Membered Heterocycles

Aziridines are the well-known, three membered cyclic amines. Their associated ring strain makes them highly reactive compounds, and they are notable for their powerful alkylating ability. Conversely, this moiety can be found in many natural products, some of which are known to display bioactivity.⁴ Thus, these highly reactive groups have seen aziridine containing compounds become recognised in their application as anticancer agents as their ability to alkylate DNA leads to toxicity *in vivo*.⁵ PBI and Mitomycin, illustrated in Figure 3.1, represent two classes of aziridine-containing natural products which exhibit anticancer activity through their ability to crosslink between DNA strands.

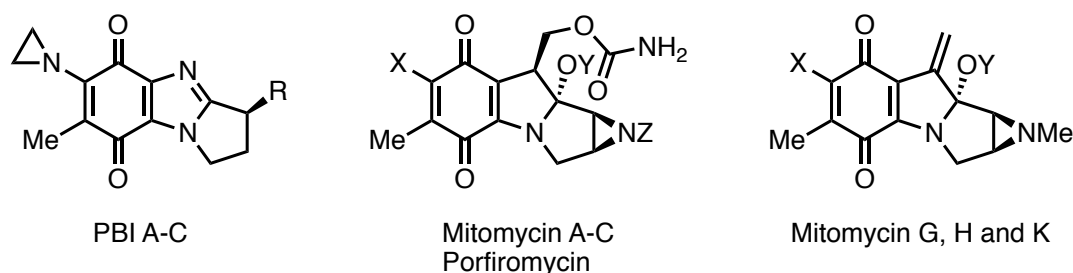
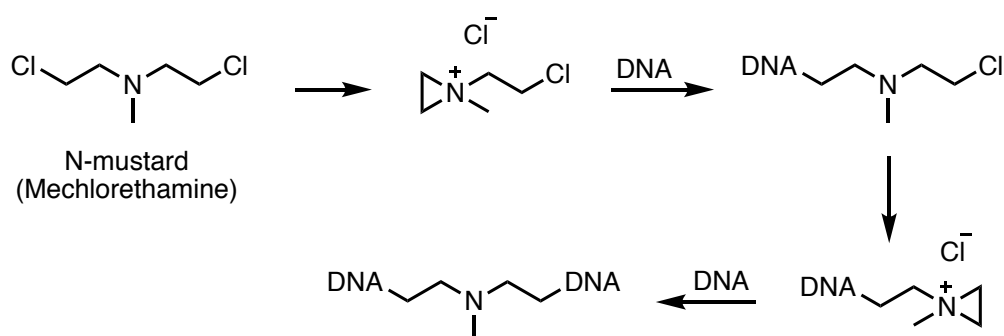


Figure 3.1 PBI-A ($R = OAc$), PBI-B ($R = OCONH_2$), PBI-C ($R = H$), Mitomycin A ($X = OMe$, $Y = Me$, $Z = H$), Mitomycin B ($X = OMe$, $Y = H$, $Z = Me$), Mitomycin C ($X = NH_2$, $Y = Me$, $Z = H$), Portiromycin ($X = NH_2$, $Y = Me$, $Z = Me$), Mitomycin G ($X = NH_2$, $Y = Me$), Mitomycin H ($X = OMe$, $Y = H$), Mitomycin K ($X = OMe$, $Y = Me$).

The aziridine moiety has been identified as essential for the bioactivity of mitomycins, through the structure-activity relationship, signifying the importance of the group.⁵

Aziridines are highly nucleophilic which enables their facile reaction to afford aziridinium ions. The enhanced reactivity of the ion in comparison to the aziridine makes them common intermediates and therefore they are not often isolated; their formation is inferred from the nature of the reaction products.⁶

Nitrogen mustard and its functionalised derivatives are a class of compounds which also form DNA interstrand crosslinks. To do so, they go via an aziridinium salt intermediate which has been illustrated in Scheme 3.1. Mechlorethamine is used to treat Hodgkin's lymphoma.⁷



Scheme 3.1 The route of N-mustard to form DNA interstrand crosslinks via the aziridinium salt.

3.1.2 Three-Membered Phosphacycles

Three membered phosphacycles – the phosphiranes are an underdeveloped class of tertiary phosphine.^{8,9} The cycles possess significant ring strain, presented by a small sum of the bond angles at the phosphorus atom ($\Sigma(\text{P}) < 275^\circ$) with a C-P-C bond angle of approximately 50° . These small bond angles give the phosphiranes increased pyramidalised structures and thus, increased s character of the phosphorus lone pair, which is exhibited by lowered HOMO and LUMO energy levels in comparison to their four, five and six membered counterparts and acyclic tertiary phosphines. These lowered orbitals give rise to unusual electronic properties, resulting in poorer σ -donor properties, but improved π -acceptor properties (Figure 3.2).

A characteristic feature of phosphiranes is their remarkably upfield ^{31}P NMR chemical shifts which commonly occur around $\delta -230$ ppm. This can be attributed to the high s character of the phosphorus lone pair which results in very strong shielding.¹⁰

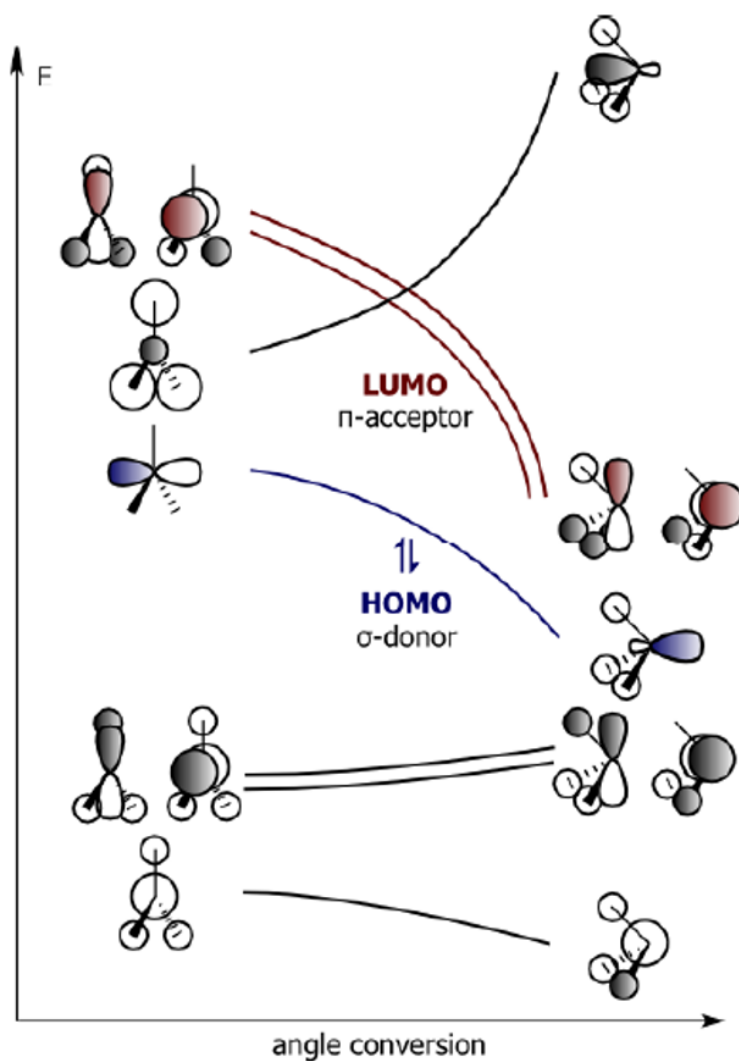
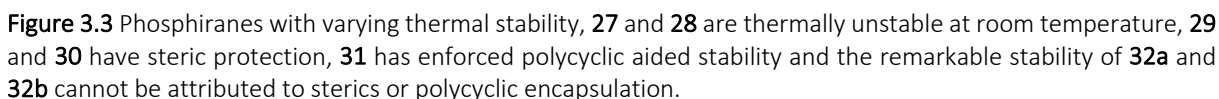


Figure 3.2 Walsh diagram showing the conversion of a trigonal planar molecule (D_{3h}) to a pyramidal molecule (C_{3v}) and its effect on the HOMO and LUMO energy levels.¹¹

Phosphiranes are often thought of as unstable, particularly when heated and degradation to secondary ethyl phosphines, ethylene and polymeric side products have been described.^{8,9,12} Parent phosphine **27**, synthesised by Wagner *et al.* in 1967, decomposes completely in 24 hours at room temperature¹³ and phenylphosphirane **28**, is only stable for one month at 0 °C and shows decomposition at higher temperatures.^{14,15,16} Bulky substituents have lent themselves to improved stability, for example, **29**, is a distillable liquid¹⁷ and **30** is a crystalline solid.¹⁸ Grützmacher *et al.* demonstrated an alternate way of increasing thermal stability, by incorporating the phosphacycle into a polycyclic structure. They developed a family of phosphiranes, coined BABAR-Phos **31**, which have demonstrated resistance to decomposition.^{19,20,11,21} This resistance to decomposition however, has hindered their reactivity and they resist alkylation with the strong methylating agent, methyl trifluoromethanesulfonate²² and display only weak coordination to metal complexes.²¹



33a-e

34a-f R = Me
34a-c R = Allyl, Bn, Et

Scheme 3.2 The alkylation of arylphosphiranes to phosphiranium salt by Gasnot *et al.*²⁵

Azetidines are four-membered nitrogen heterocycles which can be found in natural products;²⁶ they are prevalent in antibiotics as β -lactams, such as in penicillin.²⁷ They can also be found in pharmaceuticals including Calblock,²⁸ a calcium channel blocker, and Cotellic,²⁹ a targeted BRAF V600 mutation-positive advanced melanoma therapy drug. It has been reported that it is the strained nature of the ring that is responsible for the antibacterial properties.²⁶ The structures of these compounds are shown in Figure 3.4.

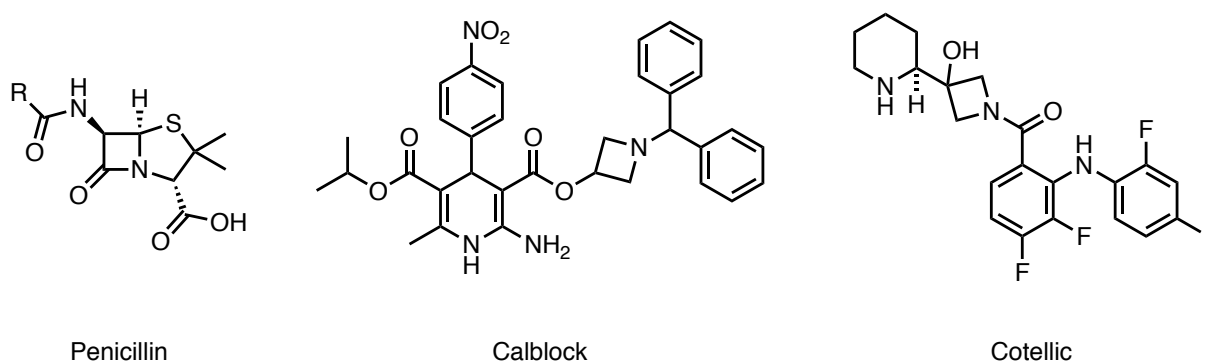
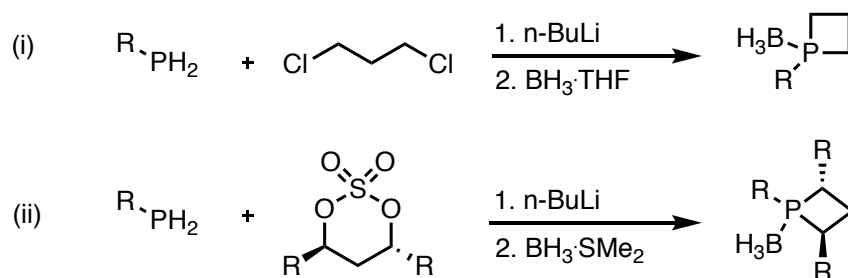


Figure 3.4 Azetidine containing pharmaceuticals, Penicillin, Calblock and Cotellic.

Phosphetanes have been discovered and developed over the last 60 years, with the first synthetic approach by McBride *et al.* in 1962.³⁰ Their electronic properties are drastically different from the phosphiranes. With the insertion of a CH₂ group, the shielding of the phosphorus lone pair is reduced to the lowest of all the phosphacycles, with a downfield shift of approximately 250 ppm in the ³¹P{¹H} NMR spectrum to δ 13.9 ppm for the phenyl derivative.¹⁰ This is the highest frequency of all the phosphacycles and can be attributed to both the hybridisation (essentially sp²) and having the smallest HOMO/LUMO gap.¹⁰ Phosphetanes exhibit partial ring strain for which intracyclic angles around the phosphorus have been reported between 72–86°.^{31–36}

The four-membered ring can be synthesised in a number of different ways, some of which are detailed by Kollár and Keglevich in their review of *P-Heterocycles as Ligands in Homogeneous Catalytic Reactions*.³⁷ This includes the double deprotonation of a primary phosphine with *n*-butyllithium, followed by the cyclisation with 1,3-dichloropropane (Scheme 3.3, (i))³⁸ or the synthesis of enantiopure cycles from primary phosphines and enantiomerically pure, cyclic sulfates (Scheme 3.3, (ii)), with each phosphetane being protected as its borane adduct in these cases.³² A more detailed synthetic review can be found in *Phosphorus-Carbon Heterocyclic Chemistry*, chapters 3.1³⁹ and 3.2.⁴⁰



Scheme 3.3 Two synthetic procedures for the synthesis of phosphetanes from primary phosphines.

The reactivity of phosphetanes is not dissimilar to acyclic tertiary phosphines. Unlike phosphiranes, phosphetanes can be readily alkylated to their corresponding phosphetanium

salts and this has been shown with benzyl bromide,⁴¹ methyl bromide⁴² and methyl iodide.⁴³ Oxidation occurs from reaction with hydrogen peroxide⁴² and phosphetane sulfides can be made from reaction with elemental sulfur.⁴⁴ Initial studies have shown that it is possible to reduce phosphetane oxides with trichlorosilane or triethylamine to their corresponding phosphetanes.⁴²

The major application of phosphetanes lies in catalysis, particularly enantiomerically pure phosphetanes for asymmetric catalysis, and in P^{III}/P^V redox cycling catalysis.⁴⁵ FerroTANE, first reported by Marinetti⁴⁶ and Burk,⁴⁷ has been used in a multitude of catalytic reactions including palladium-catalysed C–P coupling,⁴⁸ rhodium-catalysed hydrogenation,⁴⁶ ruthenium-catalysed hydrogenation⁴⁹ and iridium-catalysed [2+2+2] cycloaddition⁵⁰ with high conversions and ees of up to 99%.

Most recently, Werner *et al.* detailed a phosphetane oxide catalyst which enables phosphorus P^{III}/P^V redox cycling. This catalyst selectively reduces alkenes to alkanes in the presence of water with yields of up to 99%. Poly(methylhydrosiloxane) was used as the terminal reductant, three equivalents of water as a source of hydrogen and butylacetate as the solvent.⁵¹

Further reviews by Kollár and Keglevich,³⁷ Marinetti and Carmichael,³⁹ and Kawashima⁴⁰ can be found in the literature.

3.1.4 Five-Membered Heterocycles

Five-membered nitrogen-containing cycles, the pyrrolidines, are again found in natural products (pyrrolidine alkaloids)⁵² and pharmaceuticals. Two examples of pyrrolidine alkaloids are the highly addictive substance, nicotine, and 2,5-dihydroxymethyl-3,4-dihydropyrrolidine (DMDP), which has been tested as a glycoprotein processing inhibitor.⁵³ Furthermore, a pyrrolidine containing pharmaceutical, Levetiracetam, is used as a treatment for epilepsy.⁵⁴ These natural products are shown in Figure 3.5.

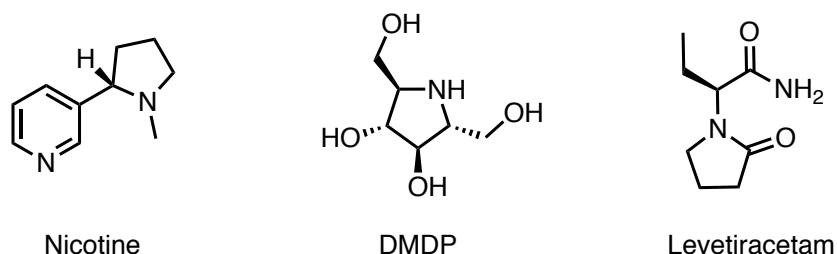
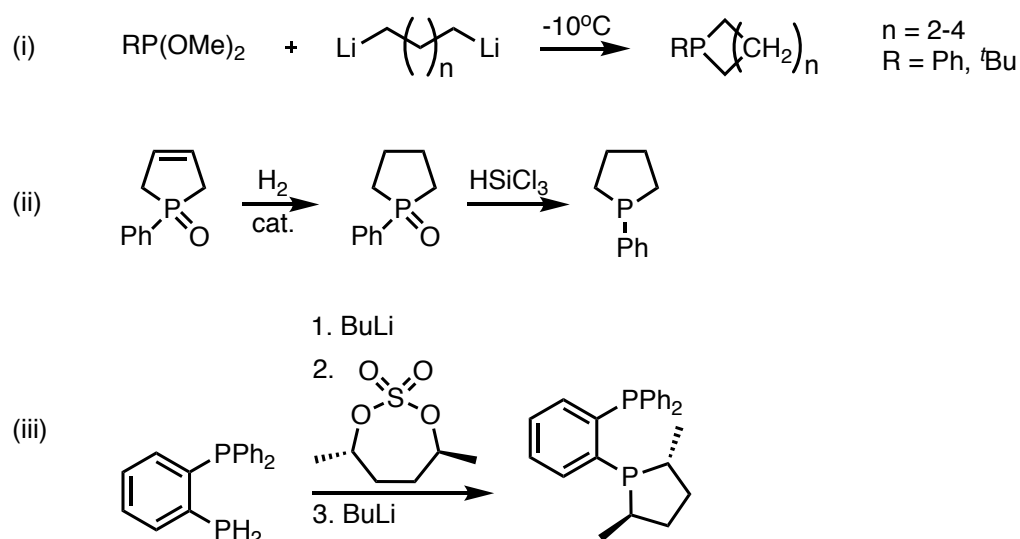


Figure 3.5 Pyrrolidine containing natural products, nicotine, DMDP and Levetiracetam (an epilepsy medication).

Phospholanes are relatively unstrained in comparison to their three- and four-membered counterparts, displaying intracyclic C–P–C bond angles of approximately 90–100°^{55,56}

(calculated optimised geometry of parent phospholane of 91.77°¹⁰). Relative to phosphiranes and phosphetanes, the 'normal' level of shielding results in a ³¹P NMR shift of ~ δ –15.3 ppm.¹⁰ The reported syntheses of phospholanes is similar to those reported for phosphetanes. A few examples are shown in Scheme 3.4. Jolly *et al.* reported the synthesis of butyl and *tert*-butyl phospholanes in a reaction between dimethylphosphite and 1,4-dilithiobutane.⁵⁷ This procedure was extended by Pringle *et al.* to the synthesis of five- to seven-membered phosphacycles with both *tert*-butyl and phenyl substituents.⁵⁸ Saturated phospholanes can also be obtained from the hydrogenation of phospholene oxides which are subsequently reduced to phospholanes with silanes ((ii) Scheme 3.4).⁵⁹ Like phosphetanes, enantiopure phospholanes can be synthesised from primary phosphines and enantiopure cyclic sulfates ((iii) Scheme 3.4).^{60,61}



Scheme 3.4 Three synthetic procedures for the synthesis of phospholanes from various starting materials.

Again, much like phosphetanes, the reactivity of phospholanes is not very different from acyclic tertiary phosphines. Phospholanes are sensitive to oxidation, yet, the reduction of the resulting oxides has been demonstrated with lithium aluminium hydride and silanes, and the resultant P(III)-cycles can be isolated and stored as their borane adducts.⁶² Phospholanium salts can be synthesised by the alkylation of phospholanes and have shown applications in asymmetric rhodium-catalysed hydrogenation reactions.⁶³

More so than their phospholanium salts, phospholanes themselves have been established as ligands in a range of catalytic reactions. Two ligands developed by Burk *et al.* are bis(dimethylphospholano)ethane (BPE) and DuPHOS (Figure 3.6) which are based on two 2,5-alkyl-substituted phospholanes, differing only by the connecting 1,2-phenylene or 1,2-ethylene bridge.^{64,65} BPE has applications in the asymmetric reduction of carbonyl bonds

under hydrogenation conditions⁶⁶ and DuPhos complexes have shown remarkable enantioselectivities in a wide range of catalytic transformations. DuPhos has been used as a ligand in a range of rhodium-catalysed enantioselective hydrogenation to form C–N, C–C and C–O stereogenic centres.⁶⁴

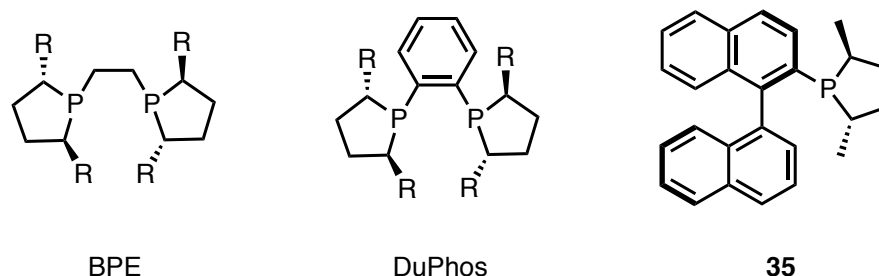


Figure 3.6 Examples of enantiopure phospholanes with applications in catalysis.

The Higham group prepared four phospholanes based on enantiopure BINAP backbones, one of which is shown in Figure 3.6. This phospholane was used as a ligand in Pd-catalysed asymmetric hydrosilylation of styrene to give 1-phenylethanol, the best result giving 100% conversion and 73% ee.⁶¹ Reviews have been published by Kee⁶⁷ and Kollár and Keglevich³⁷ which give further information on phospholanes.

3.1.5 Six-Membered Heterocycles

The six-membered azacycle, known as piperidine, can be extracted from natural products, including black pepper⁶⁸ and is a common reagent and ligand in chemistry. This structural motif can be found in a number of alkaloids and has been used as a building block in many pharmaceuticals.⁶⁹ Some examples shown in Figure 3.7 include Ritalin (ADHD medication),⁷⁰ Paxil (antidepressant),⁷¹ and Minoxidil (antihypertensive vasodilator).⁷²

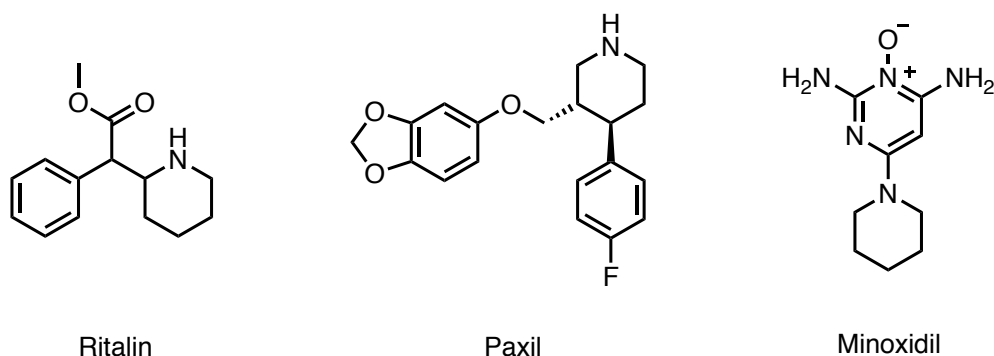
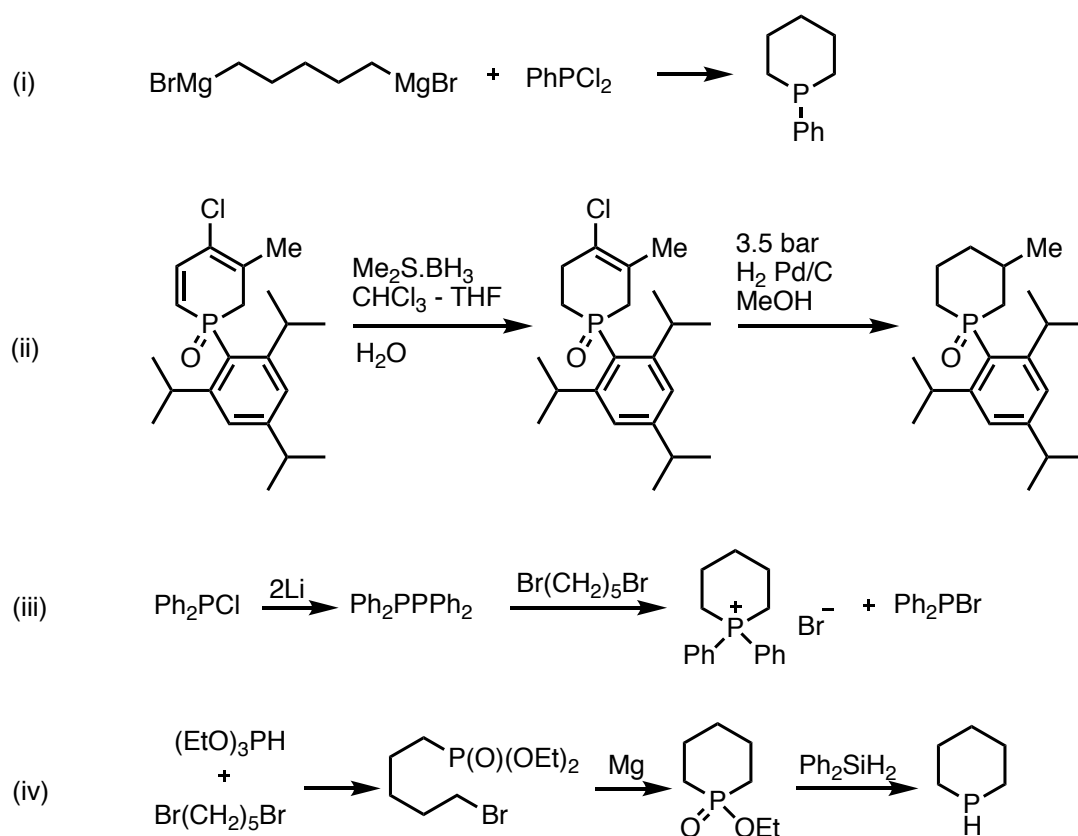


Figure 3.7 Piperidine containing pharmaceuticals: Ritalin, Paxil and Minoxidil.

According to Gallagher, phosphinanes (previously known as phosphorinanes) show no indication of ring strain and they commonly exhibit a conformationally mobile chair geometry which shows flattening at the phosphorus atom.⁷³ The optimised geometry of parent

phosphinane shows C–P–C intracyclic angles of 98.08° and the ^{31}P NMR resonance is upfield of the phosphetanes at δ –34.3 ppm.¹⁰

Much like the four- and five-membered phosphacycles, phosphinanes can be synthesised by a variety of methods. 1-phenyl-phosphinane was initially synthesised in 1915 by Grüttner, and Wiernik,⁷⁴ by reaction of 1,5-bromomagnesium pentane with dichlorophenylphosphine (Scheme 3.5, (i)). Additional synthetic procedures have since been developed, some of which are also shown in Scheme 3.5. Formation of the saturated ring can occur both from the hydrogenation of their unsaturated cycles, or from cyclisation reactions.



Scheme 3.5 Four synthetic procedures for the synthesis of phosphinanes from various starting materials.

Cyclisation reactions are commonly designed to result in the formation of either phosphinanium salts (Scheme 3.5 (iii))⁷⁵, or phosphinane oxides (Scheme 3.5 (iv))⁷⁶ which, if required, can subsequently be reduced.⁷⁷ For further information, a synthetic review has been published by Gallagher,⁷³ but it should be noted that the synthesis of enantiopure phosphinanes from primary phosphines with cyclic sulfates has not yet been reported.

There are fewer examples of phosphinanes as ligands in catalysis, with their unsaturated counterparts featuring much more heavily. Shekhar *et al.* however, reported the synthesis and application of a series of biaryl phosphinane ligands in palladium-catalysed C–N and C–O cross-coupling reactions.⁷⁸ Pringle *et al.* prepared a series of phenyl and tert-butyl

phosphacycle ligands (ring sizes: five, six and seven) and examined their activity in the rhodium-catalysed hydroformylation of 1-octene. As part of this study, platinum complexes, with the general formula $[\text{Pt}(\text{L})_2\text{Cl}_2]$ (where L = phosphacycles), were also synthesised, and a discussion of the geometries and stereoelectronic properties of the ligands was given.⁵⁸ Given the number of compounds with the piperidine motif, one would perhaps expect to see more examples of its phosphorus analogues. Further discussion of six-membered phosphacycles, containing additional heteroatoms, will be given in Section 3.9.

3.1.6 Seven-Membered Heterocycles

Unsaturated seven membered phosphacycles – the phosphepines – are sparsely reported in comparison to their nitrogen analogues, the azepines/benzoazepines which are found in synthetic drugs including i) Benazepril⁷⁹ – an antihypertensive agent, ii) Varenicline,⁸⁰ a treatment for nicotine addiction and iii) Imipramine,⁸¹ used in the treatment of depression.

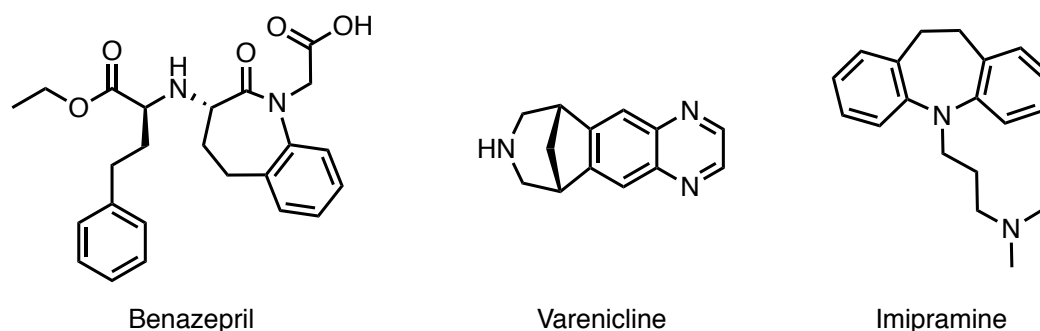


Figure 3.8 Pharmaceuticals containing the seven-membered nitrogen cycles, Benazepril, Varenicline and Imipramine.

Very few azepines with three double bonds have been reported, yet there is a motivation to synthesise new azepine systems in the hope of preparing novel biologically active compounds.⁸²

The chemistry of unsaturated seven-membered phosphacycles is very limited and research to date has predominantly focused on their synthesis and stability.^{83,84} Phosphepines can be divided into two groups, dependant on whether they have two or three carbon-carbon double bonds. The majority of research for those with two double bonds contain a binaphthyl backbone which displays axial chirality and allows for their application in asymmetric catalysis. For example, phosphepines **36** and **37** (Figure 3.9) have been reported by the Fu group for their catalytic abilities in the '*Doubly Stereoconvergent γ -Additions of Racemic Heterocycles to Racemic Allenates*'⁸⁵ and the '*Enantioselective carbon–sulfur bond formation: γ additions of aryl thiols to allenates*'⁸⁶ respectively.

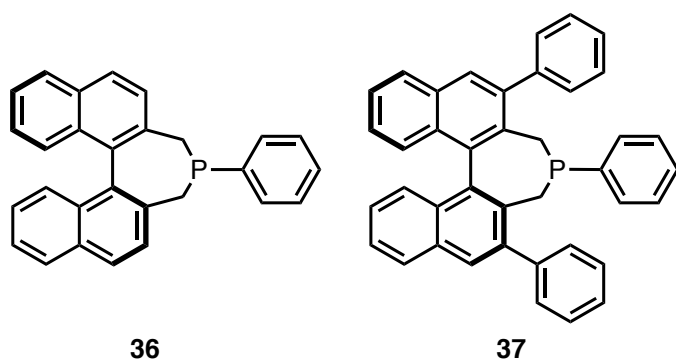


Figure 3.9 Examples of phosphepines containing binaphthyl backbones, **36** and **37**.

For our study however, we are interested in 3-benzophosphepines. Research in this area has predominantly been carried out by three groups: Märkl,⁸³ Tsuchiya^{87,88} and Lammertsma.^{84,89} However, more recent work by Delouche *et al.* has developed a series of π -extended phosphepines which show potential as semiconductors in p-type organic field-effect transistors (OFETs) and solid-state lighting applications.⁹⁰

The phosphepine, 3-phenyl-3-benzophosphepine **38** (Figure 3.10) was first synthesised by Märkl *et al.* in 1983⁸³ after his former attempts to produce it via the reduction of phenyl phosphepine oxide **39** (Figure 3.10), were unsuccessful.⁹¹ Studies were later carried out by Tsuchiya *et al.* on the synthesis of 1-benzoheteropines, inclusive of silepines, germepines, phosphepines (**40**, Figure 3.10) and arsepines. Flash vacuum pyrolysis (FVP) of 2a,7b-dihydrocyclobuta[*b*]-1-benzophosphole resulted in valence isomerisation and ring opening to form 1-benzophosphepine oxide in 85% yield which could subsequently be reduced to **40** by trichlorosilane.⁹² They later reported a milder synthesis of 1- and 3-benzometallopines via a 1,6-dilithium intermediate which will be discussed further in Section 3.15.1.^{87,93}

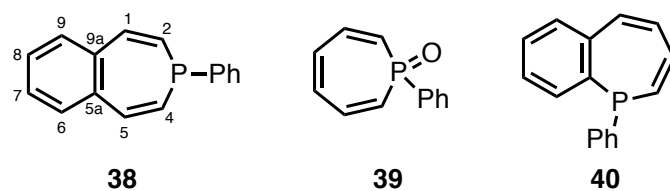
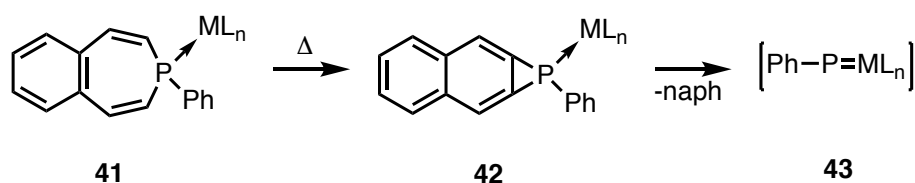


Figure 3.10 Phosphepines, 3-phenyl-3-benzophosphepine (**38**), phosphepine oxide (**39**) and 1-phenyl-1-benzophosphepine (**40**).

Both 3- and 1-benzophosphepines **38** and **40** have demonstrated thermal instability in solution, resulting in phosphorus extrusion via a norcaradiene intermediate, giving naphthalene as the degradation product. Lammertsma *et al.* took advantage of this degradation pathway and demonstrated that by introducing a transition metal to the phosphepine, the degradation of the phosphepine ligand resulted in the generation of a phosphinidene complex, as illustrated in Scheme 3.6.⁸⁴



Scheme 3.6 Proposed route of heteroatom extrusion from the 3H-benzophosphepine metal complex (**41**), via phosphanorcaradiene complex (**42**), resulting in phosphinidene complex formation (**43**).

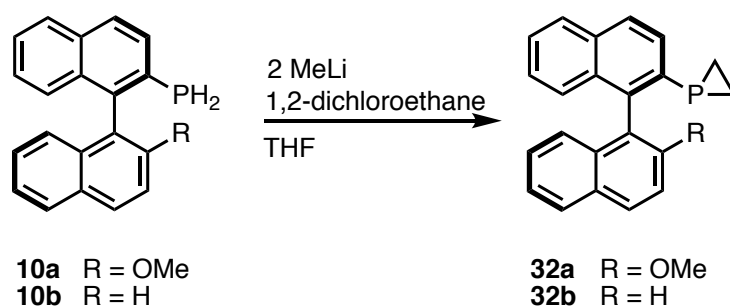
It was noted that the coordination of **38** to a transition metal destabilises the phosphanorcaradiene with respect to the 3-benzophosphepine. This is due to an antibonding interaction that weakens the C–C bond formed in the valence isomerisation, resulting in phosphaphines which are more stable in terms of decomposition. These 3-benzophosphepine complexes inspired the following work in this chapter in the synthesis of a fluorescent analogue of these uncommon seven-membered rings.

To summarise, the chemistry of the respective phosphacycles discussed above appears to vary depending on the ring size, particularly when ring strain leads to geometries at the phosphorus atom that are very different to their acyclic counterparts. Given that our group can readily access air-stable primary phosphines, which ought to be able to act as a convenient precursor in phosphacycle syntheses, we were keen to explore the possibility of accessing novel fluorescent phosphacycles as they may possess unique properties which could expand their applications in medicinal chemistry.

3.2 Results and Discussion

3.2.1 Highly Stable Phosphirane

In 2011, our group reported the synthesis of the chiral phosphiranes **32a** and **32b** (Scheme 3.7) and demonstrated that the incorporation of a backbone with extended π -conjugation resulted in phosphiranes with both remarkable air and thermal stability, and reactivity.

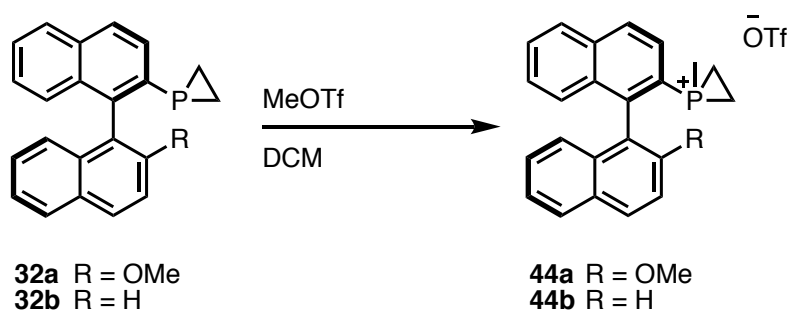


Scheme 3.7 Synthesis of MOP phosphiranes **32a/b** from primary phosphines **10a/b** with MeLi and 1,2-DCE in THF.

As with their primary phosphine precursors (**10a** and **10b**), our group^{94,95,96} demonstrated that the additional π -conjugation also led to the air and thermally stable compounds **32a** and **32b**,

which were inert towards air oxidation in both the solid and solution state over seven days. They also demonstrated thermal stability when heated in refluxing in toluene overnight and displayed no degradation by $^{31}\text{P}\{^1\text{H}\}$ NMR spectroscopy, a property which very few phosphiranes portray (Section 3.1.2). On reaction with *cis*-[Pt(η^2 : η^2 cod)Cl₂], both **32a** and **32b** resulted in rapid coordination to form the *cis*-[Pt(**32a/32b**)₂Cl₂] complexes **49a** and **49b**.²⁴

As mentioned in the earlier introduction, Section 3.1.2, the attempted quarternisation of phosphiranes often results in degradation of the cycle,⁹⁷ or in no reaction in the case of the more thermally stable phosphirane, BABAR Phos.²³ Remarkably, **32a** and **32b**, were readily alkylated, like 1-phenylphosphirane,¹⁹ by methyl trifluoromethanesulfonate to their corresponding phosphiranium salts **44a** and **44b** in quantitative yield. This is illustrated in Scheme 3.8. The phosphiranium salts displayed characteristic $^{31}\text{P}\{^1\text{H}\}$ NMR shifts at δ –101.2 and δ –102.0 ppm for **44a** and **44b** respectively.



Scheme 3.8 Alkylation of **32a** and **32b** with methyl trifluoromethanesulfonate in dichloromethane to afford the phosphiranium salts **44a** and **44b**.

The remarkable properties of these stable phosphiranes, their extremely low ^{31}P NMR spectroscopic chemical shifts, and the ability to alkylate them to give the phosphiranium salts, led to the consideration of how a fluorescent analogue based on Bodipy would behave. As Bodipy primary phosphine **14** is another example of an air stable primary phosphine, stabilised by π -conjugation, it was of interest to explore its behaviour in the attempted synthesis of the corresponding fluorescent phosphirane, in order to ascertain if the resultant product was thermally stable and could also be alkylated. A fluorescent phosphiranium salt has the potential for exploitation as a multimodal imaging agent.

3.3 Multimodal Imaging

If an external phosphorus-containing agent was to be used in ^{31}P MRS, ensuring that the signal did not overlap with endogenous phosphorus compounds in the body (*ca.* δ –5 to 25 ppm),⁹⁸ would be critical to the success of it. The phosphonium salts **45** and **46** (Figure 3.11) reported by our group have ^{31}P NMR chemical shifts of δ 34.5 and δ 22.6 ppm respectively, which come

close to the endogenous ^{31}P signals within the body. However, the MOP phosphiranium salts gave signals at $\delta -101.2$ and $\delta -102.0$ ppm for **44a** and **44b** respectively.

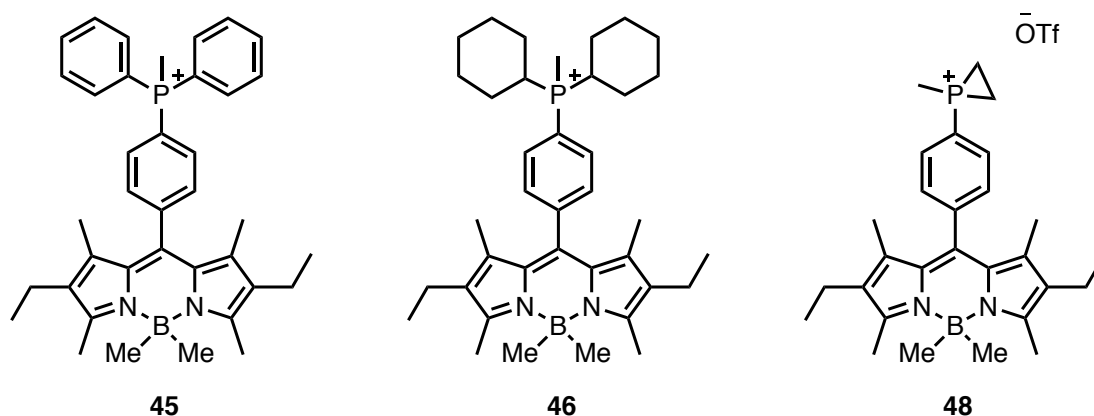
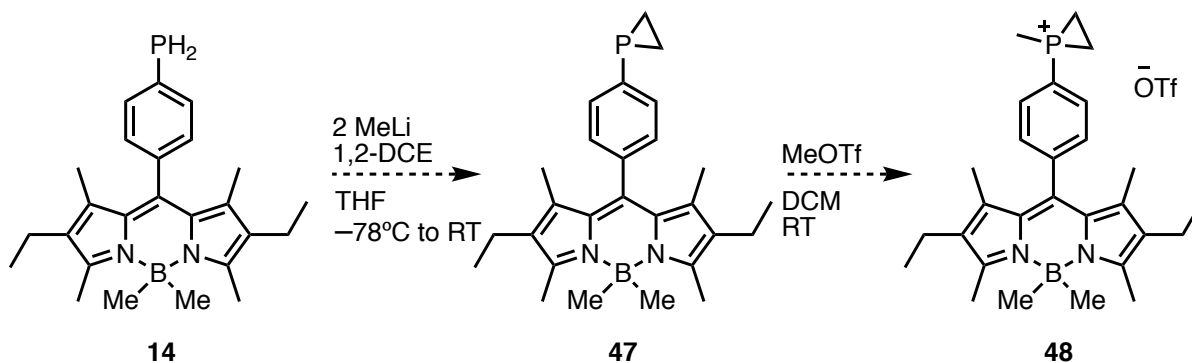


Figure 3.11 Mitochondrial specific imaging agents (**45** and **46**) and the structure of phosphiranium salt **48**.

In the following section, efforts towards the synthesis of **47** will be described (Scheme 3.9). The primary objective was to isolate and purify **47**. Structural and spectroscopic characterisation follows, which allows an investigation of whether the remarkable air- and thermal-stability displayed by MOP phosphirane **32a** and **32b** are too, present in **47**. Efforts to obtain the phosphonium salt **48**, which would have desirable multimodal imaging properties, as described above, will follow.

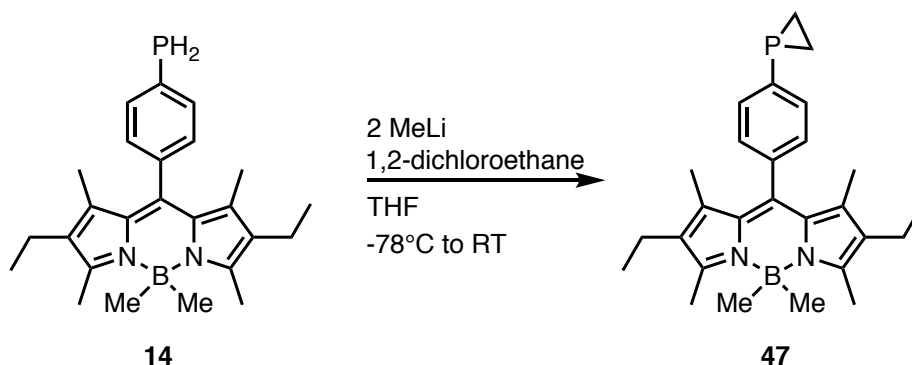


Scheme 3.9 Proposed reaction scheme for the synthesis of a fluorescent phosphiranium salt from **14**.

3.4 Synthesis of a Novel Fluorescent Phosphirane **47**

Following the procedure by our group to develop MOP phosphiranes **32a** and **32b** (Section 3.2.1, Scheme 3.7),⁹⁹ the primary phosphine **14** was dilithiated in a double deprotonation reaction with two equivalents of methyllithium at -78°C . This cooled dilithiated compound was subsequently treated with 1,2-dichloroethane and warmed to room temperature – the reaction was monitored by $^{31}\text{P}\{^1\text{H}\}$ NMR spectroscopy. Upon completion of the reaction, purification was carried out by an aqueous quench, biphasic separation and extraction with

diethyl ether. Following this, column chromatography with petroleum ether/dichloromethane (7:3) afforded the desired phosphirane compound **47** in 34% yield (Scheme 3.10).



Scheme 3.10 Synthesis of Bodipy phosphirane **47** from the fluorescent primary phosphine **14**.

The structure of Bodipy phosphirane **47** was confirmed by analysis of the $^{31}\text{P}\{^1\text{H}\}$ NMR spectrum which displayed a characteristic signal at $\delta -237.2$ ppm. This data is in line with the previously reported phenylphosphirane, which showed a signal in the $^{31}\text{P}\{^1\text{H}\}$ NMR spectrum at $\delta -237.0$ ppm and **32a** and **32b** at $\delta -235.4$ ppm and $\delta -235.0$ ppm respectively.¹⁵ Furthermore, on analysis of the $^{31}\text{P}-^1\text{H}$ NMR spectrum of **47**, a triplet of triplets at $\delta -237.2$ ppm ($J_{\text{PH}} = 15.7$ Hz and 7.6 Hz) was observed. This signal can be rationalised by the presence of *endo* and *exo* protons, as illustrated in Figure 3.12. The two *endo* protons are chemically equivalent – therefore only show one resonance – but, they are magnetically inequivalent, and the same for the two *exo* protons, thus, resulting in an AA'BB'X spin system.

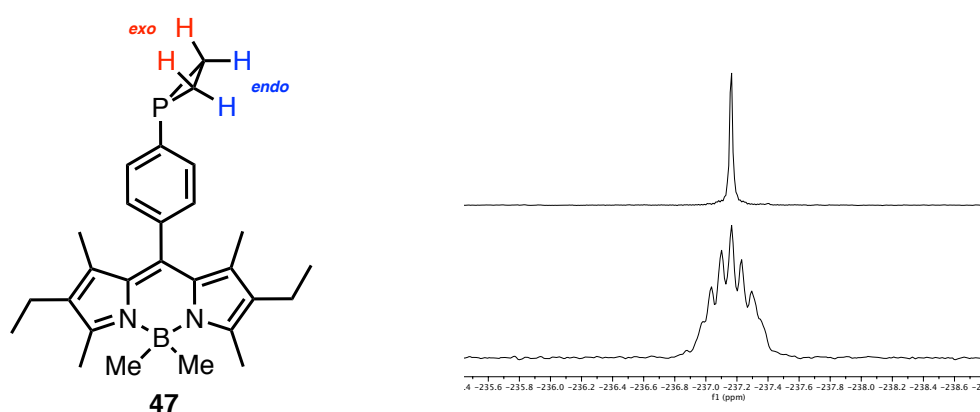
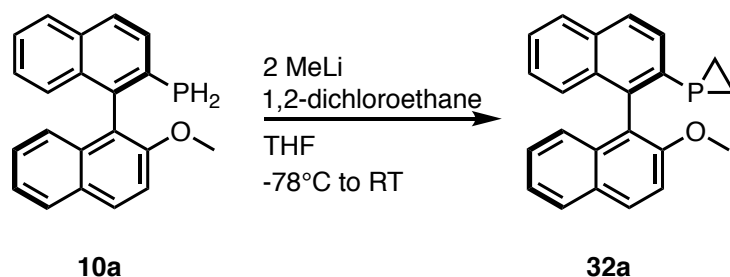


Figure 3.12 Labelling of the inequivalent *endo* and *exo* protons of phosphirane **47** (left) which is demonstrated by the triplet of triplets shown in the $^{31}\text{P}-^1\text{H}$ NMR spectrum (right).

Due to this spin system, the two CH_2 groups in the phosphirane cycle display as a complex multiplet in the ^1H NMR spectrum, further confirming the presence of *endo* and *exo* protons and likely, additional coupling to a proton on the phenyl ring. Only one environment at $\delta 10.6$ ppm (d, $J_{\text{CP}} = 39.7$ Hz) is observed in the $^{13}\text{C}\{^1\text{H}\}$ NMR spectrum for the two carbons within the ring, thus demonstrating the chemical and magnetic equivalence of the carbons. For

comparative studies, the synthesis of MOP phosphirane, **32a** was also carried out (Scheme 3.11) and the NMR spectra analysed.



Scheme 3.11 Synthesis of the MOP phosphirane **32a** from the air-stable primary phosphine **10a**.

Due to the chirality of **32a**, four separate proton environments are observed in the ^1H NMR spectrum confirming the inequivalence of the protons in the heterocycle. In this case, we observe H-*endo1*, H-*endo2*, H-*exo1* and H-*exo2*. The ^{31}P – ^1H spectrum shows an apparent, or pseudo triplet, but strictly is a doublet of doublets of doublets of doublets, with four $^2J_{\text{PH}}$ couplings. The apparent triplet can be rationalised as two of the couplings being very close to zero (*ca.* 1.5 Hz) and the other two couplings are similar to each other ($^2J_{\text{PH}} \approx 18.1$ Hz). This has been illustrated in Figure 3.13. In addition, in the ^1H NMR spectrum, we observe Nuclear Overhauser Effect (NOE) correlations of the two *endo* protons to the aromatic proton which has also been illustrated.

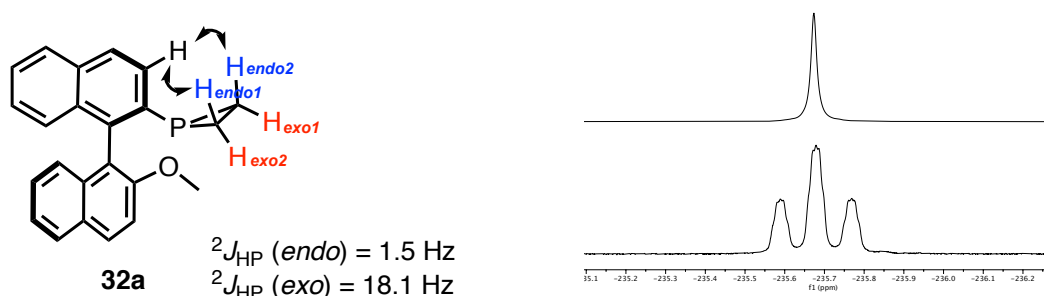


Figure 3.13 Labelling of the four inequivalent *endo1*, *endo2*, *exo1* and *exo2* protons of the phosphirane **32a** (left) which is observed as an apparent triplet in the ^{31}P – ^1H NMR spectrum (right).

In addition to the NMR spectroscopic data obtained, crystals suitable for X-ray diffraction of both **32a** and **47** were grown from slow evaporation of dichloromethane, for direct comparison of the solid-state structures of the two phosphiranes. Neither the **32a** nor **47** structures have previously been analysed by X-ray crystallography. The molecular structures are displayed in Figure 3.14.

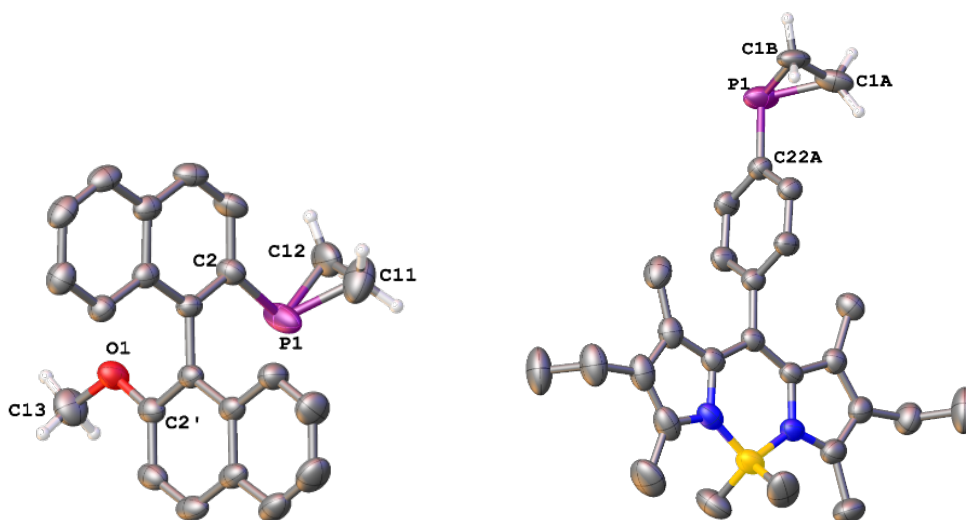


Figure 3.14 View of the molecular structure of **32a** (left). Hydrogen atoms bound to carbon have been omitted for clarity. Selected bond distances [Å] and angles [°]: P1-C1A 1.856(9), P1-C1B 1.856(9), P1-C22A 1.833(10), C1A-C1B 1.542(16), C1B-P1-C1A 49.1(1), C22A-P1-C1A 99.1(4), C22A-P1-C1B 102.6(8), C1B-C1A-P1 65.4(5), C1A-C1B-P1 65.5(5). View of the molecular structure of **47** (right). Hydrogen atoms bound to carbon have been omitted for clarity. Selected bond distances [Å] and angles [°]: P1-C2 1.841(5), P1-C11 1.830(7), P1-C12 1.804(6), O1-C2' 1.372(5), O1-C13 1.424(6), C11-C12 1.427(9), C11-P1-C2 101.8(3), C12-P1-C2 104.0(3), C12-P1-C11 46.2(3), C2'-O1-C13 118.8(4).

The solid-state structures display similar intracyclic bond angles: C1A-P1-C1B of 49.1(1)° for **32a** and C11-P1-C12, of 46.2(3)° for **47**, indicative of the expected severe ring strain. The sum of the bond angles at the phosphorus atom gave $\Sigma(P)$ 250.8° for **32a** and 252.0° for **47**.

3.5 Phosphirane Air- and Thermal-Stability Studies

Following the successful synthesis of phosphirane **47**, it was important to test its air and thermal stability. MOP phosphiranes **32a** and **32b** were air-stable in solution (CDCl₃) and in the solid state over seven days and were also found to be thermally stable at 110 °C when refluxed in toluene overnight – no degradation or oxidation products were observed. Therefore, in order to establish the air and thermal stability of **47**, the same procedures were followed.

3.5.1 Air-Stability Studies of Phosphirane **47**

For oxidation measurements in the solid state, 20 mg of **47** was weighed out into a vial in air and stored in the dark. This was then analysed by ³¹P{¹H} NMR spectroscopy, with NOE removed, on day one and on day seven. Consistent with **32a** and **32b**, **47** showed no evidence of oxidation or degradation within this time frame by ³¹P{¹H} NMR spectroscopy.

For the solution state air-stability test, 20 mg of **47** was placed in an NMR tube and dissolved in *d*-chloroform (0.6 mL). The resulting solution was stored in the dark, open to air. Analysis by ³¹P{¹H} NMR spectroscopy with NOE removed, was carried out daily for seven days; again,

like MOP phosphiranes **32a** and **32b**, the fluorescent analogue **47** showed no sign of oxidation or degradation in solution.

3.5.2 Thermal-Stability Studies of Phosphirane **47**

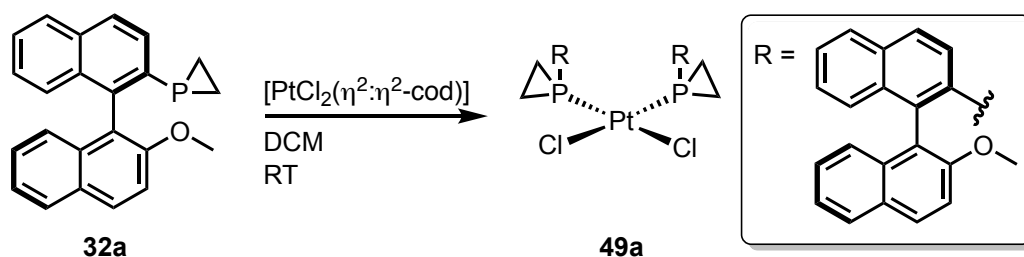
Bodipy phosphirane **47** was dissolved in anhydrous toluene and refluxed under nitrogen for 16 hours – the same conditions as those used for **32a** and **32b**. $^{31}\text{P}\{^1\text{H}\}$ NMR spectra were obtained before and after **47** was subject to reflux conditions; **47** displayed no degradation or ring opening products. This implies that, like with the binaphthyl backbone of **32a** and **32b**, the presence of extended π -conjugation provided by the aromatic system may stabilise the phosphirane towards thermal and oxidative decomposition.

3.6 Coordination Studies

To date, some examples of phosphiranes as ligands have been reported.^{9,19,21} Li *et al.* hypothesised that phosphiranes should be good ligands due to their small cone angle and reported that the coordination to a metal increases the stability of phosphiranes, allowing them to be handled in air.¹⁵ Therefore, it was anticipated that this would be the case for our novel fluorescent phosphirane **47**.

3.6.1 Synthesis of a *cis*-Platinum(II) Complex

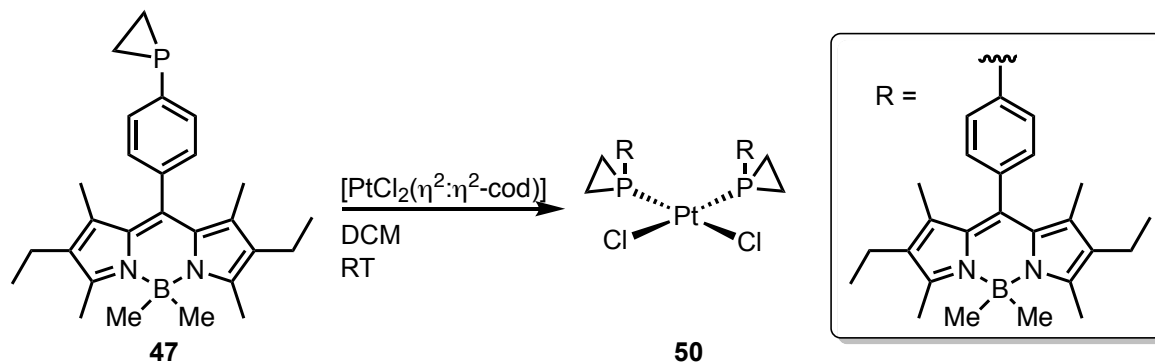
Our group synthesised the platinum MOP phosphirane complexes *cis*-[PtCl₂(**32a**/**32b**)₂] **49a** and **49b**, using two equivalents of the respective phosphirane **32a** or **32b**, and one of dichloro(1,5-cyclooctadiene)platinum(II) via the loss of the 1,5-cyclooctadiene (cod) ligand and coordination of two phosphirane ligands. This reaction occurred rapidly, and complete conversion was observed within two hours by $^{31}\text{P}\{^1\text{H}\}$ NMR spectroscopy (Scheme 3.12).²⁴



Scheme 3.12 Platinum coordination reaction between **32a** and [PtCl₂($\eta^2:\eta^2$ -cod)] at RT to afford **49a**.

The analogous reaction was carried out with Bodipy phosphirane **47**. The $^{31}\text{P}\{^1\text{H}\}$ NMR spectrum exhibited a downfield shift from δ –237.2 ppm to δ –142.8 ppm, with a doublet due to platinum satellite peaks ($^1J_{\text{Pt}} = 4071$ Hz). This very large coupling constant is larger than those observed for *cis*-[Pt(PR₃)Cl₂] complexes, which are often between 3400–3700 Hz, but it corresponds well to MOP phosphirane **49a** ($^1J_{\text{Pt}} = 4160$ Hz) and the only other known *cis*-

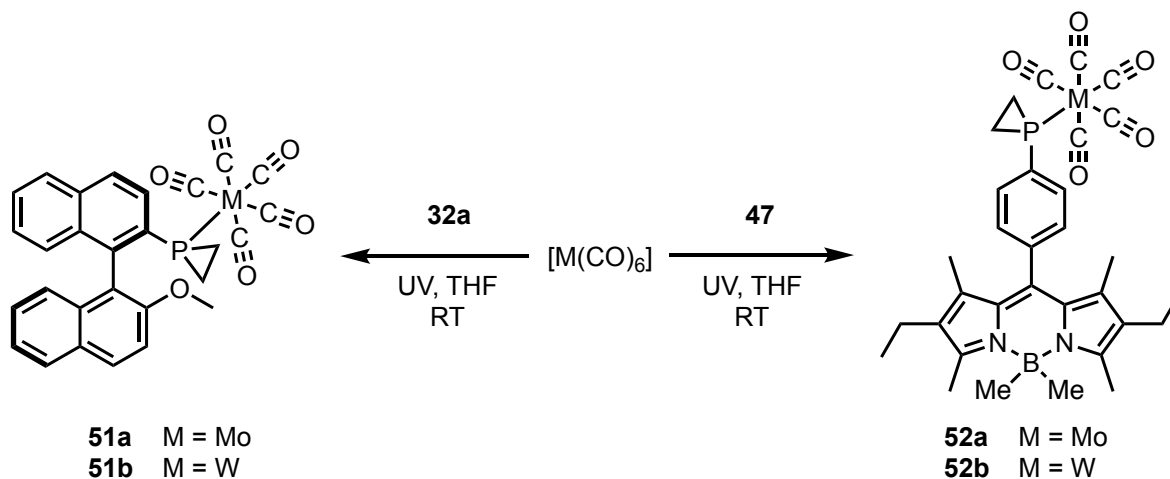
[Pt(phosphirane)Cl₂] complex, *cis*-[Pt(1-(9-anthracene)phosphirane)Cl₂] (¹J_{Pt} = 4133 Hz).¹⁰⁰ This large ³¹P-¹⁹⁵Pt coupling constant therefore also suggests that the phosphiranes are *cis* to each other in this case.¹⁰¹ The 89 Hz smaller coupling for **50** could be interpreted as the ligand having lower π-acceptor strength in comparison to **49**.^{24,102}



Scheme 3.13 Platinum coordination between **47** and [PtCl₂(η²:η²-cod)] to form the square planar complex **50**.

3.6.2 Synthesis of Metal Carbonyl Complexes

As discussed in Chapter 1, carbonyl complexes are often used to look at the donor/acceptor properties of phosphines. The higher the carbonyl IR frequency, the less σ-donating and better a π-acceptor the phosphine is. The Higham group have not previously reported the coordination of **32a** to group 6, tungsten and molybdenum, carbonyl complexes and so this was carried out in parallel to the analogous reactions with the Bodipy phosphirane **47**.



Scheme 3.14 Synthesis of [M(CO)₅(**32a**/**47**)] (**51a**, **51b** from **32a**) and (**52a**, **52b** from **47**) with [M(CO)₆] (M = Mo or W respectively) under UV conditions at room temperature.

The synthesis of these phosphirane metal complexes (Scheme 3.14) was carried out in a quartz UV vessel. [M(CO)₆] (M = Mo or W) was dissolved in anhydrous tetrahydrofuran and irradiated with UV light (365 nm) for one hour to substitute a carbonyl group for a more kinetically labile tetrahydrofuran ligand. Phosphiranes **32a** or **47** were dissolved in anhydrous tetrahydrofuran

and added to the metal complex, the resulting reaction mixture was then irradiated with UV light for a further 30 minutes. To confirm the completion of the reaction, crude $^{31}\text{P}\{^1\text{H}\}$ NMR spectroscopy was carried out and, in all cases, the reaction showed two product peaks, likely corresponding to mono- and disubstituted complexes. The volatiles were removed *in vacuo* and the complexes were purified by column chromatography.

On coordination with the group 6 metal complexes, analysis by $^{31}\text{P}\{^1\text{H}\}$ NMR spectroscopy displayed a downfield shift, from $\delta -237.2$ and $\delta -235.5$ ppm for the phosphiranes **47** and **32a** respectively to $\delta -165.5$ ppm (**52a**) and $\delta -169.3$ ppm (**51a**) for the molybdenum pentacarbonyl complexes and $\delta -163.7$ ppm and $\delta -189.6$ ppm for the tungsten pentacarbonyl complexes. Tungsten complexes **52b** and **51b** were further confirmed by tungsten satellite peaks ($J_{\text{PW}} = 259$ and 255 Hz respectively). These $^{31}\text{P}\{^1\text{H}\}$ NMR resonances are displayed in Figure 3.15.

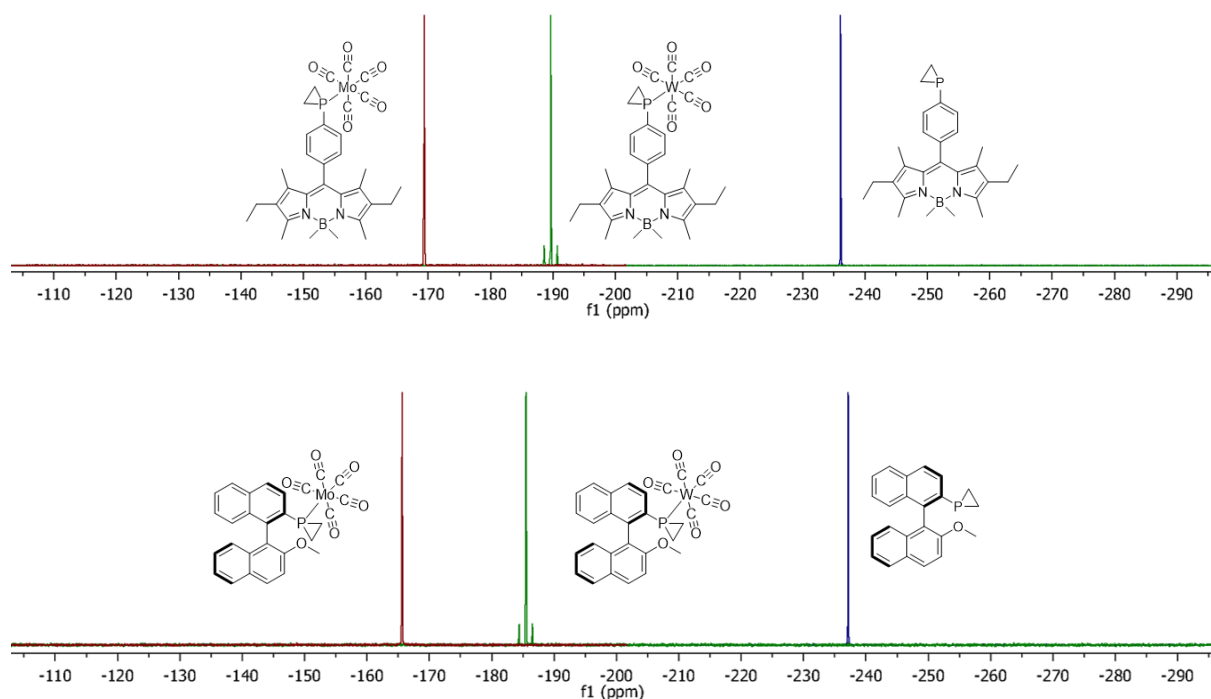


Figure 3.15 $^{31}\text{P}\{^1\text{H}\}$ NMR spectra of phosphiranes **47** and **32a** and the products of their coordination to $[\text{Mo}(\text{CO})_6]$ to give $[\text{MoCO}_5(\text{47/32a})]$ (**52a** and **51a**) and $[\text{W}(\text{CO})_6]$ to give $[\text{W}(\text{CO})_5(\text{47/32a})]$ (**52b** and **51b**).

It is clear to see from Figure 3.15 that the MOP complexes have a larger difference in chemical shift from the free ligand to the complexes than their Bodipy analogues. This may indicate the presence of increased back bonding to the phosphorus in Bodipy.

To confirm the substitution of the afforded complexes, IR spectroscopy was carried out; in each case, three carbonyl stretches were observed. IR spectroscopy can be used in conjunction with group theory symmetry calculations to determine the symmetry of the

complex and predict the number of carbonyl stretches in the IR spectra. The monosubstituted complexes have C_{4v} symmetry and thus, three carbonyl IR bands would be expected: A_1 (*cis/equatorial*), A_1 (*trans/axial*) and E. Therefore, **51a**, **51b**, **52a** and **52b** are all in accordance with being the expected, monosubstituted complexes.

The solid-state structure of **52a** was confirmed by X-ray diffraction. Crystals suitable for analysis were grown from slow diffusion of pentane into a *d*-chloroform solution of **52a**. The Mo1-P1 bond length of 2.5005(10) Å and Mo1-C28 bond length of 2.015(5) Å are in agreement with other reported monosubstituted phosphine pentacarbonyl complexes. The C25-P1-C26 bond angle of 48.9(2)° is also in agreement with reported phosphiranes.¹⁰³

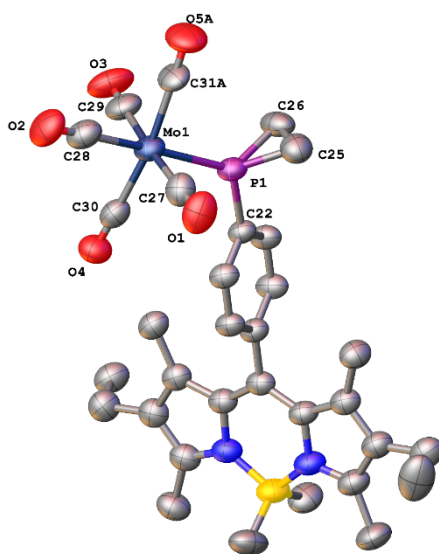


Figure 3.16 View of the molecular structure of **52a**. Hydrogen atoms bound to carbon have been omitted for clarity. Selected bond distances [Å] and angles [°]: Mo1-P1 2.5005(10), Mo1-C27 2.041(5), Mo1-C28 2.015(5), Mo1-C29 2.057(5), Mo1-C30 2.048(5), Mo1-C31A 2.043(8), P1-C22 1.824(3), P1-C25 1.820(5), P1-C26 1.800(4), O1-C27 1.140(5), O2-C28 1.134(5), O3-C29 1.137(6), O4-C30 1.140(5), O5A-C31A 1.116(9), C22-P1-Mo1 121.64(12), C25-P1-Mo1 124.28(15), C25-P1-C22 105.36(19), C26-P1-Mo1 127.79(14), C26-P1-C22 107.01(17), C26-P1-C25 48.9(2).

In addition to the monosubstituted complexes, over reaction led to side product formation of disubstituted complexes. Analysis by $^{31}\text{P}\{^1\text{H}\}$ NMR spectroscopy revealed chemical shifts further downfield to the monodentate complexes: $[\text{Mo}(\text{CO})_4(\mathbf{47})_2]$ (δ –163.7 ppm), $[\text{Mo}(\text{CO})_4(\mathbf{32a})_2]$ (δ –165.3 ppm); $[\text{W}(\text{CO})_4(\mathbf{47})_2]$ (δ –183.0 ppm, 251.4 Hz J_{PW}), $[\text{W}(\text{CO})_4(\mathbf{32a})_2]$ (δ –188.6 ppm, 247.3 Hz J_{PW}).

The diphosphirane tetracarbonyl complexes formed in each reaction could potentially be *cis* or *trans*. In analogous reactions with primary phosphines, *cis* complexes were reported and so this is likely the case here. To confirm this, IR spectroscopy was carried out on each sample. The *cis* complex would belong to the C_{2v} point group with an irreducible representation of $2A_1$, B_1 and B_2 , as all of these represent IR active bands, we would expect to see four carbonyl

stretches in the IR spectra. The *trans* complex however would belong to the D_{4h} point group with the irreducible representation A_{1g} , B_{1g} , E_u . As only E_u is IR active, we would expect to see only one carbonyl stretch. All disubstituted complexes showed four carbonyl stretches in the IR spectrum, consistent with our assumption of forming *cis*- complexes.

To further confirm the *cis* geometry, a crystalline sample of $[W(CO)_4(\mathbf{32a})_2]$ was grown from slow diffusion of diethyl ether into dichloromethane and analysed by X-ray diffraction. The solid-state structure revealed a diethyl ether disolvate *cis*-complex, as shown in Figure 3.17. The two W1-P1 and W1-P2 bond lengths of 2.506(2) and 2.492(2) Å respectively are in agreement with similar complexes within the literature.¹⁰³

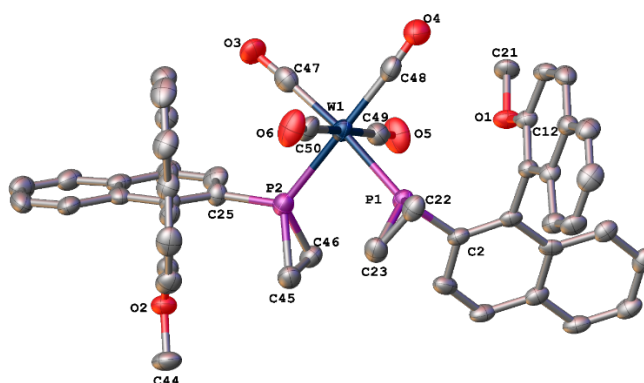


Figure 3.17 View of the molecular structure of $[W(CO)_4(\mathbf{32a})_2]$. Hydrogen atoms bound to carbon have been omitted for clarity. Selected bond distances [Å] and angles [°]: W1-P1 2.506(2), W1-P2 2.492(2), W1-C47 1.993(10), W1-C48 2.001(10), W1-C49 2.034(9), W1-C50 2.034(9), P1-C2 1.839(7), P1-C22 1.826(8), P1-C23 1.846(9), P2-C25 1.826(8), P2-C45 1.826(9), P2-C46 1.827(8), O3-C47 1.148(11), O4-C48 1.139(11), O5-C49 1.141(11), O6-C50 1.150(11), P2-W1-P1 89.1(7), C47-W1-P1 172.8(2), C47-W1-P2 86.8(3), C2-P1-W1 127.9(2), C22-P1-W1 123.9(3), C2-P1-C23 103.1(4), C22-P2-C2 105.9(4), C22-P1-C23 48.9(4), C25-P2-C46 101.1(4), C45-P2-W1 129.7, C46-P2-W1 120.1(3), C45-P2-C46 49.1(4).

When comparing the carbonyl stretching frequencies for the group 6 complexes, slight differences can be seen between the Bodipy complexes **52a** and **52b** and the MOP analogues **51a** and **51b**. Selected IR and NMR spectroscopic data are shown in Table 3.2 for comparison. Carbonyl stretching frequencies give information on the σ -donor and π -acceptor properties of the phosphines; the higher the IR frequency, the better the π -acceptor ability and therefore lower σ -donor ability the phosphine has. On comparison of the strongest carbonyl stretching frequencies (E), it is apparent that the values are slightly higher for the Bodipy complexes, more significantly in the case of the Mo complexes (1941 cm^{-1} for **52a**, in contrast to 1918 for **51b**). The higher values coincide with **47** being a poorer σ -donor.

In addition to looking at carbonyl frequencies, Grim *et al.* reported the correlation between E carbonyl stretching frequencies and J_{PW} for $LW(CO)_5$ phosphine complexes. They found that poor σ -donors have larger phosphorus-tungsten coupling constants which indeed is what is

observed here (259 Hz for **52b** and 256 Hz for **51b**) and, further indicating the weaker σ -donor abilities of Bodipy phosphirane **47**. It should be noted that a difference of 3 Hz is negligible and so this is not a strong case for comparing σ -donor ability in this instance.

Table 3.2 Selected IR and NMR spectroscopic data for the group 6 transition metal-phosphine complexes.

	$\tilde{\nu}(\text{CO})$ A ₁ Eq cm ⁻¹	$\tilde{\nu}(\text{CO})$ A ₁ Ax cm ⁻¹	$\tilde{\nu}(\text{CO})$ E cm ⁻¹	³¹ P δ ppm	¹ J _{P-W} Hz	δ (² J _{P-C}) CO Trans	δ (² J _{P-C}) CO Cis
[Mo(CO) ₅ (14)]	2076	1992	1929	-64.1	-	208.8 (24.0)	204.7 (9.1)
[Mo(CO) ₅ (47)] 52a	2075	1994	1941	-165.5	-	208.5 (31.8)	207.7 (10.5)
[W(CO) ₅ (14)]	2077	1973	1902	-85.8	223.0	198.3 (22.6)	195.5 (6.8)
[W(CO) ₅ (47)] 52b	2073	1981	1913	-185.5	259.2	197.9 (30.9)	195.7 (8.3)
[Mo(CO) ₅ (10a)]	2074	1992	1913	-79.4	-	209.4 (23.4)	204.8 (9.1)
[Mo(CO) ₅ (32a)] 51a	2073	1992	1918	-169.3	-	209.5 (31.8)	204.6 (10.8)
[W(CO) ₅ (10a)]	2072	1982	1908	-101.3	218.8	197.8 (22.0)	196.2 (6.8)
[W(CO) ₅ (32a)] 51b	2072	1984	1909	-189.6	255.6	198.8 (30.0)	195.5 (8.5)

3.6.3 Photophysical Properties

After the successful synthesis of this novel fluorescent phosphirane, and its complexation to group 6 metals, it was important to determine their photophysical properties. This data was collected for **47**, **52a** and **52b** in anhydrous, degassed tetrahydrofuran at room temperature, to minimise photobleaching and phosphine oxidation in solution and has been tabulated against primary phosphine **14** in Table 3.3.

Table 3.3 Photophysical properties of **14**, **47** and its group 6 complexes [Mo(CO)₅(**47**)] **52a** and [W(CO)₅(**47**)] **52b**.

	λ_{abs} (nm) ^a	λ_{em} (nm) ^a	Φ_{F} ^{a,b}	ϵ (M ⁻¹ cm ⁻¹) ^a
14	512	526	0.33	79,000
47	512	528	0.25	52,000
[Mo(CO) ₅ (47)] 52a	514	530	0.26	44,000
[W(CO) ₅ (47)] 52b	514	530	0.26	65,000

^a Measured in dry, degassed tetrahydrofuran at room temperature, dyes were excited at 485 nm; ^b Fluorescence quantum yields were measured with respect to 4,4-difluoro-8-phenyl-1,3,5,7-tetramethyl-2,6-diethyl-4-bora-3a,4a-diaza-s-indacene.

The absorption spectra of the phosphirane displays a typical Bodipy profile which is shown in Figure 3.18. The maximum absorbance which corresponds to the S_0-S_1 ($\pi-\pi^*$) transition was observed at 512 nm for both primary phosphine **14** and **47**. The molar absorption coefficient lowered slightly from $\epsilon = 79,000 \text{ M}^{-1} \text{ cm}^{-1}$ for **14** to $\epsilon = 52,000 \text{ M}^{-1} \text{ cm}^{-1}$ for **47**.

On coordination of **47** to afford the molybdenum and tungsten pentacarbonyl complexes, **52a** and **52b** respectively, a minor red shift of the maximum absorbance was observed (from 512 nm for **47** to 514 nm for both **52a** and **52b**).

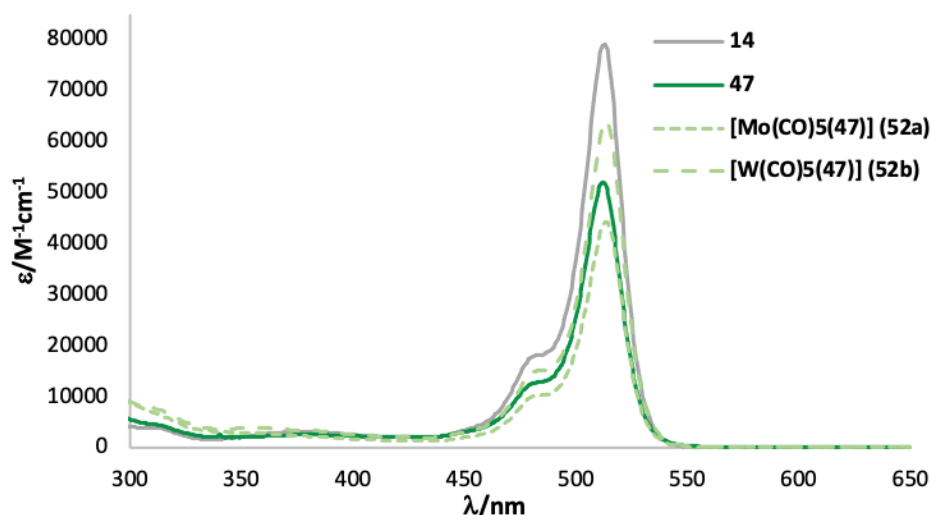


Figure 3.18 Absorption spectra of primary phosphine **14**, phosphirane **47** and its complexes $[\text{Mo}(\text{CO})_5(\text{47})]$ **52a** and $[\text{W}(\text{CO})_5(\text{47})]$ **52b** in tetrahydrofuran at room temperature.

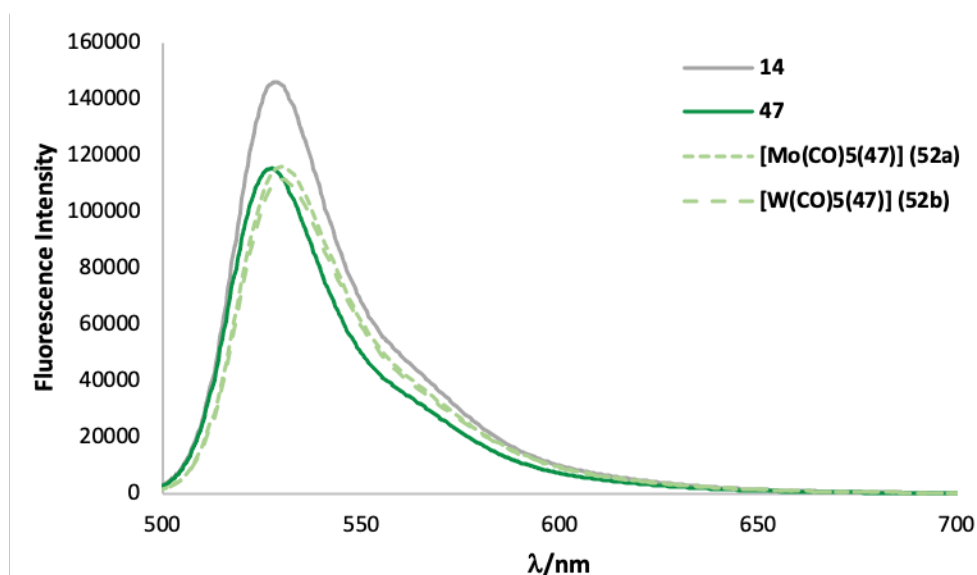


Figure 3.19 Emission spectra of primary phosphine **14**, phosphirane **47** and its complexes $[\text{Mo}(\text{CO})_5(\text{47})]$ **52a** and $[\text{W}(\text{CO})_5(\text{47})]$ **52b** in tetrahydrofuran at room temperature (excitation at 485 nm).

A slight red shift was observed in the emission spectra from primary phosphine **14** to tertiary phosphirane **47** (526 to 528 nm). A lower fluorescence quantum yield was observed for **47** (Φ_F

= 0.25) when compared to primary phosphine **14** (Φ_F = 0.33) however, the cyclic compound remains fluorescent. On coordination of **47** to molybdenum and tungsten carbonyl complexes, the spectra was again observed to red shift (530 nm for **52a** and **52b**). The quantum yields of the corresponding complexes (Φ_F of **52a** and **52b** = 0.26) were comparable with the free ligand **47**. The emission spectra of **14**, **47** and its corresponding complexes **52a** and **52b** are shown in Figure 3.19.

This data has identified that cyclisation to this three-membered phosphacycle, reduces, but does not fully quench the fluorescence quantum yield. Therefore, this phosphirane holds potential as an optical imaging agent.

3.7 Towards the Synthesis of a Fluorescent Phosphiranium Salt **48**

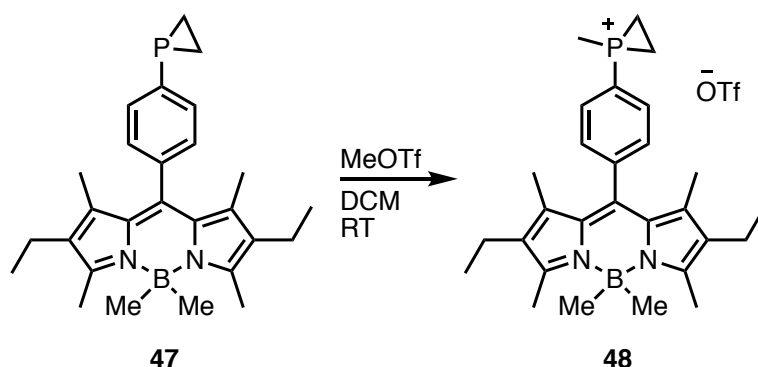
The ability of phosphonium salts to localise within the mitochondria has been well established.¹⁰⁴ This property enables their function as site specific agents and thus, proves beneficial for the design of biological probes. In addition to this organelle specific localisation, and the optical microscopy facilitated by the Bodipy group, the highly unusual chemical shift of phosphiranium salts may confer an ability for these probes to be useful in MRS. The ³¹P NMR shift should be out of range of any endogenous phosphorus present in the body. Since the ³¹P chemical shifts of **32a** and **32b** have been reported at δ -102.0 ppm and δ -101.2 respectively, this is a sufficient distance away from phosphorus within the body (*ca.* δ -5 to 25 ppm).¹⁰⁵

There are only a few examples of alkylations of phosphiranes known in the literature and until recently, all of them, including the alkylation of 1-phenylphosphirane and **32a** and **32b**, have used the strong methylating agent methyl trifluoromethanesulfonate. Therefore, to investigate the reactivity of **47** to quarternisation, this procedure was also followed.

It should be noted that very recent work by Gasnot and coworkers,²⁵ also employed two additional alkylating procedures, i) Meerwein's salt (trimethyloxonium tetrafluoroborate), and ii) generated alkyl triflate *in situ* from trifluoromethanesulfonic anhydride and allyl alcohol or benzyl alcohol in the presence of diisopropylethylamine, which facilitated the introduction of allyl and benzyl groups respectively to the phosphorus.

3.7.1 Synthesis of Phosphiranium Salt **48**

Under nitrogen, **47** was dissolved in anhydrous dichloromethane and methyl trifluoromethanesulfonate was added dropwise to the solution. Shown in Scheme 3.15.



Scheme 3.15 Synthesis of phosphiranium salt **48** by alkylation of **47** with methyl trifluoromethanesulfonate in dichloromethane at room temperature.

Co-workers in our group found that the reaction reached completion within 1 hour 30 minutes, supported by conclusive $^{31}\text{P}\{^1\text{H}\}$ NMR spectroscopic evidence ($\delta -101.6$ ppm). On repeating the reaction, and monitoring by $^{31}\text{P}\{^1\text{H}\}$ NMR spectroscopy, the same signal at a chemical shift of $\delta -101.6$ ppm was observed after one hour; however, the reaction did not reach completion until six hours (Figure 3.20). This shift coincides with the MOP phosphiranium salts **44a** and **44b** and others reported in the literature.²³

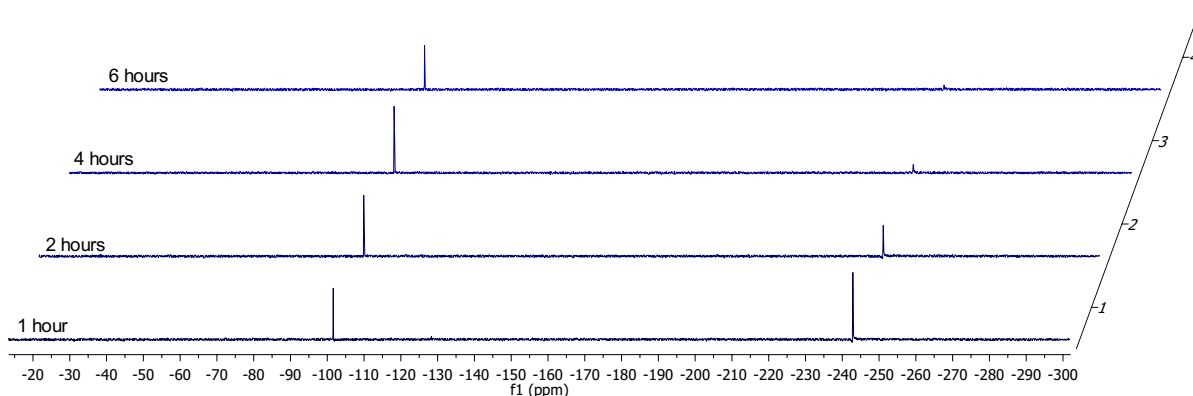
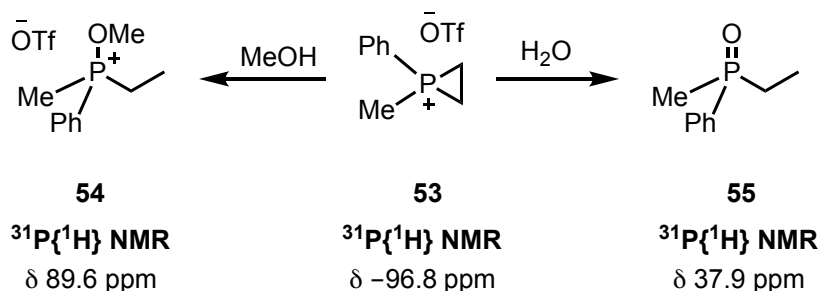


Figure 3.20 Crude $^{31}\text{P}\{^1\text{H}\}$ NMR spectra taken during the reaction of **47** with MeOTf. The peak at $\delta -237.2$ ppm gradually diminishes leaving a peak at $\delta -101.6$ ppm showing the complete conversion of **47** to **48** after 6 hours.

On completion of the reaction, confirmed by $^{31}\text{P}\{^1\text{H}\}$ NMR spectroscopy, the solvent was removed *in vacuo* to allow for analysis by crude ^1H NMR spectroscopy in *d*-chloroform, where the observation of the newly incorporated methyl peak as a doublet with $^2J_{\text{HP}}$ coupling should be apparent. Analysis of the crude product by ^1H NMR spectroscopy however, was inconclusive and when the $^{31}\text{P}\{^1\text{H}\}$ spectrum was recorded, two chemical shifts at $\delta 69.1$ ppm and $\delta 31.2$ ppm were observed, indicating the degradation of the alkylated phosphirane. The chemical shift at $\delta 69.1$ ppm later fully degraded into a peak at $\delta 31.2$ ppm.

Studies by Wild *et al.*, reported the isolation of 1-methyl-1-phenylphosphiranium triflate **53** as a crystalline product from their reaction mixture, when cooled to 5°C ,¹⁴ thus, **48** could

perhaps be unstable at room temperature but stable at lower temperatures. The reactivity of **53** with primary alcohols and water – depicted in Scheme 3.16 – was also reported by the same group; with methanol, this resulted in the formation of the acyclic phosphonium salt ethylmethoxymethylphenylphosphonium triflate **54**, with a $^{31}\text{P}\{^1\text{H}\}$ NMR chemical shift of δ 89.6 ppm. The reaction of **53** with water afforded ethylmethylphenylphosphine oxide **55** with a chemical shift of δ 37.9 ppm.



Scheme 3.16 Reaction of **53** with methanol to afford ethylmethoxymethylphenylphosphonium (**54**) or with water to afford ethylmethylphenylphosphine oxide (**55**).

Therefore, the resulting products from the degradation of **48** could perhaps be as a result of the presence of water and alcohol which possibly originated from the deuterated chloroform. As demonstrated by Wild *et al.*, this would almost certainly result in the formation of the acyclic phosphonium salt and the acyclic phosphine oxide products.

3.7.2 Density Functional Theory Calculations

In order to gain further insight into the properties of this novel phosphirane, density functional theory (DFT) calculations were carried out using Spartan'14 software.¹⁰⁶ Geometry optimised calculations were carried out at the B3LYP/6-31G* level of theory.

Phosphiranes reportedly exhibit lowered HOMO and LUMO orbitals in comparison to their less-strained and acyclic tertiary phosphine analogues.¹² This results in low σ -donor properties but an increased π -acceptor ability which is consistent with the common inability to alkylate the phosphorus centre.

Interestingly, the molecular orbitals of the Bodipy phosphirane **47** and the MeO-MOP phosphirane **32a** differed significantly. As shown in Figure 3.21, Bodipy phosphirane, **47**, demonstrates no phosphorus character until HOMO-3 at -6.44 eV, whereas MOP phosphirane, **32a**, (Figure 3.22) shows phosphorus character in the much higher energy orbital, HOMO-1 at -5.61 eV. This lower energy HOMO-3 of Bodipy phosphirane suggests a more stable, and thus, less reactive phosphorus lone pair. In the case of MOP phosphirane

32a, the higher energy of the phosphorus lone pair could explain the ease of alkylation of this compound.

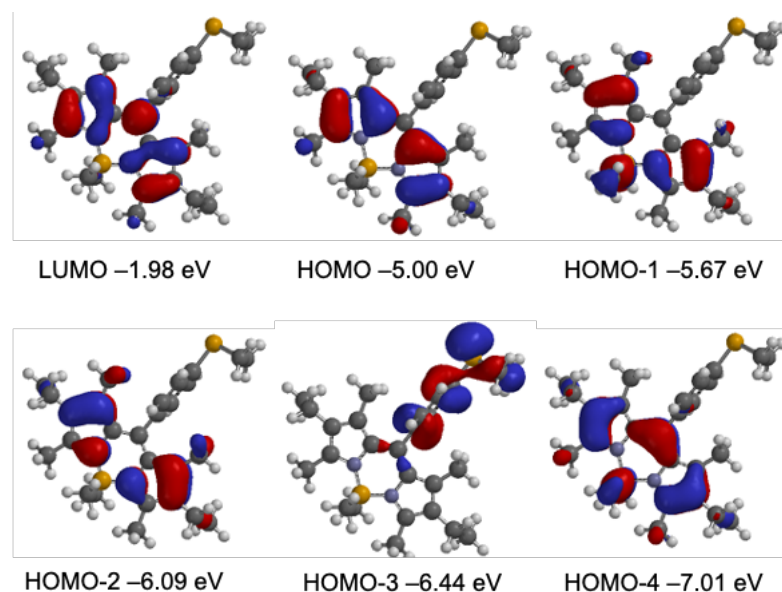


Figure 3.21 Calculated molecular orbital surfaces from the LUMO to HOMO-4 of the Bodipy phosphirane **47**

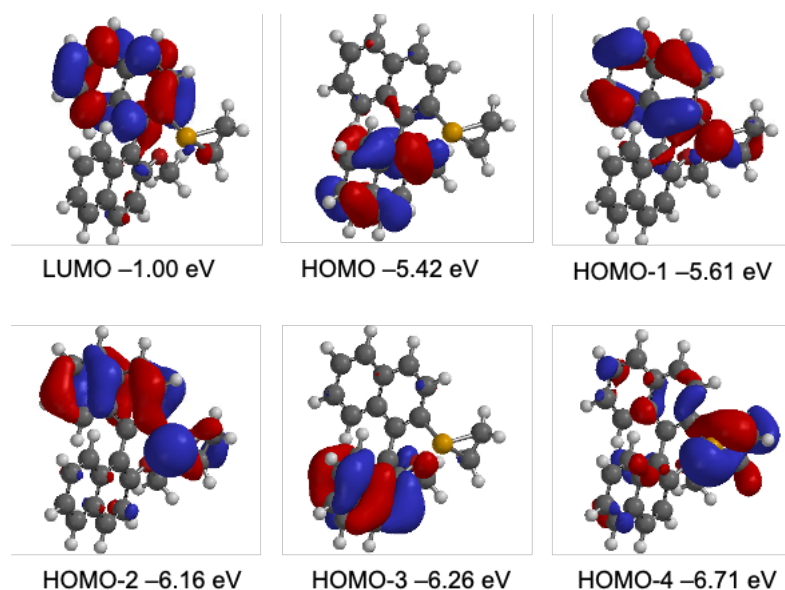


Figure 3.22 Calculated molecular orbital surfaces from the LUMO to HOMO-4 of MeO-MOP phosphirane **32a**.

As an additional benchmark, the DFT data for phenylphosphirane was calculated (Figure 3.23). Like **32a**, phenylphosphirane can also be methylated, with two equivalents of methyl trifluoromethanesulfonate in three hours to afford 1-methyl-1-phenylphosphiranium triflate.¹⁰⁷ Phenylphosphirane shows phosphorus character in the HOMO (-6.27 eV) which corresponds to its lone pair. The alkylation of phosphiranes would occur via an S_N2 reaction which involves the HOMO and thus, this data is in line with the fact that MOP phosphiranes,

32a and **32b**, and phenylphosphirane are known to alkylate but the reaction appears slower for Bodipy phosphirane **47**.

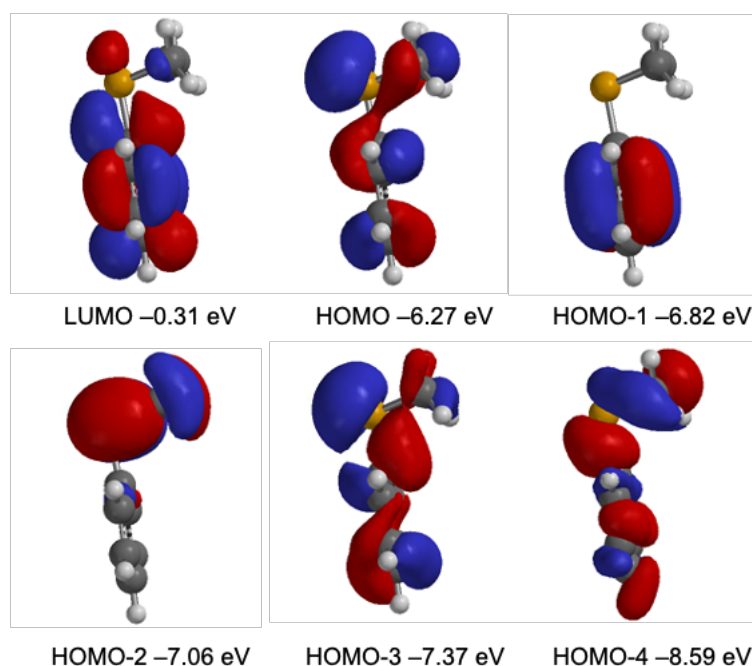


Figure 3.23 Calculated molecular orbital surfaces from the LUMO to HOMO-4 of phenylphosphirane **28**.

3.8 Phosphirane Summary

This section introduced the three membered phosphacycles, the phosphiranes, and discussed their unusual properties with respect to their air and thermal stability and nucleophilicity. The phosphiranes **32a** and **32b**, previously reported by the Higham group, display remarkable air and thermal stability, which could not be attributed to sterics, but instead, may be attributed to the electronic stabilising effects from the highly conjugated binaphthalene backbone. These compounds were also found to alkylate with ease through reaction with methyl trifluoromethanesulfonate to afford the corresponding phosphiranium triflates. Investigations were then carried out to see whether this level of stability and reactivity towards alkylation could be obtained from a highly conjugated, fluorescent backbone.

Thus, the successful synthesis of a fluorescent phosphirane **47** was carried out from primary phosphine **14**. The novel compound was characterised by NMR spectroscopy and X-ray crystallography. Air- and thermal-stability tests were carried out, which found **47** to be air-stable over seven days in both the solid and solution state, comparable to **32a** and **32b**. The phosphirane also exhibited high thermal stability when heated in refluxing toluene overnight. This remarkable stability may lend credence to the idea that again electronic conjugative effects may stabilise the three-membered ring.

The coordination of **32a** and **47** with molybdenum and tungsten carbonyl complexes was explored to gain insight into their respective reactivities and coordination chemistry. **32a** and **47** were reacted with molybdenum and tungsten hexacarbonyl which afforded the monosubstituted complexes [Mo(**32a**)(CO)₅] **51a**, [W(**32a**)(CO)₅] **51b**, [Mo(**47**)(CO)₅] **52a** and [W(**47**)(CO)₅] **52b**. These novel complexes were characterised by NMR and IR spectroscopy. In addition, the photophysical properties of **47**, **52a** and **52b** were obtained.

Preliminary alkylation experiments were carried out with the expectation to yield a fluorescent phosphiranium salt which could hold potential as a dual-functional imaging agent. **47** was reacted with methyl trifluoromethanesulfonate which resulted in the appearance of a ³¹P{¹H} NMR resonance consistent with the desired product. However, through attempted further purification and analysis, this product was found to degrade, likely to acyclic and oxide products. Density functional theory calculations were also carried out (at the B3LYP/6-31G* level of theory) to allow for visualisation of the molecular orbital boundary surfaces in order to compare between **47**, **32a** and 1-phenylphosphirane **28** to understand their differing reactivities.

Although there are many more aspects to be considered, this fluorescent phosphirane **47** could be the beginning of the development of a dual MRS and optical imaging agent.

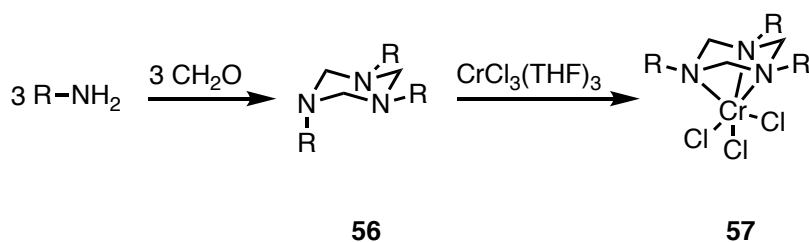
This chapter now moves its focus towards the six-membered heterocycles, the 1,3,5-diazaphosphanes.

3.9 1,3,5-Diazaphosphanes

This section was carried out in collaboration with Dr Randolph Köhn at The University of Bath. The synthesis of two six-membered fluorescent 1,3,5-diazaphosphanes from primary phosphine **14** is described and full characterisation and photophysical data are reported. Preliminary studies into the coordination of these diazaphosphanes to chromium(III) complexes were carried out to investigate their ability as ligands in catalytic hexene trimerization.

3.9.1 Six-Membered Heterocycles

A class of six-membered heterocycles, particularly well-known within the Köhn group are the 1,3,5-triazacyclohexanes **56**.^{108–112} 1,3,5-Triazacyclohexanes can be synthesised from the condensation reaction of primary amines with formaldehyde and can act as ligands through the coordination of all three nitrogen atoms to transition metals (Scheme 3.17).^{109,112–114}



Scheme 3.17 Synthesis of 1,3,5-triazacyclohexanes and their coordination to chromium(III).

Recently, Köhn *et al.* have reported the halide containing 1,3,5-triazacyclohexane compounds **58**, **59** and **60** (Figure 3.24) for their antimicrobial activity against Gram-negative and positive bacteria.

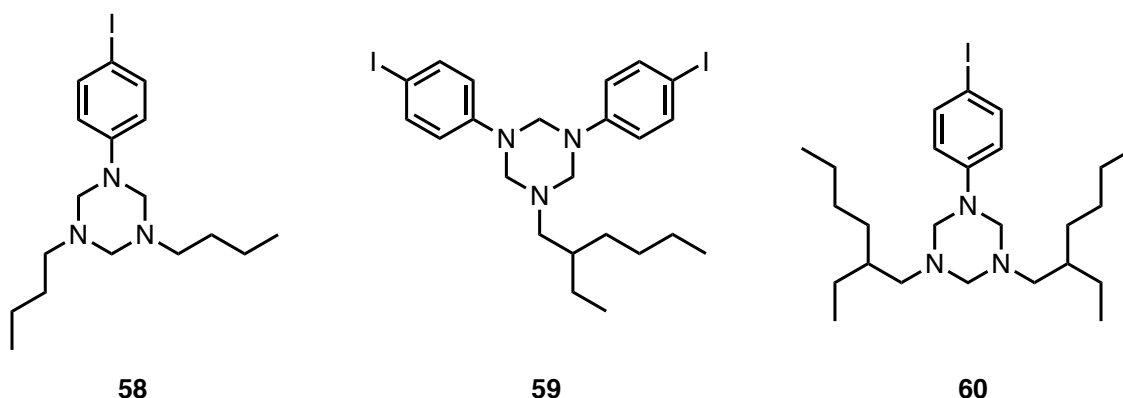
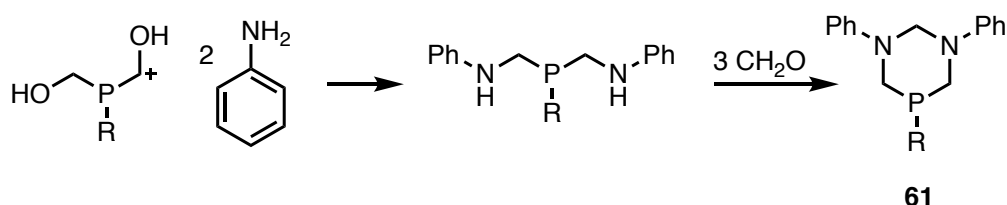


Figure 3.24 Iodo functionalised 1,3,5-triazacyclohexanes **58**, **59** and **60** reported for their antimicrobial activity against Gram-positive and Gram-negative bacteria.

All three compounds were screened for their antibacterial activity against *Staphylococcus aureus*, resistant *Staphylococcus aureus* and *Escherichia coli* by the diffusion method on agar medium. The compounds showed activity against the bacteria, displaying similar results to that of the positive control, which displays inhibition against a variety of bacteria.^{115,116}

In addition to 1,3,5-triazacyclohexanes, their phosphorus-containing analogues, the 1,3,5-diazaphosphanes are known; the first was synthesised by Märkl *et al.* in 1981.¹¹⁷ The synthesis involved a multistep procedure from bis(hydroxymethyl)-substituted phosphine and two equivalents of aniline to yield bis(anilinemethylene)-substituted phosphine. This PN_2 ligand was then subject to a condensation reaction with formalin to afford the 1,3,5-diazaphosphinane **61**, shown in Scheme 3.18.

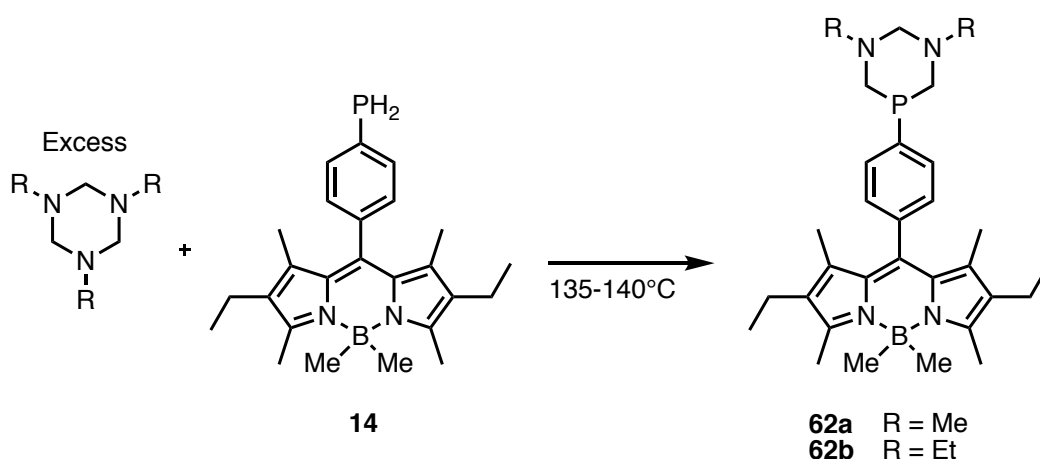


Scheme 3.18 Synthesis of 1,3,5-diazaphosphinane from bishydroxymethylphosphine and two equivalents of aniline.

Diazaphosphinanes have recently been reported for their radical reactivity resulting in hydrodehalogenation and cascade cyclization¹¹⁸ and, as hydride, hydrogen atom or proton donors, in metal-free conditions¹¹⁹ and thus, are currently attracting interest. To date, there have been no reports of fluorescent 1,3,5-diazaphosphinanes, and therefore, here we explore the synthesis of novel 1,3,5-diazaphosphinanes from our fluorescent primary phosphine **14**.

3.9.2 Synthesis of a Novel Fluorescent 1,3,5-Diazaphosphinane

In collaboration with Dr Randolph Köhn at the University of Bath, efforts towards the synthesis of two fluorescent 1,3,5-diazaphosphinanes, **62a** and **62b**, from the reaction of Bodipy primary phosphine **14** with 1,3,5-trimethyltriazacyclohexane or 1,3,5-triethyltriazacyclohexane were carried out. Thus, primary phosphine **14** was suspended in an excess of the appropriate 1,3,5-triazacyclohexane and heated to 135 °C, in the case of **62a**, and 140 °C for **62b** (Scheme 3.19). On completion of the reaction, the compounds were purified by column chromatography (alumina) and the desired compounds **62a** and **62b** were afforded in 61% and 76% yield respectively.



Scheme 3.19 Synthesis of 1,3,5-diazaphosphinanes **62a** and **62b** from the Bodipy primary phosphine **14** and 1,3,5-trimethyltriazacyclohexane or 1,3,5-triethyltriazacyclohexane.

Full characterisation of the cyclic compounds was obtained by ^1H , $^{31}\text{P}\{^1\text{H}\}$, $^{15}\text{N}\{^1\text{H}\}$ and $^{13}\text{C}\{^1\text{H}\}$ NMR spectroscopy, mass spectrometry and CHN, elemental analysis. The $^{31}\text{P}\{^1\text{H}\}$ NMR gave signals of δ –60.2 ppm and δ –58.3 ppm for **62a** and **62b** respectively. In addition, crystals suitable for X-ray diffraction were obtained by Dr Randolph Köhn; the solid-state structures are shown in Figure 3.25.

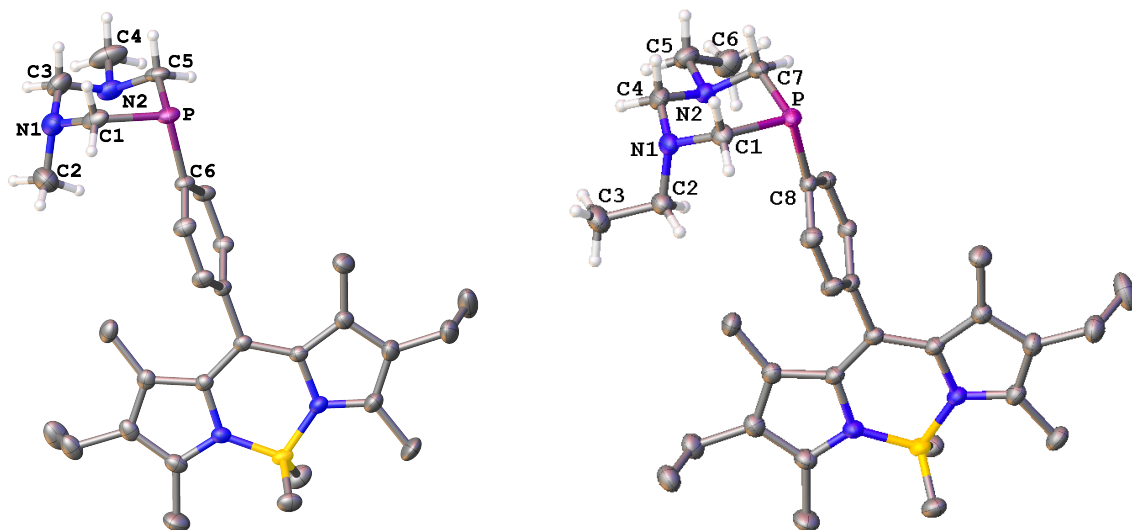
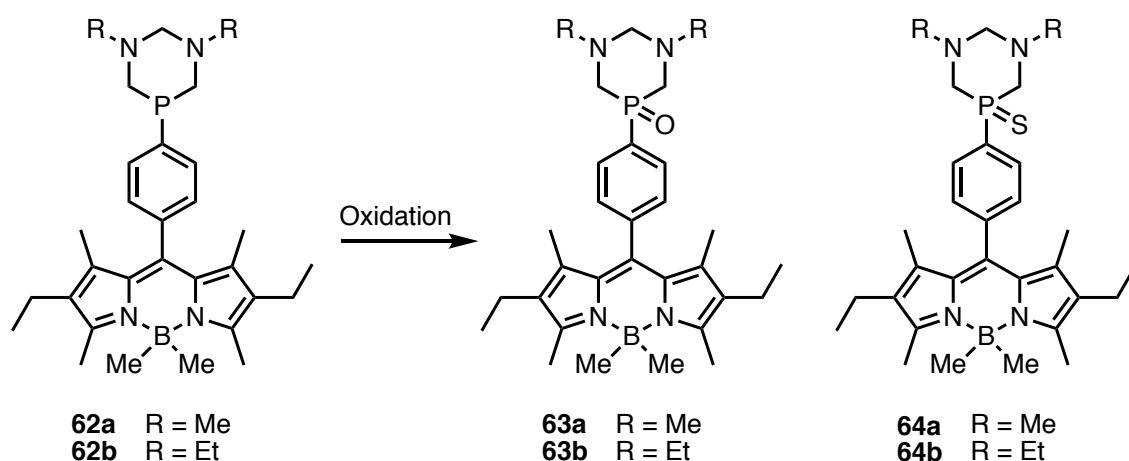


Figure 3.25 View of the molecular structure of **62a** (left). Hydrogen atoms have been omitted for clarity. Selected bond distances [Å] and angles [°]: P-C6 1.827(2), P-C5 1.838(3), P-C1 1.861(3), N1-C3 1.444(4), N1-C2 1.463(5), N1-C1 1.464(5), N2-C4 1.457(4), N2-C5 1.458(4), N2-C3 1.469(4), C6-P-C5 103.70(12), C6-P-C1 105.04(13), C5-P-C1 97.15(14), C2-N1-C1 114.3(3), C3-N1-C1 112.1(3), C3-N1-C2 112.2(3), C4-N2-C5 109.6(3), C4-N2-C3 110.3(2), C5-N2-C3 110.3(3). View of the molecular structure of **62b** (right). Hydrogen atoms have been omitted for clarity. Selected bond distances [Å] and angles [°]: P-C8 1.8322(14), P-C7 1.8313(16), P-C1 1.8647(14), N1-C4 1.443(2), N1-C1 1.4537(19), N1-C2 1.4688(19), N2-C7 1.4562(18), N2-C5 1.468(2), N2-C4 1.4730(19), C8-P-C7 102.37(7), C7-P-C1 95.98(7), C4-N1-C1 112.40(12), C4-N1-C2 114.33(12), C1-N1-C2 114.44(13), C1-N1-C2 114.48(12), C7-N2-C5 111.30(12), C7-N2-C4 109.89(12), C5-N2-C4 111.71(12).

The intracyclic bond angles around the phosphorus, 97.15(14)° for **62a** (C5-P-C1) and 95.98(7)° for **62b** (C7-P-C1) are smaller in comparison to those around the nitrogen atoms; C3-N1-C1: 112.1(3) and C5-N2-C3: 110.3(3) for **62a** and C4-N1-C1: 112.40(12), and C7-N2-C4: 109.89(12) for **62b**. A similarly related, triazacyclohexane analogue, 1,3,5-triphenyl-triazacyclohexane, has intracyclic bond angles around the nitrogens of 109.3(2)° and 109.6(2)°; much closer to the ideal chair conformation.¹²⁰ These angles highlight the higher ring strain around the phosphorus of the 1,3,5-diazaphosphinanes **62a** and **62b** in comparison to the 1,3,5-triphenyl-triazacyclohexanes.

Both compounds **62a** and **62b** oxidised slowly in solution to afford **63a** and **63b** respectively. Oxidation also occurred when the ligands were reacted with elemental sulfur to give the corresponding P=S analogues **64a** and **64b**. These reactions have been illustrated in Scheme 3.20. **64a** and **64b** have also been characterised by X-ray diffraction, and the corresponding data can be found in Appendix I, Section 6.2. It is noteworthy that **64b** is disordered between P=O and P=S.



Scheme 3.20 **62a** and **62b** can be oxidised slowly in air to form **63a** and **63b** respectively, or by reaction with elemental sulfur to form **64a** and **64b** respectively.

3.10 Photophysical Data

Following the synthesis of the fluorescent 1,3,5-diazaphosphinanes **62a** and **62b**, the photophysical properties were determined. Photophysical data was collected for the compounds **62a** and **62b** in anhydrous, degassed tetrahydrofuran at room temperature and the data is depicted in Table 3.4 alongside the relevant data for the primary phosphine **14**.

Table 3.4 Photophysical properties of primary phosphine **14** and 1,3,5-diazaphosphinane compounds **62a** and **62b**. Measured in dry, degassed tetrahydrofuran at room temperature.

	λ_{abs} (nm)	λ_{em} (nm) ^a	$\Phi_{\text{f}}^{\text{ab}}$	ϵ (M ⁻¹ cm ⁻¹)
14	512	526	0.33	79,000
62a	513	529	0.24	88,000
62b	513	529	0.28	96,000

^a Dyes were excited at 485 nm; ^b Fluorescence quantum yields were measured with respect to 4,4-difluoro-8-phenyl-1,3,5,7-tetramethyl-2,6-diethyl-4-bora-3a,4a-diaza-s-indacene.

The absorption spectra of **62a** and **62b** are displayed in Figure 3.26. Both compounds display a typical Bodipy absorption curve, with a negligible bathochromic shift (1 nm) of the absorption maxima from the primary phosphine **14** in both cases (from 512 nm for **14** to 513 nm). The cyclic compounds have a larger molar absorption coefficient (ϵ = 88,000 and 96,000 M⁻¹ cm⁻¹ for **62a** and **62b** respectively) in comparison to the primary phosphine **14** (ϵ = 79,000 M⁻¹ cm⁻¹).

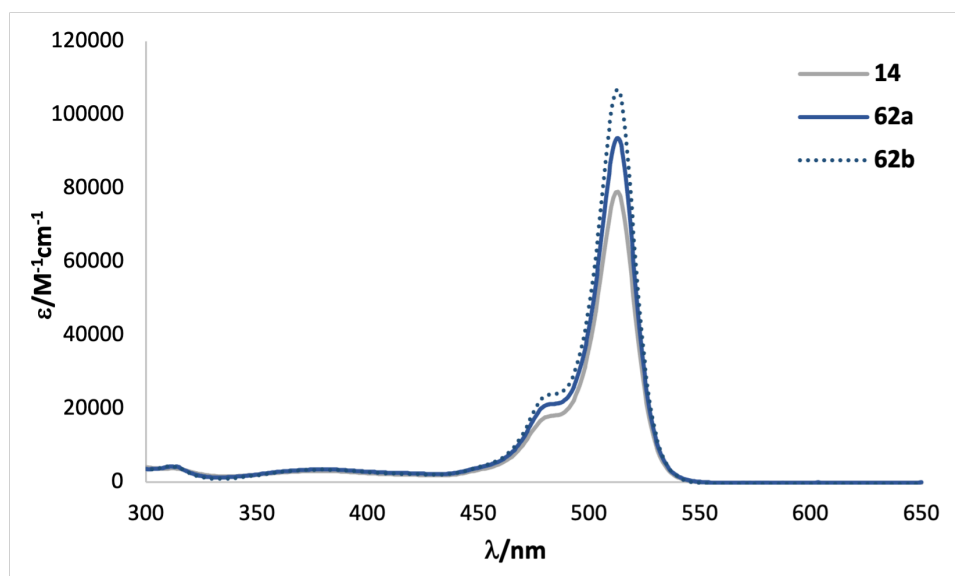


Figure 3.26 Absorption spectra of 1,3,5-diazaphosphinanes **62a** and **62b** and their precursor, primary phosphine **14**, in tetrahydrofuran at room temperature.

Room temperature fluorescence was apparent for **62a** and **62b** and the spectra are displayed in Figure 3.27. In both cases, the emission maxima showed a slight bathochromic shift (3 nm) from the primary phosphine **14** (from 526 to 529 nm). Table 3.4 shows that the quantum yields for the cyclic phosphines **62a** and **62b** were slightly lower than for the primary phosphine **14** (**62a**: $\Phi_F = 0.24$ and **62b**: $\Phi_F = 0.28$ in comparison to $\Phi_F = 0.33$ for **14**). This may indicate that slight quenching of fluorescence via reductive-PeT is occurring as a result of the nitrogens.

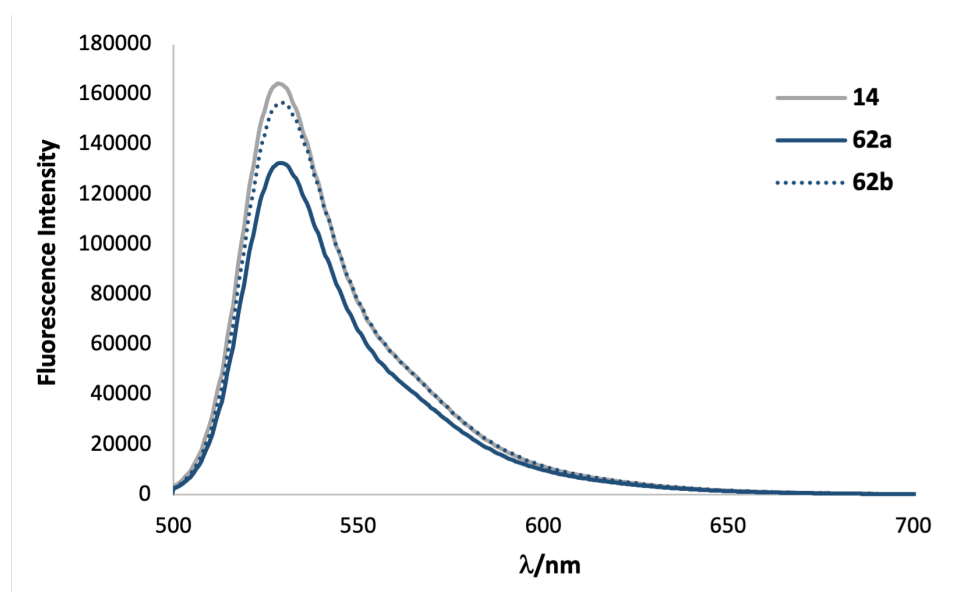


Figure 3.27 Emission spectra of the 1,3,5-diazaphosphinanes **62a** and **62b** and their precursor, primary phosphine **14** in tetrahydrofuran at room temperature (excitation at 485 nm).

The cyclisation of primary phosphine **14**, to 1,3,5-diazaphosphinanes **62a** and **62b** results in the slight reduction in their quantum yield, but both compounds demonstrate adequate photophysical properties. In addition, cyclisation had no significant influence on their

absorption or emission profiles – in fact, an increase in molar absorption coefficient is observed.

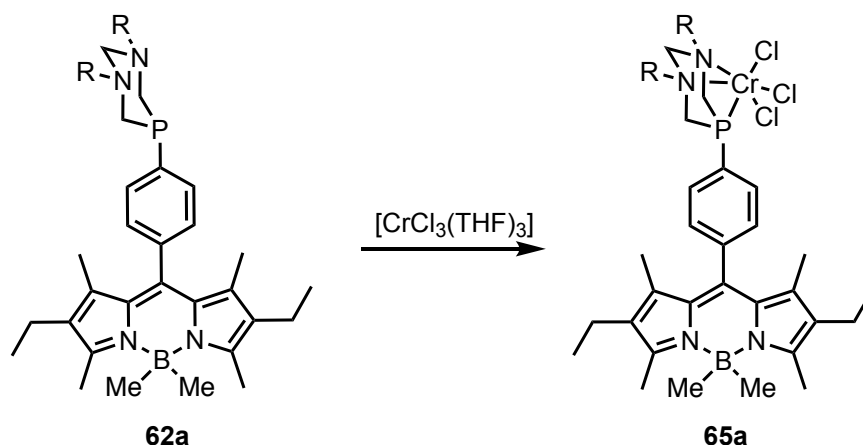
3.11 Complexation reactions with Chromium(III) Complexes

As discussed in Section 3.9.1, the 1,3,5-triazacyclohexanes **58**, **59** and **60** display antimicrobial activity, though this class of compounds have more commonly been used as ligands for complexes in catalysis. Of particular interest are their chromium complexes which have displayed activity in the catalysis of olefin trimerization.^{108,111} Köhn *et al.* have reported the synthesis of 1,3,5-triazacyclohexane chromium(III) complexes; the 1,3,5-triazacyclohexane coordinates as a tripodal ligand with *fac*-geometry, which was illustrated in Scheme 3.17. The chromium complexes can be activated with methylaluminoxane (MAO) and have shown to be effective in ethylene polymerisation,¹²¹ ethylene trimerization and α -olefin trimerization^{108,110} The polyethylene produced in these reactions displays similar branching and end group distribution of those produced by the Phillips catalyst,¹²² thus demonstrating their potential industrial applications.

It was previously reported by Köhn *et al.* that the main catalyst decomposition route for 1,3,5-triazacyclohexane complexes was ligand transfer to aluminium, likely at the chromium(I) stage of the catalytic cycle.¹¹¹ Köhn hypothesised that the introduction of a phosphine could potentially slow this decomposition route due to the improved bonding of the phosphine to the softer chromium(I) centre and less well to aluminium(III) from the catalyst activator, methylaluminoxane (MAO). Therefore, it was of interest to see if the novel 1,3,5-diazaphosphanes could – firstly, coordinate to chromium(III) – and secondly, whether the complex would demonstrate activity in the catalytic trimerization of hexene.

Initially, complexation reactions of **62a** were attempted with CrCl_3 , CrBr_3 , CrOTf_3 , $\text{Cr}(\text{CO})_3$ and $[\text{Ni}(\text{CH}_3\text{CN})_3]^{2+}$ but no firm evidence of complex formation was obtained. Thus, reactions were carried out with $[\text{CrCl}_3(\text{THF})_3]$ where the displacement of THF could be monitored by ^1H NMR spectroscopy. On the addition of **62a** with $[\text{CrCl}_3(\text{THF})_3]$, and monitoring by ^1H NMR spectroscopy, at least two equivalents of tetrahydrofuran were released. The signals corresponding to the methylene protons of the N_2P ring were not observed, due to paramagnetism of the chromium, indicating coordination. The ^1H NMR resonances corresponding to the protons of the Bodipy core (further away from the metal centre) were observed and thus, not affected by paramagnetic effects. However, on analysis of **65a** by mass spectrometry in acetonitrile, the desired complex was not observed, and it appeared that

acetonitrile de-coordinates the ligand. Thus, it is possible that the ligand is able to bind but may not be strongly bound.



Scheme 3.21 The attempted, but not confirmed coordination of Bodipy 1,3,5-diazaphosphinane **62a** to $\text{CrCl}_3(\text{THF})_3$ to afford **65a**.

As no complexation product was observed by MS for the coordination of **62a** to $[\text{CrCl}_3(\text{THF})_3]$, the reaction was explored by low-level DFT calculations (carried out by Köhn) and compared to the analogous 1,3,5-trimethyl-1,3,5-triazacyclohexane **56** coordination. The DFT calculations were performed with the ORCA software, version 3.0.0.¹²³ The geometry optimisations were done using the density functional BP86¹²⁴ employing the def2-SVP basis set.¹²⁵ The Gibbs free energy were calculated and revealed that a higher energy for the 1,3,5-diazaphosphinane **62a** ($\Delta G = +26 \text{ kJ mol}^{-1}$) was required in comparison to **56** ($\Delta G = +13 \text{ kJ mol}^{-1}$) to reach the all-equatorial conformation required for coordination. The free energy for the coordination of **62a** ($\Delta G = -33 \text{ kJ mol}^{-1}$) is much less negative in comparison to the coordination of **56** ($\Delta G = -123 \text{ kJ mol}^{-1}$). Therefore, the coordination of **62a** to chromium(III) is much less favoured than the coordination of **56**. There is however still an overall negative free coordination Gibbs free energy obtained for binding the lowest energy conformation of **62a** to $[\text{CrCl}_3(\text{THF})_3]$, which is driven by the entropy of THF displacement.

Whilst the absolute bond lengths at this level of theory will likely be inexact, they can be compared between **62a** and **56**; the calculated bond length Cr-N increases from 2.16 Å for the triazacyclohexane to 2.26 Å for the diazaphosphinane (Cr-P = 2.36 Å). Thus, **62a** is a more weakly-coordinating ligand to chromium(III) in comparison to 1,3,5-triazacyclohexanes which may explain the failure to detect a complex experimentally. However, coordination may still be possible as indicated by the calculated negative free energy.

Although at this time, it cannot be confirmed that any chromium(III) complex formed, a small amount of the resulting product or mixture was used in a reaction for selective hexene trimerization.

3.11.1 Testing in Catalytic Reactions

Initial tests were carried out to see how the product afforded from the reaction of **62a** with $[\text{CrCl}_3(\text{THF})_3]$ fared in the catalysis of selective hexene trimerization. Although slow to start, the system displayed activity; after the addition of 2000 equivalents of 1-hexene, less than 2% was converted after 10 hours. However, in 10 days, approximately 24% (500 eq) was converted and the system still showed activity at this time. Although this was much slower than their 1,3,5-triaza analogues (>50% conversion in a few hours and take only minutes to initiate) the diazaphosphinane analogue was active for much longer; 1,3,5-triazacyclohexanes do not show activity after a day. Thus, this system shows promise in turning off decomposition pathways which appears to support the above hypothesis. Further studies are being carried out to obtain firm evidence of the coordination of **62a** with $[\text{CrCl}_3(\text{THF})_3]$ following this, further catalytic studies will be carried out.

3.12 1,3,5-Diazaphosphinane Summary

1,3,5-Diazaphosphinanes **62a** and **62b** were obtained directly in 61% and 76% yield respectively, from 1,3,5-trimethyltriazacyclohexane and 1,3,5-triethyltriazacyclohexane by heating with the air-stable primary phosphine **14** (under a flow of nitrogen to remove the primary amine released). The coordination of **62a** and **62b** to $[\text{CrCl}_3(\text{THF})_3]$ has been explored and although ^1H NMR spectroscopic analysis indicates coordination, no definitive data has been obtained to confirm the structure of the complex. Nevertheless, preliminary catalytic studies were carried out with the postulated coordination complex **65a**, which proved to be active in the catalysis of selective hexene trimerization. Although the initiation was slower than their 1,3,5-triazacyclohexane analogues, **65a** proved to be active for >10 days, which is over ten-fold longer than the 1,3,5-triazacyclohexane Cr(III) complexes. This extended activity demonstrates promise in turning off decomposition routes as was hypothesised by the Köhn group due to the ligand transfer of the 1,3,5-diazaphosphinane to aluminium(III) being less likely than with the analogous 1,3,5-triazacyclohexane.

3.13 Surface Modification with a Fluorescent Label

An alternative synthetic route to the 1,3,5-diazaphosphinane would be through a condensation reaction of a hydroxymethyl phosphine with an amine (as in Scheme 3.18),

but this is yet to be explored in this system. The hydroxymethyl functional group does provide a route to further functionalisation however, which we have preliminarily investigated through a collaboration with Professor Bill Henderson at the University of Waikato, New Zealand.

Previous work by the Henderson group has explored the use of hydroxymethylphosphines in surface modification, describing the immobilisation of hydroxymethylphosphines through condensation reactions with amine modified surfaces, including: i) alcohol dehydrogenase (enzyme) immobilisation,¹²⁶ ii) chiral biopolymers: chitosan and chitin,¹²⁷ iii) polyaniline nanostructures¹²⁸ and iv) ferrocenylphosphine-modified silicon surfaces.¹²⁹

The ability to incorporate a fluorescent Bodipy group offers an important extension to this chemistry as a way of detecting amine-containing compounds such as collagen, in order to provide insight into bone taphonomic history and biological information about ancient life¹³⁰ or, for diagnostic purposes.¹³¹

Thus, Bodipy hydroxymethylphosphine **24d** was used to carry out surface modification of mesoporous silica (SBA-15), to give fluorescently labelled silica with the idea that this method could be translated to bones for collagen detection. The procedure has been illustrated in a schematic below in Figure 3.28.

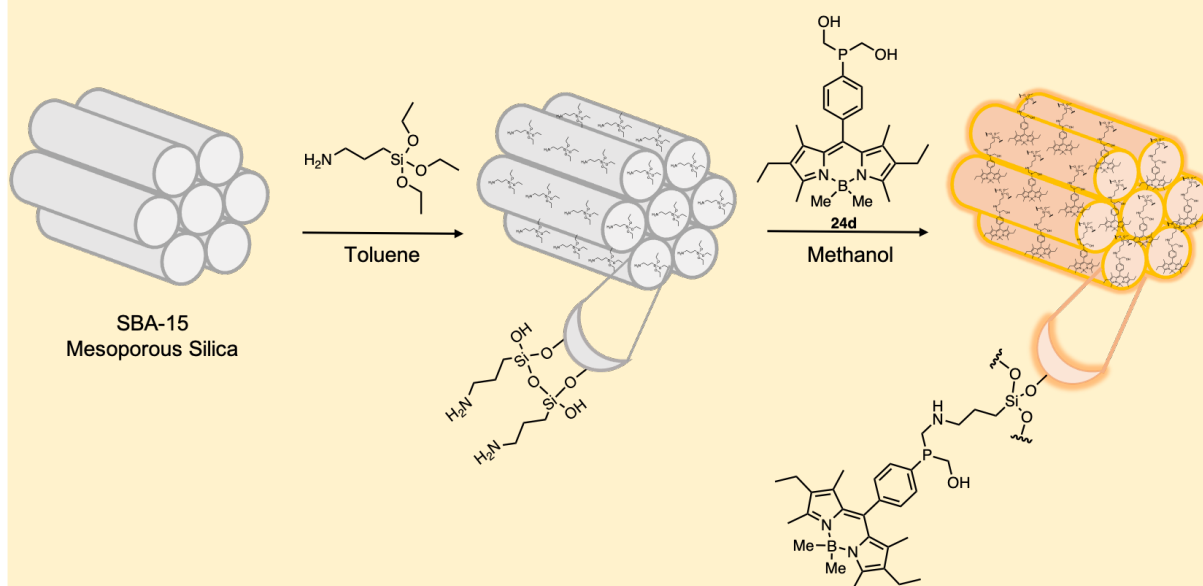


Figure 3.28 A schematic illustrating: first, the amination of SBA-15 mesoporous silica and second, the condensation reaction of **24d** with aminated SBA-15 to afford fluorescently labelled silica.

3.13.1 Surface Modification

SBA-15 was aminated through reaction with 3-aminopropyl triethoxysilane following toluene reflux over eight hours. The resulting suspension was filtered and washed with toluene and water and dried *in vacuo* for four days.

The aminated silica could then be reacted with an excess of Bodipy hydroxymethylphosphine **24d** through a condensation reaction in methanol at room temperature for three hours. The solid was filtered and washed twice with methanol, water and then acetone to ensure no unbound phosphine remained on the surface. The resulting solid was orange in colour, and after drying in air, exhibited a bright green fluorescence under UV light (365 nm), implying a successful reaction. As a control experiment, the same reaction was completed using underivatised SBA-15. The solid was washed free of unreacted Bodipy hydroxymethylphosphine **24d** as above, giving a white solid. This procedure indicated that the presence of silica-bound amine groups is necessary for immobilisation of the **24d** to occur. This solid showed no green fluorescence under UV light. A comparison of the two samples can be seen in Figure 3.29.



Figure 3.29 Left: Underivatised SBA-15 after treatment with Bodipy hydroxymethylphosphine **24d**. Right: 3-aminopropyl SBA-15 after treatment with **24d**. Image taken under visible light (left). Image taken under irradiation with UV light (365 nm) (right).

These preliminary results show promise for the use of Bodipy hydroxymethylphosphine **24d** as a way of fluorescently labelling amine modified surfaces. The future plans for this research involve the testing of **24d** for its application in the detection of residual collagen in bones. To compare this work with alternate methods and fluorophores, the treatment of bone samples with the readily available *tris*(hydroxymethyl)phosphine could be carried out. The resulting hydroxymethylphosphine derivatised bone samples could subsequently be treated with a fluorescent amine.

This chapter now turns the attention towards an uncommon seven membered phosphacycle. Focus here is directed towards the unsaturated cycle, as these are predominantly studied. Furthermore, the seven membered azepines, are well known for their biological activity and

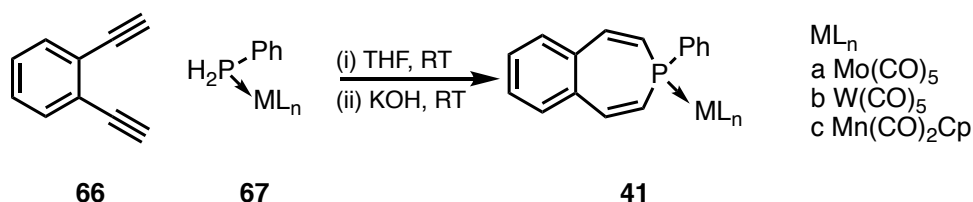
this chapter contains exploratory work towards phosphorus analogues of the azepines, the little studied, phosphepines.

3.14 Seven-Membered Phosphacycle

This section reports the synthesis of two novel 3-benzophosphepine complexes, the first known fluorescent examples, and describes our attempts at the synthesis of the free ligand.

3.14.1 Synthesis of Primary Phosphine Group 6 Carbonyl Complexes [M(CO)₅(**14**)]

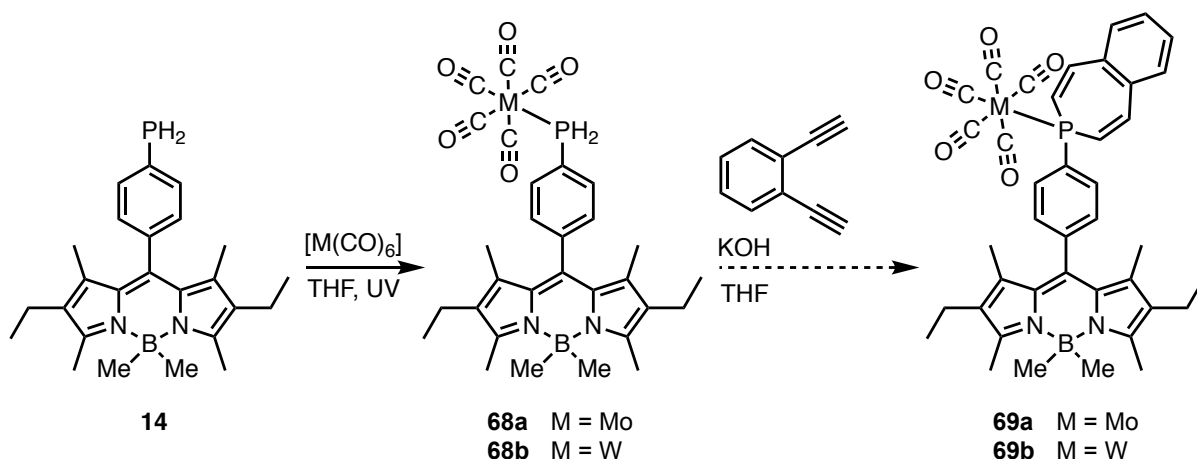
Incorporation of the phosphorus into the cycle, in the procedure by Lammertsma *et al.*, was achieved by the double hydrophosphination reaction of primary phosphine-coordinated metal complexes with 1,2-diethynylbenzene. The first hydrophosphination occurred without base whereas, the second required the addition of potassium hydroxide (Scheme 3.22).



Scheme 3.22 Synthesis of 3-phenyl-3-benzophosphine group 6 (Mo and W) and group 7 (Mn) complexes via the double hydrophosphination of 1,2-diethynylbenzene with primary phosphine metal complexes.

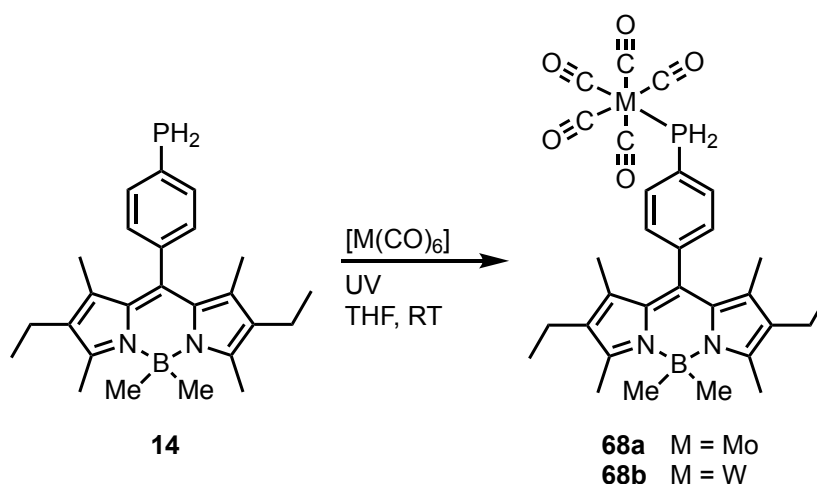
3.14.2 Synthesis of Metal Carbonyl Complexes

It was envisaged that a fluorescent 3-benzophosphepine complex could be synthesised following this method from the air-stable primary phosphine **14**, in a two-step synthesis. First coordination to a group 6 carbonyl complex would afford the transition metal complexes **68a** and **68b** (which have been synthesised previously within the Higham group) and second, the hydrophosphination of these complexes with 1,2-diethynylbenzene would aim to afford fluorescent 3-benzophosphepine complexes. The proposed route is shown in Scheme 3.23.



Scheme 3.23 Proposed route to the synthesis of two fluorescent group 6 3-benzophosphepine complexes.

To a quartz vessel, the appropriate metal hexacarbonyl complex $[M(CO)_6]$ ($M = Mo, W$), was added and dissolved in anhydrous tetrahydrofuran. The solution was irradiated with UV light under a stream of nitrogen for one hour, resulting in the replacement of a carbonyl ligand with a more labile tetrahydrofuran ligand. Primary phosphine **14** was dissolved in anhydrous tetrahydrofuran and added to the quartz vessel and the reaction mixture was irradiated with UV light for a further 30 minutes resulting in the formation of monosubstituted complexes $[Mo(CO)_5(\mathbf{14})]$ **68a** and $[W(CO)_5(\mathbf{14})]$ **68b** as precursors to the phosphepine (Scheme 3.24).

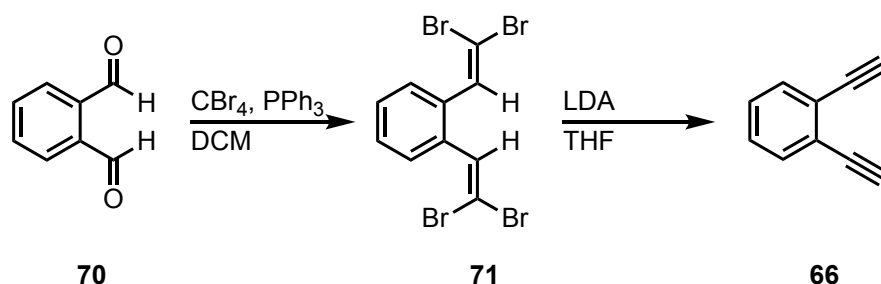


Scheme 3.24 Synthesis of $[Mo(CO)_5(\mathbf{14})]$ **68a** and $[W(CO)_5(\mathbf{14})]$ **68b** from primary phosphine **14** and the appropriate metal hexacarbonyl complexes $[Mo(CO)_6]$ and $[W(CO)_6]$.

Coordination of **14** to the metal complexes resulted in a downfield shift of the $^{31}P\{^1H\}$ NMR spectroscopic signal from $\delta -122.4$ ppm for the primary phosphine **14** to $\delta -64.1$ for **68a** and $\delta -85.9$ ppm for **68b**. The formation of the tungsten complex **68b** was further confirmed by the appearance of tungsten satellite peaks $^1J_{PW} = 223$ Hz, consistent with data reported in the literature.¹³² The volatiles were removed *in vacuo* and purification was carried out by column chromatography to yield **68a** and **68b** in 44% and 38% yield respectively. The low yields can be attributed to the additional formation of the disubstituted side products $[Mo(CO)_4(\mathbf{14})_2]$ and $[W(CO)_4(\mathbf{14})_2]$.

3.14.3 Synthesis of 1,2-Diethynylbenzene

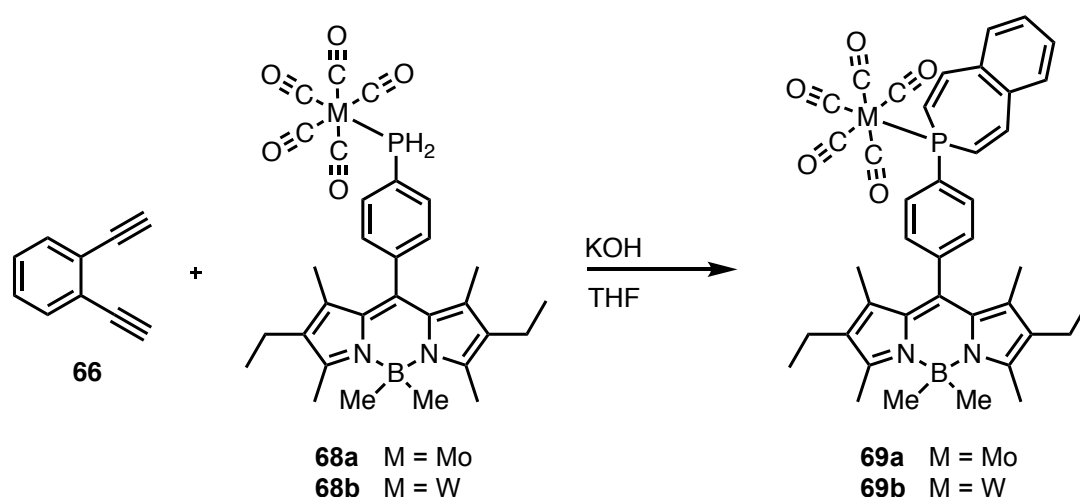
The next step in the synthesis towards a fluorescent 3-benzophosphepine required the preparation of 1,2-diethynylbenzene (**66**), which was accomplished following the procedure from Lammertsma *et al.*⁸⁹ The commercially available *o*-phthalaldehyde **70** was subject to the Corey-Fuchs one-carbon homologation reaction to give the corresponding 1,2-bis(2,2-dibromovinyl)benzene **71** in 76% yield after purification. This 1,2-dibromoalkene **71** then underwent a debromination with LDA to give **66** as a colourless liquid in 15% yield.



Scheme 3.25 Corey-Fuchs reaction from *o*-phthalaldehyde (**70**) to 1,2-bis(2,2-dibromovinyl)benzene (**71**), which is subsequently debrominated with LDA to 1,2-diethynylbenzene (**66**).

3.14.4 Synthesis of Fluorescent Group 6 3-Benzophosphepine Complexes

The original procedure to synthesise free phosphepine **38** reported by Märkl, was achieved by the use of $\text{KOH}/[18]\text{-crown-6}$ complex in a base-catalysed double hydrophosphination reaction.⁸³ Lammertsma and co-workers however, found the use of $\text{KOH}/[18]\text{-crown-6}$ inadequately reproducible and so turned to KOH/THF conditions. Thus, following this updated procedure, $[\text{M}(\text{CO})_5(\mathbf{14})]$ ($\text{M} = \text{Mo}$ or W) was stirred with 1,2-diethynylbenzene in tetrahydrofuran overnight at room temperature. Lammertsma reported that the first hydrophosphination reaction to secondary *cis*-vinylphosphine complex occurred with no additional reagents. However, in our case, analysis of the reaction mixture by $^{31}\text{P}\{^1\text{H}\}$ NMR spectroscopy displayed only starting material. Therefore, in an attempt to induce the hydrophosphination of **68a** and **68b**, potassium hydroxide was added to the stirred solution. After 30 minutes, in both cases, no starting material was observed in the $^{31}\text{P}\{^1\text{H}\}$ NMR spectra.



Scheme 3.26 Synthesis of **69a** and **69b** from the base catalysed double hydrophosphination reaction from **66** and **68a** or **68b** respectively with KOH in THF at room temperature.

The molybdenum complex showed two major peaks in the ^{31}P NMR spectrum; the first at δ 9.5 ppm (dt) gave $^{31}\text{P}\text{-}^1\text{H}$ coupling constants of 313.9 Hz and 9.7 Hz, which are similar to those reported by Lammertsma⁸⁴ for the intermediate *cis*-vinylphosphine complex which he

observed at δ –23 ppm ($J_{\text{PH}} = 345$ Hz); the second at δ –5.78 ppm, gave coupling constants consistent with the desired product **69a** (tt, $^2J_{\text{PH}} = 31.1$ Hz, $^3J_{\text{PH}} = 11.5$ Hz). Purification was carried out by filtration of the reaction mixture through silica gel which isolated the compound in 43% yield. The formation of the desired product was confirmed by analysis of the ^1H NMR spectrum. A characteristic resonance indicating the presence of protons 2 and 4 (depicted in Figure 3.30) was observed at δ 6.41 ppm with an expected doublet of doublets pattern and coupling constants of $^2J_{\text{HP}} = 31.0$ Hz and $^3J_{\text{HH}} = 12.2$ Hz.

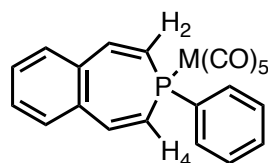


Figure 3.30 Labelling scheme used for phosphapine compounds.

Crystals suitable for X-ray crystallographic analysis were obtained from slow diffusion of pentane into a diethyl ether solution of **69a** and shown in Figure 3.31.

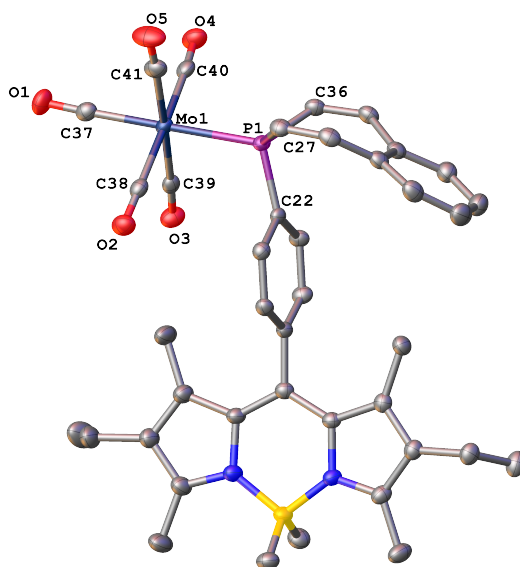


Figure 3.31 View of the molecular structure of **69a**. Hydrogen atoms have been omitted for clarity. Selected bond distances [\AA] and angles [$^\circ$]: Mo1-P1 2.5190(4), Mo1-C37 2.006(2), Mo1-C38 2.051(2), Mo1-C39 2.042(2), Mo1-C40 2.043(2), Mo1-C41 2.050(2), O1-C37 1.145(2), O2-C38 1.140(2), O3-C39 1.138(2), O4-C40 1.141(2), O5-C41 1.136(3), C37-Mo1-P1 178.26(6), C22-P1-Mo1 110.07(5), C27-P1-Mo1 118.16(6), C27-P1-C22 103.21(8), C36-P1-Mo1 117.55(6), C36-P1-C22 105.75(8), C36-P1-C27 100.47(9).

In the case of the tungsten complex, three major chemical shifts were observed in the crude $^{31}\text{P}\{^1\text{H}\}$ NMR spectrum. The largest resonance was observed at δ –26.9 ppm, which displayed coupling constants in the ^{31}P NMR spectrum consistent with the desired product (tt, with ^{183}W satellite $^1J_{\text{PW}} = 239$ Hz, $^2J_{\text{PH}} = 31.3$, $^3J_{\text{PH}} = 11.2$ Hz), **69b**. A second resonance at δ 46.6 ppm presented coupling constants consistent with a one-bond ^{31}P - ^1H coupling (313.9 Hz) and a two-bond ^{31}P - ^1H coupling (10.0 Hz). These coupling constants are indicative of a secondary

phosphine, and perhaps suggest an intermediate compound such as a *cis*-vinylphosphine complex as observed by the Lammertsma group before the addition of potassium hydroxide. A final chemical shift was displayed at $\delta -130.7$ ppm (dt, $J_{\text{PH}} = 180.8, 5.6$ Hz) with ^{183}W satellite peaks of 75.1 Hz. Discussions with Professor Lammertsma¹³³ have suggested that this could indicate the presence of an oxygen atom or perhaps the coordination of the tungsten pentacarbonyl group to a P=C bond, yet, the identity is unknown.

Similarly to the molybdenum complex, purification was carried out by filtration of the reaction mixture over silica gel which resulted only in the isolation of the compound with phosphorus resonance at $\delta -26.9$ ppm, in 30% yield. Confirmation of the desired product was realised through ^1H NMR spectroscopy, where a characteristic doublet of doublets was observed at δ 6.51 ppm with a two-bond ^{31}P - ^1H coupling constant of 31.4 Hz, and a three-bond ^1H - ^1H coupling constant of 12.1 Hz. Crystals suitable for X-ray crystallographic analysis were obtained from slow diffusion of petroleum ether into diethyl ether and is shown in Figure 3.32.

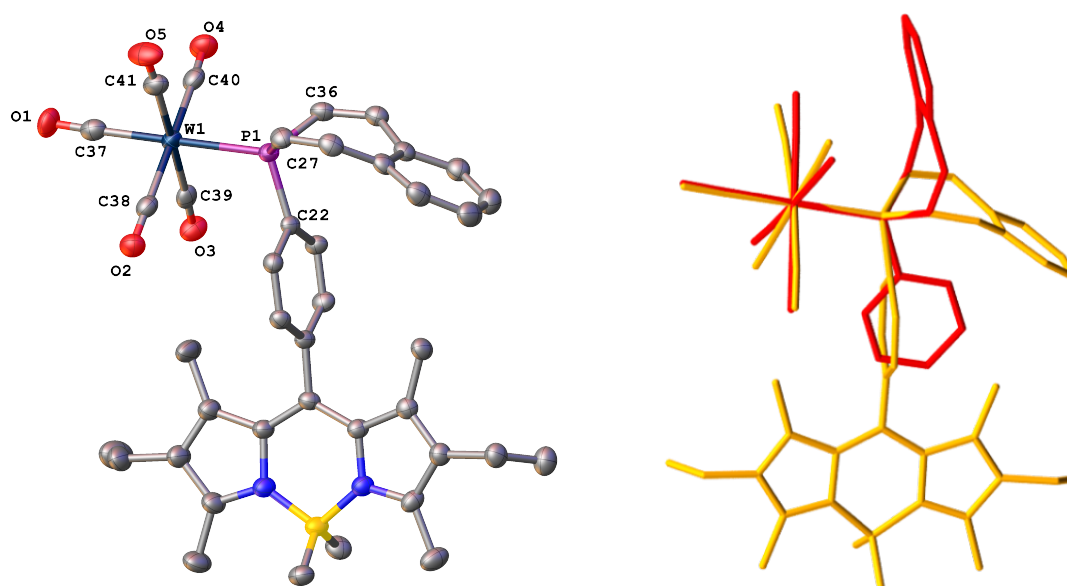


Figure 3.32 View of the molecular structure of **69b** (left). Hydrogen atoms have been omitted for clarity. Selected bond distances [Å] and angles [°]: W1-P1 2.5080(9), W1-C37 2.008(5), W1-C38 2.008(5), W1-C39 2.038(5), W1-C40 2.050(5), W1-C41 2.051(5), O1-C37 1.146(5), 1.137(5), O3-C39 1.140(5), O4-C40 1.135(6), O5-C41 1.123(6), P1-C22 1.828(4), P1-C27 1.808(4), P1-C36 1.802 (4), C37-W1-P1 178.38(14), C22-P1-W1 110.08(11), C27-P1-W1 117.87(14), C27-P1-C22 103.36(18). Overlapping crystal structures of **41b** and **69b** created in Olex2 (right).¹³⁴

Both Bodipy phosphepine complexes (**69a** and **69b**) show bond lengths and angles comparable to each other, which are also in agreement with examples from the literature.⁸⁹ When compared to the analogous tungsten complex published by Lammertsma *et al.*, the W1-P1 bond is marginally shorter for **69b** (2.5080 Å) than for Lammertsma's complex (**41b**) (2.5279 Å). This is reversed when looking at the W1-C37 bond which is 2.007(6) Å for **69b** and 2.003 Å for **41b**. A larger M1-P1-C22 angle is observed in Lammertsma's tungsten complex **41b**

(119.0°) in comparison to the Bodipy tungsten complex **69b** (110.08°) which is presumably due to the increased steric hinderance of the Bodipy backbone. The intracyclic angles around P1 are all similar with angles of 100.47(9)° (**69a**), 100.67° (**69b**) and 100.6° (**41b**). These differences and similarities can be visualised in Figure 3.32 with an overlay of the two tungsten crystal structures.

3.14.5 IR and NMR Spectroscopic Characterisation

Selected IR and NMR spectroscopic data for the primary phosphine complexes **68a** and **68b**¹³², the phosphepine complexes **69a** and **69b**, and the analogous non-fluorescent phenylphosphine complexes **67a** and **67b** and the 3-phenyl-benzophosphepine complexes **41a** and **41b**⁸⁴ have been compiled and are displayed in Table 3.5.

IR stretching frequencies of carbonyl groups in metal complexes are very distinctive within the spectra and their values provide information on the electronic properties of the phosphine, following Tolman's electronic parameter.¹³⁵ All the pentacarbonyl complexes in the table have been assigned to point group C_{4v} and therefore three carbonyl stretching frequencies A_1 (*cis/equatorial*), A_1 (*trans/axial*) and E should be observed.

Table 3.5 Selected IR and NMR spectroscopic data for group 6 transition metal-phosphine complexes.

	$\tilde{\nu}(\text{CO})$ A_1 $Eq\text{ cm}^{-1}$	$\tilde{\nu}(\text{CO})$ A_1 $Ax\text{ cm}^{-1}$	$\tilde{\nu}(\text{CO})$ E cm^{-1}	$^{31}\text{P } \delta$ ppm	$^1J_{\text{PH}}$ Hz	$^1J_{\text{PW}}$ Hz	$\delta (^2J_{\text{P-C}})$ CO <i>Trans</i>	$\delta (^2J_{\text{P-C}})$ CO <i>Cis</i>
[Mo(CO) ₅ (PhPH ₂)] 67a	2074	1945	Not reported	−66.6	312.0	-	Not reported	Not reported
[W(CO) ₅ (PhPH ₂)] 67b	2077	1948	Not reported	−87.7	343.0	224.6	Not reported	Not reported
[Mo(CO) ₅ (14)] 68a	2076	1992	1929	−64.1	327.3	-	208.8 (24.0)	204.7 (9.1)
[W(CO) ₅ (14)] 68b	2077	1973	1902	−85.8	341.4	223.0	198.3 (22.6)	195.5 (6.8)
41a	2071	1948	Not reported	5.8	-	-	210.2 (22.0)	205.2 (9.1)
41b	2070	1928	Not reported	−14.8	-	237.7	199.9 (4.2)	196.4 (7.0)
69a	2070	1984	1917	−5.8	-	-	205.4 (9.2)	Not observed
69b	2070	1979	1928	−26.9	-	239.7	199.5 (12.6)	196.6 (7.0)

IR spectra recorded neat; NMR spectra recorded in *d*-chloroform

The IR stretching frequencies of the carbonyl groups lowers from the primary phosphine complexes **67a**, **67b**, **68a** and **68b** ($\tilde{\nu}$ = 2074, 2077, 2076, 2077 cm^{-1} respectively) to their

corresponding phosphine complexes **41a**, **41b**, **69a** and **69b** ($\tilde{\nu} = 2071, 2070, 2070, 2070$ cm⁻¹ respectively). This lower frequency coincides with the phosphines being better σ -donors. The $^1J_{\text{PW}}$ coupling constants were larger for cyclic tertiary phosphine complexes **41b** and **69b**, in comparison to their primary phosphine complex precursors **67b** and **68b** yet this is contrary to the discussion on the fluorescent phosphirane complex **52b** in Section 3.6.2.

Upon cyclisation to cyclic tertiary phosphines, a downfield shift was observed in the $^{31}\text{P}\{^1\text{H}\}$ NMR spectrum. For Lammertsma's complexes (**41a/b**), this was by 72.4 ppm from **67a** to **41a** and 72.9 ppm from **67b** to **41b**, whereas, for the fluorescent complexes, this was only by 58.3 ppm and 58.9 ppm for **69a** and **69b**, respectively. This difference could perhaps suggest variances in the sigma donor properties of the Bodipy complexes **69a** and **69b** in comparison to **41a** and **41b**; the differences in the IR stretching frequencies of the A_1 *eq* carbonyl groups, however, are minimal, suggesting similar electronic properties. The incomplete data from the Lammertsma group means this is inconclusive. However, the increased steric effect of the Bodipy group, as reflected in the M1-P1-C22 bond angle (119.0° for **41b** and 110.08° for **69b**), may account for the observed differences.

3.14.6 Photophysical Properties of $[\text{M}(\text{CO})_5(\text{PR}_3)]$ Complexes **68a**, **68b**, **69a** and **69b**

After the successful synthesis of these novel fluorescent phosphine complexes, it was important to determine their photophysical properties. Photophysical data was collected for **69a** and **69b** in anhydrous, degassed tetrahydrofuran at room temperature (to minimise photobleaching and phosphine oxidation in solution). The data is shown in Table 3.6 alongside the fluorescent primary phosphine complexes **68a** and **68b**, for comparison.¹³²

Table 3.6 Photophysical properties of $[\text{M}(\text{CO})_5(\text{PR}_3)]$ complexes **68a-b** and **69a-b** (M = Mo, W respectively).

	λ_{abs} (nm) ^a	λ_{em} (nm) ^a	Φ_{F} ^{a,b}	ϵ (M ⁻¹ cm ⁻¹) ^a
$[\text{Mo}(\text{CO})_5(\mathbf{14})]$ 68a	512	527	0.25	72,000
$[\text{W}(\text{CO})_5(\mathbf{14})]$ 68b	512	527	0.20	73,000
69a	513	529	0.11	46,000
69b	514	530	0.12	35,000

^a Measured in dry, degassed tetrahydrofuran at room temperature, dyes were excited at 485 nm; ^b Fluorescence quantum yields were measured with respect to 4,4-difluoro-8-phenyl-1,3,5,7-tetramethyl-2,6-diethyl-4-bora-3a,4a-diaza-s-indacene.

The absorption spectra of the two phosphine complexes **69a** and **69b** display a typical Bodipy profile which is shown in Figure 3.33. The maximum absorbance, relating to the S_0 - S_1 (π - π^*) transition, for primary phosphine complexes **68a** and **68b** was observed at 512 nm and

upon cyclisation to the 3-benzophosphepine complexes shifted marginally to 513 and 514 nm, for **69a** and **69b**, respectively. The molar absorption coefficients lowered on cyclisation from $\epsilon = 72,000$ and $73,000 \text{ M}^{-1}\text{cm}^{-1}$ for **68a** and **68b**, to $\epsilon = 46,000$ and $35,000 \text{ M}^{-1}\text{cm}^{-1}$ for the corresponding phosphepines, **69a** and **69b**.

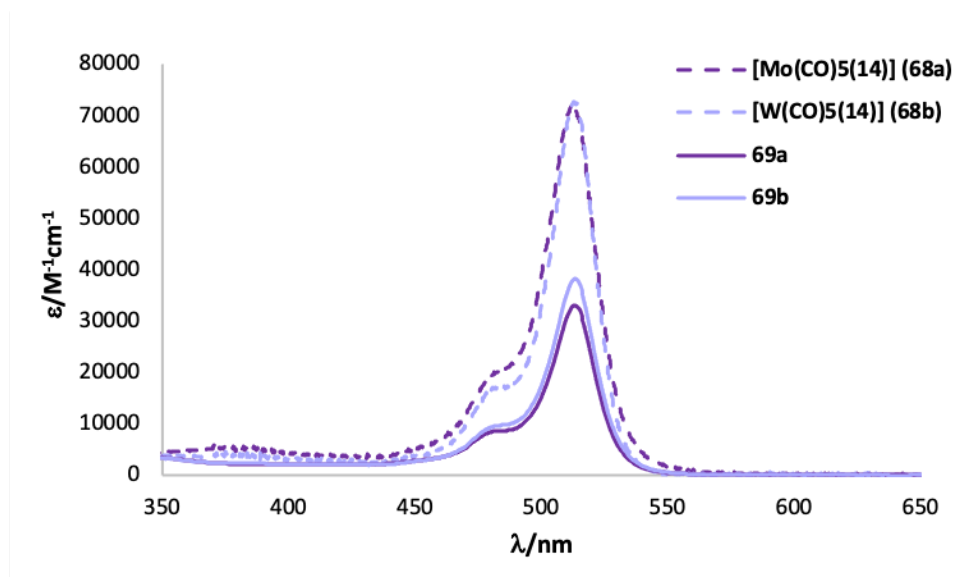


Figure 3.33 Absorption spectra of the complexes $[\text{Mo}(\text{CO})_5(14)]$ **68a**, $[\text{W}(\text{CO})_5(14)]$ **68b**, **69a** and **69b** in tetrahydrofuran at room temperature.

A slight bathochromic shift was also apparent in the emission spectra, the maxima displayed at 527 nm for both the primary phosphine complexes **68a** and **68b** shifted to 529 for **69a** and 530 for **69b**, respectively. A decrease in fluorescence quantum yield was observed upon cyclisation from $\Phi_F = 0.25$ to 0.11 for **68a** to **69a** and from $\Phi_F = 0.20$ to 0.12 for **68b** to **69b**. The emission spectra is displayed in Figure 3.34.

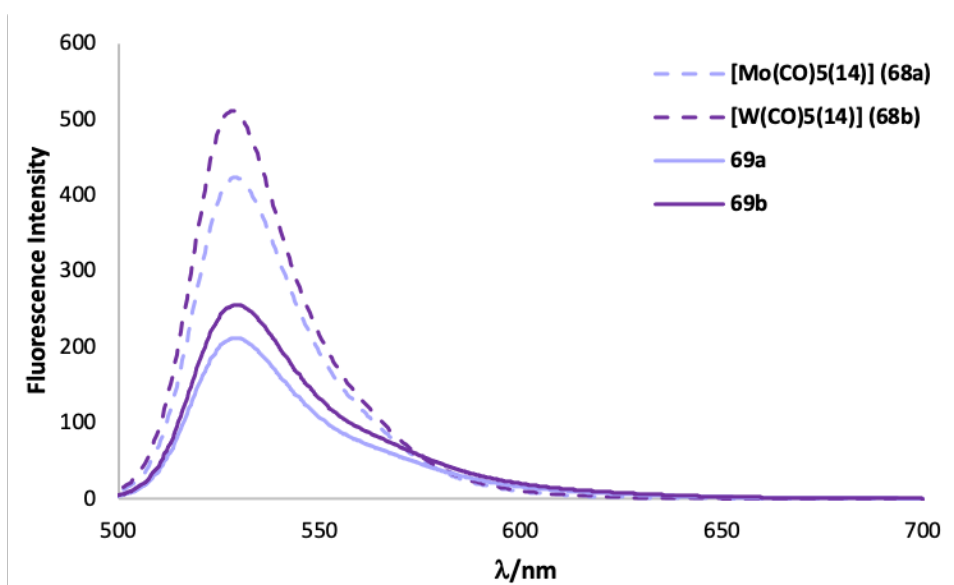


Figure 3.34 Emission spectra of the complexes $[\text{Mo}(\text{CO})_5(14)]$ **68a**, $[\text{W}(\text{CO})_5(14)]$ **68b**, **69a** and **69b** in tetrahydrofuran at room temperature (excitation at 485 nm).

This research has identified that similar to phosphirane **47**, cyclisation to a seven-membered phosphacycles in **69a** and **69b** reduces, but does not fully quench, the fluorescence quantum yield and therefore these complexes still hold potential as optical imaging agents.

3.15 Free Phosphepine

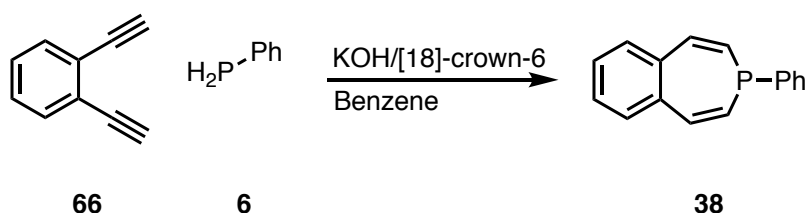
Having established the successful synthesis of the first fluorescent phosphepine complex, the next aim was to synthesise this ligand without the metal scaffold needing to be present. The highly conjugated Bodipy backbone has previously been proven to enhance the air-stability of otherwise unstable compounds, phenyl phosphirane for example, discussed in Section 3.2.1. Thus, it is possible that this could also be the case for a phosphepine.

The advantage of isolating the free phosphepine would allow for further derivatisation of this uncommon seven membered ring, both with other transition metals but also with reactive organic groups.

Quarterisation of the free phosphepine by reaction with alkylating agents such as methyl trifluoromethanesulfonate could give rise to the corresponding phosphepinium salt. As previously seen, positively charged hydrophobic cations localise within the mitochondria and thus the free phosphepine could feasibly be a precursor to a mitochondrial specific imaging agent.

3.15.1 Attempted Synthesis of a Metal-Free Phosphepine

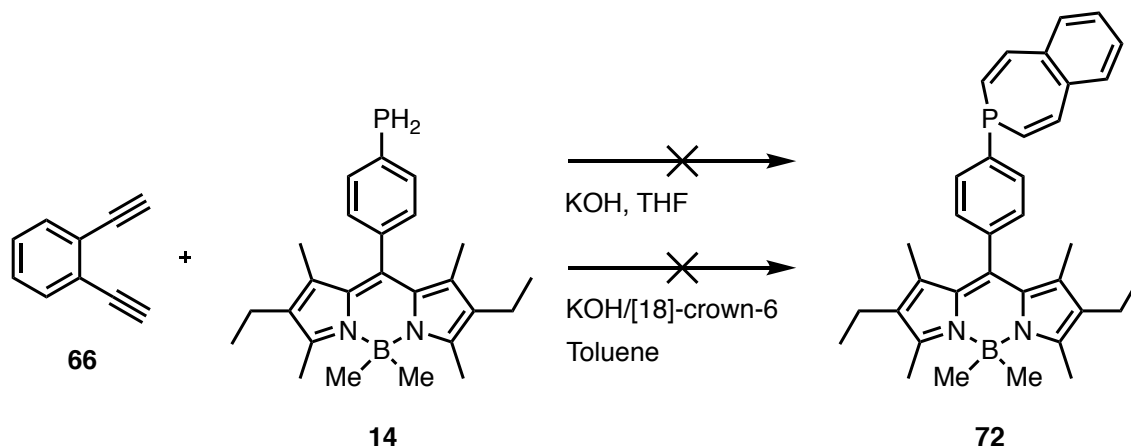
As briefly discussed in Section 3.1.6, two procedures have been reported for the synthesis of the free 3-phenyl-3-benzophosphepine compound. The first, by Märkl in 1983, is similar to the synthesis of metal carbonyl phosphepines (**41a/b** and **69a/b**) and involved the double base catalysed hydrophosphination of phenyl phosphine and 1,2-diethynylbenzene with KOH/[18]-crown-6, shown in Scheme 3.27.⁸³



Scheme 3.27 Synthesis of 3-phenyl-3-benzophosphepine from the base-catalysed hydrophosphination of 1,2-diethynylbenzene by phenylphosphine.

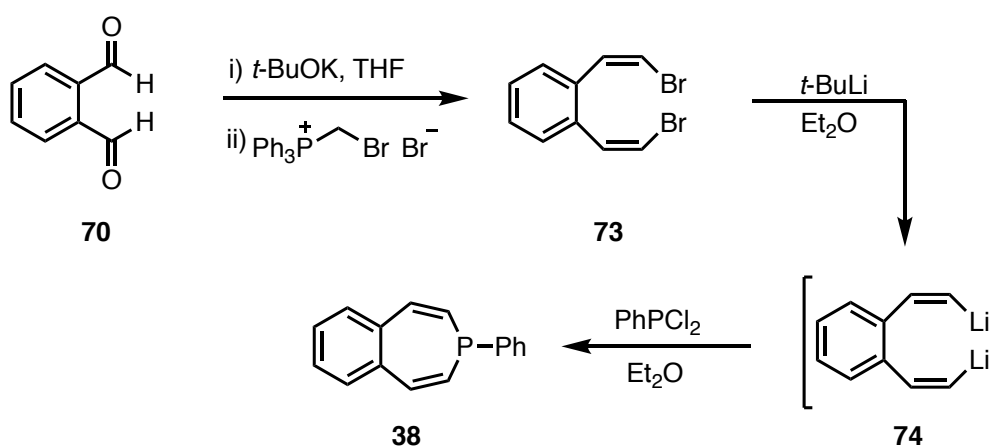
This synthesis was attempted from Bodipy primary phosphine **14** with both potassium hydroxide in tetrahydrofuran and KOH/[18]-crown-6 in toluene. Both experiments however,

resulted in no reaction by $^{31}\text{P}\{^1\text{H}\}$ NMR spectroscopy and only starting material was recovered (Scheme 3.28). Therefore, alternative procedures were considered.



Scheme 3.28 Attempted procedure for the synthesis of **72** from the base catalysed hydrophosphination of **14** with 1,2-diethynylbenzene (**66**) in tetrahydrofuran.

In 1996, Tsuchiya *et al.* reported an alternate procedure for the synthesis of 3-benzophosphepines. This method involved the lithium-halogen exchange reaction of dichlorophenylphosphine with a dilithium intermediate, (*Z,Z*)-*o*-bis(β -lithiovinyl)benzene (**74**), yielding the free 3-phenyl-3-benzophosphepine ligand **38**, shown in Scheme 3.29.⁸⁷

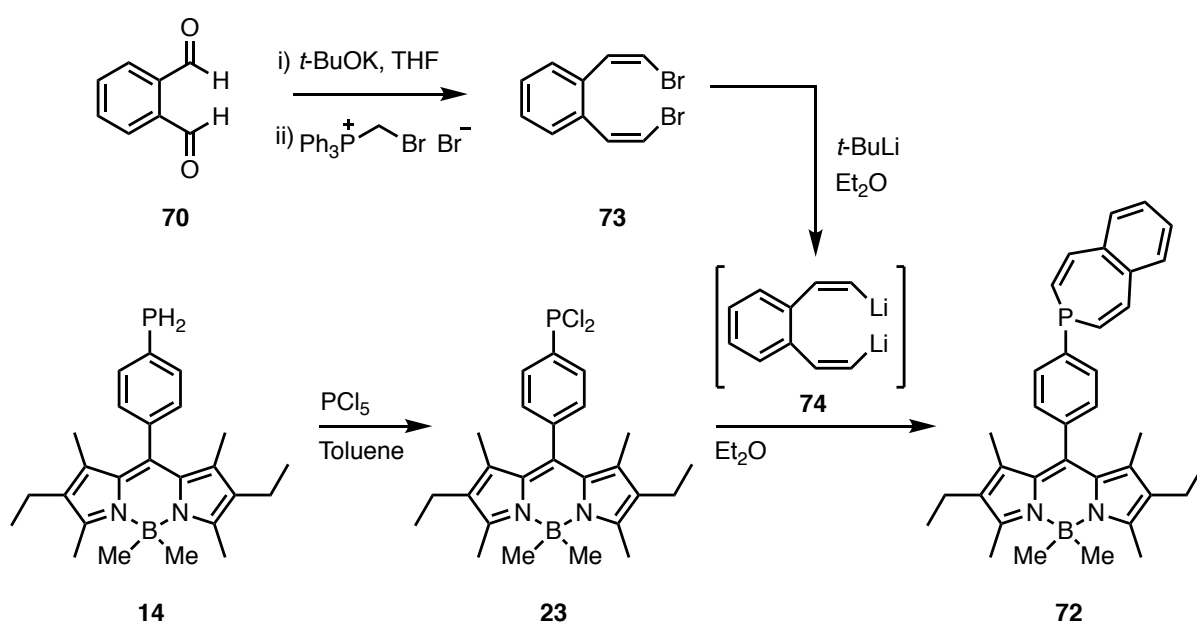


Scheme 3.29 Synthesis of 3-phenyl-3-benzophosphepine from the lithium-halogen exchange reaction of (*Z,Z*)-*o*-bis(β -lithiovinyl)benzene and dichlorophenylphosphine.

Therefore, we planned to synthesise a fluorescent analogue of 3-benzophosphepine **38** based on the work of Tsuchiya *et al.* This procedure first required the synthesis of (*Z,Z*)-*o*-bis(β -bromovinyl)benzene **73** which was prepared via a double Wittig reaction of *o*-phthalaldehyde **70**. To a cooled suspension of potassium *tert*-butoxide in diethyl ether, bromomethyltriphenylphosphonium bromide was added to generate bromomethylenetriphenylphosphorane *in-situ*. To this intermediate, a solution of *o*-phthalaldehyde **70** in tetrahydrofuran was added dropwise. Purification by aqueous work up

and column chromatography (petrol) yielded the desired *cis*-compound **73** in 37% yield (much lower than the reported 90%). This was stored in the freezer until ready to use.

Finally, for the synthesis of the target fluorescent 3-benzophosphepine **72**, the previously isolated (*Z,Z*)-*o*-bis(β -bromovinyl)benzene **73** was dilithiated with *tert*-butyllithium at -78°C in diethyl ether before being reacted with the dichloroaryl phosphine. Thus, in parallel, Bodipy primary phosphine **14** was subject to a chlorination reaction with phosphorus pentachloride in toluene to afford the Bodipy dichlorophosphine **23**. The synthesis of **23** was confirmed by $^{31}\text{P}\{^1\text{H}\}$ NMR spectroscopy by a resonance at δ 159.7 ppm. The volatiles were removed *in vacuo* and the dichlorinated compound **23** was suspended in diethyl ether. **23** was then added dropwise to the cooled dilithiated intermediate **74**. The reaction is illustrated in Scheme 3.30.



Scheme 3.30 Proposed route to synthesise the fluorescent 3-benzophosphepine **72** from (*Z,Z*)-*o*-bis(β -bromovinyl)benzene **73** and the dichlorophosphine intermediate **23**.

The reaction was monitored by $^{31}\text{P}\{^1\text{H}\}$ NMR spectroscopy and after approximately one hour, the complete consumption of dichlorophosphine **23** was apparent, and a new resonance at δ -5.9 ppm was observed. Following an aqueous work up, the appearance of a smaller, second resonance at δ 46.8 ppm was observed. Further purification by column chromatography was carried out, but only the compound with a ^{31}P NMR resonance at δ 46.8 ppm was isolated. Analysis of the non-decoupled $^{31}\text{P}-^1\text{H}$ NMR spectrum presented a doublet of multiplets, with the largest coupling of $J_{\text{PH}} = 466$ Hz consistent with a one-bond $^{31}\text{P}-^1\text{H}$ coupling. This data supports the formation of a secondary *cis*-vinylphosphine intermediate or its corresponding oxide product.

Märkl reported the ^{31}P NMR shift for the 3-phenyl-3-benzophosphepine at δ –33.3 ppm. It is possible that the resonance at δ –5.9 ppm could perhaps be desired free phosphepine (**72**) or phosphepine oxide, but further characterisation data could not be obtained.

3.16 DFT Calculations

To gain further insight into the properties of these novel 3-benzophosphepines, DFT calculations were carried out using Spartan '14 software.¹⁰⁶ Geometry optimised calculations were carried out at the B3LYP/LACVP level of theory.

Although it has not yet been successfully isolated, DFT calculations were carried out for **72**. These calculations illustrate both a Bodipy based LUMO (–1.9 eV) and HOMO (–4.9 eV) with no phosphorus character until the HOMO–2 (–5.9 eV). The calculated molecular orbitals are shown in Figure 3.35.

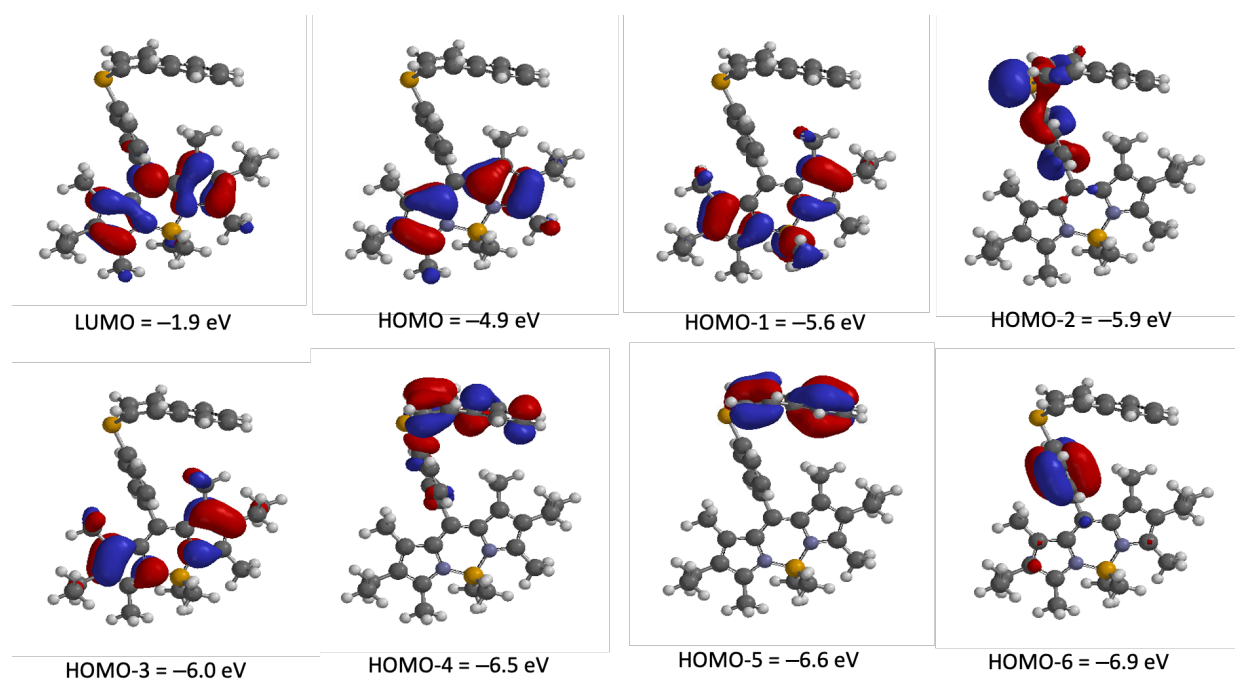


Figure 3.35 Calculated molecular orbital surfaces from the LUMO to HOMO–6 of the free phosphepine ligand **72**.

The molybdenum and tungsten complexes **69a** and **69b** were successfully synthesised and their solid-state structures derived by X-ray crystallographic diffraction. Whilst these complexes also display Bodipy based LUMO and HOMOs, there is also electron density centred around the benzophosphepines, particularly in the case of the tungsten complex **69b**. The orbital energies for their precursors **68a** and **68b**, which have previously reported,¹³⁶ also have Bodipy based HOMOs (–5.2 and –5.3 eV respectively) and LUMOs (–2.2 for both complexes). Neither **69a** nor **69b** exhibit phosphorus character until the HOMO–6 at –6.9 eV for both complexes. The calculated molecular orbitals are shown in Figures 3.36 and 3.37 respectively.

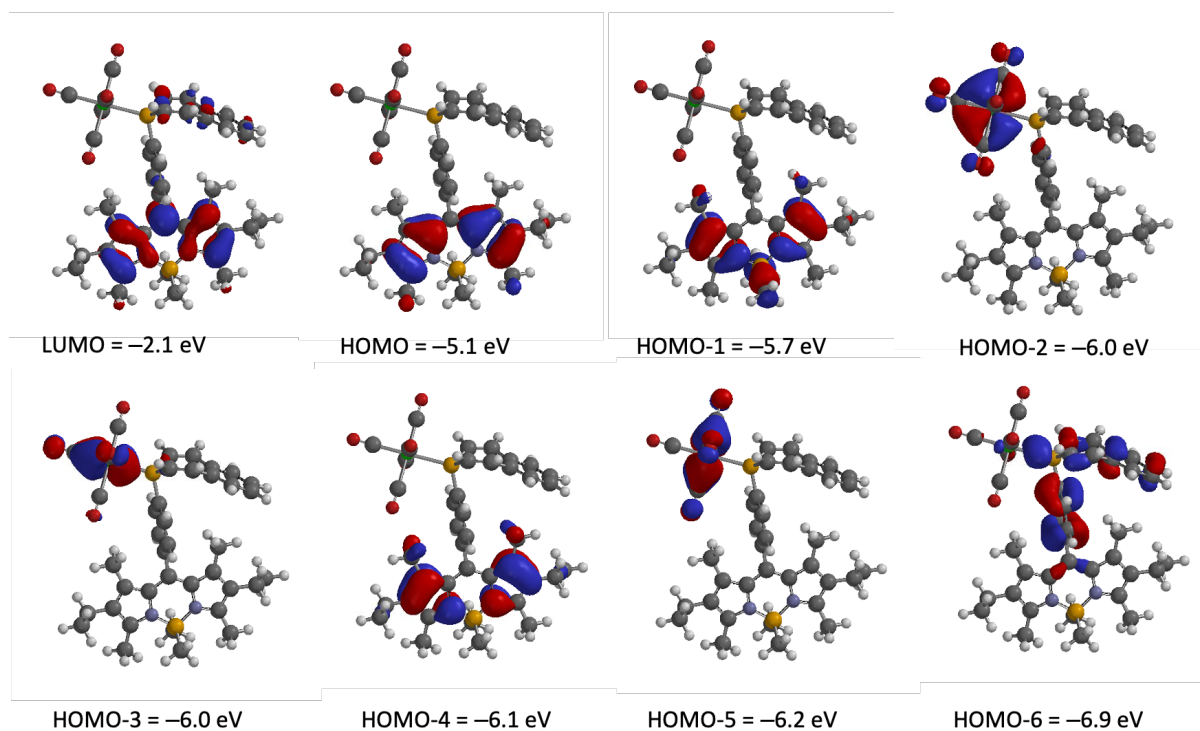


Figure 3.36 Calculated molecular orbital surfaces from the LUMO to HOMO-6 of the molybdenum pentacarbonyl phosphepine complex, **69a**.

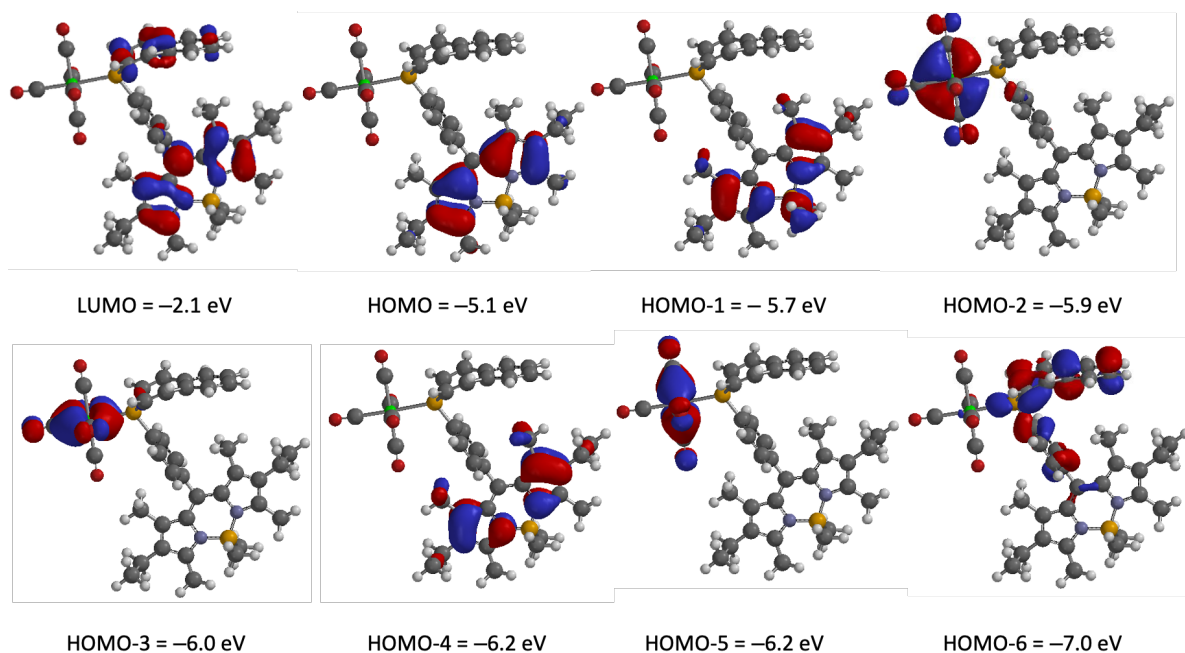


Figure 3.37 Calculated molecular orbital surfaces from the LUMO to HOMO-6 of the tungsten pentacarbonyl phosphepine complex, **69b**.

3.17 Phosphepine Summary

This section introduced the little-studied, seven-membered, unsaturated benzophosphepines. The first fluorescent 3-benzophosphepine group 6 complexes **69a** and **69b** were synthesised from the base-catalysed double hydrophosphination reaction of 1,2-

diethynylbenzene with the group 6 pentacarbonyl primary phosphine complexes **68a** and **68b**. The products were both characterised by NMR and IR spectroscopy and X-ray diffraction, and the analytical data was compared to the analogous complexes reported by Lammertsma *et al.* **41a** and **41b** and their respective primary phosphine complexes [Mo(PhPH₂)CO₅] **67a**, [W(PhPH₂)CO₅] **67b**. Photophysical measurements were obtained to establish the differences in the properties of primary phosphine complex **68a** and **68b** to their corresponding 3-benzophosphepine complexes **69a** and **69b**. The phosphepine complexes displayed lower quantum yields to their precursors, yet the fluorescence was not quenched. Preliminary experiments were carried out in an attempt to synthesise the free fluorescent phosphepine ligand. A base-catalysed hydrophosphination reaction from primary phosphine **14** with **66** resulted in no reaction and so a second approach was taken. A lithium-halogen exchange reaction using dilithio compound **74** with the fluorescent dichlorophosphine **23** resulted in promising signals in the ³¹P{¹H} NMR spectra of the crude reaction mixture. However, attempted isolation of this compound for further analysis proved unsuccessful. Further experiments could be carried out to develop the metal-free synthesis to the seven-membered phosphacycle which would expand its potential applications. Isolating the free ligand may allow for a quarternisation reaction leading to a phosphepinium salt which could also have application in the fluorescence imaging of mitochondria. It would be of particular interest to and compare the cellular activity of this cyclic tertiary phosphine to the acyclic versions reported by the Higham group to understand how the phosphacycle might affect the behaviour with respect to biodistribution within the cell, and the mitochondria in particular.

3.18 Chapter Summary

We described the synthesis of three phosphacycles of ring sizes, three (**47**), six (**62a** and **62b**), and seven (**69a** and **69b**) from the fluorescent Bodipy primary phosphine **14**. The structural properties were evaluated by X-ray crystallographic studies and in addition, the σ -donor/ π -acceptor properties of **47**, **69a** and **69b** were analysed through their coordination to tungsten and molybdenum metal carbonyl complexes. The photophysical properties of the novel phosphacycles were assessed, and showed slightly reduced quantum yields in comparison to that of their primary phosphine precursor **14**, but all of the cyclic compounds retained their fluorescent properties.

We saw that there are diverse potential applications of these phosphacycles, for example, the fluorescent phosphirane has an unusual ³¹P NMR chemical shift that could potentially be exploited in ³¹P MRS and optical imaging, while the 1,3,5-diazaphosphinane, was coordinated

to chromium(III) and the resulting complex showed activity in the catalysis of hexene trimerization. In addition, this complex showed extended activity over the triaza analogues, thus, demonstrating promise for turning off the decomposition routes that are observed for the 1,3,5-triazacyclohexanes.

When investigating the synthesis of the fluorescent 1,3,5-diazaphosphinanes **62a** and **62b**, we found that the Bodipy bis(hydroxymethyl)phosphine **24d**, which could act as a starting material in its synthesis, actually has exciting potential in the modification of amine-functionalised surfaces to produce fluorescently labelled surfaces. Preliminary experiments carried out using amine modified silica (SBA-15), proved successful, and thus, this represents a promising approach for the detection of amine-containing compounds such as residual collagen in bones.

Attempts to isolate the fluorescent phosphepine **72** proved unsuccessful, though a characteristic peak at $\delta -5.9$ ppm was observed in the ^{31}P NMR spectrum of the crude reaction mixture, leaving a strong basis for a future project. The isolation of the free ligand would open up routes for its further functionalisation, likely enabling the synthesis of corresponding phosphepinium salts which may have application in mitochondrial specific imaging. This would allow for comparisons of the cellular behaviour of a cyclic salt to the acyclic versions previously reported by our group.

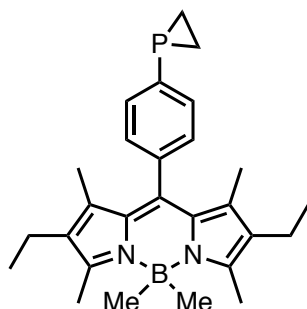
3.19 Experimental Procedures and Analytical Data

3.19.1 General Procedure

All air- and/or water-sensitive reactions were performed under a nitrogen atmosphere using standard Schlenk line techniques. Tetrahydrofuran was distilled over sodium/benzophenone, dichloromethane over calcium hydride and *d*-chloroform over phosphorus pentoxide; all solvents were distilled prior to use. $[\text{Pt}(\eta^2:\eta^2\text{-cod})\text{Cl}_2]$ was prepared according to a literature procedure.¹³⁷ All other chemicals were purchased from Sigma Aldrich, Fisher Scientific, Alfa Aesar or Fluorochem and used as received. Flash chromatography was performed on silica gel from Fluorochem (silica gel, 40-63 μ , 60 Å). Thin-layer chromatography was performed on Fisher aluminium-based plates with silica gel and fluorescent indicator (254 nm). ^1H , $^{13}\text{C}\{^1\text{H}\}$, $^{31}\text{P}\{^1\text{H}\}$, and $^{11}\text{B}\{^1\text{H}\}$ NMR spectra were recorded on a Bruker Avance III 300 MHz (^1H 300.13 MHz), Bruker Avance II 400 MHz (^1H 399.78 MHz) or Bruker Avance III HD 500 MHz (^1H 500.16 MHz) spectrometer at room temperature (21 °C) using the indicated solvent as internal reference; ^1H and ^{13}C shifts were relative to tetramethylsilane, ^{31}P relative to 80% H_3PO_4 , and ^{11}B relative to $\text{BF}_3\cdot\text{Et}_2\text{O}$. IR spectra were recorded on a Varian 800 FT-IR spectrometer and mass spectrometry was carried out by the EPSRC National Mass Spectrometry Service Centre, Swansea or the SAgE Mass Spectrometry Facility (Newcastle University) performed by Dr Rachael Dack or Dr Alex Charlton. The X-ray crystallographic data were collected on an Xcalibur, Atlas, Gemini ultra diffractometer equipped with a fine-focus sealed X-ray tube ($\lambda_{\text{CuK}\alpha} = 1.54184$ Å) and an Oxford Cryosystems CryostreamPlus open-flow N_2 cooling device. The analysis of the X-ray diffraction data of the compounds was performed by Dr Paul Waddell (Newcastle University). DFT calculations were carried out on Spartan '14 using the B3LYP functional with a 6-31G* basis set.¹⁰⁶

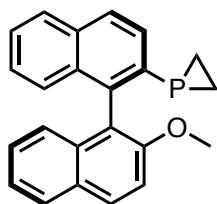
3.20 Phosphirane and Phosphiranium Experimental

3.20.1 8-((4-Phosphirane)phenyl)-4,4-dimethyl-1,3,5,7-tetramethyl-2,6-diethyl-4-bora-3a,4a-diaza-s-indacene (**47**)



Methyl lithium (1.6M, 0.97 mL, 1.60 mmol) was added to a solution of primary phosphine **14** (0.300 g, 0.74 mmol) in anhydrous tetrahydrofuran (15 mL) which had been cooled to -78°C in a dry ice/acetone bath. The reaction mixture was stirred for 30 minutes at -78°C before anhydrous 1,2-dichloroethane (0.07 mL, 0.89 mmol) was added dropwise. The reaction mixture was warmed to RT and stirred for two hours, quenched slowly with water and extracted with diethyl ether (3 x 15 mL). Purification by column chromatography (dichloromethane/petroleum ether, 3:7) afforded **47** as an orange solid (0.109 g, 34%). Crystals suitable for X-ray crystallographic analysis were obtained from slow evaporation of dichloromethane. ^1H NMR (400 MHz, CDCl_3) δ 7.44 (pseudo t, $^3J_{\text{HH}} = 7.5$ Hz, 2H), 7.19 (d, $^3J_{\text{HH}} = 7.5$ Hz, 2H), 2.44 (s, 6H), 2.30 (q, $^3J_{\text{HH}} = 7.5$ Hz, 4H), 1.36–1.12 (m, 4H), 1.21 (s, 6H), 0.97 (t, $^3J_{\text{HH}} = 7.5$ Hz, 6H), 0.26 (s, 6H) ppm; $^{31}\text{P}\{^1\text{H}\}$ NMR (162 MHz, CDCl_3) δ -237.2 (s, 1P) ppm; $^{31}\text{P}-^1\text{H}$ NMR (121 MHz, CDCl_3) δ -237.2 (tt, $J_{\text{PH}} = 7.6$ Hz, $J_{\text{PH}} = 15.7$ Hz) ppm; $^{11}\text{B}\{^1\text{H}\}$ NMR (96 MHz, CDCl_3) δ -1.2 (s, 1B) ppm; $^{13}\text{C}\{^1\text{H}\}$ NMR (75 MHz, CDCl_3) δ 150.8, 139.9, 139.9 (d, $J_{\text{CP}} = 41.2$ Hz), 137.5, 133.8, 132.6, 132.1, 131.9, 129.0, 128.7 (d, $J_{\text{CP}} = 6.2$ Hz), 17.6, 14.8, 14.5, 12.0, 10.6 (d, $J_{\text{CP}} = 39.7$ Hz) ppm; IR (neat): $\tilde{\nu} = 2959$ (w), 2928 (w), 2867 (w), 1546 (s), 1469 (w), 1402 (w), 1359 (m), 1313 (s), 1290 (m), 1261 (w), 1167 (s), 1142 (s), 1110 (m), 1062 (w), 1022 (w), 977 (m), 943 (s), 906 (m), 792 (s), 704 (w), 671 (m), 558 (w), 512 (m) cm^{-1} ; HRMS (ESI $^{+}$) calcd for $\text{C}_{27}\text{H}_{36}\text{BN}_2\text{P}$ $[\text{M}]^{+}$ requires m/z 431.2792, found m/z 431.2618.

3.20.2 (*R*)-1-(2'-Methoxy-1,1'-binaphthyl-2-yl)phosphirane (**32a**)



Methyl lithium (1.6M, 1.3 mL, 2.09 mmol) was added to a solution of primary phosphine (**10a**) (0.300 g, 0.95 mmol) in anhydrous tetrahydrofuran (6 mL) which had been cooled to $-78\text{ }^{\circ}\text{C}$ in a dry ice/acetone bath. The reaction mixture was stirred for 30 minutes at $-78\text{ }^{\circ}\text{C}$ before anhydrous 1,2-dichloroethane (0.09 mL, 1.14 mmol) was added dropwise. The reaction mixture was warmed to RT, stirred for two hours and quenched slowly with water and extracted with diethyl ether (3 x 15 mL). Purification by column chromatography (dichloromethane/petroleum ether, 3:7) to yield **32a** as a white solid (0.264 g, 81%). Crystals suitable for X-ray crystallographic analysis were obtained from slow evaporation of dichloromethane. $^1\text{H NMR}$ (300 MHz, CDCl_3) δ 8.15 (d, $^3J_{\text{HH}} = 9.0\text{ Hz}$, 1H), 8.01 (d, $^3J_{\text{HH}} = 8.2\text{ Hz}$, 1H), 7.96 (d, $^3J_{\text{HH}} = 6.1\text{ Hz}$, 1H), 7.93 (d, $^3J_{\text{HH}} = 6.2\text{ Hz}$, 1H), 7.62–7.39 (m, 5H), 7.38–7.34 (m, 1H), 7.32 (d, $^3J_{\text{HH}} = 6.5\text{ Hz}$, 1H), 7.10 (d, $^3J_{\text{HH}} = 8.5\text{ Hz}$, 1H), 3.91 (s, 3H), 1.56–1.40 (m, 1H), 1.39–1.28 (m, 1H), 1.08–0.96 (m, 1H), 0.96–0.81 (m, 1H) ppm; $^{13}\text{C}\{^1\text{H}\}$ NMR (75 MHz, CDCl_3) δ 155.0, 141.3 (d, $^2J_{\text{CP}} = 24.4\text{ Hz}$), 137.7 (d, $^1J_{\text{CP}} = 39.3\text{ Hz}$), 134.3, 133.3, 132.7, 130.2, 129.1, 128.2, 128.1, 127.8, 127.3, 126.9, 126.5, 126.1, 125.9, 125.2, 123.8, 122.0 (d, $J_{\text{CP}} = 6.6\text{ Hz}$), 113.5, 56.5, 9.3 (d, $^1J_{\text{CP}} = 11.2\text{ Hz}$), 8.8 (d, $^1J_{\text{CP}} = 11.1\text{ Hz}$) ppm; $^{31}\text{P}\{^1\text{H}\}$ NMR (121 MHz, CDCl_3) δ -235.5 ppm; $^{31}\text{P}-^1\text{H}$ NMR (121 MHz, CDCl_3) δ -235.5 (pseudo-t, $^2J_{\text{PH}} = 18.1\text{ Hz}$) ppm. IR (neat): $\tilde{\nu} = 3051$ (w), 2934 (w), 2837 (w), 1619 (w), 1591 (m), 1501 (m), 1459 (w), 1429 (w), 1331 (w), 1268 (m), 1249 (s), 1145 (w), 1077 (m), 1050 (m), 1019 (m), 906 (w), 804 (s), 741 (m), 625 (m), 594 (w), 538 (w), 465 (m), 437 (m) cm^{-1} . HRMS (ESI $^{+}$) calcd for $\text{C}_{23}\text{H}_{20}\text{OP}$ $[\text{M}]^{+}$ requires m/z 343.1278, found m/z 343.1252 (7.6 ppm). These spectroscopic data are in agreement with the literature.²⁴

3.20.3 Solid-State Oxidation Experiments

A 0.020 g aliquot of the phosphirane was placed in a glass vial, exposed to air and stored in the dark for seven days. The sample was analysed on day one and day seven by ^{31}P NMR spectroscopy in *d*-chloroform, with a relaxation time of three seconds and with NOE removed to allow for integration.

3.20.4 Solution-State Oxidation Experiments

A 0.020 g aliquot of the phosphirane, was dissolved in *d*-chloroform. The solution was placed in a glass vial, exposed to air and stored in the dark. The sample was analysed every 24 hours for seven days by ^{31}P NMR spectroscopy, with a relaxation time of three seconds and with NOE removed to allow for integration.

3.20.5 Thermal Stability Experiments

A Schlenk flask was charged with phosphirane (0.020 g, 0.05 mmol) and cycled between vacuum and nitrogen. Anhydrous toluene (3 mL) was added, and the reaction was heated to reflux (110 °C). ^{31}P NMR spectroscopy (relaxation time of 3 seconds and with NOE removed to allow for integration) was obtained before and after 16 hours of reflux conditions.

3.20.6 *cis*-[Pt(**47**)₂Cl₂] (**50**)

[Pt(η^2 : η^2 -cod)Cl₂] (0.035 g, 0.1 mmol) was added to a stirred solution of **47** (0.08 g, 0.02 mmol) in anhydrous dichloromethane (2 mL). The reaction mixture was analysed by $^{31}\text{P}\{^1\text{H}\}$ NMR spectroscopy which showed complete conversion of starting material after two hours. Solvent was removed *in vacuo* to yield the desired product (100% conversion). **$^{31}\text{P}\{^1\text{H}\}$ NMR** (121 MHz, CDCl₃) δ -142.80 (s, with ^{195}Pt satellites, $^1J_{\text{PPt}} = 4070.8$ Hz).

3.20.7 *cis*-[Pt(**32a**)₂Cl₂] (**49a**)

[Pt(η^2 : η^2 -cod)Cl₂] (0.019 g, 0.05 mmol) was added to a stirred solution of (*R*)-1-(2'-methoxy-[1,1'-binaphthalen]-2-yl)phosphirane (0.034 g, 0.10 mmol) in anhydrous dichloromethane (7 mL). The reaction mixture was analysed by $^{31}\text{P}\{^1\text{H}\}$ NMR which showed complete conversion of starting material after two hours. The solvent was removed *in vacuo* to afford the desired product (100% conversion). **^1H NMR** (300 MHz, CDCl₃) δ 8.11 (d, $^3J_{\text{HH}} = 9.1$ Hz, 1H), 7.91 (d, $^3J_{\text{HH}} = 8.2$ Hz, 1H), 7.84 (d, $^3J_{\text{HH}} = 8.2$ Hz, 1H), 7.81–7.73 (m, 2H), 7.50–7.42 (m, 2H), 7.42–7.35 (m, 1H), 7.30 (pseudo-t, $^3J_{\text{HH}} = 8.3$ Hz, 1H), 7.18 (pseudo-t, $^3J_{\text{HH}} = 8.3$ Hz, 1H), 6.87 (pseudo-t, $^3J_{\text{HH}} = 8.4$ Hz, 1H), 3.74 (s, 3H), 1.25 (m, 2H), 1.02 (m, 2H), -0.09 (m, 2H), 0.42–0.17 (m, 2H); **$^{31}\text{P}\{^1\text{H}\}$ NMR** (121 MHz, CDCl₃) δ -149.8 (s with ^{195}Pt satellites, $^1J_{\text{PPt}} = 4160.2$ Hz) ppm. These spectroscopic data are in agreement with literature values.²⁴

3.20.8 General Procedure for the Preparation of $[M(CO)_5(32a/47)]$

$[M(CO)_6]$ (0.1 mmol) was dissolved in anhydrous tetrahydrofuran (6 mL) under a stream of nitrogen and irradiated with UV light (365–366 nm) in a quartz vessel at room temperature for one hour. A solution of the corresponding phosphirane (0.1 mmol) in anhydrous tetrahydrofuran (6 mL) was added and stirred in the UV vessel for a further 30 minutes with continued irradiation. Solvent was removed and the product was purified by column chromatography.

3.20.9 $[Mo(CO)_5(47)]$ (**52a**)

Purification by column chromatography (petroleum ether/chloroform, 4:1) to yield **52a** as an orange solid (0.020 g, 30%). Crystals suitable for X-ray crystallographic analysis were obtained from slow diffusion of pentane into *d*-chloroform. **1H NMR** (300 MHz, $CDCl_3$) δ 7.70–7.54 (m, 2H), 7.42–7.32 (m, 2H), 2.45 (s, 6H), 2.30 (q, $^3J_{HH} = 7.6$ Hz, 4H), 1.78–1.69 (m, 2H), 1.46–1.29 (m, 2H), 1.20 (s, 6H), 0.98 (t, $^3J_{HH} = 7.5$ Hz, 6H), 0.27 (s, 6H) ppm; **$^{13}C\{^1H\}$ NMR** (176 MHz, $CDCl_3$) δ 208.5 (d, $J_{CP} = 31.8$ Hz), 204.7 (d, $J_{CP} = 10.5$ Hz), 151.2, 139.6, 138.8, 135.8 (d, $J_{CP} = 19.6$ Hz), 133.2 (d, $J_{CP} = 126.4$ Hz), 131.8 (d, $J_{CP} = 13.1$ Hz), 129.6 (d, $J_{CP} = 9.3$ Hz), 128.8, 29.9, 17.6, 14.8, 14.5, 12.0, 10.6 (d, $J_{CP} = 14.9$ Hz) 10.5 (s, br) ppm; **$^{31}P\{^1H\}$ NMR** (121 MHz, $CDCl_3$) δ –165.6 (s, 1P) ppm; **$^{11}B\{^1H\}$ NMR** (96 MHz, $CDCl_3$) δ –0.9 (s, 1B) ppm; **IR (neat)**: $\tilde{\nu} = 2931$ (w), 2076 (w), 1941 (s), 1551 (m), 1437 (w), 1350 (s), 1325 (m), 1179 (s), 1140 (m), 1055 (s), 945 (w), 790 (w), 738 (w), 605 (w), 514 (w) cm^{-1} . **HRMS** (ESI⁺) calcd for $C_{32}H_{36}BMoN_2O_5P$ [M] requires m/z 668.1509, found m/z 668.1626.

3.20.10 $[W(CO)_5(47)]$ (**52b**)

Purification by column chromatography (petroleum ether/chloroform, 4:1) to yield **52b** as an orange solid (0.015 g, 20%). **1H NMR** (300 MHz, $CDCl_3$) δ 7.69–7.52 (m, 2H), 7.38 (m, 2H), 2.45 (s, 6H), 2.30 (q, $^3J_{HH} = 7.5$ Hz, 4H), 1.88–1.74 (m, 2H), 1.55–1.39 (m, 2H), 1.20 (s, 6H), 0.98 (t, $^3J_{HH} = 7.5$ Hz, 6H), 0.27 (s, 6H) ppm; **$^{13}C\{^1H\}$ NMR** (126 MHz, $CDCl_3$) δ 197.9 (d, $J_{CP} = 30.9$ Hz), 195.7 (d, $J_{CP} = 8.3$ Hz), 151.3, 140.0, 138.7, 134.8 (d, $J_{CP} = 29.8$ Hz), 133.3 (d, $J_{CP} = 83.8$ Hz), 131.8 (d, $J_{CP} = 13.2$ Hz), 129.7 (d, $J_{CP} = 10.0$ Hz), 128.8, 29.9, 17.6, 14.8, 14.5, 12.0, 11.1 (d, $J_{CP} = 12.3$ Hz), 10.5 ppm; **$^{31}P\{^1H\}$ NMR** (121 MHz, $CDCl_3$) δ –185.5 (s, with W satellite peaks, $^1J_{PW} = 259.2$ Hz); **$^{11}B\{^1H\}$ NMR** (96 MHz, $CDCl_3$) δ –1.4 (s, 1B) ppm; **IR (neat)**: $\tilde{\nu} = 2961$ (w), 2927 (w), 2869 (w), 2074 (m), 1981 (w), 1913 (s), 1546 (m), 1469 (m), 1451 (m), 1316 (m), 1260 (m), 1170 (m), 1144 (m), 1021 (m), 944 (m), 906 (s), 801 (m), 731 (s), 672 (m), 570 (s), 514 (m) cm^{-1} ; **HRMS** (ESI⁺) calcd for $C_{32}H_{36}BW N_2O_5P$ [M] requires m/z 754.1964, found m/z 754.2055.

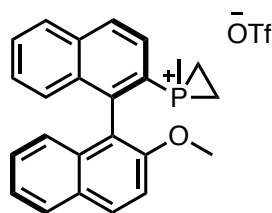
3.20.11 [Mo(CO)₅(**32a**)] (**51a**)

Purification by column chromatography (petroleum ether/chloroform, 4:1) to yield **51a** as a white solid (0.017 g, 30%). **¹H NMR** (500 MHz, CDCl₃) δ 8.07 (d, ³J_{HH} = 9.0 Hz, 1H), 7.95 (d, ³J_{HH} = 8.4 Hz, 1H), 7.94–7.87 (m, 1H), 7.87 (d, ³J_{HH} = 8.5 Hz, 1H), 7.84 (d, ³J_{HH} = 8.5 Hz, 1H), 7.51–7.46 (m, 1H), 7.50 (d, ³J_{HH} = 9.1 Hz, 1H), 7.36 (ddd, ³J_{HH} = 8.1, ³J_{HH} = 6.8, ⁴J_{HH} = 1.2 Hz, 1H), 7.30–7.21 (m, 2H), 7.07 (d, ³J_{HH} = 8.5 Hz, 1H), 6.84 (d, ³J_{HH} = 8.4 Hz, 1H), 3.80 (s, 3H) 1.71–1.58 (m, 1H), 0.98–0.73 (m, 3H) ppm; **¹³C{¹H} NMR** (126 MHz, CDCl₃) δ 209.5 (d, J_{CP} = 31.8 Hz), 204.7 (d, J_{CP} = 10.8 Hz), 154.6, 139.1 (d, J_{CP} = 7.7 Hz), 134.0, 133.9 (d, J_{CP} = 7.4 Hz), 132.8 (d, J_{CP} = 7.3 Hz), 130.7, 129.9 (d, J_{CP} = 15.3 Hz), 129.2, 128.5 (d, J_{CP} = 9.9 Hz), 128.4, 128.3, 127.5, 127.3, 127.1, 126.5, 125.0, 124.2, 120.9, 113.7, 56.3, 11.1, 10.9 (d, J_{CP} = 15.2 Hz), 10.6 (d, J_{CP} = 15.5 Hz) ppm; **³¹P{¹H} NMR** (121 MHz, CDCl₃) δ –169.3 (s, 1P) ppm; **IR** (neat): $\tilde{\nu}$ = 3058 (w), 2931 (w), 2843 (w), 2073 (m), 1992 (m), 1918 (s), 1714 (w), 1621 (w), 1594 (w), 1509 (w), 1250 (m), 1079 (w), 906 (m), 810 (m), 746 (m), 674 (w), 604 (m), 580 (m) cm^{–1}.

3.20.12 [W(CO)₅(**32a**)] (**51b**)

Purification by column chromatography (petroleum ether/chloroform, 4:1) to yield **51b** as a white solid (0.018 g, 27%). **¹H NMR** (300 MHz, CDCl₃) δ 8.07 (d, ³J_{HH} = 9.2 Hz, 1H), 7.97 (m, ³J_{HH} = 8.6 Hz, 1H), 7.95–7.89 (m, 2H), 7.85 (dd, ³J_{PH} = 11.1, ³J_{HH} = 8.5 Hz, 1H), 7.54–7.46 (m, 2H), 7.40–7.33 (m, 1H), 7.30–7.21 (m, 2H), 7.07 (d, ³J_{HH} = 8.6 Hz, 1H), 6.84 (d, ³J_{HH} = 8.5 Hz, 1H), 3.80 (s, 3H), 1.79–1.60 (m, 1H), 1.42–1.26 (m, 1H), 1.25–1.06 (m, 1H), 1.06–0.91 (m, 1H) ppm; **¹³C{¹H} NMR** (75 MHz, CDCl₃) δ 198.8 (d, ²J_{CP} = 30.0 Hz), 195.9 (d, ²J_{CP} = 8.4 Hz), 154.6, 138.9 (d, J_{CP} = 7.6 Hz), 134.1, 133.9, 133.1, 132.8, 132.7, 130.8, 129.9, 129.7, 129.2, 128.6, 128.3, 127.5 (d, J_{CP} = 2.7 Hz), 126.9 (d, J_{CP} = 43.2 Hz), 124.9, 124.2, 120.8, 120.7, 113.7, 56.4, 11.5 (d, J_{CP} = 10.0 Hz), 11.4 (d, J_{CP} = 10.5 Hz) ppm; **³¹P{¹H} NMR** (121 MHz, CDCl₃) δ –189.64 (with W satellite peaks ¹J_{PW} = 255.6 Hz) ppm; **IR** (neat): $\tilde{\nu}$ = 3058 (w), 2958 (w), 2872 (w), 2072 (m), 1984 (w), 1909 (s), 1622 (w), 1594 (w), 1509 (w), 1464 (w), 1407 (w), 1332 (w), 1251 (m), 1148 (w), 1080 (w), 1021 (w), 907 (m), 746 (m), 675 (w), 595 (m), 572 cm^{–1}; **HRMS** (ESI⁺) calcd for C₂₈H₁₉WO₆P [M] requires m/z 666.0433, found m/z 666.0491.

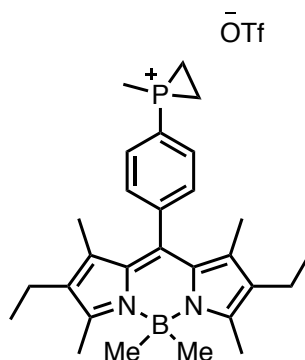
3.20.13 (R)-1-(2'-Methoxy-[1,1'-binaphthalen]-2-yl)-1-methylphosphiranium triflate (44a)



Methyl trifluoromethanesulfonate is a strong methylating agent and therefore all possible precautions should be taken when using it to avoid inhalation or absorption through the skin. Please consult the SDS before use.

Methyl trifluoromethanesulfonate (0.02 mL, 0.2 mmol) was added dropwise to a solution of (R)-1-(2'-methoxy-[1,1'-binaphthalen]-2-yl)phosphirane (0.034 g, 0.1 mmol) in anhydrous dichloromethane (7 mL). The reaction mixture was stirred at room temperature for two hours and the solvent was removed *in vacuo* to yield the desired product **44a** in quantitative conversion. $^1\text{H NMR}$ (300 MHz, CDCl_3) δ 8.16–8.06 (m, 2H), 8.05–7.93 (m, 2H), 7.89 (d, $^3J_{\text{HH}} = 8.2$ Hz, 1H), 7.69–7.59 (m, 1H), 7.46 (d, $^3J_{\text{HH}} = 9.2$ Hz, 1H), 7.42–7.29 (m, 2H), 7.23 (m, $^3J_{\text{HH}} = 9.2$, 2H), 6.66 (d, $^3J_{\text{HH}} = 8.4$ Hz, 1H), 3.75 (s, 3H), 2.31–2.16 (m, 1H), 2.16–2.03 (m, 1H), 2.03–1.89 (m, 1H), 1.87–1.70 (m, 1H), 1.58 (d, $^2J_{\text{HP}} = 18.3$ Hz, 3H) ppm; $^{13}\text{C}\{^1\text{H}\}$ NMR (75 MHz, CDCl_3) δ 155.1, 146.1 (d, $^2J_{\text{CP}} = 10.9$ Hz), 136.5 (d, $J_{\text{CP}} = 3.1$ Hz), 133.6, 133.3, 132.6 (d, $^1J_{\text{CP}} = 15.1$ Hz), 130.5, 130.3, 130.3, 129.0, 128.8, 128.6, 128.1 (d, $^3J_{\text{CP}} = 13.3$ Hz), 126.8, 124.9, 123.7, 117.7 (d, $J_{\text{CP}} = 7.4$ Hz), 115.4, 114.2, 113.0, 56.4, 7.7 (d, $^1J_{\text{CP}} = 5.2$ Hz), 7.0 (d, $^1J_{\text{CP}} = 5.9$ Hz), 5.4 (d, $^1J_{\text{CP}} = 50.3$ Hz) ppm; $^{31}\text{P}\{^1\text{H}\}$ NMR (121 MHz, CDCl_3) δ –102.5 ppm; $^{19}\text{F}\{^1\text{H}\}$ NMR (282 MHz, CDCl_3) δ –78.3 ppm. These spectroscopic data are in agreement with literature values.²⁴

3.20.14 4,4-Dimethyl-1,3,5,7-tetramethyl-2,6-diethyl-4-bora-3a,4a-diaza-s-indacene-8-methylphosphiranium triflate (**48**)



Methyl trifluoromethanesulfonate is a strong methylating agent and therefore all possible precautions should be taken when using it to avoid inhalation or absorption through the skin.

Please consult the SDS before use.

In an analogous manner to the synthesis of **44a**, using methyl trifluoromethanesulfonate (0.039 mL, 0.23 mmol), **47** (0.075 g, 0.12 mmol) in anhydrous dichloromethane (3 mL). The reaction mixture was stirred at room temperature for six hours and solvent was removed *in vacuo* to afford **48** in quantitative conversion. The resulting product decomposed on attempted isolation. $^{31}\text{P}\{^1\text{H}\}$ NMR (121 MHz, CDCl_3) δ 101.6 (s, 1P) ppm.

3.21 1,3,5-Diazaphosphinane Experimental

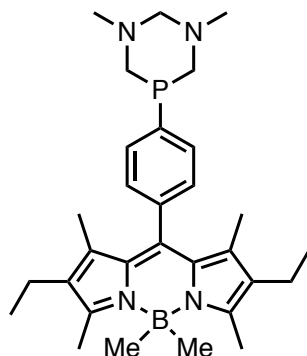
3.21.1 General Procedure

Reactions were carried out by Dr Randolph Köhn at the University of Bath. All air-sensitive manipulations were performed under nitrogen using standard Schlenk techniques or in Saffron glovebox. The solvent *o*-difluorobenzene (*o*-PhF₂) was dried over molecular sieves, vacuum transferred and stored in a glove box over molecular sieves. 1,3,5-trimethyltriazacyclohexane was prepared according to literature procedures.¹³⁸ NMR spectra were collected on a Bruker DRX 500 MHz spectrometer in CDCl_3 solution and are reported with reference to residual solvent signals (δ 7.27 and 77.0) or to an external standard of 85% H_3PO_4 (δ 0.0) for ^{31}P NMR spectra. X-Ray crystallography: Intensity data for **62a**, **62b**, **64a** and **64b** were collected at 150 K on a Nonius KappaCCD diffractometer equipped with an Oxford Cryostream, using graphite monochromated $\text{MoK}\alpha$ radiation ($\lambda = 0.71073 \text{ \AA}$).

3.21.2 Calculation Details

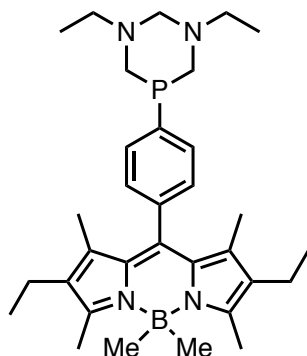
All DFT calculations were performed by Dr Randolph Köhn with the ORCA program package version 3.0.0.¹²³ The geometry optimizations were done using the density functional BP86¹²⁴ employing the def2-SVP basis set¹²⁵ and accelerated using the resolution of identity (RI) approximation¹³⁹ with the auxiliary basis set DeMon-J.¹⁴⁰ Relativistic effects were accounted for with the scalar relativistic zeroth-order regular approximation (ZORA).¹⁴¹ To include solvent effects, the conductor-like screening solvation model (COSMO)¹⁴² was applied choosing *o*-difluorobenzene ($\epsilon = 14.26$) as solvent. Dispersion correction for non-covalent interactions (D3BJ) were introduced as proposed by Grimme.¹⁴³ Harmonic vibrational frequency calculations at 298 K were performed on the optimised geometries to obtain Gibbs free energies.

3.21.3 8-(4-(1,3-Dimethyl-1,3,5-diazaphosphinan-5-yl)phenyl)-4,4-dimethyl-1,3,5,7-tetramethyl-2,6-diethyl-4-bora-3a,4a-diaza-s-indacene (**62a**)



Primary phosphine **14** (0.092 g, 0.23 mmol) was suspended in excess 1,3,5-trimethyltriazacyclohexane (1.5 g, 12 mmol) and heated to 135 °C in a stream of N₂ for five hours. After cooling to ambient temperature, all volatiles were removed *in vacuo* and the resulting bright orange oil was passed through a small alumina column with ethyl acetate. The fast-moving orange fraction was concentrated, and the residue was passed through a second alumina column with pentane as eluent (orange compound **63a** remained on the column was eluted with ethyl acetate to yield 0.036 g orange solids). The orange pentane eluent was concentrated and dried *in vacuo* at 70 °C. The residue was dissolved in a minimum amount of pentane and left in a freezer to crystallise. Orange crystals were isolated by decanting the supernatant solution, washing with cold pentane and drying *in vacuo* to yield 0.070 g of **62a** (0.14 mmol, 61%). **¹H NMR** (500 MHz, CDCl₃) δ 7.63 (dd, ³J_{HP} = 6.4 Hz, ³J_{HH} = 7.6 Hz, 2H), 7.30 (dd, ⁴J_{HP} = 0.2 Hz, ³J_{HH} = 7.6 Hz, 2H), 3.39 (dd ⁴J_{HP} = 0.5 Hz, ⁴J_{HH} = 11.0 Hz, 1H), 3.33 (dd, ²J_{HP} = 15.2 Hz, ⁴J_{HH} = 13.2 Hz, 2H), 3.30 (dd ⁴J_{HP} = 2.6 Hz, ⁴J_{HH} 11.0 Hz, 1H), 3.09 (dd, ²J_{HP} = 3.6 Hz, ⁴J_{HH} = 13.2 Hz, 2H), 2.46 (s, 6H), 2.44 (s, 6H), 2.32 (q, ³J_{HH} = 7.5 Hz, 4H), 1.27 (s, 6H), 0.99 (t, ³J_{HH} = 7.5 Hz, 6H), 0.29 (s, 6H) ppm; **¹³C{¹H} NMR** (126 MHz, CDCl₃) δ 150.1, 139.7, 138.6 (d, J_{CP} = 18.5 Hz), 136.6, 133.3, 132.0, 131.4 (d, J_{CP} = 16.5 Hz), 128.7, 128.3 (d, J_{CP} = 8.7 Hz), 78.6, 53.5 (d, J_{CP} = 13.7 Hz), 44.47 (d, J_{CP} = 6.3 Hz), 17.1, 14.4, 13.9, 11.6, 10.2 (br) ppm; **³¹P{¹H} NMR** (202 MHz, CDCl₃) δ –60.2 (br, 171 Hz wide) ppm; **¹⁵N{¹H} NMR** (51 MHz, CDCl₃) δ 203.0, 32.4 ppm; **¹¹B{¹H} NMR** (160 MHz, CDCl₃) δ –0.9 ppm; **HRMS** (ESI+) calcd for C₃₀H₄₅BN₄P [M+H] required 503.3475 m/z found m/z 503.3475. **EA** Anal. found (calcd. for C₃₀H₄₄BN₄P): C, 71.55 (71.71); H, 8.73 (8.83); N, 10.96 (11.15)%.

3.21.4 8-(4-(1,3-Diethyl-1,3,5-diazaphosphinan-5-yl)phenyl)-4,4-dimethyl-1,3,5,7-tetramethyl-2,6-diethyl-4-bora-3a,4a-diaza-s-indacene (**62b**)



Primary phosphine **14** (0.138 g, 0.341 mmol) was suspended in excess 1,3,5-triethyltriazacyclohexane (1.37 g, 8.0 mmol) and heated to 140 °C in a stream of N₂ for 2.5 hours (dissolved after one hour). After cooling to ambient temperature all volatiles were removed *in vacuo* over five hours in a warm water bath and the residue was passed through a small alumina column with hexane (orange compound **63b** remained on the column and was eluted with ethyl acetate). The orange hexane eluent was concentrated and dried under high vacuum to yield 0.138 g of **62b** (0.26 mmol, 76%). The product can be crystallised from a saturated hot hexane solution by cooling to –10 °C. ¹H NMR (500 MHz, CDCl₃) δ 7.64 (dd, ³J_{HP} = 6.4 Hz, ³J_{HH} = 8.0 Hz, 2H), 7.29 (dd, ⁴J_{HP} = 1.1 Hz, ³J_{HH} = 8.1 Hz, 2H), 3.55 (dd ⁴J_{HP} = 1.0 Hz, ⁴J_{HH} = 11.4 Hz, 1H), 3.44 (dd, ⁴J_{HP} = 2.45 Hz, ⁴J_{HH} = 11.4 Hz, 1H), 3.40 (dd, ²J_{HP} = 15.5 Hz, ⁴J_{HH} = 13.4 Hz, 2H), 3.20 (dd, ²J_{HP} = 3.4 Hz, ⁴J_{HH} = 13.4 Hz, 2H), 2.65 (dq, ⁴J_{HH} = 0.3 Hz, ⁴J_{HP} = 7.2, ³J_{HH} = 12.4, 2H), 2.61 (dq, ⁴J_{HP} = 0.2 Hz, ⁴J_{HH} = 7.2, ³J_{HH} = 12.4 Hz, 2H), 2.46 (s, 6H), 2.32 (q, ³J_{HH} = 7.5 Hz, 4H), 1.28 (s, 6H), 1.08 (t, ³J_{HH} = 7.1 Hz, 6H), 0.99 (t, ³J_{HH} = 7.5 Hz, 6H), 0.29 (s, 6H) ppm; ¹³C{¹H} NMR (126 MHz, CDCl₃) δ 150.6, 140.1, 139.2 (d, J_{CP} = 18.5 Hz), 136.9, 133.7, 132.4, 131.6 (d, J_{CP} = 16.2 Hz), 129.0, 128.6 (d, J_{CP} = 5.7 Hz), 75.1 (d, J_{CP} = 1.6 Hz), 51.7 (d, J_{CP} = 13.5), 50.1 (d, J_{CP} = 6.0), 17.4, 14.7, 14.3, 12.3, 11.9, 10.4 br (28 Hz wide) ppm; ³¹P{¹H} NMR (202 MHz, CDCl₃) δ –58.3 (br, 90 Hz wide) ppm; ¹⁵N{¹H} NMR (51 MHz, CDCl₃) δ 203.1, 44.9 ppm; ¹¹B{¹H} NMR (160 MHz, CDCl₃) δ –0.9 ppm; HRMS (ESI) calcd for C₃₂H₄₉BN₄P [M+H] required 531.3788 m/z found m/z 531.3806. EA Anal. found (calcd. for C₃₂H₄₈BN₄P): C, 72.34 (72.44); H, 9.29 (9.12); N, 10.41 (10.56)%.

3.21.5 8-(4-(1,3-Dimethyl-1,3,5-diazaphosphinane-5-oxide)phenyl)-4,4-dimethyl-1,3,5,7-tetramethyl-2,6-diethyl-4-bora-3a,4a-diaza-s-indacene (**63a**)

¹H NMR (500 MHz, CDCl₃) δ 8.20 (dd, ³J_{PH} = 11.0 Hz, ³J_{HH} = 7.9 Hz, 2H), 7.49 (dd, ⁴J_{PH} = 2.4 Hz, ³J_{HH} = 7.9 Hz, 2H), 3.56 (d, ⁴J_{HH} = 10.5 Hz, 1H), 3.34 (dd, ²J_{PH} = 10.0 Hz, ⁴J_{HH} = 14.3 Hz, 2H), 3.00 (dd, ²J_{PH} = 9.6 Hz, ⁴J_{HH} = 14.4 Hz, 2H), 3.12 (d, ⁴J_{HH} = 10.5 Hz, 1H), 2.46 (s, 6H), 2.44 (d, ⁴J_{HH} = 2.6 Hz, 6H), 2.33 (q, ³J_{HH} = 7.4 Hz, 4H), 1.25 (s, 6H), 0.99 (t, ³J_{HH} = 7.4 Hz, 6H), 0.29 (s, 6H) ppm; **¹³C{¹H} NMR** (126 MHz, CDCl₃) δ 151.0, 141.4 (d, J_{CP} = 3.0 Hz), 138.9, 133.5, 132.7, 132.7 (d, J_{CP} = 94.7 Hz), 131.6 (d, J_{CP} = 9.1 Hz), 129.1 (d, J_{CP} = 11.6 Hz), 128.6, 78.6 (d, J_{CP} = 3.0 Hz), 55.9 (d, J_{CP} = 93.2 Hz), 44.8 (d, J_{CP} = 12.3 Hz), 17.4, 14.6, 14.3, 11.9, 10.4 (br) ppm; **³¹P{¹H} NMR** (202 MHz, CDCl₃) δ 16.0 (s, 7 Hz wide) ppm; **¹⁵N{¹H} NMR** (51 MHz, CDCl₃) δ 203.3, 32.0 ppm.

3.21.6 8-(4-(1,3-Diethyl-1,3,5-diazaphosphinane-5-oxide)phenyl)-4,4-dimethyl-1,3,5,7-tetramethyl-2,6-diethyl-4-bora-3a,4a-diaza-s-indacene (**63b**)

¹H NMR (500 MHz, CDCl₃) δ 8.22 (dd, ³J_{PH} = 11.1 Hz, ³J_{HH} = 7.95 Hz, 2H), 7.48 (dd, ⁴J_{PH} = 2.68 Hz, ³J_{HH} = 7.95 Hz, 2H), 3.69 (dd, ⁴J_{PH} = 0.04 Hz, ⁴J_{HH} = 11.1 Hz, 1H), 3.47 (dd, ²J_{PH} = 10.9 Hz, ⁴J_{HH} = 14.2 Hz, 2H), 3.28 (dd, ⁴J_{PH} = 1.2 Hz, ⁴J_{HH} = 11.1 Hz, 1H), 3.03 (dd, ²J_{PH} = 9.0 Hz, ⁴J_{HH} = 14.2 Hz, 2H), 2.66 (dq, ⁴J_{PH} = 2.5 Hz, ⁴J_{HH} = 7.5, ³J_{HH} = 12.6 Hz, 2H), 2.58 (dq, ⁴J_{PH} = 0.3 Hz, ⁴J_{HH} = 7.1, ³J_{HH} = 12.6 Hz, 2H), 2.47 (s, 6H), 2.31 (q, ³J_{HH} = 7.5 Hz, 4H), 1.24 (s, 6H), 1.06 (dd, ³J_{HH} = 7.5, ³J_{HH} = 7.1 Hz, 6H), 0.99 (t, ³J_{HH} = 7.5 Hz, 6H), 0.29 (s, 6H) ppm; **¹³C{¹H} NMR** (126 MHz, CDCl₃) δ 150.9, 141.2 (d, J_{CP} = 3.0 Hz), 138.9, 133.4, 133.0 (d, J_{CP} = 93.4 Hz), 132.7, 131.7 (d, J_{CP} = 8.8 Hz), 128.9 (d, J_{CP} = 11.3 Hz), 128.6, 75.2 (d, J_{CP} = 3.8 Hz), 53.4 (d, J_{CP} = 73.4 Hz), 50.2 (d, J_{CP} = 11.4 Hz), 17.4, 14.6, 14.3, 12.7, 11.9, 10.4 (br) ppm; **³¹P{¹H} NMR** (202 MHz, CDCl₃) δ 16.9 (s, 27 Hz wide) ppm; **¹⁵N{¹H} NMR** (51 MHz, CDCl₃) δ 203.1, 44.1 ppm.

3.21.7 8-(4-(1,3-Dimethyl-1,3,5-diazaphosphinane-5-sulfide)phenyl)-4,4-dimethyl-1,3,5,7-tetramethyl-2,6-diethyl-4-bora-3a,4a-diaza-s-indacene (**64a**)

¹H NMR (500 MHz, CDCl₃) δ 8.36 (dd, ³J_{PH} = 12.5 Hz, ³J_{HH} = 8.1 Hz, 2H), 7.47 (dd, ⁴J_{HP} = 2.6 Hz, ³J_{HH} = 8.1 Hz, 2H), 3.62 (dd, ⁴J_{PH} = 1.5 Hz, ⁴J_{HH} = 10.8 Hz, 1H), 3.34 (dd, ²J_{PH} = 11.1 Hz, ⁴J_{HH} = 14.4 Hz, 2H), 3.19 (dd, ⁴J_{PH} = 3.9 Hz, ⁴J_{HH} = 10.8 Hz, 1H), 3.00 (dd, ²J_{PH} = 3.2 Hz, ⁴J_{HH} = 14.4, 2H), 2.47 (s, 6H), 2.42 (d, ⁴J_{HH} = 2.2 Hz, 6H), 2.31 (q, ³J_{HH} = 7.5 Hz, 4H), 1.25 (s, 6H), 0.99 (t, ³J_{HH} = 7.5 Hz, 6H), 0.29 (s, 6H) ppm; **¹³C{¹H} NMR** (126 MHz, CDCl₃) δ 151.0, 141.1 (d, J_{CP} = 3.0 Hz), 138.9, 133.1 (d, J_{CP} = 73.9 Hz), 133.5, 132.7, 132.3 (d, J_{CP} = 10.1 Hz), 128.9 (d, J_{CP} = 12.1 Hz), 128.6, 77.9 (d, J_{CP} = 3.2 Hz), 60.4 (d, J_{CP} = 56.0 Hz), 44.4 (d, J_{CP} = 12.4), 17.4, 14.7, 14.3, 12.0, 10.4 (br, 11 Hz wide); **³¹P{¹H} NMR** (202 MHz, CDCl₃) δ 14.7 (s, 1P) ppm; **¹⁵N{¹H} NMR** (51 MHz, CDCl₃) δ 203.3, 34.6 ppm.

3.21.8 8-(4-(1,3-Diethyl-1,3,5-diazaphosphinane-5-sulfide)phenyl)-4,4-dimethyl-1,3,5,7-tetramethyl-2,6-diethyl-4-bora-3a,4a-diaza-s-indacene (**64b**)

¹H NMR (500 MHz, CDCl₃) δ 8.37 (dd ³J_{PH} = 12.4 Hz, ³J_{HH} = 8.2 Hz, 2H), 7.45 (dd, ⁴J_{PH} = 2.8 Hz, ³J_{HH} = 8.2 Hz, 2H), 3.77 (dd, ²J_{PH} = 5.3 Hz, ⁴J_{HH} = 12.9 Hz, 2H), 3.73 (dd ⁴J_{PH} = 1.5 Hz, ⁴J_{HH} = 11.5 Hz, 1H), 3.31 (dd, ⁴J_{PH} = 3.3 Hz, ⁴J_{HH} = 11.5 Hz, 1H), 3.15 (dd, ²J_{PH} = 1.5 Hz, ⁴J_{HH} = 12.9 Hz, 2H), 2.62 (dq, ⁴J_{PH} = 2.7 Hz, ⁴J_{HH} = 7.2, ³J_{HH} = 12.6 Hz, 2H) 2.57 (dq, ⁴J_{PH} = 1.0 Hz, ⁴J_{HH} = 7.1 ³J_{HH} = 12.6 Hz, 2H), 2.46 (s, 6H), 2.31 (q, ³J_{HH} = 7.5 Hz, 4H), 1.25 (s, 6H), 1.04 (dd, ³J_{HH} = 7.2, ³J_{HH} = 7.1 Hz, 6H), 0.99 (t, ³J_{HH} = 7.5 Hz, 6H), 0.29 (s, 6H) ppm; **¹³C{¹H} NMR** (126 MHz, CDCl₃) δ 150.9, 140.9 (d, J_{CP} = 3.1 Hz), 138.9, 133.4, 133.1 (d, J_{CP} = 73.2 Hz), 132.7, 132.3 (d, J_{CP} = 9.9 Hz), 128.8 (d, J_{CP} = 12.0 Hz), 128.6, 74.4 (d, J_{CP} = 3.8 Hz), 58.2 (d, J_{CP} = 55.9 Hz), 49.8 (d, J_{CP} = 9.6 Hz), 17.4, 14.7, 14.3, 12.4, 12.0, 10.4 (br); **³¹P{¹H} NMR** (202 MHz, CDCl₃) δ 15.5 (s, 1P) ppm; **¹⁵N{¹H} NMR** (51 MHz, CDCl₃) δ 203.4, 47.1 ppm.

3.22 Surface Modification General Procedure

Mesoporous silica SBA-15 was generously donated by Professor Maria Olea, Teesside University, UK. Experiments were carried out by Professor William Henderson at the University of Waikato.

3.22.1 Synthesis of 3-Aminopropyl SBA-15

SBA-15 (2.314 g) was suspended in toluene (50 mL), and 3-aminopropyl triethoxysilane (Sigma Aldrich, 12 mL) was added. The suspension was refluxed with stirring for eight hours and allowed to cool. The solid was filtered, washed with toluene (3 x 20 mL) and then distilled water (150 mL). The solid was briefly air dried, and then dried under vacuum for four days, giving 3.192 g of a white solid.

3.22.2 Reaction of Aminopropyl SBA-15 with **24d**

Approximately 1.5 g of the above solid was suspended in methanol (30 mL) and an excess of Bodipy hydroxymethylphosphine **24d** was added, and the mixture stirred. The presence of excess phosphine was indicated by a bright orange colour to the solution. After 3 hours, the solid was filtered, washed with methanol (2 x 10 mL), water (2 x 10 mL) and then acetone (2 x 10 mL) and air-dried, to give a light orange solid. This solid fluoresces bright green under UV light (365 nm).

3.22.3 Control Experiment

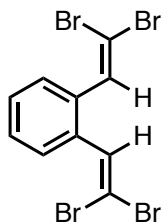
As a control experiment, the above procedure was repeated, but replacing aminopropyl SBA-15 with (underivatised) SBA-15 itself. The solid was washed free of unreacted Bodipy hydroxymethylphosphine **24d** as above, giving a white solid.

3.23 Phosphepine Experimental

3.23.1 General Procedure

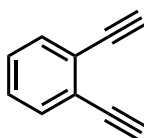
All air- and/or water-sensitive reactions were performed under a nitrogen atmosphere using standard Schlenk line techniques. Tetrahydrofuran was distilled over sodium/benzophenone and *d*-chloroform over phosphorus pentoxide; all solvents were distilled prior to use. Bromomethyltriphenylphosphonium bromide was prepared according to a literature procedure.¹⁴⁴ All other chemicals were purchased from Sigma Aldrich, Fisher Scientific, Alfa Aesar or Fluorochem and used as received. Flash chromatography was performed on silica gel from Fluorochem (silica gel, 40-63 μ , 60 Å). Thin-layer chromatography was performed on Fisher aluminium-based plates with silica gel and fluorescent indicator (254 nm). ^1H , $^{13}\text{C}\{^1\text{H}\}$, $^{31}\text{P}\{^1\text{H}\}$, and $^{11}\text{B}\{^1\text{H}\}$ NMR spectra were recorded on a Bruker Avance III 300 MHz (^1H 300.13 Hz), Bruker Avance II 400 MHz (^1H 399.78 MHz) or Bruker Avance III HD 500 MHz (^1H 500.16 MHz) spectrometer at room temperature (21 °C) using the indicated solvent as internal reference; ^1H and ^{13}C shifts were relative to tetramethylsilane, ^{31}P relative to 80% H_3PO_4 , and ^{11}B relative to $\text{BF}_3\cdot\text{Et}_2\text{O}$. Infrared spectra were recorded on a Varian 800 FT-IR spectrometer and mass spectrometry was carried out by the EPSRC National Mass Spectrometry Service Centre, Swansea or the SAgE Mass Spectrometry Facility (Newcastle University) performed by Dr Rachael Dack or Dr Alex Charlton. The X-ray crystallographic data were collected on an Xcalibur, Atlas, Gemini ultra diffractometer equipped with a fine-focus sealed X-ray tube ($\lambda_{\text{CuK}\alpha} = 1.54184 \text{ \AA}$) and an Oxford Cryosystems CryostreamPlus open-flow N_2 cooling device. The analysis of the X-ray diffraction data of the compounds was performed by Dr Paul Waddell. DFT calculations were carried out on Spartan '14 using the B3LYP functional with a 6-31G* basis set.

3.23.2 1,2-Bis(2,2-dibromovinyl)benzene (**71**)



Following the procedure reported by Lammertsma *et al.*⁸⁹ Freshly ground triphenylphosphine (9.00 g, 34.31 mmol) was added portion-wise to a cold (0 °C) solution of tetrabromomethane (5.60 g, 16.9 mmol) in dichloromethane (80 mL). The resultant red solution was warmed to room temperature and stirred for 20 minutes. A cooled (0 °C) solution of *o*-phthalaldehyde **70** (1.00 g, 7.46 mmol) in dichloromethane (32 mL) was added dropwise and the reaction mixture was stirred in the dark for two hours at room temperature. The reaction mixture was then washed with distilled water (3 x 50 mL) and extracted with dichloromethane (2 x 50 mL). The organic layers were combined and dried over MgSO₄, filtered and the solvent removed *in vacuo*. The resulting yellow oil was triturated with pentane (2 x 200 mL) and the resulting suspension was filtered and washed with pentane and the pentane fractions were combined, concentrated *in vacuo* and purified by column chromatography (1% diethyl ether in petroleum ether) to afford **71** as a yellow oil (2.53 g, 76%). ¹H NMR (300 MHz, CDCl₃) δ 7.55–7.49 (m, 2H), 7.42 (s, 2H), 7.40–7.34 (m, 2H) ppm. These spectroscopic data are in agreement with literature values.⁸⁹

3.23.3 1,2-Diethynylbenzene (**66**)⁸⁹



n-BuLi (2.5 M in hexane, 13.5 mL, 33.7 mmol) was added to a –78 °C solution of DIPA (4.73 mL, 33.7 mmol) in tetrahydrofuran (100 mL). The reducing mixture was warmed to RT and the solution was added dropwise to a –78 °C solution of **71** (2.51 g, 5.61 mmol) in tetrahydrofuran (20 mL). After 20 minutes, the reaction was quenched with saturated (NH₄)₂SO₄ (55 mL) and stirred for two hours at RT. The reaction mixture was poured into pentane (50 mL) and the organic layer was separated, washed with water, dried over MgSO₄, filtered and concentrated *in vacuo*. Purification was by column chromatography (1% diethyl ether in petroleum ether) to afford **66** (0.109 g, 15%). ¹H NMR (300 MHz, CDCl₃) δ 7.56–7.46 (m, 2H), 7.34–7.29 (m, 2H), 3.34 (s, 2H) ppm. These spectroscopic data are in agreement with literature values.⁸⁹

3.23.4 General Procedure for the Synthesis of Metal Carbonyl Complexes

[M(CO)₆] (0.25 mmol) was dissolved in anhydrous tetrahydrofuran and irradiated with UV light (365–366 nm) in a quartz vessel at room temperature under a stream of nitrogen for one hour. A solution of Bodipy primary phosphine **14** (0.25 mmol) in anhydrous tetrahydrofuran was added and stirred in the UV vessel for a further 30 minutes. Solvent was removed *in vacuo* and the product was purified by column chromatography.

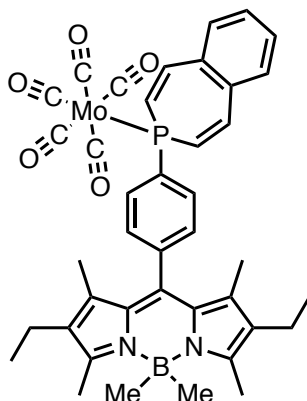
3.23.5 [Mo(CO)₅(**14**)] (**68a**)

Purification by column chromatography (petroleum ether/chloroform, 4:1) to afford **68a** as an orange solid (0.070 g, 44%). ¹H NMR (400 MHz, CDCl₃) δ 7.67 (m, 2H), 7.44 (m, 2H), 5.57 (d, ¹J_{HP} = 327.1 Hz, 2H), 2.46 (s, 6H), 2.32 (q, ³J_{HH} = 7.5 Hz, 4H), 1.25 (s, 6H), 0.99 (t, ³J_{HH} = 7.5 Hz, 6H), 0.29 (s, 6H) ppm; ¹³C{¹H} NMR (75 MHz, CDCl₃) δ 208.8 (d, ²J_{CP} = 24.0 Hz), 204.7 (d, ²J_{CP} = 9.1 Hz), 151.3, 139.9, 138.7, 133.6, 132.9, 132.8 (d, J_{CP} = 11.7 Hz), 130.0 (d, J_{CP} = 10.0 Hz), 128.9, 126.8 (d, J_{CP} = 41.7 Hz), 17.6, 14.8, 14.5, 12.1, 10.4 (br) ppm; ³¹P{¹H} NMR (162 MHz, CDCl₃) δ –64.1 (s, 1P) ppm; ³¹P-¹H NMR (162 MHz, CDCl₃) δ –64.1 (tt, ¹J_{PH} = 327.3, ³J_{PH} = 12.1 Hz, 1P) ppm; ¹¹B{¹H} NMR (96 MHz, CDCl₃) δ –0.9 (s, 1B) ppm. IR (neat): $\tilde{\nu}$ = 2928 (w), 2076 (m), 1992 (m), 1913 (s), 1549 (m), 1450 (m), 1387 (m), 1359 (m), 1318 (s), 1262 (w), 1171 (s), 1145 (m), 1112 (m), 1035 (w), 979 (m), 944 (m), 909 (m), 876 (m), 793 (m), 734 (w), 694 (w), 672 (w), 605 (m), 577 (s), 513 (m), 472 (w) cm^{–1}. These spectroscopic data are in agreement with literature values.¹³²

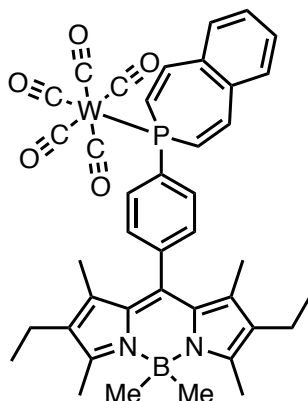
3.23.6 [W(CO)₅(**14**)] (**68b**)

Purification by column chromatography (petroleum ether/chloroform, 4:1) to yield **68b** as an orange solid (0.070 g, 38%). ¹H NMR (400 MHz, CDCl₃) δ 7.70–7.60 (m, 2H), 7.46 (dd, ³J_{HH} = 8.2, ⁴J_{HH} = 2.1 Hz, 2H), 5.90 (d, ¹J_{HP} = 340.9 Hz, 2H), 2.46 (s, 6H), 2.31 (q, ³J_{HH} = 7.5 Hz, 4H), 1.24 (s, 6H), 0.98 (t, ³J_{HH} = 7.5 Hz, 6H), 0.28 (s, 6H) ppm; ¹³C{¹H} NMR (101 MHz, CDCl₃) δ 198.3 (d, J_{CP} = 22.6 Hz), 195.5 (d, J_{CP} = 6.8 Hz), 151.3, 140.3, 138.5, 133.6, 132.9, 132.8 (d, J_{CP} = 11.6 Hz), 130.1 (d, J_{CP} = 10.5 Hz), 128.9, 126.2 (d, J_{CP} = 47.2 Hz), 17.6, 14.8, 14.5, 12.2, 10.5 (br) ppm; ³¹P{¹H} NMR (162 MHz, CDCl₃) δ –85.8 (s, with ¹⁸³W satellites ¹J_{PW} = 223 Hz, 1P) ppm; ³¹P-¹H NMR (162 MHz, CDCl₃) δ –85.8 (tt, ¹J_{PH} = 341.4, ³J_{PH} = 12.4 Hz, with ¹⁸³W satellites, ¹J_{PW} = 223.0 Hz) ppm; ¹¹B{¹H} NMR (96 MHz, CDCl₃) δ –0.8 (s, 1B) ppm. IR (neat): $\tilde{\nu}$ = 2926 (w), 2076 (m), 1985 (w), 1909 (s), 1547 (m), 1452 (w), 1318 (m), 1261 (w), 1171 (m), 1144 (m), 1111 (w), 1036 (w), 979 (m), 944 (m), 909 (w), 880 (m), 794 (m), 732 (w), 694 (w), 671 (w), 596 (m), 571 (s), 519 (m), 441 (w). These spectroscopic data are in agreement with literature values.¹³²

3.23.7 [Mo(CO)₅(72)] (69a)

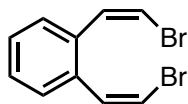


Following the procedure reported by Lammertsma *et al.*⁸⁹ Bodipy complex **68a** (0.045 g, 0.07 mmol) was stirred overnight with 1,2-diethynyl benzene (0.012 g, 0.09 mmol) in anhydrous tetrahydrofuran (1.5 mL). The following day, freshly ground KOH (0.003 g, 0.05 mmol) was added and stirred for a further 30 minutes. The complete consumption of starting material was determined by ³¹P{¹H} NMR spectroscopy and the reaction mixture was filtered over silica and concentrated. Product was further purified by column chromatography (toluene/petroleum ether, 1:4) to yield **69a** as an orange solid (0.023 g, 43%). Crystals suitable for X-ray crystallographic analysis were obtained from slow diffusion of pentane into diethyl ether. ¹H NMR (300 MHz, CDCl₃) δ 7.62–7.48 (m, 2H), 7.46–7.38 (d, 2H), 7.37–7.27 (m, 4H), 7.24–7.16 (m, 2H), 6.41 (dd, ²J_{HP} = 31.0 Hz, ³J_{HH} = 11.9 Hz, 2H), 2.43 (s, 6H), 2.28 (q, ³J_{HH} = 7.5 Hz, 4H), 0.97 (s, 6H), 0.97 (t, ³J_{HH} = 7.5 Hz, 6H), 0.24 (s, 6H) ppm; ³¹P{¹H} NMR (121 MHz, CDCl₃) δ –5.78 (s, 1P) ppm; ³¹P-¹H NMR (121 MHz, CDCl₃) δ –5.78 (tt, ²J_{PH} = 31.1 Hz, ³J_{PH} = 11.5 Hz, 1P) ppm; ¹¹B{¹H} NMR (128 MHz, CDCl₃) δ –1.45 (s, 1B) ppm; ¹³C{¹H} NMR (75 MHz, CDCl₃) δ 205.4 (d, J_{CP} = 9.2 Hz), 150.9, 142.6, 137.9, 136.5 (d, J_{CP} = 4.4 Hz), 133.7, 132.3 (d, J_{CP} = 34.3 Hz), 130.4 (d, J_{CP} = 12.1 Hz), 128.8 (d, J_{CP} = 9.6 Hz), 128.7, 128.1, 127.1 (d, J_{CP} = 9.6 Hz), 21.5, 17.4, 14.7, 14.3, 11.9, 10.4 ppm;† IR (neat): $\tilde{\nu}$ = 3658 (w), 2981 (s), 2929 (m), 2889 (m), 2070 (m), 1984 (w), 1917 (s), 1723 (w), 1591 (w), 1544 (m), 1458 (m), 1387 (m), 1361 (m), 1318 (w), 1260 (m), 1165 (m), 1145 (m), 1071 (m), 944 (s), 908 (w), 797 (m), 770 (m), 719 (w), 670 (w), 647 (m), 606 (m), 578 (s), 503 (w), 429 (w) cm⁻¹; HRMS (ESI⁺) calcd for C₄₀H₄₀BMoNaN₂O₅P [M+Na] requires *m/z* 789.1712, found *m/z* 789.2525. †Signals for the (CO)_{ax} carbons and two additional carbon atoms were not observed.

3.23.8 [W(CO)₅(72)] (69b)

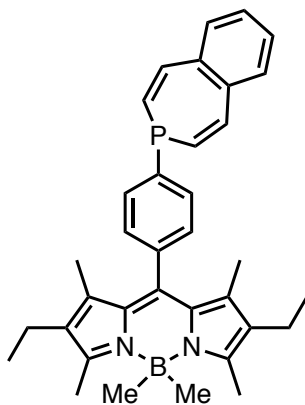
Following the procedure reported by Lammertsma *et al.*⁸⁹ Bodipy complex **68b** (0.049 g, 0.06 mmol) was stirred overnight with 1,2-diethynylbenzene (0.009 g, 0.07 mmol) in anhydrous tetrahydrofuran (1.5 mL). The next day, freshly ground KOH (0.002 g, 0.04 mmol) was added, and the reaction mixture was stirred for a further 30 minutes. Complete consumption of the starting material was determined by ³¹P{¹H} NMR spectroscopy and the reaction mixture was filtered over silica and concentrated to yield **69b** as an orange solid (0.013 g, 30%). Crystals suitable for X-ray crystallographic analysis were obtained from slow diffusion of petroleum ether into diethyl ether. ¹H NMR (500 MHz, CDCl₃) δ 7.53–7.44 (m, 2H), 7.44–7.39 (m, 2H), 7.39–7.29 (m, 4H), 7.22–7.16 (m, 2H), 6.51 (dd, ²J_{HP} = 31.3 Hz, ³J_{HH} = 12.0 Hz, 2H), 2.42 (s, 6H), 2.27 (q, ³J_{HH} = 7.5 Hz, 4H), 0.96 (t, ³J_{HH} = 7.5 Hz, 6H), 0.93 (s, 6H), 0.23 (s, 6H); ³¹P{¹H} NMR (202 MHz, CDCl₃) δ –26.9 (s, with ¹⁸³W satellite ¹J_{PW} = 239 Hz); ³¹P-¹H NMR (202 MHz, CDCl₃) δ –26.9 (tt, with ¹⁸³W satellite peaks, ¹J_{PW} = 239 Hz, ²J_{PH} = 31.3, ³J_{PH} 11.2 Hz); ¹¹B{¹H} NMR (96 MHz, CDCl₃) δ –1.0 (s, 1B) ppm; ¹³C{¹H} NMR (75 MHz, CDCl₃) δ 199.5 (d, *J*_{CP} = 12.6 Hz), 196.9 (d, *J*_{CP} = 7.0 Hz), 151.0, 143.7 (d, *J*_{CP} = 5.4 Hz), 138.9 (d, *J*_{CP} = 32.8 Hz), 136.5 (d, *J*_{CP} = 4.4 Hz), 133.8, 132.4 (d, *J*_{CP} = 34.1 Hz), 130.3 (d, *J*_{CP} = 11.3 Hz), 129.1 (d, *J*_{CP} = 16.6 Hz), 128.6 (d, *J*_{CP} = 37.9 Hz), 127.2, 119.1, 29.9, 17.6, 14.8, 14.5, 12.1, 10.4 ppm;† IR (neat): $\tilde{\nu}$ = 3658 (w), 2980 (m), 2927 (m), 2070 (m), 1979 (w), 1928 (s), 1909 (s), 1774 (w), 1723 (w), 1592 (w), 1544 (m), 1451 (m), 1387 (m), 1360 (m), 1317 (m), 1261 (m), 1171 (m), 1144 (m), 1066 (m), 1019 (m), 943 (m), 908 (w), 797 (m), 771 (m), 734 (w), 704 (w), 696 (w), 648 (m), 596 (m), 571 (s), 504 (w), 442 (w), 411 (w) cm^{–1}; HRMS (ESI⁺) calcd for C₄₀H₄₀BN₂O₅PW [M]⁺ requires *m/z* 877.2321, found *m/z* 877.2175. †Signals for two carbon atoms were not observed.

3.23.9 1,2-Bis((Z)-2-bromovinyl)benzene (**73**)



Following the procedure reported by Tsuchiya *et al.*⁸⁷ bromomethyltriphenylphosphonium bromide (1.37 g, 3.13 mmol) was added to a cooled suspension of potassium *tert*-butoxide (0.351 g, 3.13 mmol) in tetrahydrofuran (5 mL) to generate bromomethylenetriphenylphosphorane *in-situ*. To this intermediate, a solution of *o*-phthalaldehyde **70** (0.100 g, 0.75 mmol) in tetrahydrofuran (0.5 mL) was added dropwise. After stirring for three hours at room temperature, distilled water (10 mL) was added and then extraction with dichloromethane (3 x 5 mL). The organic fractions were combined and washed with brine (1 x 10 mL), dried over MgSO₄, filtered and dried *in vacuo*. Purification by column chromatography (petroleum ether) afforded **73** (0.080 g, 37%). ¹H NMR (300 MHz, CDCl₃) δ 7.68 (dd, *J*_{HH} = 5.7, *J*_{HH} = 3.5 Hz, 1H), 7.37 (dd, *J*_{HH} = 5.7, *J*_{HH} = 3.5 Hz, 1H), 7.11 (d, *J*_{HH} = 7.9 Hz, 1H), 6.55 (d, *J*_{HH} = 7.9 Hz, 1H) ppm; ¹³C{¹H} NMR (75 MHz, CDCl₃) δ 134.1, 131.4, 128.9, 127.8, 109.4 ppm. These spectroscopic data are in agreement with literature values.⁸⁷

3.23.10 Attempted Synthesis of a Metal-Free Phosphepine (**72**)



Bodipy primary phosphine **14** (0.04 g, 0.1 mmol) was subject to a chlorination reaction with phosphorus pentachloride (0.046 g, 0.22 mmol) in toluene (1.5 mL). The synthesis of **23** was confirmed by ³¹P{¹H} NMR spectroscopy by a resonance at δ 159.7 ppm. The volatiles were removed from **23** *in vacuo* over 45 minutes. In parallel, (*Z,Z*)-*o*-bis(β-bromovinyl)benzene **73** (0.014 g, 0.05 mmol) was dissolved in diethyl ether (1.5 mL) and the pale-yellow solution was cooled to −78 °C. *Tert*-butyllithium (1.7 M solution in pentane, 0.24 mL, 0.4 mmol) was added dropwise over ten minutes and stirred for a further 10 minutes, by which time, the solution had become purple in colour. The dichlorophosphine compound **23** was suspended in diethyl ether and this was then added dropwise to the cooled dilithiated intermediate **74**. The

reaction mixture was slowly warmed to room temperature and stirred for three hours. Analysis of the reaction mixture by $^{31}\text{P}\{^1\text{H}\}$ NMR spectroscopy revealed no remaining Bodipy dichlorophosphine **23** and instead, a peak at -5.9 ppm was observed. Isolation of the product was attempted by purification by an aqueous work-up and extraction with dichloromethane, however, a second resonance was observed in the $^{31}\text{P}\{^1\text{H}\}$ NMR spectrum at *ca.* δ 47 ppm, likely an oxidation product. $^{31}\text{P}\{^1\text{H}\}$ NMR (121 MHz, CDCl_3) δ -5.9 ppm.

3.24 References

- 1 A. R. Pinder, *Nat. Prod. Rep.*, 1992, **9**, 491–504.
- 2 C. T. Walsh, *Tetrahedron Lett.*, 2015, **56**, 3075–3081.
- 3 A. Gupta and A. K. Halve, *Int. J. Pharm. Sci. Res.*, 2015, **6**, 978–987.
- 4 G. S. Singh, *Adv. Heterocycl. Chem.*, 2020, **130**, 1–74.
- 5 J. B. Sweeney, *Chem. Soc. Rev.*, 2002, **31**, 247–258.
- 6 L. Kiss, A. Márió and B. Volk, in *Molecular Sciences and Chemical Engineering, Balázs B T - Reference Module in Chemistry*, Elsevier, 2019.
- 7 H. Shah, K. Sarker, R. Patel, R. Chaudhary, D. Pandit, A. Sanyal, Y. Patel, S. Rai, D. Basu, S. Patel, D. Sharma and D. Jyoti Sen, *World J. Pharm. Res.*, 2016, **5**, 433–453.
- 8 F. Mathey and M. Regitz, in *Phosphorus-Carbon Heterocyclic Chemistry The Rise of a New Domain*, ed. F. Mathey, Elsevier Science Ltd, Oxford, 2001, pp. 17–55.
- 9 F. Mathey, *Chem. Rev.*, 1990, **90**, 997–1025.
- 10 D. B. Chesnut, L. D. Quin and S. B. Wild, *Heteroat. Chem.*, 1997, **8**, 451–457.
- 11 J. Liedtke, S. Loss, C. Widauer and H. Grützmacher, *Phosphiranes as Ligands for Platinum Catalysed Hydrosilylations*, Pergamon, 2000, vol. 56.
- 12 L. D. Quin, *A Guide to Organophosphorus Chemistry*, John Wiley & Sons, Inc., New York, 2000.
- 13 R. I. Wagner, L. D. Freeman, H. Goldwhite and D. G. Rowsell, *J. Am. Chem. Soc.*, 1967, **89**, 1102–1104.
- 14 Y. B. Kang, M. Pabel, A. C. Willis and S. B. Wild, *J. Chem. Soc. Chem. Commun.*, 1994, 475–476.
- 15 X. Li, K. D. Robinson and P. P. Gaspar, *J. Org. Chem.*, 1996, **61**, 7702–7710.
- 16 D. C. R. Hockless, Y. Beng Kang, M. A. McDonald, M. Pabel, A. C. Willis and S. B. Wild, *Organometallics*, 1996, **15**, 1301–1306.
- 17 M. Baudler and J. Germeshausen, *Chem. Ber.*, 1985, **118**, 4285–4287.
- 18 T. Oshikawa and M. Yamashita, *Synthesis*, 1985, **3**, 290–291.
- 19 J. Liedtke, S. Loss, G. Alcaraz, V. Gramlich and H. Grützmacher, *Angew. Chemie Int. Ed.*, 1999, **38**, 1623–1626.
- 20 J. Liedtke, H. Rüegger, S. Loss and H. Grützmacher, *Angew. Chemie Int. Ed.*, 2000, **39**,

2478–2481.

- 21 C. Laporte, G. Frison, H. Grützmacher, A. C. Hillier, W. Sommer and S. P. Nolan, *Organometallics*, 2003, **22**, 2202–2208.
- 22 H. Jansen, F. B. Läng, J. C. Slootweg, A. W. Ehlers, M. Lutz, K. Lammertsma and H. Grützmacher, *Angew. Chemie Int. Ed.*, 2010, **49**, 5485–5488.
- 23 D. C. R. Hockless, M. A. McDonald, M. Pabel and S. B. Wild, *J. Chem. Soc. Chem. Commun.*, 1995, 257.
- 24 A. Ficks, I. Martinez-Botella, B. Stewart, R. W. Harrington, W. Clegg and L. J. Higham, *Chem. Commun.*, 2011, **47**, 8274–8276.
- 25 J. Gasnot, C. Botella, S. Comesse, S. Lakhdar, C. Alayrac, A.-C. Gaumont, V. Dalla and C. Taillier, *Synlett*, 2020, **31**, 883–888.
- 26 H. Yoda, M. Takahashi and T. Sengoku, in *Heterocycles in Natural Product Synthesis*, eds. S. K. Chattopadhyay and K. C. Majumdar, 2011, pp. 41–61.
- 27 C. C. Ruddle and T. P. Smyth, *Org. Biomol. Chem.*, 2007, **5**, 160–168.
- 28 D. S. Johnson and J. J. Li, *The Art of Drug Synthesis*, John Wiley & Sons, Incorporated, Hoboken, US, 2007.
- 29 D. L. Hughes, *Org. Process Res. Dev.*, 2016, **20**, 1855–1869.
- 30 J. J. McBride, E. Jungermann, J. V. Killheffer and R. J. Clutter, *J. Org. Chem.*, 2002, **27**, 1833–1836.
- 31 A. Marinetti, S. Jus, F. Labrue, A. Lemarchand, J. P. Genêt and L. Ricard, *Synthesis*, 2001, 2095–2104.
- 32 P. Pinto, A. W. Götz, G. Marconi, B. A. Hess, A. Marinetti, F. W. Heinemann and U. Zenneck, *Organometallics*, 2006, **25**, 2607–2616.
- 33 A. Ohashi, S. Matsukawa and T. Imamoto, *Heterocycles*, 2000, **52**, 905–910.
- 34 J. A. Campbell, C. N. Caughlan, A. Fitzgerald, C. Campana and S. E. Cremer, *Acta Crystallogr. Sect. C*, 1984, **40**, 1920–1922.
- 35 C. Moret and L. M. Trefonas, *Org. Biol. Chem.*, 1969, **91**, 2255–2259.
- 36 D. Coleman, P. G. Edwards, B. M. Kariuki and P. D. Newman, *Dalton Trans.*, 2010, **39**, 3842–3850.
- 37 L. Kollár and G. Keglevich, *Chem. Rev.*, 2010, **110**, 4257–4302.
- 38 T. Imamoto, N. Oohara and H. Takahashi, *Synthesis*, 2004, 1353–1358.

- 39 A. Marinetti and D. Carmichael, in *Phosphorus-Carbon Heterocyclic Chemistry The Rise of a New Domain*, ed. F. Mathey, Elsevier, Oxford, 2001, pp. 87–103.
- 40 T. Kawashima and R. Okazaki, in *Phosphorus-Carbon Heterocyclic Chemistry The Rise of a New Domain*, ed. F. Mathey, Elsevier Science Ltd, Oxford, 2001, pp. 105–165.
- 41 W. Hawes and S. Trippett, *J. Chem. Soc. C Org.*, 1969, 1465.
- 42 S. E. Cremer and R. J. Chorvat, *J. Org. Chem.*, 1967, **32**, 4066–4070.
- 43 S. E. Cremer and R. J. Chorvat, *Tetrahedron Lett.*, 1968, **9**, 413–416.
- 44 J. R. Corfield and S. Trippett, *J. Chem. Soc.*, 1971, 334–336.
- 45 L. Longwitz, A. Spannenberg and T. Werner, *ACS Catal.*, 2019, **9**, 9237–9244.
- 46 A. Marinetti, F. Labrue and J.-P. Genêt, *Synlett*, 1999, 1975–1977.
- 47 U. Berens, M. J. Burk, A. Gerlach and W. Hems, *Angew. Chemie Int. Ed.*, 2000, **39**, 1981–1984.
- 48 C. Korff and G. Helmchen, *Chem. Commun.*, 2004, 530–531.
- 49 A. Marinetti, F. Labrue, B. Pons, S. Jus, L. Ricard and J.-P. Genêt, *Eur. J. Inorg. Chem.*, 2003, 2583–2590.
- 50 T. Shibata, T. Uchiyama, Y. Yoshinami, S. Takayasu, K. Tsuchikama and K. Endo, *Chem. Commun.*, 2012, **48**, 1311–1313.
- 51 L. Longwitz and T. Werner, *Angew. Chemie Int. Ed.*, 2020, **59**, 2760–2763.
- 52 D. O’Hagan, *Nat. Prod. Rep.*, 2000, **17**, 435–446.
- 53 A. D. Elbein, M. Mitchell, B. A. Sanford, L. E. Fellows and S. V Evans, *J. Biol. Chem.*, 1984, **259**, 12409–12413.
- 54 A. Agrawal and A. Banerjee, *Curr. Drug Metab.*, 2017, **18**, 727–734.
- 55 Z. Galdecki, T. J. Bartczak, W. M. Wolf, H. Krawczyk and P. Majewski, *Acta Crystallogr. Sect. C*, 1985, **41**, 732–734.
- 56 A. T. Axtell, C. J. Cobley, J. Klosin, G. T. Whiteker, A. Zanotti-Gerosa and K. A. Abboud, *Angew. Chemie Int. Ed.*, 2005, **44**, 5834–5838.
- 57 R. Emrich and P. W. Jolly, *Synthesis*, 1993, 39–40.
- 58 R. Angharad Baber, M. F. Haddow, A. J. Middleton, A. Guy Orpen, P. G. Pringle, A. Haynes, G. L. Williams and R. Papp, *Organometallics*, 2007, **26**, 713–725.
- 59 G. Keglevich and T. Kovacs, *Curr. Green Chem.*, 2014, **1**, 182–188.

- 60 S. Basra, J. G. de Vries, D. J. Hyett, G. Harrison, K. M. Heslop, A. G. Orpen, P. G. Pringle and K. von der Luehe, *Dalton Trans.*, 2004, 1901.
- 61 L. J. Higham, in *Phosphorus Compounds: Advanced Tools in Catalysis and Material Sciences*, eds. M. Peruzzini and L. Gonsalvi, Springer Netherlands, Dordrecht, 2011, pp. 1–19.
- 62 M.-N. Birkholz, N. V. Dubrovina, H. Jiao, D. Michalik, J. Holz, R. Paciello, B. Breit and A. Börner, *Chem. Eur. J.*, 2007, **13**, 5896–5907.
- 63 C. Dobrota, J.-C. Fiaud and M. Toffano, *ChemCatChem*, 2015, **7**, 144–148.
- 64 M. J. Burk, *Acc. Chem. Res.*, 2000, **33**, 363–372.
- 65 I. C. Lennon and C. J. Pilkington, *Synthesis*, 2003, **4**, 1639–1642.
- 66 M. J. Burk, T. Gregory P. Harper and C. S. Kalberg, *J. Am. Chem. Soc.*, 1995, **117**, 4423–4424.
- 67 T. P. Kee, in *Phosphorus-Carbon Heterocyclic Chemistry The Rise of a New Domain*, ed. F. Mathey, Elsevier Science Ltd, Oxford, 2001, pp. 195–218.
- 68 L. Gorgani, M. Mohammadi, G. D. Najafpour and M. Nikzad, *Compr. Rev. Food Sci. Food Saf.*, 2017, **16**, 124–140.
- 69 M. Baumann and I. R. Baxendale, *Beilstein J. Org. Chem.*, 2013, **9**, 2265–2319.
- 70 S. Gottlieb, D. D. Graham and N. York, *J. Neurosci.*, 2001, **322**, 2001.
- 71 L. Czibula, A. Nemes, F. Sebök, C. Szántay and M. Mák, *European J. Org. Chem.*, 2004, 3336–3339.
- 72 E. Vitaku, D. T. Smith and J. T. Njardarson, *J. Med. Chem.*, 2014, **57**, 10257–10274.
- 73 M. J. Gallagher, in *Phosphorus-Carbon Heterocyclic Chemistry The Rise of a New Domain*, ed. F. Mathey, Elsevier, Oxford, 2001, pp. 463–483.
- 74 G. Grüttner and M. Wiernik, *Berichte der Dtsch. Chem. Gesellschaft*, 1915, **48**, 1473–1486.
- 75 G. Märkl, *Angew. Chemie Int. Ed.*, 1963, **2**, 479.
- 76 R. B. Wetzel and G. L. Kenyon, *J. Am. Chem. Soc.*, 1974, **96**, 5189–5198.
- 77 J. B. Lambert and J. W. L. Oliver, *Tetrahedron*, 1971, **27**, 4245–4254.
- 78 S. D. Laffoon, V. S. Chan, M. G. Fickes, B. Kotecki, A. R. Ickes, J. Henle, J. G. Napolitano, T. S. Franczyk, T. B. Dunn, D. M. Barnes, A. R. Haight, R. F. Henry and S. Shekhar, *ACS Catal.*, 2019, **9**, 11691–11708.

- 79 J. A. Balfour and K. L. Goa, *Drugs*, 1991, **42**, 511–539.
- 80 J. W. Coe, P. R. Brooks, M. G. Vetelino, M. C. Wirtz, E. P. Arnold, J. Huang, S. B. Sands, T. I. Davis, L. A. Lebel, C. B. Fox, A. Shrikhande, J. H. Heym, E. Schaeffer, H. Rollema, Y. Lu, R. S. Mansbach, L. K. Chambers, C. C. Rovetti, D. W. Schulz, F. D. Tingley and B. T. O'Neill, *J. Med. Chem.*, 2005, **48**, 3474–3477.
- 81 Y. Segall, E. Shirin and I. Granoth, *Phosphorus Sulfur Silicon Relat Elem*, 1980, **8**, 243–254.
- 82 A. G. Meyer, A. C. Bissember, C. J. T. Hyland, C. C. Williams, M. Szabo, M. A. Pearsall, I. K. Hyland and W. J. Olivier, in *Progress in Heterocyclic Chemistry*, eds. G. W. Gribble and J. A. Joule, Elsevier, 2020, vol. 31, pp. 597–647.
- 83 G. Märkl and W. Burger, *Tetrahedron Lett.*, 1983, **24**, 2545–2548.
- 84 M. L. G. Borst, R. E. Buló, D. J. Gibney, Y. Alem, F. J. J. de Kanter, A. W. Ehlers, M. Schakel, M. Lutz, A. L. Spek and K. Lammertsma, *J. Am. Chem. Soc.*, 2005, **127**, 16985–16999.
- 85 M. Kalek and G. C. Fu, *J. Am. Chem. Soc.*, 2015, **137**, 9438–9442.
- 86 Y. Fujiwara, J. Sun and G. C. Fu, *Chem. Sci.*, 2011, **2**, 2196–2198.
- 87 S. Yasuike, T. Kiharada, J. Kurita and T. Tsuchiya, *Chem. Commun.*, 1996, 2183–2184.
- 88 S. Yasuike, T. Kiharada, T. Tsuchiya and J. Kurita, *Chem. Pharm. Bull.*, 2003, **51**, 1283–1288.
- 89 M. L. G. Borst, R. E. Buló, C. W. Winkel, D. J. Gibney, A. W. Ehlers, M. Schakel, M. Lutz, A. L. Spek and K. Lammertsma, *J. Am. Chem. Soc.*, 2005, **127**, 5800–5801.
- 90 T. Delouche, A. Mocanu, T. Roisnel, R. Szűcs, E. Jacques, Z. Benkő, L. Nyulászi, P.-A. Bouit and M. Hissler, *Org. Lett.*, 2019, **21**, 802–806.
- 91 G. Märkl and H. Schubert, *Tetrahedron Lett.*, 1970, **11**, 1273–1276.
- 92 J. Kurita, S. Shiratori, S. Yasuike and T. Tsuchiya, *J. Chem. Soc., Chem. Commun.*, 1991, 1227–1228.
- 93 S. Yasuike, S. Shiratori, J. Kurita and T. Tsuchiya, *Chem. Pharm. Bull.*, 1999, **47**, 1108–1114.
- 94 R. M. Hiney, L. J. Higham, H. Müller-Bunz and D. G. Gilheany, *Angew. Chemie Int. Ed.*, 2006, **45**, 7248–7251.
- 95 L. H. Davies, B. Stewart and L. J. Higham, in *Organometallic Chemistry: Volume 39*, The Royal Society of Chemistry, 2014, vol. 39, pp. 51–71.

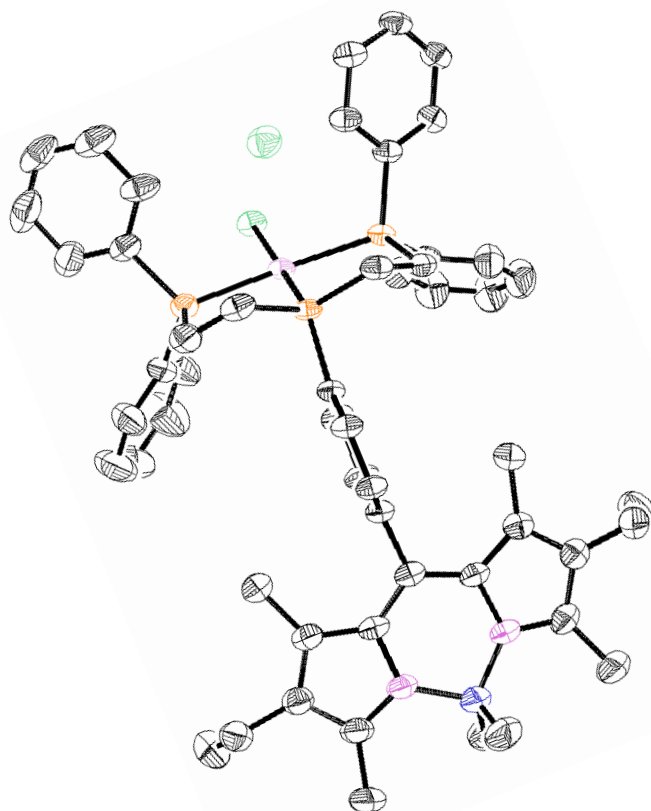
- 96 L. H. Davies, B. Stewart, R. W. Harrington, W. Clegg and L. J. Higham, *Angew. Chemie Int. Ed.*, 2012, **51**, 4921–4924.
- 97 A. Maercker and W. Brieden, *Chem. Ber.*, 1991, **124**, 933–938.
- 98 R. A. de Graaf, in *In Vivo NMR Spectroscopy: Principles and Techniques*, John Wiley & Sons Ltd., 2007, pp. 43–110.
- 99 N. Mézailles, P. E. Fanwick and C. P. Kubiak, *Organometallics*, 1997, **16**, 1526–1530.
- 100 F. Yang, P. E. Fanwick and C. P. Kubiak, *Organometallics*, 1999, **18**, 4222–4225.
- 101 W. E. Hill, D. M. A. Minahan, J. G. Taylor and C. A. McAuliffe, *J. Am. Chem. Soc.*, 2002, **104**, 6001–6005.
- 102 C. M. Haar, S. P. Nolan, W. J. Marshall, K. G. Moloy, A. Prock and W. P. Giering, *Organometallics*, 1999, **18**, 474–479.
- 103 J. Te Hung, S. Wan Yang, G. M. Gray and K. Lammertsma, *J. Org. Chem.*, 1993, **58**, 6786–6790.
- 104 M. P. Murphy, *Biochim. Biophys. Acta, Bioenerg.*, 2008, **1777**, 1028–1031.
- 105 D. E. Befroy, D. L. Rothman, K. F. Petersen and G. I. Shulman, *Diabetes*, 2012, **61**, 2669–2678.
- 106 Wavefunction Inc., 2013, Spartan 14.
- 107 D. C. R. Hockless, M. A. McDonald, M. Pabel and S. B. Wild, *J. Organomet. Chem.*, 1997, **529**, 189–196.
- 108 R. D. Köhn, M. Haufe, G. Kociok-Köhn, S. Grimm, P. Wasserscheid and W. Keim, *Angew. Chemie Int. Ed.*, 2000, **39**, 4337–4339.
- 109 R. D. Köhn, Z. Pan, G. Kociok-Köhn and M. F. Mahon, *J. Chem. Soc., Dalt. Trans.*, 2002, 2344–2347.
- 110 A. G. N. Coxon and R. D. Köhn, *ACS Catal.*, 2016, **6**, 3008–3016.
- 111 R. D. Köhn, A. G. N. Coxon, S. Chunawat, C. Heron, S. Mihan, C. L. Lyall, S. B. Reeksting and G. Kociok-Köhn, *Polyhedron*, 2020, **185**, 114572.
- 112 R. D. Köhn, D. Smith, M. F. Mahon, M. Prinz, S. Mihan and G. Kociok-Köhn, *J. Organomet. Chem.*, 2003, **683**, 200–208.
- 113 P. J. Wilson, A. J. Blake, P. Mountford and M. Schröder, *J. Organomet. Chem.*, 2000, **600**, 71–83.
- 114 A. I. Kuramshin, E. V. Kolpakova, R. N. Galimullin and V. I. Galkin, *Russ. J. Gen. Chem.*, 174

2017, **87**, 2006–2010.

- 115 L. Lefrada, R. D. Köhn, S. Malki, W. Mazouz, A. Bouchemma and M. Hadjem, *Alger. J. Nat. Prod.*, 2017, **5**, 463–468.
- 116 L. Lefrada, R. Köhn, S. Malki, W. Mazouz, A. Bouchemma and M. Hadjem, *Eur. J. Chem.*, 2017, **8**, 82–84.
- 117 G. Märkl and G. Y. Jin, *Tetrahedron Lett.*, 1981, **22**, 229–232.
- 118 J. Zhang, J.-D. Yang and J.-P. Cheng, *Chem. Sci.*, 2020, **11**, 4786–4790.
- 119 J. Zhang, J.-D. Yang and J.-P. Cheng, *Chem. Sci.*, 2020, **11**, 3672–3679.
- 120 A. G. Giumanini, G. Verardo, L. Randaccio, N. Bresciani-Pahor and P. Traldi, *J. Prakt. Chemie*, 1985, **327**, 739–748.
- 121 R. D. Köhn, M. Haufe, S. Mihan and D. Lilge, *Chem. Commun.*, 2000, 1927–1928.
- 122 M. P. McDaniel, in *Advances in Catalysis*, eds. D. D. Eley, H. Pines and P. B. Weisz, Academic Press, 1985, vol. 33, pp. 47–98.
- 123 F. Neese, *WIREs Comput. Mol. Sci.*, 2012, **2**, 73–78.
- 124 A. D. Becke, *Phys. Rev. A*, 1988, **38**, 3098–3100.
- 125 D. A. Pantazis, X.-Y. Chen, C. R. Landis and F. Neese, *J. Chem. Theory Comput.*, 2008, **4**, 908–919.
- 126 F. C. Cochrane, H. H. Petach and W. Henderson, *Enzyme Microb. Technol.*, 1996, **18**, 373–378.
- 127 W. Henderson, G. M. Olsen and L. S. Bonnington, *J. Chem. Soc. Chem. Commun.*, 1994, 1863–1864.
- 128 C. Laslau, W. Henderson, Z. D. Zujovic and J. Travas-Sejdic, *Synth. Met.*, 2010, **160**, 1173–1178.
- 129 R. D. Eagling, J. E. Bateman, N. J. Goodwin, W. Henderson, B. R. Horrocks and A. Houlton, *J. Chem. Soc. Dalt. Trans.*, 1998, 1273–1275.
- 130 B. Thomas, D. McIntosh, T. Fildes, L. Smith, F. Hargrave, M. Islam, T. Thompson, R. Layfield, D. Scott, B. Shaw, C. L. Burrell, S. Gonzalez and S. Taylor, *Bone Reports*, 2017, **7**, 137–144.
- 131 X. Sun, L. Yao, C. Fu, J. Xiao, L. Luo and J. Wang, *J. Mater. Chem. B*, 2019, **7**, 7676–7682.
- 132 L. H. Davies, J. F. Wallis, R. W. Harrington, P. G. Waddell and L. J. Higham, *J. Coord. Chem.*, 2016, **69**, 2069–2080.

- 133 K. Lammertsma, Personal Communication.
- 134 O. V. Dolomanov, L. J. Bourhis, R. J. Gildea, J. A. K. Howard and H. Puschmann, *J. Appl. Cryst.*, 2009, **42**, 339–341.
- 135 C. A. Tolman, *J. Am. Chem. Soc.*, 1970, **92**, 2953–2956.
- 136 J. F. Wallis, Newcastle University, 2018.
- 137 D. Drew, J. R. Doyle and A. G. Shaver, *Inorg. Synth.*, 1990, 346–349.
- 138 R. Lauterbach, Ed., in *Beilstein Handbook of Organic Chemistry*, Springer, Berlin, 4th edn., 1993.
- 139 K. Eichkorn, F. Weigend, O. Treutler and R. Ahlrichs, *Theor. Chem. Acc.*, 1997, **97**, 119–124.
- 140 N. Godbout, D. R. Salahub, J. Andzelm and E. Wimmer, *Can. J. Chem.*, 1992, **70**, 560–571.
- 141 C. van Wüllen, *J. Chem. Phys.*, 1998, **109**, 392–399.
- 142 A. Klamt and G. Schüürmann, *J. Chem. Soc. Perkin Trans. 2*, 1993, 799–805.
- 143 S. Grimme, S. Ehrlich and L. Goerigk, *J. Comput. Chem.*, 2011, **32**, 1456–1465.
- 144 M. Moir, R. Boyd, H. Gunosewoyo, A. P. Montgomery, M. Connor and M. Kassiou, *Tetrahedron Lett.*, 2019, **60**, 151019.

Chapter 4



A Fluorescent Tridentate Phosphine and its Coordination to Group 10 Metals

An introduction into platinum containing chemotherapeutic agents is given, and additionally, how chelating ligands have been introduced to alter their reactivity.

We introduce a fluorescent tridentate phosphine, hereafter referred to as BodP₃, which was developed by our group for its application as a dual imaging agent in fluorescence and SPECT imaging.

We then describe the coordination of BodP₃ to group 10 metals, nickel, palladium and platinum, to afford a series of fluorescent probes which have been characterised by X-ray crystallographic studies, photophysical studies and NMR spectroscopy. Further to this, we see the platinum complex tested in HeLa and PC-3 cells.

A second series of fluorescent novel platinum-containing complexes has been synthesised by varying both the ligand trans to the central phosphorus donor and the counter ion, and these have been characterised spectroscopically.

4 A Fluorescent Tridentate Phosphine and its Coordination to Group 10 Metals

Platinum(II) complexes are known for their anticancer properties and have been of significant interest since the FDA approval of cisplatin (Figure 4.1) in 1978.¹ Cisplatin is a chemotherapeutic drug that is currently used in the treatment of testicular, ovarian, bladder, head and neck, and non-small cell lung cancer by causing DNA damage through crosslinking with purine bases.² Chemotherapy with cisplatin can result in severe side effects and drug-resistance that can result in treatment failure and thus, in an attempt to overcome these associated issues, many *cis*-, square planar, platinum(II) containing analogues continue to be studied. Two platinum containing FDA approved anti-cancer agents are oxaliplatin and carboplatin (Figure 4.1). Both complexes have a bidentate ligand which prevents the formation of the inactive 'transplatin', *in vivo*, an additional problem associated with cisplatin. Furthermore, carboplatin has displayed reduced side effects when compared to cisplatin.^{1,2}

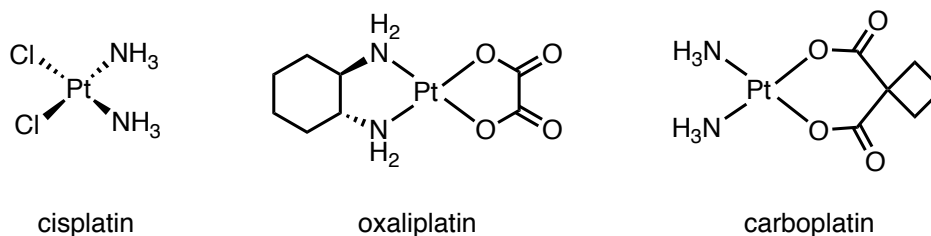


Figure 4.1 FDA approved platinum(II) containing anticancer agents.

In order to better understand the cellular mechanisms of disease and offer improved treatment, current research is investigating metals which facilitate radioimaging by PET and SPECT (e.g. ^{99m}Tc) or coordination compounds which possess a fluorescent ligand for analysis by optical imaging.^{3,4} This chapter will describe ways in which a fluorescent ligand and a bioactive metal can be incorporated into the same probe. The synthesis of fluorescent tridentate phosphine complexes of the group 10 metals will be described, and their potential applications as multimodal cell imaging agents assessed.

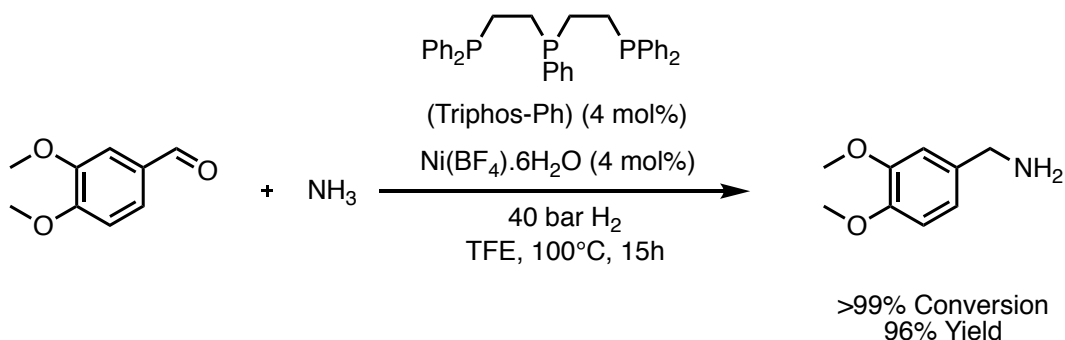
The synthesis and characterisation of three novel fluorescent platinum(II) complexes from the coordination to a fluorescent tridentate phosphine (BodP₃) is reported. The cell imaging properties of one of these complexes is explored for applications in prostate cancer (PC-3) cells. The analogous group 10 nickel(II) and palladium(II) complexes were also prepared and their structural properties and photophysical properties are described.

4.1 Polydentate Ligands

Polydentate ligands have an enhanced affinity for metals which is known as the chelate effect. This effect makes the binding of polydentate ligands more favourable than the analogous monodentate ligands for a number of reasons, including, i) the enhanced control over the coordination environment, ii) increased thermodynamic stability and kinetic inertness over a range of oxidation states, and iii) higher nucleophilicity at the metal centre. Thus, these qualities have been exploited in both catalysis^{5,6} and medicine.^{3,7}

4.1.1 Polydentate Ligands in Catalysis

A current example of tridentate phosphine-based Ni complexes serving as valuable catalysts were recently described by Jagadeesh *et al.*⁶ The group compared the reactivity and selectivity of seven tridentate ligands in the Ni-catalysed reductive amination of veratraldehyde. Only the triphos-Ph containing complex $[\text{Ni}(\text{triphos-Ph})\text{Cl}_2]$ exhibited high activity and selectivity for the reductive amination of veratraldehyde and afforded the desired product, veratrylamine in 96% yield (Scheme 4.1).



Scheme 4.1 Reductive amination of veratraldehyde to veratrylamine with triphos-Ph containing $[\text{Ni}(\text{triphos-Ph})\text{Cl}_2]$ catalyst, illustrating the high yields and conversions possible.

It was found that this Ni complex was highly selective in the amination of a library of functionalised carbonyl compounds to afford linear primary amines from aldehydes, and branched primary amines from ketones. $[\text{Ni}(\text{triphos-Ph})\text{Cl}_2]$ enabled the introduction of the primary amine moiety to the structurally complex pharmaceuticals and steroid derivatives: nabumetone, pentoxifylline, azaperone, estrone, androsterone and stanolone in yields of 80–93%, thus signifying its potential application within industrial applications. It was also found that $[\text{Ni}(\text{triphos-Ph})\text{Cl}_2]$ exhibited excellent activity in the hydrogenation of nitroarenes. $[\text{Ni}(\text{triphos-Ph})\text{Cl}_2]$ displayed high yields with nitroarenes with both electron withdrawing and donating groups, and was found to tolerate a range of functional groups including, esters, amides, ethers and halides. Thus, $[\text{Ni}(\text{triphos-Ph})\text{Cl}_2]$ was the first nickel-based homogeneous

catalyst for the reductive amination of carbonyl compounds and hydrogenation of nitroarenes.⁶

4.1.2 Polydentate Ligands in Medicine

Due to their high affinity to metals, polydentate ligands have been employed in a range of areas of medicine including both therapeutics and diagnostics.⁸ Their strong binding to metal centres has facilitated their application in the removal of toxic metals from the body in chelation therapy.⁹ In addition, an abundance of polydentate ligands are found in complexes used for *in vivo* medical imaging for diagnostic purposes.^{10,11}

One of the key roles of polydentate ligands in medical imaging is to enhance the stability of radioactive and toxic metal complexes to resist reaction with potential ligands *in vivo*. This is critical for their use in radiotracers or pharmaceuticals and thus, tridentate ligands can be found in complexes used as i) MRI contrast agents,¹² ii) PET^{13,14} and iii) SPECT¹⁵ imaging agents.

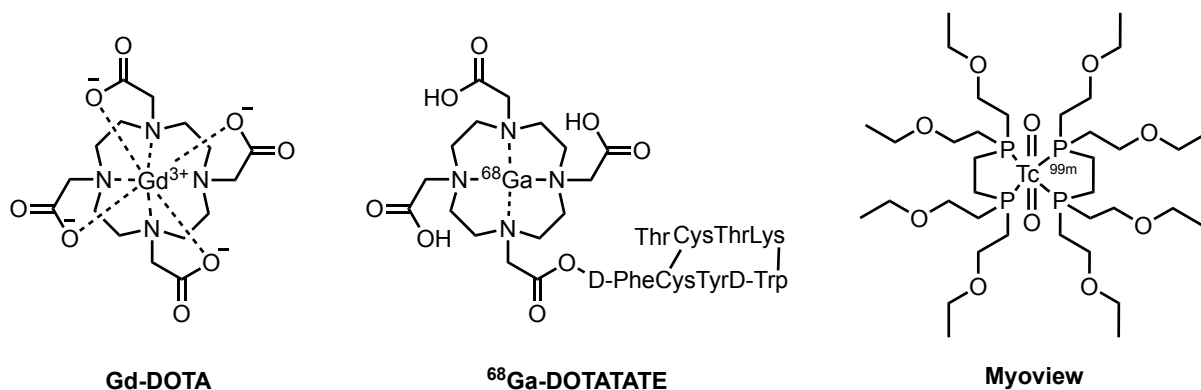


Figure 4.2 Examples of imaging agents with polydentate ligands used for different medical imaging techniques. Gadolinium complex, Gd-DOTA for use as an MRI contrast agent, ⁶⁸Ga-DOTATATE for use as a PET imaging agent and ^{99m}Tc-Tetrafosmin (commercially known as Myoview), the most popular SPECT imaging agent.

Contrast agents are used to enhance the quality of MRI images, the most commonly used examples contain gadolinium which has significant toxicities associated with it, both, *in vitro* and *in vivo*. To eliminate these toxicities, chelating ligands are often used to encapsulate the metal, consequently minimising metal leeching and toxic effects.¹⁶ An example shown in Figure 4.2 is Gd-DOTA which encapsulates gadolinium with the tetraaza macrocycle, DOTA and was found to be less toxic than its linear equivalent, Gd DTPA-BMA.¹⁷

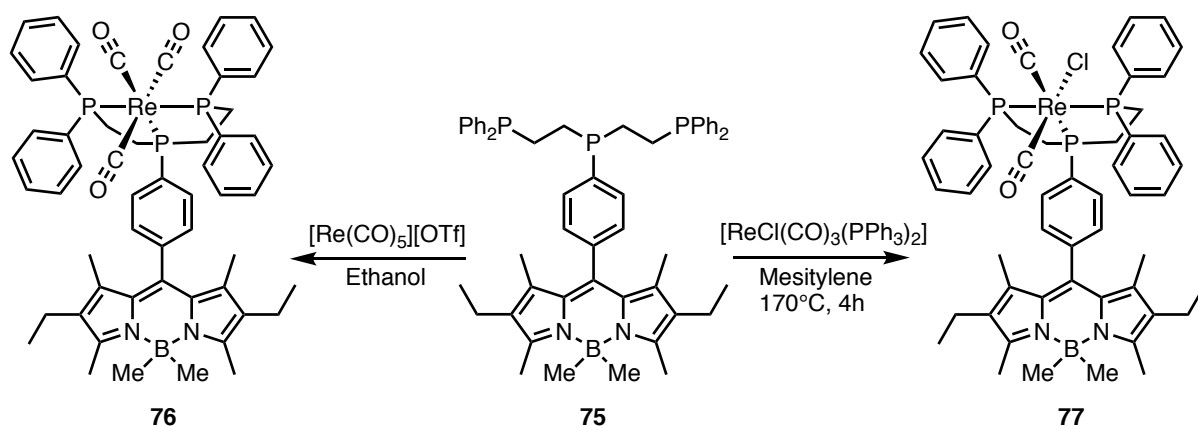
The DOTA macrocycle has also been exploited in the PET imaging agent, ⁶⁸Ga-DOTATATE, which is shown in Figure 4.2. This functionalised DOTA chelate encapsulates the radioactive metal, again to prevent leeching of this into the body.¹⁸

A further example of a polydentate ligand containing complexes is FDA approved myocardial perfusion, SPECT imaging agent, ^{99m}Tc -Tetrofosmin (Myoview, Figure 4.2). The complex is comprised of the 99m gamma emitting radioisotope, Tc(V), two chelating diphosphines and a stable trans dioxo unit.¹⁹

4.1.3 Dual-Modality Tridentate Phosphine

Taking inspiration from both Myoview and the dual functional SPECT and optical imaging probe developed by Valliant *et al.*, (introduced in Section 1.5) our group reported the synthesis of the tridentate phosphine, BodP₃, **75**²⁰ and explored its potential as both an *in vitro* imaging agent, when coordinated to rhenium, and a combined *in vitro* and *in vivo* imaging agent suitable for optical and SPECT imaging, when coordinated to the 99m-technetium radiolabel (Scheme 4.3).⁴ **75** is an example of a probe that combines features to enable its application in two imaging techniques. SPECT facilitates *in vivo* tissue imaging, but it is not capable of subcellular imaging due to a resolution limit of 1-2 mm. Although radioimaging is a useful tool for imaging organs, it does not give an insight into molecule behaviour and cellular biochemistry.²¹ Optical fluorescence imaging allows for subcellular imaging due to its sub-micron resolution, theoretically to a resolution of one molecule.²¹ Thus, used together, they could outweigh their individual limitations and complement each other to make an overall more effective imaging agent.

The fluorescent tridentate phosphine **75** could be reacted with $[\text{Re}(\text{CO})_5][\text{OTf}]$ or $[\text{ReCl}(\text{CO})_3(\text{PPh}_3)_2]$ to afford the corresponding fluorescent rhenium complexes **76** and **77** respectively (Scheme 4.2).



Scheme 4.2 Synthesis of rhenium complexes **76** and **77** from fluorescent tridentate phosphorus compound **75** and $[\text{Re}(\text{CO})_5][\text{OTf}]$ or $[\text{ReCl}(\text{CO})_3(\text{PPh}_3)_2]$ to produce a cold standard for a SPECT imaging agent.

76 and **77** were tested as optical imaging agents in a preliminary screening of prostate carcinoma (PC-3) cells. Although **76** and **77** have similar structures and differ only by one

ligand, their behaviour *in vitro* was surprisingly different. Treatment of the cells with **77** resulted in a morphological effect which was confirmed by an MMT assay as cytotoxic with an MI_{50} (the concentration required to reduce mitochondrial metabolism to 50%) of $45\ \mu\text{M} \pm 5\ \mu\text{M}$. On the other hand, treatment with **76** enabled high-resolution imaging of organelles and displayed to be innocuous up to $250\ \mu\text{M}$ after 48 hours incubation. It was noted however that, at the concentrations required for SPECT imaging, neither **76** nor **77** displayed significant cytotoxicity. Cell images are shown below, in Figure 4.3.

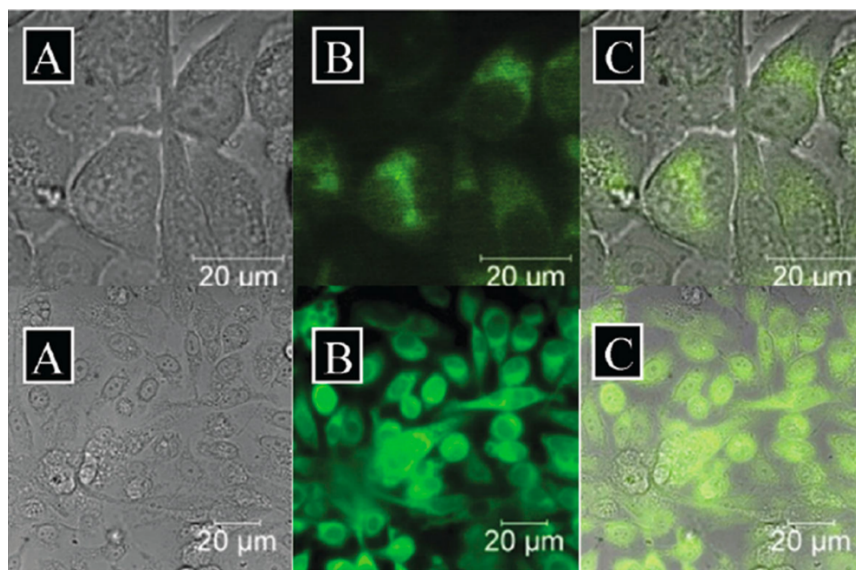
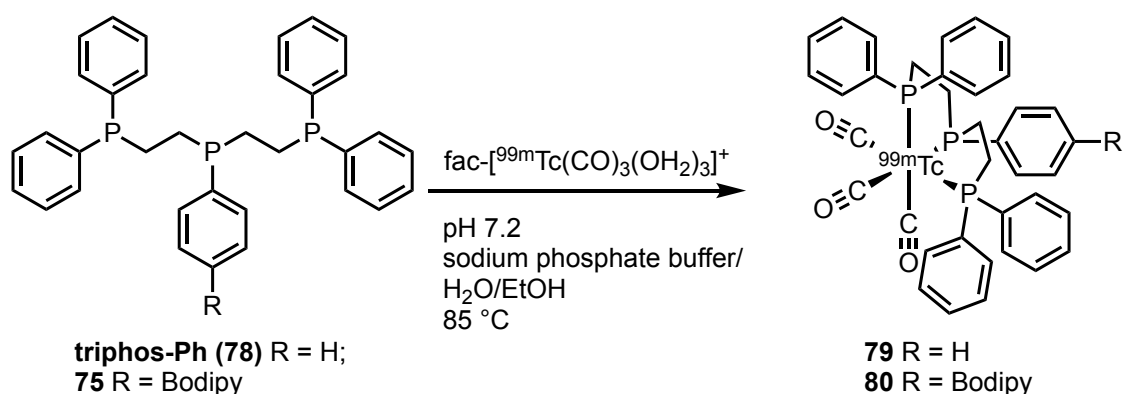


Figure 4.3 Fluorescence imaging of PC-3 living cells with compounds *cis,mer*-[ReCl(CO)₂(**75**)], **77** (Top) and *fac*-[Re(CO)₃(**75**)]⁺, **76** (Bottom). (A) DIC, (B) green channel $\lambda_{\text{ex}} = 460\text{--}500\ \text{nm}$, long pass filtered at $510\ \text{nm}$, (C) overlay of A and B. **76** allowed for high resolution imaging without cytotoxicity, whereas **77** caused morphological changes.

Due to the similar chemical properties of rhenium and technetium (atomic radii of 137 and 136 pm respectively),²² rhenium complexes serve as a cold standard for radioactive ^{99m}technetium complexes which would be applicable in SPECT imaging, and thus add an additional functionality to the existing fluorescent complex. Therefore, through collaboration with the research group of Dr Paul Benny, at Washington State University, coordination of both triphos-Ph and **75** to *fac*-[^{99m}Tc(CO)₃(OH₂)₃]⁺ afforded two complexes, [Tc(triphos-Ph)CO₃] **79** and [Tc(**75**)CO₃] **80**. These complexes both hold potential as SPECT imaging agents, but **80** has the additional function as an optical imaging agent (Scheme 4.3).



Scheme 4.3 Synthesis of $^{99\text{m}}$ -technetium complexes **79** and **80** from tridentate phosphorus compounds triphos-Ph and **75** to produce compounds suitable for SPECT imaging.

80 was the first example of a phosphine based multifunctional imaging agent which combined i) a tridentate phosphine for kinetic stability ii) a fluorophore to enable *in vitro* imaging, and iii) a radiolabel for *in vivo* imaging via SPECT.

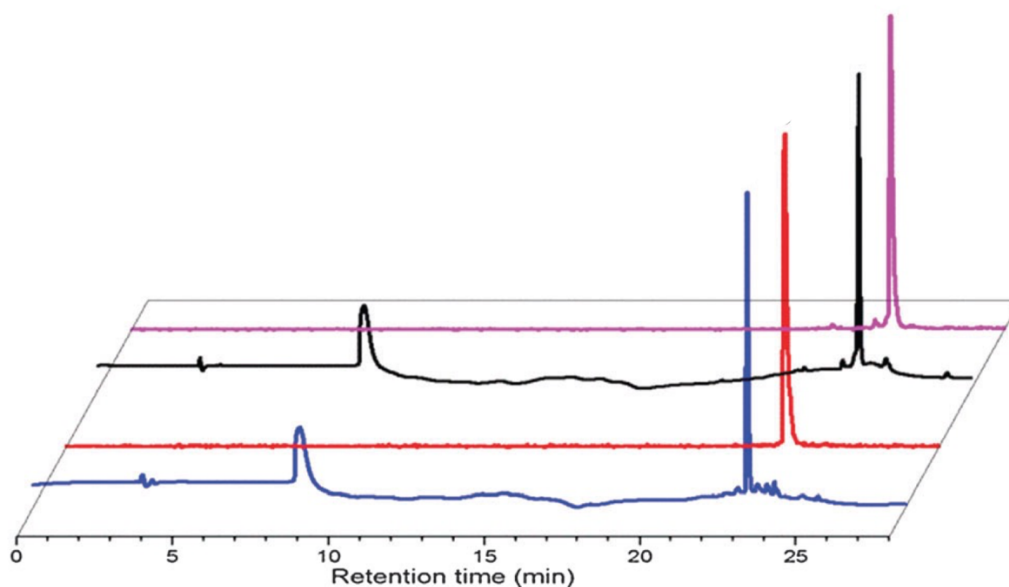


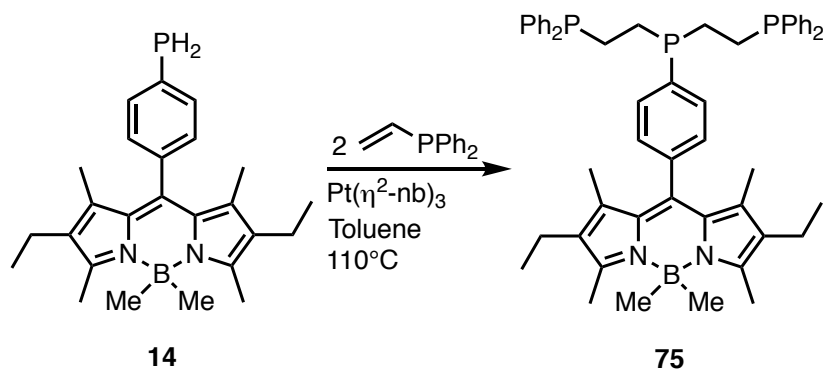
Figure 4.4 The HPLC chromatogram used for comparing the crude reactions of rhenium and $^{99\text{m}}$ -technetium complexes showing their analogous physical properties. $[\text{Re(CO)}_3(\text{triphos-Ph})]^+$ (blue), $\text{fac-[}^{99\text{m}}\text{Tc(CO)}_3(\text{triphos-Ph})]$ **79** (red), $\text{fac-[Re(CO)}_3(\textbf{75})]^+$ **76** (black), $\text{fac-[}^{99\text{m}}\text{Tc(CO)}_3(\textbf{75})]^+$ **80** (purple).

Following the success of this approach with group 7, rhenium and technetium complexes, we were keen to explore group 10 for the reasons explained earlier. It was of interest to investigate whether group 10 complexes could be synthesised that incorporate the tridentate phosphine **75** to afford fluorescent complexes with potential biological activity.

4.1.4 Synthesis of Fluorescent Tridentate Phosphine (**75**)

8-(4-(Bis-2-ethyldiphenylphosphino)-phenylphosphino)-4,4-dimethyl-1,3,5,7-tetramethyl-2,6-diethyl-4-bora-3a,4a-diaza-s-indacene (BodP_3) can be synthesised from the fluorescent primary phosphine **14** in a double hydrophosphination reaction (Scheme 4.4). Thus, primary

phosphine **14** was reacted with vinyl diphenylphosphine; this reaction was catalysed using the platinum catalyst $[\text{Pt}(\eta^2\text{-norbornene})_3]$ and showed complete conversion to **75** by $^{31}\text{P}\{^1\text{H}\}$ NMR spectroscopy after reflux conditions in toluene for five days. No indications of secondary phosphine intermediates were observed.



Scheme 4.4 The synthesis of **75** via $[\text{Pt}(\eta^2\text{-nb})_3]$ catalysed hydrophosphination of primary phosphine **14** with two equivalents of vinyl diphenylphosphine in refluxing toluene over five days.

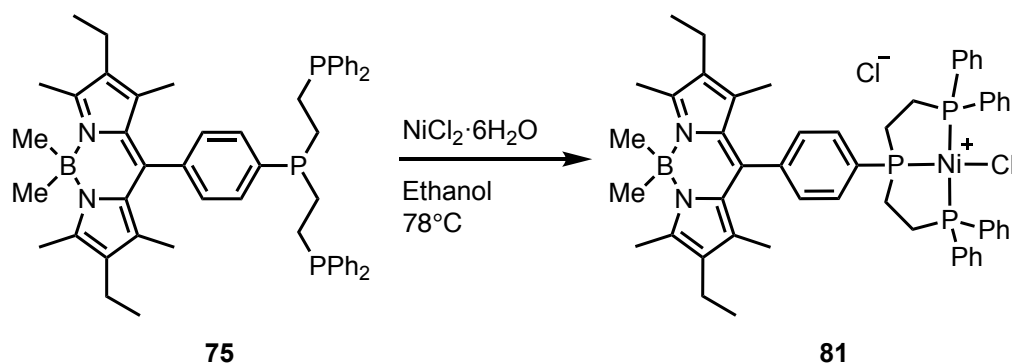
Purification by column chromatography, afforded **75** as an orange solid in 53% yield. Analysis by $^{31}\text{P}\{^1\text{H}\}$ NMR spectroscopy displayed resonances in an AX_2 spin system with a doublet at $\delta -12.9$ ($^3J_{\text{PP}} = 27.9$ Hz) ppm for the terminal phosphines and a triplet at $\delta -16.9$ ($^3J_{\text{PP}} = 27.9$ Hz) for the central phosphorus atom, consistent with the reported data.²⁰

4.2 Group 10 Metal Coordination Studies

The reader will observe that the main focus of this chapter is on the fluorescent platinum(II) complexes as the most prominent group 10 metal in medicine. However, tridentate nickel complexes have been used in catalysis and thus, it will be interesting to compare their biological activity to platinum, other researchers may want to investigate fluorescent complexes in catalysis. In addition to this, palladium complexes are emerging as an alternative to platinum complexes for their anticancer properties, therefore, the tridentate nickel and palladium complexes will also be synthesised and characterised.

4.2.1 Synthesis of Nickel(II) Complex from Fluorescent Tridentate BodP₃

An ethanol solution of $\text{NiCl}_2 \cdot 6\text{H}_2\text{O}$ was reacted with one equivalent of **75** at reflux to produce the nickel(II) complex $[\text{Ni}(\text{75})\text{Cl}]\text{Cl}$ **81**, as shown in Scheme 4.5. Removal of the solvent *in vacuo* afforded a bright orange solid in near quantitative yield (95%).



Scheme 4.5 Synthesis of the nickel(II) complex [Ni(75)Cl]Cl **81** from the coordination of **75** to NiCl₂·6H₂O.

Analysis by ³¹P{¹H} NMR spectroscopy saw a downfield shift of the AX₂ resonances for the free phosphine **75** at δ −12.9 (d, ³J_{PP} = 27.9 Hz, 2P) and δ −16.9 (t, ³J_{PP} = 27.9 Hz, 1P) ppm to a triplet at δ 112.1 ppm (³J_{PP} = 31.0 Hz) for the central phosphorus atom, and a doublet at δ 48.9 (³J_{PP} = 31.0 Hz) corresponding to the terminal phosphorus atoms for nickel(II) complex **81**. These values compare well to the [Ni(triphos-Ph)Cl]BPh₄ analogue which are shown in Table 4.1.²³

Crystals of **81** suitable for X-ray crystallography were obtained by co-worker Dr Laura Davies by slow diffusion of pentane into an ethanol solution of **81**; the molecular structure of **81** is depicted in Figure 4.5. The Ni(II) metal centre is incorporated into two fused five-membered chelate rings (NiPC₂P).

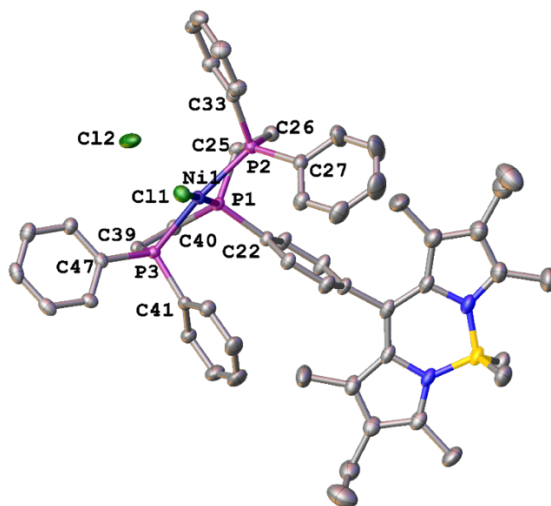


Figure 4.5 View of the molecular structure of **81**. Hydrogen atoms have been omitted for clarity. Selected bond distances [Å] and angles [°]: Ni1-P1 2.1303(6), Ni1-P2 2.2004(6), Ni1-P3 2.1852(6), Ni1-Cl1 2.1951(6), P1-C22 1.823(2), P1-C25 1.829(2), P1-C40 1.843(2), P1-Ni1-P2 85.17(2), P1-Ni1-P3 84.21(2), P2-Ni1-P3 168.62(3), P1-Ni1-Cl1 176.27(3), P2-Ni1-Cl1 94.73(2), P3-Ni1-Cl1 95.61(2), Ni1-P1-C25 107.79(7), Ni1-P2-C26 109.53(7), Ni1-P3-C39 108.49(7).

The Ni-P bond lengths of Ni1-P1 2.1303(6), Ni1-P2 2.2004(6) and Ni1-P3 2.1852(6) Å are similar to the analogous complex, [Ni(triphos-Ph)Cl]BPh₄ (Ni-P_C 2.123(2), Ni-P_T 2.214(3), Ni-P_T 2.202(3) Å).²⁴ The complex **81** has a distorted square planar geometry, apparent from the

bond angles around the nickel centre of P1-Ni1-P2 85.17(2), P1-Ni1-P3 84.21(2), P2-Ni1-Cl 94.73(2) and P3-Ni1-Cl 95.61(2)° again, similar to the non-fluorescent derivative (P_T-Ni-P_C 85.6(1), P_C-Ni-P_T 85.8(1), P_T-Ni-Cl 93.8(1) and P_T-Ni-Cl 97.4(1)°).²⁴

Although nickel is not known for its biological properties and applications, tridentate nickel complexes are currently attracting attention as catalysts as discussed earlier, and thus **81** may hold potential in a catalytic applications as a fluorescent catalyst which may prove useful in aspects such as investigating mechanistic cycles by optical spectroscopy.

4.2.2 Palladium

Due to toxicities associated with platinum chemotherapeutics, this has led to the investigation of alternative metal complexes as anticancer agents.²⁵ The chemical and physical similarities between platinum and palladium have resulted in palladium complexes becoming the target of many studies.²⁵ It was established early on however, that *cis*-palladium was not active as an anticancer agent due to the inferior reactivity and kinetics of the metal complexes.²⁶ Palladium(II) complexes display high lability and are ~10⁵ more reactive than their platinum(II) analogues, which commonly results in the rapid hydrolysis of the metal centre, forming reactive species before reaching their biological targets.²⁷ Thus, strongly binding or polydentate ligands have been utilised to reduce the reactivity of palladium(II) complexes.²⁵

In recent literature, studies by Aydemir and co-workers evaluated two bis(phosphinite)-palladium(II) complexes, **82a** and **82b** in their activity as anticancer agents as part of a small study of novel ruthenium and palladium complexes.²⁸ These palladium(II) complexes contained one bidentate phosphinite ligand and two chloride ligands in a square planar geometry, mimicking the structure of cisplatin and were tested against non-small- (NSCLC) and small-cell lung cancers (SCLC) cell lines.

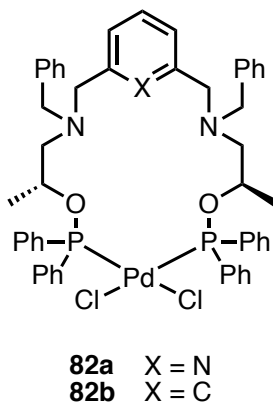


Figure 4.6 Palladium(II) complexes **82a** and **82b** with a bidentate bis(phosphinite) ligand, tested for their anticancer activity.

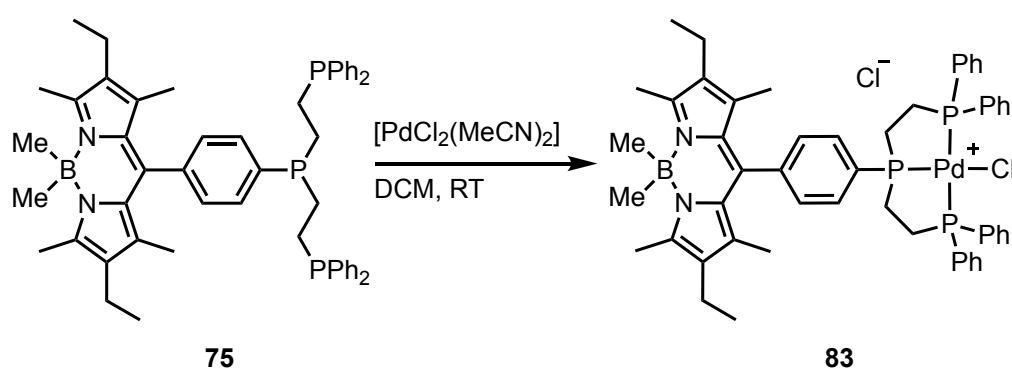
Both complexes displayed cytotoxic effects against the cell lines, demonstrating effective cell antiproliferation effects. They were shown to inhibit cellular viability and induce apoptosis at low concentrations, supporting their potential as anticancer agents and warranting their further investigation.²⁸

A current study from Serebryanskaya and coworkers discovered the first example of a palladium(II)-based acyclic diaminocarbene complex that displayed antiproliferation activity which was comparable or better than the activity of the analogous platinum complex. They highlighted that in this case, platinum could be replaced by the cheaper metal, palladium, resulting in more commercially available anticancer agents.²⁹

Although initial studies presented unpromising bioactivity for palladium, more recent studies have revealed compelling advantages over platinum complexes including: i) lower toxicity, ii) lower cost, and iii) better structure–activity relationships which merits their further development.^{25,30}

4.2.3 Synthesis of Palladium(II) Complex **83** from Fluorescent Tridentate BodP₃

Synthesis of the fluorescent [Pd(**75**)Cl]Cl **83** was achieved via the reaction of BodP₃ (**75**) and [PdCl₂(MeCN)₂] in dichloromethane. The reaction mixture was stirred for two hours at room temperature to afford palladium complex, **83**, as depicted in Scheme 4.6. All three phosphorus donors of the tridentate ligand coordinate to the palladium(II) centre displacing two labile acetonitrile groups and one chloride ligand. The volatiles were removed *in vacuo* to afford **83** as an orange solid in near quantitative yield (96%).



Scheme 4.6 Synthesis of the palladium(II) complex [Pd(**75**)Cl]Cl **83** from the coordination of **75** to [PdCl₂(MeCN)₂].

Subsequent analysis by ³¹P{¹H} NMR spectroscopy showed downfield signals from **75**, similar to those observed for the [Ni(**75**)Cl]Cl complex **83**; an AX₂ spin system was evident, displaying a triplet at δ 112.4 ppm for the central phosphine, and a doublet for the two terminal phosphorus atoms at δ 45.8 ppm. A small coupling constant of 9.9 Hz was observed which

corresponds to a two bond ^{31}P - ^{31}P coupling ($^2J_{\text{PP}}$). The values compare well to the analogous triphos-Ph complex, $[\text{Pd}(\text{triphos-Ph})\text{Cl}]\text{Cl}$ which are displayed in Table 4.1.³¹

Crystals of **83** suitable for X-ray crystallography were obtained by slow diffusion from ethanol/pentane by co-worker, Dr Davies; the molecular structure is illustrated in Figure 4.7.

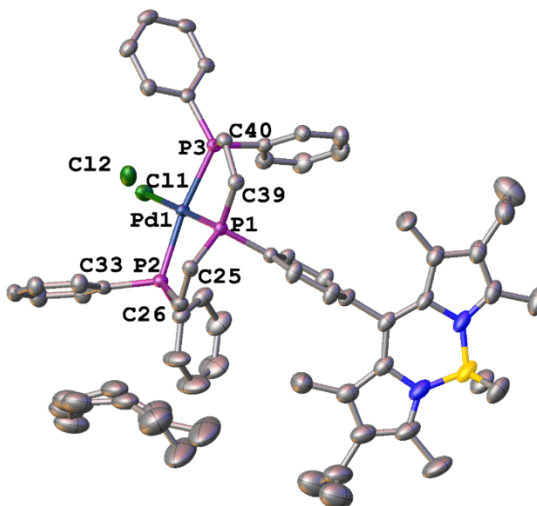
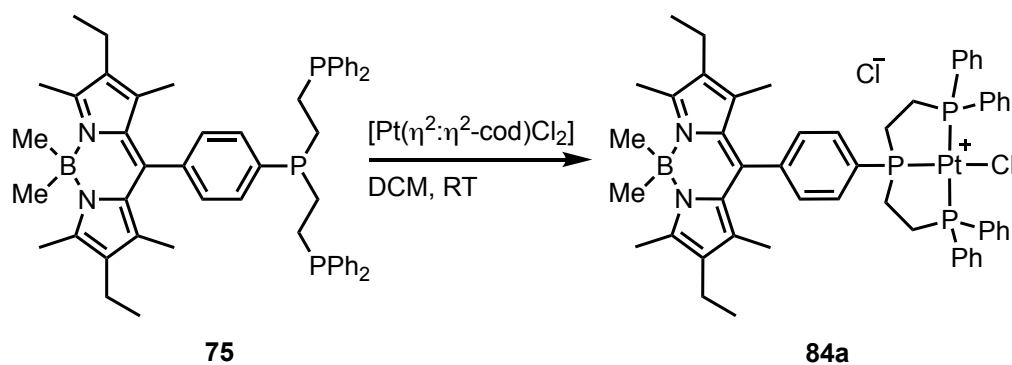


Figure 4.7 View of the molecular structure of **83**. Hydrogen atoms have been omitted for clarity. Selected bond distances [Å] and angles [°]: Pd1-Cl1 2.3519(8) Pd1-P1 2.2143(8) Pd1-P2 2.3130(8) Pd1-P3 2.2993(8) P1-C22 1.816(3), P1-C25 1.822(3), P1-C39 1.84(3), P1-Pd1-Cl1 177.94(3), P1-Pd1-P2 83.65(3), P1-Pd1-P3 83.05(3), P2-Pd1-Cl1 96.05(3), P3-Pd1-Cl1 97.24(3), P3-Pd1-P2 166.70(3), Pd1-P1-C25 107.12(11), Pd1-P1-C39 113.09(11), Pd1-P2-C26 107.85(11), Pd1-P3-C40 107.23(11).

The Pd-P bond lengths of Pd1-P1 2.2143(8), Pd1-P2 2.3130(8) and Pd1-P3 2.2993(8) Å are typical for palladium(II) complexes. Again, this palladium(II) complexes adopts a distorted square planar geometry (bond angles: P1-Pd1-P2 83.65(3), P1-Pd1-P3 83.05(3), P2-Pd1-Cl1 96.05(3) and P3-Pd1-Cl1 97.24(3)°) which compares well to palladium(II) triphos-Ph analogue, $[\text{Pd}(\text{triphos-Ph})\text{Cl}]\text{Cl}$ (bond angles: $\text{P}_\text{T}\text{-Pd-P}_\text{C}$ 83.8(1), $\text{P}_\text{T}\text{-Pd-P}_\text{C}$ 84.1(1), Cl-Pd-P_T 98.5(1), Cl-Pd-P_T 93.6(1)° T to denote the terminal phosphorus atoms and C for the central phosphorus).³²

4.2.4 Synthesis of Platinum(II) Complex **84a** from Fluorescent Tridentate BodP_3

75 was added to a dichloromethane solution of $[\text{Pt}(\eta^2\text{:}\eta^2\text{-cod})\text{Cl}_2]$ at room temperature and monitored by $^{31}\text{P}\{^1\text{H}\}$ NMR spectroscopy. On completion of the reaction, the solvent was removed *in vacuo* and subsequent washing of the solid with petroleum ether to remove 1,5-cyclooctadiene afforded $[\text{Pt}(\textbf{75})\text{Cl}]\text{Cl}$ **84a** as an orange solid (90% yield) (Scheme 4.7).



Scheme 4.7 Synthesis of the platinum(II) complex **84a** from **75** and $[\text{Pt}(\eta^2:\eta^2\text{-cod})\text{Cl}_2]$ in dichloromethane at RT.

On analysis by $^{31}\text{P}\{^1\text{H}\}$ NMR spectroscopy, downfield shifts from the free ligand were observed at δ 86.3 ppm ($^1J_{\text{Pt}} = 3010$ Hz) for the central phosphorus atom and δ 41.8 ppm ($^1J_{\text{Pt}} = 2485$ Hz) for the two terminal phosphorus atoms. These large satellite peaks confirmed the coordination to platinum and are typical for such complexes, with comparable couplings observed for the analogous $[\text{Pt}(\text{triphos-Ph})\text{Cl}]\text{Cl}$ complex (δ 83.7 ppm ($^1J_{\text{Pt}} = 3015$ Hz), δ 39.8 ppm ($^1J_{\text{Pt}} = 2484$ Hz)).³³

Interestingly, only a very small coupling of 3.0 Hz was observed for the J_{PP} coupling constant which was consistent with that observed for the triphos-Ph analogue ($J_{\text{PP}} = 3.1$ Hz). It has been suggested that these small ^{31}P - ^{31}P coupling constants are dependent on two properties, i) the monodentate ligand trans to the central phosphorus atom and ii) the chelate ring size.

García-Fernández *et al.* reported on the dependency of the coupling constant on the monodentate ligand in the series of $[\text{Pt}(\text{triphos})\text{X}]^+$ complexes. The size of the ^{31}P - ^{31}P coupling constant (J_{PP}) decreased in the order $\text{X} = \text{NO}_3^- > \text{CN}^- > \text{Cl}^- > \text{I}^- \approx \text{Br}^- \approx \text{PPh}_3$, and no $^2J_{\text{PP}}$ coupling was observed for I^- , Br^- or PPh_3 .³³

Meek *et al.* observed an increase in the coupling constant from a five-membered chelate ring to a six-membered one.³⁴ They attributed this to an idea which was first suggested by Grim *et al.*³⁵ where there are coupling contributions from both the backbone ($^{\text{B}}J_{\text{PP}}$) and through the metal ($^{\text{M}}J_{\text{PP}}$) which can be totalled to give J_{PP} . In a five-membered chelate ring, the magnitudes of $^{\text{B}}J_{\text{PP}}$ and $^{\text{M}}J_{\text{PP}}$ are approximately equal, but of opposite sign, leading to the smaller coupling constant. For a six-membered ring however, no $^{\text{B}}J_{\text{PP}}$ coupling is observed for the free ligand and so the value for J_{PP} can be attributed entirely to $^{\text{M}}J_{\text{PP}}$.

X-ray crystallographic data from co-worker Davies shows **84a** as an isostructural complex to the nickel and palladium complexes **81** and **83** respectively, displaying a distorted square planar complex confirmed by the bond angles around the platinum centre (Figure 4.8). This complex however, displayed less distorted angles than the analogous nickel and palladium

complexes **81** and **83**. The Pt-P_{central} bond is shorter than the two Pt-P_{terminal} due to the double chelate effect and lower trans effect of the chlorine in comparison to the phosphorus donor.

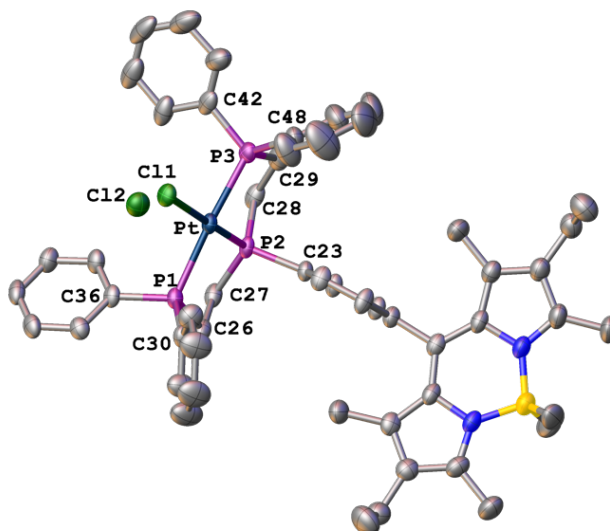


Figure 4.8 View of the molecular structure of **84a** with 50% probability displacement ellipsoids. Hydrogen atoms have been omitted for clarity. Selected bond distances [Å] and angles [°]: Pt-P1 2.3121(11), Pt-P2 2.2058(10), Pt-P3 2.3057(11), Pt-Cl1 2.3613(10), P2-C23 1.803(4), P2-C28 1.803(5), P2-C27 1.812(5), P3-C29 1.854(5); P1-Pt-P2 85.32(4), P1-Pt-P3 168.70(4), P2-Pt-P3 83.80(4), P1-Pt-Cl1 95.85(4), P2-Pt-Cl1 176.59(4), P3-Pt-Cl1 94.84(4), Pt-P1-C26 105.92(16), Pt-P2-C27 108.68(15), Pt-P3-C29 107.14(17), Pt-P2-C23 113.61(14), Pt-P1-C30 118.86(15), Pt-P1-C36 112.37(15).

4.2.5 Cell Imaging Studies

Prior to this work, through collaboration of Dr Laura Davies (Higham group) with Professor Sofia I. Pascu at the University of Bath, initial cell uptake studies of **84a** in HeLa and prostate cancer (PC-3) cells were carried out. The platinum(II) complex demonstrated limited toxicity effects when incubated for 15 minutes at 37 °C in both HeLa and PC-3 cells. Energy dependant uptake resulted in the localisation of **84a** within the endoplasmic reticulum (ER) of both HeLa (Figure 4.9) and PC-3 cells (Figure 4.10) which could be confirmed by overlay images showing co-localisation of the ER tracker dye and **84a**.

The ER is the largest organelle which is responsible for many functions within the cell including calcium storage, protein synthesis and lipid metabolism.³⁶ The strategy for targeting the ER is not as well-defined as that for mitochondria,³⁷ nevertheless, a recent review by King and Wilson has revealed the ER as a promising target for anticancer agents; cytotoxic compounds have displayed selectivity for cancer cells over non-cancer cells.³⁸ In particular, many metal-based anticancer agents have been reported to cause ER stress induction, resulting in apoptosis.

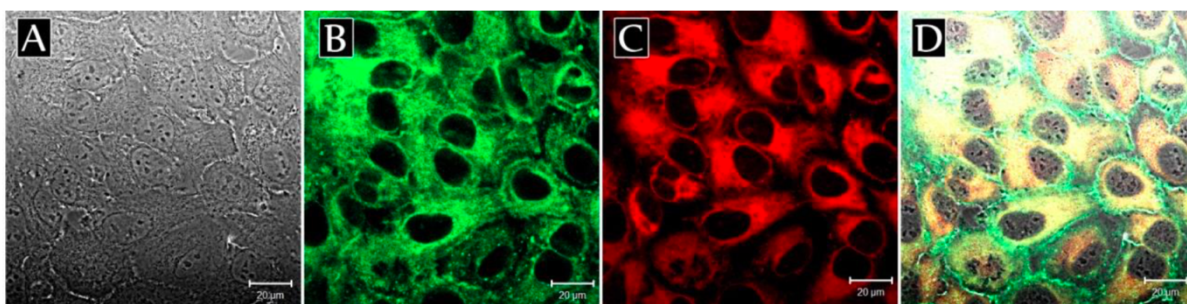


Figure 4.9 1-Photon confocal microscopy images of 10 μM solution of $[\text{Pt}(\mathbf{75})\text{Cl}]\text{Cl}$ **84a** with ER Tracker in HeLa cells (A) DIC image; (B) excitation at 488 nm, emission at 505-550 nm; (C) excitation at 543 nm, emission 593-657 nm; (D) an overlay of the previous three images.

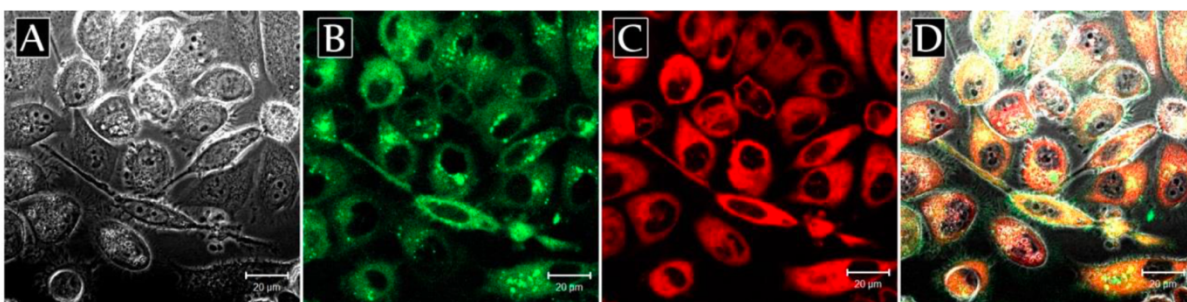


Figure 4.10 1-Photon confocal microscopy images of 10 μM solution of $[\text{Pt}(\mathbf{75})\text{Cl}]\text{Cl}$ **84a** with ER Tracker in PC-3 cells (A) DIC image; (B) excitation at 488 nm, emission at 505-550 nm; (C) excitation at 543 nm, emission 593-657 nm; (D) an overlay of the previous three images.

These preliminary results looked promising and thus, formed the basis for further studies of this Pt(II) complex to establish full cytotoxicity data and expand its application as a cell imaging probe. To further this research, it was of interest to assess the significance of the halogen ligand and counterion in the platinum(II) complex. Thus, two novel complexes, $[\text{Pt}(\mathbf{75})\text{Br}]\text{Br}$ **84b** and $[\text{Pt}(\mathbf{75})\text{I}]\text{I}$ **84c** were synthesised.

4.2.6 Effect of the Halide Ligand on Platinum(II) Complexes

Platinum iodo complexes have commonly been overlooked for their bioactivity due to early studies which deemed these analogues biologically inactive; studies inclusive of the cisplatin iodo analogue, $[\text{Pt}(\text{NH}_3)_2\text{I}_2]$, carried out in separate studies by Cleare³⁹ and Aggarwal⁴⁰, were to this effect. However, more recent work is beginning to challenge this opinion and in a recent series of papers by Marzo *et al.*, they have studied the chemical and biological profile of cisplatin and oxaliplatin analogues where the chloride ligands of cisplatin are replaced by bromide or iodide, whilst the oxalate ligand of oxaliplatin are replaced by halides (chloride, bromide or iodide) have been investigated.^{41–43}

Cisplatin analogues $[\text{Pt}(\text{NH}_3)_2\text{Br}_2]$ and $[\text{Pt}(\text{NH}_3)_2\text{I}_2]$, were found to have similar solution behaviour to cisplatin in which the sequential release of the halide ligands results in their replacement by water molecules. For $[\text{Pt}(\text{NH}_3)_2\text{Br}_2]$, this occurred with similar kinetics to

cisplatin, whereas for $[\text{Pt}(\text{NH}_3)_2\text{I}_2]$ slower kinetics were observed. Weakly acidic conditions ($\text{pH} = 4.5$) resulted in an alternative hydrolysis path for $[\text{Pt}(\text{NH}_3)_2\text{I}_2]$, where the ammonia ligands instead are exchanged for water, affording $[\text{Pt}(\text{OH}_2)(\text{NH}_3)\text{I}_2]$ and $[\text{Pt}(\text{OH}_2)_2\text{I}_2]$, yet this is not observed in cisplatin or $[\text{Pt}(\text{NH}_3)_2\text{Br}_2]$. All three complexes displayed a similar DNA platination pattern however, again, the kinetics of DNA metalation were much slower for $[\text{Pt}(\text{NH}_3)_2\text{I}_2]$. Log P experiments were carried out, and as expected, $[\text{Pt}(\text{NH}_3)_2\text{Br}_2]$ and $[\text{Pt}(\text{NH}_3)_2\text{I}_2]$ exhibited increased lipophilicity when compared to cisplatin.

Both complexes were tested against a selection of cancer cell lines; $[\text{Pt}(\text{NH}_3)_2\text{Br}_2]$ displayed cytotoxic activity comparable with that of cisplatin and displayed a slight improvement when tested against the FLG 29.1 (leukaemia) cell line. Remarkably, $[\text{Pt}(\text{NH}_3)_2\text{I}_2]$ demonstrated higher cytotoxicity than cisplatin in three out of four cisplatin-sensitive cancer cell lines and was effective in overcoming resistance in the cisplatin-resistant colon carcinoma cell line, HCT116-R. The cell uptake was much higher than cisplatin, which could partially explain the improved activity. The increased cellular uptake did not display a linear correlation with the cytotoxicity of the complex however. Thus, it is likely that there are additional targets and mechanisms of action occurring. The improved cytotoxic effects over cisplatin, particularly of the iodo substituted analogue, $[\text{Pt}(\text{NH}_3)_2\text{I}_2]$, merit the further studies and the assessment of its full pharmacological profile.^{41,42}

Similar studies were carried out by the same group on analogues of oxaliplatin, these complexes are shown in Figure 4.11. The replacement of the oxalate group with halide ligands resulted in a display of a similar solution property profile of the halido complexes **85**, **86** and **87** to the parent complex, oxaliplatin.

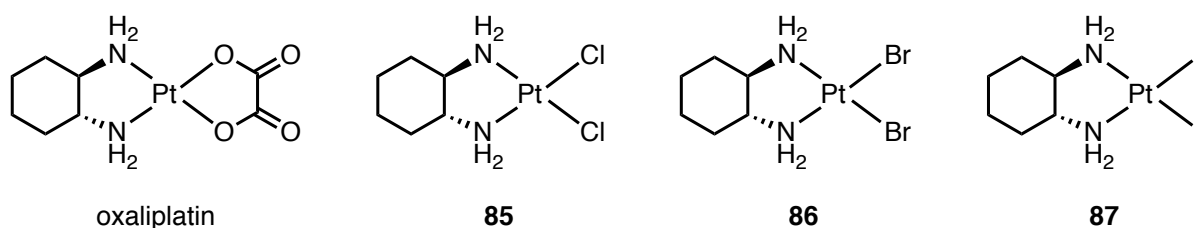


Figure 4.11 Oxaliplatin and three analogues **85-87** which have been tested for their anticancer activity against colorectal cancer cell lines. It was demonstrated that the oxalate ligand was not necessary for anticancer activity.

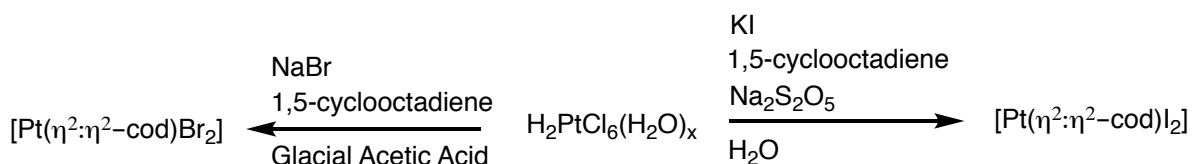
The studies demonstrated that the bidentate oxalate ligand was not essential for the anticancer activity of the drug, and by changing the ligands to halogens, a large increase in lipophilicity of the complex resulted which is recognised as a highly important factor in drug development.⁴⁴

Interestingly, in contrast to cisplatin and its corresponding analogues, these new complexes exhibited almost no reactivity with model proteins.^{43,45} This unexpected result could be of significant importance in their pharmacological profile and thus, acknowledges the need for further studies.

A full review of platinum iodo complexes, their anticancer properties and mechanisms of action was carried out by Trávníček *et al.* in 2019. The overview merits the further development of these complexes as new platinum-based anticancer agents and classified them as highly active, more specific and potentially safer alternatives to the current platinum-based therapeutics available.⁴⁶ Thus, it was of interest to synthesise the two iodo and bromo fluorescent platinum complexes, analogues to **84a**, which could demonstrate different cellular behaviour.

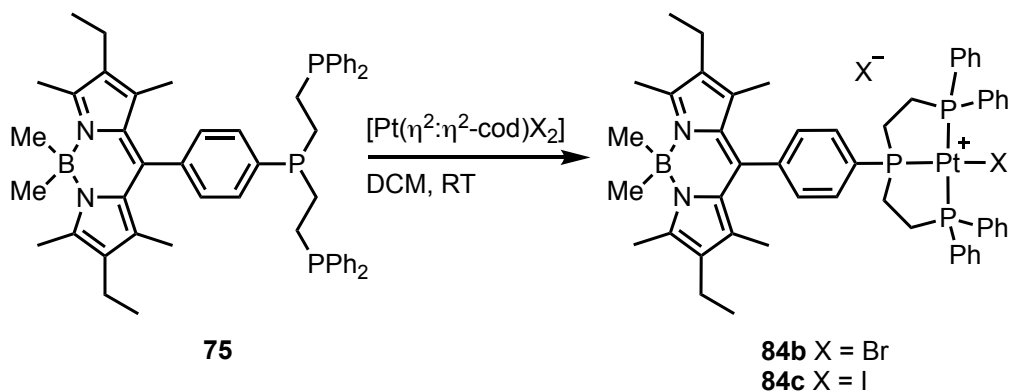
4.2.7 Synthesis of Novel Platinum(II) Complexes from Fluorescent Tridentate BodP₃

To synthesise the fluorescent bromo and iodo substituted platinum(II) complexes, **84b** and **84c**, the corresponding dihalo(1,5-cyclooctadiene)platinum(II) complexes, [Pt(η^2 : η^2 -cod)Br₂] and [Pt(η^2 : η^2 -cod)I₂] were first synthesised following procedures by Drew and Doyle (Scheme 4.8). These complexes could be formed from hydrated chloroplatinic acid, 1,5-cyclooctadiene and sodium bromide or potassium iodide respectively as shown in Scheme 4.8.⁴⁷



Scheme 4.8 Synthesis of dibromo(1,5-cyclooctadiene)platinum(II) and diiodo(1,5-cyclooctadiene)platinum(II) complexes, [Pt(η^2 : η^2 -cod)Br₂] and [Pt(η^2 : η^2 -cod)I₂] from hydrated chloroplatinic acid.

Following the synthesis of the dihalo(1,5-cyclooctadiene)platinum(II) complexes, **84b** and **84c** were synthesised in an analogous manner to **84a** in dichloromethane at room temperature.



Scheme 4.9 Synthesis of the platinum(II) complexes **84b** and **84c** from **75** and [Pt(η^2 : η^2 -cod)X₂] in DCM at RT.

The reactions were monitored by $^{31}\text{P}\{^1\text{H}\}$ NMR spectroscopy and in both cases, downfield chemical shifts with platinum satellite peaks confirmed complete conversion of **75** to **84b** and **84c** after one hour. Like **84a**, both **84b** and **84c** complexes presented downfield chemical shifts to **75** upon coordination. The $^{31}\text{P}\{^1\text{H}\}$ NMR spectrum showed the central phosphorus atom at δ 89.2 ($^1J_{\text{PPt}} = 2996$ Hz) and at δ 92.7 ($^1J_{\text{PPt}} = 2900$ Hz) ppm respectively, as well as terminal phosphorus atoms at δ 42.2 ($^1J_{\text{PPt}} = 2458$ Hz) and δ 42.4 ($^1J_{\text{PPt}} = 2416$ Hz) respectively for **84b** and **84c**. This data has been illustrated in Figure 4.12.

Unlike **84a**, no $^2J_{\text{PP}}$ coupling was observed for **84b** and **84c**, yet this was in line with the reported data by García-Fernández *et al.* as discussed in Section 4.2.4.

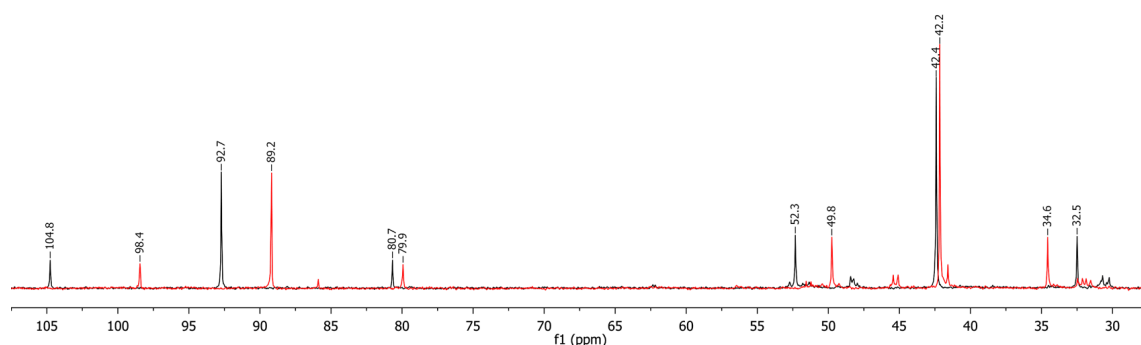


Figure 4.12 Overlay of the $^{31}\text{P}\{^1\text{H}\}$ NMR spectra of $[\text{Pt}(\mathbf{75})\text{Br}]\text{Br}$ **84b** (red) and $[\text{Pt}(\mathbf{75})\text{I}]\text{I}$ **84c** (black); the chemical shifts at δ 89.2 ppm and 92.7 ppm are assigned to the central phosphorus atoms and the resonances at δ 42.2 ppm and 42.4 ppm are assigned to the terminal phosphorus donors for the respective complexes.

Table 4.1 $^{31}\text{P}\{^1\text{H}\}$ NMR spectroscopic data for tridentate phosphine group 10 complexes.

	ppm (δ_{Central})	J_{PP} (Hz)	J_{PPt} (Hz)	ppm (δ_{Terminal})	J_{PPt} (Hz)
$[\text{Ni}(\text{triphos-Ph})\text{Cl}]\text{BPh}_4^{\text{a}}$	111.5	31.0	-	47.5	-
$[\text{Pd}(\text{triphos-Ph})\text{Cl}]\text{Cl}^{\text{b}}$	109.3	9.4	-	44.2	-
$[\text{Pt}(\text{triphos-Ph})\text{Cl}]\text{Cl}^{\text{c}}$	83.7	3.1	3015	39.8	2484
$[\text{Pt}(\text{triphos-Ph})\text{Br}]\text{Br}^{\text{c}}$	86.7	-	2992	40.2	2464
$[\text{Pt}(\text{triphos-Ph})\text{I}]\text{I}^{\text{c}}$	89.9	-	2895	40.1	2424
$[\text{Ni}(\mathbf{75})\text{Cl}]\text{Cl}$ (81)	112.1	47.1	-	48.9	-
$[\text{Pd}(\mathbf{75})\text{Cl}]\text{Cl}$ (83)	112.4	9.9	-	46.8	-
$[\text{Pt}(\mathbf{75})\text{Cl}]\text{Cl}$ (84a)	86.3	3.0	3010	41.8	2485
$[\text{Pt}(\mathbf{75})\text{Br}]\text{Br}$ (84b)	89.2	-	2996	42.2	2458
$[\text{Pt}(\mathbf{75})\text{I}]\text{I}$ (84c)	92.7	-	2900	42.4	2416

^aData reported by Henderson *et al.*²³ ^bData reported by Sadler *et al.*³¹ ^cData reported by García-Fernández *et al.*³³

Crystals of **84c** suitable for X-ray crystallographic analysis were grown from slow diffusion of petroleum ether into dichloromethane. These samples have been submitted for analysis and are awaiting results.

4.3 Photophysical Data

As previously reported by the Higham group, on coordination of **75** to rhenium, the fluorescence of the BodP₃ ligand was not fully quenched as might have been expected (from $\Phi_F = 0.34$ for **75** to $\Phi_F = 0.27$ and 0.20 for **76** and **77** respectively).⁴ Therefore, following the synthesis of the group 10 metal complexes **81**, **83**, **84a**, **84b** and **84c**, it was important to determine their photophysical properties to see if they could also have applications in cell imaging, bearing in mind the success of cisplatin. Thus, photophysical data was collected for the tridentate ligand **75** and complexes **81**, **83**, **84a**, **84b** and **84c** in dry, degassed tetrahydrofuran (to minimise photobleaching and phosphine oxidation in solution). The data is shown in Table 4.2.

Table 4.2 Photophysical data for the tridentate phosphine **75** and group 10 complexes [Ni(**75**)Cl]Cl **81**, [Pd(**75**)Cl]Cl **83**, [Pt(**75**)Cl]Cl **84a**, [Pt(**75**)Br]Br **84b** and [Pt(**75**)I]I **84c**.

	λ_{abs} (nm) ^a	λ_{em} (nm) ^a	$\Phi_F^{a,b}$	ϵ (M ⁻¹ cm ⁻¹) ^a
BodP ₃ (75)	513	527	0.34	90,000
[Ni(75)Cl]Cl (81)	513	528	0.09	85,000
[Pd(75)Cl]Cl (83)	514	530	0.19	63,000
[Pt(75)Cl]Cl (84a)	514	532	0.23	61,000
[Pt(75)Br]Br (84b)	514	532	0.48	49,000
[Pt(75)I]I (84c)	514	531	0.55	65,000

^aMeasured in dry, degassed tetrahydrofuran at room temperature, dyes were excited at 485 nm; ^bFluorescence quantum yields were measured with respect to 4,4-difluoro-8-phenyl-1,3,5,7-tetramethyl-2,6-diethyl-4-bora-3a,4a-diaza-s-indacene.

The absorption spectra of the tridentate phosphine **75** and the complexes **81**, **83**, **84a**, **84b** and **84c** (shown in Figure 4.13) display a strong absorbance relating to the S₀-S₁ (π - π^*) transition, with maxima at either 513 or 514 nm, which can be assigned to the Bodipy core. A second, lower intensity, broader absorption band is visible between 370 and 380 nm which can be assigned to the S₀-S₂ (π - π^*) transition of the Bodipy core. Tridentate phosphine **75** has a high molar absorption coefficient of 90,000 M⁻¹cm⁻¹, characteristic of Bodipy compounds, which is lowered on coordination to the group 10 complexes ($\epsilon = 49,000$ -85,000 M⁻¹cm⁻¹).

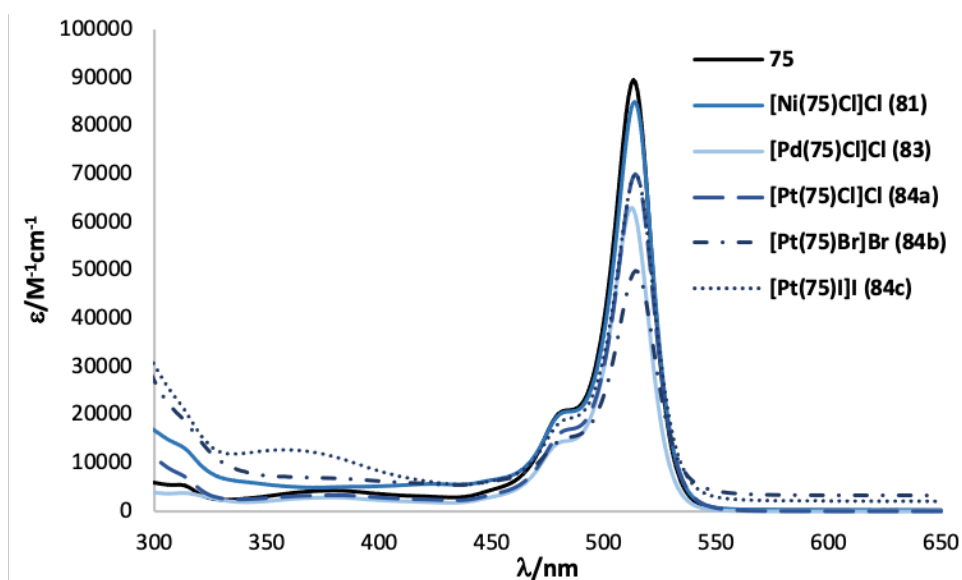


Figure 4.13 Absorption spectra of tridentate phosphine **75**, and complexes **[Ni(75)Cl]Cl** **81**, **[Pd(75)Cl]Cl** **83**, **[Pt(75)Cl]Cl** **84a**, **[Pt(75)Br]Br** **84b** and **[Pt(75)I]I** **84c**, in tetrahydrofuran at room temperature.

On coordination to the group 10 metals, Ni, Pd and Pt, to afford **81**, **83**, **84a**, **84b** and **84c**, the emission maxima were shifted slightly, by 1–5 nm, to a lower frequency (Figure 4.14). The Stokes shifts observed for the complexes are small (15–18 nm) which is common for Bodipy fluorophores, signifying minimal structural change on excitation. The data is displayed in Table 4.2.

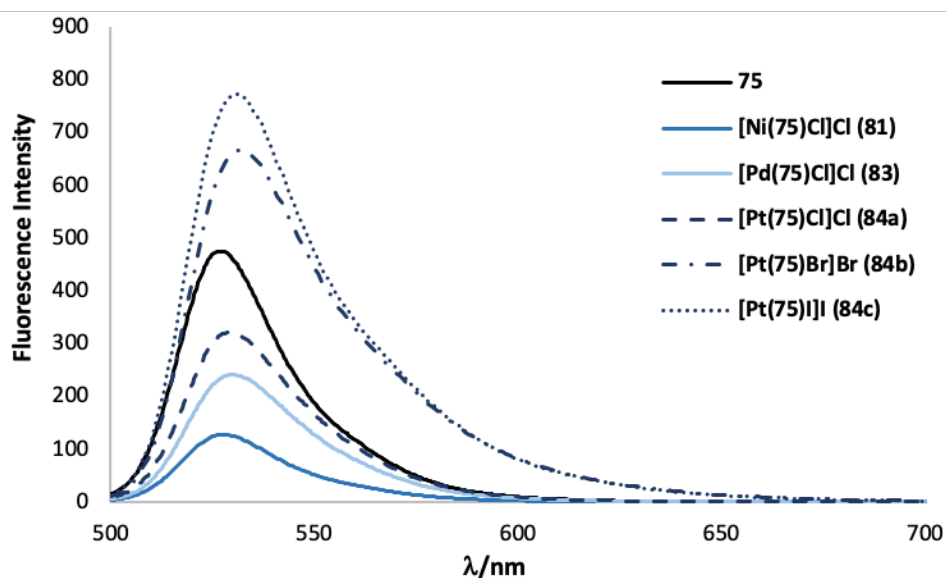


Figure 4.14 Emission spectra of the tridentate phosphine **75** and its complexes **[Ni(75)Cl]Cl** **81**, **[Pd(75)Cl]Cl** **83**, **[Pt(75)Cl]Cl** **84a**, **[Pt(75)Br]Br** **84b** and **[Pt(75)I]I** **84c**, in tetrahydrofuran at RT (excitation at 485 nm).

The quantum yield of BodP₃ **75**, ($\Phi_F = 0.34$) in tetrahydrofuran was similar to the reported values for primary phosphine, **14** ($\Phi_F = 0.33$) showing that the addition of two phosphorus donors has minimal effect on the photophysical properties. DFT calculations had not been carried out to aid in the understanding of this phenomenon, and thus were calculated as part

of this study. The minimised structure and calculated molecular orbitals are illustrated in Figure 4.15 and these will be discussed in Section 4.4.

On coordination to the chloro-substituted metals, the fluorescence quantum yields were lowered, **81** ($\Phi_F = 0.09$), **83** ($\Phi_F = 0.19$) and **84a** ($\Phi_F = 0.23$), but not quenched. For the second trend that was investigated, of replacing the halide trans to the central phosphorus atom, the quantum yield for the resulting complexes *increased*, **84b** ($\Phi_F = 0.48$) and **84c** ($\Phi_F = 0.55$). These data were unexpected, as previous to this, all of our complexation reactions have displayed reductions in quantum yield (although often small) in comparison to the free ligands. In addition, as a result of the heavy atom effect,⁴⁸ one might have expected a decrease in fluorescence quantum yield down the group, but clearly the reverse is observed. The relative solubilities of the complexes may have an effect on the quantum yields, but we also cannot rule out that there might be a highly fluorescent impurity present, so these results should be repeated to eliminate any possibility of anomalies. To gain further insight, DFT calculations of the metal complexes were carried out to afford the calculated molecular orbitals and their relative orbital energies. These are discussed in the following section.

4.4 DFT Calculations

The DFT calculations of the tridentate phosphine ligand, **75** (Figure 4.15) illustrate a Bodipy-based HOMO, consistent with the photophysical data. Interestingly, no significant phosphorus character is displayed until the HOMO-5 (-6.28 eV), with an energy difference of 1.23 eV from the HOMO. This phosphorus containing orbital is much lower in energy than the HOMO which implies that the electron density localised on phosphorus is not involved in the transitions responsible for the observed fluorescence. Furthermore, the large difference in energy between the phosphorus-containing HOMO-5 and the HOMO (localised on the Bodipy core) suggests that reductive-PeT, a mechanism of self-quenching, common for systems with donor atoms, will be disfavoured; thus, the excited state is not quenched. To further investigate this point, DFT calculations were carried out on 4-(2-diphenylphosphinoethylamino)-7-nitro-2,1,3-benzoxadiazole, a weakly fluorescent phosphorus-containing ligand which is known to undergo self-quenching via reductive-PeT.⁴⁹ From these calculations, it was apparent that the phosphorus character was most pronounced in the HOMO-1, with an energy difference of only 0.5 eV from the HOMO. The fact that the electron density on phosphorus is much higher in energy than in the example of **75** supports the idea that the energy of the phosphorus containing orbital is influential on the prevalence of reductive-PeT. For reference, the corresponding orbital energies can be found in Appendix II.

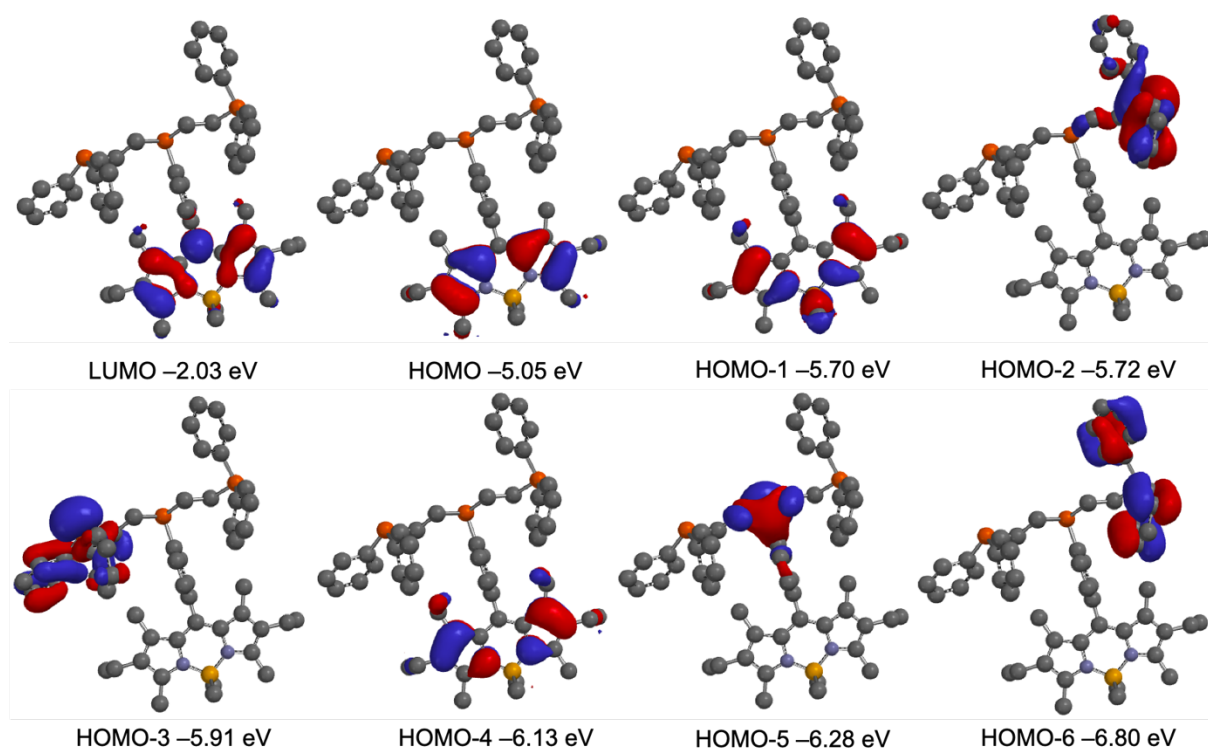


Figure 4.15 Calculated molecular orbital surfaces from the LUMO to HOMO-6 of BodP₃ **75**.

DFT calculations were also carried out for the group 10 metal complexes **81**, **83**, **84a**, **84b** and **84c**, and Figures illustrating the minimised structures and calculated molecular orbitals of **81**, **83** and **84a** are shown in Figures 4.16, 4.17 and 1.18 respectively, and those of **84b** and **84c**, in Appendix II Section 6.6.

The DFT calculations of the complexes display a metal and phosphorus-based LUMO, the values increasing from **81** (-4.82 eV) to **83** (-4.76 eV) to **84a** (-4.19 eV) as we go down group 10. In contrast, as the halogen ligand is changed in the platinum series, a decrease in the energy of the LUMO is observed from **84a** (-4.19 eV) to **84b** (-4.21 eV) to **84c** (-4.32 eV). The HOMO of the complexes and unbound ligand **75** (-5.05 eV) is spatially very similar, therefore, binding to metals resulted in minimal change. The HOMO energies of **81** (-6.77 eV), **83** (-6.77 eV), **84a** (-6.76 eV), **84b** (-6.76 eV) and **84c** (-6.77 eV) are near identical, irrespective of the metal and the halogen ligand and therefore, the reduction in energy of the HOMO exhibited on coordination is likely a result of the formation of a complex and the change in charge associated with this. Similar to the free ligand, the HOMOs down to the HOMO-3 or -4 of **81**, **83**, **84a**, **84b** and **84c** display no phosphorus incorporation and are solely on the Bodipy core. The photophysical data obtained for these complexes displayed a reduction in quantum yield (for **81**, **83** and **84a**) from the free ligand, however, the fluorescence was not fully quenched. Binding to a metal would further reduce the ability for reductive-PeT to occur, and thus, it

would not be expected for coordination to metal complexes to quench the fluorescence via this mechanism. An alternative, well known quenching mechanism, is the heavy atom effect which could perhaps account for the reduction in quantum yield in the series **81**, **83** and **84a**. The addition of heavy atoms in a compound promotes intersystem crossing, thus, resulting in a reduction of fluorescence. However, we see an increase in the quantum yield from **84a** to **84c** which cannot be explained.

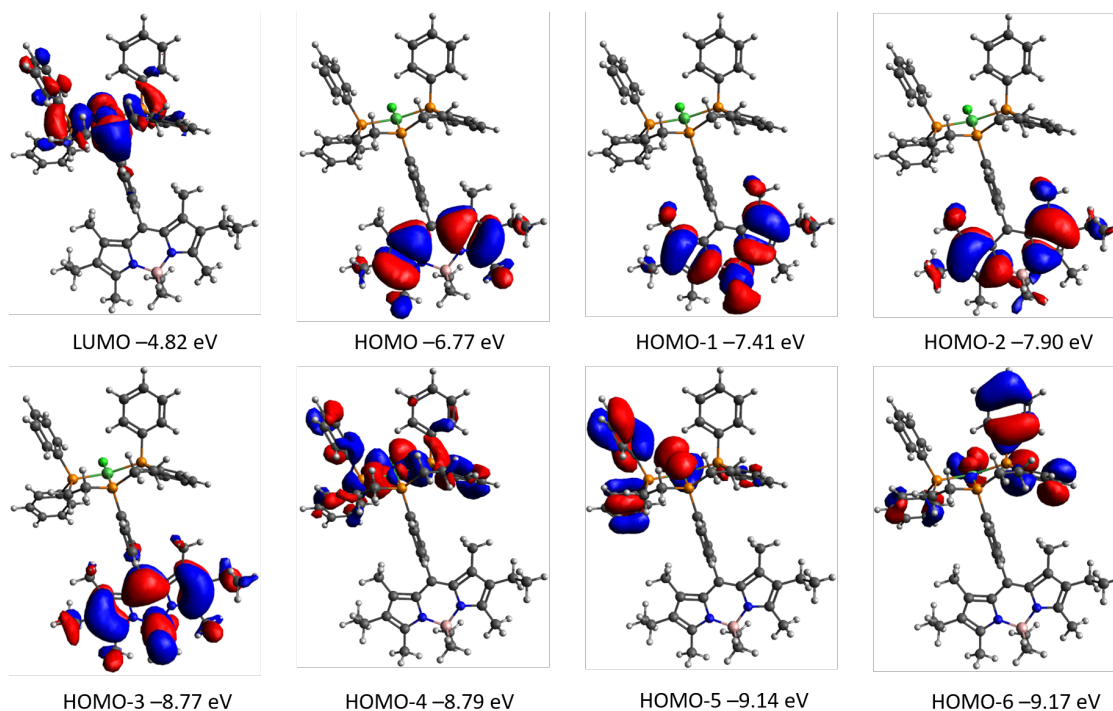


Figure 4.16 Calculated molecular orbital surfaces from the LUMO to HOMO-6 of the [Ni(**75**)Cl]Cl complex, **81**.

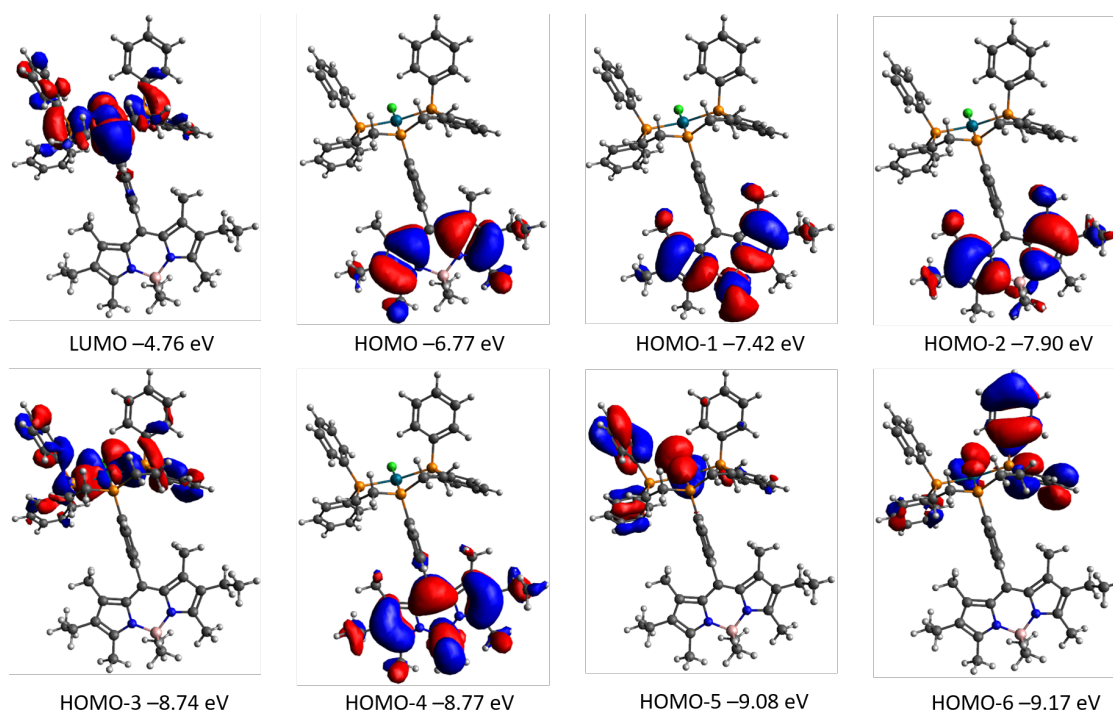


Figure 4.17 Calculated molecular orbital surfaces from the LUMO to HOMO-6 of the [Pd(**75**)Cl]Cl complex, **83**.

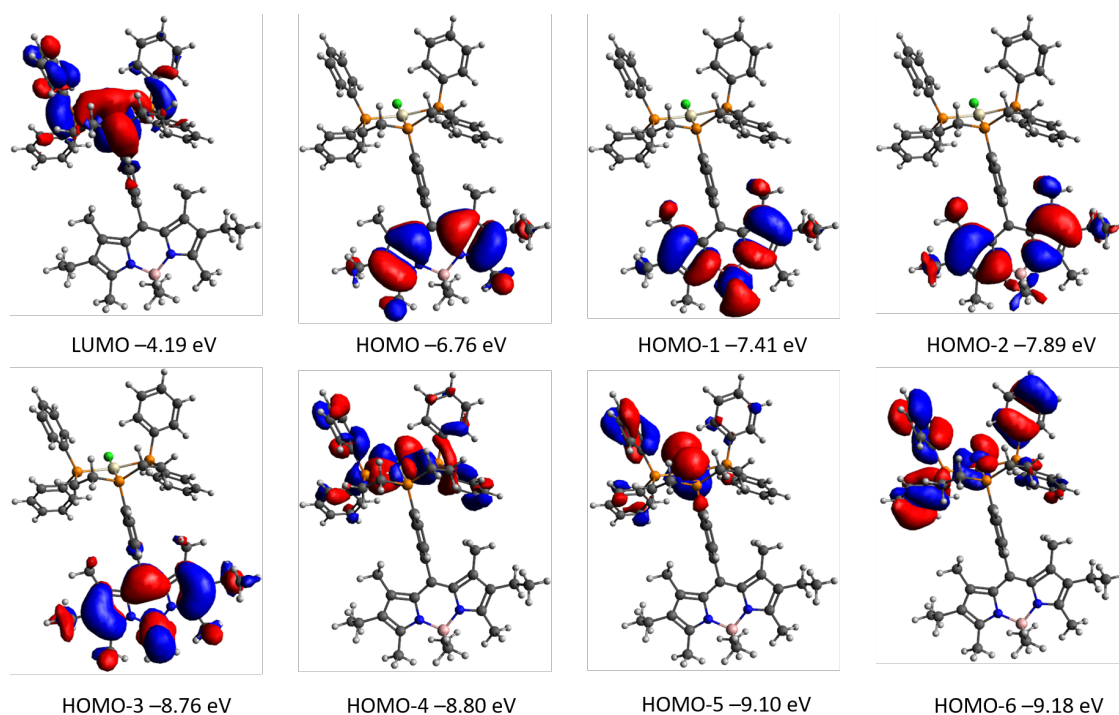


Figure 4.18 Calculated molecular orbital surfaces from the LUMO to HOMO-6 of the [Pt(**75**)Cl]Cl complex, **84a**.

4.5 Summary and Future Work

The Bodipy tridentate phosphine, BodP₃ **75** was synthesised via a double hydrophosphination reaction with two equivalents of vinyl diphenyl phosphine and [Pt(η^2 -norbornene)₃] as previously reported by the group. The tridentate phosphine **75** coordinates to the group 10 metals to form square planar complexes **81**, **83** and **84a**. Crystal structures of **81**, **83** and **84a** were obtained by coworker, Laura Davies, and the bond angles and lengths were comparable to analogous triphos-Ph complexes.

84a was previously tested in a collaboration with the research group of Professor Sofia I. Pascu in HeLa and PC-3 cells and showed uptake and localisation within the endoplasmic reticulum as confirmed through co-localisation with an ER tracker dye.

As square planar platinum(II) complexes are of significant importance in medicine, two additional novel platinum(II) complexes were synthesised from tridentate phosphine **75** and [Pt(η^2 : η^2 -cod)Br₂] and [Pt(η^2 : η^2 -cod)I₂] to afford **84b** and **84c** respectively. By substituting the chloride ligand and counter-ion for bromide or iodide, this generated a novel series of fluorescent platinum(II) complexes which warrant further studies to determine their bioactive properties via cell testing and *in vitro* studies. The lability of the halide and subsequent generation of a vacant coordination site for DNA binding is important to study. By having two series of probes, **81**, **83** and **84a** and **84a**, **84b** and **84c**, it will allow for the assessment of the cellular behaviour of changing both the metal and the halide ligand.

All compounds exhibited remarkable photophysical properties with high molar extinction coefficients of 49,000-85,000 M⁻¹ cm⁻¹ and the coordination to group 10 metals did not significantly quench their fluorescence; all complexes displayed quantum yields of >18% with the exception of [Ni(**75**)Cl]Cl **81** (Φ_F = 0.09).

In collaboration with Professor Sofia I. Pascu at The University of Bath, samples of the bromo and iodo analogues, **84b** and **84c** could be tested *in vitro* to determine their cell uptake and bioactivities. The studies could be compared to **84a** to assess how their cellular behaviour alters by changing the halide ligand.

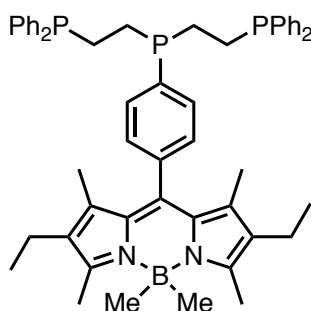
4.6 Experimental Procedures and Analytical Data

4.6.1 General Procedure

All air- and/or water-sensitive reactions were performed under a nitrogen atmosphere using standard Schlenk line techniques. Toluene was dried over sodium, dichloromethane over calcium hydride, and *d*-chloroform over phosphorus pentoxide; all solvents were distilled prior to use. [Pt(η^2 -norbornene)₃],⁵⁰ [Pt(η^2 : η^2 -cod)Cl₂],⁵¹ [Pt(η^2 : η^2 -cod)Br₂]⁴⁷ and [Pt(η^2 : η^2 -cod)I₂]⁴⁷ were prepared according to literature procedures. All other chemicals were purchased from Sigma Aldrich, Fisher Scientific, Alfa Aesar or Fluorochem and used as received. Flash chromatography was performed on silica gel from Fluorochem (silica gel, 40-63 μ , 60 Å). Thin-layer chromatography was performed on Fisher aluminium-based plates with silica gel and fluorescent indicator (254 nm). ¹H, ¹³C{¹H}, ³¹P{¹H}, and ¹¹B{¹H} NMR spectra were recorded on a Bruker Avance III 300 MHz (¹H 300.13 Hz), Bruker Avance II 400 MHz (¹H 399.78 MHz) or Bruker Avance III HD 500 MHz (¹H 500.16 MHz) spectrometer at room temperature (21 °C) using the indicated solvent as internal reference; ¹H and ¹³C shifts were relative to tetramethylsilane, ³¹P to 80% H₃PO₄, and ¹¹B to BF₃·Et₂O. IR spectra were recorded on a Varian 800 FT-IR spectrometer and mass spectrometry was carried out by the EPSRC National Mass Spectrometry Service Centre, Swansea or the SAgE Mass Spectrometry Facility (Newcastle University) performed by Dr Rachael Dack or Dr Alex Charlton. The X-ray crystallographic data were collected on an Xcalibur, Atlas, Gemini ultra diffractometer equipped with a fine-focus sealed X-ray tube ($\lambda_{\text{CuK}\alpha}$ = 1.54184 Å) and an Oxford Cryosystems CryostreamPlus open-flow N₂ cooling device. The analysis of the X-ray diffraction data of the compounds was performed by Dr Paul Waddell. DFT calculations of **75** were carried out on Spartan 14 using the B3LYP functional with a 6-31G* basis set.⁵² All other calculations were carried out using Gaussian 6 software⁵³ by Dr Magda Pascual Borrás, and the molecular orbital surfaces were visualised

using Avogadro.^{54,55} Full geometry optimisations of the studied compounds were performed using density functional theory with a B3LYP function with a 6-31G* basis set for **75** and B3LYP function with 6-31G* basis set with the LANL2DZ effective core basis set for **81**, **83**, **84a**, **84b** and **84c**. A vibrational analysis was performed at the same level to characterise calculated structures as minima.

4.6.2 8-(4-(Bis-2-ethyldiphenylphosphino)-phenylphosphino)-4,4-dimethyl-1,3,5,7-tetramethyl-2,6-diethyl-4-bora-3a,4a-diaza-s-indacene (**75**)



To a stirred solution of 8-((4-phosphino)phenyl)-4,4-dimethyl-1,3,5,7-tetramethyl-2,6-diethyl-4-bora-3a,4a-diaza-s-indacene (**14**) (0.150 g, 0.37 mmol) in anhydrous toluene (10 mL), [Pt(η^2 -norbornene)₃] (0.018 g, 0.04 mmol) was added, followed by vinylidiphenylphosphine (0.16 mL, 0.78 mmol). The reaction mixture was heated to reflux and stirred for five days until consumption of the starting material was confirmed by ³¹P{¹H} NMR spectroscopy. Solvent was removed *in vacuo* and purification was carried out by column chromatography on silica gel (petrol/dichloromethane 1:1) (0.163 g, 53%). ¹H NMR (300 MHz, CDCl₃) δ 7.46–7.36 (m, 2H), 7.35–7.28 (m, 22H), 2.45 (s, 6H), 2.27 (q, ³J_{HH} = 7.5 Hz, 4H), 2.02–1.75 (m, 8H), 1.16 (s, 6H), 0.96 (t, ³J_{HH} = 7.5 Hz, 6H), 0.28 (s, 6H) ppm; ¹³C{¹H} NMR (75 MHz, CDCl₃) δ 150.9, 139.9, 139.2–137.4 (overlapping signals), 133.7–132.9 (overlapping signals), 132.9–132.6 (overlapping signals), 24.3–22.5 (overlapping signals), 17.6, 14.8, 14.5, 12.0, 10.4 (br) ppm; ³¹P{¹H} NMR (121 MHz, CDCl₃) δ –12.9 (d, ³J_{PP} = 27.9 Hz, 2P) –16.9 (t, ³J_{PP} = 27.9 Hz, 1P) ppm; IR (neat): $\tilde{\nu}$ = 3054 (w), 2960 (w), 2928 (w), 1549 (s), 1471 (m), 1433 (m), 1404 (m), 1360 (m), 1319 (s), 1263 (w), 1172 (s), 1146 (s), 1112 (m), 1066 (w), 981 (m), 945 (s), 907 (s), 800 (m), 729 (s), 695 (s), 646 (w), 530 (w) cm⁻¹; HRMS (AP⁺) calcd for C₅₃H₆₁B₁N₂P₃ [M+H]⁺ requires *m/z* 828.4171, found *m/z* 828.4166 (0.7 ppm). These spectroscopic data are in agreement with literature.²⁰

4.6.3 [Ni(75)Cl]Cl (**81**)

8-(4-(bis-2-ethyldiphenylphosphino)-phenylphosphino)-4,4-dimethyl-1,3,5,7-tetramethyl-2,6-diethyl-4-bora-3a,4a-diaza-s-indacene (0.100 g, 0.121 mmol) and NiCl₂·6H₂O (0.029 g, 0.121 mmol) were dissolved in ethanol (9 mL) and stirred at reflux for 3 hours. After removal of the solvent *in vacuo* a bright orange solid was produced (0.110 g, 95%). A sample suitable for X-ray crystallographic analysis was obtained from ethanol/pentane. **¹H NMR** (400 MHz, CDCl₃) δ 8.53 (m, 1H), 7.79 (m, 3H), 7.57–7.32 (m, 20H), 3.67 (m, 2H), 3.10–2.90 (br, 4H), 2.39 (s, 6H), 2.20 (q, ³J_{HH} = 7.8 Hz, 4H), 2.00 (br, 2H), 0.99 (s, 6H), 0.92 (t, ³J_{HH} = 7.8 Hz, 6H), 0.21 (s, 6H) ppm; **¹³C{¹H} NMR** (100 MHz, CDCl₃) δ 151.3, 142.7, 137.5, 134.7 (d, J_{CP} = 10.5 Hz), 133.8 (pseudo t, J_{CP} = 5.3 Hz), 132.8, 132.5 (m), 131.8 (d, J_{CP} = 7.7 Hz), 130.3 (d, J_{CP} = 10.5 Hz), 129.2 (pseudo dt, J_{CP} = 28.8 Hz, J_{CP} = 4.8 Hz), 128.2, 127.8 (pseudo dt, J_{CP} = 132.3 Hz, J_{CP} = 20.0 Hz), 126.6 (d, J_{CP} = 45.1 Hz), 28.7 (m), 17.2, 14.5, 14.2, 11.8, 10.2 ppm; **³¹P{¹H} NMR** (162 MHz, CDCl₃) δ 112.1 (t, ²J_{PP} = 47.1 Hz, 1P), 48.9 (d, ²J_{PP} = 47.1 Hz, 2P) ppm; **¹¹B{¹H} NMR** (128 MHz, CDCl₃) δ -0.9 ppm; **IR** (neat): $\tilde{\nu}$ = 2965 (w), 2928 (w), 2871 (w), 1551 (s), 1435 (m), 1404 (w), 1361 (w), 1320 (s), 1264 (w), 1173 (s), 1145 (s), 1103 (m), 1028 (w), 982 (m), 945 (s), 910 (w), 800 (s), 746 (m), 689 (s) cm⁻¹; **HRMS** (ESI⁺) calcd for C₅₃H₆₀B₁Cl₁N₂P₃Ni₁ [M]⁺ requires m/z 920.3141 found m/z 920.3130 (1.2 ppm).

4.6.4 [Pd(75)Cl]Cl (**83**)

8-(4-(bis-2-ethyldiphenylphosphino)-phenylphosphino)-4,4-dimethyl-1,3,5,7-tetramethyl-2,6-diethyl-4-bora-3a,4a-diaza-s-indacene (0.050 g, 0.060 mmol) was dissolved in anhydrous dichloromethane (2 mL) and added to a stirred solution of [PdCl₂(MeCN)₂] (0.016 g, 0.060 mmol) in anhydrous dichloromethane (2 mL); the mixture was stirred at room temperature for two hours. After removal of the solvent *in vacuo* an orange solid was produced (0.058 g, 96%). A sample suitable for X-ray crystallographic analysis was obtained from ethanol/pentane. **¹H NMR** (500 MHz, CDCl₃) δ 8.43 (dd, ³J_{HP} = 12.3 Hz, ³J_{HH} = 8.0 Hz, 2H), 7.83 (pseudo q, ³J_{HH} = 6.3 Hz, 4H), 7.68 (pseudo q, ³J_{HH} = 6.3 Hz, 4H), 7.57–7.42 (m, 14H), 4.15 (m, 2H), 3.24 (d, ³J_{HP} = 13.5 Hz, 1H), 3.12 (d, ³J_{HP} = 14.0 Hz, 1H), 2.89 (m, 2H), 2.42 (s, 6H), 2.26 (q, ³J_{HH} = 7.6 Hz, 4H), 2.25 (m, 2H), 1.01 (s, 6H), 0.95 (t, ³J_{HH} = 7.6 Hz, 6H), 0.26 (s, 6H) ppm; **¹³C{¹H} NMR** (126 MHz, CDCl₃) δ 151.6, 143.5, 137.5, 134.8 (d, J_{CP} = 11.6 Hz), 133.4 (pseudo t, J_{CP} = 6.7 Hz), 133.1, 132.8–132.4 (br m), 130.8 (d, J_{CP} = 11.6 Hz), 129.7 (dt, J_{CP} = 24.1 Hz, J_{CP} = 4.8 Hz), 128.5, 128.4 (d, J_{CP} = 49.1 Hz), 128.3, 127.1 (pseudo t, J_{CP} = 24.1 Hz), 125.3 (d, J_{CP} = 51.9 Hz), 30.3 (dt, J_{CP} = 33.6 Hz, J_{CP} = 5.8 Hz), 28.6 (m), 17.5, 14.9, 14.4, 11.8, 10.4 ppm; **³¹P{¹H} NMR** (202 MHz, CDCl₃) δ 112.4 (t, ²J_{PP} = 9.9 Hz, 1P), 46.8 (d, ²J_{PP} = 9.9 Hz, 2P) ppm; **¹¹B{¹H} NMR** (160

MHz, CDCl₃) δ -0.9 ppm; **IR** (neat): $\tilde{\nu}$ = 2960 (w), 2924 (w), 1556 (m), 1430 (m), 1363 (w), 1321 (m), 1265 (m), 1171 (s), 1143 (m), 1107 (s), 1021 (m), 980 (m), 945 (m), 802 (s), 685 (s) cm⁻¹; **HRMS** (ESI⁺) calcd for C₅₃H₆₀B₁Cl₁N₂P₃Pd₁ [M]⁺ requires *m/z* 964.2838 found *m/z* 964.2813 (2.6 ppm).

4.6.5 [PtCl₂(η^2 : η^2 -cod)]

¹H NMR (300 MHz, DMSO-*d*₆) 5.50 (m with ¹⁹⁵Pt satellites, ²*J*_{HPt} = 68.2 Hz, 4H), 2.60 (m, 4H), 2.38–2.09 (m, 4H) ppm; **¹³C{¹H} NMR** (75 MHz, DMSO) δ 101.3 (s, with ¹⁹⁵Pt satellites, ¹*J*_{CPt} = 152.2 Hz), 30.4 ppm; **IR** (neat): $\tilde{\nu}$ = 3008 (w), 2943 (w), 1476 (m), 1450 (w), 1423 (w), 1339 (s), 1311 (w), 1226 (w), 1179 (m), 1087 (w), 1008 (s), 911 (w), 872 (m), 832 (s), 810 (m), 780 (m), 695 (m), 582 (m) cm⁻¹. These spectroscopic data are in agreement with literature.⁴⁷

4.6.6 [PtBr₂(η^2 : η^2 -cod)]

¹H NMR (300 MHz, DMSO-*d*₆) 5.63 (m with ¹⁹⁵Pt satellites, ²*J*_{HPt} = 67.8 Hz, 4H), 2.54 (m, 4H), 2.29–1.99 (m, 4H) ppm; **¹³C{¹H} NMR** (75 MHz, DMSO) δ 102.3 (s, with ¹⁹⁵Pt satellites, ¹*J*_{CPt} = 140.2 Hz), 30.7 ppm; **IR** (neat): $\tilde{\nu}$ = 3004 (w), 1474 (m), 1449 (w), 1425 (w), 1340 (s), 1309 (w), 1178 (m), 1006 (s), 908 (w), 869 (s), 829 (s), 808 (m), 779 (m), 694 (m), 577 (m) cm⁻¹. These spectroscopic data are in agreement with literature.⁴⁷

4.6.7 [PtI₂(η^2 : η^2 -cod)]

¹H NMR (300 MHz, DMSO-*d*₆) 5.59 (m with ¹⁹⁵Pt satellites, ²*J*_{HPt} = 67.3 Hz, 4H), 2.45–2.27 (m, 4H), 2.10–1.80 (m, 4H) ppm; **¹³C{¹H} NMR** (75 MHz, DMSO) δ 104.2 (s, with ¹⁹⁵Pt satellites, ¹*J*_{CPt} = 122.8 Hz), 31.2 ppm; **IR** (neat): $\tilde{\nu}$ = 2932 (w), 2878 (w), 1500 (m), 1477 (w), 1423 (s), 1376 (w), 1339 (s), 1309 (s), 1227 (m), 1176 (s), 1088 (m), 1070 (m), 1039 (m), 998 (s), 903 (w), 869 (s), 823 (s), 799 (s), 776 (s), 694 (w), 567 (w) cm⁻¹. These spectroscopic data are in agreement with literature.⁴⁷

4.6.8 General Procedure for the Synthesis of Platinum Complexes (**84a-c**)

8-(4-(Bis-2-ethyldiphenylphosphino)-phenylphosphine)-4,4-dimethyl-1,3,5,7-tetramethyl-2,6-diethyl-4-bora-3a,4a-diaza-*s*-indacene (**75**) (0.050 g, 0.06 mmol) was dissolved in anhydrous dichloromethane and added to a stirred solution of appropriate Pt(II) complex (0.06 mmol) and stirred for one hour by which time ³¹P{¹H} NMR spectroscopy showed complete consumption of the starting material. The solvent was removed and the solid was washed with hexane (3 x 5 mL) to remove 1,5-cyclooctadiene and dried *in vacuo*.

4.6.9 [Pt(75)Cl]Cl (**84a**)

(0.060 g, 92% Yield); $^1\text{H NMR}$ (400 MHz, CDCl_3) δ 8.44 (dd, $^3J_{\text{HP}} = 12.2$ Hz, $^3J_{\text{HH}} = 7.7$ Hz, 2H), 7.80 (m, 4H), 7.71 (m, 4H), 7.62–7.30 (m, 14H), 4.38–3.74 (m, 2H), 3.29 (d, $^3J_{\text{HP}} = 13.9$ Hz, 1H), 3.13 (d, $^3J_{\text{HP}} = 15.7$ Hz, 1H), 2.88–2.62 (m, 2H), 2.44 (s, 6H), 2.27 (q, $^3J_{\text{HH}} = 7.5$ Hz, 4H), 2.19–2.05 (m, 2H), 1.02 (s, 6H), 0.95 (t, $^3J_{\text{HH}} = 7.5$ Hz, 6H), 0.26 (s, 6H) ppm; $^{13}\text{C}\{^1\text{H}\}$ NMR (75 MHz, CDCl_3) δ 151.6, 133.6–133.1 (overlapping signals), 133.3–132.8 (overlapping signals), 132.7–132.3 (overlapping signals), 130.3–129.2 (overlapping signals), 28.1, 22.8, 17.6, 14.8, 14.5, 11.8, 10.6 (br) ppm; $^{31}\text{P}\{^1\text{H}\}$ NMR (121 MHz, CDCl_3) δ 86.3 (s, with satellite peaks $J_{\text{PPt}} = 3010.2$ Hz), 41.8 (s, with satellite peaks $J_{\text{PPt}} = 2485.2$ Hz) ppm; $^{11}\text{B}\{^1\text{H}\}$ NMR (160 MHz, CDCl_3) δ –0.83 ppm; IR (neat): $\tilde{\nu} = 2962$ (w), 2925 (w), 1553 (m), 1436 (m), 1404 (w), 1361 (w), 1321 (m), 1173 (s), 1146 (m), 1102 (s), 1021 (s), 982 (m), 946 (m), 801 (s), 691 (s), 516 (m) cm^{-1} ; HRMS (ESI⁺) calcd for $\text{C}_{53}\text{H}_{61}\text{BClN}_2\text{P}_3\text{Pt}$ $[\text{M}+\text{H}]^+$ requires m/z 1059.3412 found m/z 1059.3396.

4.6.10 [Pt(75)Br]Br (**84b**)

(0.063 g, 89% Yield); $^1\text{H NMR}$ (400 MHz, CDCl_3) δ 8.37 (dd, $^3J_{\text{HP}} = 12.2$ Hz, $^3J_{\text{HH}} = 7.7$ Hz, 2H), 7.82–7.73 (m, 4H), 7.74–7.62 (m, 4H), 7.58–7.46 (m, 14H), 7.46–7.37 (m, 2H), 4.19–3.79 (m, 2H), 3.30 (d, $^3J_{\text{HP}} = 17.1$ Hz, 1H), 3.17 (d, $^3J_{\text{HP}} = 17.5$ Hz, 1H), 2.93–2.76 (m, 2H), 2.44 (s, 6H), 2.28 (q, $^3J_{\text{HH}} = 7.6$ Hz, 4H), 2.20–2.04 (m, 2H), 1.01 (s, 6H), 0.97 (t, $^3J_{\text{HH}} = 7.5$ Hz, 6H), 0.26 (s, 6H) ppm; $^{13}\text{C}\{^1\text{H}\}$ NMR (75 MHz, CDCl_3) δ 151.6, 133.8–133.4 (overlapping signals), 133.3–133.0 (overlapping signals), 132.7–132.4 (overlapping signals), 129.8–129.3 (overlapping signals), 28.2, 21.3, 17.6, 14.8, 14.5, 11.8, 10.5 ppm; $^{31}\text{P}\{^1\text{H}\}$ NMR (121 MHz, CDCl_3) δ 89.2 (s, with satellite peaks $J_{\text{PPt}} = 2996.4$ Hz), 42.2 (s, with satellite peaks $J_{\text{PPt}} = 2458.2$ Hz) ppm; $^{11}\text{B}\{^1\text{H}\}$ NMR (160 MHz, CDCl_3) δ 0.59 ppm; IR (neat): $\tilde{\nu} = 2962$ (w), 2927 (w), 1551 (m), 1435 (m), 1320 (m), 1261 (m), 1173 (s), 1102 (s), 1019 (s), 908 (m), 799 (s), 726 (s), 689 (s), 616 (w), 515 (s), 483 (m) cm^{-1} . HRMS (ESI⁺) calcd for $\text{C}_{53}\text{H}_{60}\text{B}_1\text{Br}_1\text{N}_2\text{P}_3\text{Pt}_1$ $[\text{M}]^+$ requires m/z 1102.2894 found m/z 1102.1536.

4.6.11 [Pt(75)I]I (**84c**)

(0.069 g, 90% Yield); $^1\text{H NMR}$ (300 MHz, CDCl_3) δ 8.27 (dd, $^3J_{\text{HP}} = 12.1$ Hz, $^3J_{\text{HH}} = 7.8$ Hz, 2H), 7.75 (m, 4H), 7.66 (m, 4H), 7.60–7.32 (m, 14H), 3.88–3.59 (m, 2H), 3.40 (d, $^3J_{\text{HP}} = 17.5$ Hz, 1H), 3.27 (d, $^3J_{\text{HP}} = 17.5$ Hz, 1H), 2.97 (m, 2H), 2.45 (s, 6H), 2.28 (q, $^3J_{\text{HH}} = 7.7$ Hz, 4H), 2.12–1.95 (m, 2H), 1.00 (s, 6H), 0.96 (t, $^3J_{\text{HH}} = 7.5$ Hz, 6H), 0.27 (s, 6H) ppm; $^{13}\text{C}\{^1\text{H}\}$ NMR (75 MHz, CDCl_3) δ 151.7, 133.9–133.6 (overlapping peaks), 133.6–133.3 (overlapping peaks), 133.2, 132.8, 132.6–132.4 (overlapping peaks), 31.7, 22.8, 17.6, 14.8, 14.5, 11.8, 10.4 (br) ppm; $^{31}\text{P}\{^1\text{H}\}$ NMR

(121 MHz, CDCl₃) δ 92.7 (s, with satellite peaks $J_{\text{PPt}} = 2900.4$ Hz), 42.4 (s, with satellite peaks $J_{\text{PPt}} = 2416.1$ Hz) ppm; **¹¹B{¹H} NMR** (160 MHz, CDCl₃) δ -0.82 ppm; **IR** (neat): $\tilde{\nu} = 3053$ (w), 2960 (w), 2928 (w), 1552 (s), 1471 (w), 1435 (s), 1387 (w), 1321 (s), 1173 (s), 1146 (m), 1111 (m), 1026 (w), 946 (m), 910 (w), 801 (m), 691 (m), 516 (m) cm⁻¹; **HRMS** (ESI⁺) calcd for C₅₃H₆₀B₁I₁N₂P₃Pt₁ [M]⁺ requires m/z 1150.2755 found m/z 1150.1360.

4.7 References

- 1 D. Shaloam and P. B. Tchounwou, *Eur. J. Pharmacol.*, 2014, **740**, 364–378.
- 2 T. Makovec, *Radiol. Oncol.*, 2019, **53**, 148–158.
- 3 T. Kanagasundaram, C. S. Kramer, E. Boros and K. Kopka, *Dalton Trans.*, 2020, **49**, 7294–7298.
- 4 L. H. Davies, B. B. Kasten, P. D. Benny, R. L. Arrowsmith, H. Ge, S. I. Pascu, S. W. Botchway, W. Clegg, R. W. Harrington and L. J. Higham, *Chem. Commun.*, 2014, **50**, 15503–15505.
- 5 C. Bianchini, A. Meli, M. Peruzzini, F. Vizza, P. Frediani and J. A. Ramirez, *Organometallics*, 1990, **9**, 226–240.
- 6 K. Murugesan, Z. Wei, V. G. Chandrashekhar, H. Jiao, M. Beller and R. V. Jagadeesh, *Chem. Sci.*, 2020, **11**, 4332–4339.
- 7 C. J. Smith, N. Li, K. V Katti, C. Higginbotham and W. A. Volkert, *Nucl. Med. Biol.*, 1997, **24**, 685–691.
- 8 G. J. Kontoghiorghes, *Int. J. Mol. Sci.*, 2020, **21**, 1–8.
- 9 S. J. S. Flora and V. Pachauri, *Int. J. Environ. Res. Public Health*, 2010, **7**, 2745–2788.
- 10 F. Silva, C. Fernandes, M. P. C. Campello and A. Paulo, *Polyhedron*, 2017, **125**, 186–205.
- 11 C. J. Jones and J. R. Thornback, in *Medicinal Applications of Coordination Chemistry*, Royal Society of Chemistry, Cambridge, 2007, pp. 101–200.
- 12 D. Schühle and P. Caravan, in *Comprehensive Inorganic Chemistry II*, eds. J. Reedijk and K. Poeppelemeier, Elsevier Ltd, 2013, pp. 901–932.
- 13 C. J. Jones and J. R. Thornback, in *Medicinal Applications of Coordination Chemistry*, 2007, pp. 324–339.
- 14 R. Alberto and H. Braband, in *Comprehensive Inorganic Chemistry II*, eds. J. Reedijk and K. Poeppelemeier, Elsevier Ltd, 2013, pp. 785–817.
- 15 J. R. Dilworth and S. I. Pascu, in *The Chemistry of Molecular Imaging*, eds. N. J. Long and W. Wing-Tak, John Wiley & Sons, Inc, Hoboken, NJ, 2014, pp. 165–178.
- 16 W. A. Gibby, K. A. Gibby and W. A. Gibby, *Invest. Radiol.*, 2004, **39**, 138–142.
- 17 Y. D. Xiao, R. Paudel, J. Liu, C. Ma, Z. S. Zhang and S. K. Zhou, *Int. J. Mol. Med.*, 2016, **38**, 1319–1326.
- 18 M. Brandt, J. Cardinale, M. L. Aulsebrook, G. Gasser and T. L. Mindt, *J. Nucl. Med.*, 2018,

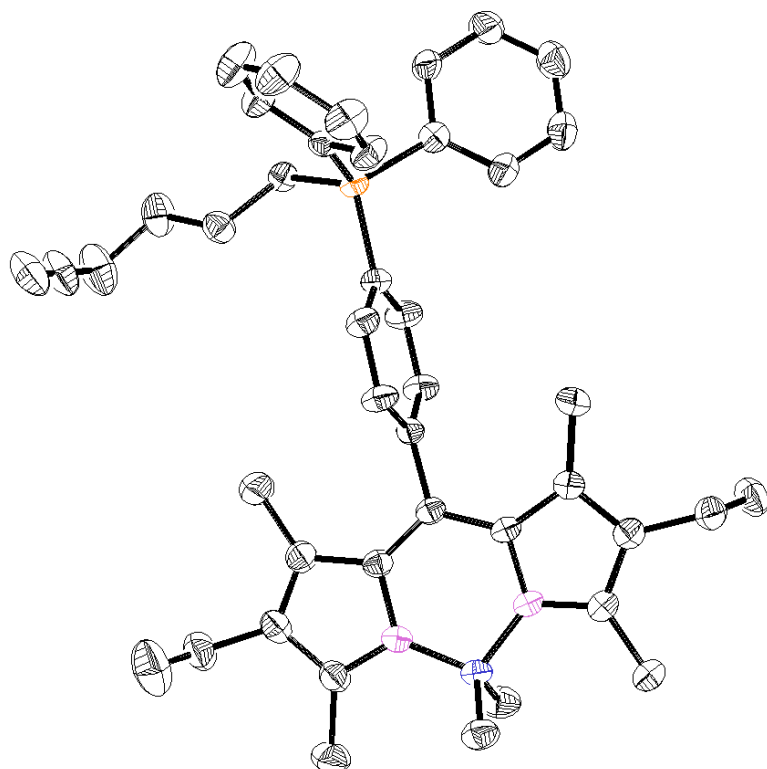
59, 1500–1506.

- 19 J. D. Kelly, A. M. Forster, B. Higley, C. M. Archer, F. S. Booker, L. R. Canning, K. Wai Chiu, B. Edwards, H. K. Gill, M. McPartlin, K. R. Nagle, I. A. Latham, R. D. Pickett, A. E. Storey and P. M. Webbon, *J. Nucl. Med.*, 1993, **34**, 222–227.
- 20 L. H. Davies, B. Stewart, R. W. Harrington, W. Clegg and L. J. Higham, *Angew. Chemie Int. Ed.*, 2012, **51**, 4921–4924.
- 21 J. R. Lakowicz, *Principles of Fluorescence Spectroscopy*, Springer, 3rd edn., 2006.
- 22 A. J. West, in *Chemistry of the Elements*, Elsevier, 1997, vol. 105, pp. 1040–1069.
- 23 A. Alwaaly, W. Clegg, R. W. Harrington, A. L. Petrou and R. A. Henderson, *Dalton Trans.*, 2015, **44**, 11977–11983.
- 24 G.-I. Bertinsson, *Acta Crystallogr. Sect. C*, 1983, **39**, 563–567.
- 25 S. Prince, S. Mapolie and A. Blanckenberg, in *Encyclopedia of Cancer*, ed. M. Schwab, Springer Berlin Heidelberg, Berlin, Heidelberg, 2014, pp. 1–9.
- 26 J. V. Burda, M. Zeizinger and J. Leszczynski, *J. Chem. Phys.*, 2004, **120**, 1253–1262.
- 27 N. K. Sharma, R. K. Ameta and M. Singh, *Int. J. Med. Chem.*, 2016, 1–10.
- 28 O. Tokgun, D. E. Karakas, S. Tan, E. R. Karagür, B. İnal, H. Akca, F. Durap, A. Baysal and M. Aydemir, *Chem. Pap.*, 2020, **74**, 2883–2892.
- 29 T. V. Serebryanskaya, M. A. Kinzhalov, V. Bakulev, G. Alekseev, A. Andreeva, P. V. Gushchin, A. V. Protas, A. S. Smirnov, T. L. Panikorovskii, P. Lippmann, I. Ott, C. M. Verbilo, A. V. Zuraev, A. S. Bunev, V. P. Boyarskiy and N. A. Kasyanenko, *New J. Chem.*, 2020, **44**, 5762–5773.
- 30 M. Vojtek, M. P. M. Marques, I. M. P. L. V. O. Ferreira, H. Mota-Filipe and C. Diniz, *Drug Discov. Today*, 2019, **24**, 1044–1058.
- 31 P. Sevillano, A. Habtemariam, S. Parsons, A. Castiñeiras, M. E. García and P. J. Sadler, *J. Chem. Soc., Dalt. Trans.*, 1999, **4**, 2861–2870.
- 32 C. E. Housecroft and B. A. M. Shaykh, *Acta Crystallogr. Sect. C*, 1990, **46**, 1549–1551.
- 33 D. Fernández, P. Sevillano, M. I. García-Seijo, A. Castieiras, L. János, Z. Berente, L. Kollár and M. E. García-Fernández, *Inorg. Chim. Acta*, 2001, **312**, 40–52.
- 34 K. D. Tau, R. Uriarte, T. J. Mazanec and D. W. Meek, 1979, **101**, 6614–6619.
- 35 S. O. Grim, W. L. Briggs, R. C. Barth, C. A. Tolman and J. P. Jesson, *Inorg. Chem.*, 1974, **13**, 1095–1100.

- 36 D. S. Schwarz and M. D. Blower, *Cell. Mol. Life Sci.*, 2016, **73**, 79–94.
- 37 Y. Zhao, H. Li, Z. Chai, W. Shi, X. Li and H. Ma, *Chem. Commun.*, 2020, **56**, 6344–6347.
- 38 A. P. King and J. J. Wilson, *Chem. Soc. Rev.*, , DOI:10.1039/D0CS00259C.
- 39 M. J. Cleare and J. D. Hoeschele, *Bioinorg. Chem.*, 1973, **2**, 187–210.
- 40 S. K. Aggarwal, J. A. Broomhead, D. P. Fairlie and M. W. Whitehouse, *Cancer Chemother. Pharmacol.*, 1980, **4**, 249–258.
- 41 T. Marzo, S. Pillozzi, O. Hrabina, J. Kasparkova, V. Brabec, A. Arcangeli, G. Bartoli, M. Severi, A. Lunghi, F. Totti, C. Gabbiani, A. G. Quiroga and L. Messori, *Dalton Trans.*, 2015, **44**, 14896–14905.
- 42 T. Marzo, G. Bartoli, C. Gabbiani, G. Pescitelli, M. Severi, S. Pillozzi, E. Michelucci, B. Fiorini, A. Arcangeli, A. G. Quiroga and L. Messori, *BioMetals*, 2016, **29**, 535–542.
- 43 T. Marzo, A. Pratesi, D. Cirri, S. Pillozzi, G. Petroni, A. Guerri, A. Arcangeli, L. Messori and C. Gabbiani, *Inorg. Chim. Acta*, 2018, **470**, 318–324.
- 44 J. A. Arnott and S. L. Planey, *Expert Opin. Drug Discov.*, 2012, **7**, 863–875.
- 45 D. Cirri, S. Pillozzi, C. Gabbiani, J. Tricomi, G. Bartoli, M. Stefanini, E. Michelucci, A. Arcangeli, L. Messori and T. Marzo, *Dalton Trans.*, 2017, **46**, 3311–3317.
- 46 P. Štarha, J. Vančo and Z. Trávníček, *Coord. Chem. Rev.*, 2019, **380**, 103–135.
- 47 D. Drew, J. R. Doyle and A. G. Shaver, in *Inorganic Syntheses*, ed. F. A. Cotton, McGraw-Hill, Inc., 2007, vol. 13, pp. 47–55.
- 48 B. Valeur and M. N. Berberan-Santos, *Molecular Fluorescence*, Wiley-VCH Verlag GmbH & Co. KGaA, Weinheim, Germany, 2012.
- 49 M. Onoda, S. Uchiyama, A. Endo, H. Tokuyama, T. Santa and K. Imai, *Org. Lett.*, 2003, **5**, 1459–1461.
- 50 L. E. Craswell, J. L. Spencer, R. A. Doyle and R. J. Angelici, *Inorg. Synth.*, 1990, 126–132.
- 51 D. Drew, J. R. Doyle and A. G. Shaver, *Inorg. Synth.*, 1990, 346–349.
- 52 Wavefunction Inc., 2013, Spartan 14.
- 53 M. J. Frisch, G. W. Trucks, H. B. Schlegel, G. E. Scuseria, M. A. Robb, J. R. Cheeseman, G. Scalma, V. Barone, G. A. Petersson, H. Nakatsuji, X. Li, M. Caricato, A. Marenich, J. Bloino, B. G. Janesko, R. Gomperts, B. Mennucci, H. P. Hratchian, J. V. Ortiz, A. F. Izmaylov, J. L. Sonnenberg, D. Williams-Young, F. Ding, F. Lipparini, F. Egidi, J. Goings, B. Peng, A. Petrone, T. Henderson, D. Ranasinghe, V. G. Zakrzewski, J. Gao, N. Rega, G.

- Zheng, W. Liang, M. Hada, M. Ehara, K. Toyota, R. Fukuda, J. Hasegawa, M. Ishida, T. Nakajima, Y. Honda, O. Kitao, H. Nakai, T. Vreven, K. Throssell, J. A. J. Montgomery, J. E. Peralta, F. Ogliaro, M. Bearpark, J. J. Heyd, E. Brothers, K. N. Kudin, V. N. Staroverov, T. Keith, R. Kobayashi, J. Normand, K. Raghavachari, A. Rendell, J. C. Burant, S. S. Iyengar, J. Tomasi, M. Cossi, J. M. Millam, M. Klene, C. Adamo, R. Cammi, J. W. Ochterski, R. L. Martin, K. Morokuma, O. Farkas, J. B. Foresman and D. J. Fox, 2016, Gaussian, Inc.
- 54 *Avogadro: an open-source molecular builder and visualization tool. Version 1.2.0.*
<http://avogadro.cc/>.
- 55 M. D. Hanwell, D. E. Curtis, D. C. Lonie, T. Vandermeersch, E. Zurek and G. R. Hutchison,
J. Cheminform., 2012, **4**, 17.

Chapter 5



The Development of a Multimodal Mitochondrial Imaging Agent

The importance of targeting the mitochondria and how this can be achieved using lipophilic cations such as phosphonium salts is detailed. Fluorescent phosphonium salts were synthesised and characterised, and we see one of these compounds tested in PDAC cells in collaboration with the University of California, San Diego.

We then introduce the concept of the addition of an ^{18}F radiolabel (through collaboration with Prof. Steve Archibald at the University of Hull) to enable application in Positron Emission Tomography (PET). Our group previously developed fluorescent phosphonium salts with applications in mitochondrial-specific fluorescence imaging with the intention of radiolabelling these to afford a multimodal imaging agent. We follow on from this work and look towards alternative methods of radiolabelling and synthesise two series of alkyne functionalised phosphonium salts to enable further functionalisation by azide-alkyne click chemistry.

5 Towards a Trifunctional Mitochondrial Imaging Agent

This chapter focuses on the synthesis of phosphonium salts with the principal target of developing a trifunctional imaging agent that incorporates i) a fluorescent Bodipy core to facilitate *in vitro* fluorescence imaging, ii) a phosphonium cation to target the mitochondria and iii) an ^{18}F radiolabel for applications in *in vivo* positron emission tomography (PET).

The reader will notice that the initial route of ^{18}F radiolabelling by direct exchange of a halide group did not result in successful radiolabelling. Therefore, this led to the development of alkyne functionalised phosphonium salts.

The addition of an alkyne moiety to a phosphine to generate phosphonium salts expands their potential as reagents for click chemistry, where it will become apparent that they have possible application as i) radiolabelled phosphonium salts for PET imaging and ii) phosphonium biomolecule carriers.

5.1 Mitochondria

Mitochondria are organelles found in every complex organism and are essential in the generation of energy in the form of adenosine triphosphate (ATP) via the oxidative phosphorylation pathway. This vital pathway also results in the formation of reactive oxygen species (ROS) as a side product; an imbalance of these can lead to oxidative stress, a key factor in a number of diseases. Their dysfunction has been widely studied and has been found to be associated with several diseases, such as Alzheimer's,¹ diabetes,² a number of cancers^{3–5} and Parkinson's.⁶

Lipophilic cations have the ability to penetrate the mitochondrial membrane and thus accumulate within the mitochondrial matrix due to its negative membrane potential.⁷ The hyperpolarisation of the mitochondrial membrane potential (MMP) has been reported as a key factor in cardiac failure⁸ and cancer,⁹ and as a result, the accumulation of MMP-dependent compounds was demonstrated to increase by almost tenfold in comparison to their healthy counterparts.^{9,10}

By conjugating a bioactive molecule to the cation, this ability to cross the membrane has been exploited and resulted in the accumulation of the active molecule within the matrix. Thus, this has seen lipophilic cations developed for their application as anticancer agents,¹¹ antioxidants¹² and myocardial imaging agents.⁸

5.1.1 Phosphonium Cations

Neamati *et al.* developed a series of phosphonium salts (Figure 5.1) that have potential as anti-cancer agents against a panel of tumours. This ability seemingly derives from the localisation of the drugs within the mitochondria which resulted in increased superoxide production, and a decreased rate of cellular oxygen consumption. The inhibition of tumour growth was apparent from the arresting of cell cycle progression.¹¹ In 2013, Neamati and co-workers then evaluated the mechanism of TP421 in pancreatic cancer cells, validating that the cytotoxicity could be attributed to its localisation within the mitochondria.¹³

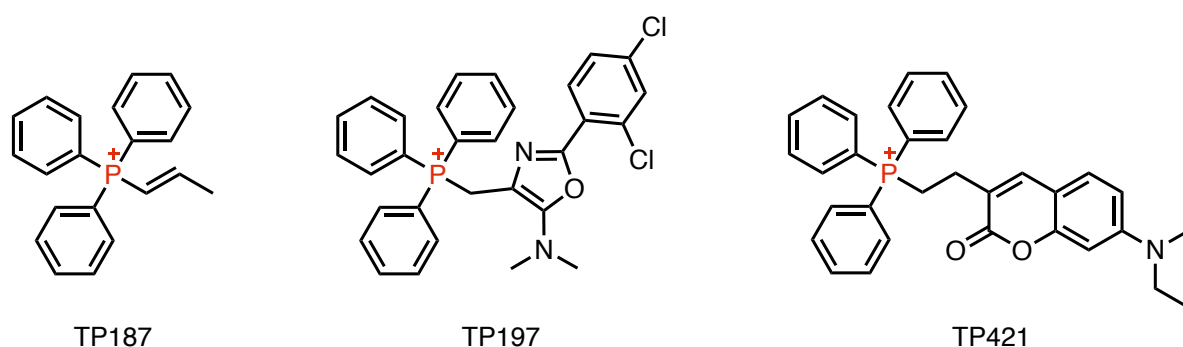


Figure 5.1 A series of triphenylphosphonium salts with anti-cancer activity developed by Neamati *et al.*

Murphy *et al.* prepared a series of mitochondria-targeted antioxidants based on triphenylphosphonium-labelled, vitamin E derivatives with a range of linker lengths, to facilitate variation in the lipophilicity of the compounds (Figure 5.2). This change in lipophilicity was utilised to assess the effect of lipophilicity on the bioactivity of the compounds. When the compounds were tested in rat brain homogenates, it was found that the change in lipophilicity did not significantly alter their bioactivity and that their differences could instead be assigned to variations in their uptake ability. The efficiency of these compounds as antioxidants far outweighed that of Trolox, a commercially available water-soluble analogue of Vitamin E (Figure 5.2), validating the importance of the triphenylphosphonium moiety.¹²

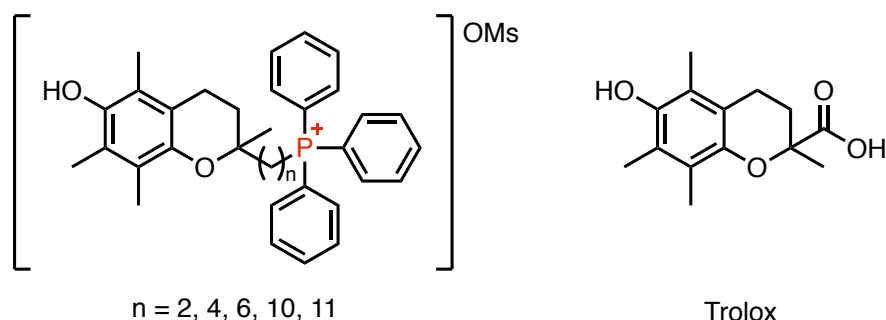


Figure 5.2 A series of triphenylphosphonium-labelled vitamin E derivatives, with a range of linker lengths, as mitochondria-targeted antioxidants.

The MMP is higher for cardiomyocytes than for normal epithelial cells.¹⁴ In addition to this, the loss of MMP is an early sign for cell death in myocardial ischemia and thus, phosphonium salts have been exploited in myocardial imaging. The incorporation of an ^{18}F radiolabel to triphenylphosphonium salts enables imaging via PET scans, resulting in dual-functional imaging agents for myocardial imaging. Three examples given in Figure 5.3 have all shown applications in myocardial imaging; ^{18}F -BnTP has shown additional potential as a myocardial perfusion agent.⁸

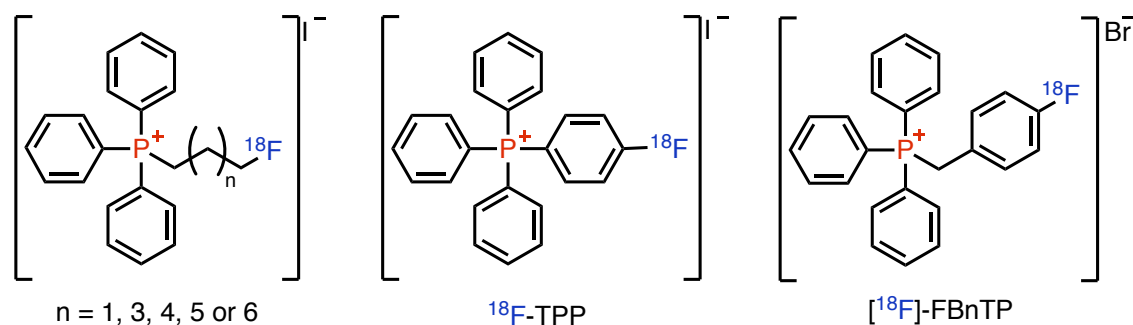


Figure 5.3 Examples of ^{18}F radiolabelled triphenylphosphonium salts with applications in myocardial imaging.

5.2 Towards a Multimodal Imaging Agent

Previous work within the Higham group has led to the development of the fluorescent phosphonium salts **45** and **46** (Figure 5.4). These salts were synthesised from fluorescent tertiary phosphines (diphenyl **24a** or dicyclohexyl **24b**) which were alkylated to their corresponding phosphonium salts with methyl trifluoromethanesulfonate (MeOTf).

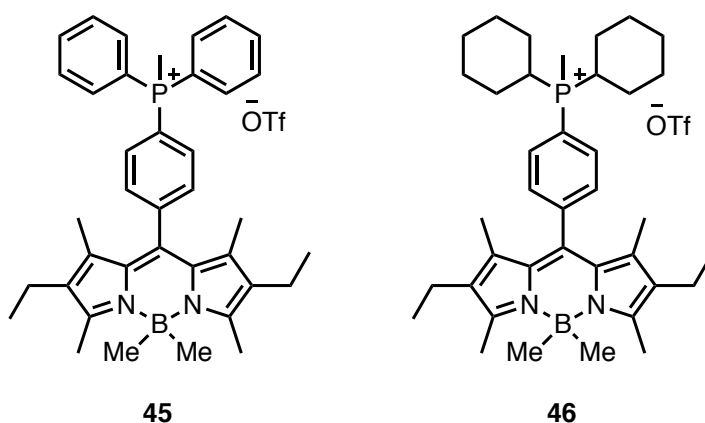


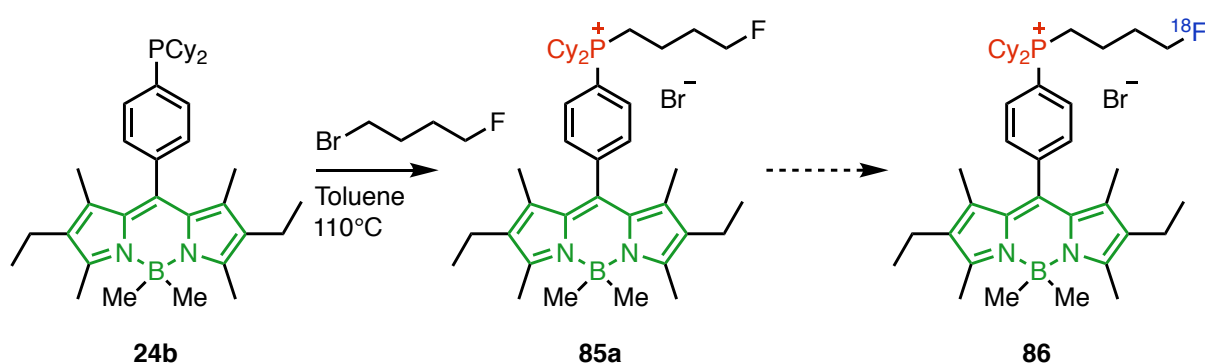
Figure 5.4 Fluorescent phosphonium salts developed by the Higham group for mitochondria-specific cell imaging.

Through collaboration with the Archibald group at the University of Hull, these salts were tested in human breast cancer cells (MCF-7) and rat cardiomyocytes (H9c2) and exhibited localisation within the mitochondria of both, confirmed when overlaid with MitoTracker Deep Red. The fluorescent phosphonium salts showed uptake dependency on the MMP, presenting

a reduction in the fluorescence intensity when the cells were treated with carbonyl cyanide *m*-chlorophenylhydrazone (CCCP), a protonophore which removes the membrane potential. The use of the fluorescent phosphine backbone added a second modality to the mitochondrial specific compound which allowed for the visualisation of the mitochondria by fluorescence optical imaging. The MMP dependency offered the capability for dynamic live fluorescence imaging which could aid in the detection of mitochondrial dysfunction in disease, together with the potential for monitoring therapeutic responses.¹⁵

As introduced in Chapter 3, compounds with multi-modalities are becoming increasingly common due to the limitations of the individual imaging techniques. Fluorescence, for example, has exceptional *in vitro* resolution (μm) with the ability to image specific organelles. However, due to its low spatial resolution, the technique has its downfalls when it comes to *in vivo*, deep tissue imaging. PET probes have high spatial resolution and are capable of deep tissue imaging, yet they lack the resolution to image at a submicron level. Combined, these techniques can outweigh the respective limitations in a complementary manner.¹⁶

Therefore, the fluorescent phosphonium salt probes could be further developed by the addition of a third modality; with the incorporation of a radiolabel suitable for PET imaging in mind, the group synthesised a fluorobutyl-substituted, fluorescent phosphonium salt with the anticipation that this could act as a precursor to a radioactive ^{18}F -substituted probe. The proposed route to radiolabel **85a** to afford **86** is outlined in Scheme 5.1.



Scheme 5.1 Proposed synthetic route for the synthesis of a trifunctional mitochondrial imaging agent (**86**).

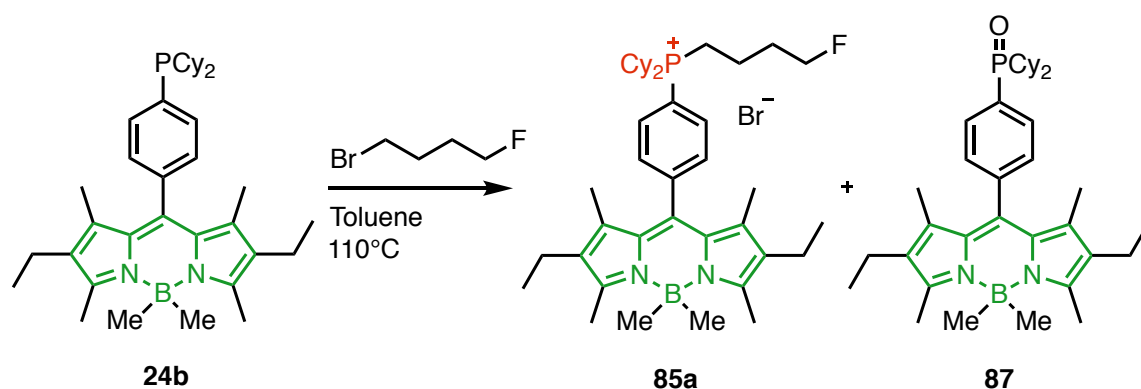
This second-generation probe **85a** (prior to attempted radiolabelling reactions) was also tested in MCF-7 and H9c2 cells and displayed increased MMP dependency when compared to **45** and **46**, thus validating its potential as a trifunctional probe.

This chapter continues on from the work published in this paper, initially to further assess the MMP dependency of this probe through cell imaging experiments (in collaboration with The University of California, San Diego). Moreover, efforts towards the synthesis of a fluorescent,

mitochondrial-specific and radiolabelled probe will be further explored, and the advantages and disadvantages of different synthetic routes will be described.

5.3 Synthesis of Fluorescent Phosphonium Salt **85a**

The synthesis of the phosphonium salt **85a** was achieved following the procedure reported by our group in 2016 and is shown in Scheme 5.2.¹⁵ 1-Fluoro-4-bromobutane was added to a solution of **24b** in toluene and the reaction mixture was stirred at reflux overnight. Analysis by $^{31}\text{P}\{^1\text{H}\}$ NMR spectroscopy confirmed the completion of the reaction after approximately 16 hours where the consumption of **24b** (δ 2.2 ppm) was observed. A new resonance was seen at δ 32.6 ppm, consistent with the reported values for **85a**, and a small amount of the phosphine oxide **87** at *ca.* δ 46 ppm. Purification was achieved by the layering of pentane over a crude solution of **85a** in *d*-chloroform which afforded a crystalline sample.



Scheme 5.2 Synthesis of the fluorescent phosphonium salt **85a** from **24b** with 1-fluoro-4-bromobutane.

5.4 Cell Imaging Studies of **85a** in Pancreatic Ductal Adenocarcinoma Cells

As part of a one-year Capstaff fellowship, a collaboration with the Wang group at the University of California, San Diego was established, and the author spent this time learning the techniques associated with live cell imaging. During this time, the fluorescent phosphonium salt **85a** was tested for mitochondrial uptake studies in pancreatic ductal adenocarcinoma (PDAC) cells.

5.4.1 Pancreatic Cancer

Pancreatic cancer is the 5th most fatal cancer in the UK with only 25.4% of people diagnosed surviving for a year or more, and a five year survival rate of 7.3%.¹⁷ The poor survival statistics can be attributed to i) an absence of symptoms in the early stages of the disease which commonly results in its late diagnosis, meaning it is often too widespread to be treated with surgery and ii) the alternative treatment of chemotherapy has been shown to be ineffective

in many cases, with the cancer displaying high levels of resistance. Thus, there is motivation to find new methods of detection and treatment.^{18,19}

Mitochondrial dysfunction is apparent in many cancers including pancreatic cancer, where it has been reported to shift cellular metabolism, resulting in increased tumour proliferation.²⁰

Neamati *et al.* identified the mitochondria as an untargeted area for therapy in pancreatic cancer and thus tested the mitochondrial-targeting phosphonium salt, TP421 (Figure 5.1), for its activity in MIA PaCa-2, PANC-1 and HPAC cells. From the treatment of these cell lines with TP421, they observed an inhibition of mitochondrial respiration which consequently led to the inhibition of cell growth and cell death. These preliminary results warrant their further studies and development.¹³

The limited studies and understanding of the involvement of the mitochondria in pancreatic cancer makes for an attractive target for the testing of the fluorescent mitochondrial imaging agent **85a**. Therefore, preliminary studies were carried out.

5.4.2 Mitochondrial Uptake Tests

Compound **85a** was tested using fluorescence microscopy in murine pancreatic adenocarcinoma (PDAC) cells. Initial studies confirmed the localisation of **85a** within the mitochondria of the PDAC cells, consistent with our previous studies in collaboration with the Archibald group in breast cancer cells (MCF-7) and rat cardiomyocytes (H9c2).¹⁵ Localisation images are shown in Figure 5.5.

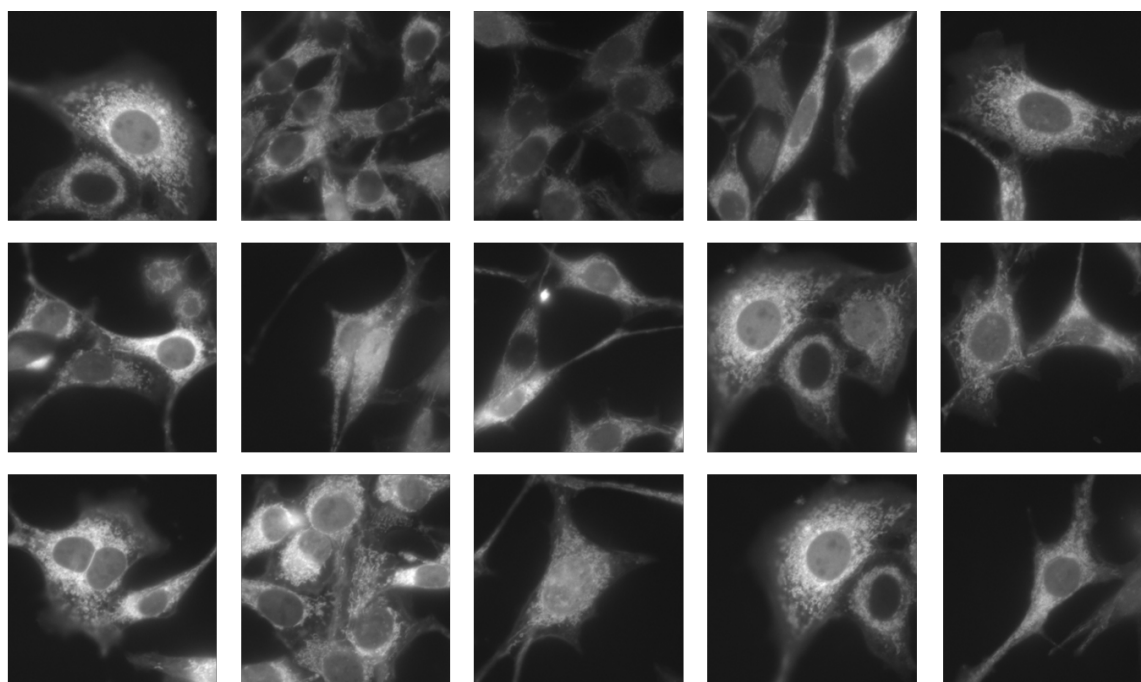


Figure 5.5 Images illustrating the localisation of phosphonium salt **85a** in murine pancreatic ductal adenocarcinoma cells (PDAC p53 R172H).

Since compound **85a** displayed MMP dependant uptake in MCF-7 and H9c2 cells, it was decided to test these properties through live cell imaging in PDAC cells. It was of interest to understand how the MMP differed between gemcitabine-resistant, and non-resistant cell lines. Gemcitabine (2',2'-difluoro-2'deoxyctidine) is a chemotherapy drug used in first line pancreatic cancer therapy, either alone, or as part of a combination of drugs.²¹ Therefore, to aid in understanding the effects of gemcitabine on the MMP, **85a** was applied to two cell lines. The first cell line was a murine pancreatic ductal adenocarcinoma cell line (PDAC p53 R172H) which will herein be referred to as the non-resistant (NR) cell line. The second was derived from the NR cell line and it was cultured with 100 nM gemcitabine to build a drug resistant cell line. These cells will be referred to as the gemcitabine-resistant (R100) cell line.

The MMP specific uptake of compound **85a** in the two cell lines was measured by the average intensity value taken across 30 images per cell line. The R100 cell line had a 75% lower uptake to the NR cell line, by fluorescence intensity, indicating a decreased membrane potential. Cancer cells reportedly have a more hyperpolarised MMP¹⁰ and thus, the lower uptake of **85a** in the R100 cells indicates that their drug-resistant nature may have an effect on the MMP. The mitochondria are highly plastic organelles which enables their adaptation in response to their changing environment.²² The results are shown in Figure 5.6.

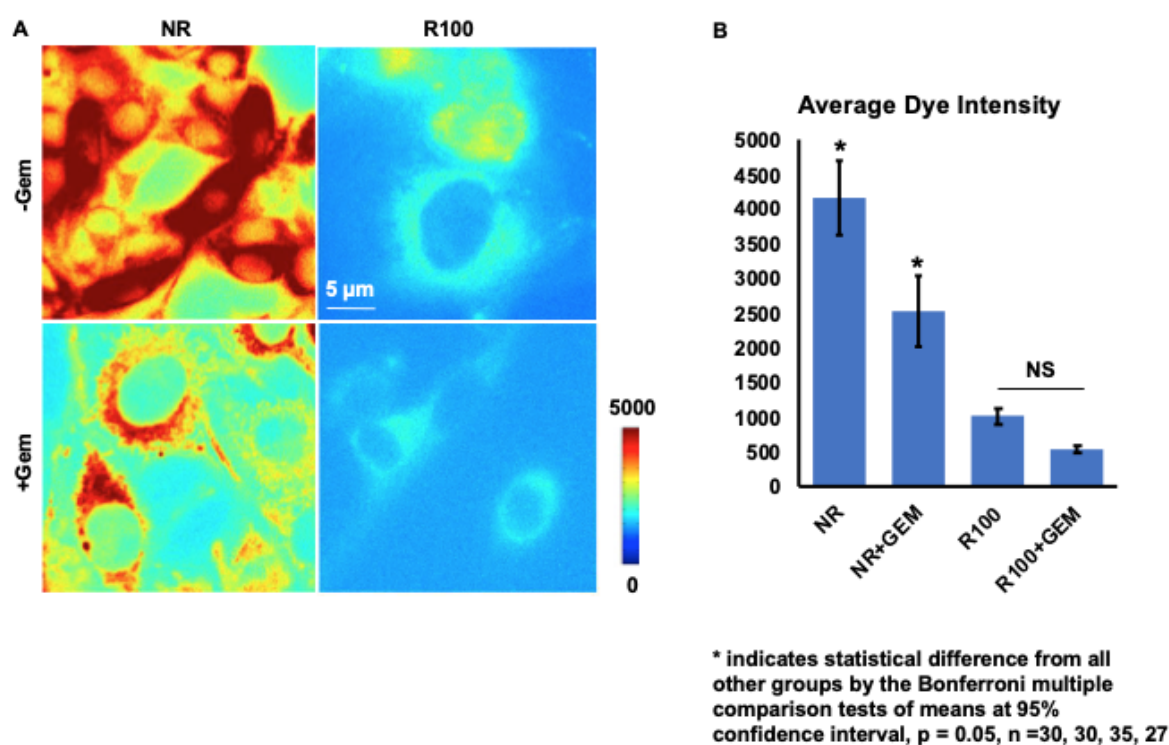


Figure 5.6 Ratio images of PDAC cells with the phosphonium salt probe **85a** for both the NR and R100 cell lines, before and after 2.5 µM gemcitabine treatment (A). The average intensities of the cells in a single frame for both the NR and R100 cell lines, before and after 2.5 µM gemcitabine treatment (B).

To monitor how the MMP of the two cell lines adapted to treatment, both cell lines were subsequently treated with gemcitabine, to give a final concentration of 2.5 μ M, and incubated for 12 hours before imaging. As with the previous experiments, approximately 30 positions were manually selected and images were taken and analysed to give an average intensity value for each position. Following the treatment with gemcitabine, a decrease in the uptake of **85a** was observed; the NR cells displayed a 37.5% lower uptake than before treatment and a 50% lower uptake was observed for the R100 cell line. These results are shown in Figure 5.6. These results demonstrated that when the drug was administered and used in conjunction with the fluorescent probe, the dynamic nature of the MMP could be monitored via the fluorescence intensity of **85a**. The R100 cell line appears to adapt more significantly than the NR cell line, signifying a more plastic mitochondrial membrane potential. These preliminary results are encouraging for the continued research of this probe in mitochondrial studies.

The work carried out in Section 5.4 was done in collaboration with the research group of Professor Peter (Yingxiao) Wang, as part of a larger project at the University of California, San Diego from January to December 2017 whilst on the Capstaff Fellowship.

The Capstaff Fellowship enables one postgraduate science student to undertake research at the University of California, San Diego for one year. The scholarship was bequeathed in 1968 by alumnus John G. Capstaff.

This fellowship gave me the opportunity to join a Bioengineering laboratory where I was able to learn a range of new techniques, mainly cell culture and live cell imaging but also inclusive of RNA isolation, transfection and virus infection.

Further research on a project entitled '*Epigenetic mechanisms of cancer drug resistance*' can be found in Appendix III

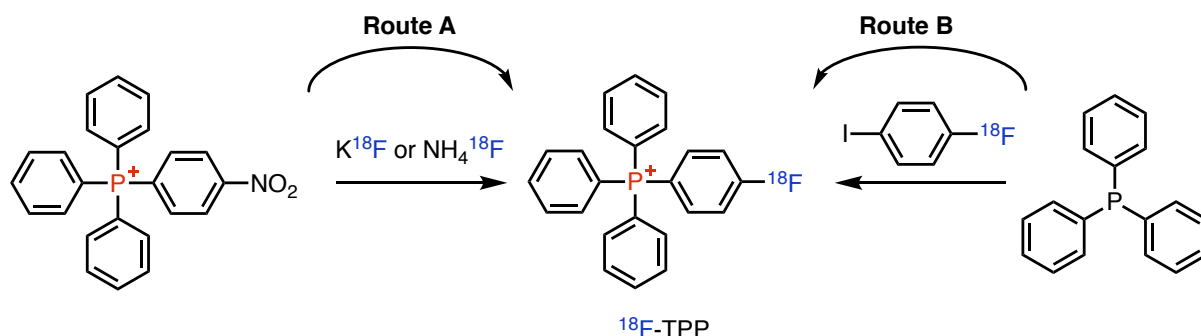


5.5 Radiolabelling of the Fluorescent Phosphonium Salt to Convert **85a** into a PET Probe

The introduction of an ^{18}F radiolabel to a molecule of interest can be achieved in a number of ways including both nucleophilic and electrophilic substitution, which allows for direct or indirect introduction.²³

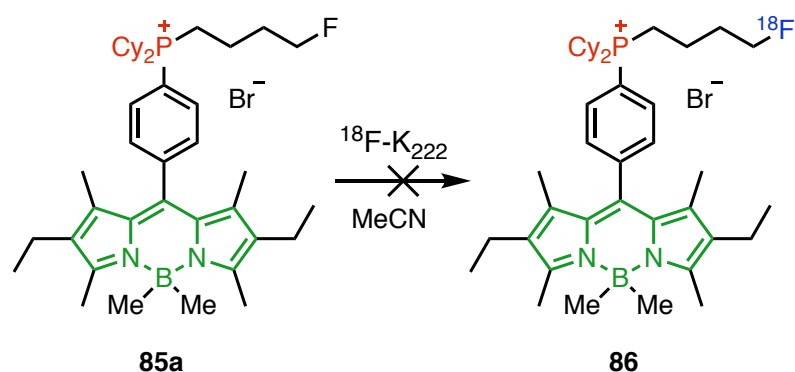
The synthesis of ^{18}F -TPP (introduced in Section 1.4.1) has been achieved by nucleophilic fluorination. Two methods have been reported and are illustrated in Scheme 5.3. Route A involves a direct exchange reaction of a 4-nitrophenyltriphenylphosphonium cation with a nucleophilic source of ^{18}F , where the nitro moiety acts as a leaving group. Route B follows a

two-step labelling method with the first step to radiolabel 1-fluoro-4-iodobenzene (not shown) before reacting it with triphenylphosphine in a nucleophilic substitution reaction.^{24,8,25}



Scheme 5.3 Methods of radiolabelling via nucleophilic fluorination. Route A illustrates the direct exchange of NO_2 to ^{18}F . Route B shows the two-step radiolabelling procedure, from the reaction of pre ^{18}F -radiolabelled 1-fluoro-4-iodobenzene and triphenylphosphine.

In collaboration with Professor Steve Archibald at The University of Hull, efforts were made to radiolabel **85a** via direct exchange through the addition of a nucleophilic source of ^{18}F (^{18}F - K_{222}); this would facilitate its application in PET imaging and afford a multimodal imaging agent. **85a** was dissolved in anhydrous acetonitrile and added to ^{18}F - K_{222} (~ 280 MBq) (Scheme 5.4). The reaction mixture was heated to 80°C and subsequently analysed by radio-TLC at 5, 10, 20, 30, and 60-minute timepoints. Unfortunately, no radiolabelled product was detected at any time point. It was hypothesised that these problems were caused by difficulties in the C–F bond cleavage due to the strong C–F bond ($105.4\text{ kcal mol}^{-1}$).²⁶ Therefore, potential solutions and alternative halogen leaving groups were considered.



Scheme 5.4 The attempted radiolabelling of fluorescent phosphonium salt **85a**.

5.6 Development of Probes for Radiolabelling by the Direct Exchange Method

The work described in this section (5.6) was done with an MChem student, Miss R. A. Dalton.

^{18}F has a half-life of only 109.7 minutes, and therefore to have applications in PET imaging, it is crucial that the radiolabelling reaction occurs rapidly. Therefore, a good leaving group is essential for this method. As the attempted radiolabelling of **85a** to synthesise a trifunctional

imaging agent was unsuccessful, efforts were made to improve the design of this phosphonium salt to aid the radiolabelling procedure.

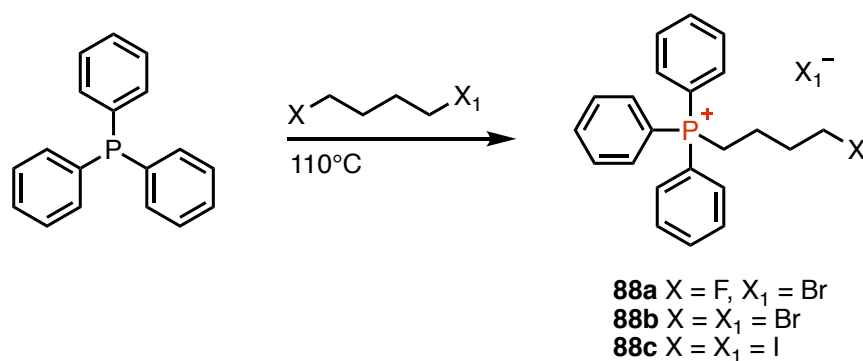
Initial experiments were carried out with triphenylphosphine, a readily available and easy-to-handle system for the optimisation of the quarternisation reactions, before transferring the procedure to the more complex fluorescent Bodipy phosphine.

5.6.1 Synthesis of Triphenylphosphonium Salts

The previously reported phosphonium salt **85a** developed in the group was synthesised from tertiary phosphine **24b** by refluxing in toluene with one equivalent of 1-fluoro-4-bromobutane. However, this led to long reaction times (16 hours) and afforded a mixture of the tertiary phosphine oxide **87** and the desired salt **85a**.

To aid in the halogen/ ^{18}F exchange reaction, alternative halide leaving groups were investigated. In addition, a literature search was carried out to find improved conditions for the alkylation of phosphines. A procedure for the synthesis of (4-iodobutyl)triphenylphosphonium, **88c**, from triphenylphosphine and 1,4-diiodobutane by Lin *et al.*²⁷ was followed. This method yielded the phosphonium salt after 1.5 hours in a solvent-free reaction at 100 °C in light-free conditions.

This procedure was applied for substitution reactions using 1-fluoro-4-bromobutane, 1,4-dibromobutane and 1,4-diiodobutane to afford the phosphonium salts **88a-c**. An excess of 1,4-dihalobutane was added to a Schlenk flask containing triphenylphosphine under an inert atmosphere. The flask was darkened with foil and heated for 1.5 hours at 100 °C. By this time, a precipitate had formed which was filtered off and washed with toluene. The resulting compounds were purified by recrystallisation, which afforded the corresponding phosphonium salts in good yields (69-80%). These reactions have been illustrated in Scheme 5.5.²⁷



Scheme 5.5 Synthesis of triphenylphosphonium salts (**88a-c**) from triphenylphosphine and the corresponding dihalobutane in toluene under refluxing conditions.

The synthesis of the alkylated products **88a-c** was confirmed by a downfield shift in the $^{31}\text{P}\{^1\text{H}\}$ NMR spectra from triphenylphosphine at $\delta -5.3$ ppm to $\delta 24.6$ ppm for **88a** and 24.7 ppm for **88b** and **88c**. The addition of peaks for the alkyl chain were observed in the ^1H NMR spectra, which were in agreement with those reported in the literature.^{28,29,30} Samples suitable for analysis by X-ray diffraction were obtained by the slow diffusion of diethyl ether into a solution of the corresponding phosphonium salt in dichloromethane. The structures are shown in Figure 5.7.

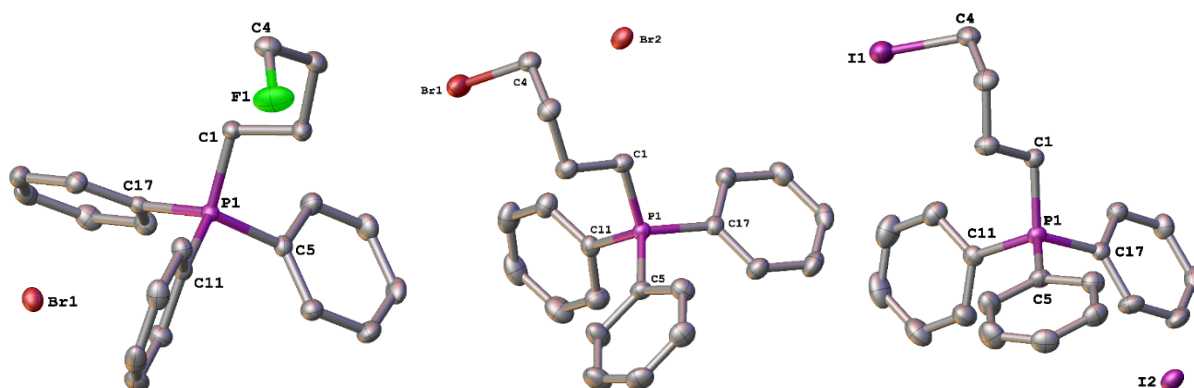


Figure 5.7 Molecular structure of **88a** (left). Hydrogen atoms have been omitted for clarity. Selected bond distances [Å] and angles [°]: P1-C1 1.7976 (14), P1-C5 1.7949 (14), P1-C11 1.7984 (14), P1-C17 1.8018 (14), F1-C4 1.4169 (18); C1-P1-C11 110.35 (7), C1-P1-C17 110.63 (7), C5-P1-C1 108.62 (6), C5-P1-C11 111.56 (7), C5-P1-C17 108.65 (7), C11-P1-C17 107.02 (6), F1-C4-C3 109.88 (13). Molecular structure of **88b** (middle). Hydrogen atoms have been omitted for clarity. Selected bond distances [Å] and angles [°]: Br1-C4 1.9585 (19), P1-C1 1.7968 (18), P1-C5 1.7966 (18), P1-C11 1.7989 (18), P1-C17 1.7973 (18); C1-P1-C11 110.94 (9), C1-P1-C17 110.35 (8), C5-P1-C1 108.35 (8), C5-P1-C11 110.60 (8), C5-P1-C17 109.30 (8), C17-P1-C11 107.30 (8). Molecular structure of **88c** (right). Hydrogen atoms have been omitted for clarity. Selected bond distances [Å] and angles [°]: P1-C1 1.794 (3), P1-C5 1.795 (3), P1-C11 1.798 (4), P1-C17 1.793 (3), I1-C4 2.148 (4); C1-P1-C5 108.61 (15), C1-P1-C11 111.03 (16), C5-P1-C11 109.84 (16), C17-P1-C1 111.16 (16), C17-P1-C5 109.02 (15), C17-P1-C11 107.16 (15), C3-C4-I1 113.2 (3).

The three crystal structures of **88a-c** are analogous to each other, with the only notable difference being the length of the halogen-carbon bond which has been illustrated in Figure 5.8 by an overlay of the structures. As expected, the bond lengthens on descending group 17: C–F < C–Br < C–I (F1-C4 1.4169 (18), Br1-C4 1.9585 (19), I1-C4 2.148 (4) Å).

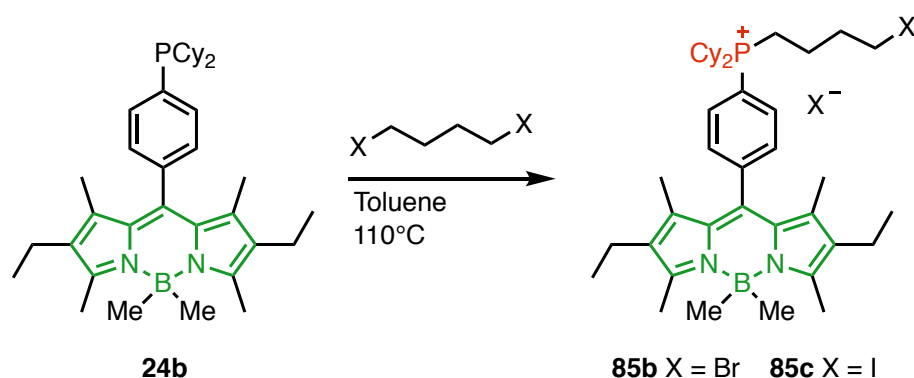


Figure 5.8 An overlay of the three crystal structures **88a-c**. Green (**88a**), orange (**88b**), purple (**88c**).

5.6.2 Synthesis of the Third-Generation Fluorescent Triphenylphosphonium Salts **85b-c**

Following the success of the synthesis of the triphenylphosphonium salts, the next step was to transfer this to the analogous fluorescent Bodipy system to advance towards the aim of synthesising a trifunctional mitochondrial imaging agent.

Bodipy tertiary phosphine **24b** was reacted with the corresponding 1,4-dihalobutane in refluxing toluene (Scheme 5.6). The reactions were monitored by $^{31}\text{P}\{^1\text{H}\}$ NMR spectroscopy, where reaction completion was confirmed by downfield shifts from δ 2.2 ppm for **24b** to δ 33.0 ppm for compounds **85b** and **85c**.



Scheme 5.6 The synthesis of fluorescent phosphonium salts **85b** and **85c**, from **24b** with 1,4-dibromobutane 1,4-diiodobutane respectively.

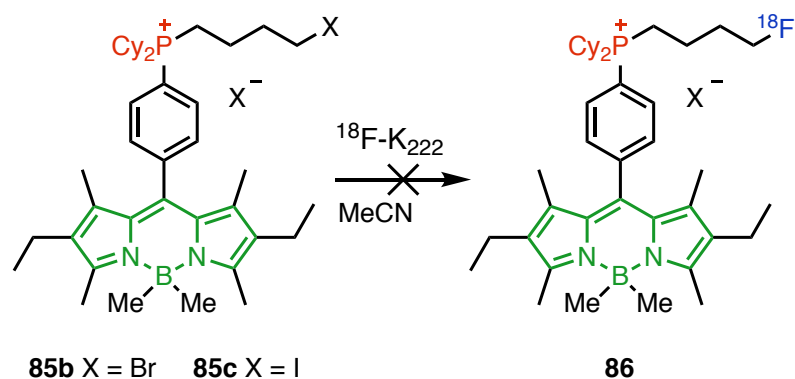
In both cases, purification was achieved by crystallisation from a *d*-chloroform solution of the corresponding phosphonium salt, layered with pentane to afford **85b** and **85c** as crystalline solids. Analysis of **85c** by X-ray crystallography was carried out, but unfortunately, only weak diffraction was observed, resulting in low resolution data which was insufficient for full data collection. Crystalline samples of the phosphonium salts **85b** and **85c**, along with their tertiary phosphine precursor **24b** were sent to Professor Steve Archibald to attempt the radiolabelling with ^{18}F in a nucleophilic substitution reaction.

5.7 Attempted ^{18}F Radiolabelling Reactions

This work was carried out by Dr Juozas Domarkas (Postdoctoral Research Fellow in Professor Steve Archibald's group) at the University of Hull.

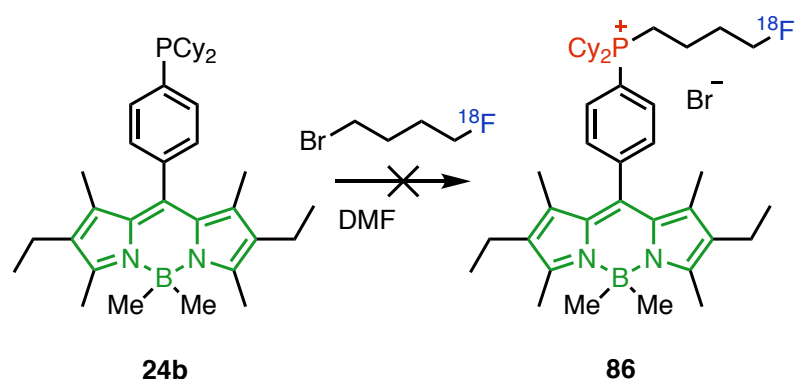
As was seen in Section 5.5, radiolabeling can be achieved by direct exchange (Route A) or by a two-step labelling method (Route B). First, the direct exchange method of **85b** and **85c** was attempted using a nucleophilic source of ^{18}F , $^{18}\text{F}\text{-K}_{222}$. The $^{18}\text{F}\text{-K}_{222}$ was formed from cyclotron produced ^{18}F -fluoride in H_2^{18}O , which was trapped and subsequently eluted into a vessel containing Kryptofix-222. The resulting radioactive compound was dried by azeotropic evaporation and used for the following reactions.

Radiolabeling of both **85b** and **85c** was tested by dissolving the respective phosphonium salt in anhydrous acetonitrile and adding to the dry $^{18}\text{F}\text{-K}_{222}$ (~280 MBq) (Scheme 5.7). The reaction mixtures were heated to 80 °C and subsequently analysed by radio-TLC at 5, 10, 20, 30, and 60-minute timepoints. In both cases, no radiolabelled product was detected at any time point, which was confirmed by HPLC. A second reaction was carried out at the higher temperature of 100 °C, yet again, no radiolabeled product was detected at any timepoint up to 60 minutes.



Scheme 5.7 The attempted radiolabelling of fluorescent phosphonium salts **85b** and **85c** with $^{18}\text{F}\text{-K}_{222}$ in MeCN.

As the radiolabelling of the phosphonium salts **85b** and **85c** by direct exchange was unsuccessful, a two-step method was attempted instead from the tertiary phosphine **24b** with 1- ^{18}F -4-bromobutane. The 1- ^{18}F -4-bromobutane was first generated by reacting 1,4-dibromobutane with $^{18}\text{F}\text{-K}_{222}$. The resulting ^{18}F -labelled haloalkane was subsequently reacted with **24b** in anhydrous DMF (Scheme 5.8). The reaction mixture was heated to 130 °C for 60 min and analysed by radio-TLC and radio-HPLC at 5, 10, 20, 30, and 60-minute timepoints. Unfortunately, again, no radiolabeled product was detected at any timepoint.



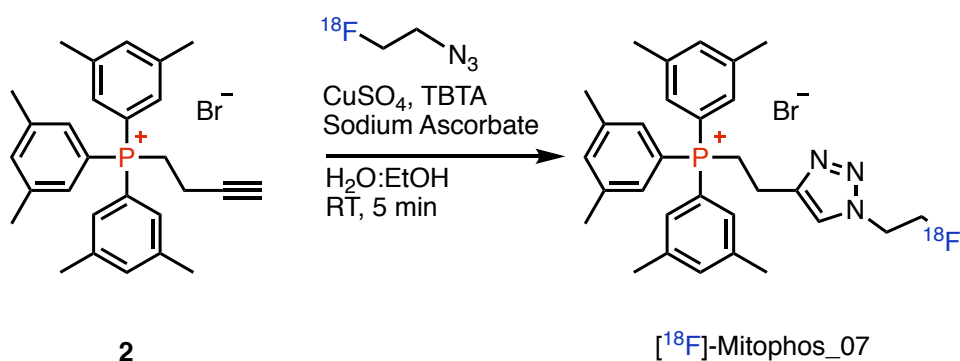
Scheme 5.8 The attempted radiolabelling of **24b** in a two-step procedure with 1- ^{18}F -4-bromobutane.

As these direct exchange radiolabelling reactions proved to be unsuccessful, alternative methods were sought.

5.8 Radiolabelling by Click Chemistry

Click chemistry is a concept coined by Barry Sharpless (Nobel Prize winner) used to describe reactions that 'click' two reagents together through a heteroatom. These reactions are high yielding, use mild conditions and have a fast reaction rate and therefore have been exploited for their application in radiolabelling.^{31–33}

Haslop *et al.* employed a copper-catalysed azide-alkyne cycloaddition (CuAAC) click reaction to synthesise a small library of phosphonium salts called [¹⁸F]-Mitophos. These were constructed from different (but-3-ynyl)triarylphosphonium bromide salts and an ¹⁸F substituted ethyl azide. Scheme 5.9 shows the synthesis of [¹⁸F]-Mitophos_07; the click reaction is carried out under aqueous conditions in five minutes in a fully automated synthesis, providing an exceptional method to radiolabel rapidly.^{31,32}



Scheme 5.9 The radiolabelling of an alkyne-substituted phosphonium salt via a copper-catalysed azide-alkyne cycloaddition click chemistry reaction to yield the cardiac imaging agent, [¹⁸F]-Mitophos_07.

The same group have recently evaluated [¹⁸F]-Mitophos_07 as a cardiac imaging agent, comparing it to the leading ¹⁸F labelled lipophilic cation, ¹⁸F-FBnTP (Figure 5.3). [¹⁸F]-Mitophos_07 was tested in perfused rat hearts to evaluate its ability in the imaging of chemotherapy-induced cardiotoxicity where it showed improvement in comparison to ¹⁸F-FBnTP. With its favourable pharmacokinetic properties and improved efficiency of washout from the liver, it demonstrates promise as an agent for early detection of cardiotoxicity, yet further studies are required for a comprehensive understanding. The success of [¹⁸F]-Mitophos_07 as a cardiac imaging agent bodes well for the synthesis of a fluorescent analogue via click chemistry.

Click chemistry provides the rapid reaction times that are critical to radiolabelling because of the short half-lives of the radioactive nuclides. Thus, this could be a valid route for the rapid labelling of the fluorescent derivatives to afford a trifunctional probe containing: i) a

fluorescent Bodipy core to facilitate fluorescence imaging, ii) a phosphonium cation to target the mitochondria, and iii) an ^{18}F radiolabel for application in PET imaging.

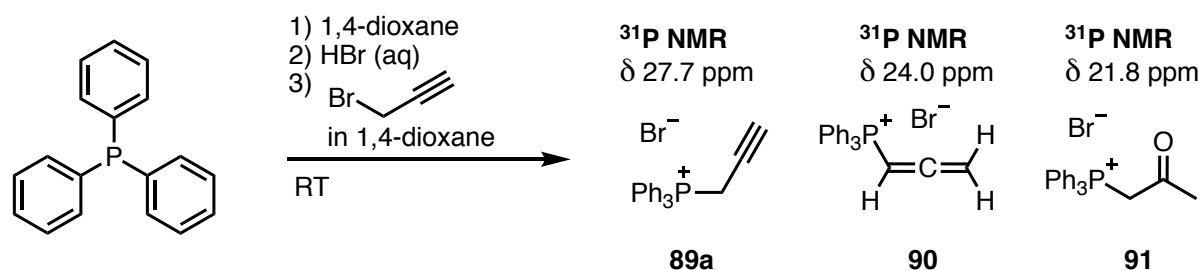
5.9 Development of Probes for Radiolabelling by Click Chemistry

As was described for the haloalkane phosphonium salts **85a-c**, initial experiments to attach the alkyne moiety were carried out with non-fluorescent phosphines, before transferring to the fluorescent Bodipy backbone.

5.9.1 Synthesis of Alkynyl Triphenylphosphonium Salts

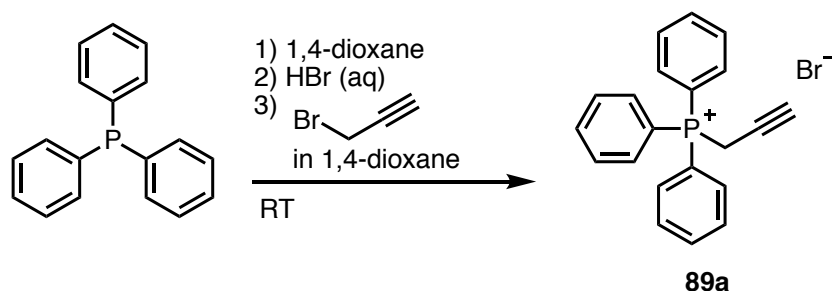
The first approach that was taken to synthesise an alkynyl phosphonium salt used propargyl bromide as the alkylating agent. In an analogous method to the synthesis of the haloalkyl phosphonium salts **85a-c**, propargyl bromide was added to a toluene solution of triphenylphosphine and heated to reflux. A colour change was observed almost instantly, from colourless to yellow, and the flask was coated with a brown insoluble residue within one hour. The reaction was monitored by $^{31}\text{P}\{^1\text{H}\}$ NMR spectroscopy, where the appearance of a single peak at δ 24.2 ppm after 24 hours confirmed the completion of the reaction. This resonance is similar to those that were observed for the triphenylphosphonium salts **88a-c**, implying the synthesis of a phosphonium salt. However, on removal of the solvent and the subsequent analysis by ^1H NMR spectroscopy, no peak consistent with a terminal alkyne proton was observed and the signal in the $^{31}\text{P}\{^1\text{H}\}$ NMR spectrum was now consistent with that of triphenylphosphine oxide (*ca.* δ 29 ppm). Reports in the literature suggested the acidic conditions that were essential for this preparation, are likely to prevent the prototropic isomerisation of the alkyne to an allene.^{34,35} Thus, an alternative synthesis was explored.

Bagdasaryan *et al.* reviewed the reported syntheses of propargyltriphenylphosphonium bromide and adapted them to improve the overall yield (from 17% to 76%). In all cases, the synthesis resulted in the formation of the isomeric allenic salt **90** and acetonyltriphenylphosphonium bromide **91** side-products (Scheme 5.10).³⁶ As a result of difficulties with our previously successful procedure, this improved procedure was followed.



Scheme 5.10 The improved synthesis of propargyltriphenylphosphonium bromide **89a** and reported side products **90** and **91** described by Bagdasaryan and co-workers.³⁶

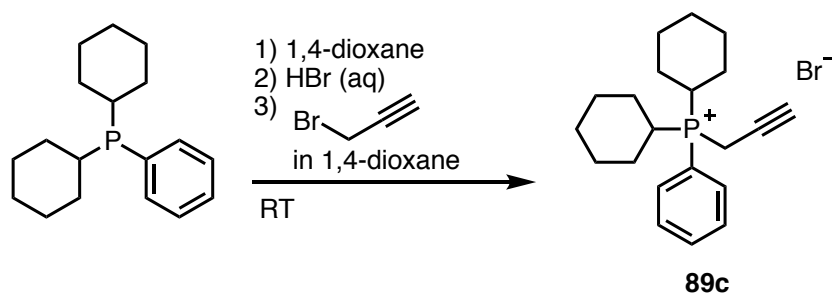
An aqueous solution of hydrogen bromide was added dropwise to a solution of triphenylphosphine in 1,4-dioxane, which resulted in the formation of a precipitate. To this, a solution of propargyl bromide in 1,4-dioxane was added and the reaction mixture was allowed to stir at room temperature overnight. The following day, a white precipitate had formed which was isolated by filtration, washed and dried *in vacuo* to afford **89a** in 61% yield. (Scheme 5.11).



Scheme 5.11 The synthesis of propargyltriphenylphosphonium bromide **89a** from triphenylphosphine and propargyl bromide in acidic conditions.

Analysis of the white precipitate by $^{31}\text{P}\{^1\text{H}\}$ NMR spectroscopy showed a downfield shift from *ca.* $\delta -5.3$ ppm for triphenylphosphine to $\delta 22.0$ ppm for the isolated product. A chemical shift corresponding to the terminal alkyne proton was observed at $\delta 3.46$ (dt, $^4J_{\text{HH}} = 6.9$, $^4J_{\text{HP}} = 2.7$ Hz) which was consistent with the data reported in the literature.³⁶

It was important to understand whether this procedure was transferrable to other tertiary phosphines, and so the experiment was carried out with dicyclohexylphenylphosphine as an analogous compound to the fluorescent tertiary phosphine **24b** (Scheme 5.12).



Scheme 5.12 The synthesis of propargyldicyclohexylphenylphosphonium bromide (**89c**) from dicyclohexylphenylphosphine and propargyl bromide in acidic conditions.

An aqueous solution of hydrogen bromide was added dropwise to a solution of dicyclohexylphenylphosphine in 1,4-dioxane. In this case, no precipitate was observed. A solution of propargyl bromide in 1,4-dioxane was then added and the reaction mixture was allowed to stir at room temperature overnight. The following day, unlike with triphenylphosphine, no precipitate was observed, thus $^{31}\text{P}\{^1\text{H}\}$ NMR spectroscopy was used to

analyse the crude reaction mixture. A phosphorus resonance was observed at δ 21.1 ppm, but following an aqueous work up, a new resonance was observed at δ 32.0 ppm. Purification was achieved by dissolving the crude sample of **89c** in dichloromethane and precipitating out the desired product with diethyl ether. **89c** was isolated in 77% yield (Scheme 5.12). Crystals suitable for analysis by X-ray diffraction were formed from the slow evaporation of a solution of **89c** in *d*-chloroform. The structure is shown in Figure 5.9.

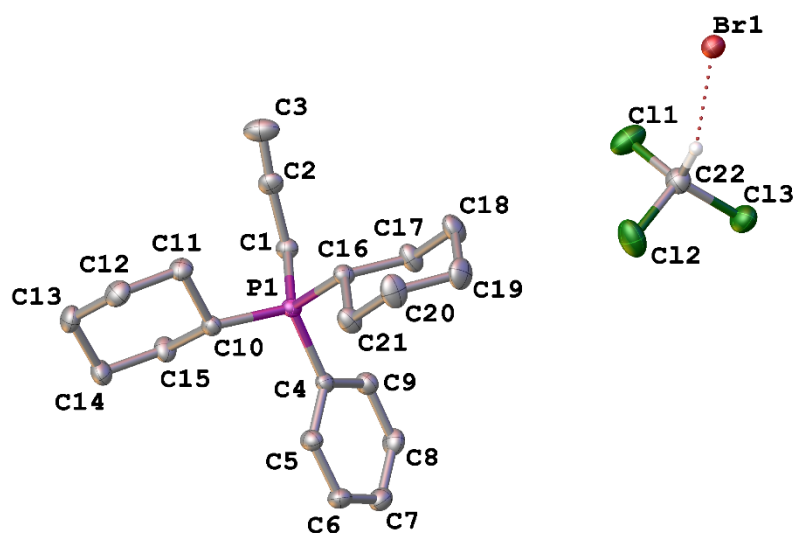
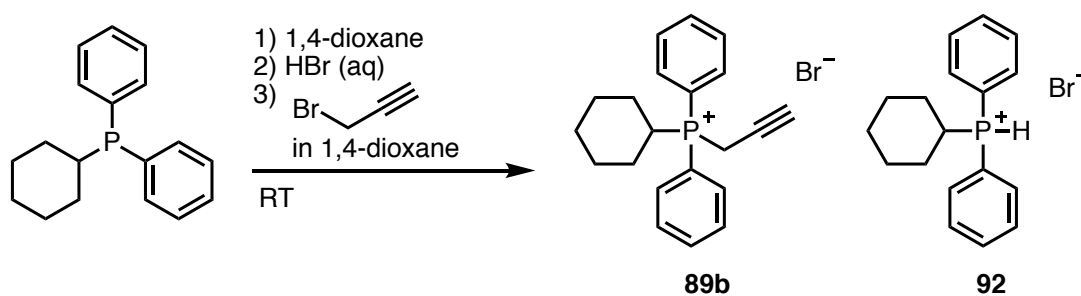


Figure 5.9 Molecular structure of **89c**. Hydrogen atoms have been omitted for clarity. Selected bond distances [Å] and angles [°]: P1-C1 1.828(2), P1-C4 1.796(3), P1-C10 1.815(2), P1-C16 1.808(3), C2-C3 1.181(4), C1-C2-C3 176.2(3).

The P1-C1 bond length of 1.828(2) Å and C2-C3 bond length of 1.181(4) Å are in agreement with examples reported in the literature.³⁷

An analogous reaction was set up using cyclohexyldiphenylphosphine. After overnight stirring in 1,4-dioxane at room temperature, analysis by $^{31}\text{P}\{^1\text{H}\}$ NMR spectroscopy was carried out. The major chemical shift was observed at δ 29.6 ppm, consistent with the expected signal for the product, however, an additional chemical shift was observed at δ 10.4 ppm which has not been assigned. Purification was by an aqueous work-up and extraction with dichloromethane. Both layers were subsequently analysed by $^{31}\text{P}\{^1\text{H}\}$ NMR spectroscopy. The organics showed the major resonance at δ 2.4 ppm – likely starting material. On analysis of the evaporated aqueous fraction, the major resonance was observed at δ 20.5 ppm. This product was isolated by crystallisation from slow diffusion of diethyl ether into a dichloromethane solution. The subsequent analysis of these crystals by X-ray diffraction showed that they were of the intermediate product, cyclohexyldiphenylphosphonium bromide **92** which is shown in Scheme 5.13 and Figure 5.10. Unfortunately, the desired product was not isolated.



Scheme 5.13 The synthesis of propargylcyclohexyldiphenylphosphonium bromide (**89b**) and intermediate, cyclohexyldiphenylphosphonium bromide (**92**) from cyclohexyldiphenylphosphine and propargyl bromide in acidic conditions.

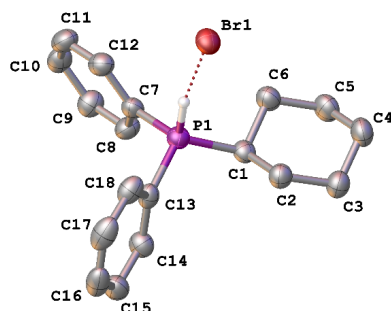
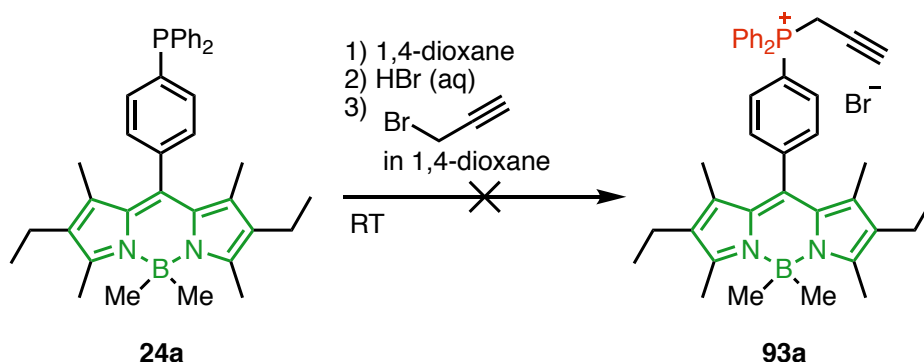


Figure 5.10 Molecular structure of **92**. Hydrogen atoms have been omitted for clarity. Selected bond distances [Å] and angles [°]: P1-C1 1.803(2), P1-C7 1.793(2), P1-C13 1.791(2), P1-H1 1.289, H1-Br1 2.434, C1-P1-C7 112.73(10), C7-P1-C13 111.04(9), C13-P1-C1 112.47(9).

The P1–H bond length of 1.289 Å is shorter than that observed for the analogous compound, triphenylphosphonium bromide, previously reported, with a bond length of 1.61(9). However, the precise location of hydrogen atoms cannot be determined by X-ray diffraction. The proton bound to the P1, directed towards Br1 is also observed in the analogous structure.³⁸

5.9.2 Synthesis of Fluorescent Alkynyl Phosphonium Salts

To create a fluorescent compound suitable for click chemistry, the translation of this procedure to the fluorescent Bodipy backbone was attempted. Thus, the fluorescent tertiary phosphine **24a** was reacted first with hydrogen bromide and subsequently with propargyl bromide in an analogous method to **89a** and **89c** (Scheme 5.14).



Scheme 5.14 The attempted synthesis of propargyl-functionalised fluorescent phosphonium salt (**93a**) from **24a** and propargyl bromide under acidic conditions.

After overnight stirring at room temperature, analysis by $^{31}\text{P}\{^1\text{H}\}$ NMR spectroscopy revealed three signals. Two minor resonances were observed at $\delta -5.1$ ppm (br) and $\delta -6.2$ ppm, both indicating the presence of tertiary phosphines, and the major signal was seen at $\delta 22.7$ ppm, indicative of a phosphonium salt. Following purification by aqueous work-up and analysis by ^1H NMR spectroscopy, no shifts characteristic of the propargyl substituted product were observed. It appeared by $^{31}\text{P}\{^1\text{H}\}$ NMR spectroscopy that the product had reverted back to a tertiary phosphine ($\delta -5.6$ ppm) and a phosphine oxide product ($\delta 29.4$ ppm). Following crystallisation of the resulting product, it was discovered that a dechelation reaction of the Bodipy core had occurred, resulting in the formation of the dipyrin compound **94** – shown in Figure 5.11.

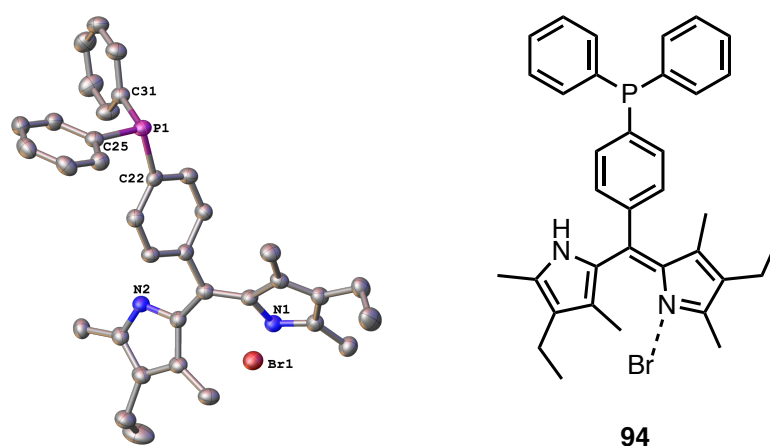


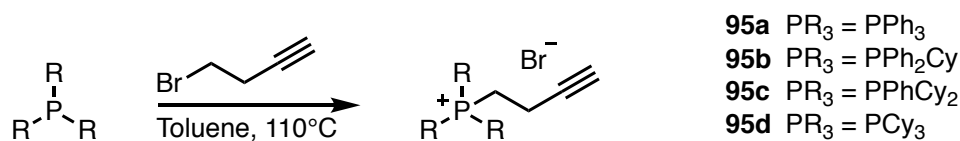
Figure 5.11 Molecular structure of **94**. Hydrogen atoms have been omitted for clarity. Selected bond distances [Å] and angles [°]: P1-C22 1.837(3), P1-C25 1.831(3), P1-C31 1.827(3), C25-P1-C22 105.61(12), C31-P1-C22 101.52(12), C31-P1-C25 102.22(13).

Dechelation of the Bodipy core by removal of the BF_2 group has previously been reported using bronsted acids. Amat-Guerri *et al.* found this to occur under deacetylation conditions of ethanolic hydrogen chloride³⁹ and Rutledge *et al.* demonstrated the dechelation occurred with both hydrochloric acid and trifluoroacetic acid.⁴⁰ As this procedure was found to be inadequately transferrable to the Bodipy phosphine system, this was not pursued further and instead, attention was focused towards finding alternative methods.

As introduced in Chapter 1 (Section 1.4.2), Haslop and coworkers reported the synthesis of (butyl)triarylphosphonium bromide from a triarylphosphine and 1-bromo-4-butyne. Thus, this procedure was followed to synthesise a small library of phosphonium salts (Scheme 5.15).³¹

The tertiary phosphines were dissolved in anhydrous toluene and heated to 110°C . 1-Bromo-4-butyne was added dropwise and the reaction mixture was stirred until the desired product

precipitated out of solution as a white solid. In each case, the solid was filtered off, washed with toluene, and the solid was dried *in vacuo*. No further purification was required.



Scheme 5.15 The synthesis of a series of butyne-functionalised phosphonium salts (**95a-d**) from tertiary phosphines with 1-bromo-4-butyne in toluene at 110 °C, overnight.

Characterisation of this series of phosphonium salts was achieved by a combination of NMR spectroscopy, IR spectroscopy and mass spectrometry. In all cases, the ^1H NMR spectra showed characteristic signals for the two sets of alkyl protons in the butyne chain, along with a triplet for the terminal proton ($^4J_{\text{HH}} = 2.5\text{--}2.7$ Hz) (Figure 5.12). Analysis by $^{31}\text{P}\{^1\text{H}\}$ NMR spectroscopy displayed signals with downfield shifts from their corresponding tertiary phosphines (from $\delta -5.3$ to 11.2 ppm for the tertiary phosphines to $\delta 23.7$ to 33.4 ppm for **95a-d**) and the ^{13}C NMR spectra showed signals at *ca.* $\delta 70$ ppm and $\delta 80$ ppm for the two alkynyl carbons. The IR spectra displayed absorptions for the alkyne C-H stretch at $\sim 3200\text{ cm}^{-1}$ and the $\text{C}\equiv\text{C}$ stretch at $\sim 2100\text{ cm}^{-1}$ in all cases and the mass spectra showed the corresponding M^+ ion.

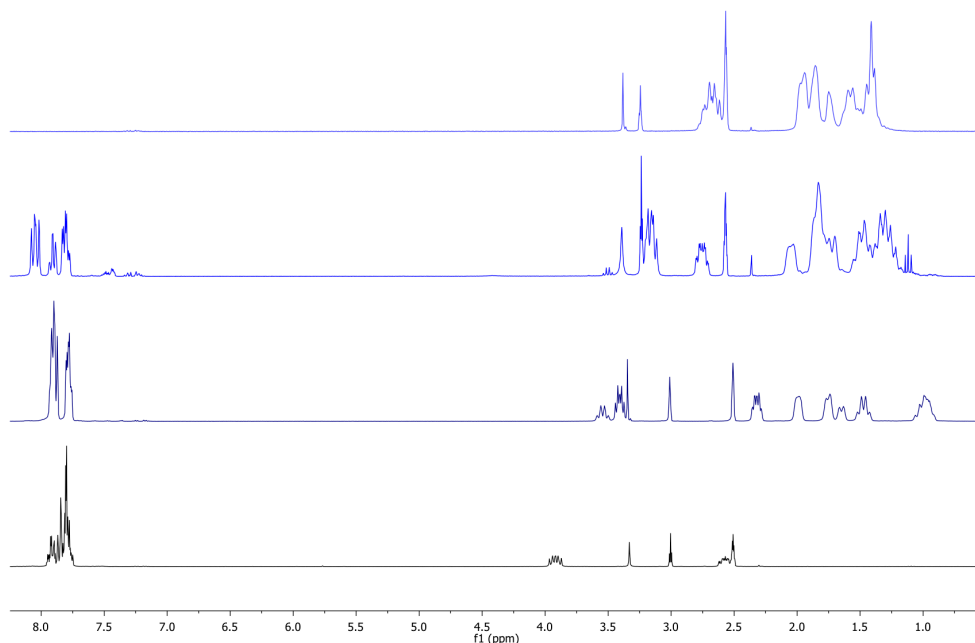


Figure 5.12 ^1H NMR spectra of the butyne-functionalised phosphonium salts **95a-d**, taken in d_6 -dimethylsulfoxide.

In each case, the corresponding products were crystallised by slow diffusion of diethyl ether into a dichloromethane solution of the phosphonium salt to afford samples suitable for analysis by X-ray diffraction. These structures are analogous to each other; their molecular structures are shown in Figures 5.13-15. The $\text{C}\equiv\text{C}$ triple bond (C3-C4) lengthens with the

substitution of phenyl groups for cyclohexyl groups. From 1.178(3) Å for **95b**, to 1.185(3) Å for **95c** and to 1.194(5) Å for **95d**. However, these bond lengths are not statistically different.

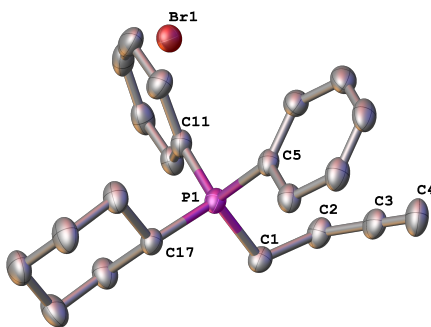


Figure 5.13 Molecular structure of **95b**. Hydrogen atoms have been omitted for clarity. Selected bond distances [Å] and angles [°]: P1-C1 1.8028(16), P1-C5 1.7955(17), P1-C11 1.7961(17), P1-C17 1.8116(17), C3-C4 1.178(3), C1-P1-C17 108.24(8), C5-P1-C1 108.34(7), C5-P1-C11 110.91(8), C5-P1-C17 110.80(8), C11-P1-C1 109.52(9), C11-P1-C17 108.97(8), C4-C3-C2 176.51(19).

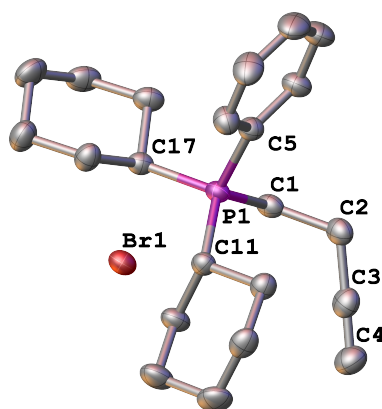


Figure 5.14 Molecular structure of **95c**. Hydrogen atoms have been omitted for clarity. Selected bond distances [Å] and angles [°]: P1-C1 1.8058(17), P1-C5 1.7984(17), P1-C11 1.8154(17), P1-C17 1.8137(18), C3-C4 1.185(3), C1-P1-C17 106.03(8), C5-P1-C1 110.32(8), C5-P1-C11 108.81(8), C5-P1-C17 108.64(8), C11-P1-C1 113.65(8), C11-P1-C17 109.25(8), C4-C3-C2 179.3(2).

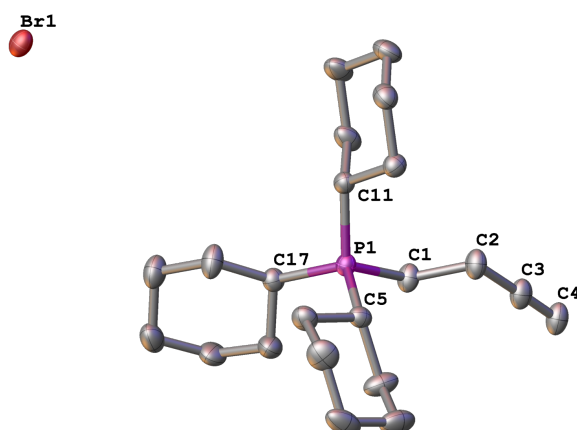
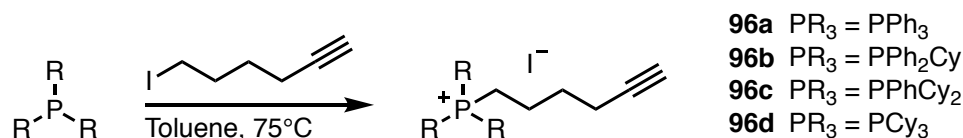


Figure 5.15 Molecular structure of **95d**. Hydrogen atoms have been omitted for clarity. Selected bond distances [Å] and angles [°]: P1-C1 1.803(3), P1-C5 1.822(3), P1-C11 1.825(3), P1-C17 1.831(3), C3-C4 1.194(5), C1-P1-C17 103.96(13), C5-P1-C1 107.51(13), C5-P1-C11 109.78(13), C5-P1-C17 116.20(13), C11-P1-C1 111.42(14), C11-P1-C17 107.87(12), C4-C3-C2 179.0(3).

To synthesise additional alkyne-functionalised phosphonium salts, as a result of searching the literature and the commercially available haloalkynes, the hexyne derivatives were targeted. By using 1-iodo-6-hexyne for the alkylation reactions, the resulting phosphonium salts may possess higher lipophilicity to the butyne derivatives **95a-d**. Lipophilicity is an essential property of bioactive compounds to enable their cellular uptake.⁴¹ McIndoe and co-workers demonstrated the synthesis of (hexyne)triphenylphosphonium iodide with 1-iodo-6-hexyne and thus, this procedure was followed (Scheme 5.16).⁴²



Scheme 5.16 The synthesis of a series of hexyne-functionalised phosphonium salts (**96a-d**) from tertiary phosphines with 1-bromo-6-hexyne in toluene at 75 °C, overnight.

The reaction of the tertiary phosphines with 1-iodo-6-hexyne was carried out in a similar method as with 1-bromo-4-butyne, however these reactions only required temperatures of 75 °C as demonstrated by McIndoe *et al.*⁴² Again, the reaction mixture was stirred until the desired products precipitated out of solution as white solids. The suspensions were filtered, washed with toluene and dried *in vacuo*. No further purification was required.

The characterisation of the hexyne-functionalised phosphonium salts **96a-d** was accomplished using a combination of ^1H , $^{31}\text{P}\{^1\text{H}\}$ and $^{13}\text{C}\{^1\text{H}\}$ NMR spectroscopy, IR spectroscopy and mass spectrometry. In all cases, the ^1H NMR spectra showed signals for the four sets of alkyl protons in the hexyne chain, with a characteristic triplet for the terminal proton ($^4J_{\text{HH}} = 2.5\text{-}2.6\text{ Hz}$).

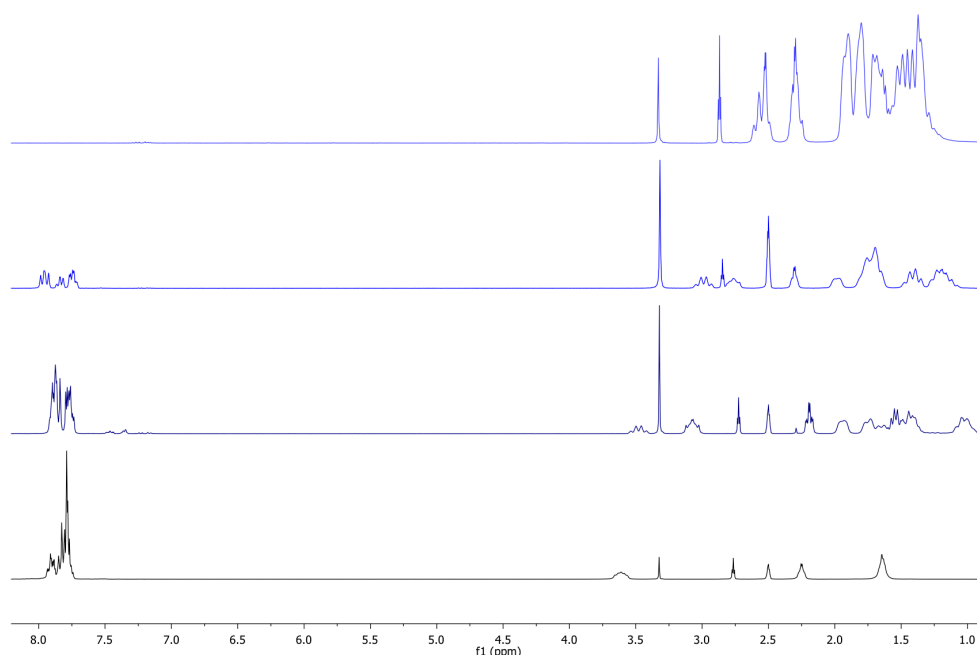


Figure 5.16 ^1H NMR spectra of the hexyne functionalised phosphonium salts **96a-d** taken in d_6 -dimethylsulfoxide.

A downfield shift in the $^{31}\text{P}\{^1\text{H}\}$ NMR spectra was observed from the corresponding tertiary phosphine (δ –5.3 ppm to 11.2 ppm) to their respective phosphonium salts **96a-d** (δ 24.0 ppm to 32.9 ppm). Analysis by $^{13}\text{C}\{^1\text{H}\}$ NMR spectroscopy displayed characteristic signals for the two alkynyl carbons at *ca.* δ 70 ppm and δ 80 ppm and the mass spectra showed the corresponding M^+ ion in all cases.

The IR spectra displayed absorptions for the alkyne C-H stretch at approximately 3200 cm^{-1} , however, the absorptions expected for the alkyne $\text{C}\equiv\text{C}$ stretch were not observed. Therefore, to confirm the desired structures were obtained, crystals suitable for analysis by X-ray diffraction were grown by slow diffusion of either diethyl ether (for **96b**) or petroleum ether (**96c** and **96d**) into dichloromethane. The molecular structures are shown in Figures 5.17-19.

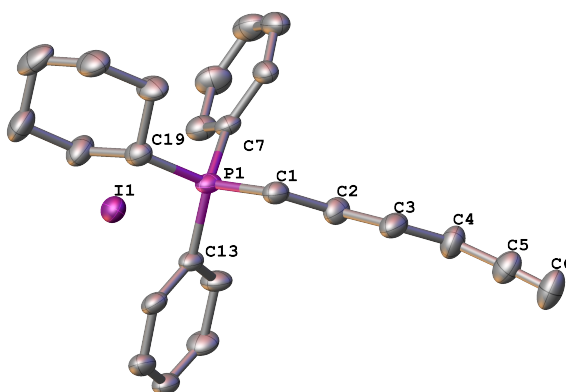


Figure 5.17 Molecular structure of **96b**. Hydrogen atoms have been omitted for clarity. Selected bond distances [Å] and angles [°]: P1-C1 1.810(5), P1-C7 1.797(5), P1-C13 1.803(4), P1-C19 1.823(5), C5-C6 1.174(8), C4-C5-C6 176.6(7).

The P1-C1 bond length of 1.810(5) Å and the alkyne C5-C6 bond length of 1.174(8) Å are in agreement with the data for **96a** which has previously been reported in the literature.⁴²

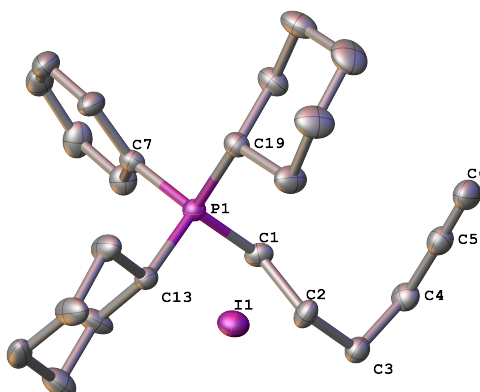


Figure 5.18 Molecular structure of **96c**. Hydrogen atoms have been omitted for clarity. Selected bond distances [Å] and angles [°]: P1-C1 1.795(6), P1-C7 1.796(6), P1-C13 1.814(6), P1-C19 1.821(6), C5-C6 1.174(9), C4-C5-C6 178.6(7).

The P1-C1 bond length of 1.795(6) Å and the alkyne C5-C6 bond length of 1.174(9) Å are consistent with the data for **96a** which has previously been reported in the literature.⁴²

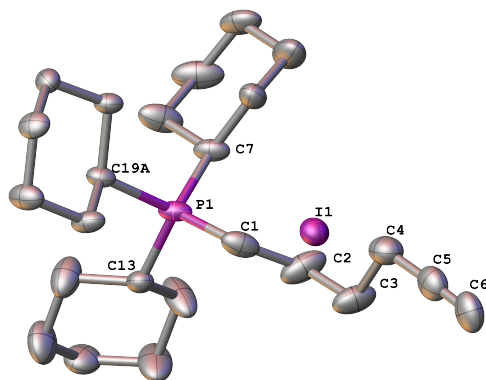
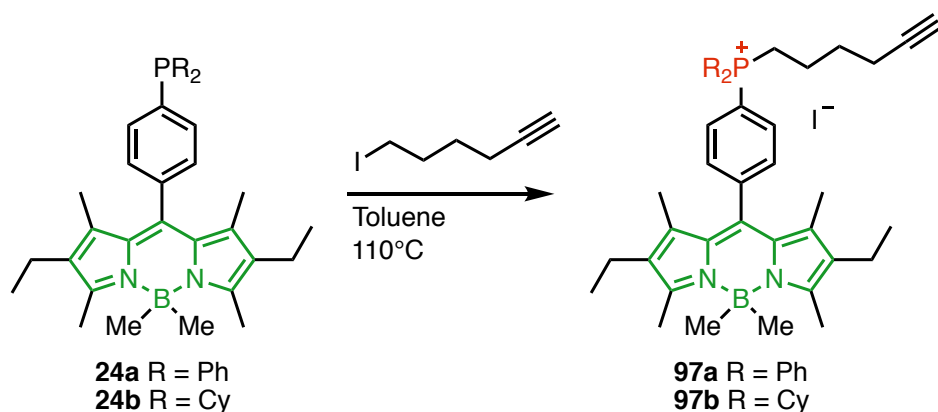


Figure 5.19 Molecular structure of **96d**. Hydrogen atoms have been omitted for clarity. Selected bond distances [Å] and angles [°]: P1-C1 1.804(4), P1-C7 1.817(3), P1-C13 1.821(3), P1-C19A 1.891(6), C5-C6 1.197(6), C4-C5-C5 177.7(5).

The P1-C1 bond length of 1.804(4) Å and the alkyne C5-C6 bond length of 1.197(6) Å is comparable to **96b** and **96c** and is consistent with the analogue **96a** which has been reported in the literature.⁴²

5.9.3 Synthesis of Fluorescent Alkynyl Phosphonium Salts (**97a** and **97b**)

Following the successful synthesis of a library of alkynyl phosphonium salts, the next step was to translate this to a fluorescent tertiary phosphine to afford a fluorescent phosphonium salt suitable for click chemistry. Thus, the Bodipy tertiary phosphines **24a** and **24b** were reacted with 1-iodo-6-hexyne in refluxing toluene, overnight (Scheme 5.17). On analysis of the crude reaction mixture by $^{31}\text{P}\{^1\text{H}\}$ NMR spectroscopy, a major resonance was observed at δ 24.9 ppm for the diphenyl phosphine derivative and at δ 33.1 ppm for the dicyclohexyl phosphine analogue, indicating the successful formation of the desired phosphonium salts **97a** and **97b** respectively.



Scheme 5.17 The synthesis of fluorescent hexyne-functionalised phosphonium salts **97a** and **97b** from fluorescent tertiary phosphines **24a** and **24b** respectively, with 1-iodo-6-hexyne in refluxing toluene overnight.

On further analysis of the novel phosphonium salts **97a** and **97b**, new chemical shifts consistent with the alkyl chain were observed in the ^1H NMR spectra, and a triplet indicative of the terminal alkynyl proton was observed in each spectrum, at δ 1.98 ppm ($^4J_{\text{HH}} = 6.6$ Hz) for **97a** and at δ 1.95 (t, $^4J_{\text{HH}} = 2.6$ Hz, 1H) for **97b**. The presence of an alkyne moiety could also be seen in the $^{13}\text{C}\{^1\text{H}\}$ NMR spectra from the two chemical shifts at δ 83.7 and δ 71.8 ppm for **97a** and at δ 83.4 and δ 69.7 ppm for **97b**. Furthermore, absorptions corresponding to the alkyne C-H stretch were observed at $\tilde{\nu} = 3306\text{ cm}^{-1}$ and 3308 cm^{-1} for **97a** and **97b** respectively and, in addition, those corresponding to the alkyne $\text{C}\equiv\text{C}$ stretch were seen at $\tilde{\nu} = 2189\text{ cm}^{-1}$ and 2192 cm^{-1} for **97a** and **97b** respectively. In both cases, analysis by mass spectrometry displayed peaks corresponding to the molecular ions $[\text{M}]^+$ ($m/z = 637.3238$ for **97a** and 649.4942 for **97b**) confirming the formation of the desired products.

In addition, crystals of **97a** suitable for analysis by X-ray diffraction were grown by slow evaporation of a saturated diethyl ether solution. The molecular structure is shown in Figure 5.20 and has been compared to the analogous hex-5-yn-1-yltriphenylphosphonium iodide structure reported in the literature.⁴² The $\text{C}\equiv\text{C}$ alkyne bond length was reported as 1.118 \AA in the literature, in comparison to $1.178(14)\text{ \AA}$ for the fluorescent analogue **97a**. Both structures showed a slightly distorted linear geometry across the alkyne bond: C28-C29-C30 $177.9(11)^\circ$ for **97a** and 177.51° for the non-fluorescent analogue.

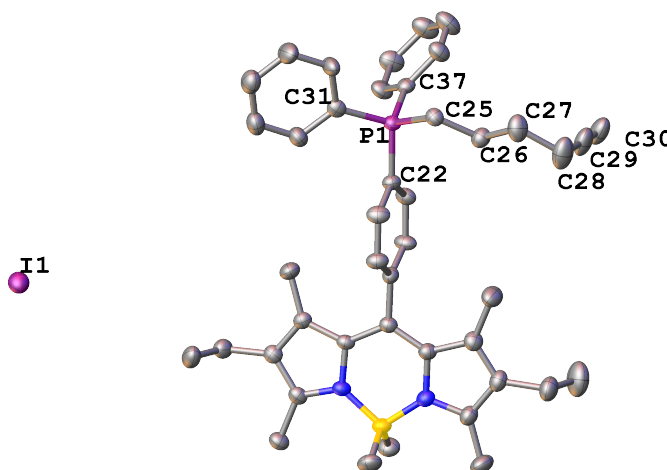


Figure 5.20 Molecular structure of **97a**. Hydrogen atoms have been omitted for clarity. Selected bond distances [\AA] and angles [$^\circ$]: P1-C22 1.805(6), P1-C25 1.804(7), P1-C31 1.789(8), P1-C37 1.803(7), C28-C29 1.455(14), C29-C30 1.178(14), C25-P1-C22 $107.7(3)$, C31-P1-C22 $108.7(4)$, C37-P1-C22 $111.1(3)$, C28-C29-C30 $177.9(11)$.

5.10 Photophysical Data

Following the successful synthesis and purification of the alkyne functionalised phosphonium salts **97a** and **97b**, their photophysical properties were determined to ensure the salts would be suitable in fluorescence cell imaging. Thus, photophysical measurements were collected

for **97a** and **97b**. Measurements were taken in dry degassed tetrahydrofuran in all cases to minimise photobleaching and phosphine oxidation in solution. The data is shown in Table 5.1 alongside their respective tertiary phosphine precursors **24a** and **24b**.

Table 5.1 Photophysical data for tertiary phosphines **24a**, **24b**, and their corresponding hexyne functionalised phosphonium salts **97a** and **97b**.

	λ_{abs} (nm) ^a	λ_{em} (nm) ^a	$\Phi_F^{\text{a,b}}$	ϵ (M ⁻¹ cm ⁻¹) ^a
BodPPh ₂ 24a ⁴³	513	527	0.29	92,000
BodPCy ₂ 24b ⁴³	512	526	0.44	82,000
[BodPPh ₂ (hexyne)]I 97a	514	531	0.23	68,000
[BodPCy ₂ (hexyne)]I 97b	514	532	0.24	64,000

^a Measured in dry, degassed tetrahydrofuran at room temperature, dyes were excited at 485 nm; ^b Fluorescence quantum yields were measured with respect to 4,4-difluoro-8-phenyl-1,3,5,7-tetramethyl-2,6-diethyl-4-bora-3a,4a-diaza-s-indacene.

Both the phosphonium salts, **97a** and **97b**, show typical Bodipy absorption profiles with a maxima at 514 nm which corresponds to the S₀-S₁ (π - π^*) transition and is assigned to the Bodipy core. The molar extinction coefficients lowered for the phosphonium salts **97a** and **97b** (ϵ = 68,000 and 64,000 M⁻¹ cm⁻¹ respectively) from 92,000 for **24a** and 82,000 M⁻¹ cm⁻¹ for **24b**. The absorption spectra for the tertiary phosphines **24a** and **24b** and their corresponding hexyne phosphonium salts **97a** and **97b** are shown in Figure 5.21.

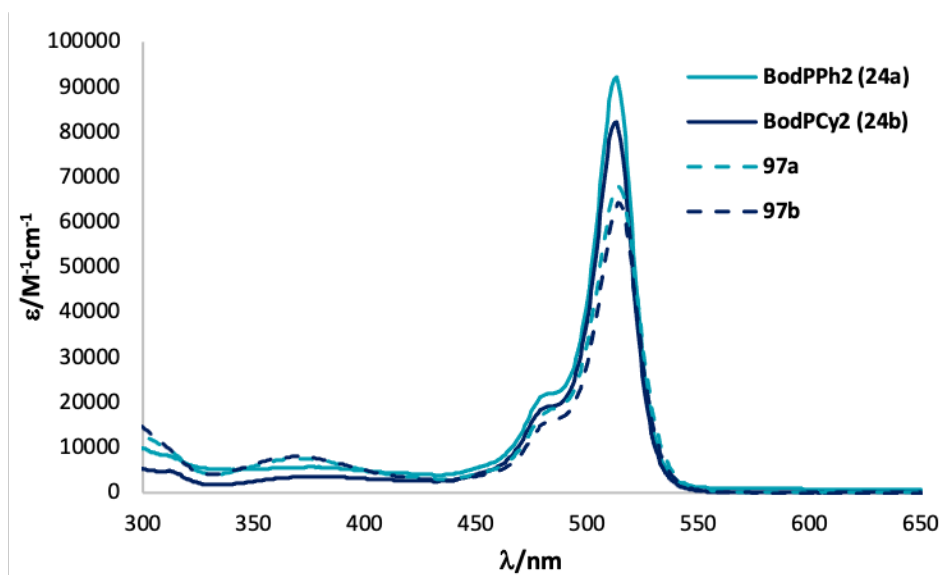


Figure 5.21 Absorption spectra of the tertiary phosphines, **24a** and **24b** and their respective hexyne functionalised phosphonium salts, **97a** and **97b**, in tetrahydrofuran at room temperature.

Fluorescence of the phosphonium salts **97a** and **97b** was detected at room temperature and the compounds displayed maxima at 531 nm and 532 nm, respectively (Figure 5.22). These maxima were slightly red shifted in comparison to their precursors which were observed at

527 nm for **24a** and 526 nm for **24b**. The fluorescence quantum yields of the phosphonium salts **97a** ($\Phi_F = 0.23$) and **97b** ($\Phi_F = 0.24$) are slightly lower than those measured for the tertiary phosphines (**24a**: $\Phi_F = 0.29$, **24b**: $\Phi_F = 0.44$); nevertheless, the quantum yields are suitable for fluorescence optical imaging.⁴⁴

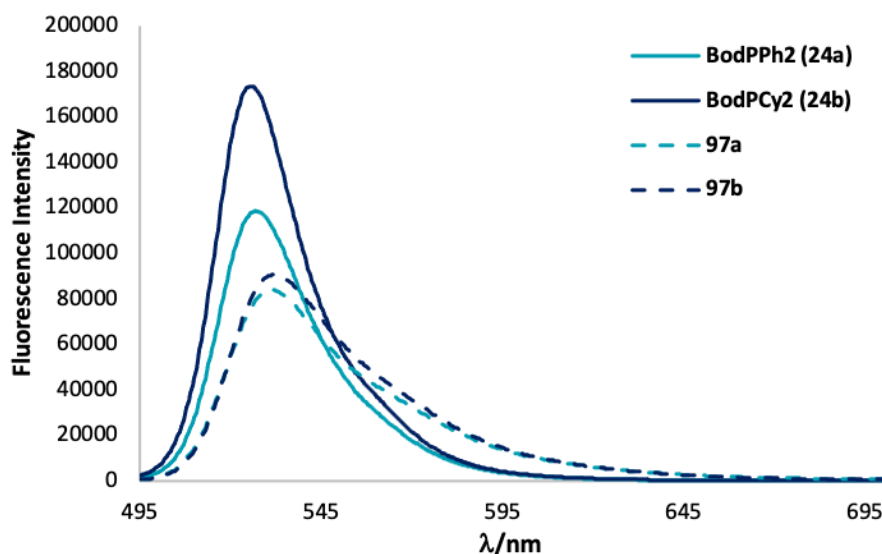


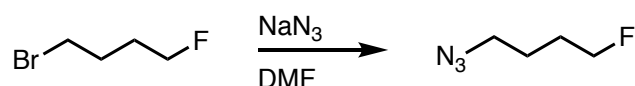
Figure 5.22 Emission spectra of the tertiary phosphines **24a** and **24b** and their respective hexyne functionalised phosphonium salts **97a** and **97b**, in tetrahydrofuran at room temperature (excitation at 485 nm).

This photophysical data confirms that phosphonium salts that possess suitable fluorescent properties required for optical imaging have been synthesised. Thus, these compounds bring the project in line with the original aim to synthesise a fluorescent, mitochondrial specific probe which has the potential to be radiolabelled. Having the alkyne functional group should allow for the addition of an ^{18}F radiolabel by a CuAAC click reaction, which would afford a trifunctional mitochondrial imaging agent suitable for combined optical and PET imaging.

5.11 Preliminary Copper-Catalysed Azide-Alkyne Cycloaddition Experiments

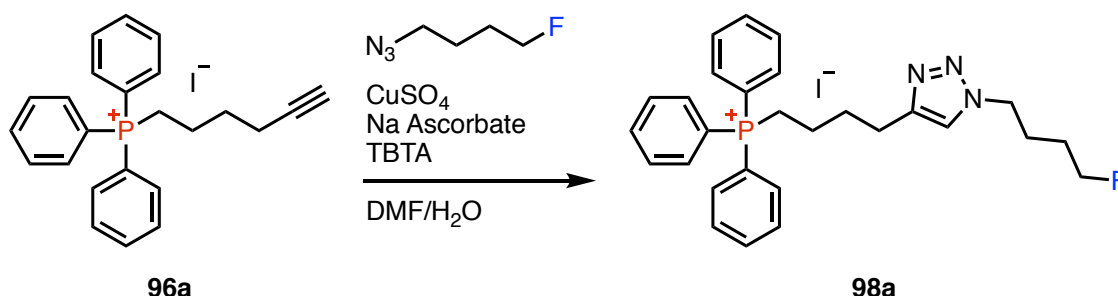
In an attempt to synthesise a cold standard to the radiolabelled imaging agent, we sought to synthesise a fluoroalkylazide which could be used to attach the fluoro moiety to the alkyne-functionalised phosphonium salt via a CuAAC click chemistry reaction.

Therefore, 1-bromo-4-fluorobutane was reacted with sodium azide in dimethylformamide at room temperature overnight (Scheme 5.18). The reaction afforded a white precipitate of sodium bromide, indicating the success of the reaction. Due to the explosive nature of azides,⁴⁵ the resulting 1-azido-4-fluorobutane was not isolated but instead was used for the following click reactions, without further purification.



Scheme 5.18 Synthesis of 1-azido-4-fluorobutane from the reaction of 1-bromo-4-fluorobutane with sodium azide in dimethylformamide.

The click reaction was first attempted with the simple triphenylphosphonium system to allow for the testing of the CuAAC click reaction conditions. Water and diethyl ether were added to the reaction mixture containing 1-azido-4-fluorobutane in dimethylformamide. The organic layer was then transferred via cannula to the phosphonium salt **96a** which had been suspended in water. To this reaction mixture, the click reagents: copper sulfate, sodium ascorbate and TBTA were added. Finally, to ensure all the reagents were in solution, additional dimethylformamide was added (Scheme 5.19).



Scheme 5.19 CuAAC of hex-5-yn-1-yltriphenylphosphonium iodide **96a** with 1-azido-4-fluorobutane to afford **98a**.

The reaction mixture was stirred overnight at room temperature, and the following day was analysed by $^{31}\text{P}\{^1\text{H}\}$ and $^{19}\text{F}\{^1\text{H}\}$ NMR spectroscopy. A single resonance was observed at δ 24.4 ppm in the $^{31}\text{P}\{^1\text{H}\}$ NMR spectrum and multiple resonances between δ –217 to –219 ppm in the $^{19}\text{F}\{^1\text{H}\}$ NMR spectrum, consistent with the occurrence of a reaction. To isolate and purify the product, the dimethylformamide was first removed by heating under vacuum. The resulting residue was then extracted with methanol and subsequently filtered, and the solvent removed *in vacuo*. Chloroform was added and the suspension was filtered to remove solid and the solvent was removed *in vacuo*. The resulting yellow oil was analysed by ^1H NMR spectroscopy where the presence of a peak at δ 7.92 ppm was observed, indicative of a triazole proton. Both the $^{31}\text{P}\{^1\text{H}\}$ and $^{19}\text{F}\{^1\text{H}\}$ NMR spectra showed single resonances which were split in the respective proton non-decoupled spectra; the ^{31}P NMR resonance splits into a multiplet and the ^{19}F NMR peak appears as a triplet of triplets ($^2J_{\text{FH}} = 47.5$ Hz, $^3J_{\text{FH}} = 25.9$ Hz). The $^1\text{H}\{^{31}\text{P}\}$ and $^1\text{H}\{^{19}\text{F}\}$ NMR spectra were recorded, and it became apparent that the fluorine atom was responsible for the doublet splitting in the doublet of triplets observed at δ 4.53 ppm; this signal displays as a single triplet in the $^1\text{H}\{^{19}\text{F}\}$ NMR spectrum. In addition, the

multiplet at δ 3.81–3.58 ppm showed a simpler splitting pattern in the $^1\text{H}\{^{31}\text{P}\}$ NMR spectrum consistent with this being the CH_2 adjacent to the phosphonium centre (Figure 5.23).

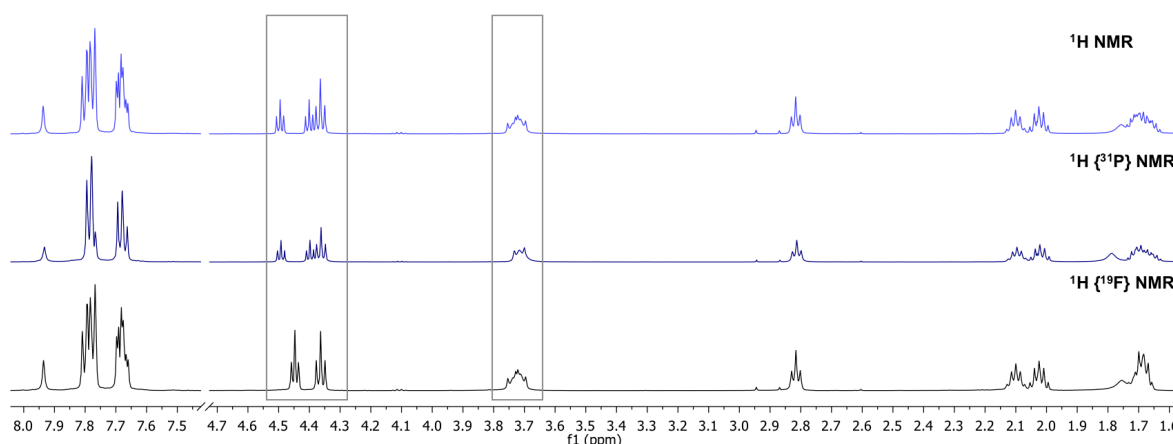
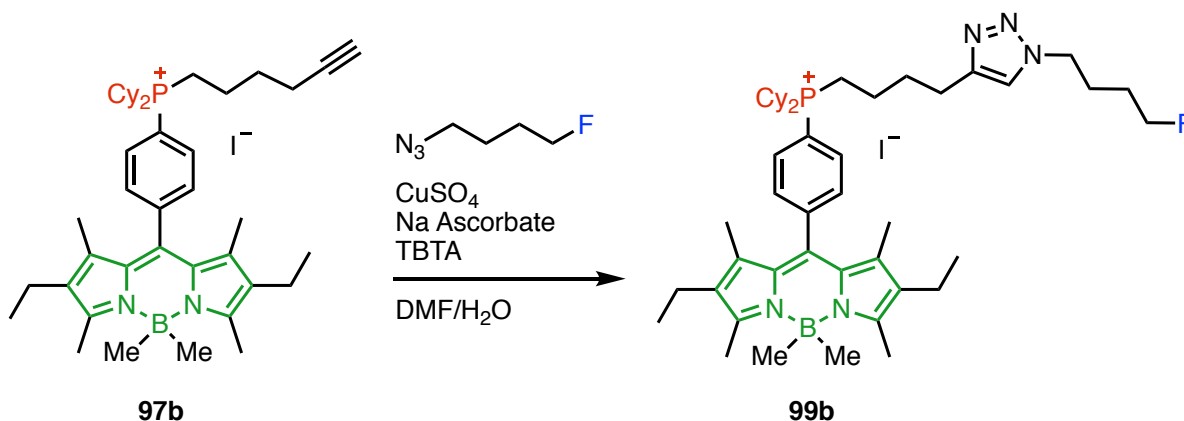


Figure 5.23 NMR studies to deduce the resonance corresponding the protons adjacent to the fluorine atom.

In addition, on analysis by mass spectrometry, a peak corresponding to the molecular ion $[\text{M}]^+$ was observed ($m/z = 460.2305$). Thus, all data supports the formation of the desired product.

Due to the success of this click reaction, the procedure was then transferred to the fluorescent analogue **97b**. In an analogous method to that used to synthesise **98a**, **97b** was subject to the CuAAC click reaction conditions. After overnight stirring at room temperature, the reaction mixture was analysed by $^{31}\text{P}\{^1\text{H}\}$ and $^{19}\text{F}\{^1\text{H}\}$ NMR spectroscopy. A major resonance was observed at δ 32.7 ppm in the $^{31}\text{P}\{^1\text{H}\}$ NMR spectrum and at δ –218.9 ppm in the $^{19}\text{F}\{^1\text{H}\}$ NMR spectrum, consistent with the data obtained for the non-fluorescent analogue **98a**. An analogous work-up to **98a** was carried out and the resulting crude product was analysed by mass spectrometry. This displayed a peak at m/z 766.5457 corresponding to the molecular ion $[\text{M}]^+$, confirming the success of the reaction. Given time constraints, this sample was not further purified and thus, full NMR spectroscopic characterisation could not be obtained.



Scheme 5.20 Reaction of **97b** with 1-azido-4-fluorobutane under CuAAC conditions gave **99b** as a cold-standard of a potential future radiolabelled product suitable for both optical and PET imaging.

Not only does the alkynyl motif allow for the addition of a radiolabel via click chemistry, it will also allow for the binding of bioactive species such as proteins and antibodies, opening up a route to a wide variety of new compounds. In a recent collaboration with Dr James Knight at Newcastle University, plans have been outlined to use this alkynyl phosphonium salt to fluorescently label antibodies.

5.12 Summary and Future Work

A fluorescent phosphonium salt **85a** was synthesised from a reaction of the Bodipy tertiary phosphine **24b** with 1-fluoro-4-bromobutane. This compound was successfully imaged in PDAC cells where it displayed localisation within the mitochondria. Initial studies were carried out to compare the uptake of salt **85a** in gemcitabine-resistant (R100) and non-resistant (NR) PDAC cell lines to test the MMP dependency of the salt. This highlighted differences in the MMP of the drug resistant and non-resistant cell lines.

An unsuccessful attempt by the Archibald group to substitute the alkyl fluorine for an ^{18}F radiolabel, directed the project towards the alteration of the phosphonium salt in order to aid in this substitution reaction. Thus, alternative halogen leaving groups with increased leaving group ability in comparison to fluorine were considered. Reaction conditions were optimised using triphenylphosphine and then translated to the fluorescent Bodipy system to afford **85b** and **85c**.

85b and **85c** were sent to the Archibald group and further attempts were made to substitute the halogen group with an ^{18}F radiolabel by direct exchange. Again, this proved unsuccessful, and efforts were refocused towards the synthesis of a probe suitable for click chemistry instead. The incorporation of an alkynyl moiety enables the application of these compounds in click chemistry and would also allow for the conjugation of bioactive molecules to these phosphonium salts.

A library of phosphonium salts with an alkynyl moiety were synthesised from non-fluorescent tertiary phosphines and three different alkylating agents. **89a** and **89c** using propargyl bromide, **95a-d** with 1-bromo-4-butyne and **96a-d** with 1-iodo-6-hexyne.

Once the procedure had been established for the alkylation of tertiary phosphines with an alkyne moiety, the method was translated to the fluorescent Bodipy backbone. **97a** and **97b** were synthesised from the reaction of fluorescent tertiary phosphines **24a** and **24b** with 1-iodo-6-hexyne, to afford two novel phosphonium salts suitable for click chemistry. The compounds were characterised by NMR spectroscopy, IR spectroscopy and mass

spectrometry. In addition, crystals of **97a** suitable for analysis by X-ray crystallography were grown and the structure determined.

To test the CuAAC click chemistry reaction conditions, a simple alkyl azide was synthesised and a preliminary click reaction was tested using the triphenylphosphonium system. The reaction successfully resulted in the 1,2,3-triazole **98a** which was fully characterised. This click reaction was then translated to the fluorescent Bodipy system and **97b** was subject to CuAAC click chemistry reaction conditions. The success of this reaction was confirmed by high resolution mass spectrometry in which a peak corresponding to the molecular ion of **99b** was observed. In addition, **99b** was partially characterised by NMR spectroscopy.

In an attempt to radiolabel these phosphonium salts by CuAAC click chemistry, samples of **95a**, **95c**, **96a**, **96c**, **97a** and **97b**, have been sent to Professor Steve Archibald at the University of Hull where radiolabelling experiments will be carried out with an ^{18}F -PEG-azide. If successful, this would result in a multimodal imaging agent containing i) a fluorescent Bodipy core to enable fluorescence imaging, ii) a phosphonium cation to target the mitochondria and iii) an ^{18}F radiolabel for application in PET imaging.

5.13 Experimental Procedures and Analytical Data

5.13.1 General Procedure

All air- and/or water-sensitive reactions were performed under a nitrogen atmosphere using standard Schlenk line techniques. Tetrahydrofuran was distilled over sodium/benzophenone, toluene over sodium, dichloromethane over calcium hydride and *d*-chloroform over phosphorus pentoxide; all solvents were distilled prior to use. All other chemicals were purchased from Sigma Aldrich, Fisher Scientific, Alfa Aesar or Fluorochem and used as received. Flash chromatography was performed on silica gel from Fluorochem (silica gel, 40–63 μ , 60 Å). Thin-layer chromatography was performed on Fisher aluminium-based plates with silica gel and fluorescent indicator (254 nm). ^1H , $^{13}\text{C}\{^1\text{H}\}$, $^{31}\text{P}\{^1\text{H}\}$, and $^{11}\text{B}\{^1\text{H}\}$ NMR spectra were recorded on a Bruker Avance III 300 MHz (^1H 300.13 Hz), Bruker Avance II 400 MHz (^1H 399.78 MHz) or Bruker Avance III HD 500 MHz (^1H 500.16 MHz) spectrometer at room temperature (21 °C) using the indicated solvent as internal reference; ^1H and ^{13}C shifts were relative to tetramethylsilane, ^{31}P relative to 80% H_3PO_4 , and ^{11}B relative to $\text{BF}_3\cdot\text{Et}_2\text{O}$. IR spectra were recorded on a Varian 800 FT-IR spectrometer and mass spectrometry was carried out by the EPSRC National Mass Spectrometry Service Centre, Swansea or the SAgE Mass Spectrometry Facility (Newcastle University) performed by Dr Rachael Dack and Dr Alex Charlton. The X-ray crystallographic data were collected on an Xcalibur, Atlas, Gemini ultra diffractometer equipped with a fine-focus sealed X-ray tube ($\lambda_{\text{CuK}\alpha} = 1.54184$ Å) and an Oxford Cryosystems CryostreamPlus open-flow N_2 cooling device. The analysis of the X-ray diffraction data of the compounds was performed by Dr Paul Waddell (Newcastle University).

5.14 Cell Imaging Studies of **85a** in Pancreatic Ductal Adenocarcinoma Cells

This work was carried out in the School of Engineering, Bioengineering, at the University of California, San Diego in Professor Peter (Yingxiao) Wang's lab.

5.14.1 Cell Culture

Cell culture reagents were purchased from Thermo Fisher Scientific. The murine pancreatic cancer cells (LSL-Trp53^{R172H/+}) were cultured in Dulbecco's Modified Eagle's Medium (DMEM) (Thermo Fisher Scientific, Cat. No. 11995073), supplemented with 10% (v/v) fetal bovine serum (FBS) (Thermo Fisher Scientific, Cat. No. 10438026), 100 units/mL of penicillin and 100 $\mu\text{g}/\text{mL}$ of streptomycin, at 37 °C with 5% CO_2 . The R100 murine pancreatic cancer cells (LSL-Trp53^{R172H/+} 100 nM gemcitabine resistant) were cultured in the same media with the addition of gemcitabine hydrochloride (final concentration of 100 nM), at 37 °C with 5% CO_2 .

5.14.2 Cell Plating for Microscopy

The murine pancreatic cancer cells were cultured in a glass bottom dish (Cell E&G) coated with 20 µg/mL fibronectin for 16-20 hours before imaging. The cells were then incubated in starvation medium (DMEM 0.5% FBS) with phenol red at 37 °C for 30 min, washed twice using PBS, and maintained in the starvation medium (DMEM with 0.5% FBS) for image acquisition.

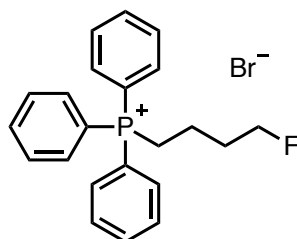
5.14.3 Image Acquisition and Analysis

Cell imaging was done using a Nikon ECLIPSE-Ti microscope equipped with a charge-coupled device (CCD) camera, a unique Perfect Focus System (PFS) that automatically corrects focus drift in real time during a prolonged period of time-lapse imaging, as well as a 420DF20 excitation filter, a 450DRLP dichroic mirror, and two emission filters controlled by a filter changer (480DF30 for ECFP and 535DF35 for YPet). Time-lapse fluorescence images were acquired at 5-minute intervals by MetaMorph 7.8.6.0 software (Molecular Devices, Sunnyvale, California). The ECFP and FRET images were processed and quantified by in-house developed image analysis software package Fluocell, which is developed in MATLAB. The Fluocell source code and documents for Windows and Mac systems can be downloaded from Github (<http://github.com/lu6007/fluocell>). All the ECFP and FRET images were background-subtracted and smoothed with a median filter defined by a 3 × 3 pixel size window. The pixelwise ECFP/FRET ratio images were then calculated and visualized with the intensity modified display (IMD) method, before being subjected to quantification and analysis by Excel.

5.15 General Procedure for the Synthesis of the Triphenylphosphonium Salts **88a-c**

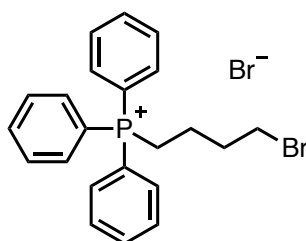
Triphenylphosphine (0.24 mmol) was dissolved in the appropriate dihaloalkane (1.20 mmol) and heated to 100 °C for 1.5 hours. The resulting product was washed with diethyl ether and dried *in vacuo*. Samples suitable for analysis by X-ray diffraction were obtained by the slow diffusion of diethyl ether into a dichloromethane solution of the salt.

5.15.1 (4-Fluorobutyl)triphenylphosphonium bromide (**88a**)



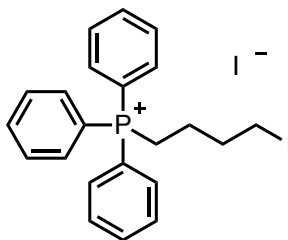
88a (82 mg, 80%). $^1\text{H NMR}$ (400 MHz, CDCl_3) δ 7.92–7.66 (m, 15H), 4.54 (dt, $^2J_{\text{HF}} = 47.5$, $^3J_{\text{HH}} = 5.3$ Hz, 2H), 4.10–3.97 (m, 2H), 2.27–2.12 (m, 2H), 1.87–1.75 (m, 2H) ppm; $^{13}\text{C}\{^1\text{H}\}$ NMR (75 MHz, CDCl_3) δ 135.1 (d, $J_{\text{CP}} = 3.0$ Hz), 133.8 (d, $J_{\text{CP}} = 10.0$ Hz), 130.6 (d, $J_{\text{CP}} = 12.6$ Hz), 118.4 (d, $^1J_{\text{CP}} = 86.0$ Hz), 83.0 (d, $^1J_{\text{CF}} = 164.1$ Hz), 30.5 (d, $^2J_{\text{CP}} = 17.2$ Hz), 22.6, 21.9 ppm; $^{31}\text{P}\{^1\text{H}\}$ NMR (162 MHz, CDCl_3) δ 24.6 ppm; $^{19}\text{F}\{^1\text{H}\}$ NMR (282 MHz, CDCl_3) δ –221.5; IR (neat): $\tilde{\nu} = 2888$ (w), 1587 (w), 1486 (w), 1436 (m), 1111 (s), 761 (s), 751 (s), 736 (m), 721 (s), 689 (s) cm^{-1} . These spectroscopic data are in agreement with literature values.⁴⁶

5.15.2 (4-Bromobutyl)triphenylphosphonium bromide (**88b**)



88b (82 mg, 70%). $^1\text{H NMR}$ (400 MHz, CDCl_3) δ 7.90–7.68 (m, 15H), 3.94–3.83 (m, 2H), 3.55 (pseudo-t, $^3J_{\text{HH}} = 6.0$ Hz, 2H), 2.34–2.22 (m, 2H), 1.81 (pseudo-p, $^3J_{\text{HH}} = 7.9$ Hz, 2H); $^{13}\text{C}\{^1\text{H}\}$ NMR (101 MHz, CDCl_3) δ 135.1 (d, $J_{\text{CP}} = 3.0$ Hz), 133.9 (d, $J_{\text{CP}} = 10.1$ Hz), 130.6 (d, $J_{\text{CP}} = 12.5$ Hz), 118.2 (d, $^1J_{\text{CP}} = 82.8$ Hz), 32.3, 31.7 (d, $^2J_{\text{CP}} = 17.6$ Hz), 30.8, 20.6 ppm; $^{31}\text{P}\{^1\text{H}\}$ NMR (162 MHz, CDCl_3) δ 24.7 ppm; IR (neat): $\tilde{\nu} = 2885$ (w), 2862 (w), 1587 (w), 1485 (w), 1436 (m), 1108 (s), 767 (m), 749 (m), 735 (s), 721 (s), 689 (s) cm^{-1} . These spectroscopic data are in agreement with literature values.⁴⁷

5.15.3 (4-Iodobutyl)triphenylphosphonium iodide (**88c**)

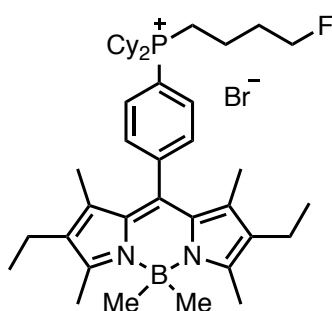


88c (95 mg, 69%). $^1\text{H NMR}$ (400 MHz, CDCl_3) δ 7.91–7.67 (m, 15H), 3.90–3.80 (m, 2H), 3.35 (pseudo-t, $^3J_{\text{HH}} = 6.1$ Hz, 2H), 2.23 (pseudo-q, $^3J_{\text{HH}} = 6.5$ Hz, 2H), 1.80 (dt, $^2J_{\text{HP}} = 15.4$ Hz, $^3J_{\text{HH}} = 7.7$ Hz, 2H) ppm; $^{13}\text{C}\{^1\text{H}\}$ NMR (101 MHz, CDCl_3) δ 135.3 (d, $J_{\text{CP}} = 3.0$ Hz), 133.9 (d, $J_{\text{CP}} = 10.0$ Hz), 130.7 (d, $J_{\text{CP}} = 12.5$ Hz), 118.2 (d, $^1J_{\text{CP}} = 86.0$ Hz), 32.9 (d, $^2J_{\text{CP}} = 17.0$ Hz), 23.7, 20.1, 8.1 ppm; $^{31}\text{P}\{^1\text{H}\}$ NMR (162 MHz, CDCl_3) δ 24.7 ppm; IR (neat): $\tilde{\nu} = 2889$ (w), 2856 (w), 1586 (w), 1483 (w), 1434 (m), 1106 (m), 748 (m), 722 (s), 6889 (vs) cm^{-1} . These spectroscopic data are in agreement with literature values.²⁷

5.16 General Procedure for the Synthesis of the Halobutane Phosphonium Salts **85a-c**

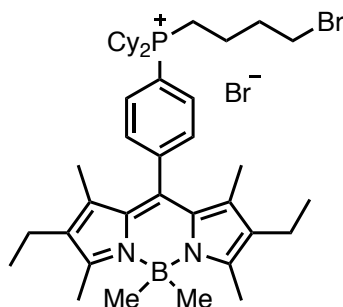
The synthesis of the phosphonium salts **85a**, **85b** and **85c** was carried out by Dr Jennifer F. Wallis or Miss Rosie Dalton. Bodipy dicyclohexylphosphine **24b** (0.27 mmol) was dissolved in anhydrous toluene (7 mL), the appropriate dihalogenated species (1.35 mmol) was added and the mixture heated to reflux (110 °C) until the complete consumption of the starting materials was observed by $^{31}\text{P}\{^1\text{H}\}$ NMR spectroscopy (*ca.* 16 hours). The desired product was crystallised out of solution using a layered mixture of deuterated chloroform and pentane.

5.16.1 8-((4-Dicyclohexylphosphino)(fluorobutyl)phenyl)-4,4-dimethyl-1,3,5,7-tetramethyl-2,6-diethyl-4-bora-3a,4a-diaza-s-indacene (**85a**)¹⁵



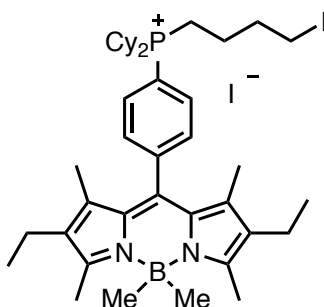
^1H NMR (300 MHz, CDCl_3) δ 8.09 (m, 2H), 7.70 (m, 2H), 4.65 (t, $^3J_{\text{HH}} = 5.2$ Hz, 2H), 4.50 (t, $^3J_{\text{HH}} = 5.2$ Hz, 2H), 3.20 (m 4H), 2.44 (s, 6H), 2.28 (q, $^3J_{\text{HH}} = 7.6$ Hz, 4H), 2.22–1.73 (m, 12H), 1.58–1.32 (m, 10H), 1.17 (s, 6H), 0.96 (t, $^3J_{\text{HH}} = 7.5$ Hz, 6H), 0.26 (s, 6H) ppm; $^{13}\text{C}\{^1\text{H}\}$ NMR (176 MHz, CDCl_3) δ 151.8, 144.4, 136.9, 133.4 (d, $J_{\text{CP}} = 7.5$ Hz), 133.4, 132.8, 131.3 (d, $J_{\text{CP}} = 11.4$ Hz), 128.4, 83.7, 82.8, 31.2, 30.4 (d, $J_{\text{CP}} = 43.5$ Hz), 26.6 (dd, $J_{\text{CF}} = 13.0$ Hz, $J_{\text{CP}} = 2.9$ Hz), 26.3, 25.6, 19.5, 17.5, 15.9 (d, $J_{\text{CP}} = 44.4$ Hz), 14.8, 14.5, 12.1, 10.4 (br) ppm; $^{31}\text{P}\{^1\text{H}\}$ NMR (121 MHz, CDCl_3) δ 32.6 ppm; $^{19}\text{F}\{^1\text{H}\}$ NMR (470 MHz, CDCl_3) δ -221.3 ppm; $^{11}\text{B}\{^1\text{H}\}$ NMR (96 MHz, CDCl_3) δ -0.4 ppm; HRMS (ESI⁺) calcd. for $\text{C}_{41}\text{H}_{62}\text{BFN}_2\text{P}$ [M]⁺ requires m/z 643.4722, found m/z 643.4719.

5.16.2 8-((4-Dicyclohexylphosphino)(bromobutyl)phenyl)-4,4-dimethyl-1,3,5,7-tetramethyl-2,6-diethyl-4-bora-3a,4a-diaza-s-indacene (**85b**)



^1H NMR (400 MHz, CDCl_3) δ 8.02–7.94 (m, 2H), 7.73–7.63 (m, 2H), 3.57 (pseudo-t, $^3J_{\text{HH}} = 5.1$ Hz, 1H), 3.37 (pseudo-t, $^3J_{\text{HH}} = 5.1$ Hz, 1H), 3.29–3.19 (m, 4H), 2.40 (s, 6H), 2.23 (q, $^3J_{\text{HH}} = 7.3$ Hz, 4H), 2.18–1.65 (m, 16H), 1.60–1.32 (m, 10H), 1.12 (s, 6H), 0.91 (t, $^3J_{\text{HH}} = 7.5$ Hz, 6H), 0.21 (s, 6H) ppm; **$^{13}\text{C}\{^1\text{H}\}$ NMR** (101 MHz, CDCl_3) δ 151.7, 144.3, 136.8, 133.4, 133.2, 132.6, 131.2, 128.3, 33.8, 32.5, 30.6, 30.0, 26.4, 26.2, 25.5, 19.5, 17.4, 15.6, 14.7, 14.4, 11.9, 10.4 (br) ppm; **$^{31}\text{P}\{^1\text{H}\}$ NMR** (162 MHz, CDCl_3) δ 33.0 ppm; **$^{11}\text{B}\{^1\text{H}\}$ NMR** (128 MHz, CDCl_3) δ –1.1 ppm; **IR** (neat): $\tilde{\nu}$ 2929, 2857, 1555, 1448, 1323, 1174, 946, 728, 640 cm^{-1} ; **HRMS** (ESI+) calcd. for $\text{C}_{41}\text{H}_{66}\text{BN}_2\text{P}$ $[\text{M}]^+$ requires m/z 705.3901, found m/z 705.3919.

5.16.3 8-((4-Dicyclohexylphosphino)(iodobutyl)phenyl)-4,4-dimethyl-1,3,5,7-tetramethyl-2,6-diethyl-4-bora-3a,4a-diaza-s-indacene (**85c**)



^1H NMR (400 MHz, CDCl_3) δ 8.00–7.93 (m, 2H), 7.69–7.64 (m, 2H), 3.33 (pseudo-t, $^3J_{\text{HH}} = 5.6$ Hz, 1H), 3.32 (pseudo-t, $^3J_{\text{HH}} = 5.1$ Hz, 1H), 3.16–2.90 (m, 4H), 2.39 (s, 6H), 2.23 (q, $^3J_{\text{HH}} = 7.6$ Hz, 4H), 1.96–1.72 (m, 16H), 1.58–1.29 (m, 10H), 1.12 (s, 6H), 0.91 (t, $^3J_{\text{HH}} = 7.5$ Hz, 6H), 0.21 (s, 6H) ppm; **$^{13}\text{C}\{^1\text{H}\}$ NMR** (101 MHz, CDCl_3) δ 151.9, 144.6, 135.3, 133.6 (d, $^1J_{\text{CP}} = 10.3$ Hz), 133.5, 133.4, 132.7, 131.4, 128.3, 33.9, 33.1 (d, $^2J_{\text{CP}} = 17.0$ Hz), 30.7, 30.3, 26.4, 26.2, 25.6, 17.5, 15.8, 14.8, 14.5, 12.2, 10.4 (br) ppm; **$^{31}\text{P}\{^1\text{H}\}$ NMR** (162 MHz, CDCl_3) δ 33.0 ppm; **$^{11}\text{B}\{^1\text{H}\}$ NMR** (128 MHz, CDCl_3) δ –19.3 ppm; **IR** (neat): $\tilde{\nu}$ 2930, 2857, 1552, 1443, 1320, 1171, 945, 801, 731, 674, 601 cm^{-1} .

5.17 Attempted ^{18}F -Radiolabelling Experiments by Direct Exchange

5.17.1 ^{18}F Generation

Cyclotron-produced ^{18}F -fluoride in H_2^{18}O was trapped on a weak anion SPE Cartridge (Sep-Pak Light QMA (Waters)), activated beforehand with 8.4% NaHCO_3 (5 mL), followed by water (20 mL) and finally air (20 mL). Trapped ^{18}F -Fluoride was eluted with 0.5 mL of K_2CO_3 (3.6 mg/mL) solution into a reaction vessel containing 10 mg of Kryptofix-222 in acetonitrile (1 mL) and the resulting ^{18}F - K_{222} complex was dried by azeotropic evaporation at 100 °C, under a gentle stream of argon.

5.17.2 Direct Exchange Experiments

Approximately 1 mg of the phosphonium salt (**85a**, **85b** or **85c**) was dissolved in anhydrous acetonitrile (0.5 mL) and added to the anhydrous ^{18}F - K_{222} (ca. 280 MBq) and the reaction vessel was heated at 80 °C. The reaction mixture was analysed at 5, 10, 20, 30 and 60-minute time points by radio-TLC on silica gel, developed in acetonitrile, or a mixture of dichloromethane/methanol/acetone 8:1:1 and confirmed by HPLC (ACE5, C18, 4.6*250 mm, 5A, 1 mL/min of 90% acetonitrile, 0.1%TFA). No radiolabelled product was detected at any time point.

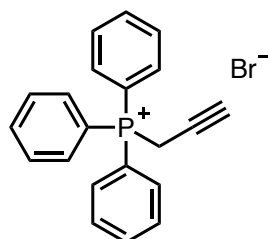
Approximately 5 mg of the phosphonium salt (**85a**, **85b** or **85c**) was dissolved in anhydrous DMF (0.5 mL) and added to the dry ^{18}F - K_{222} (ca. 130 MBq) and the reaction vessel was heated to 100 °C. The reaction mixture was then analysed as described above but no product was detected at any time point up to 60 minutes.

5.17.3 Attempted Two-step Radiolabelling with a ^{18}F -Bu-Br Prosthetic Group

The 1- ^{18}F -4-bromobutane (^{18}F -Bu-Br) prosthetic group was prepared from a 1,4-dibromobutane precursor, as described in Section 5.16.1, starting with 1500 MBq of ^{18}F - K_{222} and 10 μL of the dibromo precursor in acetonitrile (0.5 mL). This reaction mixture was heated at 90 °C for 20 minutes, followed by semi-preparative HPLC purification. To approximately 130 MBq of dried ^{18}F -Bu-Br, **24b** (0.3 mg) in anhydrous DMF (0.5 mL) was added. The reaction mixture was heated at 130 °C for 60 min and was analysed by radio-TLC and radio-HPLC as described above, but no radiolabelled product was detected at any time point.

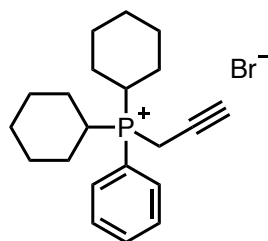
5.18 Synthesis of the Propyne Phosphonium Bromide Salts

5.18.1 Prop-2-yn-1-yltriphenylphosphonium bromide (**89a**)



Triphenylphosphine (5.00 g, 19.1 mmol) was added to a Schlenk flask and cycled three times between vacuum and nitrogen, before dissolving in anhydrous 1,4-dioxane (9 mL). To this stirred solution, hydrogen bromide (48%, 1.7 mL) was added dropwise, which resulted in the formation of a white precipitate. This suspension was stirred for one hour before the dropwise addition of propargyl bromide (80 wt% in toluene, 2.13 mL) in 1,4-dioxane (2.5 mL). This now homogenous solution was stirred overnight at room temperature. The following day, the resultant white precipitate was filtered off, washed with diethyl ether and dried *in vacuo* to afford **89a** as a white solid (4.46 g, 61%). ¹H NMR (300 MHz, DMSO-*d*₆) δ 7.98–7.90 (m, 3H), 7.89–7.76 (m, 12H), 5.14 (dd, ²J_{HP} = 16.6 Hz, ⁴J_{HH} = 2.8 Hz, 2H), 3.46 (dt, ⁴J_{HP} = 6.9 Hz, ⁴J_{HH} = 2.7 Hz, 1H) ppm; ¹³C{¹H} NMR (75 MHz, DMSO-*d*₆) δ 135.4 (d, *J*_{CP} = 3.1 Hz), 133.7 (d, *J*_{CP} = 10.2 Hz), 130.2 (d, *J*_{CP} = 12.7 Hz), 117.6 (d, *J*_{CP} = 87.3 Hz), 78.4 (d, ³*J*_{CP} = 9.8 Hz), 72.6 (d, ²*J*_{CP} = 12.7 Hz), 14.7 (d, ¹*J*_{CP} = 54.6 Hz) ppm; ³¹P{¹H} NMR (121 MHz, DMSO-*d*₆) δ 22.0 ppm; IR (neat): $\tilde{\nu}$ = 3149 (alkyne C-H), 2819 (w), 2741 (w), 1588 (w), 1484 (w), 1439 (m), 1322 (w), 1113 (m), 997 (w), 868 (w), 726 (s), 739 (s), 718 (s), 687 (s), 539 (s), 508 (s), 491 (s), 426 (m) cm⁻¹. These spectroscopic data are in agreement with literature values.³⁶

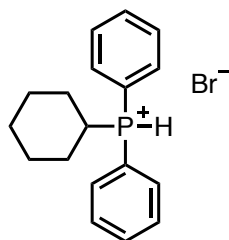
5.18.2 Prop-2-yn-1-ylcyclohexylphenylphosphonium bromide (**89c**)



Dicyclohexylphenylphosphine (0.27 g, 0.98 mmol) was added to a Schlenk flask and cycled three times between vacuum and nitrogen before dissolving in anhydrous 1,4-dioxane (0.5 mL). To this stirred solution, hydrogen bromide (48%, 0.1 mL) was added (no precipitate formed), and the reaction mixture was stirred for one hour before the dropwise addition of propargyl bromide (80 wt% in toluene, 0.1 mL) in 1,4-dioxane (0.2 mL). The reaction mixture

was stirred overnight at room temperature, unlike **89a**, no precipitate was observed. The solvent was removed *in vacuo* and purification was achieved by trituration with dichloromethane and diethyl ether to afford **89c** as a white solid (0.298 g, 77%). **¹H NMR** (300 MHz, DMSO-*d*₆) δ 8.12–7.95 (m, 2H), 7.94–7.45 (m, 3H), 4.26 (dd, ²*J*_{HP} = 14.7 Hz, ⁴*J*_{HH} = 2.8 Hz, 2H), 3.44 (dt, ⁴*J*_{HP} = 5.5 Hz, ⁴*J*_{HH} = 2.7 Hz, 1H), 3.19–3.00 (m, 2H), 2.12–1.97 (m, 2H), 1.92–1.54 (m, 8H), 1.52–1.26 (m, 8H), 1.22–0.99 (m, 2H) ppm; **¹³C{¹H} NMR** (75 MHz, DMSO-*d*₆) δ 134.6, 133.3 (d, *J*_{CP} = 8.0 Hz), 129.9 (d, *J*_{CP} = 11.8 Hz), 77.5 (d, ³*J*_{CP} = 8.7 Hz), 73.2, 28.9 (d, ²*J*_{CP} = 43.1 Hz), 26.9–24.1 (overlapping peaks), 6.5 (d, ¹*J*_{CP} = 50.5 Hz) ppm; **³¹P{¹H} NMR** (121 MHz, DMSO-*d*₆) δ 32.0 (s) ppm; **IR** (neat): $\tilde{\nu}$ = 3152 (alkyne C-H), 2930 (m), 2851 (m), 1437 (m), 1177 (w), 1113 (m), 1006 (w), 891 (w), 852 (w), 753 (s), 721 (m), 694 (s), 556 (m), 537 (m), 519 (s), 493 (m), 471 (m), 5410 (m) cm⁻¹; **HRMS** (TOF MS ES+) calcd for C₂₁H₃₀P⁺ [*M*⁺] 313.2080, found *m/z* 313.1710.

5.18.3 Cyclohexyldiphenylphosphonium bromide (**92**)



92 was isolated following the attempted synthesis of prop-2-yn-1-ylcyclohexyldiphenylphosphonium bromide (**89b**).

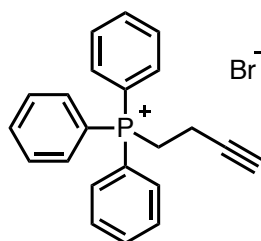
Cyclohexyldiphenylphosphine (0.10 g, 0.373 mmol) was added to a Schlenk flask and cycled three times between vacuum and nitrogen before dissolving in anhydrous 1,4-dioxane (1 mL). To this stirred solution, hydrogen bromide (48%, 0.1 mL) was added, and the reaction mixture was stirred for one hour before the dropwise addition of propargyl bromide (80 wt% in toluene, 0.1 mL) in 1,4-dioxane (0.5 mL). The reaction mixture was stirred overnight at room temperature and subsequently analysed by ³¹P{¹H} NMR spectroscopy which showed two peaks at δ 29.6 ppm and δ 10.4 ppm. Following an aqueous work up, and extraction with dichloromethane, the layers were separated, the organics were dried over MgSO₄, filtered and the solvent was removed from both layers. The organics were trituated with diethyl ether and on analysis of this solid by ³¹P{¹H} NMR spectroscopy, showed the major resonance at δ 2.4 ppm – likely starting material. On analysis of the aqueous layer by ³¹P{¹H} NMR spectroscopy, the major resonance was observed at δ 20.5 ppm. Crystallisations were set up

and crystals of **92** suitable for X-ray diffraction were obtained from slow diffusion of diethyl ether into a dichloromethane solution of **92**. $^{31}\text{P}\{^1\text{H}\}$ NMR (121 MHz, H_2O) δ 20.5 (s) ppm.

5.19 General Procedure for the Synthesis of the Butyne Phosponium Bromide Salts

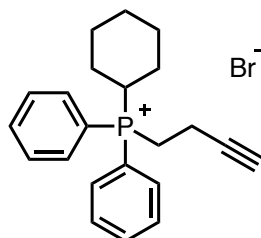
4-Bromo-1-butyne (1 eq) was added dropwise to a solution of tertiary phosphine (2 eq) in anhydrous toluene at 110 °C. The reaction mixture was stirred at reflux overnight by which time, precipitation of a white solid had occurred. The precipitate was filtered, washed with toluene and dried *in vacuo*.

5.19.1 But-3-yn-1-yltriphenylphosphonium bromide (**95a**)



Reacting 0.500 g (1.91 mmol) of triphenylphosphine with 0.10 mL (0.96 mmol) 4-bromo-1-butyne in 1 mL of toluene afforded **95a** as a white solid (0.221 g, 58%). ^1H NMR (300 MHz, $\text{DMSO}-d_6$) δ 8.00–7.68 (m, 15H), 3.99–3.84 (m, 2H), 3.00 (t, $^4J_{\text{HH}} = 2.7$ Hz, 1H), 2.62–2.52 (m, 2H) ppm; $^{13}\text{C}\{^1\text{H}\}$ NMR (75 MHz, $\text{DMSO}-d_6$) δ 135.5 (d, $J_{\text{CP}} = 3.0$ Hz), 134.2 (d, $J_{\text{CP}} = 10.3$ Hz), 130.7 (d, $J_{\text{CP}} = 12.5$ Hz), 118.4 (d, $J_{\text{CP}} = 86.1$ Hz), 81.5 (d, $J_{\text{CP}} = 17.4$ Hz), 74.5, 20.3 (d, $^1J_{\text{CP}} = 50.8$ Hz), 12.5 (d, $J_{\text{CP}} = 2.5$ Hz) ppm; $^{31}\text{P}\{^1\text{H}\}$ NMR (121 MHz, $\text{DMSO}-d_6$) δ 23.7 (s, 1P) ppm; IR (neat): $\tilde{\nu} = 3189$ (alkyne C-H), 3048 (w), 2888 (w), 2109 ($\text{C}\equiv\text{C}$), 1588 (w), 1435 (m), 1329 (w), 1112 (m), 946 (m), 798 (w), 732 (m), 685 (s), 556 (m), 503 (s) cm^{-1} ; HRMS (TOF MS ES^+) calcd for $\text{C}_{22}\text{H}_{20}\text{P}^+$ [M^+] 315.1297, found m/z 315.1799. These spectroscopic data are in agreement with literature values.³¹

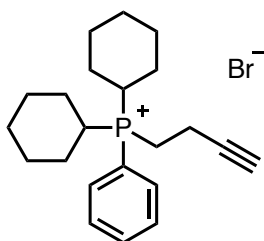
5.19.2 But-3-yn-1-ylcyclohexyldiphenylphosphonium bromide (**95b**)



Reacting 0.150 g (0.56 mmol) of cyclohexyldiphenylphosphine with 0.025 mL (0.28 mmol) 4-bromo-1-butyne in 0.5 mL of toluene afforded **95b** as a white solid (0.067 g, 60%). Crystals suitable for X-ray diffraction were formed by the slow diffusion of diethyl ether into a solution of **95b** in dichloromethane. ^1H NMR (300 MHz, $\text{DMSO}-d_6$) δ 7.95–7.83 (m, 6H), 7.82–7.72 (m,

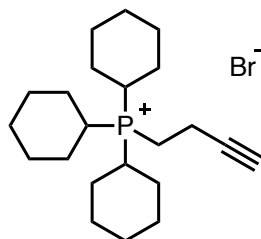
4H), 3.61–3.46 (m, 1H), 3.40 (dt, $^2J_{\text{HP}} = 12.3$ Hz, $^3J_{\text{HH}} = 7.4$ Hz, 2H), 2.99 ($^4J_{\text{HH}} = 2.6$ Hz, 1H), 2.31 (dtd, $^3J_{\text{HP}} = 14.5$ Hz, $^3J_{\text{HH}} = 7.4$ Hz, $^4J_{\text{HH}} = 2.7$ Hz, 2H), 2.05–1.92 (m, 2H), 1.78–1.57 (m, 4H), 1.55–1.38 (m, 2H), 1.10–0.86 (m, 2H) ppm; $^{13}\text{C}\{^1\text{H}\}$ NMR (75 MHz, DMSO- d_6) δ 134.8 (d, $J_{\text{CP}} = 3.0$ Hz), 133.9 (d, $J_{\text{CP}} = 9.1$ Hz), 129.9 (d, $J_{\text{CP}} = 11.9$ Hz), 115.3 (d, $J_{\text{CP}} = 80.6$ Hz), 81.0 (d, $J_{\text{CP}} = 14.5$ Hz), 73.6, 29.4 (d, $J_{\text{CP}} = 45.9$ Hz), 25.3–24.6 (overlapping peaks), 17.7 (d, $^1J_{\text{CP}} = 48.4$ Hz), 11.3 (d, $J_{\text{CP}} = 2.6$ Hz) ppm; $^{31}\text{P}\{^1\text{H}\}$ NMR (121 MHz, DMSO- d_6) δ 30.7 (s, 1P) ppm; IR (neat): $\tilde{\nu} = 3184$ (alkyne C-H), 3022 (w), 2926 (w), 2911 (w), 2877 (w), 2842 (w), 2115 (C \equiv C), 1589 (w), 1439 (m), 1328 (w), 1110 (m), 942 (w), 812 (m), 742 (s), 727 (s), 699 (s), 685 (s), 552 (s), 498 (s), 487 (s), 465 (s) cm^{-1} ; HRMS (TOF MS ES+) calcd. for $\text{C}_{22}\text{H}_{26}\text{P}^+$ [M] 321.1767, found m/z 321.2153.

5.19.3 But-3-yn-1-ylidicyclohexylphenylphosphonium bromide (**95c**)



Reacting 0.150 g (0.55 mmol) of dicyclohexylphenylphosphine with 0.025 mL (0.27 mmol) 4-bromo-1-butyne in 0.5 mL of toluene afforded **95c** as a white solid (0.064 g, 58%). Crystals suitable for X-ray diffraction were formed by the slow diffusion of diethyl ether into a solution of **95c** in dichloromethane. ^1H NMR (300 MHz, DMSO- d_6) δ 8.04–7.93 (m, 2H), 7.84 (m, 1H), 7.78–7.69 (m, 2H), 3.17 (t, $^4J_{\text{HH}} = 2.6$ Hz, 1H), 3.15–3.04 (m, 4H), 2.68 (m, 2H), 2.06–1.92 (m, 2H), 1.88–1.58 (overlapping peaks, 8H), 1.52–1.12 (overlapping peaks, 10H) ppm; $^{13}\text{C}\{^1\text{H}\}$ NMR (75 MHz, DMSO- d_6) δ 134.8 (d, $J_{\text{CP}} = 2.7$ Hz), 133.6 (d, $J_{\text{CP}} = 7.9$ Hz), 130.3 (d, $J_{\text{CP}} = 11.1$ Hz), 115.2 (d, $J_{\text{CP}} = 75.1$ Hz), 82.5 (d, $J_{\text{CP}} = 13.2$ Hz), 74.2, 29.1, 28.6, 26.2–25.1 (overlapping peaks), 14.4 (d, $^1J_{\text{CP}} = 44.9$ Hz), 12.4 (d, $J_{\text{CP}} = 3.0$ Hz) ppm; $^{31}\text{P}\{^1\text{H}\}$ NMR (121 MHz, DMSO- d_6) δ 32.7 (s, 1P) ppm; IR (neat): $\tilde{\nu} = 3187$ (alkyne C-H), 2933 (m), 2847 (m), 2110 (C \equiv C), 1449 (m), 1435 (m), 1311 (w), 1225 (w), 1009 (w), 853 (w), 802 (m), 742 (s), 709 (s), 695 (s), 552 (s) cm^{-1} ; HRMS (TOF MS ES+) calcd. for $\text{C}_{22}\text{H}_{32}\text{P}^+$ [M] 327.2236, found m/z 327.2535.

5.19.4 But-3-yn-1-yltricyclohexylphosphonium bromide (**95d**)

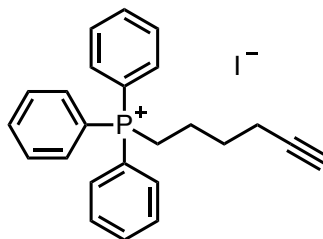


Reacting 0.150 g (0.53 mmol) of tricyclohexylphosphine with 0.024 mL (0.27 mmol) 4-bromo-1-butyne in 0.5 mL of toluene afforded **95d** as a white solid (0.063 g, 56%). Crystals suitable for X-ray diffraction were formed by the slow diffusion of diethyl ether into a solution of **95d** in dichloromethane. **¹H NMR** (300 MHz, DMSO-*d*₆) δ 3.18 (t, ⁴*J*_{HH} = 2.5 Hz, 1H), 1.94–1.84 (overlapping peaks, 8H), 1.84–1.73 (overlapping peaks, 9H), 1.73–1.61 (overlapping peaks, 4H), 1.60–1.19 (overlapping peaks, 16H) ppm; **¹³C{¹H} NMR** (75 MHz, DMSO-*d*₆) δ 82.2 (d, *J*_{CP} = 12.0 Hz), 73.4, 28.7 (d, *J*_{CP} = 40.4 Hz), 26.2, 25.7, 24.8, 13.6 (d, ¹*J*_{CP} = 42.4 Hz), 11.6 (d, *J*_{CP} = 2.8 Hz) ppm; **³¹P{¹H} NMR** (121 MHz, DMSO-*d*₆) δ 33.4 (s, 1P) ppm; **IR** (neat): $\tilde{\nu}$ = 3166 (alkyne C-H), 2931 (s), 2850 (s), 2107 (C≡C), 1448 (s), 1408 (m), 1308 (m), 1183 (m), 1006 (m), 849 (m), 743 (s), 667 (m), 482 (s) cm⁻¹; **HRMS** (TOF MS ES+) calcd for C₂₂H₃₈P⁺ [M] 333.2706, found *m/z* 333.3019.

5.20 General Procedure for the Synthesis of the Hexyne Phosphonium Iodide Salts

6-Iodo-1-hexyne (1 eq.) was added dropwise to a solution of the relevant tertiary phosphine (4 eq.) in anhydrous toluene at 75 °C. The reaction mixture was stirred overnight, in which time a white solid had precipitated. The precipitate was filtered, washed with toluene and dried *in vacuo*.

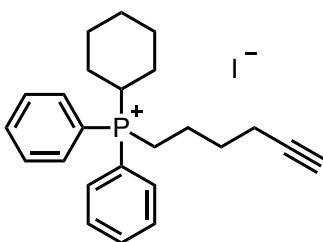
5.20.1 Hex-5-yn-1-yltriphenylphosphonium iodide (**96a**)



Reacting 0.50 g (1.91 mmol) of triphenylphosphine with 0.062 mL (0.48 mmol) 6-iodo-1-hexyne in 1 mL of toluene afforded **96a** as a white solid (0.181 g, 89%). **¹H NMR** (300 MHz, DMSO-*d*₆) δ 7.96–7.88 (m, 3H), 7.88–7.73 (m, 12H), 3.70–3.54 (m, 2H), 2.77 (t, ⁴*J*_{HH} = 2.6 Hz, 1H), 2.30–2.21 (m, 2H), 1.75–1.56 (overlapping peaks, 4H) ppm; **¹³C{¹H} NMR** (75 MHz, DMSO-*d*₆) δ 134.9 (d, *J*_{CP} = 3.0 Hz), 133.6 (d, *J*_{CP} = 10.1 Hz), 130.2 (d, *J*_{CP} = 12.4 Hz), 118.4 (d, *J*_{CP} = 85.7

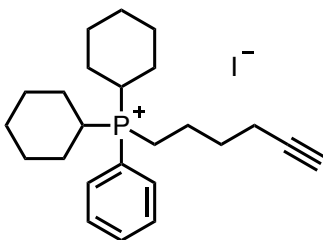
Hz), 83.7, 71.7, 28.5 (d, $J_{CP} = 17.4$ Hz), 20.7 (d, $J_{CP} = 4.0$ Hz), 19.6 (d, $^1J_{CP} = 50.3$ Hz), 16.8 ppm; $^{31}\text{P}\{^1\text{H}\}$ NMR (121 MHz, DMSO- d_6) δ 24.0 (s, 1P) ppm; IR (neat): $\tilde{\nu} = 3228$ (alkyne C-H), 2893 (w), 2858 (w), 1586 (w), 1435 (s), 1329 (w), 1192 (w), 1108 (s), 995 (m), 809 (m), 741 (m), 734 (s), 719 (s), 686 (s), 616 (w), 552 (m) cm^{-1} ; HRMS (TOF MS ES+) calcd. for $\text{C}_{24}\text{H}_{24}\text{P}^+$ [M] 343.1610, found m/z 343.2189.

5.20.2 Hex-5-yn-1-ylcyclohexyldiphenylphosphonium iodide (**96b**)



Reacting 0.150 g (0.56 mmol) of cyclohexyldiphenylphosphine with 0.018 mL (0.14 mmol) 6-iodo-1-hexyne in 0.5 mL of toluene afforded **96b** as a white solid (0.043 g, 72%). Crystals suitable for X-ray diffraction were formed by the slow diffusion of diethyl ether into a solution of **96b** in dichloromethane. ^1H NMR (300 MHz, DMSO- d_6) δ 7.93–7.85 (m, 6H), 7.81–7.73 (m, 4H), 3.48 (dt, $^2J_{HP} = 14.3$ Hz, $^3J_{HH} = 10.3$ Hz, 1H), 3.07 (td, $^2J_{HP} = 12.6$ Hz, $^3J_{HH} = 7.5$ Hz, 2H), 2.72 (t, $^4J_{HH} = 2.6$ Hz, 1H), 2.19 (td, $^3J_{HH} = 6.9$, $^4J_{HH} = 2.7$ Hz, 2H), 2.03–1.90 (m, 2H), 1.71–1.33 (overlapping peaks, 10H), 1.13–0.93 (m, 2H) ppm; $^{13}\text{C}\{^1\text{H}\}$ NMR (75 MHz, DMSO- d_6) δ 134.7 (d, $J_{CP} = 3.1$ Hz), 133.7 (d, $J_{CP} = 8.9$ Hz), 129.9 (d, $J_{CP} = 11.8$ Hz), 116.0 (d, $J_{CP} = 80.2$ Hz), 83.6, 71.7, 29.3 (d, $^1J_{CP} = 46.8$ Hz), 28.2 (d, $J_{CP} = 16.3$ Hz), 25.3–24.7 (overlapping peaks), 20.1 (d, $J_{CP} = 4.0$ Hz), 17.3, 17.1, 16.7 ppm; $^{31}\text{P}\{^1\text{H}\}$ NMR (121 MHz, DMSO- d_6) δ 30.6 (s, 1P) ppm; IR (neat): $\tilde{\nu} = 3235$ (alkyne C-H), 3008 (w), 2946 (w), 2849 (w), 1586 (w), 1438 (m), 1432 (m), 1327 (w), 1114 (m), 994 (m), 868 (w), 749 (s), 757 (s), 696 (s), 667 (m), 551 (s), 512 (m), 475 (s) cm^{-1} ; HRMS (TOF MS ES+) calcd. for $\text{C}_{24}\text{H}_{30}\text{P}^+$ [M] 349.2080, found m/z 349.2666.

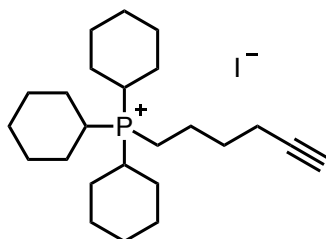
5.20.3 Hex-5-yn-1-ylcyclohexylphenylphosphonium iodide (**96c**)



Reacting 0.150 g (0.55 mmol) of dicyclohexylphenylphosphine with 0.018 mL (0.14 mmol) 6-iodo-1-hexyne in 0.5 mL of toluene afforded **96c** as a white solid (0.054 g, 88%). Crystals suitable for X-ray diffraction were formed by the slow diffusion of diethyl ether into a solution

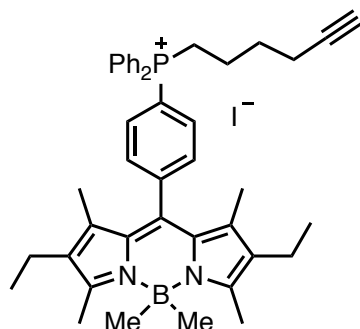
of **96c** in dichloromethane. ^1H NMR (300 MHz, DMSO- d_6) δ 8.02–7.91 (m, 2H), 7.84 (m, 1H), 7.79–7.70 (m, 2H), 3.08–3.89 (m, 2H), 2.85 (t, $^4J_{\text{HH}} = 2.6$ Hz, 1H), 2.82–2.70 (m, 2H), 2.36–2.24 (m, 2H), 2.05–1.91 (m, 2H), 1.85–1.60 (overlapping peaks, 12H), 1.41 (pseudo-q, $^3J_{\text{HH}} = 12.7$ Hz, 4H), 1.31–1.05 (m, 6H) ppm; $^{13}\text{C}\{^1\text{H}\}$ NMR (101 MHz, DMSO- d_6) δ 134.7, 133.6 (d, $J_{\text{CP}} = 7.6$ Hz), 130.3 (d, $J_{\text{CP}} = 11.0$ Hz), 115.0 (d, $J_{\text{CP}} = 74.8$ Hz), 83.9, 71.8, 28.8 (d, $J_{\text{CP}} = 15.2$ Hz), 28.3 (d, $^1J_{\text{CP}} = 44.5$ Hz), 25.8–24.6 (overlapping peaks), 20.9, 16.7, 13.9, 13.5 ppm; $^{31}\text{P}\{^1\text{H}\}$ NMR (121 MHz, DMSO- d_6) δ 32.5 (s, 1P) ppm; IR (neat): $\tilde{\nu} = 3202$ (alkyne C-H), 2926 (m), 2853 (m), 1444 (m), 1435 (s), 1109 (m), 996 (w), 855 (m), 759 (s), 696 (s), 559 (m) cm^{-1} ; HRMS (TOF MS ES+) calcd. for $\text{C}_{24}\text{H}_{36}\text{P}^+$ [M] 355.2551, found m/z 355.3093.

5.20.4 Hex-5-yn-1-yltricyclohexylphosphonium iodide (**96d**)



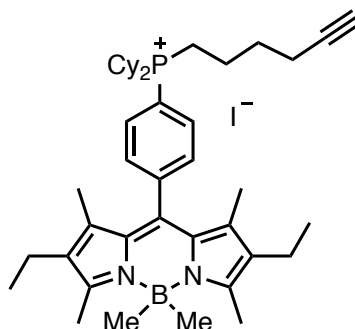
Reacting 0.150 g (0.53 mmol) of tricyclohexylphosphine with 0.018 mL (0.13 mmol) 6-iodo-1-hexyne in 0.5 mL of toluene afforded **96d** as a white solid (0.047 g, 82%). Crystals suitable for X-ray diffraction were formed by the slow diffusion of petroleum ether into a solution of **96d** in dichloromethane. ^1H NMR (300 MHz, DMSO- d_6) δ 2.85 (t, $^4J_{\text{HH}} = 2.5$ Hz, 1H), 2.61–2.43 (overlapping peaks, 4H), 2.32–2.21 (overlapping peaks, 4H), 2.00–1.19 (overlapping peaks, 33H) ppm; $^{13}\text{C}\{^1\text{H}\}$ NMR (75 MHz, DMSO- d_6) δ 84.4, 72.3, 29.5–29.2 (overlapping peaks), 26.3, 25.4, 20.9 (d, $J_{\text{CP}} = 4.6$ Hz), 17.1, 14.1 (d, $^1J_{\text{CP}} = 43.7$ Hz) ppm; $^{31}\text{P}\{^1\text{H}\}$ NMR (121 MHz, DMSO- d_6) δ 32.9 (s, 1P) ppm; IR (neat): $\tilde{\nu} = 3231$ (alkyne C-H), 2934 (s), 2854 (s), 1444 (s), 1331 (w), 1176 (m), 1122 (w), 1045 (w), 895 (m), 854 (s), 764 (w), 692 (s) cm^{-1} ; HRMS (TOF MS ES+) calcd. for $\text{C}_{24}\text{H}_{42}\text{P}^+$ [M] 361.3019, found m/z 361.3611.

5.20.5 8-((4-Diphenylphosphino)(hex-5-yn-1-yl)phenyl)-4,4-dimethyl-1,3,5,7-tetramethyl-2,6-diethyl-4-bora-3a,4a-diaza-s-indacene iodide (**97a**)



6-Iodo-1-hexyne (0.023 mL, 0.18 mmol) was added dropwise to a solution of **24a** (0.100 g, 0.18 mmol) in anhydrous toluene (1 mL) at 110 °C. The reaction was monitored by $^{31}\text{P}\{^1\text{H}\}$ NMR spectroscopy until the complete consumption of the starting materials was observed by $^{31}\text{P}\{^1\text{H}\}$ NMR spectroscopy (after *ca.* 16 hours). On completion of the reaction, the solvent was removed *in vacuo* to afford a dark orange solid. The resulting solid was triturated with pentane to afford an orange solid. Crystals suitable for X-ray diffraction were formed by the slow evaporation of a solution of **97a** in diethyl ether. ^1H NMR (300 MHz, CDCl_3) δ 8.01–7.79 (m, 8H), 7.79–7.66 (m, 6H), 3.92–3.69 (m, 2H), 2.37 (s, 6H), 2.24 (q, $^3J_{\text{HH}} = 7.5$ Hz, 4H), 1.98 (t, $^4J_{\text{HH}} = 6.6$ Hz, 1H), 1.98–1.64 (m, 2H), 1.67–1.50 (m, 2H), 1.41–1.21 (m, 2H), 1.19 (s, 6H), 0.90 (t, $^3J_{\text{HH}} = 7.5$ Hz, 6H), 0.20 (s, 6H) ppm; $^{13}\text{C}\{^1\text{H}\}$ NMR (75 MHz, CDCl_3) δ 151.0, 135.1, 134.2 (d, $J_{\text{CP}} = 10.1$ Hz), 133.5 (d, $J_{\text{CP}} = 10.1$ Hz), 132.9 (d, $J_{\text{CP}} = 19.9$ Hz), 131.5 (d, $J_{\text{CP}} = 9.7$ Hz), 130.8, 130.3 (d, $J_{\text{CP}} = 12.4$ Hz), 128.9, 127.8, 126.7, 118.9, 117.8, 83.7, 71.8, 32.0, 30.4, 20.8, 16.8, 14.6, 14.0, 11.7, 11.5, 10.4 ppm; $^{31}\text{P}\{^1\text{H}\}$ NMR (121 MHz, CDCl_3) δ 24.9 (s, 1P) ppm; IR (neat): $\tilde{\nu} = 3306$ (alkyne C-H), 2961 (m), 2929 (m), 2869 (m), 2189 ($\text{C}\equiv\text{C}$), 1549 (s), 1437 (s), 1320 (s), 1172 (s), 1112 (s), 946 (s), 801 (m), 727 (s) cm^{-1} . HRMS (TOF MS ES^+) calcd. for $\text{C}_{43}\text{H}_{51}\text{BN}_2\text{P}^+$ [M] 637.3890, found m/z 637.3238.

5.20.6 8-((4-Dicyclohexylphosphino)(hex-5-yn-1-yl)phenyl)-4,4-dimethyl-1,3,5,7-tetramethyl-2,6-diethyl-4-bora-3a,4a-diaza-s-indacene iodide (**97b**)

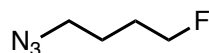


6-Iodo-1-hexyne (0.016 mL, 0.12 mmol) was added dropwise to a solution of **24b** (0.068 g, 0.12 mmol) in anhydrous toluene (1 mL) at 110 °C. The reaction was monitored by $^{31}\text{P}\{^1\text{H}\}$ NMR spectroscopy until the complete consumption of the starting materials was observed by $^{31}\text{P}\{^1\text{H}\}$ NMR spectroscopy (*ca.* 16 hours). On completion of the reaction, the solvent was removed *in vacuo* and the resulting solid was triturated with pentane to afford an orange solid. ^1H NMR (300 MHz, CDCl_3) δ 8.11 (m, 2H), 7.71 (m, 2H), 3.25–3.11 (m, 2H), 3.10–2.96 (m, 4H), 2.44 (s, 6H), 2.28 (q, $^3J_{\text{HH}} = 7.5$ Hz, 4H), 2.22–1.98 (m, 4H), 1.95 (t, $^4J_{\text{HH}} = 2.6$ Hz, 1H), 1.92–1.20 (m, 20H), 1.18 (s, 6H), 0.96 (t, $^3J_{\text{HH}} = 7.5$ Hz, 6H), 0.26 (s, 6H) ppm; $^{13}\text{C}\{^1\text{H}\}$ NMR (75 MHz, CDCl_3) δ 151.7, 144.3, 136.9, 133.8 (d, $J_{\text{CP}} = 7.7$ Hz), 131.3 (d, $J_{\text{CP}} = 11.0$ Hz), 128.4, 114.8 (d, $J_{\text{CP}} = 75.0$ Hz), 83.4, 69.7, 30.3 (d, $J_{\text{CP}} = 43.2$ Hz), 26.9–25.2 (overlapping peaks), 17.5, 14.8, 14.5, 12.1, 10.4 (br) ppm; $^{31}\text{P}\{^1\text{H}\}$ NMR (121 MHz, CDCl_3) δ 33.1 (s, 1P) ppm; IR (neat): $\tilde{\nu} = 3308$ (alkyne C-H), 2961 (m), 2929 (m), 2855 (m), 2192 ($\text{C}\equiv\text{C}$), 1796 (w), 1550 (s), 1448 (m), 1403 (m), 1320 (s), 1261 (m), 1172 (s), 1146 (s), 1111 (m), 1022 (m), 981 (s), 944 (s), 911 (m), 801 (s), 733 (m), 703 (m) cm^{-1} ; HRMS (TOF MS ES^+) calcd. for $\text{C}_{43}\text{H}_{63}\text{BN}_2\text{P}^+ [\text{M}]$ 649.4816, found m/z 649.4842.

5.21 General Procedure for the Copper-Catalysed Azide-Alkyne Cycloaddition³¹

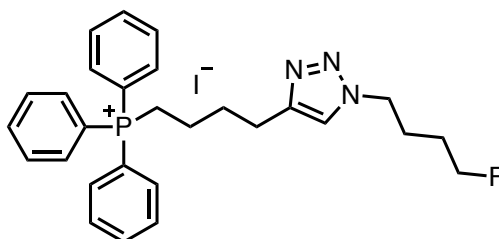
1-Azido-4-fluorobutane (1 eq) was added to the relevant hexyne functionalised phosphonium salt (**96a** or **97b**, 0.5 eq) which had been suspended in water, followed by the addition of CuSO₄ (0.05 eq), TBTA (0.06 eq) and sodium ascorbate (0.9 eq). To ensure all reagents were in solution, dimethylformamide (2 mL) was added. The reaction mixture was stirred overnight at room temperature and the resulting products were analysed by ³¹P{¹H} and ¹⁹F{¹H} NMR spectroscopy. The following day, the solvents were removed under reduced pressure and methanol was added. The suspension was transferred to a new Schlenk flask by cannula filtration to remove solid impurities, then the methanol was removed *in vacuo*. Chloroform was then added, and cannula filtration was carried out a second time to remove further solid impurities. The solvent was removed *in vacuo* to yield the desired product.

5.21.1 1-Azido-4-fluorobutane⁴⁸



1-Bromo-4-fluorobutane (0.1 mL, 1.00 mmol) was dissolved in dimethylformamide (0.5 mL) and sodium azide (0.098 g, 1.50 mmol) was added. The mixture was stirred overnight at room temperature by which time, a white precipitate had formed. The precipitate was dissolved in water (1 mL) and the desired product was extracted with diethyl ether (1 mL). The organic layer was used without further purification for the following CuAAC click reactions.

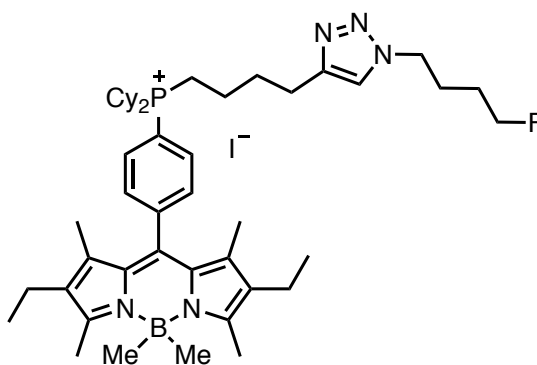
5.21.2 (4-(1-(4-Fluorobutyl)-1H-1,2,3-triazol-4-yl)butyl)triphenylphosphonium iodide (**98a**)



Afforded as a yellow oil (0.199 g, 68%). ¹H NMR (300 MHz, CDCl₃) δ 7.92 (s, 1H), 7.85–7.72 (m, 10H), 7.72–7.61 (m, 5H), 4.53 (dt, ²J_{HF} = 47.3 Hz, ³J_{HH} = 5.8 Hz, 2H), 4.36 (t, ³J_{HH} = 7.8 Hz, 2H), 3.81–3.58 (m, 2H), 2.82 (t, ³J_{HH} = 7.1 Hz, 2H), 2.05 (m, 4H), 1.80–1.56 (m, 4H) ppm; ¹³C{¹H} NMR (75 MHz, CDCl₃) δ 147.1, 135.2 (d, J_{CP} = 3.0 Hz), 133.8 (d, J_{CP} = 10.0 Hz), 130.6 (d, J_{CP} = 12.5 Hz), 128.8, 118.2 (d, J_{CP} = 85.9 Hz), 83.4 (d, J_{CF} = 165.2 Hz), 49.8, 29.7 (d, J = 16.9 Hz), 27.5 (d, J = 20.1 Hz), 26.6 (d, J = 4.6 Hz), 24.7, 22.7 (d, J = 50.1 Hz), 21.7 (d, J = 4.2 Hz) ppm; ³¹P{¹H} NMR (121 MHz, CDCl₃) δ 24.4 (s, 1P) ppm; ¹⁹F{¹H} NMR (282 MHz, CDCl₃) δ –218.9 (s, 1F) ppm; ¹⁹F NMR (282 MHz, CDCl₃) δ –218.9 (tt, ²J_{FF} = 47.5 Hz, ³J_{FF} = 25.9 Hz, 1F) ppm; IR (neat): $\tilde{\nu}$ =

3426 (br), 3055 (w), 2933 (w), 2867 (w), 1578 (w), 1438 (s), 1214 (w), 1112 (s), 1052 (m), 996 (w), 750 (m), 723 (s), 691 (s), 531 (s), 509 (m) cm^{-1} ; **MS** (TOF MS ES+) calcd for $\text{C}_{28}\text{H}_{32}\text{FN}_3\text{P}^+$ $[\text{M}]^+$ 460.2312, found m/z 460.2305.

5.21.3 8-((4-Dicyclohexylphosphino)phenyl)-4,4-dimethyl-1,3,5,7-tetramethyl-2,6-diethyl-4-bora-3a,4a-diaza-s-indacene(4-(1-(4-fluorobutyl)-1H-1,2,3-triazol-4-yl)butyl)phosphonium iodide (**99b**)



Afforded as a crude orange solid. $^{31}\text{P}\{^1\text{H}\}$ NMR (121 MHz, CDCl_3) δ 32.7 (s, 1P) ppm; ^{31}P NMR (121 MHz, CDCl_3) δ 33.7–31.6 (m, 1P) ppm; $^{19}\text{F}\{^1\text{H}\}$ NMR (282 MHz, CDCl_3) δ –218.9 (s, 1F) ppm; ^{19}F NMR (282 MHz, CDCl_3) δ –218.9 (tt, $^2J_{\text{FH}} = 47.1$ Hz, $^3J_{\text{FH}} = 25.9$ Hz, 1F) ppm; **IR** (neat): $\tilde{\nu}$ 2961 (w), 2929 (m), 2855 (w), 1550 (s), 1449 (m), 1404 (w), 1360 (m), 1320 (s), 1261 (s), 1172 (s), 1111 (s), 1018 (s), 945 (s), 910 (m), 800 (s), 699 (m), 673 (m) cm^{-1} ; **MS** (TOF MS ES+) calcd. for $\text{C}_{47}\text{H}_{71}\text{BFN}_5\text{P}^+$ $[\text{M}]^+$ 766.5519, found m/z 766.5485.

5.22 References

- 1 J. M. Perez Ortiz and R. H. Swerdlow, *Br. J. Pharmacol.*, 2019, **176**, 3489–3507.
- 2 S. H. Kwak, K. S. Park, K.-U. Lee and H. K. Lee, *J. Diabetes Investig.*, 2010, **1**, 161–169.
- 3 G. Kroemer, *Oncogene*, 2006, **25**, 4630–4632.
- 4 N. Hail, *Apoptosis*, 2005, **10**, 687–705.
- 5 D. C. Wallace, *Science*, 1999, **283**, 1482–1488.
- 6 J.-S. Park, R. L. Davis and C. M. Sue, *Curr. Neurol. Neurosci. Rep.*, 2018, **18**, 21.
- 7 M. P. Murphy, *Biochim. Biophys. Acta, Bioenerg.*, 2008, **1777**, 1028–1031.
- 8 D.-Y. Kim and J.-J. Min, *Nucl. Med. Mol. Imaging*, 2016, **50**, 185–195.
- 9 J. S. Modica-Napolitano and J. R. Aprile, *Adv. Drug Deliv. Rev.*, 2001, **49**, 63–70.
- 10 M. D. Forrest, *bioRxiv*, 2015, 25197.
- 11 M. Millard, D. Pathania, Y. Shabaik, L. Taheri, J. Deng and N. Neamati, *PLoS One*, 2010, **5**, e13131.
- 12 V. J. A. Jameson, H. M. Cochemé, A. Logan, L. R. Hanton, R. A. J. Smith and M. P. Murphy, *Tetrahedron*, 2015, **71**, 8444–8453.
- 13 Y. H. Shabaik, M. Millard and N. Neamati, *PLoS One*, 2013, **8**, e54346.
- 14 B. Kadenbach, R. Ramzan, R. Moosdorf and S. Vogt, *Mitochondrion*, 2011, **11**, 700–706.
- 15 S. Nigam, B. P. Burke, L. H. Davies, J. Domarkas, J. F. Wallis, P. G. Waddell, J. S. Waby, D. M. Benoit, A.-M. Seymour, C. Cawthorne, L. J. Higham and S. J. Archibald, *Chem. Commun.*, 2016, **52**, 7114–7117.
- 16 J. Zhao, J. Chen, S. Ma, Q. Liu, L. Huang, X. Chen, K. Lou and W. Wang, *Acta Pharm. Sin. B*, 2018, **8**, 320–338.
- 17 Cancer Research UK, <https://www.cancerresearchuk.org/health-professional/cancer-statistics/statistics-by-cancer-type/pancreatic-cancer/>, (accessed 19 May 2020).
- 18 P. E. Oberstein and K. P. Olive, *Therap. Adv. Gastroenterol.*, 2013, **6**, 321–337.
- 19 S. P. Pereira, L. Oldfield, A. Ney, P. A. Hart, M. G. Keane, S. J. Pandol, D. Li, W. Greenhalf, C. Y. Jeon, E. J. Koay, C. V. Almario, C. Halloran, A. M. Lennon and E. Costello, *Lancet Gastroenterol. Hepatol.*, 2020, **5**, 698–710.
- 20 R.-A. Hardie, E. van Dam, M. Cowley, T.-L. Han, S. Balaban, M. Pajic, M. Pinese, M. Iconomou, R. F. Shearer, J. McKenna, D. Miller, N. Waddell, J. V Pearson, S. M.

- Grimmond, L. Sazanov, A. V Biankin, S. Villas-Boas, A. J. Hoy, N. Turner and D. N. Saunders, *Cancer Metab.*, 2017, **5**, 2.
- 21 M. Hidalgo, *N. Engl. J. Med.*, 2010, **362**, 1605–1617.
- 22 S. A. Detmer and D. C. Chan, *Nat Rev Mol Cell Biol*, 2007, **8**, 870–879.
- 23 O. Jacobson, D. O. Kiesewetter and X. Chen, *Bioconjug. Chem.*, 2014, **26**, 1–18.
- 24 Z. Zhao, Q. Yu, T. Mou, C. Liu, W. Yang, W. Fang, C. Peng, J. Lu, Y. Liu and X. Zhang, *Mol. Pharm.*, 2014, **11**, 3823–3831.
- 25 D.-Y. Kim, H.-S. Kim, U. N. Le, S. N. Jiang, H.-J. Kim, K.-C. Lee, S.-K. Woo, J. Chung, H.-S. Kim, H.-S. Bom, K.-H. Yu and J.-J. Min, *J. Nucl. Med.*, 2012, **53**, 1779–1785.
- 26 D. O'Hagan, *Chem. Soc. Rev.*, 2008, **37**, 308–319.
- 27 T.-K. Lin, G. Hughes, A. Muratovska, F. H. Blaikie, P. S. Brookes, V. Darley-Usmar, R. A. J. Smith and M. P. Murphy, *J. Biol. Chem.*, 2002, **277**, 17048–17056.
- 28 M. Thelakkat, J. Ostrauskaite, A. Leopold, R. Bausinger and D. Haarer, *Chem. Phys.*, 2002, **285**, 133–147.
- 29 J. Wang, J. Zhang, B. Arbogast and C. S. Maier, *J. Am. Soc. Mass Spectrom.*, 2011, **22**, 1771.
- 30 Y. Fujiwara, J. Sun and G. C. Fu, *Chem. Sci.*, 2011, **2**, 2196–2198.
- 31 A. Haslop, A. Gee, C. Plisson and N. Long, *J. Label. Compd. Radiopharm.*, 2013, **56**, 313–316.
- 32 A. Haslop, L. Wells, A. Gee, C. Plisson and N. Long, *Mol. Pharm.*, 2014, **11**, 3818–3822.
- 33 J. C. Knight and B. Cornelissen, in *Radiopharmaceutical Chemistry*, eds. J. S. Lewis, A. D. Windhorst and B. M. Zeglis, Springer International Publishing, 2019, pp. 467–479.
- 34 H. J. Bestmann and R. Zimmermann, *Encycl. Reagents Org. Synth.*, 2001, 1–2.
- 35 K. Eiter and H. Oediger, *Justus Liebigs Ann. Chem.*, 1965, **682**, 62–70.
- 36 G. B. Bagdasaryan, P. S. Pogosyan, G. A. Panosyan and M. G. Indzhikyan, *Russ. J. Gen. Chem.*, 2008, **78**, 1177–1183.
- 37 A. L. Colebatch, I. A. Cade, A. F. Hill and M. M. Bhadbhade, *Organometallics*, 2013, **32**, 4766–4774.
- 38 N. Bricklebank, S. M. Godfrey, C. A. McAuliffe and R. G. Pritchard, *Acta Crystallogr. Sect. C*, 1993, **49**, 1017–1018.

- 39 M. Liras, J. Bañuelos Prieto, M. Pintado-Sierra, I. García-Moreno, Á. Costela, L. Infantes, R. Sastre and F. Amat-Guerri, *Org. Lett.*, 2007, **9**, 4183–4186.
- 40 M. Yu, J. K. H. Wong, C. Tang, P. Turner, M. H. Todd and P. J. Rutledge, *Beilstein J. Org. Chem.*, 2015, **11**, 37–41.
- 41 J. A. Arnott and S. L. Planey, *Expert Opin. Drug Discov.*, 2012, **7**, 863–875.
- 42 J. Luo, A. G. Oliver and J. Scott McIndoe, *Dalton Trans.*, 2013, **42**, 11312–11318.
- 43 L. H. Davies, R. W. Harrington, W. Clegg and L. J. Higham, *Dalton Trans.*, 2014, **43**, 13485–13499.
- 44 A. Kumar, How do you choose the right fluorophore?, <https://www.enzolifesciences.com/science-center/technotes/2018/august/how-do-you-choose-the-right-fluorophore?/>, (accessed 23 December 2020).
- 45 G. Evano, *Angew. Chemie Int. Ed.*, 2010, **49**, 6025–6025.
- 46 V. P. Prasad, S. Wagner, P. Keul, S. Hermann, B. Levkau, M. Schäfers and G. Haufe, *Bioorg. Med. Chem.*, 2014, **22**, 5168–5181.
- 47 P. C. Saha, T. Chatterjee, R. Pattanayak, R. S. Das, A. Mukherjee, M. Bhattacharyya and S. Guha, *ACS Omega*, 2019, **4**, 14579–14588.
- 48 A. Testa, S. Dall’Angelo, M. Mingarelli, A. Augello, L. Schweiger, A. Welch, C. S. Elmore, P. Sharma and M. Zanda, *Bioorg. Med. Chem.*, 2017, **25**, 963–976.

Chapter 6

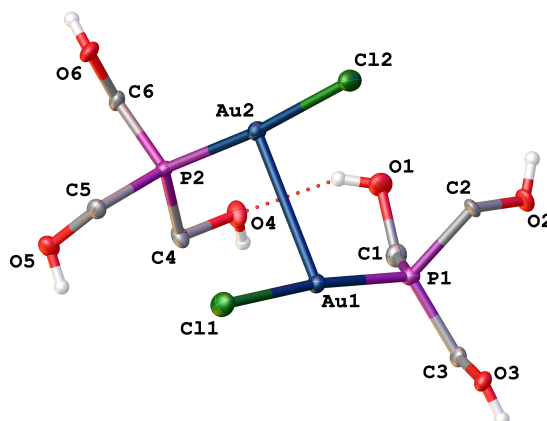
Appendices

Appendix I

X-Ray Crystallographic Data

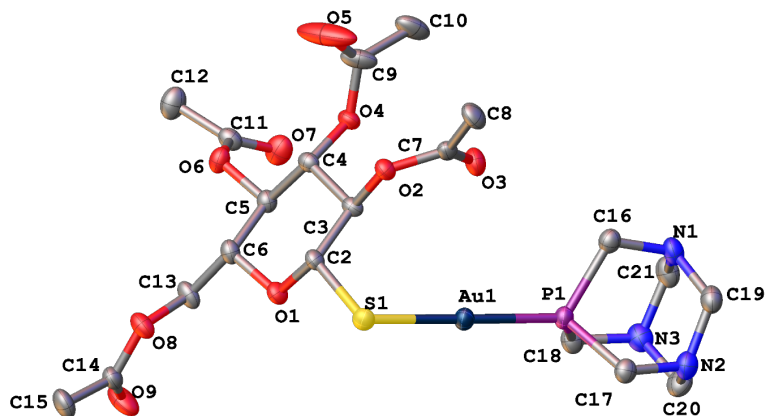
6.1 Chapter 2 X-ray Crystallographic Data

6.1.1 [Au(16g)Cl] (17g)



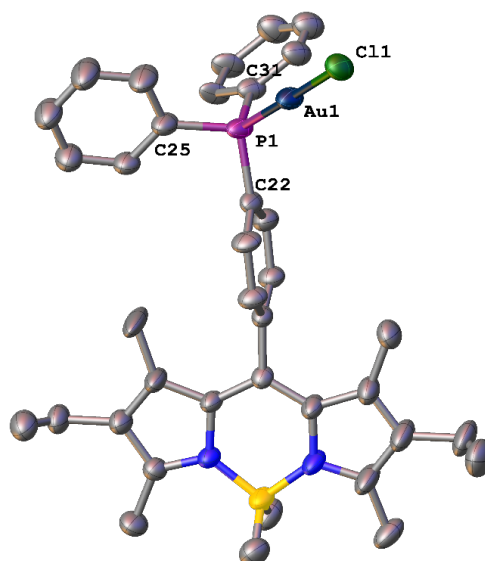
Identification code	ljh200005_3_fa
Empirical formula	C ₃ H ₉ AuClO ₃ P
Formula weight	356.49
Temperature/K	150.0(2)
Crystal system	tetragonal
Space group	P4 ₁
a/Å	8.04630(10)
b/Å	8.04630(10)
c/Å	23.2428(6)
α/°	90
β/°	90
γ/°	90
Volume/Å ³	1504.81(5)
Z	8
ρ _{calc} /cm ³	3.147
μ/mm ⁻¹	41.577
F(000)	1296.0
Crystal size/mm ³	0.22 × 0.16 × 0.09
Radiation	CuKα (λ = 1.54184)
2θ range for data collection/°	10.996 to 133.562
Index ranges	-9 ≤ h ≤ 9, -9 ≤ k ≤ 9, -27 ≤ l ≤ 27
Reflections collected	10908
Independent reflections	2674 [R _{int} = 0.0619, R _{sigma} = 0.0496]
Data/restraints/parameters	2674/127/170
Goodness-of-fit on F ²	1.055
Final R indexes [I ≥ 2σ (I)]	R ₁ = 0.0335, wR ₂ = 0.0764
Final R indexes [all data]	R ₁ = 0.0370, wR ₂ = 0.0791
Largest diff. peak/hole / e Å ⁻³	1.03/-0.89
Flack parameter	-0.06(3)

6.1.2 [Au(16f)SR] (18f)



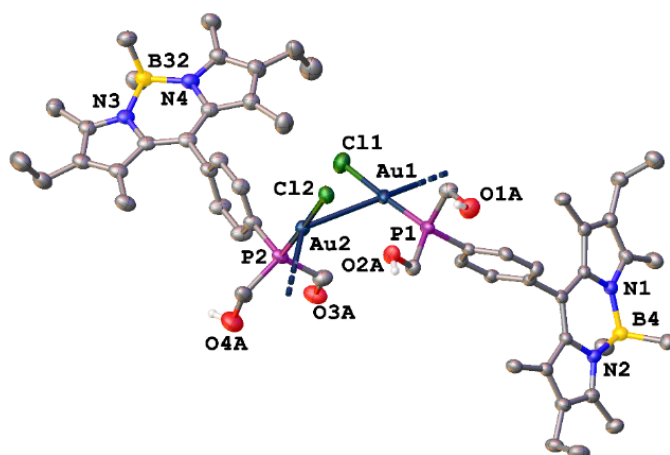
Identification code	ljh190006_fa
Empirical formula	C ₂₀ H ₃₁ AuN ₃ O ₉ PS
Formula weight	717.47
Temperature/K	150.0(2)
Crystal system	orthorhombic
Space group	P2 ₁ 2 ₁ 2 ₁
a/Å	7.25520(10)
b/Å	17.8111(3)
c/Å	19.8493(3)
α/°	90
β/°	90
γ/°	90
Volume/Å ³	2564.99(7)
Z	4
ρ _{calc} /cm ³	1.858
μ/mm ⁻¹	12.604
F(000)	1416.0
Crystal size/mm ³	0.41 × 0.06 × 0.04
Radiation	CuKα (λ = 1.54184)
2θ range for data collection/°	8.91 to 133.67
Index ranges	-8 ≤ h ≤ 8, -21 ≤ k ≤ 18, -23 ≤ l ≤ 23
Reflections collected	18371
Independent reflections	4541 [R _{int} = 0.0417, R _{sigma} = 0.0334]
Data/restraints/parameters	4541/282/320
Goodness-of-fit on F ²	1.045
Final R indexes [I ≥ 2σ (I)]	R ₁ = 0.0224, wR ₂ = 0.0492
Final R indexes [all data]	R ₁ = 0.0261, wR ₂ = 0.0510
Largest diff. peak/hole / e Å ⁻³	0.54/-0.63
Flack parameter	-0.032(8)

6.1.3 [Au(24a)Cl] (25a)



Identification code	ljh190003
Empirical formula	C ₃₇ H ₄₂ AuBClN ₂ P
Formula weight	788.92
Temperature/K	150.0(2)
Crystal system	orthorhombic
Space group	Pnma
a/Å	28.9698(6)
b/Å	8.6996(3)
c/Å	13.3119(3)
α/°	90
β/°	90
γ/°	90
Volume/Å ³	3354.94(15)
Z	4
ρ _{calc} /cm ³	1.562
μ/mm ⁻¹	9.629
F(000)	1576.0
Crystal size/mm ³	0.42 × 0.06 × 0.03
Radiation	CuKα (λ = 1.54184)
2θ range for data collection/°	7.308 to 134.278
Index ranges	-34 ≤ h ≤ 34, -10 ≤ k ≤ 10, -15 ≤ l ≤ 15
Reflections collected	45882
Independent reflections	3191 [R _{int} = 0.0545, R _{sigma} = 0.0179]
Data/restraints/parameters	3191/472/394
Goodness-of-fit on F ²	1.454
Final R indexes [I ≥ 2σ (I)]	R ₁ = 0.0534, wR ₂ = 0.0951
Final R indexes [all data]	R ₁ = 0.0600, wR ₂ = 0.0972
Largest diff. peak/hole / e Å ⁻³	0.81/-1.06

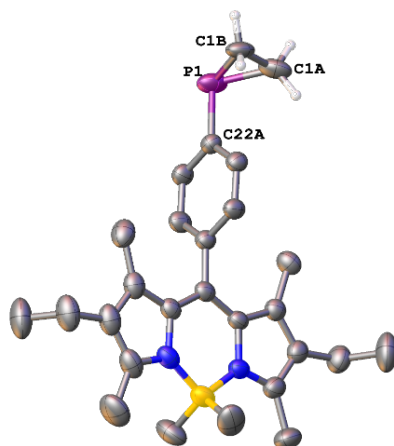
6.1.4 [Au(24d)Cl] (25d)



Identification code	ljh180037
Empirical formula	C ₅₄ H ₇₆ Au ₂ B ₂ Cl ₂ N ₄ O ₅ P ₂
Formula weight	1409.61
Temperature/K	100.0(2)
Crystal system	orthorhombic
Space group	Pbca
a/Å	11.7417(7)
b/Å	20.4489(12)
c/Å	47.312(3)
α/°	90
β/°	90
γ/°	90
Volume/Å ³	11359.8(12)
Z	8
ρ _{calc} /cm ³	1.648
μ/mm ⁻¹	4.944
F(000)	5600.0
Crystal size/mm ³	0.127 × 0.03 × 0.008
Radiation	Synchrotron (λ = 0.6889)
2θ range for data collection/°	3.338 to 51.218
Index ranges	-14 ≤ h ≤ 14, -25 ≤ k ≤ 25, -59 ≤ l ≤ 59
Reflections collected	123497
Independent reflections	11742 [R _{int} = 0.0778, R _{sigma} = 0.0468]
Data/restraints/parameters	11742/1052/802
Goodness-of-fit on F ²	1.217
Final R indexes [I ≥ 2σ (I)]	R ₁ = 0.0495, wR ₂ = 0.1082
Final R indexes [all data]	R ₁ = 0.0588, wR ₂ = 0.1119
Largest diff. peak/hole / e Å ⁻³	2.30/-1.91

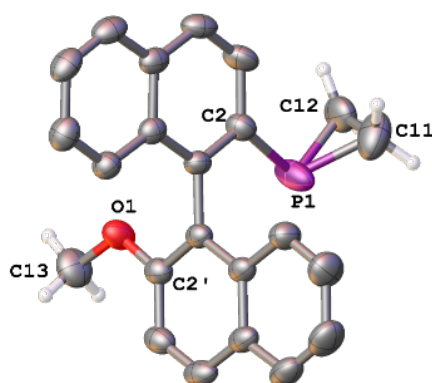
6.2 Chapter 3 X-ray Crystallographic Data

6.2.1 8-((4-Phosphirane)phenyl)-4,4-dimethyl-1,3,5,7-tetramethyl-2,6-diethyl-4-bora-3a,4a-diaza-s-indacene (47)



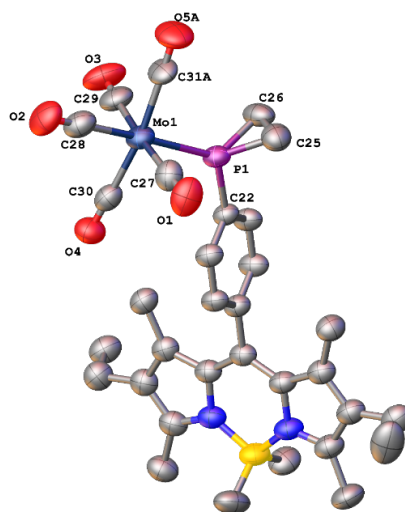
Identification code	ljh180033
Empirical formula	C ₂₇ H ₃₆ BN ₂ P
Formula weight	430.36
Temperature/K	200.0(2)
Crystal system	monoclinic
Space group	P2 ₁ /n
a/Å	8.2386(3)
b/Å	11.2137(4)
c/Å	26.6069(9)
α/°	90
β/°	91.089(3)
γ/°	90
Volume/Å ³	2457.65(14)
Z	4
ρ _{calc} /g/cm ³	1.163
μ/mm ⁻¹	1.093
F(000)	928.0
Crystal size/mm ³	0.27 × 0.18 × 0.01
Radiation	CuKα (λ = 1.54184)
2θ range for data collection/°	8.558 to 133.708
Index ranges	-9 ≤ h ≤ 9, -13 ≤ k ≤ 11, -31 ≤ l ≤ 31
Reflections collected	18143
Independent reflections	4356 [R _{int} = 0.0409, R _{sigma} = 0.0301]
Data/restraints/parameters	4356/37/324
Goodness-of-fit on F ²	1.109
Final R indexes [I ≥ 2σ (I)]	R ₁ = 0.0766, wR ₂ = 0.2039
Final R indexes [all data]	R ₁ = 0.0903, wR ₂ = 0.2145
Largest diff. peak/hole / e Å ⁻³	0.35/-0.59

6.2.2 (R)-1-(2'-Methoxy-1,1'-binaphthyl-2-yl)phosphirane (**32a**)



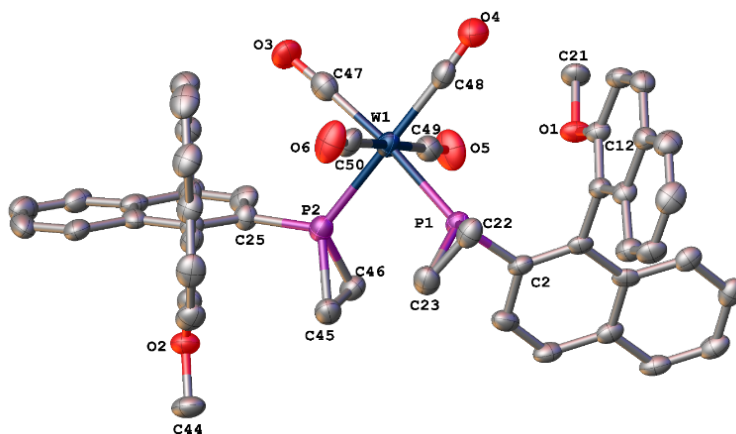
Identification code	ljh190005_2_fa
Empirical formula	C ₂₃ H ₁₉ OP
Formula weight	342.35
Temperature/K	150.0(2)
Crystal system	triclinic
Space group	P1
a/Å	7.9341(2)
b/Å	13.8312(4)
c/Å	16.2556(5)
α/°	90.078(2)
β/°	91.717(2)
γ/°	98.250(2)
Volume/Å ³	1764.58(9)
Z	4
ρ _{calc} /cm ³	1.289
μ/mm ⁻¹	1.420
F(000)	720.0
Crystal size/mm ³	0.15 × 0.1 × 0.06
Radiation	CuKα (λ = 1.54184)
2θ range for data collection/°	8.422 to 134.842
Index ranges	-9 ≤ h ≤ 9, -16 ≤ k ≤ 16, -19 ≤ l ≤ 19
Reflections collected	48480
Independent reflections	12123 [R _{int} = 0.0396, R _{sigma} = 0.0328]
Data/restraints/parameters	12123/933/932
Goodness-of-fit on F ²	1.023
Final R indexes [I ≥ 2σ (I)]	R ₁ = 0.0484, wR ₂ = 0.1244
Final R indexes [all data]	R ₁ = 0.0609, wR ₂ = 0.1337
Largest diff. peak/hole / e Å ⁻³	0.40/-0.36
Flack parameter	0.008(9)

6.2.3 [Mo(CO)₅(47)] (52a)



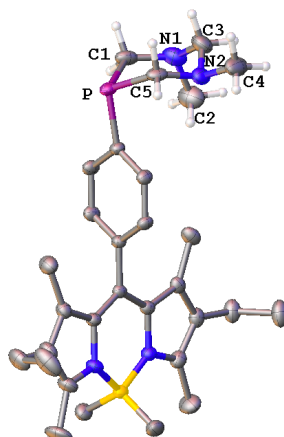
Identification code	ljh190022_fa
Empirical formula	C _{32.45} H _{36.45} BCl _{1.35} MoN ₂ O ₅ P
Formula weight	720.24
Temperature/K	150.0(2)
Crystal system	triclinic
Space group	P-1
a/Å	8.1775(4)
b/Å	14.8204(8)
c/Å	15.2531(7)
α/°	69.164(5)
β/°	85.743(4)
γ/°	87.296(4)
Volume/Å ³	1722.51(15)
Z	2
ρ _{calc} /g/cm ³	1.389
μ/mm ⁻¹	4.852
F(000)	740.0
Crystal size/mm ³	0.17 × 0.07 × 0.04
Radiation	CuKα (λ = 1.54184)
2θ range for data collection/°	7.162 to 133.504
Index ranges	-9 ≤ h ≤ 9, -17 ≤ k ≤ 17, -18 ≤ l ≤ 18
Reflections collected	24475
Independent reflections	6082 [R _{int} = 0.0589, R _{sigma} = 0.0448]
Data/restraints/parameters	6082/467/441
Goodness-of-fit on F ²	1.031
Final R indexes [I ≥ 2σ (I)]	R ₁ = 0.0431, wR ₂ = 0.1006
Final R indexes [all data]	R ₁ = 0.0604, wR ₂ = 0.1128
Largest diff. peak/hole / e Å ⁻³	0.87/-0.61

6.2.4 [W(CO)₄(32a)₂] (51b)



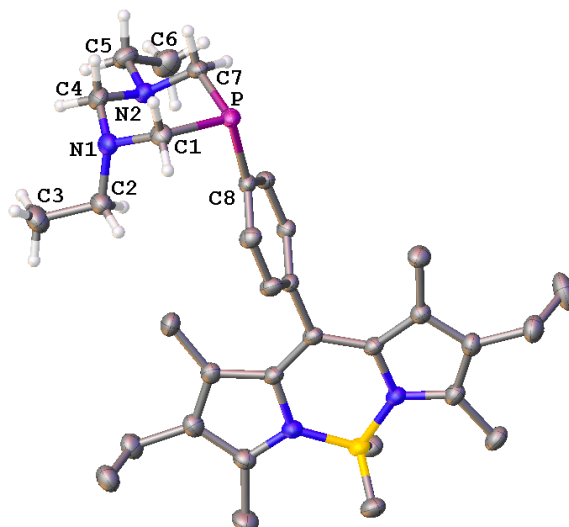
Identification code	ljh180038_fa
Empirical formula	C ₅₈ H ₅₈ O ₈ P ₂ W
Formula weight	1128.83
Temperature/K	150.0(2)
Crystal system	monoclinic
Space group	P2 ₁
a/Å	11.7532(2)
b/Å	8.3918(2)
c/Å	26.4488(4)
α/°	90
β/°	100.984(2)
γ/°	90
Volume/Å ³	2560.87(9)
Z	2
ρ _{calc} /cm ³	1.464
μ/mm ⁻¹	5.213
F(000)	1148.0
Crystal size/mm ³	0.17 × 0.04 × 0.03
Radiation	CuKα (λ = 1.54184)
2θ range for data collection/°	7.662 to 133.738
Index ranges	-13 ≤ h ≤ 13, -9 ≤ k ≤ 9, -31 ≤ l ≤ 27
Reflections collected	35490
Independent reflections	8799 [R _{int} = 0.0507, R _{sigma} = 0.0424]
Data/restraints/parameters	8799/1/628
Goodness-of-fit on F ²	1.051
Final R indexes [I ≥ 2σ (I)]	R ₁ = 0.0376, wR ₂ = 0.0893
Final R indexes [all data]	R ₁ = 0.0419, wR ₂ = 0.0919
Largest diff. peak/hole / e Å ⁻³	2.83/-0.62
Flack parameter	-0.036(6)

6.2.5 8-(4-(1,3-Dimethyl-1,3,5-diazaphosphinan-5-yl)phenyl)-4,4-dimethyl-1,3,5,7-tetramethyl-2,6-diethyl-4-bora-3a,4a-diaza-s-indacene (**62a**)



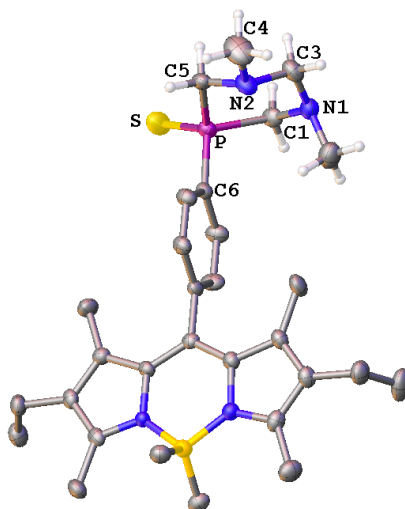
Identification code	publication
Empirical formula	C ₃₀ H ₄₄ BN ₄ P
Formula weight	502.47
Temperature/K	150.0(3)
Crystal system	monoclinic
Space group	P2 ₁
a/Å	12.1460(3)
b/Å	6.06240(10)
c/Å	20.2987(3)
α/°	90
β/°	104.2603(18)
γ/°	90
Volume/Å ³	1448.62(5)
Z	2
ρ _{calc} /g/cm ³	1.152
μ/mm ⁻¹	1.013
F(000)	544.0
Crystal size/mm ³	0.250 × 0.080 × 0.040
Radiation	Cu Kα (λ = 1.54184)
2θ range for data collection/°	7.51 to 146.178
Index ranges	-13 ≤ h ≤ 14, -7 ≤ k ≤ 7, -24 ≤ l ≤ 16
Reflections collected	9791
Independent reflections	5201 [R _{int} = 0.0314, R _{sigma} = 0.0494]
Data/restraints/parameters	5201/1/335
Goodness-of-fit on F ²	1.011
Final R indexes [I ≥ 2σ (I)]	R ₁ = 0.0402, wR ₂ = 0.0984
Final R indexes [all data]	R ₁ = 0.0444, wR ₂ = 0.1018
Largest diff. peak/hole / e Å ⁻³	0.17/-0.19
Flack parameter	0.01(2)

6.2.6 8-(4-(1,3-Diethyl-1,3,5-diazaphosphinan-5-yl)phenyl)-4,4-dimethyl-1,3,5,7-tetramethyl-2,6-diethyl-4-bora-3a,4a-diaza-s-indacene (**62b**)



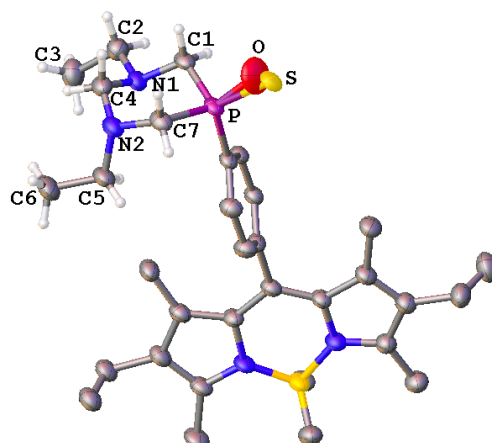
Identification code	publication
Empirical formula	C ₃₂ H ₄₈ BN ₄ P
Formula weight	530.52
Temperature/K	150.00(10)
Crystal system	triclinic
Space group	P-1
a/Å	8.4942(3)
b/Å	9.9788(4)
c/Å	18.8467(8)
α/°	75.427(4)
β/°	80.480(4)
γ/°	89.625(3)
Volume/Å ³	1523.77(11)
Z	2
ρ _{calc} /cm ³	1.156
μ/mm ⁻¹	0.987
F(000)	576.0
Crystal size/mm ³	0.269 × 0.158 × 0.048
Radiation	Cu Kα (λ = 1.54184)
2θ range for data collection/°	9.164 to 144.238
Index ranges	-10 ≤ h ≤ 6, -12 ≤ k ≤ 12, -23 ≤ l ≤ 22
Reflections collected	12769
Independent reflections	5994 [R _{int} = 0.0269, R _{sigma} = 0.0381]
Data/restraints/parameters	5994/0/353
Goodness-of-fit on F ²	1.044
Final R indexes [I >= 2σ (I)]	R ₁ = 0.0396, wR ₂ = 0.1024
Final R indexes [all data]	R ₁ = 0.0465, wR ₂ = 0.1083
Largest diff. peak/hole / e Å ⁻³	0.31/-0.24

6.2.7 8-(4-(1,3-Dimethyl-1,3,5-diazaphosphinane-5-sulfide)phenyl)-4,4-dimethyl-1,3,5,7-tetramethyl-2,6-diethyl-4-bora-3a,4a-diaza-s-indacene (**64a**)



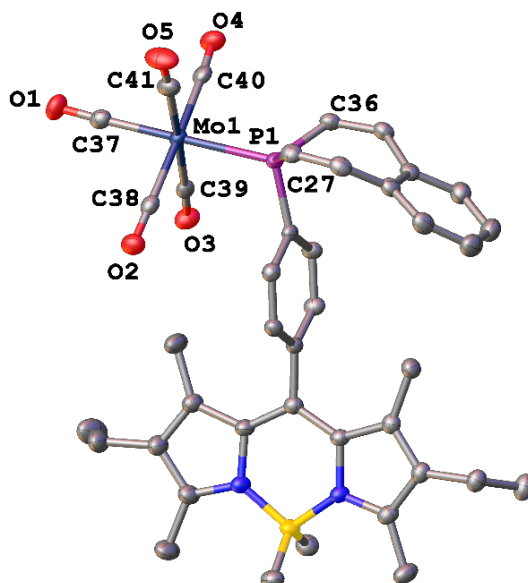
Identification code	publication
Empirical formula	C ₃₀ H ₄₄ BN ₄ PS
Formula weight	534.53
Temperature/K	150.0(2)
Crystal system	monoclinic
Space group	P2 ₁ /n
a/Å	15.8683(17)
b/Å	8.3750(7)
c/Å	24.0681(19)
α/°	90
β/°	108.622(10)
γ/°	90
Volume/Å ³	3031.1(5)
Z	4
ρ _{calc} /cm ³	1.171
μ/mm ⁻¹	0.185
F(000)	1152.0
Crystal size/mm ³	0.251 × 0.128 × 0.094
Radiation	Mo Kα (λ = 0.71073)
2θ range for data collection/°	6.734 to 50.728
Index ranges	-19 ≤ h ≤ 14, -10 ≤ k ≤ 10, -24 ≤ l ≤ 28
Reflections collected	16601
Independent reflections	5524 [R _{int} = 0.0715, R _{sigma} = 0.1136]
Data/restraints/parameters	5524/0/344
Goodness-of-fit on F ²	1.025
Final R indexes [I ≥ 2σ (I)]	R ₁ = 0.0619, wR ₂ = 0.1286
Final R indexes [all data]	R ₁ = 0.1207, wR ₂ = 0.1535
Largest diff. peak/hole / e Å ⁻³	0.42/-0.36

6.2.8 8-(4-(1,3-Diethyl-1,3,5-diazaphosphinane-5-sulfide)phenyl)-4,4-dimethyl-1,3,5,7-tetramethyl-2,6-diethyl-4-bora-3a,4a-diaza-s-indacene (**64b**)



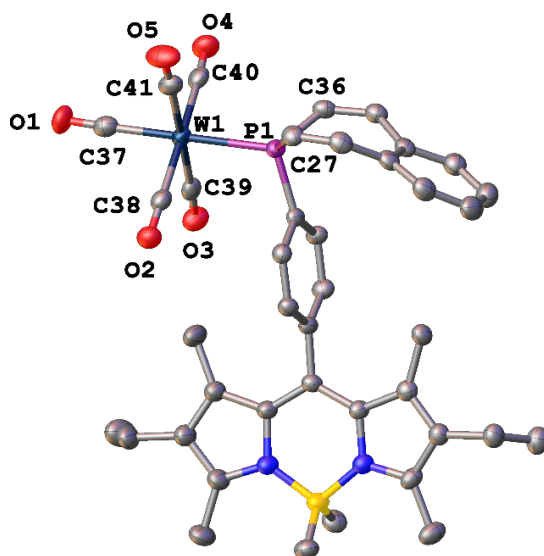
Identification code	publication
Empirical formula	C ₃₂ H ₄₈ BN ₄ O _{0.13} PS _{0.87}
Formula weight	560.54
Temperature/K	150.00(10)
Crystal system	triclinic
Space group	P-1
a/Å	8.6708(7)
b/Å	9.9266(5)
c/Å	19.1197(14)
α/°	75.334(5)
β/°	78.321(7)
γ/°	89.149(5)
Volume/Å ³	1557.93(19)
Z	2
ρ _{calc} /g/cm ³	1.195
μ/mm ⁻¹	1.528
F(000)	606.0
Crystal size/mm ³	0.180 × 0.050 × 0.030
Radiation	Cu Kα (λ = 1.54184)
2θ range for data collection/°	9.216 to 137.424
Index ranges	-7 ≤ h ≤ 10, -11 ≤ k ≤ 11, -23 ≤ l ≤ 23
Reflections collected	16794
Independent reflections	5691 [R _{int} = 0.0688, R _{sigma} = 0.0672]
Data/restraints/parameters	5691/6/372
Goodness-of-fit on F ²	1.042
Final R indexes [I ≥ 2σ (I)]	R ₁ = 0.0644, wR ₂ = 0.1666
Final R indexes [all data]	R ₁ = 0.0852, wR ₂ = 0.1858
Largest diff. peak/hole / e Å ⁻³	0.66/-0.54

6.2.9 [Mo(CO)₅(72)] (69a)



Identification code	ljh180016_fa
Empirical formula	C ₄₀ H ₄₀ BMoN ₂ O ₅ P
Formula weight	766.46
Temperature/K	150.0(2)
Crystal system	monoclinic
Space group	P2 ₁ /n
a/Å	14.83580(16)
b/Å	10.81968(11)
c/Å	23.4064(2)
α/°	90
β/°	99.8849(10)
γ/°	90
Volume/Å ³	3701.38(7)
Z	4
ρ _{calc} /g/cm ³	1.375
μ/mm ⁻¹	3.675
F(000)	1584.0
Crystal size/mm ³	0.27 × 0.24 × 0.02
Radiation	CuKα (λ = 1.54184)
2θ range for data collection/°	7.668 to 133.85
Index ranges	-17 ≤ h ≤ 17, -12 ≤ k ≤ 12, -27 ≤ l ≤ 27
Reflections collected	52138
Independent reflections	6555 [R _{int} = 0.0355, R _{sigma} = 0.0191]
Data/restraints/parameters	6555/0/459
Goodness-of-fit on F ²	1.046
Final R indexes [I ≥ 2σ (I)]	R ₁ = 0.0239, wR ₂ = 0.0585
Final R indexes [all data]	R ₁ = 0.0287, wR ₂ = 0.0619
Largest diff. peak/hole / e Å ⁻³	0.30/-0.35

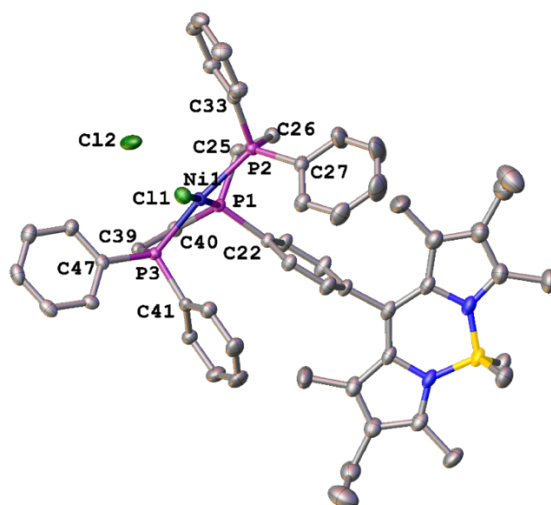
6.2.10 [W(CO)₅(72)] (69b)



Identification code	ljh180020_fa
Empirical formula	C ₄₀ H ₄₀ BN ₂ O ₅ PW
Formula weight	854.37
Temperature/K	150.0(2)
Crystal system	monoclinic
Space group	P2 ₁ /n
a/Å	14.8190(2)
b/Å	10.79147(18)
c/Å	23.3552(3)
α/°	90
β/°	100.2420(12)
γ/°	90
Volume/Å ³	3675.43(9)
Z	4
ρ _{calc} /g/cm ³	1.544
μ/mm ⁻¹	6.607
F(000)	1712.0
Crystal size/mm ³	0.24 × 0.1 × 0.02
Radiation	CuKα (λ = 1.54184)
2θ range for data collection/°	7.694 to 133.652
Index ranges	-15 ≤ h ≤ 17, -12 ≤ k ≤ 12, -27 ≤ l ≤ 25
Reflections collected	26905
Independent reflections	6506 [R _{int} = 0.0450, R _{sigma} = 0.0383]
Data/restraints/parameters	6506/0/459
Goodness-of-fit on F ²	1.092
Final R indexes [I ≥ 2σ (I)]	R ₁ = 0.0310, wR ₂ = 0.0711
Final R indexes [all data]	R ₁ = 0.0420, wR ₂ = 0.0765
Largest diff. peak/hole / e Å ⁻³	0.87/-0.64

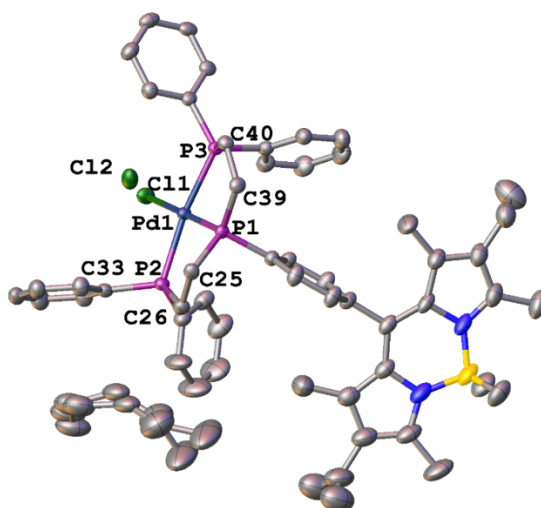
6.3 Chapter 4 X-ray Crystallographic Data

6.3.1 [Ni(75)Cl]Cl (**81**)



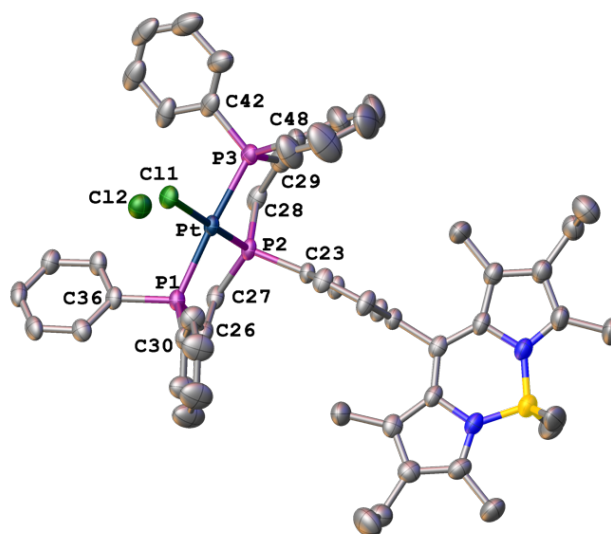
Identification code	LJH130025
Empirical formula	C ₅₃ H ₆₀ BN ₂ P ₃ Cl ₂ Ni
Formula weight	958.36
Temperature/K	150.01(10)
Crystal system	monoclinic
Space group	P2 ₁ /c
a/Å	14.3455(2)
b/Å	9.76590(15)
c/Å	40.0734(7)
α/°	90
β/°	99.0515(15)
γ/°	90
Volume/Å ³	5544.24(16)
Z	4
ρ _{calc} /cm ³	1.148
μ/mm ⁻¹	2.458
F(000)	2016.0
Crystal size/mm ³	0.6 × 0.08 × 0.05
Radiation	CuKα (λ = 1.54184)
2θ range for data collection/°	4.466 to 133.326
Index ranges	-16 ≤ h ≤ 14, -11 ≤ k ≤ 11, -46 ≤ l ≤ 47
Reflections collected	47716
Independent reflections	9773 [R _{int} = 0.0624, R _{sigma} = 0.0475]
Data/restraints/parameters	9773/543/567
Goodness-of-fit on F ²	1.030
Final R indexes [I ≥ 2σ (I)]	R ₁ = 0.0411, wR ₂ = 0.0994
Final R indexes [all data]	R ₁ = 0.0527, wR ₂ = 0.1047
Largest diff. peak/hole / e Å ⁻³	0.41/-0.28

6.3.2 [Pd(75)Cl]Cl (83)



Identification code	LJH130027
Empirical formula	C ₅₈ H ₇₂ BN ₂ P ₃ Cl ₂ Pd
Formula weight	1078.19
Temperature/K	150.00(10)
Crystal system	monoclinic
Space group	P2 ₁ /c
a/Å	14.57350(17)
b/Å	9.66970(12)
c/Å	40.4564(5)
α/°	90
β/°	99.3270(11)
γ/°	90
Volume/Å ³	5625.80(12)
Z	4
ρ _{calc} /g/cm ³	1.273
μ/mm ⁻¹	4.619
F(000)	2256.0
Crystal size/mm ³	0.172 × 0.13 × 0.113
Radiation	CuKα (λ = 1.54184)
2θ range for data collection/°	4.426 to 133.55
Index ranges	-17 ≤ h ≤ 17, -11 ≤ k ≤ 11, -48 ≤ l ≤ 46
Reflections collected	43359
Independent reflections	9962 [R _{int} = 0.0330, R _{sigma} = 0.0263]
Data/restraints/parameters	9962/634/568
Goodness-of-fit on F ²	1.087
Final R indexes [I ≥ 2σ (I)]	R ₁ = 0.0440, wR ₂ = 0.1269
Final R indexes [all data]	R ₁ = 0.0490, wR ₂ = 0.1320
Largest diff. peak/hole / e Å ⁻³	1.76/-1.18

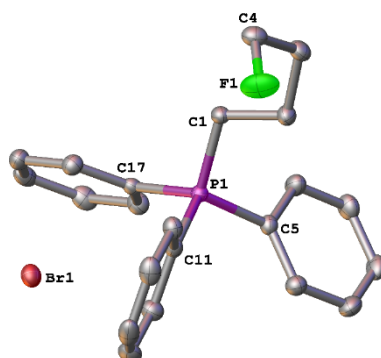
6.3.3 [Pt(75)Cl]Cl (**84a**)



Identification code	LJH12
Empirical formula	C ₅₈ H ₇₂ BN ₂ P ₃ Cl ₂ Pt+Cl-
Formula weight	1040.81
Temperature/K	150.(2)
Crystal system	monoclinic
Space group	P12 ₁ /n1
a/Å	12.7863(2)
b/Å	10.5363(2)
c/Å	40.7616(8)
α/°	90
β/°	94.746(2)
γ/°	90
Volume/Å ³	5472.59(17)
Z	4
ρ _{calc} /cm ³	1.385
μ/mm ⁻¹	6.812
F(000)	2320.0
Crystal size/mm ³	0.20 × 0.15 × 0.15
Radiation	CuKα (λ = 1.54184)
2θ range for data collection/°	2.2 to 66.7°
Index ranges	h −13 to 15, k −12 to 8, l −40 to 48
Reflections collected	22182
Independent reflections	9521 (R _{int} = 0.0270)
Data/restraints/parameters	9521/0/567
Goodness-of-fit on F ²	1.130
Final R indexes [I ≥ 2σ (I)]	R ₁ = 0.0386, wR ₂ = 0.0923
Final R indexes [all data]	R ₁ = 0.0433, wR ₂ = 0.0948
Largest diff. peak/hole / e Å ⁻³	2.47/−1.37

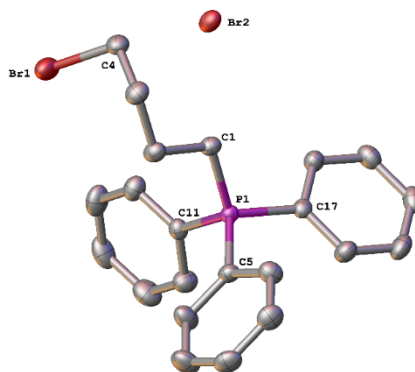
6.4 Chapter 5 X-ray Crystallographic Data

6.4.1 (4-Bromobutyl)triphenylphosphonium fluoride (**88a**)



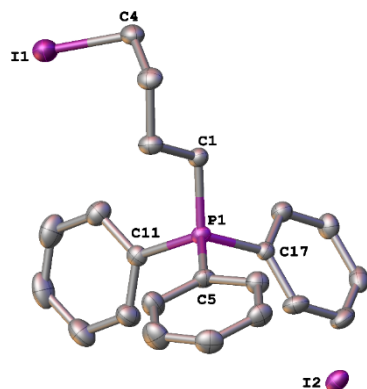
Identification code	ljh180009_fa
Empirical formula	C ₂₂ H ₂₃ BrFP
Formula weight	417.28
Temperature/K	150.0(2)
Crystal system	monoclinic
Space group	P2 ₁ /c
a/Å	11.29009(9)
b/Å	10.04406(8)
c/Å	17.36789(11)
α/°	90
β/°	103.9162(7)
γ/°	90
Volume/Å ³	1911.68(2)
Z	4
ρ _{calc} /g/cm ³	1.450
μ/mm ⁻¹	3.802
F(000)	856.0
Crystal size/mm ³	0.34 × 0.25 × 0.19
Radiation	CuKα (λ = 1.54184)
2θ range for data collection/°	8.068 to 133.66
Index ranges	-13 ≤ h ≤ 13, -11 ≤ k ≤ 11, -20 ≤ l ≤ 18
Reflections collected	13696
Independent reflections	3381 [R _{int} = 0.0171, R _{sigma} = 0.0137]
Data/restraints/parameters	3381/0/227
Goodness-of-fit on F ²	1.103
Final R indexes [I ≥ 2σ (I)]	R ₁ = 0.0198, wR ₂ = 0.0491
Final R indexes [all data]	R ₁ = 0.0208, wR ₂ = 0.0497
Largest diff. peak/hole / e Å ⁻³	0.32/-0.23

6.4.2 (4-Bromobutyl)triphenylphosphonium bromide (**88b**)



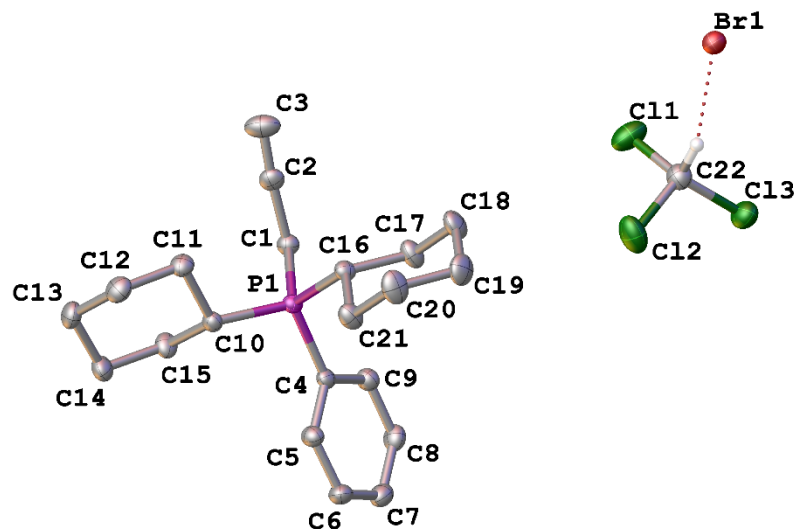
Identification code	ljh180008_fa
Empirical formula	C ₂₂ H ₂₃ Br ₂ P
Formula weight	478.19
Temperature/K	150.0(2)
Crystal system	monoclinic
Space group	P2 ₁ /c
a/Å	11.99184(15)
b/Å	10.37013(12)
c/Å	17.0047(2)
α/°	90
β/°	104.5832(13)
γ/°	90
Volume/Å ³	2046.53(4)
Z	4
ρ _{calc} /cm ³	1.552
μ/mm ⁻¹	5.761
F(000)	960.0
Crystal size/mm ³	0.2 × 0.1 × 0.02
Radiation	CuKα (λ = 1.54184)
2θ range for data collection/°	7.618 to 133.47
Index ranges	-14 ≤ h ≤ 14, -11 ≤ k ≤ 12, -20 ≤ l ≤ 20
Reflections collected	27932
Independent reflections	3629 [R _{int} = 0.0315, R _{sigma} = 0.0162]
Data/restraints/parameters	3629/0/226
Goodness-of-fit on F ²	1.064
Final R indexes [I ≥ 2σ (I)]	R ₁ = 0.0200, wR ₂ = 0.0454
Final R indexes [all data]	R ₁ = 0.0236, wR ₂ = 0.0472
Largest diff. peak/hole / e Å ⁻³	0.32/-0.36

6.4.3 (4-Iodobutyl)triphenylphosphonium iodide (**88c**)



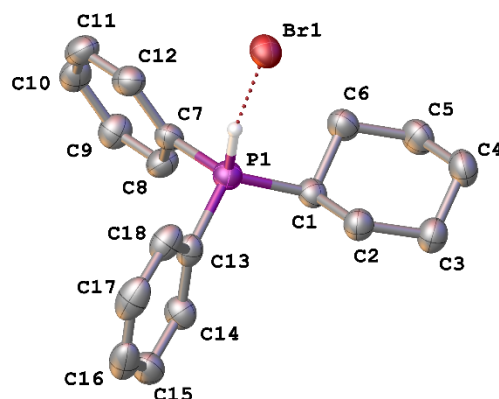
Identification code	ljh180006
Empirical formula	C ₂₂ H ₂₃ I ₂ P
Formula weight	572.17
Temperature/K	150.0(2)
Crystal system	monoclinic
Space group	P2 ₁ /c
a/Å	12.6352(5)
b/Å	10.7329(3)
c/Å	16.9032(6)
α/°	90
β/°	106.272(4)
γ/°	90
Volume/Å ³	2200.46(14)
Z	4
ρ _{calc} /g/cm ³	1.727
μ/mm ⁻¹	2.933
F(000)	1104.0
Crystal size/mm ³	0.25 × 0.22 × 0.15
Radiation	MoKα (λ = 0.71073)
2θ range for data collection/°	6.438 to 57.604
Index ranges	-16 ≤ h ≤ 15, -12 ≤ k ≤ 13, -20 ≤ l ≤ 22
Reflections collected	18196
Independent reflections	5017 [R _{int} = 0.0401, R _{sigma} = 0.0459]
Data/restraints/parameters	5017/0/226
Goodness-of-fit on F ²	1.075
Final R indexes [I ≥ 2σ (I)]	R ₁ = 0.0332, wR ₂ = 0.0541
Final R indexes [all data]	R ₁ = 0.0558, wR ₂ = 0.0620
Largest diff. peak/hole / e Å ⁻³	0.80/-0.91

6.4.4 Prop-2-yn-1-ylidicyclohexylphenylphosphonium bromide (89c)



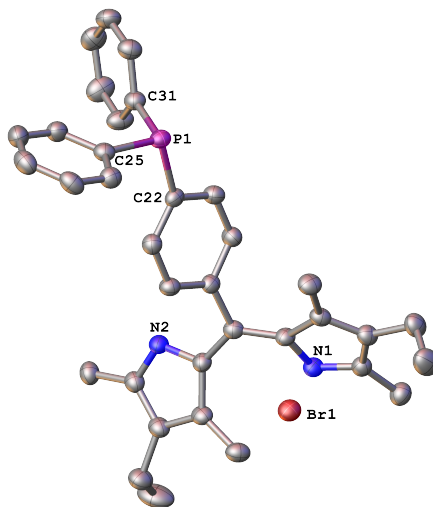
Identification code	ljh200002
Empirical formula	C ₂₂ H ₃₁ BrCl ₃ P
Formula weight	512.70
Temperature/K	150.0(2)
Crystal system	monoclinic
Space group	P2 ₁ /n
a/Å	11.3828(2)
b/Å	15.6560(3)
c/Å	13.5591(3)
α/°	90
β/°	90.4662(18)
γ/°	90
Volume/Å ³	2416.26(8)
Z	4
ρ _{calc} /cm ³	1.409
μ/mm ⁻¹	6.026
F(000)	1056.0
Crystal size/mm ³	0.31 × 0.17 × 0.06
Radiation	CuKα (λ = 1.54184)
2θ range for data collection/°	8.628 to 133.714
Index ranges	-13 ≤ h ≤ 13, -18 ≤ k ≤ 18, -12 ≤ l ≤ 16
Reflections collected	17516
Independent reflections	4277 [R _{int} = 0.0535, R _{sigma} = 0.0442]
Data/restraints/parameters	4277/0/244
Goodness-of-fit on F ²	1.053
Final R indexes [I ≥ 2σ (I)]	R ₁ = 0.0303, wR ₂ = 0.0643
Final R indexes [all data]	R ₁ = 0.0446, wR ₂ = 0.0724
Largest diff. peak/hole / e Å ⁻³	0.34/-0.37

6.4.5 Cyclohexyldiphenylphosphonium bromide (92)



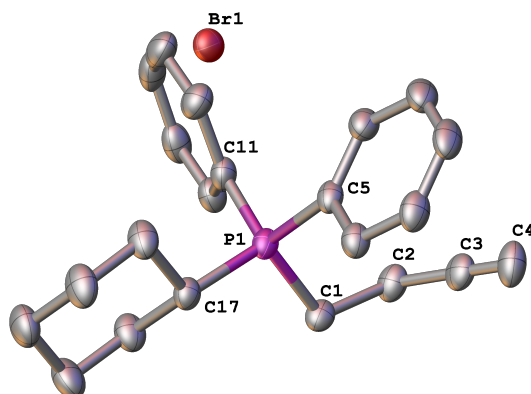
Identification code	ljh200006_fa
Empirical formula	C ₁₈ H ₂₂ BrP
Formula weight	349.23
Temperature/K	150.0(2)
Crystal system	monoclinic
Space group	C2/c
a/Å	14.6572(2)
b/Å	13.70807(17)
c/Å	18.1063(3)
α/°	90
β/°	108.5440(15)
γ/°	90
Volume/Å ³	3449.07(9)
Z	8
ρ _{calc} /g/cm ³	1.345
μ/mm ⁻¹	4.016
F(000)	1440.0
Crystal size/mm ³	0.24 × 0.16 × 0.03
Radiation	CuKα (λ = 1.54184)
2θ range for data collection/°	9.062 to 133.556
Index ranges	-17 ≤ h ≤ 14, -16 ≤ k ≤ 16, -21 ≤ l ≤ 21
Reflections collected	23624
Independent reflections	3038 [R _{int} = 0.0327, R _{sigma} = 0.0159]
Data/restraints/parameters	3038/0/184
Goodness-of-fit on F ²	1.064
Final R indexes [I ≥ 2σ (I)]	R ₁ = 0.0271, wR ₂ = 0.0716
Final R indexes [all data]	R ₁ = 0.0301, wR ₂ = 0.0743
Largest diff. peak/hole / e Å ⁻³	0.77/-0.30

6.4.6 1-Bromo-2-((4-(diphenylphosphaneyl)phenyl)(4-ethyl-3,5-dimethyl-3H-pyrrol-2-yl)methyl)-4-ethyl-3,5-dimethyl-1H-pyrrole (**94**)



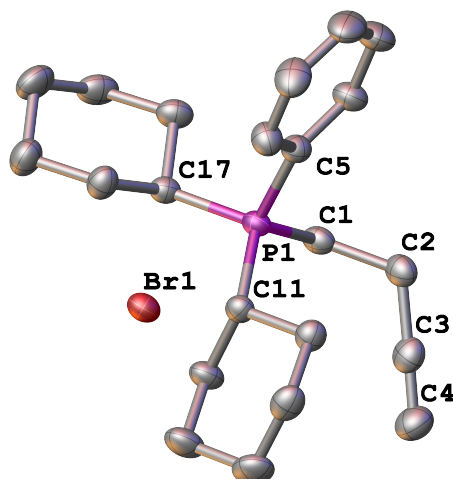
Identification code	ljh200016_fa
Empirical formula	C ₃₅ H ₃₈ BrN ₂ P
Formula weight	597.55
Temperature/K	150.0(2)
Crystal system	monoclinic
Space group	P2 ₁ /n
a/Å	19.1861(4)
b/Å	8.25760(10)
c/Å	20.4664(5)
α/°	90
β/°	110.467(3)
γ/°	90
Volume/Å ³	3037.83(12)
Z	4
ρ _{calc} /cm ³	1.307
μ/mm ⁻¹	2.528
F(000)	1248.0
Crystal size/mm ³	0.25 × 0.08 × 0.02
Radiation	CuKα (λ = 1.54184)
2θ range for data collection/°	7.83 to 133.798
Index ranges	-20 ≤ h ≤ 22, -9 ≤ k ≤ 9, -24 ≤ l ≤ 23
Reflections collected	22104
Independent reflections	5371 [R _{int} = 0.0441, R _{sigma} = 0.0369]
Data/restraints/parameters	5371/1/364
Goodness-of-fit on F ²	1.032
Final R indexes [I ≥ 2σ (I)]	R ₁ = 0.0391, wR ₂ = 0.0905
Final R indexes [all data]	R ₁ = 0.0540, wR ₂ = 0.0996
Largest diff. peak/hole / e Å ⁻³	0.79/-0.34

6.4.7 But-3-yn-1-ylcyclohexyldiphenylphosphonium bromide (95b)



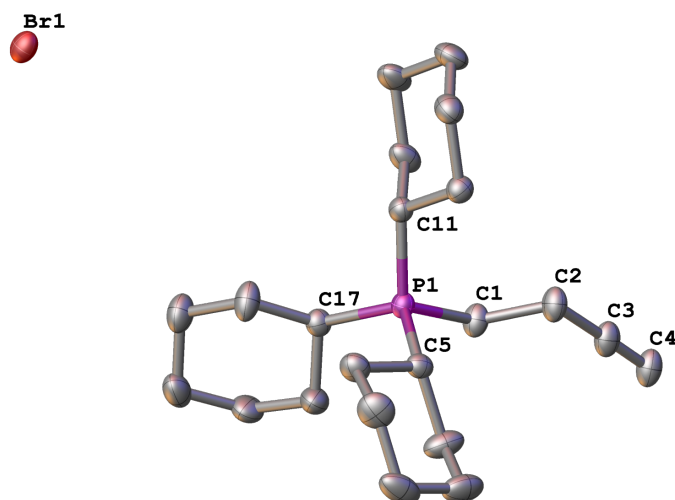
Identification code	ljh200021_fa
Empirical formula	C ₂₂ H ₂₆ BrP
Formula weight	401.31
Temperature/K	150.0(2)
Crystal system	monoclinic
Space group	C2/c
a/Å	20.4786(3)
b/Å	10.19910(10)
c/Å	20.2238(3)
α/°	90
β/°	106.9700(10)
γ/°	90
Volume/Å ³	4040.09(10)
Z	8
ρ _{calc} /g/cm ³	1.320
μ/mm ⁻¹	3.500
F(000)	1664.0
Crystal size/mm ³	0.21 × 0.17 × 0.1
Radiation	CuKα (λ = 1.54184)
2θ range for data collection/°	9.03 to 133.656
Index ranges	-23 ≤ h ≤ 24, -12 ≤ k ≤ 12, -23 ≤ l ≤ 24
Reflections collected	27983
Independent reflections	3587 [R _{int} = 0.0305, R _{sigma} = 0.0159]
Data/restraints/parameters	3587/0/217
Goodness-of-fit on F ²	1.030
Final R indexes [I ≥ 2σ (I)]	R ₁ = 0.0222, wR ₂ = 0.0533
Final R indexes [all data]	R ₁ = 0.0257, wR ₂ = 0.0554
Largest diff. peak/hole / e Å ⁻³	0.26/-0.23

6.4.8 But-3-yn-1-ylidicyclohexylphenylphosphonium bromide (95c)



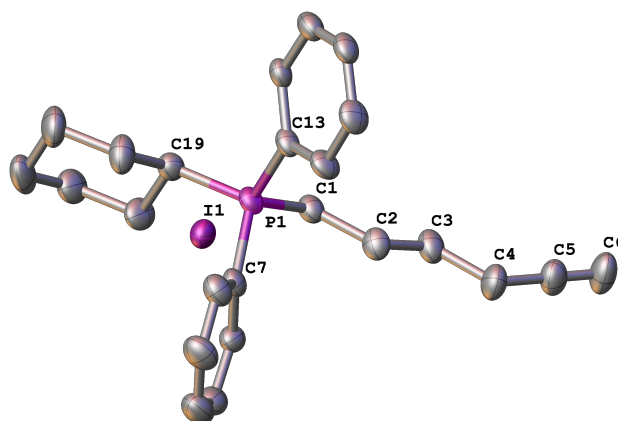
Identification code	ljh200014_fa
Empirical formula	C ₂₂ H ₃₂ BrP
Formula weight	407.35
Temperature/K	150.0(2)
Crystal system	monoclinic
Space group	P2 ₁ /n
a/Å	10.11280(10)
b/Å	14.5469(2)
c/Å	14.4493(2)
α/°	90
β/°	95.0520(10)
γ/°	90
Volume/Å ³	2117.38(5)
Z	4
ρ _{calc} /g/cm ³	1.278
μ/mm ⁻¹	3.340
F(000)	856.0
Crystal size/mm ³	0.2 × 0.16 × 0.11
Radiation	CuKα (λ = 1.54184)
2θ range for data collection/°	8.642 to 133.846
Index ranges	-12 ≤ h ≤ 11, -17 ≤ k ≤ 17, -17 ≤ l ≤ 16
Reflections collected	29498
Independent reflections	3749 [R _{int} = 0.0365, R _{sigma} = 0.0198]
Data/restraints/parameters	3749/0/217
Goodness-of-fit on F ²	1.097
Final R indexes [I ≥ 2σ (I)]	R ₁ = 0.0233, wR ₂ = 0.0530
Final R indexes [all data]	R ₁ = 0.0284, wR ₂ = 0.0557
Largest diff. peak/hole / e Å ⁻³	0.30/-0.24

6.4.9 But-3-yn-1-yltricyclohexylphosphonium bromide (95d)



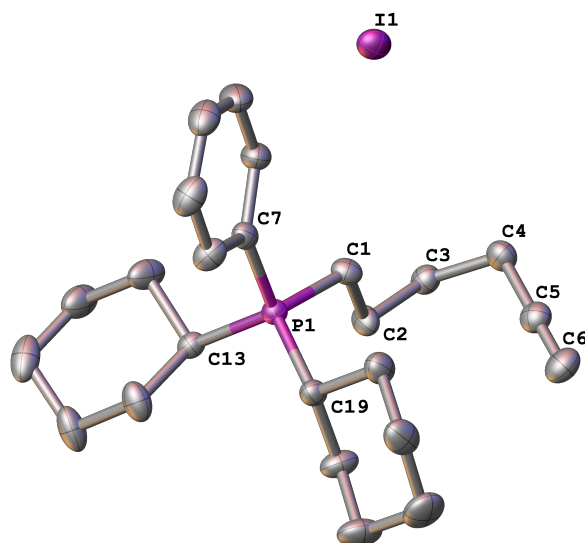
Identification code	ljh200026
Empirical formula	C ₂₃ H ₄₀ BrCl ₂ P
Formula weight	498.33
Temperature/K	100.0(2)
Crystal system	orthorhombic
Space group	Pbca
a/Å	21.02030(10)
b/Å	15.98300(10)
c/Å	14.87910(10)
α/°	90
β/°	90
γ/°	90
Volume/Å ³	4998.89(5)
Z	8
ρ _{calc} /cm ³	1.324
μ/mm ⁻¹	1.794
F(000)	2096.0
Crystal size/mm ³	0.137 × 0.055 × 0.045
Radiation	Synchrotron (λ = 0.6889)
2θ range for data collection/°	3.756 to 53.146
Index ranges	-27 ≤ h ≤ 27, -20 ≤ k ≤ 20, -19 ≤ l ≤ 19
Reflections collected	68947
Independent reflections	5737 [R _{int} = 0.0828, R _{sigma} = 0.0407]
Data/restraints/parameters	5737/0/244
Goodness-of-fit on F ²	1.077
Final R indexes [I ≥ 2σ (I)]	R ₁ = 0.0498, wR ₂ = 0.1432
Final R indexes [all data]	R ₁ = 0.0563, wR ₂ = 0.1489
Largest diff. peak/hole / e Å ⁻³	2.61/-0.66

6.4.10 Hex-5-yn-1-ylcyclohexyldiphenylphosphonium iodide (**96b**)



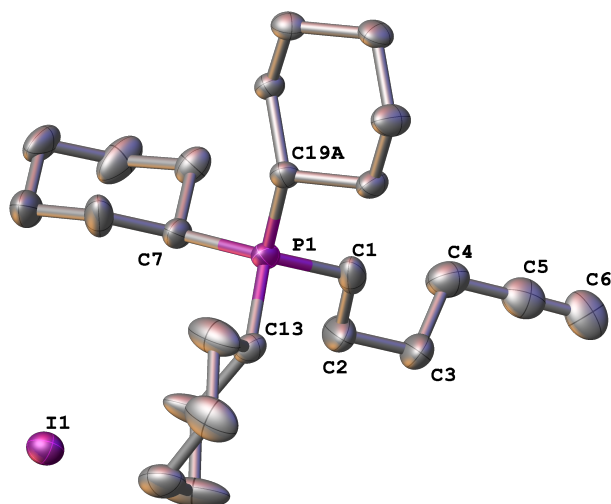
Identification code	ljh200012_fa
Empirical formula	C ₂₄ H ₃₀ IP
Formula weight	476.35
Temperature/K	150.0(2)
Crystal system	monoclinic
Space group	P2 ₁ /c
a/Å	9.0689(4)
b/Å	14.0649(5)
c/Å	18.0327(5)
α/°	90
β/°	94.688(3)
γ/°	90
Volume/Å ³	2292.43(14)
Z	4
ρ _{calc} /g/cm ³	1.380
μ/mm ⁻¹	11.648
F(000)	968.0
Crystal size/mm ³	0.11 × 0.06 × 0.04
Radiation	CuKα (λ = 1.54184)
2θ range for data collection/°	7.982 to 133.824
Index ranges	-10 ≤ h ≤ 9, -14 ≤ k ≤ 16, -21 ≤ l ≤ 19
Reflections collected	16754
Independent reflections	4057 [R _{int} = 0.0659, R _{sigma} = 0.0545]
Data/restraints/parameters	4057/0/235
Goodness-of-fit on F ²	1.020
Final R indexes [I ≥ 2σ (I)]	R ₁ = 0.0398, wR ₂ = 0.0975
Final R indexes [all data]	R ₁ = 0.0587, wR ₂ = 0.1091
Largest diff. peak/hole / e Å ⁻³	0.98/-1.04

6.4.11 Hex-5-yn-1-ylidicyclohexylphenylphosphonium iodide (96c)



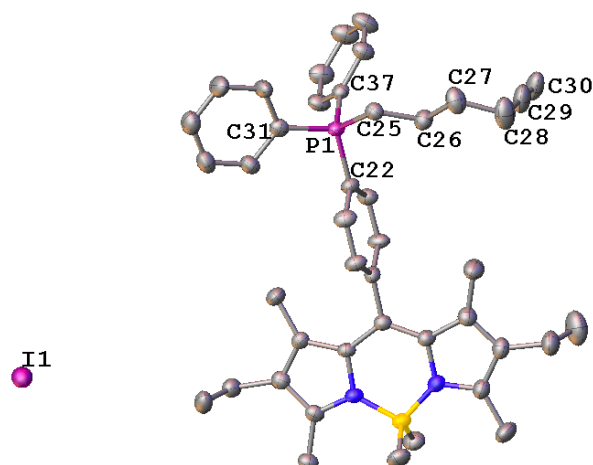
Identification code	ljh200011_fa
Empirical formula	C ₂₄ H ₃₆ IP
Formula weight	482.40
Temperature/K	150.0(2)
Crystal system	trigonal
Space group	P3 ₁
a/Å	10.3175(2)
b/Å	10.3175(2)
c/Å	18.9715(4)
α/°	90
β/°	90
γ/°	120
Volume/Å ³	1748.96(8)
Z	3
ρ _{calc} /g/cm ³	1.374
μ/mm ⁻¹	11.452
F(000)	744.0
Crystal size/mm ³	0.34 × 0.11 × 0.04
Radiation	CuKα (λ = 1.54184)
2θ range for data collection/°	9.9 to 133.668
Index ranges	-12 ≤ h ≤ 12, -12 ≤ k ≤ 12, -22 ≤ l ≤ 22
Reflections collected	15083
Independent reflections	4130 [R _{int} = 0.0547, R _{sigma} = 0.0512]
Data/restraints/parameters	4130/1/235
Goodness-of-fit on F ²	1.043
Final R indexes [I ≥ 2σ (I)]	R ₁ = 0.0295, wR ₂ = 0.0591
Final R indexes [all data]	R ₁ = 0.0350, wR ₂ = 0.0621
Largest diff. peak/hole / e Å ⁻³	0.54/-0.27
Flack parameter	-0.024(5)

6.4.12 Hex-5-yn-1-yltricyclohexylphosphonium iodide (96d)



Identification code	ljh200013
Empirical formula	C ₂₄ H ₄₂ IP
Formula weight	488.44
Temperature/K	150.0(2)
Crystal system	orthorhombic
Space group	Pbca
a/Å	14.47686(19)
b/Å	15.6449(2)
c/Å	21.1906(3)
α/°	90
β/°	90
γ/°	90
Volume/Å ³	4799.44(12)
Z	8
ρ _{calc} /g/cm ³	1.352
μ/mm ⁻¹	11.129
F(000)	2032.0
Crystal size/mm ³	0.18 × 0.12 × 0.08
Radiation	CuKα (λ = 1.54184)
2θ range for data collection/°	8.346 to 133.832
Index ranges	-17 ≤ h ≤ 17, -18 ≤ k ≤ 15, -24 ≤ l ≤ 21
Reflections collected	33950
Independent reflections	4258 [R _{int} = 0.0476, R _{sigma} = 0.0254]
Data/restraints/parameters	4258/435/290
Goodness-of-fit on F ²	1.071
Final R indexes [I ≥ 2σ (I)]	R ₁ = 0.0336, wR ₂ = 0.0646
Final R indexes [all data]	R ₁ = 0.0461, wR ₂ = 0.0700
Largest diff. peak/hole / e Å ⁻³	0.70/-0.63

6.4.13 8-((4-Diphenylphosphino)(hex-5-yn-1-yl)phenyl)-4,4-dimethyl-1,3,5,7-tetramethyl-2,6-diethyl-4-bora-3a,4a-diaza-s-indacene iodide (**97a**)



Identification code	ljh200018_fa
Empirical formula	C ₄₇ H ₆₁ BN ₂ OP
Formula weight	838.65
Temperature/K	150.0(2)
Crystal system	orthorhombic
Space group	Pna2 ₁
a/Å	54.6161(15)
b/Å	9.5757(3)
c/Å	16.8791(5)
α/°	90
β/°	90
γ/°	90
Volume/Å ³	8827.6(5)
Z	8
ρ _{calc} /cm ³	1.262
μ/mm ⁻¹	6.302
F(000)	3504.0
Crystal size/mm ³	0.3 × 0.05 × 0.03
Radiation	CuKα (λ = 1.54184)
2θ range for data collection/°	8.33 to 133.802
Index ranges	-64 ≤ h ≤ 64, -11 ≤ k ≤ 11, -20 ≤ l ≤ 18
Reflections collected	37457
Independent reflections	13260 [R _{int} = 0.0559, R _{sigma} = 0.0643]
Data/restraints/parameters	13260/1132/1062
Goodness-of-fit on F ²	1.029
Final R indexes [I ≥ 2σ (I)]	R ₁ = 0.0427, wR ₂ = 0.0879
Final R indexes [all data]	R ₁ = 0.0562, wR ₂ = 0.0941
Largest diff. peak/hole / e Å ⁻³	0.63/-0.37
Flack parameter	0.484(6)

Appendix II

Calculated Molecular Orbital Surfaces

6.5 Calculated Molecular Orbital Surfaces for 4-(2-Diphenylphosphinoethylamino)-7-nitro-2,1,3-benzoxadiazole

4-(2-Diphenylphosphinoethylamino)-7-nitro-2,1,3-benzoxadiazole is a fluorescent phosphorus containing ligand which is known to undergo reductive-PeT.¹ Here we report the calculated molecular orbital surfaces from LUMO to HOMO-6 and the respective orbital energies and orbital energy differences (Figure 6.1). The DFT calculations were carried out on Gaussian 6 software using B3LYP/6-31G and the molecular orbital surfaces visualised using Avogadro.²

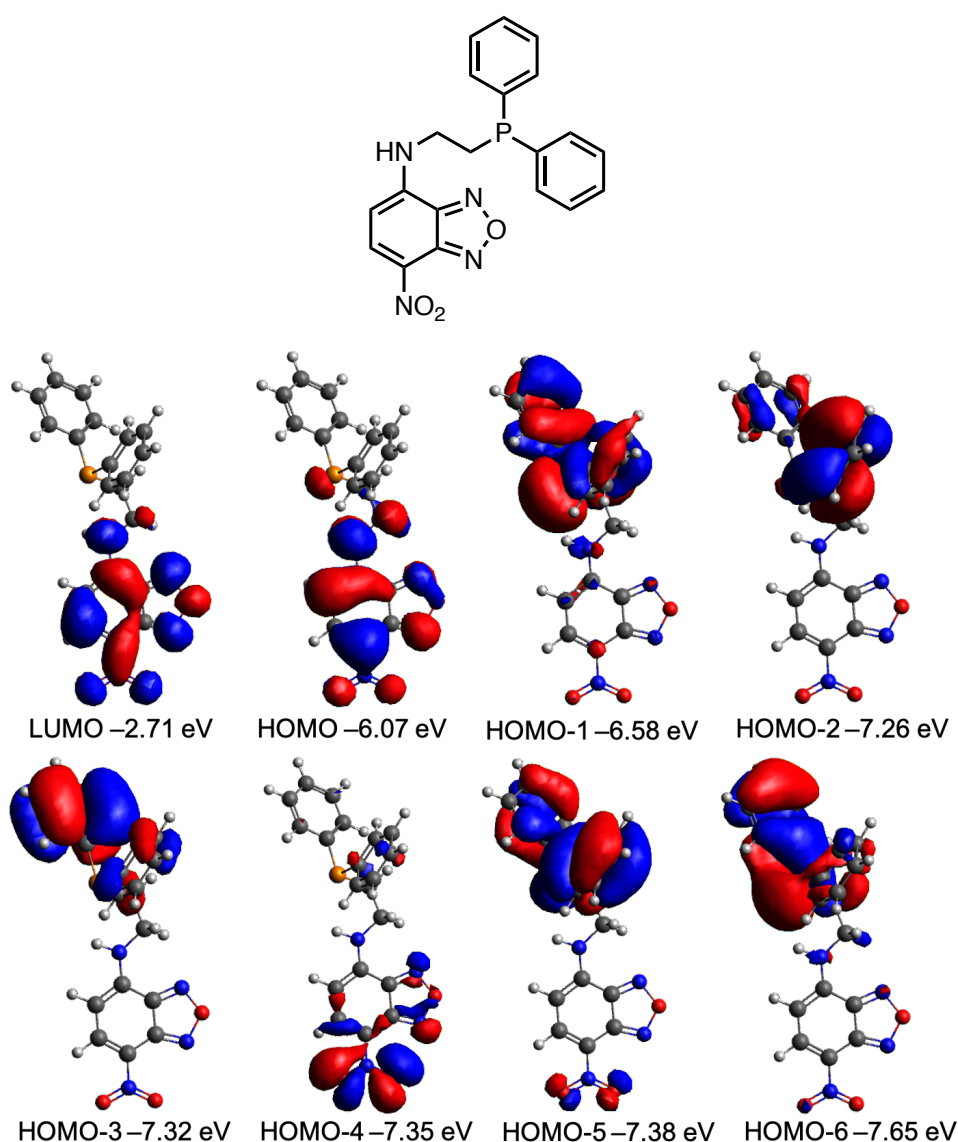


Figure 6.1 Calculated molecular orbital surfaces from the LUMO to HOMO-5 of 4-(2-diphenylphosphinoethylamino)-7-nitro-2,1,3-benzoxadiazole, a fluorescent phosphorus containing ligand which is known to undergo reductive-PeT.

6.6 Calculated Molecular Orbital Surfaces for BodP₃ Complexes

Here we report the calculated orbital energies for BodP₃ **75** and its group 10 complexes, **81**, **83**, **84a**, **84b** and **84c**. The data has been compiled and are shown in Table 6.1. In addition, the calculated molecular orbital surfaces from LUMO to HOMO–6 of BodP₃ complexes **84b** and **84c** are shown in Figures 6.2 and 6.3 respectively.

All calculations were carried out using Gaussian 6 software³ and the molecular orbital surfaces were visualised using Avogadro.² Full geometry optimisations of the studied compounds were performed using density functional theory with a B3LYP function with a 6-31G* basis set for **75** and B3LYP function with 6-31G* basis set with the LANL2DZ effective core basis set for **81**, **83**, **84a**, **84b** and **84c**. A vibrational analysis was performed at the same level to characterise calculated structures as minima.

Table 6.1 Calculated orbital energies for BodP₃ **75** and its group 10 complexes, **81**, **83**, **84a**, **84b** and **84c**.

Orbital	Energy (eV)					
	BodP ₃ (75)	[Ni(75)Cl]Cl (81)	[Pd(75)Cl]Cl (83)	[Pt(75)Cl]Cl (84a)	[Pt(75)Br]Br (84b)	[Pt(75)I]I (84c)
LUMO	–2.03	–4.82	–4.76	–4.19	–4.21	–4.32
HOMO	–5.05	–6.77	–6.77	–6.76	–6.76	–6.77
HOMO-1	–5.70	–7.41	–7.42	–7.41	–7.41	–7.41
HOMO-2	–5.72	–7.90	–7.90	–7.89	–7.89	–7.90
HOMO-3	–5.91	–8.77	–8.74	–8.76	–8.55	–8.21
HOMO-4	–6.13	–8.79	–8.77	–8.80	–8.76	–8.35
HOMO-5	–6.28	–9.14	–9.08	–9.10	–8.79	–8.77
HOMO-6	–6.80	–9.17	–9.17	–9.18	–9.12	–9.08

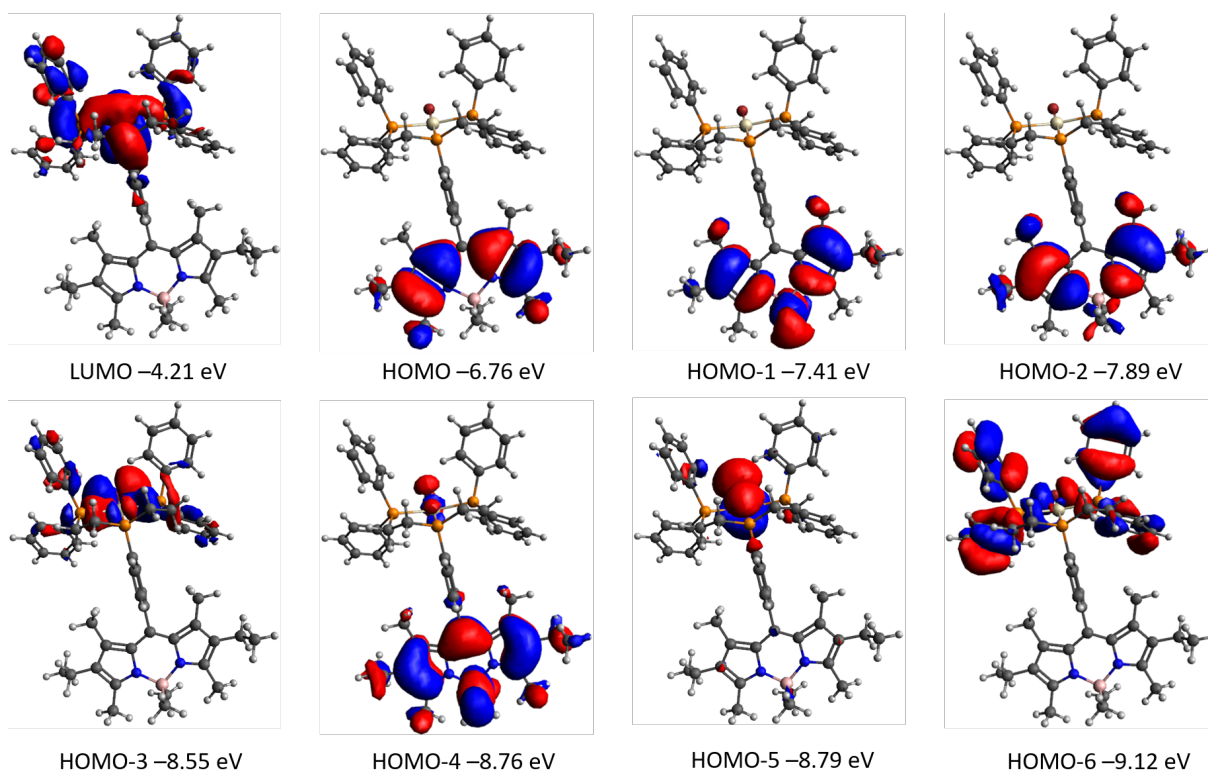


Figure 6.2 Calculated molecular orbital surfaces from the LUMO to HOMO-6 of the [Pt(**75**)Br]Br complex, **84b**.

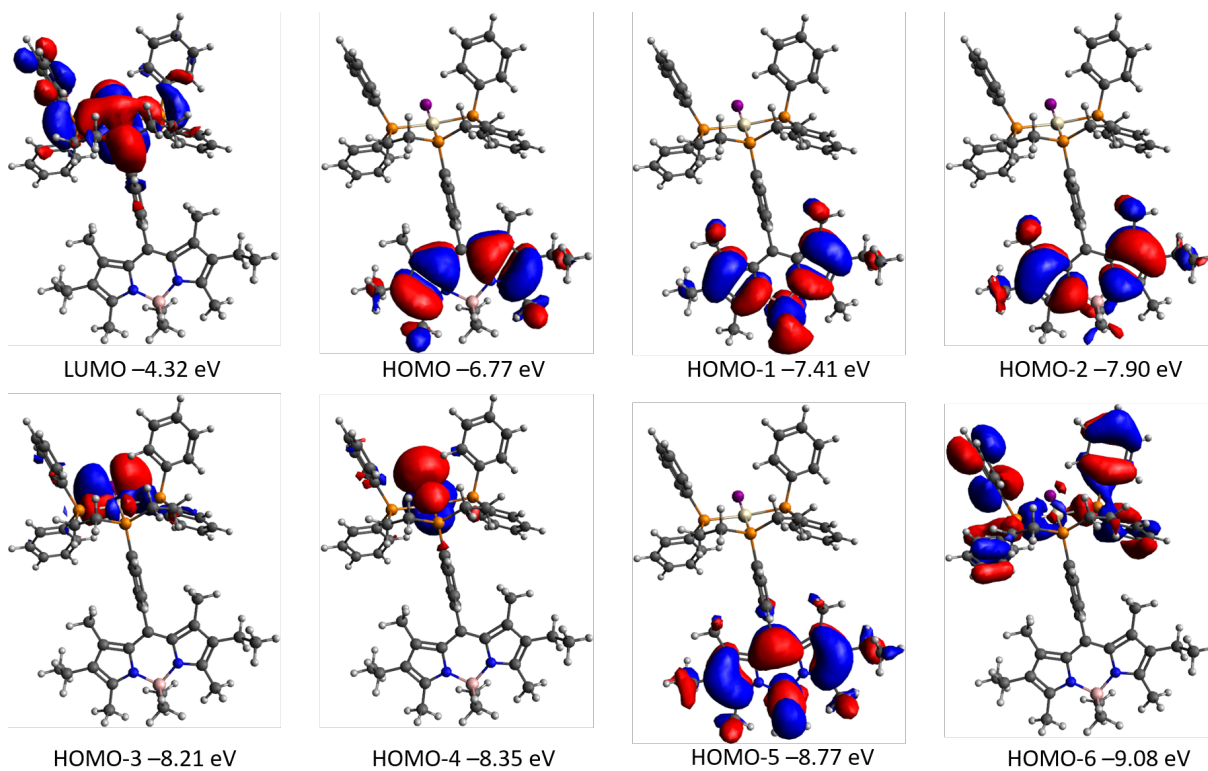


Figure 6.3 Calculated molecular orbital surfaces from the LUMO to HOMO-6 of the [Pt(**75**)I]I complex, **84c**.

Appendix III

Epigenetic Mechanisms of Cancer Drug Resistance

6.7 Epigenetic Mechanisms of Cancer Drug Resistance

This chapter describes the imaging of pancreatic ductal adenocarcinoma (PDAC) murine cells with histone H3 Lys-9 trimethylation (H3K9me3) FRET biosensor to monitor dynamic epigenetic changes within the cells. The effects of pancreatic cancer drug, gemcitabine on the methylation levels of H3K9 are also reported.

6.7.1 Pancreatic Cancer

Pancreatic cancer is the 10th most common cancer in the UK with approximately 9800 new cases every year. It is however, the 5th most fatal with only 25% of people surviving for a year or more. The poor survival statistics can be accounted to i) late diagnosis; associated with very few initial symptoms, and ii) a lack of screening tests. Due to the frequent late diagnosis of pancreatic cancer, only 10% of patients in the UK will receive surgery, 28% have chemotherapy and 5% will receive radiotherapy in comparison to 69% of people with other cancers will receive at least one of the treatments.⁴ The first line of treatment is chemotherapy using either: gemcitabine, gemcitabine with nab-paclitaxel, gemcitabine with capecitabine or a combination of five chemotherapy drugs known as FOLFIRINOX.⁵ Although there are many treatments options available, the cancer is persistent and becomes drug resistant in many patients. Research is ongoing to develop screening tests which would allow for earlier diagnosis, and research into additional treatment options is ongoing.⁶

6.7.2 Treatments for Pancreatic Cancer

This work focuses on the epigenetic effect of gemcitabine (Figure 6.4) on pancreatic ductal adenocarcinoma murine (PDAC p53 R172H) cells. Gemcitabine is an FDA approved drug for the treatment of pancreatic, metastatic breast, bladder, ovarian and non-small cell lung cancers. Gemcitabine must be phosphorylated by deoxycytidine once in the cell to its active forms, gemcitabine diphosphate (dFdCDP) and gemcitabine triphosphate (dFdCTP) (Figure 6.4), these active forms work by inhibiting mitosis and DNA and RNA synthesis.⁷

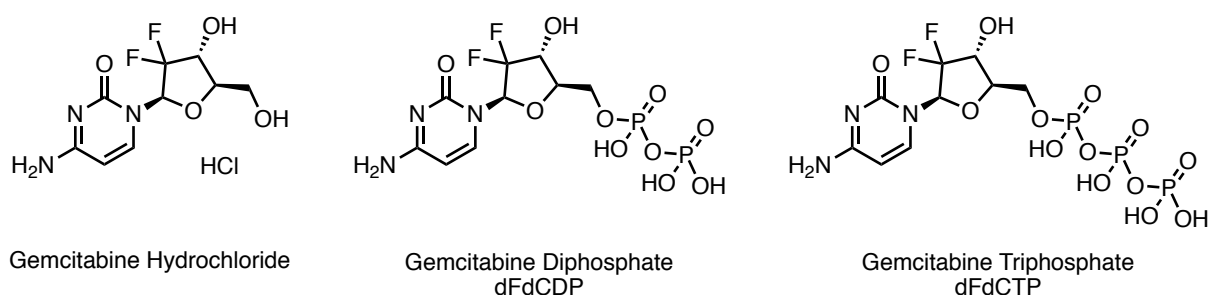


Figure 6.4 Chemical Structure of Pancreatic Cancer Treatment – gemcitabine hydrochloride and its active forms, gemcitabine diphosphate and gemcitabine triphosphate.

Ribonucleotide reductase is inhibited by gemcitabine diphosphate and in turn inhibits DNA synthesis by the lack of deoxynucleotide triphosphate formation. Gemcitabine triphosphate works as a pyrimidine antagonist, it is incorporated into DNA in the S phase and terminates chain elongation.⁷

6.7.3 Epigenetics

Epigenetics is the study of the changes in the expression of genes that do not alter the DNA sequence, a phenotype modification, in contrast to a genotype modification. It can result in the switching of genes on or off, determining which proteins are transcribed, and which are silenced. In some cases, genes are activated or silenced incorrectly, and this can lead to diseases such as Alzheimer's or cancer.⁸

There are three main epigenetic mechanisms: histone modifications, DNA methylation and RNA-associated silencing (Figure 6.5).⁹ This project focuses on histone modifications and, more specifically, H3K9 trimethylation in pancreatic cancer cells. Any additional information on histone modifications could improve the understanding around epigenetic modifications in pancreatic cancer cells and ultimately lead to hypotheses to perhaps reverse the effects.

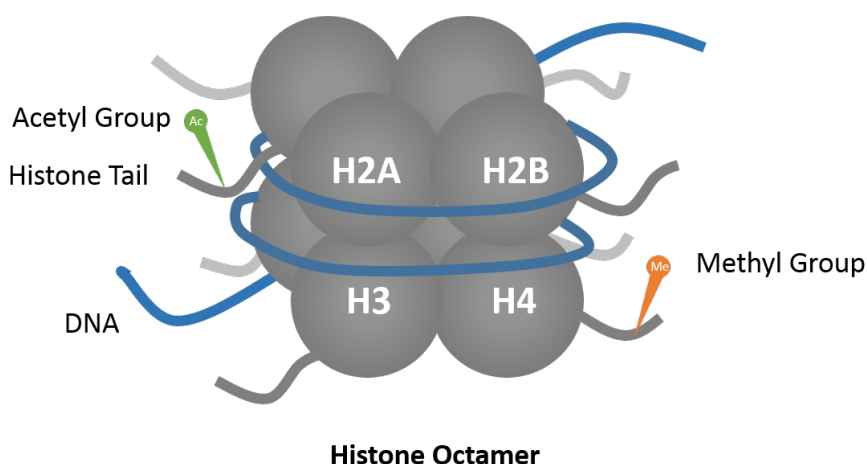


Figure 6.5 Schematic representation of histone modifications

Detection of the differences in methylation levels between cancerous and non-cancerous cells or drug resistant and non-resistant cells could provide valuable information in the progress of diagnostics and therapeutics of pancreatic cancer. Thus, histone H3, lysine 9 (H3K9) trimethylation FRET biosensor, developed by Dr Qin Peng whilst at the University of San Diego, was used for this project.¹⁰

6.7.4 Förster Resonance Energy Transfer (FRET)

Förster (or fluorescence) resonance energy transfer (FRET) is a process in which energy is transferred from a donor fluorophore to an acceptor fluorophore in a non-radiative

mechanism. This process has been illustrated on the Jablonski diagram, shown in Figure 6.6. FRET is a distance dependant phenomenon which allows for energy transfer from a donor molecule to an acceptor molecule. For FRET to occur, the donor and acceptor molecules must be close in proximity, approximately 10-100 Å apart. There must also be spectral overlap; the absorption or excitation spectrum of accepter must overlap with the emission spectrum of the donor for FRET to occur.¹¹

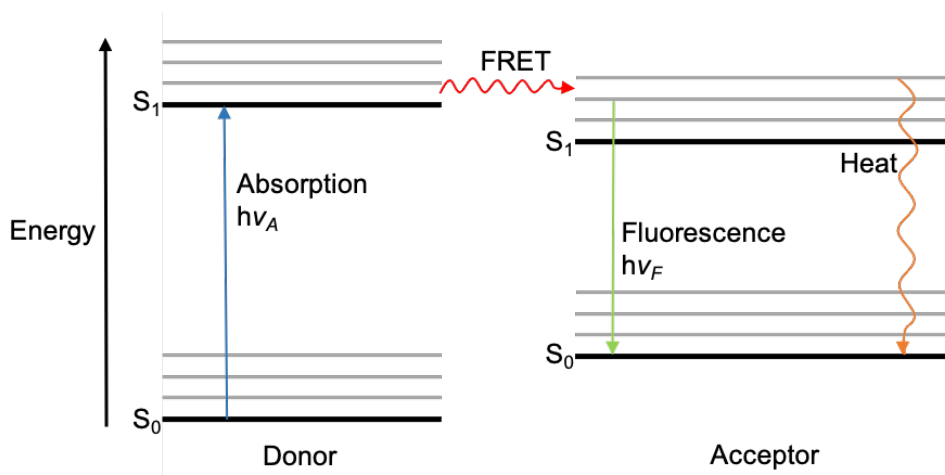


Figure 6.6 Jablonski diagram to show Förster Resonance Energy Transfer (FRET).

6.7.5 Histone H3K9me3 FRET Biosensor

In this project, studies are looking particularly at the levels of trimethylation of histone H3, lysine 9 (H3K9); the loss of the trimethylation of H3K9 has been associated with the metastatic progression of pancreatic cancer.^{12,13} This histone can be methylated or acetylated which can cause changes in chromatin structure. The FRET biosensor used, measures the dynamic trimethylation of H3K9. This methylation can be monitored by quantifying the intensity ratio between yellow fluorescent protein (YPet) and cyan fluorescent protein (CFP) ratio through live cell fluorescence imaging.¹⁰

The biosensor is made up of a Histone H3 core attached to an ECFP (cyan fluorescent protein), an EV linker, HP1 and YPet (yellow fluorescent protein). The biosensor works by the ECFP absorbing light at 433 nm and emitting at either 476 nm (ECFP) or 527 nm (YPet) dependant on the orientation of the chain. When HP1 does not bind to a methyl group, the donor (ECFP) absorbs light at 433 nm and emits at 476 nm, in the cyan region. When methylated, this changes the orientation of the chain, bringing the acceptor fluorescent protein closer to the donor fluorescent protein and the fluorescence emitted is from the acceptor (YPet). This has been illustrated in Figure 6.7. The phenomena can be visualised by fluorescence microscopy and quantified as an intensity ratio.

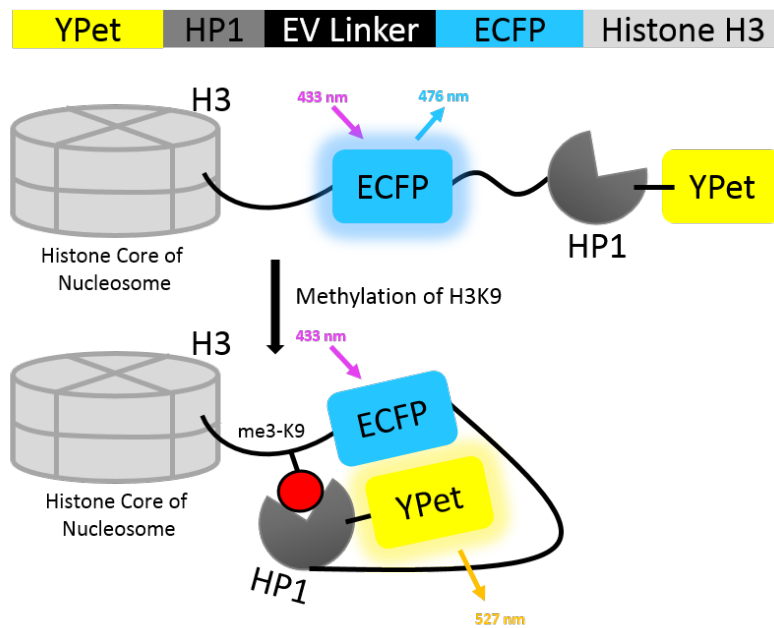


Figure 6.7 Histone H3 Lysine 9 (H3K9) trimethylation FRET biosensor.

6.7.6 Live Cell Fluorescence Imaging

Fluorescence imaging can be used to visualise proteins and specific organelles by selective labelling with fluorescent tags or stains. Specialist fluorescence microscopes must be used to image. For FRET imaging, two separate fluorescent channels must be monitored to visualise both emission wavelengths.

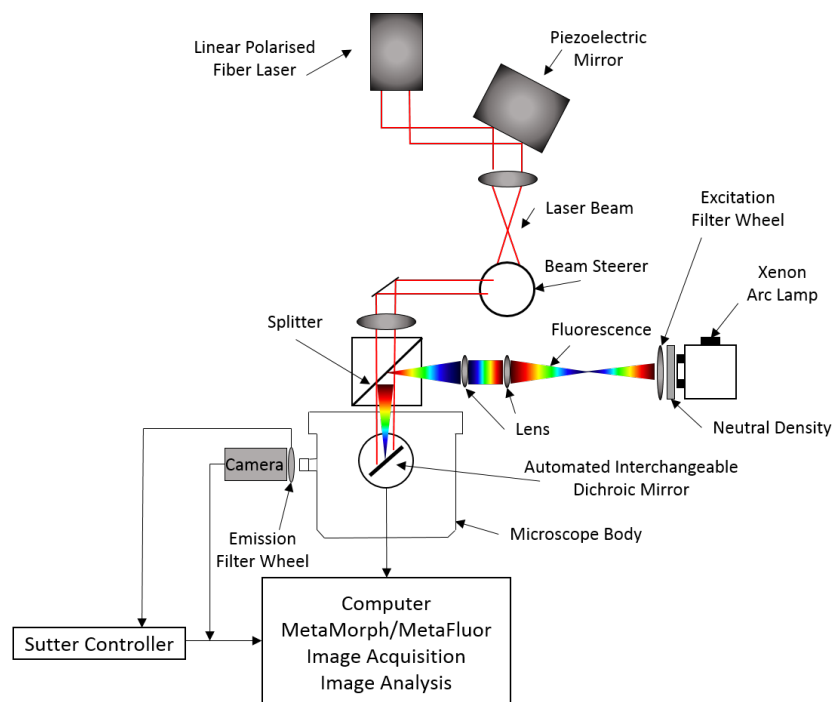


Figure 6.8 Diagram of a fluorescence confocal microscope.

This data can then be taken as a ratio and compared to other relevant data. In the case of the H3K9 trimethylation FRET biosensor, data from both ECFP (476 nm) and YPet (527 nm) channels should be collected and converted to a ratio.

As it has been reported that the loss of trimethylation of H3K9 leads to an increase in metastatic progression in pancreatic cancer,^{12,13} it was sought to explore and compare the differences of histone-3 lysine-9 trimethylation (H3K9me3) levels in two pancreatic ductal adenocarcinoma cell lines: A gemcitabine resistant (up to 100 nM) cell line (R100), and a non-resistant cell line (NR). It was also of interest to determine how these methylation levels would change when the cell lines were subsequently treated with gemcitabine, thus, the cells were subject to gemcitabine treatment over a number of days (no treatment, after 24-, 48- and 72-hours treatment), and monitored to understand how the cells adapted to the treatment.

Having further insight about how cells, both R100 and NR, respond when treated with gemcitabine could aid in an improved understanding of how the cancer can progress and develop resistance.

6.8 Results and Discussion

A series of experiments were carried out to determine the epigenetic differences in two different pancreatic cancer cell lines. The first cell line was PDAC p53 R172H (NR) and the second, a variation of this that had been treated daily with 100 nM gemcitabine to build a resistant cell line (R100).

6.8.1 Initial Comparative Studies

The two cell lines were first measured in parallel, without treatment, to compare their basal H3K9me3 levels. Figure 6.9 displays the H3K9 methylation level by FRET ratio of the two cells lines. It is apparent that the R100 cell line has an overall lower methylation level. This could perhaps be interpreted as the R100 cell line having a faster metastatic progression than the NR cell line.

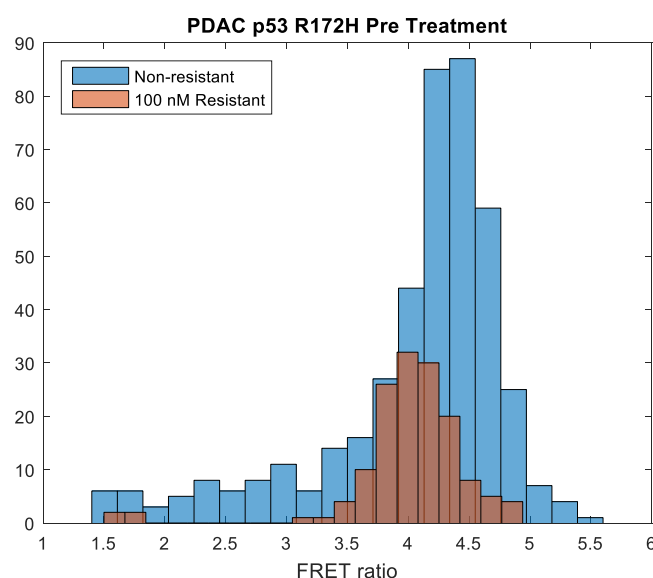


Figure 6.9 Histogram to illustrate the relative baseline FRET ratios of the two PDAC cell lines (R100 (red) and NR (blue)) demonstrating their different H3K9 trimethylation levels.

6.8.2 Effect of Gemcitabine Treatment

Once the basal levels were established the effect of drug treatment on the H3K9me3 level was then explored. As it is the first line of treatment in pancreatic cancer, we looked at the effect of gemcitabine on the epigenetics to determine its effect on the H3K9 trimethylation. To allow for the monitoring of the H3K9me3 level, two sets of PDAC cells; R100 and NR were infected with the H3K9me3 biosensor to allow for the monitoring of changes in this specific histone by fluorescence imaging. Cells to image were chosen manually using MetaMorph imaging software where 20 positions were chosen and monitored every five minutes over six hours.

6.8.3 Time Series Experiments

Time series experiments were carried out to follow the H3K9me3 levels of the R100 and NR pancreatic cancer cell lines. The cells were cultured and then transferred to imaging dishes to collect fluorescence data. The cells were initially imaged without gemcitabine as a control to acquire a basal level. Following the control imaging experiments, gemcitabine was added (to give a final concentration of 2.5 μ M) and the cells were incubated for 24 hours before imaging again. This was repeated twice more until 72 hours had passed. The imaging data was quantified and analysed using the in-lab software, fluocell.¹⁴ Fluocell gives the data as an intensity ratio where blue shows low H3K9 trimethylation and red shows high H3K9 trimethylation (Figure 6.10). The intensity ratio has also been quantified numerically (Figure 6.11).

The H3K9 trimethylation level of the NR cell line initially increased on treatment with gemcitabine, and then stayed constant (no statistical difference) after 48 hours.

For comparison, R100 cells were also treated daily with 2.5 μ M gemcitabine and monitored over 72 hours. An initial increase in FRET ratio (increased trimethylation) was observed as the cells were treated with gemcitabine, however, after 72 hours, the H3K9 trimethylation level had lowered returned almost to the level observed pre-treatment.

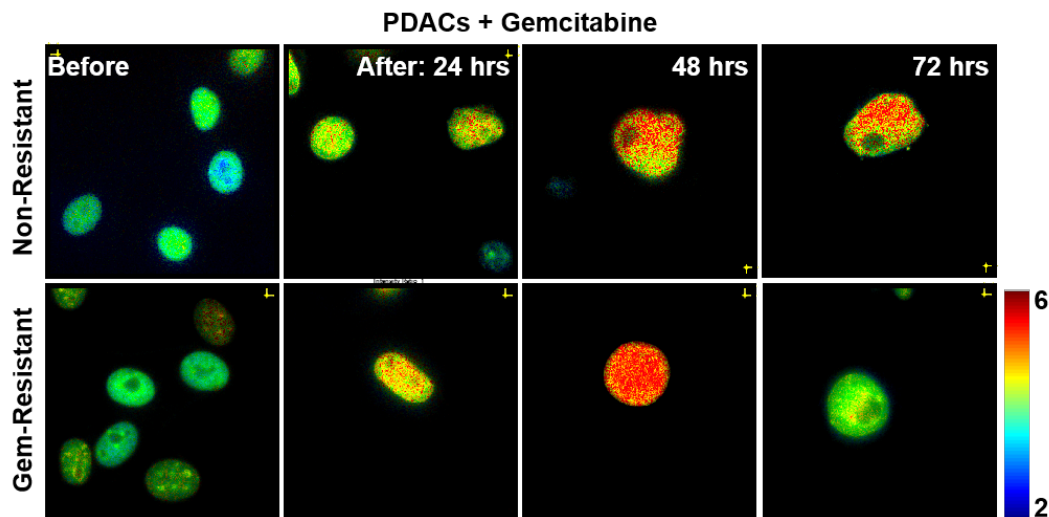


Figure 6.10 Ratio images to show the FRET intensity ratios which correspond to the H3K9 trimethylation levels of the two cell lines (NR – top and R100 – bottom) before and after treatment with gemcitabine over three days. (Red = high levels, Blue = low levels).

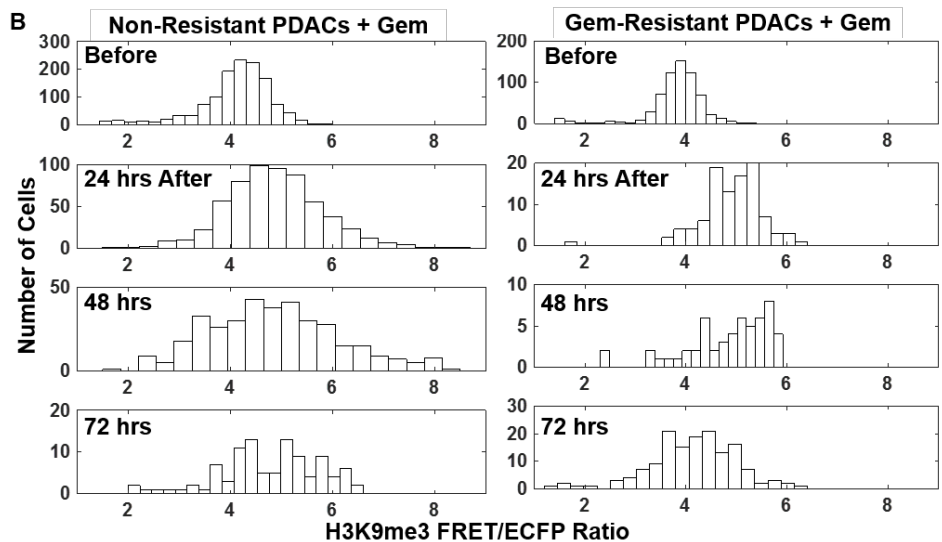


Figure 6.11 Histogram to show the FRET intensity ratios which correspond to the H3K9 trimethylation levels of the two cell lines (NR – left and R100 – right) before and after treatment with gemcitabine over three days.

The results suggest that the R100 cells may have more plastic nuclear chromatin and epigenetics. Thus, these cells can undergo epigenetic adaptation, as evidenced by the clear histone methylation changes upon inhibitor treatment. This treatment may lead to the

reorganisation of the genome architecture and hence the genetic adaption to evade from the drug treatment. The initial H3K9methylation increase and then reduction displays the plastic nature of the 100 nM gemcitabine-resistant cells, indicating an unpacking event of chromatin structures and the exposure and activation of a global scale of genes for adaption.

Future work may involve the inhibition of the histone epigenetic enzymes to examine whether this will prevent the drug-resistant cells from undergoing epigenetic adaption and cause them to become vulnerable to drug treatments.

6.8.4 RNA Sequencing

An additional way to observe the differences of the cell lines is to monitor their gene expression. To do so, RNA sequencing can be carried out or to look specifically at the histone, Chromatin Immunoprecipitation (ChIP) sequencing is available.

Thus, as a preliminary experiment, RNA sequencing was carried out to check for differences in gene expression between the R100 and NR cell lines. Extraction of the RNA was carried out using RNeasy Mini Kit by QIAGEN. The cells at each stage of the time series were collected and their RNA was extracted separately to yield six separate sets of RNA – pre gemcitabine treatment, 48 hours treatment and 72 hours treatment for both the R100 and NR cell lines. Agarose gels were then run to confirm the RNA was intact and not contaminated with DNA. As shown in Figure 6.12, each run shows clear bands corresponding to 28S and 18S (rRNA), confirming that the RNA was intact and uncontaminated.

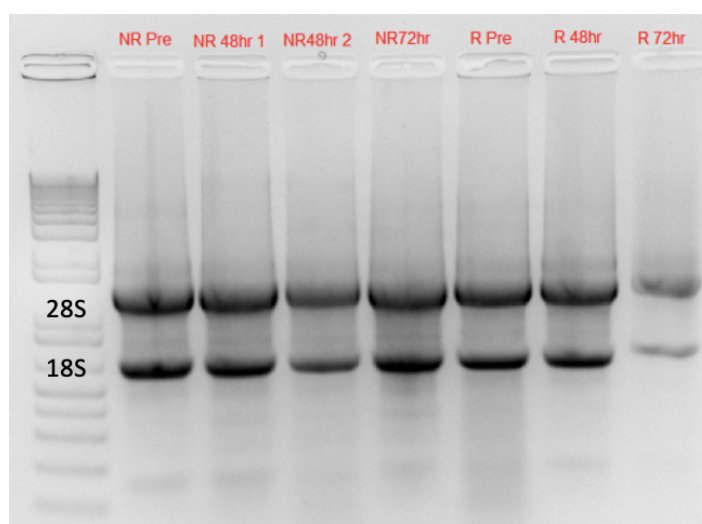


Figure 6.12 From left to right: Ladder, Non-resistant pre-treatment, non-resistant 48-hour treatment (1), non-resistant 48-hour treatment (2), non-resistant 72-hour treatment, 100 nM gemcitabine-resistant pre-treatment, 100 nM gemcitabine-resistant 48-hour treatment, gemcitabine-resistant 72-hour treatment.

These samples were then submitted to UCSD's IGM Genomics Center for RNA sequencing where we are currently awaiting sequencing results. Once the mRNA sequencing has been

completed, the raw data (fastq format) will be aligned to the UCSC reference genome by BOWTIE. The reads that are aligned will then be further analysed for their differential gene expression using DESeq2.

6.8.5 Summary

To summarise, two murine PDAC cell lines (R100 and NR) were used to compare the trimethylation levels of H3K9. H3K9 trimethylation levels were monitored using a FRET biosensor which displays a dynamic FRET/CFP ratio corresponding to the trimethylation. This ratio was monitored through live cell fluorescence imaging.

The cell lines were treated with gemcitabine to monitor how the H3K9 trimethylation levels of the two cell lines adapted to treatment. It was found that both cell lines displayed an initial increase in the trimethylation level, however, the NR cell line stayed high and the R100 cell line lowered almost back to the level observed pre-treatment. These results suggest that the R100 cells are able to adapt on treatment with gemcitabine.

6.9 Experimental Procedures and Analytical Data

6.9.1 Cell lines

LSL-Trp53^{R172H/+} were grown in DMEM (Thermo Fisher Scientific, Cat. No. 11995073) supplemented with 10% FBS (Thermo Fisher Scientific, Cat. No. 10438026) plus 100 units/mL penicillin, 100 µg/mL streptomycin (Thermo Fisher Scientific, Cat. No. 15140122) at 37°C with 5% CO₂. The R100 cell line had the additional reagent 100 nM gemcitabine.

6.10 Cell Culture

Cell culture reagents were purchased from Thermo Fisher Scientific. The murine pancreatic cancer cells (LSL-Trp53^{R172H/+}) were cultured in Dulbecco's Modified Eagle's Medium (DMEM) supplemented with 10% (v/v) fetal bovine serum, 100 units/mL of penicillin, 100 µg/mL of streptomycin, at 37°C with 5% CO₂.

The murine pancreatic cancer cells (LSL-Trp53^{R172H/+} (R100)) were cultured in Dulbecco's Modified Eagle's Medium (DMEM) supplemented with 10% (v/v) fetal bovine serum, 100 units/mL of penicillin, 100 µg/mL of streptomycin, with the additional reagent of 100 nM gemcitabine at 37°C with 5% CO₂.

6.10.1 Cell Plating for Microscopy

Cells were cultured in a glass bottom dish (Cell E&G) coated with 20 µg/mL fibronectin for 16-20 hours before imaging. Cells were then incubated in starvation medium (DMEM 0.5% FBS)

with phenol red at 37°C for 30 minutes, washed twice using PBS, and maintained in the starvation medium (DMEM with 0.5% FBS) for image acquisition.

6.10.2 Image Acquisition and Analysis

Imaging was taken using Nikon ECLIPSE-Ti microscope equipped with a charge-coupled device (CCD) camera, a unique Perfect Focus System (PFS) that automatically corrects focus drift in real time during a prolonged period of time-lapse imaging, as well as a 420DF20 excitation filter, a 450DRLP dichroic mirror, and two emission filters controlled by a filter changer (480DF30 for ECFP and 535DF35 for YPet). Time-lapse fluorescence images were acquired at 5 min interval by MetaMorph 7.8.6.0 software (Molecular Devices, Sunnyvale, California). The ECFP and FRET images were processed and quantified by in-house developed image analysis software package Fluocell, which is developed in MATLAB. The Fluocell source code and documents for Windows and Mac systems can be downloaded from Github (<http://github.com/lu6007/fluocell>). All the ECFP and FRET images were background-subtracted and smoothed with a median filter defined by a 3 × 3 pixel size window. Then the pixelwise ECFP/FRET ratio images were calculated and visualized with the intensity modified display (IMD) method before subjected to quantification and analysis by Excel.

6.10.3 RNA Extraction and Isolation

RNA extraction and isolation was achieved using QIAGEN RNeasy mini kit.

1 × 10⁷ PDAC cells (100 nM gemcitabine resistant and non-resistant) were harvested at the following timepoints: pre-treatment, after 24 hours gemcitabine treatment, after 48 hours gemcitabine treatment and after 72 hours gemcitabine treatment). All cell media and PBS was removed following centrifugation. The cells were then lysed using buffer RLT and homogenised by vortexing for 1 minute. 1 volume of 70% ethanol was added, and this was applied to the column and spun down. The flow through was discarded. Buffer RW1 was added to the column, spun down and the flow through was again discarded. To remove genomic DNA, RQ1 and RNase-free DNase were mixed together and added to the column. The column was then incubated at 37°C for 15 minutes. RNA was then washed with RW1 and Buffer RPE and the flow through discarded. Finally, RNase free water (30-50 µL) was added, and the column was incubated at room temperature for two minutes before being spun down into a clean Eppendorf tube to obtain RNA.

6.11 References

- 1 M. Onoda, S. Uchiyama, A. Endo, H. Tokuyama, T. Santa and K. Imai, *Org. Lett.*, 2003, **5**, 1459–1461.
- 2 *Avogadro: an open-source molecular builder and visualization tool. Version 1.2.0.* <http://avogadro.cc/>.
- 3 M. J. Frisch, G. W. Trucks, H. B. Schlegel, G. E. Scuseria, M. A. Robb, J. R. Cheeseman, G. Scalma, V. Barone, G. A. Petersson, H. Nakatsuji, X. Li, M. Caricato, A. Marenich, J. Bloino, B. G. Janesko, R. Gomperts, B. Mennucci, H. P. Hratchian, J. V. Ortiz, A. F. Izmaylov, J. L. Sonnenberg, D. Williams-Young, F. Ding, F. Lipparini, F. Egidi, J. Goings, B. Peng, A. Petrone, T. Henderson, D. Ranasinghe, V. G. Zakrzewski, J. Gao, N. Rega, G. Zheng, W. Liang, M. Hada, M. Ehara, K. Toyota, R. Fukuda, J. Hasegawa, M. Ishida, T. Nakajima, Y. Honda, O. Kitao, H. Nakai, T. Vreven, K. Throssell, J. A. J. Montgomery, J. E. Peralta, F. Ogliaro, M. Bearpark, J. J. Heyd, E. Brothers, K. N. Kudin, V. N. Staroverov, T. Keith, R. Kobayashi, J. Normand, K. Raghavachari, A. Rendell, J. C. Burant, S. S. Iyengar, J. Tomasi, M. Cossi, J. M. Millam, M. Klene, C. Adamo, R. Cammi, J. W. Ochterski, R. L. Martin, K. Morokuma, O. Farkas, J. B. Foresman and D. J. Fox, 2016, Gaussian, Inc.
- 4 Cancer Research UK, <https://www.cancerresearchuk.org/health-professional/cancer-statistics/statistics-by-cancer-type/pancreatic-cancer/>, (accessed 19 May 2020).
- 5 M. Hidalgo, *N. Engl. J. Med.*, 2010, **362**, 1605–1617.
- 6 C. Gromisch, M. Qadan, M. A. Machado, K. Liu, Y. Colson and M. W. Grinstaff, *Cancer Res.*, 2020, **80**, 3179–3192.
- 7 L. De Sousa Cavalcante and G. Monteiro, *Eur. J. Pharmacol.*, 2014, **741**, 8–16.
- 8 M. Shah and C. Allegrucci, in *Epigenetics: Development and Disease*, ed. T. K. Kundu, Springer Netherlands, Dordrecht, 2013, pp. 545–565.
- 9 M. Ayars and M. Goggins, *Mol. Genet. Pancreat. Cancer*, 2009, **2**, 310–326.
- 10 Q. Peng, S. Lu, Y. Shi, Y. Pan, P. Limsakul, A. V Chernov, J. Qiu, X. Chai, Y. Shi, P. Wang, Y. Ji, Y.-S. J. Li, A. Y. Strongin, V. V Verkhusha, J. C. Izpisua Belmonte, B. Ren, Y. Wang, S. Chien and Y. Wang, *Proc. Natl. Acad. Sci.*, 2018, **115**, E11681–E11690.
- 11 B. Valeur and M. N. Berberan-Santos, *Molecular Fluorescence*, Wiley-VCH Verlag GmbH & Co. KGaA, Weinheim, Germany, 2012.
- 12 C. R. Vakoc and D. A. Tuveson, *Nat. Genet.*, 2017, **49**, 323–324.

- 13 B. D. Paradise, W. Barham and M. E. Fernandez-Zapico, *Cancers (Basel)*., 2018, **10**, 128.
- 14 K. Lu, 2017, Fluocell.